İZMİR KÂTİP ÇELEBİ UNIVERSITY

UDEF ULUSLARARASI ÖĞRENCİ DERNEKLERİ FEDERASYONU
FEDERATION OF INTERNATIONAL STUDENT ASSOCIATIONS
الاتحاد العالمي للمنظمات الطلابية

İZMİR Uluslararası Misafir Öğrenci Derneği

5th International Students Science Congress

Izmir-Turkey

21-22 MAY 2021

Proceedings Book

fenkongre@gmail.com

www.sciencecon.org

5th International Students Science Congress
Proceedings Book

5. Uluslararası Öğrenciler Fen Bilimleri Kongresi
Tam Metin Kitabı

Editor-in-Chief / Sorumlu Editör
Mehmet Çevik

Co-editors / Yardımcı Editörler
Alif Diambu Ngimbi
Furkan Emrem

https://doi.org/10.52460/issc.2021.p

İzmir Kâtip Çelebi Üniversitesi Yayın No: 23

Bu eserin, İzmir Kâtip Çelebi Üniversitesi Yönetim Kurulu'nun 26.10.2021 tarih ve 2021-38 sayılı toplantısında alınan 03 numaralı kararı uyarınca, elektronik kitap olarak yayımlanmasına karar verilmiştir.

Sertifika No: 46629

Editör : Mehmet ÇEVİK
Yardımcı Editörler : Alif Diambu NGIMBI
Furkan EMREM

E-ISBN: 978-605-70737-2-3

International Students Science Congress (5th: İzmir: 2021)
5th International Students Science Congress: Proceedings, 21-22 May 2021 = 5. Uluslararası Öğrenciler Fen Bilimleri Kongresi: Tam Metin Kitabı, 21-22 Mayıs 2021 / Sorumlu editör: Mehmet Çevik; Yardımcı editörler: Alif Diambu Ngimbi, Furkan Emrem — İzmir : İzmir Kâtip Çelebi Üniversitesi, 2021.
Çevrimiçi (IX, 431 Sayfa; 26 cm.). -- (İzmir Kâtip Çelebi Üniversitesi; Yayın No: 23)
ISBN: 978-605-70737-2-3

1. Fen Bilimleri – Kongreler 2. Öğrenciler – Kongreler
I. Çevik, Mehmet – II. Ngimbi, Alif Diambu – III. Emrem, Furkan

Adres : İzmir Kâtip Çelebi Üniversitesi Rektörlüğü, Balatçık Yerleşkesi, 35620 Çiğli İzmir, Türkiye
Telefon : +90 232 329 3535 / 1255 **E-posta** : ykb@ikcu.edu.tr
Belge-geçer : +90 232 386 0888 **Web** : ykb.ikcu.edu.tr

Preface

Dear Participants, Colleagues, and International Students,

It is a great honor and privilege for us to present the Proceedings Book of the 5th International Students Science Congress to the authors and participants of the event. We hope that you will find it useful, exciting and inspiring.

In the last four years we organized our congresses in order to bring together young international researchers working in various science areas and this has really motivated all of us. Due to the ongoing global Covid-19 pandemic, we organized the fifth congress online on May 21-22 this year. This was our second online congress experience. The congress was performed over Zoom and live-streamed on YouTube; you may access videos of the sessions on our Youtube channel. (İzmir Uluslararası Misafir Öğrenci Derneği)

Though it was an online event, we accomplished the fifth congress again with great enthusiasm. About one hundred young researchers from about twenty-five countries gathered for this congress and ninety papers were presented in 17 sessions. In addition to the contributed papers, two intriguing presentations were given by invited speakers: Prof. Dr. Murat Yülek, the Rector of OSTIM Technical University, who spoke about the "University Industry Cooperation & Industry University", and Prof. Dr. Durmuş Günay, former member of Council of Higher Education - YÖK, who spoke about the "Philosophy of Innovation".

The congress particularly encouraged the interaction of international research students and developing academics with the more established academic community in an informal setting to present and to discuss new and current work. Their contributions helped to make the Congress as outstanding as it has been. The Congress provided a setting for discussing recent developments in a wide variety of topics including Agricultural Engineering, Architecture, Biology and Bioengineering, Chemistry and Chemical Engineering, Civil Engineering, Computer Science and Engineering, Electrical, Electronics and Communication Engineering, Food Engineering, Geology Engineering, Mechanical Engineering, Mathematics, Materials Science, Metallurgical and Materials Engineering, Mechatronics Engineering, Nanotechnology, Energy, Textile engineering, Urban and Regional Planning.

We would like to thank all participants for their contributions to the Congress program and for their contributions to these Proceedings Book. It is our pleasant duty to acknowledge the support from İzmir Kâtip Çelebi University, Federation of International Student Associations (UDEF) and İzmir International Guest Student Association.

I would like to express my sincere gratitude and appreciation to our organizing committee and all the students who worked voluntarily during the event.

The continuing success of this congress series means that planning can now proceed with confidence for the 6th International Students Science Congress to be held in 2022; probably both online and in-person.

We thank all authors, participants, and volunteers for their contributions.

Prof. Dr. Mehmet Çevik
Congress Chair

Önsöz

Değerli Katılımcılar, Meslektaşlarım ve Uluslararası Öğrenciler,

5. Uluslararası Öğrenciler Fen Bilimleri Kongresi Tam Metin Kitabını etkinliğin yazarlarına ve katılımcılarına sunmak bizler için büyük bir onur ve ayrıcalıktır. Bunu yararlı, heyecan ve ilham verici bulacağınızı umuyoruz.

Son dört yıldır çeşitli bilim dallarında çalışan genç uluslararası araştırmacıları bir araya getirmek amacıyla kongrelerimizi düzenledik ve bu hepimizi gerçekten motive etti. Devam eden küresel Covid-19 salgını nedeniyle bu yıl beşinci kongremizi 21-22 Mayıs tarihlerinde çevrimiçi olarak gerçekleştirdik. Bu bizim ikinci çevrimiçi kongre deneyimimizdi. Kongre Zoom üzerinden yapıldı ve YouTube'da canlı yayınlandı; İzmir Uluslararası Misafir Öğrenci Derneği Youtube kanalımızdan oturumların videolarına ulaşabilirsiniz.

Çevrimiçi bir etkinlik olmasına rağmen beşinci kongremizi de yine büyük bir istek ve heyecanla gerçekleştirdik. Bu kongre için yirmi beş ülkeden yaklaşık yüz genç araştırmacı bir araya geldi ve 17 oturumda doksan bildiri sunuldu. Bildirilere ek olarak, iki davetli konuşmacımız tarafından gerçekten ilgi çekici sunumlar yapıldı: OSTİM Teknik Üniversitesi Rektörü Prof. Dr. Murat Yülek "Üniversite Sanayi İşbirliği ve Sanayi Üniversitesi" hakkında konuştu; Yükseköğretim Kurulu Yürütme Kurulu eski üyesi Prof. Dr. Durmuş Günay ise "İnovasyon Felsefesi" başlıklı bir sunum gerçekleştirdi.

Kongre, özellikle fen bilimleri alanında eğitimlerine devam eden uluslararası öğrencilerin ve genç akademisyenlerin önlerindeki akademik camia ile etkileşimlerini gayet samimi bir ortam sunarak teşvik ederken, yeni ve güncel çalışmalarını sunmaları ve tartışmaları için de güzel bir fırsat sağlamış oldu. Onların katkıları sayesinde Kongre olabildiğince seçkin ve nitelikli bir düzeye ulaşmış oldu. Kongre, Ziraat Mühendisliği, Mimarlık, Biyoloji ve Biyomühendislik, Kimya ve Kimya Mühendisliği, İnşaat Mühendisliği, Bilgisayar Bilimi ve Mühendisliği, Elektrik, Elektronik ve Haberleşme Mühendisliği, Gıda Mühendisliği, Jeoloji Mühendisliği, Makine Mühendisliği, Matematik, Malzeme Bilimi, Metalürji ve Malzeme Mühendisliği, Mekatronik Mühendisliği, Nanoteknoloji, Enerji, Tekstil Mühendisliği, Kentsel ve Bölgesel Planlama, vb. çok çeşitli konulardaki son gelişmeleri tartışmak için keyifli bir ortam sağladı.

Tüm katılımcılara kongre programımıza ve dolayısıyla Tam Metin kitabımıza yaptıkları katkılardan dolayı teşekkür ederiz. Ayrıca verdikleri destek ile bu kongrenin gerçekleşmesine katkı sağlayan İzmir Kâtip Çelebi Üniversitesi'ne, Uluslararası Öğrenci Dernekleri Federasyonu'na (UDEF) ve ana organizatörümüz İzmir Uluslararası Misafir Öğrenci Derneği'ne teşekkürlerimizi arz ederiz.

Organizasyon komitemize ve etkinlik süresince gönüllü olarak çalışan tüm öğrencilere içten şükran ve takdirlerimi sunuyorum.

Bu kongre dizisinin devam eden başarısı, 2022'de düzenlenmeyi hedeflediğimiz 6. Uluslararası Öğrenciler Fen Bilimleri Kongresi için planlamanın artık güvenle ilerleyebileceği anlamına geliyor; bu kongre muhtemelen hem çevrimiçi hem de yüz yüze olacak.

Katkılarından dolayı tüm yazarlara, katılımcılara ve gönüllülere teşekkür ederiz.

Prof. Dr. Mehmet Çevik
Kongre Başkanı

Organizing Committee / Düzenleme Kurulu

Prof. Dr. Mehmet Çevik (Congress Chair)

Alif Diambu Ngimbi (Congress Secretary)

Furkan Emrem

Assist. Prof. Dr. Ahmet Aykaç

Assoc. Prof. Dr. Faruk Özger

Assist. Prof. Dr. Ayşe Kalaycı Önaç

Assoc. Prof. Dr. Gökçen Bombar

Ahenk Karcı Demirkol

Hande Gündel

Ala Jehad

Mustafa Öncül

Scientific Committee / Bilim Kurulu

Prof. Dr. Abdelraouf A. Elmanama (Islamic University of Gaza, Palestine)
Prof. Dr. Adnan Kaya (İzmir Kâtip Çelebi University, Turkey)
Prof. Dr. Ahmed Hussein Kamel Ahmed Elshafie (University of Malaya, Malaysia)
Prof. Dr. Ahmet Koyu (İzmir Kâtip Çelebi University, Turkey)
Prof. Dr. Ahmet Türk (Manisa Celal Bayar University, Turkey)
Prof. Dr. Akeel H. Ali Al-Assie (Tikrit University, Iraq)
Prof. Dr. Ali Mohammed Ibrahim (Jimma University, Ethiopia)
Prof. Dr. Amin Solaiman Badawy (Tikrit University, Iraq)
Prof. Dr. Antonio Vargas-Berenguel (Universidad de Almería, Spain)
Prof. Dr. Aydın Akan (İzmir Kâtip Çelebi University, Turkey)
Prof. Dr. Aydoğan Savran (Ege University, Turkey)
Prof. Dr. Ayşegül Alaybeyoğlu (İzmir Kâtip Çelebi University, Turkey)
Prof. Dr. Bayram Şahin (Ege University, Turkey)
Prof. Dr. Buket Okutan Baba (İzmir Kâtip Çelebi University, Turkey)
Prof. Dr. Ekrem Alimi ("Kadri Zeka" University – Gjilan, Kosovo)
Prof. Dr. Erdal Çelik (Dokuz Eylül University, Turkey)
Prof. Dr. Fatih Erdoğan Sevilgen (Gebze Technical University, Turkey)
Prof. Dr. Figen Kırkpınar (Ege University, Turkey)
Prof. Dr. Issa M. El Nahhal (Al Azhar University-Gaza, Palestine)
Prof. Dr. Md. Ashraful Hoque (Islamic University of Technology, Bangladesh)
Prof. Dr. Mehmet Ali Yurdusev (Manisa Celal Bayar University, Turkey)
Prof. Dr. Mehmet Çevik (İzmir Kâtip Çelebi University, Turkey)
Prof. Dr. Mehmet Sezer (Manisa Celal Bayar University, Turkey)
Prof. Dr. Musa Alcı (Ege University, Turkey)
Prof. Dr. Nazar Mohammad Halim (Kabul University, Afghanistan)
Prof. Dr. Nihat Sami Çetin (İzmir Kâtip Çelebi University, Turkey)
Prof. Dr. Nilgül Çetin (İzmir Kâtip Çelebi University, Turkey)
Prof. Dr. Nurcan Baykuş Savaşaneril (Dokuz Eylül University, Turkey)
Prof. Dr. Ramazan Karakuzu (Dokuz Eylül University, Turkey)
Prof. Dr. Sahib Jumaa Abdurrahman (Tikrit University, Iraq)
Prof. Dr. S. Bahadır Yüksel (Konya Technical University, Turkey)
Prof. Dr. Şerafettin Demiç (İzmir Kâtip Çelebi University, Turkey)
Prof. Dr. Roberta Katlen Fusco Marra (Universidade Salgado de Oliveira, Brazil)
Prof. Dr. Tevfik Tansel Tanrıkul (İzmir Kâtip Çelebi University, Turkey)
Assoc. Prof. Dr. Ali Konuralp (Manisa Celal Bayar University, Turkey)
Assoc. Prof. Dr. Ali Yurddaş (Manisa Celal Bayar University, Turkey)
Assoc. Prof. Dr. Aytuğ Onan (Manisa Celal Bayar University, Turkey)
Assoc. Prof. Dr. Berra Gültekin Sınır (Manisa Celal Bayar University, Turkey)
Assoc. Prof. Dr. Cem Tozlu (İzmir Kâtip Çelebi University, Turkey)
Assoc. Prof. Dr. Ceyhun Araz (Manisa Celal Bayar University, Turkey)
Assoc. Prof. Dr. Ersin Aslan (Manisa Celal Bayar University, Turkey)
Assoc. Prof. Dr. Fabienne Anne Chantal Dumoulin (Gebze Technical University, Turkey)
Assoc. Prof. Dr. Fethullah Güneş (İzmir Kâtip Çelebi University, Turkey)

Assoc. Prof. Dr. Gökçen Bombar (İzmir Kâtip Çelebi University, Turkey)
Assoc. Prof. Dr. Hubert Chapuis (Université de Lorraine, France)
Assoc. Prof. Dr. Kamil Şirin (Manisa Celal Bayar University, Turkey)
Assoc. Prof. Dr. Levent Aydın (İzmir Kâtip Çelebi University, Turkey)
Assoc. Prof. Dr. Levent Çetin (İzmir Kâtip Çelebi University, Turkey)
Assoc. Prof. Dr. Merih Palandöken (İzmir Kâtip Çelebi University, Turkey)
Assoc. Prof. Dr. Mücahit Sütçü (İzmir Kâtip Çelebi University, Turkey)
Assoc. Prof. Dr. Muhammad Mukhlisin (Politeknik Negeri Semarang, Indonesia)
Assoc. Prof. Dr. Mustafa Akyol (Manisa Celal Bayar University, Turkey)
Assoc. Prof. Dr. Mustafa Can (İzmir Kâtip Çelebi University, Turkey)
Assoc. Prof. Dr. Mustafa Erkan Turan (Manisa Celal Bayar University, Turkey)
Assoc. Prof. Dr. Mustafa Erol (Dokuz Eylul University, Izmir, Turkey)
Assoc. Prof. Dr. Neritan Shkodrani (Polytechnic University of Tirana, Albania)
Assoc. Prof. Dr. Nesrin Horzum Polat (İzmir Kâtip Çelebi University, Turkey)
Assoc. Prof. Dr. Ozan Karaman (İzmir Kâtip Çelebi University, Turkey)
Assoc. Prof. Dr. Ömer Öztürkoğlu (Yaşar University, Turkey)
Assoc. Prof. Dr. Özlem Çağındı (Manisa Celal Bayar University, Turkey)
Assoc. Prof. Dr. Sercan Acarer (İzmir Kâtip Çelebi University, Turkey)
Assoc. Prof. Dr. Süleyman Murat Bağdatlı (Manisa Celal Bayar University, Turkey)
Assoc. Prof. Dr. Utku Kürşat Ercan (İzmir Kâtip Çelebi University, Turkey)
Assoc. Prof. Dr. Ümit İşci (Gebze Technical University, Turkey)
Assoc. Prof. Dr. Z. Haktan Karadeniz (İzmir Kâtip Çelebi University, Turkey)
Assist. Prof. Dr. Abdelkhalk Aboulouard (Université Sultan Moulay Slimane, Morocco)
Assist. Prof. Dr. Abdulfetah Shobole (Istanbul Sabahattin Zaim University, Turkey)
Assist. Prof. Dr. Adil Ali Haydir Hassan (Tikrit University, Iraq)
Assist. Prof. Dr. Ahmet Aykaç (İzmir Kâtip Çelebi University, Turkey)
Assist. Prof. Dr. Ayşe Kalaycı Önaç (İzmir Kâtip Çelebi University, Turkey)
Assist. Prof. Dr. Aytunga Bağdatlı (Manisa Celal Bayar University, Turkey)
Assist. Prof. Dr. Daniel Hatungimana (Université du Burundi, Burundi)
Assist. Prof. Dr. Ebubekir Atan (İzmir Kâtip Çelebi University, Turkey)
Assist. Prof. Dr. Emine Kemiklioğlu (Manisa Celal Bayar University, Turkey)
Assist. Prof. Dr. Faruk Özger (İzmir Kâtip Çelebi University, Turkey)
Assist. Prof. Dr. Fatih Cemal Can (İzmir Kâtip Çelebi University, Turkey)
Assist. Prof. Dr. İlker Polatoğlu (Manisa Celal Bayar University, Turkey)
Assist. Prof. Dr. Mabvuto Mwanza (University of Zambia, Zambia)
Assist. Prof. Dr. Mehmet Alper Çankaya (İzmir Kâtip Çelebi University)
Assist. Prof. Dr. Mohammed Wadi (Istanbul Sabahattin Zaim University, Turkey)
Assist. Prof. Dr. Moustapha Maman Mounirou (Abdou Moumouni University, Niger)
Assist. Prof. Dr. Muhammad Imran Shakir (King Saud University, Saudi Arabia)
Assist. Prof. Dr. Muhammad Shahid (The Islamia University of Bahawalpur, Pakistan)
Assist. Prof. Dr. Mutlu Seçer (İzmir Kâtip Çelebi University, Turkey)
Assist. Prof. Dr. Nihad A. Jafar (Tikrit University, Iraq)
Assist. Prof. Dr. Onur Ertuğrul (İzmir Kâtip Çelebi University, Turkey)
Assist. Prof. Dr. Özgün Yücel (Gebze Technical University, Turkey)
Assist. Prof. Dr. Saim Kural (Manisa Celal Bayar University, Turkey)
Assist. Prof. Dr. Samuel Bunani (Karlsruhe Institute of Technology, Germany)

Assist. Prof. Dr. Sedat Yalçınkaya (İzmir Kâtip Çelebi University, Turkey)
Assist. Prof. Dr. Sema Demirci Uzun (İzmir Kâtip Çelebi University, Turkey)
Assist. Prof. Dr. Selçuk Saatcı (İzmir Institute of Technology, Turkey)
Assist. Prof. Dr. Şeyma Aykaç (Ege University, Turkey)
Assist. Prof. Dr. Takhi Belkacem (University of Amar Telidji, Algeria)
Assist. Prof. Dr. Tamara Kawther Hussein (Al-Mustansiriyah University, Iraq)
Assist. Prof. Dr. Tarkan Akderya (Bakırçay University, Turkey)
Assist. Prof. Dr. Umut Ceyhan (İzmir Kâtip Çelebi University, Turkey)
Assist. Prof. Dr. Violeta Rodriguez-Ruiz (The University of Cergy-Pontoise, France)
Assist. Prof. Dr. Waleed Fadel (Girne American University, TRNC)
Assist. Prof. Dr. Walid Sharmoukh Ahmed Moustafa (National Research Centre, Egypt)
Assist. Prof. Dr. Yiğit Aksoy (Manisa Celal Bayar University, Turkey)
Dr. Alex Modi Lomoro Wani (Management System International, South Sudan)
Dr. Amir Shirzadi (University of Cambridge, United Kingdom)
Dr. Ansoumana Noumou Djite (Senegal)
Dr. Ayşe Kurt Bahşı (Manisa Celal Bayar University, Turkey)
Dr. Fakhra Liaqat (Pakistan)
Dr. Habibu Aminu Hussain (Kano University of Science and Technology, Nigeria)
Dr. Hiba Yahyaoui (University of Tunis, Tunisia)
Dr. Ibrahim Karidio Diori (Niger)
Dr. Ismael Abdou Souley (Niger)
Dr. Juan Manuel Casas-Solvas (University of Almeria, Spain)
Dr. Khalid Abdalla Abdelhalim (Dokuz Eylül University, Turkey)
Dr. M. Malick Diallo Nethehi (Guinea)
Dr. M. Mustafa Bahşı (Manisa Celal Bayar University, Turkey)
Dr. Muhammad İlyas Khazi (State Key Laboratory, China)
Dr. Shadman Tariq Sadiq (Tikrit University, Iraq)
Dr. Sivarama Krishna Lakkaboyana (Universiti Teknologi Malaysia, Malaysia)
Dr. Sümeyye Sınır (İzmir Kâtip Çelebi University, Turkey)
Dr. Zoltán Fülöp (Budapest, Hungary)

Invited Speakers / Davetli Konuşmacılar

University Industry Cooperation and Industry University

Prof. Dr. Murat Yülek

Rector of OSTİM Technical University

Philosophy of Innovation

Prof. Dr. Durmuş Günay

Former Member of Turkish Council of Higher Education (YÖK)

Maltepe University Faculty Member

Table of Contents

Revaluation of Ksar El-Haouita in Laghouat, Algeria

*Fatiha Imane Mahcar**, *Belkacem Takhi*
Department of Architecture, Amar Thelidji University of Laghouat, Laghouat, Algeria
**Corresponding author: mouniimy6@gmail.com*

Abstract

Algeria has a rich urban and architectural heritage, which presents regional specificities. Once the ksour was a symbol of balance and perfect harmony with its environment, unfortunately today they no longer reflect their former function.

The Ksourian architecture, including that of Laghouat is a prestigious heritage of high value; it is the testimony of genius knowledge and the capacity of their occupants to adapt to the difficult environment. The housing is considered the essential core of this architecture it represents the entire composition of the ksar, its design is inspired by the immediate environment and respects ancestral social values. It is characterized by a simple architecture and simple construction techniques which are based on the construction in load-bearing walls, the construction materials used are local materials of great resistance and less expensive.

This study addresses the theme revaluation of heritage, particularly our case study ksar El-Haouita which has experienced a neglecting and depopulation due to several factors. The ksar El-Haouita is among the most famous ksour located in the south of Algeria and exactly in the region of Laghouat. It is built with simple materials and techniques of construction. The construction materials used are local materials like stones and lime found in the environmental surroundings of the ksar.

The aim of this study is to identify the major causes of the degradation of ksar, also to preserve ksar El-Haouita through specific operations and to improve the tourist attractiveness of ksar El-Haouita in order to promote heritage, to convert it back into sustainable Saharan tourism.

Our study based in the first place; on a theoretical underpinning which contains the notions that have a relation with our theme, the problematic and the envisaged objective, then a presentation of ksar followed by a morphological analysis accompanied by identification of the problems to identify the phenomena of damage and its disfigurement. The last step is to treat an aspect for the development of ksar, this aspect is devoted to the restitution of the defensive system (doors, ramparts, ramparts of houses and towers) of the ksar, through a diagnostic and several operations like (rehabilitation and reconstruction).

The aim result of this study is to show that the revaluation of the ksar is a very vast operation and proposes interventions that allow the preservation of the ksar and also to understand the elements that help the success of interventions and to put some of the parameters considered as reference elements and basic principles for the operations on the ksar and among these operations it is (the case study, which is the restitution of the defensive system of ksar El-Haouita).

Keywords: revaluation, ksar el-haouita, morphological analysis

Introduction

The rich urban and architectural heritage of Algeria which presents regional specificities: Mozabite in the South, Kabyle in the center, Arab-Muslim in the North, mainly in the cities of Algiers and Oran. However, urban policies have largely favored the urban expansion of cities and little supports for this heritage, in particular that of the central fabrics of cities. [1]

Despite the climate, arid and difficult nature of the Algerian desert territory which occupies four-fifths of the total area of the country, populations have chosen to settle there, to live and to adapt in this aggressive environment. These populations have invented all their knowledge and their genius to create human settlements that can protect them against the disturbing factors of this region, these settlements are known as "ksour" and they are the product of a culture and of a set of moral values. The ksour thus represent a highly qualified heritage due to its values and its architectural and urban qualities, they are characterized by a typical architecture strongly linked in history by the availability of water, building materials and also the geological and morphological environment, it is homogeneous, its foundations and its characteristics being inspired by the genius of man to adapt to his environment. [2] Formerly the ksour were a symbol of balance and perfect harmony with the arid environment, unfortunately today

they no longer reflect their old function, in recent decades the Algerian ksour and in particular those of Laghouat the "ksar of El-Haouita" have experienced degradation, this heritage is constantly neglected and depopulated which can lead to its total disappearance, several factors come together, contributing and accelerating the degradation of this prestigious heritage.

To remedy this situation, interventions such as a rehabilitation operation are more than necessary, in order to allow future generations to understand the culture of their ancestors and why not reintegrate them again into these heritage dwellings or quite simply reconvert them, as part of sustainable Saharan tourism, this contributes to local development and comes back by the benefit to the country.

Materials and Methodology

Study Area

The town of Laghouat shares its limits with two towns of the highlands (Tiaret and Djelfa) and two others of the South which are (El Bayadh and Ghardaia). (See Fig. 1). So, the town of Laghouat constitutes an open door to the great south. It is located at: 410 km from Algiers (capital); 103 km from Djelfa 187 km from Ghardaïa, 270 km from Tiaret and 230 km from El Bayadh. [3]

Figure 1. The situation of Laghouat [4]

The ksar of El-Haouita is located northeast of the city of El-Haouita 40 km southwest of Laghouat, limited to the north by the river and the gardens and to the south by the houses of the city of El-Haouita. (See Fig. 2). [3]

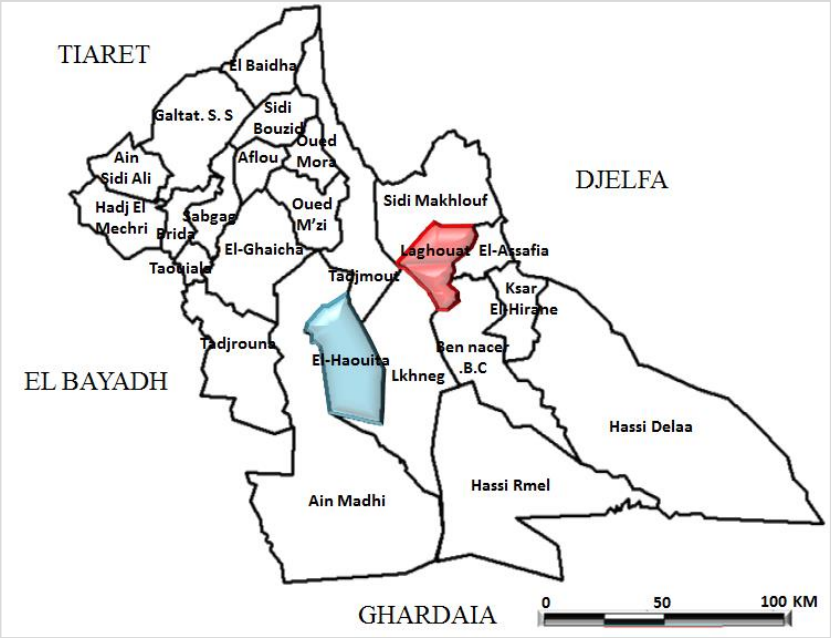

Figure 2. The situation of the town of El-Haouita

Research Methodology

The morphological approach is defined as a tool for understanding traditional fabrics in a clear and explicit way the complexity of the morphological relationships that reign in old neighborhoods through two modes which are:

The mode of distribution (parcel and street system) and the mode of occupation (built and open spaces system) [5]. We can present the processes of this approach in the following diagram: (See Fig. 3)

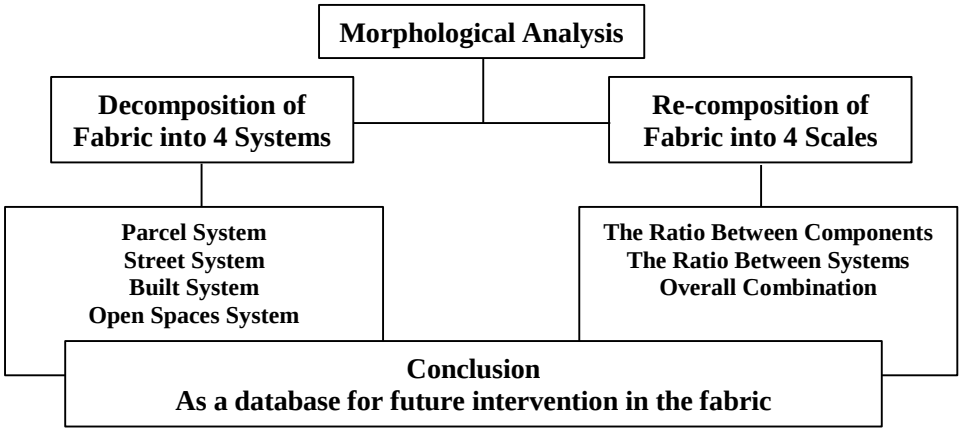

Figure 3. The processes of morphological analysis

Results and Discussion

Morphological Analysis of Ksar El-Haouita

Among the traditional fabrics we have our case study; it is the ksar El-Haouita which is characterized by its seniority which allows us to take it as a conceptual landmark of traditional architecture. The morphological analysis of ksar El-Haouita is shown in Tables 1 and 2.

After this morphological analysis, we can emerge the characteristics that present the identity of ksar El-Haouita which must be taken into account in each intervention:

- The fabric characterized by a no ramified planar built.
- Introverted architecture with the courtyard in the house as the basic unit.
- Hierarchical street system from public to private (street, alley and blind alley).
- The blind alley is between 1.35m to 2m and for the commercial street is 4.20m.

- The template is limited between (ground floor to the first floor).
- Blind facades.

The notion of privacy is presented by:

- The use of a public to private crossing space provided by the places.
- The arrangement of the entrance doors in relation to each other.

Table 1. The decomposition of ksar El-Haouita

Decomposition			
Parcel System	Street System	Built System	Open Spaces System
▪Typology of parcels systems: are found in the form of a combination of not deformed rectangular parcel and fan-shaped rectangular parcel. ▪Articulation of the dif-ferent parcels systems: the whole urban fabric presents a juxtaposition of different parcel (large and small parcel).	▪The encounter is orthogonal: the hier-archy of the streets is not changed. ▪The frontal continuity of space prevails over the lateral side.	▪Planar built: the buildings are attached to each other on all sides to form a continuous mass. ▪No ramified planar built. ▪The type of volumes: building with a central courtyard.	▪The built elements are continuous (contiguous) and the open space is discontinuous.

Table 2. The re-composition of ksar El-Haouita

Re-composition		
Topological Ratio Between Systems	The Ratio Between the 4 Systems	The Ratio Between Systems
The parcels are positioned in relation to each of the streets that form the street system.	The nature of open space: The open space is very clearly subdivided into a public zone (P) and a private zone (p), in this case the private space is isolated from all sides and without any communication with the other private spaces.	The different types of street system combine with the different types of occupation: buildings and open space. This involves making an inventory of the possible combinations between: ▪The variety of distribution systems: parcel system + street system. ▪The variety of occupancy systems: built system + open spaces system.

This study has allowed us to understand the elements that help the success of the interventions and to put certain parameters considered as reference elements and basic principles for the operations on the ksar.

Also, shows that the revaluation of the ksar is a very large operation and proposes interventions that allow the preservation of the ksar.

Study of the Defensive System (Rampart, Towers, Doors and Rampart Houses) of Ksar El-Haouita:

The ksar El-Haouita is characterized by its defensive system through its fabric which is closed and compact formed by houses which are rampart houses.

The defensive system of ksar El-Haouita contained ramparts, rampart houses, towers and doors.

The Current State of the Defensive System of Ksar El-Haouita:
For the current state of the defensive system of ksar El-Haouita we note that the majority of the system

in bad condition such as the houses ramparts and doors. For the ramparts and towers are in ruins. (See Fig. 4)

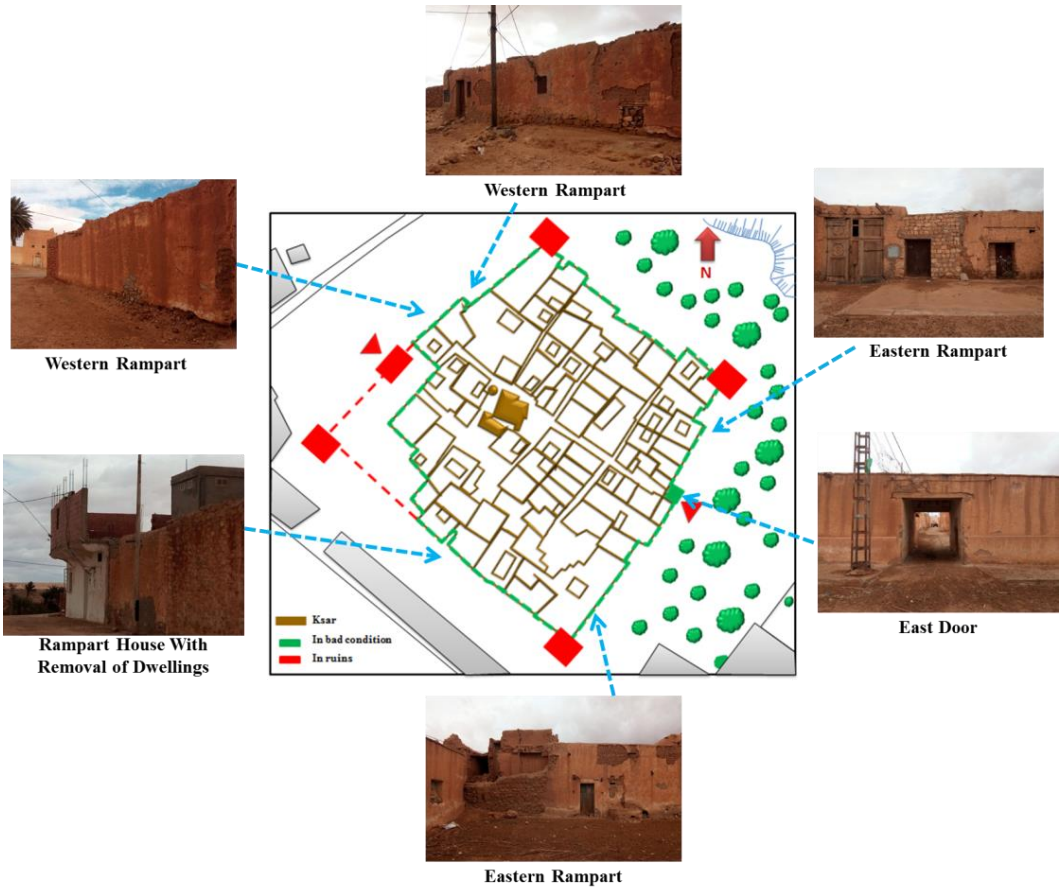

Figure 4. The current state of the defensive system of ksar El-Haouita

Diagnosis

According to several visits to the ksar, the pathologies noticed in the ksar El-Haouita are as follows:
The use of heterogeneous materials (cement).
Superficial cracks.
The degradation of the plaster.
Degradation of the base of walls.
The capillary rise.
Degradation of doors.
Collapse of walls.
The most of the causes of these pathologies are:

- Water stratification.
- Absence of maintenance.
- Rainwater infiltration.

The Restitution of the Defensive System of the Ksar El-Haouita
According to the diagnosis, the following interventions are proposed: (See Fig. 5)

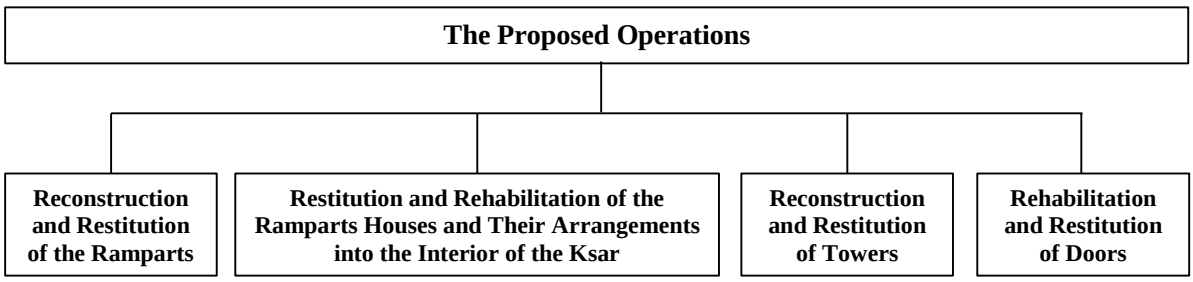

Figure 5. Diagram of the proposed operations for the defensive system of ksar El-Haouita

The study of the defensive system of ksar El-Haouita which contains a diagnosis, interventions and operations for the restitution of the defensive system.

While keeping the architectural aspect of the ksar, basing it on historical data in order to revalue it and restore it to its initial appearance.

The Proposed Strategy

The main objective of our study is the revaluation of the ksar El-Haouita through the valuation of its tourist potential and the attraction of its inhabitants who have deserted it for other new neighborhoods better equipped with basic infrastructure and local services.

Experience has shown that any architectural heritage conservation policy which consists solely of to clog the cracks, renew the plasters and make new the buildings, finds it difficult to fix the population which resides there and did not allow the return of the population which had left it.

For this reason, we are proposing a renovation plan which includes various planning operations, in the objective of which is to provide. Firstly, the Ksar with a basic infrastructure which allows the inhabitants who still reside there to lead a life of descent. On the other hand, to make it find its cultural and spiritual role through the creation of three tourist routes (territorial, regional and on the scale of the ksar) intended to receive nationals who come to visit it at times of religious holidays, such as attracting international tourists by encouraging cultural tourism.

Also, it aims to, the inclusion of gardens and beautiful landscapes in the renovation plan of the Ksar.

Highlighting the scientific tourism value in El-Haouita through the funerary monuments that are located near to El-Haouita.

It was also suggested that part of the existing residences in the Ksar be like a residence for tourists.

Promoting and valorization of the intangible heritage of El-Haouita because it is the one that brings tourists. It is represented by the weaving of carpets, traditional clothes, holidays and popular events. Especially the traditional methods of construction, as El-Haouita was famous in the past for the manufacture of stone machines, by the found of kilns for preparing lime and mortars (for restoration).

Conclusion

The Ksourian architecture of Laghouat such as the ksar of El-Haouita represents a prestigious heritage of high value; it is the testimony of genius to know and the capacity of their occupants to adapt to the difficult environment. Unfortunately, this image does not exist today, this heritage is constantly subject to depopulation which causes its degradation and accelerates its decline, various factors (natural and human factors...) generate the disorder of these ksour. Safeguarding this heritage is more than necessary in order to enhance it and improve its condition, to define the future generations of the architectural values of this heritage and to benefit from it to the tourism sector.

For the preservation and revaluation of ksar El-Haouita in Laghouat, the implementation of an intervention methodology for the rehabilitation of the ksar is necessary. This led us to touch on the aspect, of the restitution of the defensive system of ksar El-Haouita.

All these proposals and solutions were brought from the desirable theoretical framework to be applied in reality. The final objective that we wish to achieve of keeping the historical and architectural aspect of the ksar of El-Haouita as a testimony of a rich civilization in order to ensure its conservation and transmission to future generations.

References

[1] Mazouz F. Le renouvellement du patrimoine bâti vétuste (le cas du centre-ville d'Oran). Doctoral thesis. Université des Sciences et Technologie Mohamed Boudiaf-Oran. 2015.
[2] Brik B, Smaali A. La réhabilitation des ksour de la veille ville de Nigrine, Cas d'études : (Types de maisons ksouriennes). Master thesis. Université Larbi Tébessi-Tébessa, 2015.
[3] PPMVSA. Plan Permanent de Mise en Valeur et de Sauvegarde des Sites Archéologiques, la direction de la culture de la wilaya de Laghouat, 2018.
[4] Anonymous. The guardian, https://guardian.ng/news/algeria-reconciliation-proves-elusive-decade-after-deal/, 2015. (Date of access: 24.04.2021)
[5] Borie A, Denieul F. Etude et document sur le patrimoine culturel, Méthode d'analyse morphologique des tissus urbains traditionnels, UNESCO. Paris, France, 1984.

Globalization Processes in Architecture

*Nadjla Fellahi**
Izmir Institute of Technology, Dept. of Architecture, Izmir, Turkey
**Corresponding author: nadjlafellahi14@gmail.com*

Abstract

The beginning of globalization according to Karl Marx's anticipation when the Bourgeoisie class were expending their products to reach the whole globe starting from the mid of the 19th century, other scholars assume that globalization can be seen as a thread run through all the past humanities starting from our ancestors and their migration across the world which makes no fixed beginning nor an expected end of it. Globalization changed the relations between producers and consumers, also it broken various links between labor with family, daily life, as well as national attachments. The objective of this article is to discuss the progress of the globalization in the field of architecture, its signs, and its processes. The article also demonstrates how the aspect of localities has been affected by the global forces which will be done through two case studies: Algiers and Istanbul. The results expose that Globalization approach can be defined from various perspectives, but what common in these viewpoints is the "Mobility" of thoughts, objects, people, and ideas between regions, nations, and continents. The stereotype aspect of global cities which characterized by tall-sized buildings, the new materials, the sophisticated facades, new technologies etc., has impacted on the priorities of people and authorities of various countries like Algeria, and Turkey.

Keywords: globalization, localities, processes, architecture, Istanbul, Algiers

Introduction

"*It comprises a set of historical changes that are leading to an ever higher degree of interdependence and interconnectedness. A consciousness of these changes is widely shared around the globe, as is an awareness that they are affecting human experience, in varying ways, in every part of the globe.*" [1].

In order to begin discussing about globalization, it is essentially to highlight Karl Marx anticipation on the current process of globalization by describing historically how modern industry established the world market by the bourgeoisie class who were expanding their products to reach the whole globe and making connections everywhere which led to create a cosmopolitan character of production and consumption. Mazlich assumes that globalization can be seen as a thread run through all the past humanities starting from our ancestors and their migration across the world which makes no fixed beginning nor an expected end of globalization. He believes in an earlier globalization where merchant empires shifts are a part from it, and a new globalization which emerged after the World War II when "Globalization" becomes a word in human vocabulary which deals with issues and problems that can be solved only by global efforts. Globalization can be defined according to Sklair by three different aspects: generic globalization which is related to electronic and postcolonial revolution which are the most significant phenomena in the mid of 20th century, capitalist globalization which is related to the dominance of capitalism as a global system in the start of 21st century, alternative globalization which supports global participations and human values and opposes the negative aspects of globalization's aspects [2]. Different perspectives about how globalization occurred and can be identified, it can be seen according to the very fist the transmission operations of goods and people and its processes, or according to the Industrial and technological Revolutions with the emergence of political phenomena of the recent centuries.

Localities, Architecture, & Globalization

Globalization changed the relations between producers and consumers, also it broken various links between labour with family, daily life, as well as national attachments [3]. Nowadays, there is a contemporary condition for the identity's representation which resulted by the increasing production of a contemporary culture by cinema, writing, visual art, or architectural design, with the existed popular culture [4]. Social and cultural aspects can be easily affected by the strong approach of globalization where localities of nations are facing it and exposed to the danger of getting disappeared over time.

"*Globalization destabilizes and redefines both the way architecture is produced and that which architecture produces. Architecture is no longer a patient transaction between known quantities that share cultures, no longer the manipulation of established possibilities, no longer a possible judgment in rational terms of investment and return, no longer something experienced in person-by the public or critics. Globalization lends virtuality to real buildings, keeps them indigestible, forever fresh*." [5]

According to Koolhaas, globalization depletes, destabilizes and redefines the architectural imagination, it extends the sphere of possibility between better and worse, as well as it leads to the collisions of cultures, and fundamentally reshapes the architectural discourse [6]. In the last decades, competition for supremacy is one of the architectural phenomena of global icon which is represented by the race between nations to build the world's tallest building or skyscrapers as between china and Malaysia, also the tendency of building phenomena prestige which started by Frank Gehry after the second world war is also a way to see architecture at a global level by using principles of high design of museums and opera houses for economic aims as for example Qatar's recently constructed museums [7]. Also, one of the important features of global architecture practice is the growth of a global networks of firm's offices in many cities around the world starting from the 1990s as Nikken Sekkei from Japan and Gensler in the United States [8]. Without forgetting the role of internet which has been and still the leading cause of the current global community due to how it helps spreading the new digital networks and enabling the national transactions which are the engines of globalization [9].In reference to global architecture, internet also contributed in this aspect by the growth of architectural media and the migration of architectural publication to the network platforms like Arkitera, Archdaily, and others, this leads to a worldwide virtual circulation of ideas, products, and images of architecture [10]. In this regard, it is also significant to note how Sklair relates the transformation of cities in the last decades into globalizing cities with both iconic architecture aspect which is one of the drivers of global architecture and attached to the projects and buildings of famous and professional architects with global reputation, as well as with the capitalist class driver which consists the people and the firms from many countries who own and control the transnational corporation, these two aspects become interconnected in the field of architecture for the urban megaprojects in the era of globalization [11]. The force of globalization on the field of architecture has multiple factors, drivers, and images, and reached almost worldwide, though its impact varies from a nation to another in accordance with the political, economic, and social aspects of every region.

Ching indicates that in this world where globalization is extremely involved, it is hard to describe nowadays' architecture particularly with the existence of local aspect as well, this leads to use the new term glocal to a better description of today's design of architects [12]. In this sphere, Erten points out that searching for national and local identity in architecture is not the same anymore like how it was dominated and prevailed in the 1980s, it did not continue after the 2000s due to the domination of other priorities which emerged in the architectural scenes like constructing without the use of local materials, the big interest in the advanced technologies of materials and building constructions, and the use of computer technologies [13]. Marketing as well had and still having an impact on creating new life styles and forms presented as a "fashion" leaded to the loss of the locality and the local products and their importance due to the global competition of the powerful aspect of globalization which is almost in all parts of the world which detached many cities from their locality.

Algeria, Architecture, & Globalization

This detachment from the local and the tendency into global aspect can be seen in various regions around the world, in Northern Africa like in Algeria, after Phoenicians and Romans, Algiers city experienced continuous urban transformations which can be seen by urban fabrics staring from the Casbah (by the Ottoman Empire), the colonial large urban housing projects for the colonials (by the French colonial), and ZHUN (New Urban Housing Zone, in the post-colonial era), in addition to the development of private builders in individual plots of lands which is the result of informal houses areas. Buildings constructed by the French colonial era were influenced by the ideas of Le Corbusier, Zehrfuss, Miquel, and Pouillon, but this did not fit with the existed urban fabric which characterized by the low-rise buildings [15]. The area of Bab Azzoun in Algiers constructed as a European quarter, Bugeaud neighbourhood was designed by the German architect M. Lichtenstein. However, cultural, historical, and racial differences are the aspects which dominated in the building operations during the French

colonialism in addition to both contradiction with hybridity, and maintaining the dominance of difference, colonial architecture ignored the local sociocultural factors like family structure, the place and the privacy of women. In the 1970s (the Socialist period), Algeria performs the idea of industrialization in the building sector [14]. Thus, influential and important architects like Oscar Niemeyer and Kenzo Tange were invited to participate in designing universities and housing projects like Bab Ezzouar University and Faculty of Law in Ben Aknoun (in Algiers). Later on, there was a need for more housing which pushed the government to encourage and gave the freedom for self-building by private firms or by individual properties which leaded to further implications related to global and local aspects. During post-independence era over the impact of capitalism and the political and economic shifts by the late 1980s which contributed in changing Algerian people's perception on cultural preferences of their domestic places, for example of "the courtyard" which was an important space in Algerian families before the 80s due its primary role for privacy (as a women's private place), even though it is inserted anymore in the plans or among their listed criteria of the domestic spaces.

Turkey, Architecture, & Globalization

In Turkey, as in Istanbul which is also an example of a global city and similar to so many global cities by the global design of housing regions, apartments, the transportation systems, international airports, etc. It started after the 1980s when upper classes wanted to move away from the massive centre of the metropolis, forests surrounded by the city where the suitable area to build this new communities which belong to versions of global models because city administration works with famous architects like Zaha Hadid, and global capital as Sheikh Maktoum of Dubai. One of the reasons which developed the aspect of globalization in Istanbul is marketing strategies where usually advertisements related to housing contain a representation of Western suburban lifestyles. High-rise buildings which are the main sign of globalization, by the foreign investments of foreign companies' various tall buildings were built which made a change in the structure of the city by creating new central business and different living spaces [15].

Conclusion

Globalization approach can be defined from various perspectives, but what common in these viewpoints is the "Mobility" of thoughts, objects, people, and ideas between regions, nations, and continents as it is all connected without separation regardless under which circumstances it happens (colonial, business, goods, etc.).

The stereotype aspect of global cities which characterised by tall-sized buildings, the new materials, the sophisticated facades, new technologies etc., has impacted on the priorities of people and authorities of various countries like Algeria, and Turkey. Algeria, experienced both earlier as considered a "forced" globalization by the presence of successive colonials which brought their beliefs, concepts, cultures, and designs. And, new "unforced" globalization in the post-colonial ear by bringing foreign thoughts and realize projects in Algeria by foreign architects' designs. In Turkey, it looks more a "mutual consent" globalization with the West with both Turkish authorities along with Turkish people.

Regardless its advantages, globalization is affecting on localities of nations, this can be seen in the inner changes which are taking place in the use of original spaces, its particular features, certain cultures, the way of living, of thinking, and the way of seeing just for the sake of "new and modern". However, it needs to be said that targeted nations cannot run away from globalization, but it can face it by preserving their localities by the possible ways, authorities and architects are the main responsible for this issue.

References

[1] Mazlish, B. The New Global History. New York: Routledge; 2006.
[2] Ayna A. The Impact of Globalization on Architecture - Environment Relations: Housing Projects and Design Approaches, in the Scale of Globalization. Think Globally, Act Locally, Change Individually in the 21st Century. Ostrava : University of Ostrava, 2011.
[3] Çelik Z. Urban Forms and Colonial Confrontations: Algiers under French rule. Berkeley and Los Angeles: University of California Press, 1997.
[4] Ching F, Jarzombek M, Prakash V. A Global History of Architecture. New Jersey: Hoboken, 2017.

[5] Djiar KA. Locating architecture, post-colonialism and culture: contextualisation in Algiers. The Journal of Architecture 2009; 14(2): 161-183.
[6] Erten E. İzmir in the Dilemma of Globalization and the Rise of Architecture. Izmir: Vitra, 2018.
[7] Gültekin AT. Globalisation Reflected onto Architecture: Tall Buildings of Ankara-Turkey. IOP Conference Series : Materials Science and Engineering 2017: 02.
[8] Hadjri K, Osmani M. The spatial development and urban Transformation of colonial and postcolonial Algiers. 2004: 1-15.
[9] King A. Culture, Globalization and the World-System Contemporary Conditions for the Representation of Identity. New York: Palgrave, 1991.
[10] Knox P, Taylor P. Toward a Geography of the Globalization of Architecture Office Networks. Journal of Architectural Education, 75; 2005: 23-24.
[11] Koolhaas R, Mau B. S M L XL: OMA. New York : The Monacelli Press, 1995.
[12] Mazlish B. The New Global History. New York: Routledge, 2006.
[13] Sklair L. Iconic architecture and capitalist globalization. City 2006; 10(1): 21-47.
[14] Sklair L. Iconic architecture in globalizing cities. International Critical Thought 2012; 2(3): 349-361.
[15] Ülkü GK, Erten E. Global image hegemony: Istanbul's gated Communities as the new marketing icons. International Journal of Architectural Research 2013; 7(2): 244-257.

Assessment of the Last Decades Studies and Developments in Broilers Nutrition

Eric Niyonshuti[1], *Figen Kırkpınar*[2]
[1]*Ege University, The Graduate School of Natural and Applied Sciences, Department of Animal Science, Izmir, Turkey*
[2]*Ege University, Department of Animal Science, Faculty of Agriculture, Ege University, İzmir, Turkey*
**Corresponding author: niyonshuti344@gmail.com*

Abstract

The poultry industry has advanced remarkably over the past 30 years. In particular, broiler production has been the most successful than any other sector in the animal industry. Production standards of broilers have continuously improved over this period, with modern broilers reaching a live average weight of 2.5 kg at 33 – 35 days. Today, under normal conditions, a broiler chicken can gain an average weight of 65 g per day and can attain 1.5 feed conversion ratio (FCR). Genetic selection brought about by breeding companies has played a big part in the improvements of broiler growth, and advances in nutritional management have provided about 10 to 15% of these changes. In conclusion, future broiler nutrition studies are going to be continued on the plane of economic criteria, determination of alternative feedstuffs and their cultivation, production of new feed additives, sustainability, and food or product quality. However, broiler nutrition studies are expected to contain not only pure and applied nutrition but also to answer and to enlighten some discussed issues such as to support animal welfare, consumer health, and ecological equilibrium. In this review, the latest improvements in feed formulation with much attention on metabolizable energy (ME) and crude protein (CP), feeding systems and feed presentation, use of feed additives to enhance feed use and broiler performance are discussed.

Keywords: broiler nutrition, feeds, feeding program, new technologies

Introduction

The poultry industry has advanced considerably over the past 30 years. In particular, broiler production has been the most successful than any other sector in the animal industry. Production standards of broilers and layers have continually improved over this period, with modern male broilers currently reaching a live weight of 2.5 kg at 33 – 35 days [1] and can attain a feed convention ratio of 1.5 [2]. According to Havenstein et al. [3], genetic selection brought about by breeding companies is responsible for 85 – 90% of the improvements in broiler growth, and advances in nutritional management have provided about 10 – 15% of the changes. The need to achieve and sustain these improvements in genetic potential of the birds was the driving force behind recent advances in poultry nutrition, and there has been continuous refinement in the nutrition and feeding practices of commercial poultry [1]. Nutrition is the major impacting variable upon broiler productivity, profitability, and welfare. Although ration formulation requires special nutritional skills, farmers and feed manufacturers should be aware of the nutritional content of their feeds. The main objective of the modern poultry enterprise is to reduce feed cost for optimal economic returns because feed constitutes approximately 70% of the total production cost. One of the ways used for reducing the feed cost is to improve the feed efficiency of birds. While formulating a broiler's diet, main concerns are placed on metabolizable energy (ME) and crude protein (CP), because ME itself comprises 70% of the total cost of feed and protein have major cost components in broiler diets [4]. Nonetheless, great improvements in the management of broilers have also played a significant part in the efficiency of broiler production. The modern broiler is much less tolerant to environmental errors than the bird of a few years ago. This makes broiler management more challenging than ever before [5]. Moreover, today's society, contrary to the past 20 years, is demanding more information on food safety and animal welfare, and there is an emphasis on sustainable broiler production. In the future, nutritionists will need to participate in sustainability initiatives by giving more attention to ingredient quality; working on phase and sex feeding differentiation; concentrating on particle size and pellet quality, utilizing feed additives more efficiently, and at the same time coping throughly with behaviours and welfare of the birds. Antibiotic growth promoter (AGP)-free broiler meat will be more demanded by consumers. Therefore, new methods of feeding will need to be developed to meet the market demand [6].

Basic Concept of Broiler Nutrition

Feeds account over 70% of the total cost of broiler production, with energy sources being the largest in terms of quantity (70%). One of the objectives of any poultry producer is to feed the chickens with a balanced diet at least cost and also generate products that will attract premium prices in order to maximise profit. For many decades, farmers and feed manufacturers worldwide have been facing the challenge of effectively reducing the cost of poultry production and produce quality products. However, several factors such as genotype, diet composition, digestible nutrient content, energy to protein ratio, feed form, feed processing, environment, and disease could also influence the cost of production and broiler meat quality [7].

Feed Ingredients and Quality

To support optimum performance, broiler diet should be formulated to provide the correct balance of energy, amino acids, minerals, vitamins, and essential fatty acids. The feed ingredients used for broiler diets should be fresh and of high quality both in terms of digestibility of nutrients and physical quality. The main ingredients commonly used in the formulation of broiler diets are maize, soya meal, wheat, full fat soya, sunflower meal, rapeseed meal, oils and fat, limestone, phosphate, salt, mineral and vitamins, and feed additives. Quality management is vital in any feed industry. Only quality raw materials can deliver the quality feed. Today some rapid tests and inspection methods are being applied to determine the quality of raw ingredients. These include moisture, insect, smell, fungus, hull test, urease activity test, particle size test etc. and thereafter the samples from raw materials are taken to the feed mill laboratory for proximate analysis. In case the raw materials satisfy the necessary quality standards, they can be then entered to the production cycle [8].

Energy and Protein Requirements

Broilers require energy for tissue growth, maintenance, and activity. The major sources of energy in poultry feeds are typically cereal grains (primarily carbohydrates) and fats. Dietary energy levels are expressed in Megajoules (MJ/kg), kilocalories (kcal/kg or kcal/lb) of metabolizable energy (ME). ME corresponds to the energy available to the broiler chicken. The modern broiler is responsive to dietary digestible amino acids (AA) density and will respond well, in terms of growth, feed efficiency, and carcass component yield to a diet properly balanced in AA as recommended. Niu *et al.* [9] studied the effects of dietary energy and protein on growth performance and carcass quality of broilers during starter phase. It has been concluded that the optimum dietary ME requirement of broilers from 1-21 days of age is 12.97 MJ/kg and the CP requirement is 21-22%. Researchers suggest that farmers should feed diets containing a balanced AA and energy-dense ingredients to sustain the rapid growth of modern broilers. It is vital to formulate diets with neither a deficiency or excess in AA and energy [10]. The under supply of the nutrient leads to a depressed growth rate, while over supply results in inefficient use of nutrient. Both cases are costly for the broiler industry [11]. It has been concluded that programs that incorporate higher AA density during early growth phases followed by lower AA density diets may support acceptable performance and carcass composition and reduce overall feed costs. The introduction of Ideal Protein Concept has been an important progress in animal nutrition because it enables the nutritionist to immediately adjust amino acid supply with regard to the production conditions. This concept takes Lysine as the reference amino acid and all remaining essential amino acids are related to it. These amino acids can be adjusted to changing lysine requirements by simple calculation [12].

Table 1. Ideal amino acid ratios of meat chickens at three growth periods [1]

Amino acid	1-21 days	22-42 days	43-56 days
Lysine[1]	100	100	100
Arginine	105	108	108
Histidine	35	35	35
Isoleucine	65	69	69
Leucine	109	109	109
Metionine + cystine	72	72	72
Phenylalanine+ tryosine	105	105	105
Threonine	67	68.5	68.5
Tryptophan	16	17	17
Valine	77	80	80

Minerals and Vitamins

Providing the proper levels and balance of macro minerals are important to support growth, skeletal development, the immune system, and feed conversion ratio (FCR), as well as the litter quality. The macro minerals involved in broiler nutrition are calcium, phosphorus, sodium, potassium, and chloride. The available phosphorus (AP) and calcium (Ca) are fundamental for growth and bone formation and are responsible for its rigidity and compressive strength. However, Phosphorus (P) contained in plant ingredients is present as phytate which forms complexes with multivalent cations, such as Ca, to produce insoluble salts. In addition, inorganic sources of P significantly increases the feed cost. Recent nutritional strategies to enhence the use of this mineral, reduce excretion, avoid overdosing, and to decrease costs have include the use of low P levels in the feed and inclusion of phytase (PHY) enzyme. The effect of PHY on the availability of P and Ca is well recognized for improving bone quality, as it increases bone weight and ash concentration [13]. On the other hand, a lot of research has been conducted to deal with feed levels of sodium, phosphorus, and chloride in the broiler diet as their excess can cause increased water excretion and subsequent litter quality issues.

Trace minerals and vitamins are crucial for all metabolic functions. Recent investigations on trace minerals and vitamins enlightened their role to alleviate the effect of heat stress in broiler chicken. For instance, studies have reported that vitamin C or electrolyte supplementation could palliate the effects of heat stress in broiler chickens. Saiz del Barrio *et al*. [14] investigated the effect of mineral and vitamin C mix on the growth performance and blood corticosterone concentrations in heat-stressed broilers. The results of these studies showed that a combination of electrolytes and vitamin C in drinking water improved growth performance in a dose related way in heat-stressed broiler chickens under standard animal density conditions. Supplementation of vitamin C improved growth performance in heat-stressed broiler chickens but results were intermediate compared with the control and the highest level of inclusion of the mineral and vitamin mix C (2 kg/1000 l) supplementation. Both the mineral and vitamin C mix and vitamin C alone added to drinking water reduced corticosterone level in the blood serum.

Water

Water is involved in many functions of poultry metabolism including, but not limited to, body temperature control, digestion and absorption of nutrients, transport of nutrients, and the elimination of waste products, via urine, from the body [15]. Water intake of broilers can be highly variable and depends on diet composition and feed form, production performance, intestinal health, stress and on environmental conditions. High water consumption under moderate climate conditions will generally result in high water excretion, wet litter problems, and increased ammonia production. Wet litter in poultry houses poses considerable economic and pathological problems [16]. Hygienic drinking water is also important for disease prevention, food safety, and reduction of antibiotic use. Recent studies emphasized on the impact of drinking water sanitation on performance and welfare outcomes in broiler chickens kept on fresh or used litter. Jacobs *et al.* [17] found that water sanitation provides some benefits

[1] Recommended digestible lysine requirements for meat chickens during 1-21 days, 22-42 days, and 43-56 days are 1.070, 0.865 and 0.745 % respectively.

for production (body weight, average daily gain) and welfare outcomes (decrease in footpad dermatitis and chronic stress).

Broiler Feeding Program

Nutrient requirements of broilers decrease as they grow older due to changes in growth and maintenance requirements. Therefore, it is a common practice to reduce dietary protein (amino acid) content and increase energy whilst keeping other nutrients constant throughout the feeding programme of broilers. The strategies through which these changes are implemented vary. The classical feeding programmes of the National Research Council (NRC), usually define the nutrient requirements of broiler chickens based upon age within three fixed phases namely starter, grower and finisher. This programme does not match with the grow-out periods that are used in modern production practices. Broilers have evolved a lot since the early 1960s, when it used to take 60 days with a feed efficiency of 3.5 for a broiler chicken to reach 2 kg weight. Broilers now reach the same body weight at half of that time and may attain 1.5 feed efficiency ratio [18]. Today, under normal conditions, a broiler chicken can gain an average weight of 65 g per day [19] and hence, a 2.44 kg broiler is produced on 3.66 kg of feed [2].

Table 2. Body weight and feed conversion ratio to 35 days age [2]

Year	Live weight (g)	FCR
1985	1400	2.30
1990	1700	2.26
1995	2010	2.08
2000	2140	1.96
2005	2310	1.65
2010	2440	1.50

With all this evolution in broilers, replacing classical NRC feeding schedules with alternatives appear interesting, but the idea is often controversial. Many claims of benefits come from single groups of researchers and not all the merits proposed have been confirmed by other researchers or applied commercially. Conclusively, many variables affect the outcome of alternative feed phasing and further research needs to be carried out before implementation in the field [18].

Improvement in Feed Formulation

The main objective of feed formulation is to derive a balanced diet that will provide appropriate quantity of all required nutrients at least cost. Considering all possible ingredients and nutrients involved, a large number of arithmetical calculations are needed to produce a least-cost diet. Over the years, feed formulation has evolved from a simple balancing of few feedstuffs for a limited number of nutrients to computer-aided linear programming systems. Currently, brand new systems of stochastic nonlinear programmes are becoming popular with the commercial availability of this formulation software. Because variability in ingredient composition is non-linear, stochastic programmes address this issue in the most cost-effective manner possible. New approaches, which predict the maximum profit for a given ingredient combination and price of the broiler/special cuts, are being increasingly used by the commercial industry [1]. Maximum Profit Feed Formulation (MPFF) is proposed as a new approach to formulation of broiler diets which predicts the best profit for given feed ingredient and broiler prices, nutrient requirements and performance. While the least cost feed formulation keeps the nutrient requirement constant for a given performance and for a given profit. MPFF considers a mean of Dietary Nutrient Density (DND) of feeding phases which represents the energy content of starter, grower, and finisher. İt ensure the production of good quality carcasses. In addition to price variations of ingredients and broiler meat that can change nutrient requirements in order to obtain best profits, factors such as livability, temperature and processing cost that may affect nutrient requirements are considered in MPFF model [20].

Feed Form and Pelleting

Nowadays, various commercial feed mills are producing different forms of broiler feed for different age groups of bird. The physical form of feed (mash, pellet, and crumble) is a crucial factor in meat yield of broilers. Researchers suggest that ground feed is not so palatable and does not retain their nutritive value so well as ungrounded feed or pellet. Feeding pellets reduce feed wastage, increase feed intake, improved feed conversion ratio, and promote better growth performance [21,22]. Limitations in beak size of newly hatched chicks have led the majority of broiler farmers to feed crumbles during the starter period. Recent studies have showed improved growth performance on birds fed micro pellets during the starter period. Rubio *et al*. [23] studied the effects of feed form and amino acid density on productive and processing performance of broilers. They concluded that feeding 3.3mm micro pellets to broilers can improve FCR during the starter period from 1 to 14days of age. However, a larger pellet size may be required during the finisher period.

Use of Feed Additives in Broiler Nutrition

The partial or complete abolition in the use of antibiotics for poultry production have positive effects in the control of antimicrobial resistance and public health. However, the antibiotic-free production of poultry could increase public health problems caused by common foodborne pathogens such as C. perfringens, E. coli, and S. aureus. Bacterial infections increase production costs, impair the birds health, and decrease productive parameters. It was for the poultry producers to find viable alternatives with similar benefits to antibiotics. Many specific alternatives have been evaluated and are marketed. These include: enzymes, prebiotics, probiotics, organic acids, herbs, spices, essential oils, and vaccines [24].

Prebiotics and probiotics have been reported to alter the immune system, improve the growth of beneficial gastrointestinal microflora, and reduce pathogen invasion including pathogens such as *E.coli* and Salmonella. Recent studies revealed that the combinations of probiotics and prebiotics (synbiotic) results in better performance on broilers than the two additives when fed alone. The results on broilers qualitative and quantitative traits are inconsistent. Shulukh *et al.* [25] studied the effect of probıotıcs and prebıotıcs on carcass, cut yıelds and some qualıtatıve traits of broiler chickens. They concluded that the addition of probiotics and prebiotics did not influence the qualitative and quantitative parameters of carcass and breast meat of broiler chickens, and their combination improves moisture, crude protein and water holding capacity of broilers meat.

Phytase, nonstarch polysaccharide degrading enzymes (NSPase) and proteases comprise the vast majority of feed enzyme classes used in the feed industry at the present. Enzymes significantly improve nutrient digestibility. Enzymes inclusion allows the formulator to reduce energy density of the diet by 100 kcals, which is equivalent to substituting 2% of fat (high cost ingredient) with 2% corn (much lower cost ingredient) [26]. Phytase in particular is currently used in broiler diets to improve the digestion of phosphorus present in the form phytate (60 to 80%) in the feedstuffs of plant origins. Recent studies evaluated the effect of different phytase levels in diets formulated based on vegetables, vegetables plus animal, and animal origin feedstuffs on live performance and bone characteristics of broiler chickens during different growing stages. De Souza *et al.* [27] evaluate phytase and phytate interactions on broilers diet at 21 days of age. They found that diets with reduced calcium and phosphorus levels without phytase supplementation had negative effects on broilers performance. The study findings also revealed that phytase supplementation improves broilers' performance and bones quality.

In the animal feed industry, organic acids are added to reduce the action of bacteria such as Escherichia coli, Campylobacter spp. and Salmonella spp. in contaminated feed, thereby reducing subclinical infections in birds. Organic acids may be exploited as growth promoters in broiler chickens due to their beneficial antimicrobial effects and positive effects on the histology of the small intestine. Recently, butyric acid and its sodium salt have received attention as feed additives, and some studies have demonstrated positive effects on the growth performance of chickens, such as decreased tissue catabolism, intestinal integrity, and trophic effects on the gastrointestinal tract in broilers [28].

Phyto feed additives are plant-based feed additives or botanicals that are used in natural substances used in poultry nutrition. These substances are derived from herbs, spices, other plants and their extracts, like essential oils. Most common herbs and spices used as phyto feed additives in poultry production are oregano, thyme, garlic, horseradish, chili, cayenne, pepper, peppermint, cinnamon, anise, clove, rosemary and sage. Many beneficial properties of phytogenic compounds derive from their bioactive

molecules; carvacrol, thymol, cineole, linalool, anethole, eugenol, allicin, capsaicin, allyl isothiocyanate and piperine. Phyto feed additives have antimicrobial, antifungal, antiviral, antitoxigenic, antiparasitic and insecticidal properties. The benefits of using phyto feed additives in poultry nutrition are increased feed intake, stimulation of digestion, increased growth performance, reduced incidence of disease, improved reproductive parameters, feed efficiency, profitability and reducing poultry house emissions. Conclusively, in order to maximize the overall performance of poultry, phyto feed additives should be used as an alternative feed additives in poultry production because of the absence of side effects, residual effects, non-hazardous and eco-friendly [29].

Automated Feeding and Drinking System

The cost of poultry production is aggravated sometimes due to the challenge of manual pattern of feeding. Wastage of feed, improper administration of feed, stressful manual labour, disease outbreak, fatigue are some of the defects prevalent in the manual system of feeding. These flaws triggered the development of technologies that could tackle and solve some of the flaws in the most current system of feeding poultry [30]. The mode and pattern of poultry feeding and drinking systems have evolved to conform to the increasingly sophisticated production systems. Actually, nipple drinkers, flat chain and pan feeders are being used worldwide.

Figure 1. Manual versus automatic feeding systems

However, pan feeders offer a number of advantages over chain type trough feeders. Pan feeders increase the ability of birds to move over the whole floor area. Also, pan feeders offer about one third more feeder space than the same length of chain trough [31]. The use of nipple drinkers into floor housing systems are generally accepted as they have the biggest impact on the reduction in spreading of diseases (especially respiratory disease). Compared to open watering systems, nipple drinkers promote overall litter integrity, lessen growth of pathogenic organisms, improve broiler carcass quality and reduce ammonia emissions thereby lowering the birds' susceptibility to respiratory infections.

Precision Feeding

Currently precision livestock feeding is a topic under investigation. Precision livestock feeding aims to match nutrient supply precisely with the nutrient requirements of an individual animal, based on real time feedback from the sensors. The benefits include greater economic returns, reduced nutrient excretion to the environment, and improved efficiency of feed resources utilization. İt is suggested that animal models need to be further developed and integrated with new and existing smart machines designed to deliver the right amount of the right feed to the right bird at the right time. Precision livestock will strengthen the economic, environment, and social pillars of sustainability [32].

Feeding Strategies of Birds under Heat Stress

Heat stress is one of the most important environmental stressors that affect commercial poultry. It has been reported that broilers exposed to excess heat decrease feed intake to reduce metabolic heat production and maintain homeothermy. This results in slower growth, reduced breast muscle yield, higher fat deposition and higher feed conversion ratio. Jahejo *et al.* [33] studied the effects of heat stress on the performance of Hubbard broiler chicken. The results revealed that feed intake, weight gain, water

intake, feed conversion ratio and dressing percentage were significantly higher in the heat free group compared to the heat stress group.

Strategies to reduce the negative effects of heat stress can be based on a specific feeding strategy, such as restricted feeding, choice feeding, feeding wet and large particle sized feeds etc. Feeding wet diets may facilitate an increased water intake and larger particle sizes can limit water excretion in droppings, resulting in more water being available for evaporation during panting, hence cooling the bird [34]. Besides, studies suggest that diets containing high vitamin A (9000–15000 IU/kg diet), vitamin E (150–500 mg/kg diet), vitamin C (150–500 mg/kg diet) and Zn (30/60 mg/kg diet) and Se (0.1–1 mg/kg diet) can decrease the amounts of free radicals, support enzyme activity and prevent lipid peroxidation in poultry. According to Horváth & Babinszky [35], application of antioxidant vitamins and micro minerals in poultry nutrition is more effective in combination than separately. Mohamed *et al.* (2019) found that dietary supplementation with 200 mg Vit. C+200 mg Vit. E + 1.5 mg Cr + 100 mg Zn /kg diet for stressed broilers, can significantly alleviate heat stress effects by improved performance parameters, safety, serum blood biochemistry, carcass yield and carcass quality.

Conclusion and Future Considerations

The poultry, especially broiler, industry has advanced remarkably over the past 30 years. This enhancement resulted from improvements in good genetic selection and nutrition strategies. Different formulation models have been studied to decrease the cost of production and to maximize profit. A lot has been done to improve feed quality, feed intake, feed digestibility, and feed conversion efficiency to optimize meat production and to reduce feed excreted in the environment. Feeds additives have been an integral part in maintaining feed safety, improving feed digestibility, and in preventing gastrointestinal diseases hence promoting animal welfare. Future broiler nutrition studies are going to be continued on the plane of economic criteria, determination of alternative feedstuffs and their cultivation, production of new feed additives, sustainability, and food or product quality. Analytical technologies, such as near-infrared spectroscopy (NIRS), advanced in vitro fermentation modelling, nutrigenomics and bioinformatics will intervene in feed formulation so that nutritional value is defined, and feed formulation and manufacturing is no longer an ‘art’ but a more precise science. The same technologies will be used to detect contaminants and allow a new level of food safety. In order to achieve increased animal performance while minimising feed costs, new nutritional strategies, such as novel raw materials and feed additives, must be employed to optimize feed conversion and digestibility.

References

[1] Ravindran V, Abdollahi MR. Advances and future directions in poultry feeding. 2017;95–112.
[2] Siegel PB. Evolution of the modern broiler and feed efficiency. Annu. Rev. Anim. Biosci. 2014;2(1):375–85.
[3] Havenstein GB, Ferket PR, Qureshi MA. Growth, livability, and feed conversion of 1957 versus 2001 broilers when fed representative 1957 and 2001 broiler diets. Vol. 82, Poultry Science. 2003. p. 1500–8.
[4] Sarwar G, Akhter S, Khan SH, Anjum MA, Nadeem MA. Effect of different dietary protein and energy levels on the growth performance, meat and body fat composition in broiler chicks. Pakistan J. Agric Sci. 2015;52(4):1121–5.
[5] Lacy MP. Broiler Management. Commercial Chicken Meat and Egg Production. Ed. Bell DD and Weaver WD, JR. 2002;829–68.
[6] Feeding broilers of the future-Zootecnica International. [Accessed 2021 Apr 16]. https://zootecnicainternational.com/poultry-facts/feeding-broilers-future/
[7] Ahiwe EU, Omede AA, Abdallh MB, Iji PA. Managing dietary energy ıntake by broiler chickens to reduce production costs and improve product quality. Anim. Husb. Nutr. 2018;(July 2018).
[8] Wakabayashi K. Quality control of raw materials. Handb. Adhes. Technol. Second Ed. 2018;2–2(December):1129–50.
[9] Niu Z, Shi J, Liu F, Wang X, Gao C, Yao L. Effects of dietary energy and protein on growth performance and carcass quality of broilers during starter phase. Int. J. Poult Sci. 2009;8(5):508–11.
[10] Johnson CA, Duong T, Latham RE, Shirley RB, Lee JT. Effects of amino acid and energy density

on growth performance and processing yield of mixed-sex Cobb 700×MV broiler chickens. J Appl Poult Res. 2020;29(1):269–83. https://doi.org/10.1016/j.japr.2019.10.014
[11] Moss AF, Chrystal P V., Cadogan DJ, Wilkinson SJ, Crowley TM, Choct M. Precision feeding and precision nutrition: A paradigm shift in broiler feed formulation? Asian-Australasian J. Anim. Sci. 2021;34(3):354–62.
[12] Lemme A, Industries E, View AO. The "ideal protein concept" in broiler nutrition. Methodological aspects - opportunities and limitations. Amino News 2003;4(1)1–10.
[13] Ribeiro TP, Dal Pont GC, Dahlke F, da Rocha C, Sorbara JOB, Maiorka A. Available phosphorus and calcium reduction in the finisher phase and phytase utilization on broilers. J. Appl. Poult. Res. 2019;28(2):263–70.
[14] Saiz del Barrio A, Mansilla WD, Navarro-Villa A, Mica JH, Smeets JH, den Hartog LA, et al. Effect of mineral and vitamin C mix on growth performance and blood corticosterone concentrations in heat-stressed broilers. J. Appl. Poult. Res. 2020;29(1):23–33. https://doi.org/10.1016/j.japr.2019.11.001
[15] Manning L, Chadd SA, Baines RN. Water consumption in broiler chicken: a welfare indicator. World's Poult. Sci. J. 2007;63(1):63–71.
[16] Dirk Van Der Klis J, De Lange L. Water intake of poultry. Proc. 19th Eur. Symp. Poult. Nutr. 2013;(July). http://www.wpsa.com/index.php/publications/wpsa-proceedings/2013/19th-european-symposium-on-poultry-nutrition/1375-water-intake-of-poultry/file
[17] Jacobs L, Persia ME, Siman-Tov N, McCoy J, Ahmad M, Lyman J, Good L. Impact of water sanitation on broiler chicken production and welfare parameters. J. Appl. Poult. Res. 2020;29(1):258–68. https://doi.org/10.1016/j.japr.2019.10.013
[18] Shariatmadari F. Feeding schedules for broiler chickens. World's Poult. Sci. J. 2009;65(3):393–400.
[19] Butcher GD, Nilipour AH. Broiler production goals—important numbers. University of Florida Extension, VM134.
[20] Cerrate S, Waldroup P. Maximum profit feed formulation of broilers: development of a feeding program model to predict profitability using non linear programming. Int. J. Poult. Sci. 2009;8(3):205–15.
[21] Chehraghi M, Zakeri A, Taghinejad-Roudbaneh M. Effects of different feed forms on performance in broiler chickens. Eur J Exp Biol. 2013;3(4):66–70.
[22] Massuquetto A, Panisson JC, Marx FO, Surek D, Krabbe EL, Maiorka A. Effect of pelleting and different feeding programs on growth performance, carcass yield, and nutrient digestibility in broiler chickens. Poult. Sci. 2019;98(11):5497–503.
[23] Rubio AA, Hess JB, Berry WD, Dozier WA, Pacheco WJ. Effects of feed form and amino acid density on productive and processing performance of broilers. J. Appl. Poult. Res. 2020;29(1):95–105. http://dx.doi.org/10.3382/japr/pfz032
[24] Solis-Cruz B, Hernandez-Patlan D, Hargis BM, Tellez G. Use of prebiotics as an alternative to antibiotic growth promoters in the poultry industry. 2019. DOI: 10.5772/intechopen.89053
[25] Shulukh EA, Gibril S, Habib A, Abubakr A. Effect of probiotics and prebiotics on carcass, cut yields and some qualitative traits of broiler chickens. Asian Academic Research Journal of Multidisciplinary. 2017. https://www.researchgate.net/publication/321836766
[26] Bedford MR, Cowieson AJ. Matrix values for exogenous enzymes and their application in the real world. J. Appl. Poult. Res. 2020;29(1):15–22. https://doi.org/10.1016/j.japr.2019.10.011
[27] Broch J, dos Santos EC, Damasceno JL, Nesello P de O, de Souza C, Eyng C, Pesti GM, Nunes GV. Phytase and phytate interactions on broilers' diet at 21 days of age. J. Appl. Poult. Res. 2020;29(1):240–50. https://doi.org/10.1016/j.japr.2019.10.010
[28] Aristimunha PC, Mallheiros RD, Ferket PR, Cardinal KM, Filho ALBM, Santos ET, Cavalcante DT, Riberio AML. Effect of dietary organic acids and humic substance supplementation on performance, immune response and gut morphology of broiler chickens. J. Appl. Poult. Res. 2020;29(1):85–94. http://dx.doi.org/10.3382/japr/pfz031
[29] Madhupriya V, Shamsudeen P, Manohar GR, Senthilkumar S. Phyto feed additives in poultry nutrition – A review. Int. J. Sci. Environ. Technol. 2018;7(3):815–22.
[30] Olaniy OM, Salami AF, Adewumi OO, Ajibola OS. Design of an intelligent poultry feed and water

dispensing system using fuzzy logic control technique. Control Theory Informatics. 2014;4(9):61–72.
[31] Samer SM. Poultry Farms: Housing Systems, Mechanization, and Technology. 2002; (January 2002). Publisher: Cairo University, DOI: 10.13140/RG.2.1.2599.3766
[32] Zuidhof MJ. Precision livestock feeding: matching nutrient supply with nutrient requirements of individual animals. J. Appl. Poult. Res. 2020; 29(1):11–4. https://doi.org/10.1016/j.japr.2019.12.009
[33] Jahejo AR, Rajput N, Rajput NM, Leghari IH, Kaleri RR. Effects of heat stress on the performance of Hubbard broiler chicken. Cells Anim Ther. 2016;2(1):1–5.
[34] Syafwan S, Kwakkel RP, Verstegen MWA. Heat stress and feeding strategies in meat-type chickens. World's Poult. Sci. J. 2011;67(4):653–74.
[35] Horváth M, Babinszky L. Impact of selected antioxidant vitamins (Vitamin A, E and C) and micro minerals (Zn, Se) on the antioxidant status and performance under high environmental temperature in poultry. Acta Agric. Scand. Section A—Anim. Sci. 2018;68(3):152–60.

Current Situation, Future Goals, and Strategies of the Feed Sector in Rwanda

*Eric Niyonshuti**
Ege University, The Graduate School of Natural and Applied Sciences, Department of Animal Science, Izmir, Turkey
**Corresponding author: niyonshuti344@gmail.com*

Abstract

In Rwanda, livestock plays an integral part in the national economy. It contributes to improve the socio-economic status and wellbeing of Rwandans, fight malnutrition, and promote food and nutrition security. Over the past 2 decades, the government of Rwanda, in collaboration with different actors and stakeholders, has put in place strategic and implementation plans to strengthen livestock production in Rwanda. Although a remarkable step has been made in increasing animal productivity, there are still a lot of constraints and challenges in this sector. The scarcity of animal feeds is one of the main challenges that impair the development of the animal sector in Rwanda. In this review, the current status of the feed sector, future goals, and strategies to tackle and sustain animal feed resources in Rwanda are highly discussed. To the end of this article, some recommendations are made to the farmers, feed manufacturers and the government. Considering the available data, investment opportunities for feed production in Rwanda should be evaluated. In addition, there are significant shortcomings in the field of food safety and the provision. The development of the needs in this sector includes entrepreneurship opportunities.

Keywords: Rwanda, feed resources, animal products, strategies, implementation plan

Introduction

Rwanda is a country located in central east Africa. It has a surface area of 26,338 km^2 and is landlocked. The population of Rwanda is approximately 13 millions, with about 83% of this population living in the countryside [1] and most of them (87%) working in the agriculture sector [2]. The economy of Rwanda has swiftly grown over the past decade, averaging 7.46% between 2008 and 2017. Agriculture accounts for 34% of the total GDP, with livestock sector contributing 10% of agricultural GDP. Livestock plays an important part in the socio-economic development agenda in Rwanda as a key pillar to economic growth and poverty reduction. Livestock farming in Rwanda is practiced under three main production systems: extensive, semi-intensive and intensive zero-grazing systems. Due to reduced grazing land, zero grazing system, is most prevalent system all over the country. Cattle is the main livestock reared, with local breeds, basically Ankole and their crosses, being the most dominant. Sahiwal and other exotic breeds are also reared. Goats, sheep, pigs, rabbits, fishery, and poultry are also important in Rwanda [3]. Over the past two decades, the government of Rwanda has put in place different policies to strengthen the livestock production and productivity in Rwanda. Some of these agriculture-related initiatives developed by the Government of Rwanda are included in The Vision 2020, Economic Development and Poverty Reduction Strategy (EDPRS), National Agricultural Policy (NAP), Strategic Plan for Agricultural Transformation (PSTA), National Dairy Strategy (NDS), and Rwanda Livestock Master Plan. The outcomes from these policies are increased livestock contribution to the economic growth, reduced poverty, and improved nutritional security of many rural people. The Girinka program (One cow per poor family program) has been an integral part in transforming dairying in Rwanda, and sustained vegetable and legume production on infertile hillsides by providing substantial manure [4]. However, a number of constraints; namely insufficient breed stock, scarcity of feeds, shortage of land, incidence of transboundary diseases etc., have largely restrained the development of the animal sector in Rwanda. This review enormously highlights the present situation, future goals, and strategies to strengthen the feed sector in Rwanda.

Livestock Population and Productivity

Livestock contributes to food security by providing high value protein in the form of milk, eggs, and meat. It also serves as an additional source of income to the household and as a way to store wealthfor the farmer. Cattle is a major livestock species reared and accounts for about 71% of the livestock value

added showing the continuing importance of the family cattle production system in Rwanda. In the livestock survey analysis carried out in 2016/2017, the national herd was found to consist of about 1.39 million cattle, 700 thousand sheep, 2.94 million goats, 1.8 million pigs and about 7 million layers, broilers and indigenous chicken. The production was about 94.2 thousand Metric Tons (MT) of meat, 747 thousand MT of milk, and 243 million eggs in that season. Furthermore, the herd provided about 6.8 million MT of organic fertilizer. About half (46%) of the dressed meat in Rwanda came from cattle, followed by swine (21%). Chicken and goats made up 17% and 13% of dressed meat respectively, and sheep only 3%. Sixty five percent (65%) of domestically consumed beef came from crossbred cattle. Meanwhile, for mutton and goat meat only 26 and 8% came from crossbreds, respectively. The contribution of the local cattle breeds to total milk production was only 9%, though they represent 43% of the national cattle herd. Although the local, indigenous chicken constituted 75% of the chicken population, they produced only 32% of the chicken meat and 34% of the eggs in the village chicken systems. Sixty eight percent (68%) of the chicken meat came now from specialized broilers and layers and 66% of the eggs from specialized layers [4]. Recently poultry has been the fast-growing sector in Rwanda than any other sector, growing from 1.2 M chickens in 1990s to 5.4M chicken in 2017 [5]. Fish production has also shown the potential for growth. In 2016, the country produced just 26,581 tons of fish before increasing to 31,465 and 43,632 tons in 2017 and 2018 respectively. Rwanda targets to produce 112,000 tons of fish every year by 2024 [6]. According to the Rwanda Livestock Master Plan (RLMP) roodmap (2017-2022) the production of meat, milk, and eggs is projected to 663 thousand metric tons, 2.2 billion liters of milk, and 1.9 billion eggs respectively in 2031/2032. Although recently a remarkable effort has been made, livestock production is still low compared to some countries in East Africa as it is visible in the table below.

Table 1. Livestock products production in the East Africa countries [7]

Country	Eggs	Milk	Beef	Chicken meat
Kenya	1970888	3983250	462125	88719
Rwanda	222900	174149	33924	19125
D R. Congo	237596	7978	20663	10406
Burundi	62100	55000	14935	7414
Uganda	1046512	1793040	166670	68510

*Eggs data are in number*1000*
Meat and Milk data in tons

Commercial System and Consumption of Animal Products

Livestock plays a crucial role in the household and national economies of Rwanda. Most of the farmers sell animal products to the local markets, hotels, restaurants, supermarkets with little being sold to the processing companies and neighboring countries. Livestock value chain policy is not well developed in Rwanda, except for milk value chain. This is because milk is a strategic commodity targeted by the Government of Rwanda to address the economic situation in the country. Milk primarily plays a significant role in the fight against child malnutrition and underfeeding. The surplus milk is sold to the milk collection centers, who in turn deliver milk to the milk processing plants. The cost of milk production is higher in Rwanda than the neighboring countries, such as Kenya and Uganda. Therefore, the only opportunity exists for Rwanda to export milk to DRC and Burundi where the milk sector is underdeveloped and cost of production is relatively higher [8].

Meat and egg consumption in Rwanda are on the rise. National production volumes do not always meet the market demand. However, Rwanda does not have the production capacity to compete with its neighbouring countries like Uganda, Tanzania, and Kenya, where the poultry industry is much more advanced. Poultry farms, mostly in the western province of the country, informally sell meat, eggs, and sometimes live chickens across the border with the DRC, where the price is relatively higher compared to local markets. Some farmers also sell their animal products in Burundi [5]. In 2020, the Government of Rwanda has launched a project on meat value chain competitiveness with the objective to improve meat production, expand the value chain, improve market and cross-border trade in the sector and increase the contribution of the meat value chain in Rwanda's economy.

Most of the meats consumed in Rwanda were found to come from cattle. This is partly caused by the decreased contribution with time of beef, goat, and mutton meat due to declining grazing land. On the other hand, the proportions of the annual meat available from chicken and pork were found to be on the rise [9]. Generally animal products consumption in Rwanda is far below the FAO nutritionally recommended levels. In 2014/15 the per capita meat consumption for the people of Rwanda was only 7.9 kg/year for meat, 59 liters/year for milk and 0.63 kg per year for eggs[4]. Low production, low purchasing power, outdated eating habits, and socio-cultural beliefs are the main reasons among others that lead to the underconsumption of animal products [9].

Livestock Farming Systems

In Rwanda the prevalent livestock production system is a smallholder crop-livestock mixed farming system with average land holding of 0.76 ha for the majority of farmers [10]. Livestock production in Rwanda follows three main production systems: extensive, semi-intensive and intensive zero-grazing systems with zero grazing being the most prevalent system [3]. Cattle feeding is mostly based on a zero-grazing system in which fodder is carried to the animal kept in confinement. Some of the reasons for this practice largely include land-scarcity and limited forage resources, minimizing the risk of overgrazing and environmental degradation. Although cattle grazing outside the farm is restricted, small ruminants may be tethered outside the farms to browse on roadside vegetation. Crops and cultivated grasses provide the bulk of feed for cattle, small ruminants (goats and sheep), pigs and to some extent rabbits, which return soil nutrients to the cycle through the supply of organic manure [11]. On the other hand, there are two coexisting poultry production systems in Rwanda: traditional village poultry and commercial poultry. The traditional village poultry is the predominant system and is relatively well-distributed throughout rural, urban and peri-urban areas. Most of the eggs and chicken meat produced in this system are consumed by the farmers themselves. The commercial poultry sector in Rwanda is still in its development phase. It is characterized by larger flock sizes than village poultry and marketing of chicken meat and eggs produced in the farm. Commercial poultry farms, in addition to selling eggs and meat, generate some income from selling chicken manure to farmers and the remains of chicken processing (heads, innards and feet) to pig growers [5]. In Rwanda, pigs and poultry, are now being emphasized because they require less land, quick return on investment, high growth rate, and short generation interval. According to Mbuza *et al*. [12] the main pig breeds kept are landrace (37.7%), followed by nondescript crosses (28.1%), large white (22.9%), Pietrain (7.3%), Duroc (1.6%) and local breeds (2.3%). Pig production systems are shifting from subsidence to modern semi-intensive to intensive production systems. However, in order to improve production, the characteristics of the existing systems must be known and well documented. Rwanda's fish production is still low though, it is growing quickly. Most of the production comes from capture fisheries as aquaculture only started recently in Rwanda. Fishing is conducted on a total of 17 inland lakes but is largely confined to the lakes of Kivu, Cyohoha and Mugesera. The lake fisheries are all artisanal in nature and the main fish species caught are: *Limnothrissa miodon* (Isambaza), *Haplochromis spp* (Haplochromines), *Oreochromis niloticus L*. (Nile tilapia), and *Clarias gariepinus* (Catfish). Following the realization that capture fisheries only could not be sufficient to provide enough fish to the growing Rwandan population, a big investment is being done in the commercial production of fishmeal from haplochromines, for both human consumption and animal feed manufacture (as an ingredient in the production of feeds for poultry, pigs and farmed fish), and in the aquaculture of Nile tilapia and catfish both in cage and tanks [13].

Status of Animal Feed Resources

Forage

Forages are the main source of feed for all ruminant animals. In Rwanda, most of the forages used to feed ruminants particularly cattle, goats, and sheep come from crops and cultivated grasses. Although small ruminants may be tethered outside the farms to browse on roadside vegetation, cattle feeding is largely based on a zero-grazing system in which fodder is cut and carried to the animal kept in confinement. The reasons for this practice are land-scarcity and limited forage resources, minimizing the risk of overgrazing and environmental degradation [11]. In their survey on the innovation opportunities for dairy milk production, Kalibwani *et al.*[8] reported that 70% of the respondents were

engaged in zero grazing, 21% were engaged in semi-grazing, whereas 9% were engaged in open range grazing. The main feeds available for the cattle include grasses, legumes, crop residues, brewers' and home wastes, and nonconventional feeds [14]. The majority of the farmers have access to natural pasture, while a small but significant number use fodder banks of Napier or Kikuyu grasses as well as a variety of crop residues [9]. Generally, Napier grass and natural pastures form the bulk of feed resources during both the wet and dry seasons. During the dry season commonly utilized feeds are crop by-products like maize stover, wheat/rice straws, bean haulms, purchased hay and in some cases Napier grass. A smaller number of farmers feed compounded dairy concentrate or feed supplements to dairy cattle regularly. Commercial feeds are very expensive; hence their use increases the production cost. Therefore, farmers usually invest in concentrate use during the dry season only when feeds are scarce. The use of conserved feed such as hay and silage is low among small dairy holders and higher among dairy holders in peri-urban and urban areas [9,14,15].

Commercial feeds

In Rwanda, farmers can either buy commercial feed or produce it themselves. The main feed manufacturers are Premier Animal Feed Industries (PAFI), Gorilla Feed, Poultry East Africa Limited (PEAL) and Zamura Feeds, which together account for 60% of the total poultry feeds produced and sold in the country. The remaining 40% is covered by ten other smaller non-specialized units [5]. The production of commercial feeds for other livestock animals other than poultry is low because these feeds are marginally used by farmers. The feedstuffs often used in poultry feed manufacturing are maize, rice, wheat and their by-products, soybean meal, cottonseed meal, and fish meal plus vitamins and minerals. Mbuza et al. [16] reported that the majority of broiler chicken farmers (92%) buy feedstuffs from commercial supplies and mix the feeds at farm level. Only 8% of broiler farmers purchase premixed commercial feeds. Maize bran is the main basal feedstuff used (97.06 %), followed by rice bran (35.29%) and wheat bran (17.65%). With regard to protein sources, cotton seed cake and fish meal (79.41%) are the most commonly used followed by soybean meal (67%).

Bone meal is most reported as a source of minerals (70.59%) followed by lake shell (29.41%). Most of the feedstuffs such as cottonseed cake, fish meal, lake shells and others are being imported since the raw materials are not produced in Rwanda or are produced in very small quantities. On the other hand, pig farmers use different types of feedstuffs as basal feed or supplements. The choice on feed type and quantity is dictated by the availability and price of the feed. The majority of the farmers tended to use maize bran and swill. In their study Mbuza et al. [12] found that a large number of pig farmers (65.9%) buy commercial feedstuffs for supplementary feeding and at times on-farm ration formulation; 30.2% of the farmers feed the pigs on home grown feedstuffs, while 58.6% feed swill (chicken remains) as a sole feed or a supplement to other feedstuffs. They also found that the quantity of feed given to pigs is below or close to the FAO (2009) recommendations. However, the quality of the feeds remains very low. Fish feeds are in high demand in Rwanda and their sourcing has long been the most significant constraint for the development of aquaculture in the country as until the year 2014 fish feeds could not be sourced locally. Thanks to PAFI, now fish feed is produced in Rwanda even though it is very expensive. Fish feed, like other animal feeds, is made from a variety of ingredients such as maize bran, wheat bran, soybean meal, cassava flour, vitamin and mineral premixes.

Challenges of Rwandan Animal Feed Sector

The main constraint to livestock production in many developing countries in the tropics especial Rwanda is the inadequate quantity and quality of both forage and concentrate feeds. The reasons for forage shortage are land scarcity, inadequacy of forage planting material, and lack of knowledge on forage production and utilisation [17]. Crop Intensification Program (2007) has enormously decreased the surface area needed for forage production. Today, forage is only produced in the public woodlots, marshlands; field and farm boundaries; intercropping with annual crops; roadsides; and forest buffer zones [18]. There is also limited knowledge on forage conservation as hay or silage which leads to the wastage of forage in the periods of surplus production. There is also scarcity of raw materials such as maize and soybean, and dependency on their imports. This has resulted to the price fluctuation of commercial feeds, particularly poultry feeds. There is a big competition of these feed ingredients between man and feed sector. The situation is even worsened by export and import bans that countries

in the region are implementing due to political issues [5]. Some manufactured feeds are of low quality, due to low institutional capacity to control feed quality. In addition, the number of available feeds companies and feed laboratories in the country are also insufficient [4].

Strategies and Implementation Plan for Feed Sector

The Rwanda Livestock Master Plan (RLMP 2017/2022) sets out the investment interventions which will help meet the national development plan targets of Rwanda by improving productivity and total production in the key livestock value chains for cow dairy, red meat, milk, poultry, and pork. In this 5 years roadmap, the strategies to mitigate feed challenges have been well described. Although the implementation of these strategies is ongoing, successful results have been remarkably observed. There has been a considerable improvement in forage production resulting from the effort made in introduction, characterization, and evaluation of exotic forage species based on their agro-ecological zones. There have been also improvements in forage conservation and grazing pasture management [19]. Some of the strategies to tackle animal feeds constraints include:

- Rehabilitation of grazing land through over-sowing with improved grass and legumes.
- Training and capacity building and skill development to increase the use and conservation of forage.
- Increase number of specialists well trained in animal nutrition, feed production and feed quality control
- Increased and better use of agro-industrial by-products from the processing of cereals/grains as concentrates for animal feeding.
- Promotion of appropriate storage and marketing of concentrates and feed supplements
- Training of farmers on forage seed multiplication, proper feeding, and availing improved plant materials.
- Create an industry for producing feed additives (minerals, vitamins, amino acids).

Table 2. Some investment interventions to reinforce feeds production and productivity [4]

Investment intervention	Quantity	Total budget	Source of budget
Support to forage seed multipliers	0.7 Ha	18,700,000.00	Public -30%, Private -70%
Support small scale feed processing units	Building new 25 processing units	62,300,000.00	Public -30%, Private -70%
Construction of 3 commercial animal feed plants	3 feed plants each of 40.000MT	-	100% private
Improve the capacity of existing feed quality control laboratories	Building 2 new laboratories	1,328,000,000.00	Public - 50%, Private - 50%
Rangeland rehabilitation	1000 Ha	41,600,000.00	Public - 20%, Private - 80%

Budget money is in Rwandan francs

Conclusion

It is obvious that livestock production in Rwanda has considerably improved especially in the last 2 decades. A lot has been done to improve animal genetic resources, animal health and welfare, and animal feed production. However, despite all those reinforcements made in the improvement and development of the feed sector in Rwanda, farmers still face feed shortages in both wet and dry seasons. Farmers and manufacturing companies have been importing feed and feed ingredients from neighboring countries to support locally available feed resources, but many reasons prove that importation is not a long-term solution. There is a need to sustain the animal feed sector based on locally available feedstuffs in order to minimize feed production cost, maximize profit and be able to compete at the regional markets. More research efforts to integrate home-grown forages, crop residues and other non-conventional feed resources into different feed formulation systems are needed. Therefore, in vitro and in vivo experimental researches are needed to reveal the feed quality and value of these alternative feed resources. There is also a need to slightly introduce the use of non feed additives to enhance the use of

available feeds. More funds have to be mobilized to support research projects in the area of the animal feed industry in Rwanda.

References

[1] Population by Country in 2020. Worldometer. https://www.worldometers.info/world-population/population-by-country/ [Accessed 2021 April 4]
[2] Beyi AF, Dahl EG. Feed the Future Innovation Lab for Livestock Systems Rwanda: Animal Source Foods Production and Marketing Brief. 2016;(May):3–4.
[3] Enahoro D, Njuri N, Thornton P, Staal SJ. A review of projections of demand and supply of livestock-derived foods and the implications for livestock sector management in LSIL focus countries. Mid-Project Research Report of the Feed the Future Innovation Lab for Livestock Systems (LSIL) Futures Fo. 2019;(262):64.
[4] Shapiro BI, Gebru G, Desta S, Nigussie K. Rwanda Livestock Master Plan. Int Livest Res Inst Livest Master Plan. 2017. http://extwprlegs1.fao.org/docs/pdf/rwa172923.pdf
[5] Cocchini S, Steeg E. Poultry Sector Analysis Rwanda based on the Poultry Learning Event 2019. Traide. 2019.
[6] Strategıc plan for agrıculture transformatıon in Rwanda 2018-24. http://extwprlegs1.fao.org/docs/pdf/rwa180543.pdf [Accessed 2021 Apr 30].
[7] FAOSTAT 2019. http://www.fao.org/faostat/en/#home [Accessed 2021 Apr 4].
[8] Kalibwani RM, Kakuru M, Tenywa M, Mugabo J, Nyamwaro S, Buruchara R. Innovation opportunities for milk production in Rwanda with lessons from the Mudende innovation platform. African J Rural Dev. 2018;3(1):651–64.
[9] Claire D`A H, Cyprian E, Jules M, Mupenzi M, Felix N, Paul Ampon W. Livestock Farming and Management: The Case of Meat Production and Processing in Rwanda. Asian J Anim Sci. 2017;11(2):96–107.
[10] Mutimura M, Lussa AB, Mutabazi J, Myambi CB, Cyamweshi RA, Ebong C. Status of animal feed resources in Rwanda. Trop Grasslands-Forrajes Trop. 2013;1(1):109–10.
[11] Klapwijk CJ, Bucagu C, van Wijk MT, Udo HMJ, Vanlauwe B, Munyanziza E, et al. The "One cow per poor family" programme: Current and potential fodder availability within smallholder farming systems in southwest Rwanda. Agric Syst. 2014;131:11–22. http://dx.doi.org/10.1016/j.agsy.2014.07.005
[12] Francis M, Denis M, Jean DDA, Marie FD. Inventory of pig production systems in Rwanda. Int J Livest Prod. 2016;7(7):41–7.
[13] Busıness case for fısh meal productıon and aquaculture in Rwanda. https://rwandatrade.rw/media/2015%20MINICOM%20Business%20Case%20Dried%20Fish.pdf [Accessed 2021 June 15]
[14] Mutimura M, Ebong C, Rao IM, Nsahlai IV. Nutritional values of available ruminant feed resources in smallholder dairy farms in Rwanda. Trop Anim Health Prod. 2015;47(6):1131–7.
[15] Lukuyu BA, Kitalyi A, Franzel S, Duncan A, Baltenweck I. Constraints and options to enhancing production of high quality feeds in dairy production in Kenya, Uganda and Rwanda. ICRAF Working Paper no. 95. Nairobi, Kenya: World Agroforestry Centre. 2009;34.
[16] Mbuza F, Manishimwe R, Mahoro J, Simbankabo T, Nishimwe K. Characterization of broiler poultry production system in Rwanda. Trop Anim Health Prod [Internet]. 2017;49(1):71–7. Available from: http://dx.doi.org/10.1007/s11250-016-1160-0
[17] Kamanzi M, Mapiye C. Feed inventory and smallholder farmers' perceived causes of feed shortage for dairy cattle in Gisagara District, Rwanda. Trop Anim Health Prod. 2012;44(7):1459–68.
[18] Umunezero O, Mwendia S, Paul BK, Maass BL, Ebong C, Kagabo D, et al. Identifying and Characterizing Areas for Potential Forage Production in Rwanda. 2016;(417).
[19] Uwituze S. Animal resources research In Rwanda https://livestocklab.ifas.ufl.edu/media/livestocklabifasufledu/pdf-/Uwituze,-S-(2019_04_02)-Animal-Resources-Research-in-Rwanda.pdf [Accessed 2021 May 15].

Fertilizer Rate for Optimum Growth and Yield of Egusi Melon (*Colocynthis citrullus* L.)/ Hot Pepper (*Capsicum chinense*, Jackquin cv. rodo) Intercrop

*Anjola S. Aninkan**, *Eyitayo A. Makinde*
Federal University of Agriculture Abeokuta, Department of Horticulture, College of Plant Science and Crop Production (COLPLANT), P.M.B. 2240, Abeokuta, Nigeria
**Corresponding author: anjolaaninkan@gmail.com*

Abstract

The use of chemical fertilizers as a supplemental source of nutrients has been on the increase but they are not applied in balanced proportion by most farmers [1]. Also, fertilizer requirements of the mixed intercropping systems have been a matter of conjecture; some studies had suggested that fertilizer requirements of the dominant component be applied [2], others recommend that the sum of the sole crop requirements, be applied [3]. Teriah [4], however, stated that both practices have proved either inadequate or wasteful. In this experiment the effects of different rates of NPK 15-15-15 fertilizer application on growth and yield of hot pepper and Egusi melon in an intercropping system was examined to determine optimum rate for production. The experiment was carried out at the Teaching and Research Farm of the Federal University of Agriculture Abeokuta, in the south western part of Nigeria. It took place from March to October 2017 during the growing season. The experiment was laid out in a Randomized Complete Block Design (RCBD) with 5 treatments (fertilizer rates) and 3 replicates. Treatments were; 0, 100, 200, 300 and 400 kg/ha of NPK 15-15-15 applications. Plot size was 3m by 3m with a 1.5m gang way round each plot to reduce inter-plot effect. Data were collected on growth parameters at 6 weeks after treatment (WAT) and continued at two-week intervals until 10 WAT. Four plants each of pepper and Egusi melon from the inner rows were randomly selected and tagged for the purpose of data collection. Data on yield were also collected at ripening. Analysis of variance (ANOVA) was carried out on each observation and the Least Significant Difference (LSD) was used for means separation ($P \leq 0.05$). The effects of fertilizer rates showed significant difference on pepper plant height, number of leaves, number of branches and leaf area. However, there was no significant difference in the effect of fertilizer rate on days to 50% flowering of pepper. Number of vines and vine length of Egusi melon were significantly different in their responses to fertilizer rates but the leaf area and days to 50% flowering of melon were similar at the various treatment levels. Meanwhile, total fruit yield of pepper, number of Egusi melon pods per hectare and the dry matter yield of Egusi melon showed significant difference. It was concluded from the study that the growth and yield of pepper and Egusi melon in intercrop increased with increase in fertilizer rate up to 400Kg/ha of NPK (15:15:15). However, higher fertilizer application rates should be explored in future studies for a better yield increase. These studies should be carried out with various compositions of inorganic and organic fertilizer application rates to ensure sustainable fertilizer application and to also preserve the natural fertility of the soil.

Keywords: inorganic fertilizers, NPK 15-15-15, fertilizer application rate

Introduction

Pepper (*Capsicum chinense*, Jackquin) also called King Chili finds importance in human diets as condiments, processed meat flavor, colorant and medicinal purposes [5]. Nigeria produces 50% of total pepper production in Africa. It is cultivated over a wide range of production practices which vary greatly from region to region. A warm humidity climate favors growth while warm and dry weather enhances fruit maturity [6]. Plants are established by seedling or transplanting.

Egusi melon (*Colocynthis citrullus* L.) is a member of the family *Cucurbitaceae* and belongs to the tribe Benicaseae. The *colocynthis* is a small genus of 4 to 5 species found in Africa, one of which is the *C. citrullus*. Egusi melon originated in Africa and has been cultivated in the drier part of the continent for many centuries [7]. It thrives in hot regions with rich light soil and can tolerate periods of low rainfall. The crop is cultivated for its seeds which are prepared into condiments used especially in preparing soup. The Egusi melon seed, like soya bean (*Glycine maxima*), is rich in oil and protein, about 51.3% and 33.8% respectively. Fertilizers are sources of plant nutrients that can be added to the soil to supply its natural fertility [8]. Profitable responses to NPK fertilization were reported by Conover and Poole [9]. Organic matter also has been reported to act as a reservoir of plant nutrients especially NPK and

micronutrients and also prevents leaching of nutrients. Karim et al. [10] reported that due to poor management and intensive manipulation of soil, organic matter content is getting reduced day by day. Available data according to Karim et al. [10] and Ali et al, [11] showed that the fertility of most soils has deteriorated over the years. The reduction in the soil fertility level is responsible for stagnating and, in some cases even declining crop yields [12],[13],[14]. John et al. [15] reported that inorganic fertilizers are the most important sources of nutrient N and adequate supply of N is associated with high photosynthetic activity, vigorous vegetative growth and a dark green color of the leaves.

The use of chemical fertilizers as a supplemental source of nutrients has been on the increase but they are not applied in balanced proportion by most farmers [1]. Also, fertilizer requirements of the mixed intercropping systems have been a matter of conjecture; some workers suggest that fertilizer requirements of the dominant component be applied [2], others recommend that the sum of the sole crop requirements, be applied [3]. Teriah [4], however, stated that both practices have proved either inadequate or wasteful. It is on this backdrop that this research focuses on the effects of fertilizer rates on the growth and yield of Egusi melon and pepper in intercrop. The objective therefore was to establish the optimum NPK 15:15:15 fertilizer application rate for the growth and yield of Egusi melon and pepper in intercrop.

Materials and Method

The experiment was carried out at the Teaching and Research farm of the Federal University of Agriculture, Abeokuta located on Latitude $7^0$15'N; longitude $3^0$25'E at an elevation of 141m above sea level. The experiment commenced when the rains were steady for 2017 planting season and it ran through the beginning of the dry season. An Egusi melon cultivar, the black-edged 'Bara' [16] was used. Pepper variety used was the medium corrugated fruited hot pepper ('Rodo'). The pepper seedlings were raised at a nursery behind the College of Veterinary Medicine Teaching Hospital, Federal University of Agriculture Abeokuta from extracted seeds of the pepper fruit. The seeds were air- dried after extraction to improve viability. There was shade provision for the seedling at the nursery so as to reduce water loss due to evapotranspiration. The shade was removed gradually at four weeks after sowing (WAS) to harden the seedlings before transplanting.

The experimental site was double-ploughed, followed by harrowing operation, so as to plough nutrients from resident vegetation back into the soil and to reduce weed incidence. Soil samples were collected from the experimental site at 15cm depth for nutrient content analysis, making use of the Judgmental Random Sampling method by dividing the site into strata based on its major slope i.e., upper slope, middle slope, and slope bottom. The experiment was laid out in a Randomized Complete Block Design (RCBD) with 5 treatments (fertilizer rates) and 3 replicates. The plot size was 3m by 3m with a 1.5m gang way round each plot to reduce inter-plot effect.

The Egusi melon seeds were planted at a spacing of 1m by 1m at 3cm depth. The sowing rate was 3 seeds per hole. The pepper seedlings were transplanted 6 weeks after sowing (WAS) at 1m by 0.5m spacing and 1 seedling per stand. The melon stands were thinned to one plant per stand at 2 WAS and missing stands supplied for both melon and pepper.

Weeding was done a week after planting/transplanting to ensure fertilizer efficiency and it was repeated regularly to check pest and weed impact on crop growth and yield. Fertilizer was weighed and applied at treatment rates (0, 100, 200, 300, 400, kg/ha of NPK 15:15:15) to each treatment plot on a wet soil so as to avoid desiccation of the growing plant tissue due to the hygroscopic nature of the fertilizer

Data were collected on growth parameters at 6 weeks after treatment (WAT) and continued at two-week intervals until 10 WAT. Four plants each of pepper and *Egusi* melon from the inner rows were randomly selected and tagged for the purpose of data collection. Vine length of Egusi melon were determined by measuring with a flexible tape**.** Number of vines and number of leaves was determined by counting from each sample**.** Leaf area (cm^2) was calculated using the linear model according to Wahua [17]: Area = -30.53 + 7.43X - where 'X' is the mid rib length of the central lobe. Plant height for pepper was measured as the distance from the soil surface to the tip of the top most leaf. Leaf area was determined using linear equation described by Salau *et al.* [18]: Y=1.45+0.65 (L*B) - where 'Y' is the estimated leaf area; 'L' is the leaf length and 'B' is breadth of the leaf. Pepper stem girth was determined with the use of a veneer caliper at 10cm height above the soil. Days to attain 50% flowering

for both pepper and Egusi melon were determined by counting the number of days from sowing to when 50 % population flowered.

Data on yield were also collected at ripening. Ripe pepper fruits (evident by red coloration and size increase) were hand-picked at five-days interval, counted and weighed. Egusi melon was harvested at about 16 WAS, when the leaves turned yellowish and fell off with stem drying, which were signs of senescence and crop maturity [19]. Dry seed yield (kg/ha) was determined by measuring weight of seed yield per unit area of each treatment plot. Weights of fruit per plot (kg) were measured from random samples of fruits on a plot. Fruit yield (kg/ha) was determined by measuring weight of yield per unit area of each treatment plot.

Analysis of variance (ANOVA) was carried out on each observation and the Least Significant Difference (LSD) was used for means separation ($P \leq 0.05$).

Results

The rainfall had its onset in April with a rainfall of 112.80mm and reached its peak in May with a rainfall of 156.10mm after which there was a decline in total monthly rainfall. The total rainfall for the experimental period was 788.4mm. The lowest minimum temperature was recorded in the month of June with a temperature of 21.30°c, relative humidity of 83.5 and 4.33 hours of sunshine. (Table 1). The soil was near neutral and sandy with very low organic matter, total N and available P contents, very low to low exchangeable cations and Effective Cation Exchangeable Capacity (ECEC). However, the soil has a high base saturation of 99.17%. (Table 2).

The effect of different NPK fertilizer rates on pepper plant height in intercrop with melon was significant throughout the weeks. The application rate of 200kg/ha and 400kg/ha gave plants that were significantly taller 8 weeks after transplanting (WAT) while at 10 WAT, application rate of 400kg/ha had the tallest plant. (Table 3). The effect of different NPK fertilizer rates on pepper stem girth in intercrop with melon was significant from 6 to 8 WAT. Application rate of 200kg/ha and 400kg/ha of NPK showed comparable stem thickness that was thicker than application rate of 300kg/ha at 8 WAT. The thickest plants were obtained at 10 WAT from application rate of 400kg/ha of NPK with an average thickness of 9.3cm followed by application rate of 300kg/ha with an average thickness of 6.10cm. (Table 3). There was significant difference in the number of leaves of pepper among the treatments throughout the weeks. Application rates of 300kg/ha and 400kg/ha of NPK had comparable number of leaves per plant that were higher than those from other treatments at 10 WAT. (Table 4). There were significant differences in the number of branches of pepper among the treatment throughout the weeks. At 10 WAT the highest number of branches per plant were obtained from application rate of 400kg/ha of NPK and it was comparable to that of 300kg/ha only. (Table 4). The effect of NPK fertilizer rates on average leaf area showed significant difference at 10 WAT when fertilizer rate of 400kg/ha gave leaf area that was significantly wider (17.77cm^2 per plant) than that of the other rates. This was followed by application rate of 300kg/ha that gave average leaf area of 13.95cm^2 per plant. (Table 5).

There was no significant difference among the treatment means for days to 50% flowering. However, application rates of 200kg/ha and 300kg/ha of NPK attained the earliest days to 50% flowering at 44 days after transplanting (DAT) while the longest of 46 DAT was from the unfertilized plants. (Table 5)

Table 1. Weather report of the experimental area from March to October (2017)

Month	Total rainfall (mm)	Min. temp. (^{0}c)	Max. temp. (^{0}c)	Relative humidity (%)	Sunshine hours
March	34.30	24.20	35.80	68.10	6.10
April	112.80	23.70	33.40	73.80	5.60
May	146.00	23.10	27.80	80.90	5.20
June	111.00	21.30	31.40	83.50	4.33
July	156.10	22.80	29.20	85.70	2.10
August	90.50	21.80	28.30	86.30	1.27
September	50.00	22.10	32.10	79.20	3.00
October	87.70	23.30	29.90	84.80	4.30

Table 2. Pre-cropping physical and chemical properties of the soil

Properties	**Value**
pH	7.07
Total organic carbon	0.53%
Total nitrogen	0.06%
Available Phosphorus	8.82 mg/kg
Exchangeable bases	
K	0.26cmol
Ca	4.12cmol
Mg	1.10cmol
Na	0.48cmol
Al+H	0.05cmol
ECEC	6.01cmol
Mn	49.95 mg/kg
Fe	10.20 mg/kg
Cu	0.86 mg/kg
ZN	2.76 mg/kg
Base saturation	99.17%
Particle size	
Sand	93.2%
Silt	3.2%
Clay	3.2%

Table 3. Pepper average stem girth and average shoot height as influenced by NPK fertilizer rates in intercrop with Egusi melon

	Average stem girth (mm)			Average plant height (cm)		
	Weeks after transplanting					
Treatments	6	8	10	6	8	10
*0	1.80	2.40	5.70	12.98	16.03	35.76
100	1.90	2.40	4.90	11.97	17.83	38.66
200	2.50	3.60	5.70	20.33	27.33	52.75
300	2.20	3.30	6.10	19.1	22.22	43.5
400	2.50	3.70	9.30	22.67	28.03	61.93
LSD, 5%	0.40	0.20	NS	3.77	4.33	5.53

*kg/ha of NPK 15:15:15

Table 4. Number of leaves and number of branches as influenced by NPK fertilizer rates in intercrop with Egusi melon

	Number of leaves/plants			Number of branches/plants		
	Weeks after transplanting					
Treatments	6	8	10	6	8	10
*0	7.92	13.75	118.92	0.08	0.58	5.00
100	9.25	16.42	101.42	0.33	1.17	4.25
200	20.5	37.50	143.92	0.83	1.58	4.58
300	19.42	36.00	214.75	0.67	1.42	5.67
400	21.17	42.33	253.58	1.42	2.08	5.75
LSD, 5%	5.31	5.31	49.64	0.25	0.51	0.85

*kg/ha of NPK 15:15:15

Table 5. Pepper average leaf area and days to 50% flowering as influenced by NPK fertilizer rates in intercrop with Egusi melon

	Average leaf area (cm^2)			
	Weeks after transplanting			
Treatment	6	8	10	Days to 50% flowering
*0	5.02	11.85	13.37	46.33
100	4.12	9.73	10.18	45.00
200	6.53	18.95	6.90	44.00
300	6.42	17.59	13.95	43.67
400	6.26	20.45	17.77	45.33
LSD, 5%	NS	NS	3.72	NS

*kg/ha of NPK 15:15:15

The effect of NPK fertilizer rates on Egusi melon number of vines per plant showed significant difference, with application of 200kg/ha, 300kg/ha and 400kg/ha of NPK giving a comparable number which was significantly higher than other levels. (Table 6). The effect of NPK fertilizer rates on Egusi melon vine length per plant showed significant difference when treatment level of 400kg/ha gave significantly longer vines than others at 141.75cm per plant. Treatment levels of 100kg/ha, 200kg/ha and 300kg/ha, however, gave a comparable result (Table 6). The effect of NPK fertilizer rates on Egusi melon number of leaves per plant showed no significant difference. Treatment level of 400kg/ha NPK 15:15:15 however gave plants with the highest number of leaves (21 leaves per plant) (Table 6). There

was no significant difference in the effect of the treatment levels on the average leaf area of Egusi melon. However, application of 400kg/ha gave the widest leaf area of 66.66cm^2 per plant followed by application of 200kg/ha that had 65.43cm^2 per plant. (Table 6). There was no significance difference in the effect of the treatment levels on days to 50% flowering of Egusi melon. However, application of treatment level of 400kg/ha of NPK attained the earliest days to 50% flowering at 34 days after transplanting while the longest of 36 days was from the unfertilized plants. (Table 7)

Table 6. Egusi melon number of vines, vine length, number of leaves and average leaf area as influenced by NPK fertilizer rates in intercrop with pepper

Treatments	Number of vines/plants	Vine length/plant (cm)	Number of leaves/plants	Average leaf area (cm^2)
*0	4.00	86.33	16.67	49.68
100	3.92	109.39	18.00	58.88
200	5.17	118.71	18.67	65.43
300	4.58	117.00	19.33	59.19
400	5.33	141.75	20.67	66.66
LSD, 5%	0.77	15.05	NS	NS

*kg/ha of NPK 15:15:15

Table 7. Egusi melon days to 50% flowering as influenced by NPK fertilizer rates in intercrop with pepper

Treatments	Days to 50% flowering (days after transplanting)
*0	35.67
100	34.67
200	35.00
300	35.00
400	34.33
LSD, 5%	NS

*kg/ha of NPK 15:15:15

Average fruit lengths of pepper per plant were all comparable. However, application rate of 200kg/ha gave the longest fruits of 3.1cm per plant followed by application of 400kg/ha that had 3.03cm per plant. (Table 8). Average pepper fruit diameters per plant were all comparable. However, application rate of 400kg/ha gave the widest fruits at 3.56cm per plant followed by application rate of 200kg/ha that had 3.02cm diameter per plant. (Table 8). There was significant difference in the average pepper fruit weights per plant. Application rate of 400kg/ha gave fruits that were significantly heavier (38.17g per plant) than those of other treatments. (Table 8). There was significant difference among the treatment means for pepper total fruit yield per hectare. Application rate of 400kg/ha gave the highest fruit yield of 4.69t/ha of pepper fruits and that was significantly higher than the yields obtained from the other treatments. (Table 9). There was no significant difference among the treatment means for percentage marketable pepper fruit yield per hectare. Application rate of 300kg/ha, however, gave 89.48% marketable fruits (i.e., four in every five fruits) which was the highest recorded. (Table 9). Percentage unmarketable pepper fruit yield per hectare were all comparable. (Table 9)

Table 8. Yield parameters of pepper as influenced by fertilizer rates in intercrop with Egusi melon

Treatments	Average fruit length/plant (cm)	Average fruit diameter/plant (cm)	Average fruit weight/plant (g)
*0	2.47	2.83	14.04
100	2.77	2.89	11.71
200	3.03	3.02	20.37

300	2.20	3.01	26.98
400	3.10	3.56	38.17
LSD, 5%	NS	NS	7.23

*kg/ha of NPK 15:15:15

Table 9. Total fruit yield, % marketable fruit yield and % unmarketable fruit yield of pepper as influenced by NPK fertilizer rates in intercrop with Egusi melon

Treatment	Total fruit yield (t/ha)	% Marketable fruit yield	% Unmarketable fruit yield
*0	1.17	76.817	23.183
100	1.69	84.131	15.869
200	2.26	85.110	14.890
300	2.99	89.479	10.521
400	4.69	86.664	13.336
LSD, 5%	1.13	NS	NS

*kg/ha of NPK 15:15:15

The effect of fertilizer rates on number of melon pods per hectare showed significant difference when application rate of 300kg/ha and 400kg/ha gave a comparable number that was significantly higher than others. Application rate of 400kg/ha gave the highest number of pods per hectare (62,348). (Table 10). There was significant difference in the effects of fertilizer rates on dry seed yield of Egusi melon per hectare. Application rate of 400kg/ha gave seed yield (339.28kg/ha) that was significantly higher than those of other treatments. (Table 10)

Table 10. Yield of Egusi melon as influenced by NPK fertilizer rates in intercrop with pepper

Treatments	Number of pods per hectare	Dry seed yield per hectare (kg/ha)
*0	28000	104.77
100	32778	107.42
200	36278	124.36
300	59384	231.71
400	62348	339.28
LSD, 5%	14987	51.73

Discussion

The pepper shoot height, stem girth, number of leaf and number of branches that were observed increased with increase in fertilizer rate and reached a peak at 400kg/ha of NPK, this was in agreement with Olaniyi [20] who recorded that all the growth parameters measured were influenced by the combined N and P fertilizers application with the highest mean values recorded at 80 kg N and 13.2 kg P ha^{-1}. Also, Ayodele *et al.* [21] recorded that at each sampling period, N application increased pepper plant heights significantly and at 10 WAT 75 kg N. ha^{-1} produced the tallest plants which averaged 35.64 and 34.86 cm while plants in the control were shortest at 23.75 and 21.44 cm in 2010 and 2011 respectively. Johnson and William [22] noted that the improvement in vegetative growth was due to increased N availability in the soil nutrient pool and its uptake. Adequate N induces growth and fruit yield of vegetables than other nutrients and mature pepper plants, especially, have a relatively high demand of the nutrient for vegetative growth and fruit formation and development [21]. The results from this study showed that NPK 15:15:15 application enhanced the growth performance of pepper in terms of increase in plant height, more branches and leaves with larger leaves. This is probably due to the presence of N nutrient in the complete fertilizer combination.

The yield parameters of pepper as observed from fruits harvested over a period of 10 weeks also showed significant difference as increase in fertilizer rate resulted in increased pepper fruit yield up to

400kg/ha NPK application. Ayodele et al., [21] has also reported a linear increase in yield with increasing N fertilizer application. The highest yield obtained in this study at 400kg/ha NPK 15-15-15 treatment level was 4.69 tons. Although this was similar to a yield of 4.28 tons recorded by Lawal et al. [23] his findings showed that yield declines when the same fertilizer rate was applied the following season in 2004. This decline can be attributed to the lack of residual effect common to the use of inorganic fertilizer. It can also be suggested that continuous use of inorganic fertilizer will have to take place with constantly increasing rate in order to increase yield, a condition which might cause damage to the natural fertility of the soil.

Vine length of Egusi melon increased with increase in fertilizer rate and reached a peak at 400kg/ha of NPK which was similar to result obtained by Muoneke et al. [24], when he recorded that in 2010 the vine length progressively increased as the NPK rate increased from zero to 400 kg/ha and thereafter declined with 600 kg/ha application. He also suggested that the decline of the vine length with application of 600 kg/ha NPK indicated that this rate could represent the toxic level of the nutrients to the plant.

Seed yield per hectare also increased with increase in fertilizer rate and it reached a peak at 400kg/ha of NPK. This is in agreement with the results obtained by Ekwere et al. [25]. However, Muoenke et al. [24] recorded higher yield per hectare when okra was intercropped with egusi melon. This might be due to a stiffer competition in favor of the pepper crop.

Conclusion

Although the various fertilizer inputs in the intercrop favors more of the yield of pepper than of Egusi melon, the growth and yield of pepper and Egusi melon in intercrop increases with increasing fertilizer rate up to 400Kg/ha of NPK 15:15:15. However, studies have shown that continuous use of inorganic fertilizers is injurious to the natural fertility of the soil.

Recommendation

Therefore, it is recommended that more studies should be carried out on various inorganic and organic fertilizer application rates to ensure the Optimum rate for growth and yield of Egusi melon and pepper intercrop and to also preserve the natural fertility of the soil.

References

[1] Okonwu K, Mensah SI. Effects of NPK (15:15:15) Fertilizer on Some Growth Indices of Pumpkin. Asian Journal of Agricultural research. 2012; 6(3): 137-143.
[2] Ahmed S, Gunasena HPM. Nitrogen Utilization and economics of some intercrop systems in tropical countries. Tropical Agriculture. 1979; 56(2):115-123.
[3] Haizel KA. The agronomic significance of mixed cropping: maize interplanted with cowpea. Ghana Journal of Science. 1994; 7(3):163-178.
[4] Terriah NM. Effect of intercropping maize and cowpea on nutrient balance and soil nutrient status. Nigerian Journal of Agricultural Technology. 1990; 2:50-58.
[5] Alabi DA. Effects of Fertilizer Phosphorus and Poultry Droppings Treatments on Growth and Nutrient Components of Pepper (*Capsicum annum* L.), African Journal of Biotechnology. 2006; 5(8).
[6] Denton L, Makinde MJ. Variation among landraces of pepper in Nigeria Capsicum and Eggplant, Newsletter, 1993; 12, 42-44.
[7] Cobley LS. An Introduction to Botany of Tropical Crops. Food and Agriculture Organization of the United Nation, 1967.
[8] El Aziz NG. Stimulatory Effects of NPK Fertilizer and Benzyl adenine on Growth and Chemical Constituent of Codiaeum variegatum L. plant. Am-Eurasian Journal of Agriculture and Environmental Science. 2007; 2:711-719.
[9] Conover CA, Poole RT. Light and Fertilizer Recommendation for Production Acclimatized Potted Foliage Plants. CFREC-A Research Report RH-90-1. Apopka, FL., USA: Central Florida Research and Education Center; 1990.
[10] Karim Z, Miah MMU, Razia S. Fertilizer in the National Economy and Sustainable Environmental Development. Asia Pacific Journal of Environmental Development. 1994; 2: 48-67.

[11] Ali MM, Saheed SM, Kubota D, Masunaga T, Wakatsuki T. Soil degradation from the period of 1967-1995 in Bangladesh, II, selected chemical characters. Soil Science and Plant Nutrition. 1997; 43: 879-890.
[12] Fertilizer Recommendation Guide. Bangladesh Agricultural Research Council, Dakah, Bangladesh. 1997.
[13] Land Degradation Situation in Bangladesh. Soil Division, Bangladesh Agricultural Research Council. Dakah, Bangladesh. 1999.
[14] Cassman KG, De Datta Sk, Olk DC, Alcantra J, Sason M, Descalsota J, Dizon M. Yield decline and Nitrogen economy of long-term experiment on continuous, irrigated rice system in the tropics. In: Soil Management: Experimental Basis for Sustainability and Environmental Quality, Lal, R. and Stewart, B.A., (Eds.). London, UK: Lewis Publisher; 1995. 181-222.
[15] John LW, Jamer DB, Samuel LT, Warner LW, Soil Fertility and Fertilizers: An Introduction to Nutrient Management. India: Pearson Education; 2004. 106-153.4.
[16] Olaniyi JO, Growth. Seed Yield and Nutrient Use Efficiency of Egusi Melon (*Citrullus lanatus* Thunb. Mansf) Cultivars as affected by NPK 15-15-15 Fertilization. Journal of Agricultural biotechnology and Environment. 2000; 2(1/2): 11-16.
[17] Wahua TAT. Effects of melon (*Colocynthis vulgaris*) population density on inter cropped maize (*Zea mays* L.) and melon. Experimental Agriculture. 1985; 21: 281-289.
[18] Salau AW, Olasantan FO, Oloriade GA, Rapid leaf area estimation in capsicum. Nigeria Journal of Horticultural Science. 2008; 13: 128-136.
[19] Ijoyah MO, Alexander A, Fanen FT. Yield performance of Okra (Abelmoschus esculentus L. Moench) and maize (*Zea mays* L.) as Affected by Time of Planting Maize in Makurdi, Nigeria. Agriculture and Biology Journal of Northern America. 2012; 6: 1328-1332.
[20] Olaniyi JO. Growth and Seed Yield Response of Egusi Melon to Nitrogen and Phosphorus Fertilizer Application. Am. Eurasian Journal of Sustainable Agriculture. 2008; 2(3): 255-260.
[21] Ayodele O, Alabi EO, Aluko M. Nitrogen Fertilizer Effects on Growth, Yield and Chemical Composition of Hot pepper (Rodo). International Journal of Agriculture and Crop Science. 2015; 8(5): 666-673.
[22] Johnson GA, William CM. Multiple Cropping in the Humid Tropics of Asia. Canada : IDRC Publication; 1997; 176-248.
[23] Lawal Ab, Rahman SA. Effect of irrigation, fertiliser and manure on yield and economic return of okra/pepper intercrops. Tropical Science. 2007; 47(1): 45–48.
[24] Muoneke CO, Ndukwe OO, Amih CA, Eka MJ. Cropping System and NPK Fertilizer Rate Influenced Productivity of Garden Egg (Solanum gilo) and Egusi melon (*Colocynthis citrulllus*) in garden egg/Egusi melon Intercropping System. International Journal of Agronomy Research. 2016; 9(6): 1-14.
[25] Ekwere OJ, Muoneke CO, Eka MJ, Osodeke VE. Growth and Yield Parameters of Maize and Egusi Melon in Intercrop as Influenced by The Cropping System and Different Rates of NPK Fertilizer. Journal of Agriculture and Crop Research. 2013; 1(5): 69-75.

Application of *In-Ovo* Injection of Some Substances for Manipulation of Sex and Improving Performance in Chicken

*Abdol Hossain Ataei**, *Figen Kırkpınar*
Ege University, Faculty of Agriculture, Department of Animal Science, Izmir, Turkey
**Corresponding author: ab.ataei@gmail.com*

Abstract

In intensive production, freshly hatched cockerels are culled in the layer hatchery (7 billion males each year), On the other hand, for meat production rearing female birds has not economic benefits because of male broiler chicks have a faster growth rate and better feed efficiency than females. In this regards several methods are being developed for sex determination in the chick embryo during the incubation period. But these methods need to be rapid, cost-efficient, and suitable practical for commercial use. Additionally, sex determination should be done before pain perception has evolved in chick embryos. Biotechnology by *in ovo* technique to sex determination of between male and female chicks or sex reversal could improve production and eliminate ethical dilemmas for poultry industries. In birds, the differentiation of embryonic gonads is not determined by genetic gender with the certainty that occurs in mammals and can be affected by early treatment with a steroid hormone. During the development of the chick embryo, the genotype of the zygote determines the nature of the gonads, which then caused male or female phenotype. The differentiation of gonads during the period called the "critical period of sexual differentiation" is accompanied by the beginning of secretion of sexual hormones. Namely, any change in the concentration of steroid hormones during the critical period affects the structure of the gonads. Many synthetic anti-aromatases such as federazole and non-synthetic in plants, mushrooms, and fruits containing natural flavonoids have been used in the experiments *in ovo* injection of anti-aromatase had no negative effect on the growth performance of sexual reversal female chickens.

In conclusion, administration of an aromatase inhibitor causes testicular growth in the genetic female gender, and estrogen administration leads to the production of the left ovotestis in the genetic male gender. Therefore, in the early stages of embryonic development, sexual differentiation can be affected by changing the ratio of sexual hormones.

In this review, effects of some substances applied by *in ovo* injection technique on sex reversal and performance in chicks.

Keywords: *In ovo* technique, performance, sex reversal

Introduction

Genetics has played a major role in the domestication of poultry, which in intensive production, commercial hybrid chickens selected for one purpose only; either eggs or meat. Accordingly, freshly hatched cockerels are culled in the layer hatchery (7 billion males each year [1]). Chick culling or unwanted chick killing is a result of advanced specialization in poultry production with layer strains which are characterized by a slim physique and low fattening performance, while male broiler chicks have a faster growth rate and better feed efficiency than females. Consequently, it does not make economic sense to raise male chicks, because of the differences in the sale prices and care costs of male and female avian species and the time spent in the reproduction process causes significant financial losses [2]. In addition, sperm sexing as is performed for other species is not feasible for poultry [3]. Therefore, superfluous chicks are eliminated either by some methods of culling that do not involve anesthetics include: cervical dislocation, asphyxiation by CO_2 gas, or by maceration using a high-speed grinder. In this regards several methods are being developed for sex determination in the chick embryo during the incubation period. But these methods need to be rapid, cost-efficient, and suitable practical for commercial use. Additionally, sex determination should be done before pain perception has evolved in chick embryos.

An increasing number of initiatives are working on a solution for this challenge. For example, detection of estrogen versus androgen in incubated eggs, microscopic cytogenetic analysis of

chromosomes, ultrasonography *in ovo*, embryonic heartbeat, and temperature variation during incubation are used to determine the sex of the chick in the egg [4]. An alternative to circumvent chick culling is the so-called "*in ovo*" (inside the egg). Biotechnology by *in ovo* technique to sex determination of between male and female chicks or sex reversal could improve production and eliminate ethical dilemmas for poultry industries. Successful manipulation of sex ratios in birds depends on a better understanding of the sex control mechanisms and gonadal development in early embryogenesis [5]. In birds, the differentiation of embryonic gonads is not determined by genetic gender with the certainty that occurs in mammals and can be affected by early treatment with a steroid hormone. Chicken embryonic gonads at an early stage have the potential to convert to both sexes (male and female). During the development of the chick embryo, the genotype of the zygote determines the nature of the gonads, which then caused male or female phenotype. The differentiation of gonads during the period called the "critical period of sexual differentiation" is accompanied by the beginning of secretion of sexual hormones. Namely, any change in the concentration of steroid hormones during the critical period affects the structure of the gonads. Estrogens and their receptors are crucial for female sexual differentiation. This sexual differentiation occurs as a result of aromatase expression in the left gonad at day 6.5 and the production of estrogen from testosterone, and experimental sex reversal has been performed using anti-estrogens, aromatase inhibitors, and synthetic steroids [6]. Many synthetic anti-aromatases such as federazole and non-synthetic in plants, mushrooms, and fruits containing natural flavonoids have been used in the experiments *in ovo* injection of anti-aromatase had no negative effect on the growth performance of sexual reversal female chickens.

This review includes attempts to provide an insight on some substances applied by *in ovo* injection technique on sex reversal and performance in chicks.

Sex Determination and Sexual Differentiation in the Birds

The sex is determined genetically in mammals and birds, and genetic sex is determined at fertilization, although gonads are indistinguishable. According to the genetic sex, gonads develop into testes or ovaries. In birds, the gonads of both sexes are not differentiated during the first week of the embryo. After this stage, the male gonad becomes the testis and the female gonad becomes the ovary [7]. However, the sex chromosomes of birds are different from those of other mammals. Unlike mammals, genetically male birds are homozygous (ZZ) and the females are heterozygous (ZW) [8]. This system is unrelated to the XX and XY system seen in mammals, hence birds lack the mammalian sex determination is initiated by the expression of the Y-chromosomal SRY gene [9]. Gender may be controlled by the dominance of sex chromosomes W the ovary, the number of Z chromosomes, or a combination of both mechanisms. The dominant W assumes that the female sex chromosome carries a dominant-acting ovary determinant [10]. However, due to the inactivity of Z chromosomes in birds [11, 12], the main mechanism controlling sex determination is the dosage of the Z gene [13, 14]. Under this mechanism, the ratio of the Z chromosome to asexual chromosomes is very important. As global Z dosage compensation is absent in birds, Z-linked genes may direct sexual development [15]. The onset of sex differentiation of gonads in birds is sensitive to steroid hormones [16]. But determinants of more masculinity are involved in the gonads or other glands such as the brain glands [17]. Study analysis of gynandromorphic chickens and experimental chimeras indicate that sexual phenotype is at least partly cell-autonomous [18]. Although neither mechanism has so far been definitely proven, most evidence now favors the Z dosage hypothesis [19, 20].

Despite sex determination in the embryonic stage, genes involved in gonadal differentiation are also active later in the developmental stage. A large number of studies focusing on sex determination in vertebrates have focused on gender differentiation in the gonadal period, on the shape of the testicles and ovaries during embryonic life. However, evidence from avian (and other vertebrate) embryos suggests that genes that control sex differentiation may be active in some cases before gonads, in other tissues such as the brain [21, 22]. For example, homogenous gene expression is present in the blastoderm of chickens, early embryos, and in the primary brain before the formation of the reproductive system [22]. This shows that sex differentiation is at least partially dependent on the "sex differentiation genes" active in different parts of the fetus, not just the gonads [23]. These genes are different from the genes expressed in the gonads. Thus, sexual differentiation may depend on both direct genetic components and hormonal mechanisms [16, 17].

Estrogen and Gonadal Aromatase Activity

In birds, the genotype of the embryo in the fertilized egg determines the nature of the sexual gonads, leading to the evolution of the male or female phenotype [5]. But differentiation of embryonic gonads can be affected by early treatment with a steroid hormone [6]. In contrast to mammals, The W chromosome positively controls early aromatase synthesis and consequently, estrogen production [6]. In the male genotype and both gonads develop into 2 testes. In females, extensive expression of the aromatase gene after 6.5 days of incubation, leading to estrogen synthesis [24] and specific expression of the estrogen receptor RNA in the left gonad [25], results in the development of a functional left ovary. The P_{450} enzyme, aromatase, is essential for estrogen synthesis. In birds, aromatase is strictly expressed in female gonads at the onset of embryonic sexual differentiation. Administration of aromatase inhibitor prevents the synthesis of estrogen (the hormone responsible for the ovarian structure and the secondary sex characteristics) in genetic material and causes the production of roosters with female genotype. Also, experimental manipulation of blood levels of progesterone [26], testosterone [27, 28, 29], and corticosterone [27, 30, 31] has been reported to induce sex ratio bias in various avian species. Estrogen is required for ovarian development, the left gonad differentiates to a single ovary, and the right gonad regresses, and developing a permanent female phenotype [5]. Moreover, 17b-Hydroxysteroid dehydrogenase and aromatase enzymes which are responsible for the conversion of androgens to estradiol-17 b are only detectable in the female embryos' gonads [25].

Nowadays, researchers have been able to change the sex ratio of chickens and roosters during hatching with genetic and nutritional strategies. Although aromatase has been studied for decades, the crystallographic structure of this enzyme was reported in 2009 [32]. The importance of aromatase is underscored by many studies showing that aromatase inhibitors, such as Fadrozole, induce female-to-male sex reversal in ZW females when administered before or during sexual differentiation [33, 34].

Aromatase inhibitors that inhibit estrogen production from testosterone dispart into two categories: synthetic and non-synthetic. The nonsynthetic anti-aromatase are natural biochemical compounds that are found in fungi, vegetables, fruits, and other plants. Flavonoids are natural anti-aromatase compounds that are abundantly found in plants [35]. Synthetic aromatase inhibitors are classified into two types, steroidal and non-steroidal. Steroid inhibitors such as Androstenedione and its derivatives, Hydroxybromo and Methyl androstenedione, Formestin, and Exemestane bind irreversibly to the aromatase receptor, destroying the combination of protein and drug [36]. Non-steroidal inhibitors such as Fadrazole, Aminoglutamides, Anastrozole, and Letrozole bind to aromatase in the P_{450} region so that they can adhere without degradation [37].

Chick Culling and Approaches to Avoid the Killing of Male Chickens

Methods that are used to cull chicks include: Maceration (also called 'grinding') [38], Electrocution; An electric current passes through the chick's body until it dies [39], Asphyxiation (also called 'gassing'); carbon dioxide (CO_2) is used to induce unconsciousness and then death [40], and suffocation; The chickens are placed in plastic bags [41].

The culling of day-old male chicks is a much-regarded topic in today's politics. Several approaches to the animal welfare problems and chicken egg sexing have been proposed in the attempt to solve the dilemma between economy and ethics by providing an alternative to day-old chick culling. I) Rearing of a dual-purpose breed, II) Fattening of male layer hybrids and, III) *in ovo*-sex identification.

I) The aim is that both sexes gain economic value. The selection for growth efficiency in broiler strains has resulted in negative effects concerning several reproduction traits, such as reduction of fertility and a higher percentage of defective eggs [42]. However, due to the negative correlation between reproduction and fattening traits, their fattening performance is less profitable than in broilers.

II) Rearing and fattening of male layers

Koenig et al. [43] demonstrated that rearing male layers as cockerels improves the fattening performance and thus increases economic efficiency. However, since these efforts are in their infancy, the hens which are in the present breeding and selection process are still valued for their laying performance, and the males are reared without distinct economic value [44].

III) The *in ovo* sex determination during incubation: Are based on endocrinological or optical methods, the sex of the chick embryo is determined, at a preferably early phase of incubation [1]. The *in ovo* are including noninvasive methods (reflectance spectroscopy [45], egg shape [46], hyperspectral

imaging [47]) and, invasive methods, require extraction of samples, (molecular sexing [17], measurement of hormones in egg fluids [48], Infrared absorption spectroscopy of blastoderm cells [49], DNA analysis [50]). However, these methods could not be exploited commercially because shell windowing of the unincubated egg strongly affects the hatching rate and chick health.

Application of *in ovo* technique

More recently, *in ovo* sexing, an application of this technology, has been proposed to solve important animal welfare and ethics issues the culling by maceration or suffocation of male chicks in commercial layer production [41].

In-ovo sex determination has the potential to bring an end to the unnecessary killing of billions of chicks. However, the technology raises new ethical concerns which relate to the sensitivity of the embryo, as well as how the screened-out eggs will be used afterward and the accuracy of gender determination [51].

In addition, sex determination should be performed before pain perception has evolved in chick embryos [1]. Synaptic connection of sensory afferent nerves connected to the spinal cord is not present before d 7 of incubation [52]. Therefore, no sense of the chick embryo is to be expected before d 7 of incubation [53].

The history of *in ovo* (Latin for "inside the egg") technology is traceable to the works of Sharma and Burmester [54], which revealed that embryonic vaccination confers superior immunity against Marek disease in chickens. *In ovo* technology can be defined as the direct inoculation of bioactive substances to the developing embryo to elicit superior lifelong effects while considering the dynamic physiology of the chicken embryo [41].

In ovo applications are applied for different purposes in incubation. This technique is used to improvement of hatching [55], vaccination of chicks, increase digestive capacity and intestinal development [56], skeletal system [57], immune system [58], improving body weight and feed efficiency [59], reducing first-week mortality [60], increasing muscle growth [61], have all been reported in the literature.

Studies of Some Substances by *In Ovo* Injection for Chicken Sex Reversal

The importance of aromatase inhibitors is reported by several studies; induce female-to-male sex reversal in females when administered before or during sexual differentiation. It has been reported that *in ovo* injection of Fadrozole to 5-day-old embryos in the incubation period, conversion of androgens to estrogen is inhibited and phenotypic males are formed from genetic females, especially due to decreased P_{450} aromatase mRNA expression in the right ovary. Genetic females exhibited mating behaviors similar to normal roosters at 10 months of age. While there was no abnormality in spermatogenesis in genetic females mating with chickens, only the amount of sperm was found to be low, and this caused the problem of infertility in eggs [6].

In a study by *in ovo* injection of two different anti-aromatases, 14- α hydroxy androstone 3, 6, 17-trione (NKSO1), (1 and 2 mg) and Fadrazole (0.05, 0.1, and 0.15 mg) were applied to 5-day old embryos of eggs) to chicken sex determination, it was indicated that, as compared to NKSO1, Fadrazol resulted in a significant increase in male birds ($p<0.05$). It has shown that, *in ovo* injection of Fadrazol, no negative effects on either hatchability, chick viability, and/or economic performances such as feed efficiency, live weight, and carcass cuts [62]. In a similar study by Burke and Henry [63], injection of 0.15 mg of Fadrazole resulted in the highest percentage of male chicks compared to 0.05 and 0.45 mg. While the report of Shimada et al. [64], showed the highest percentage of males in eggs treated with 0.1 mg of Fadrazole.

Mohammadrezaei et al. [65] assessed the effects of *in ovo* injection of fadrozole hydrochloride (FH) and insulin-like growth factor 1 (IGF-I), on sexual differentiation and growth performance of broiler chickens. They reported that all the chicks in IGF-I and FH groups were male chicks in phenotypically, and *in ovo* administration of IGF-I and FH can to a great extent improve productive traits (feed conversion ratio, Body weight) of broiler, while, *in ovo* exposure of treatment did not influence hatchability and mortality ($P>0.05$). In agreement, Fuxjager et al. [66] showed that the positive effects of androgens on muscle mass could be mediated through IGF-I expression in bird's muscles. Matsushita et al. [67] also reported that *in ovo* injection of atrazine (an aromatase inhibitor) has no effect on the

hatchability. However, injection of higher doses of Fadrozole led to a remarkable decrease in hatchability [68, 63].

Female birds have been shown to manipulate offspring sex ratio under natural as well as experimental conditions. However, mechanisms of sex ratio bias are not well understood and it is often not clear whether a skewed sex ratio is due to primary or secondary sex ratio bias; Although, in contrast to wild bird species, the laying hen maybe after severe selection for egg production, have lost the ability to manipulate offspring sex ratio [69].

In another study, after a treatment on the 3rd day of egg incubation with 1-methyl-androstendion (steroidal aromatase inhibitor), or with Fadrozole (nonsteroidal aromatase inhibitor), gonads of 12-day-old female embryos looked like the testis and exhibited different grades of sex reversal [70]. Li et al. [71] also reported that *in ovo* injection of Fadrozole, before gonadal sex differentiation can induce female-to-male sex reversal in broiler chickens. On the other hand, the male-to-female chicken sex reversal can be directed by estrogen [5] or aromatase over expression [72] during sexual differentiation.

The results of an experiment by Mokarrami et al. [73] showed that *in ovo* injection of 0.1 mg mushroom extract, nettle extract or Fadrozole had no effect significant differences on hatchability, dressing percentage and internal organ weights, embryo mortality during incubation, and the weight of hatching chicks, they concluded that mushroom extract and Fadrozole hydrochloride by creating a sex reversal and increase the ratio of males in flock improved the average production traits.

Fazli et al. [74], the influence of *in ovo* injection of aromatase inhibitors, clomiphen citrate (0.05 mg/egg), tomoxifen (0.05 mg/egg), and both garlic and tomato extracts (0.1 mL/egg) at day 5 of the incubation period on sex differentiation in broiler chickens investigated. The results showed that *in ovo* injection of garlic and tomato extracts caused the highest percentage of male chicks. In addition, the percentage of thighs and wings of the males was significantly higher than those of females. However, *in ovo* injection of garlic extract, tomato extract, tomoxifen, and clomiphene citrate numerically reduced hatchability compared to the control group.

In a similar study, *in ovo* injection of tomato alcoholic extract and tomato aqueous extract (0.3 and 0.6 mL) lead to a significant increase in male chicken percentage at hatching compared to the control group, without any negative effect on hatchability and performance ($P < 0.05$) [75]. In agreement, Mokarrami et al. [73], showed that, broiler sex reversal by using mushroom extract and fadrozole resulting to increase in the growth rate of broilers. Also, the high anti-aromatase characteristics of the mushroom extract can be a good alternative to chemical drugs such as fadrozole hydrochloride. In contrast, Sarbozi et al. [76] reported that *in ovo* injection of Pine pollen extract had no significant effect on hatchability, economic characteristics, and sex differentiation.

More results by *in ovo* injection of green tea extract and/or fadrozole hydrochloride at 5th day of incubation period indicated that *in ovo* injection of 0.1 mL of fadrozole hydrochloride and green tea extract led to 100 and 80 percent sex reversal, respectively. Also, During the whole, experimental period, daily feed intake and daily weight gain of chickens of fadrozole hydrochloride and green tea extract treatments were higher than those in the control group [77].

Conclusion

In conclusion, administration of an aromatase inhibitor causes testicular growth in the genetic female gender, and estrogen administration leads to the production of the left ovotestis in the genetic male gender. Therefore, in the early stages of embryonic development, sexual differentiation can be affected by changing the ratio of sexual hormones. In addition, this technique is a potential and ethically justifiable alternative to the culling of day-old male layer chicks, and allows a reliable sex reversal, and causes the production performance of avians. Also, it is concluded that natural plant compounds with anti-aromatase properties can compete with synthetic anti-aromatases, without adversely affecting bird development from the embryonic period to the end of the rearing period.

References

[1] Krautwald-Junghanns ME, Cramer K, Fischer B, Förster A, Galli R, Kremer F, Mapesa EU, Meissner S, Preisinger R, Preusse G, Schnabel C. Current approaches to avoid the culling of day-old male chicks in the layer industry, with special reference to spectroscopic methods. Poultry science. 2018; 97(3):749-57.
[2] Cerit H, Avanus K. Sex determination by CHDW and CHDZ genes of avian sex chromosomes in Nymphicus hollandicus. Turkish Journal of Veterinary and Animal Sciences. 2008; 31(6):371-4.
[3] Vishwanath R, Moreno JF. Semen sexing–current state of the art with emphasis on bovine species. Animal. 2018; 12(1):85-96.
[4] Kaleta EF, Redmann T. Approaches to determine the sex prior to and after incubation of chicken eggs and of day-old chicks. World's Poultry Science Journal. 2008; 64(3):391-9.
[5] Elbrecht A, Smith RG. Aromatase enzyme activity and sex determination in chickens. Science. 1992; 255(5043): 467-70.
[6] Shimada K. Gene expression of steroidogenic enzymes in chicken embryonic gonads. Journal of experimental zoology. 1998; 281(5): 450-6.
[7] Ellegren H. Dosage compensation: do birds do it as well? Trends in Genetics. 2002; 18(1):25-8.
[8] Bellott DW, Skaletsky H, Pyntikova T, Mardis ER, Graves T, Kremitzki C, Brown LG, Rozen S, Warren WC, Wilson RK, Page DC. Convergent evolution of chicken Z and human X chromosomes by expansion and gene acquisition. Nature. 2010; 466(7306):612-6.
[9] Koopman, P., Munsterberg, A., Capel, B., Vivian, N. and Lovell Badge, R. (1990) Expression of a candidate sex-determining gene during mouse testis differentiation. Nature 348, 450-452.
[10] Smith CA, Roeszler KN, Hudson QJ, Sinclair AH. Avian sex determination: what, when and where? Cytogenetic and Genome Research. 2007; 117(1-4):165-73.
[11] Arnold AP, Chen X, Link JC, Itoh Y, Reue K. Cell-autonomous sex determination outside of the gonad. Developmental Dynamics. 2013; 242(4): 371-9.
[12] Uebbing S, Künstner A, Mäkinen H, Ellegren H. Transcriptome sequencing reveals the character of incomplete dosage compensation across multiple tissues in flycatchers. Genome biology and evolution. 2013; 5(8):1555-66.
[13] Chue J, Smith CA. Sex determination and sexual differentiation in the avian model. The FEBS journal. 2011; 278(7): 1027-34.
[14] Ayers KL, Davidson NM, Demiyah D, Roeszler KN, Grützner F, Sinclair AH, Oshlack A, Smith CA. RNA sequencing reveals sexually dimorphic gene expression before gonadal differentiation in chicken and allows comprehensive annotation of the W-chromosome. Genome biology. 2013; 14(3):1-7.
[15] Hirst CE, Major AT, Smith CA. Sex determination and gonadal sex differentiation in the chicken model. International Journal of Developmental Biology. 2018; 62(1-2-3):153-66.
[16] Zhao D, McBride D, Nandi S, McQueen HA, McGrew MJ, Hocking PM, Lewis PD, Sang HM, Clinton M. Somatic sex identity is cell autonomous in the chicken. Nature 2010; 464(7286): 237-42.
[17] Clinton M, Nandi S, Zhao D, Olson S, Peterson P, Burdon T, McBride D. Real-time sexing of chicken embryos and compatibility with *in ovo* protocols. Sexual Development 2016;10(4):210-6.
[18] Ellegren H. Emergence of male-biased genes on the chicken Z-chromosome: sex-chromosome contrasts between male and female heterogametic systems. Genome Research. 2011; 21(12): 2082-6.
[19] Nanda I, Schlegelmilch K, Haaf T, Schartl M, Schmid M. Synteny conservation of the Z chromosome in 14 avian species (11 families) supports a role for Z dosage in avian sex determination. Cytogenetic and genome research. 2008;122(2):150-6.
[20] Smith CA, Roeszler KN, Ohnesorg T, Cummins DM, Farlie PG, Doran TJ, Sinclair AH. The avian Z-linked gene DMRT1 is required for male sex determination in the chicken. Nature. 2009 Sep;461(7261):267-71.
[21] Nef S, Schaad O, Stallings NR, Cederroth CR, Pitetti JL, Schaer G, Malki S, Dubois-Dauphin M, Boizet-Bonhoure B, Descombes P, Parker KL. Gene expression during sex determination reveals a robust female genetic program at the onset of ovarian development. Developmental biology. 2005 Nov 15; 287(2):361-77.

[22] Ayers KL, Sinclair AH, Smith CA. The molecular genetics of ovarian differentiation in the avian model. Sex Dev 7: 80-94, 2013.
[23] Arnold AP, Itoh Y. Factors causing sex differences in birds. Avian biology research. 2011; 4(2):44-51.
[24] Zhang C, Saito, N, Matsuda, Y, Shimada, K. Identification of sperm-bearing female-specific chromosome in the sex-reversed chicken. Journal of Experimental Zoology 1998, 280(1), 65-72.
[25] Nakabayashi O, Kikuchi H, Kikuchi T, Mizuno S. Differential expression of genes for aromatase and estrogen receptor during the gonadal development in chicken embryos. Journal of Molecular Endocrinology. 1998 Apr 1;20(2):193-202.
[26] Bagheri-Fam S, Bird AD, Zhao L, Ryan JM, Yong M, Wilhelm D, Koopman P, Eswarakumar VP, Harley VR. Testis determination requires a specific FGFR2 isoform to repress FOXL2. Endocrinology. 2017 Nov 1;158(11):3832-43.
[27] Bowles J, Feng CW, Ineson J, Miles K, Spiller CM, Harley VR, Sinclair AH, Koopman P. Retinoic acid antagonizes testis development in mice. Cell reports. 2018 Jul 31;24(5):1330-41.
[28] Baetens D, Stoop H, Peelman F, Todeschini AL, Rosseel T, Coppieters F, Veitia RA, Looijenga LH, De Baere E, Cools M. NR5A1 is a novel disease gene for 46, XX testicular and ovotesticular disorders of sex development. Genetics in Medicine. 2017 Apr;19(4):367-76.
[29] Baroiller JF, d'Cotta H. The reversible sex of gonochoristic fish: insights and consequences. Sexual Development. 2016;10(5-6):242-66.
[30] Baronio F, Ortolano R, Menabò S, Cassio A, Baldazzi L, Di Natale V, Tonti G, Vestrucci B, Balsamo A. 46, XX DSD due to androgen excess in monogenic disorders of steroidogenesis: genetic, biochemical, and clinical features. International journal of molecular sciences. 2019 Jan;20(18):4605.
[31] Barrionuevo F, Bagheri-Fam S, Klattig J, Kist R, Taketo MM, Englert C, Scherer G. Homozygous inactivation of Sox9 causes complete XY sex reversal in mice. Biology of reproduction. 2006; 74(1):195-201.
[32] Ghosh D, Griswold J, Erman M, Pangborn W. Structural basis for androgen specificity and estrogen synthesis in human aromatase. Nature. 2009 Jan;457(7226):219-23.
[33] Smith CA, Katz M, Sinclair AH. DMRT1 is upregulated in the gonads during female-to-male sex reversal in ZW chicken embryos. Biology of reproduction. 2003 Feb 1;68(2):560-70.
[34] Vaillant S, Dorizzi M, Pieau C, Richard-Mercier N. Sex reversal and aromatase in chicken. Journal of Experimental Zoology. 2001 Dec 1;290(7):727-40.
[35] Grove JF. Volatile compounds from the mycelium of the mushroom Agaricus bisporus. Phytochemistry. 1981 Jan 1;20(8):2021-2.
[36] Hong J, Wang Y, Kumagai H, Tamaki H. Construction of thermotolerant yeast expressing thermostable cellulase genes. Journal of biotechnology. 2007 Jun 15;130(2):114-23.
[37] Haynes BF, Hale LP, Patton KL, Martin ME, McCallum RM. Measurement of an adhesion molecule as an indicator of inflammatory disease activity: Up-regulation of the receptor for hyaluronate (CD44) in rheumatoid arthritis. Arthritis & Rheumatism. 1991 Nov;34(11):1434-43.
[38] Ćujić N, Šavikin K, Janković T, Pljevljakušić D, Zdunić G, Ibrić S. Optimization of polyphenols extraction from dried chokeberry using maceration as traditional technique. Food chemistry. 2016; 194:135-42.
[39] Gregory NG. Stunning and slaughter. processing of poultry 1995 (31-63). Springer, Boston, MA.
[40] Nieuwenhuis M. Atmospheric governance: Gassing as law for the protection and killing of life. Environment and Planning D: Society and Space. 2018 Feb;36(1):78-95.
[41] Oladokun S, Adewole DI. *In ovo* delivery of bioactive substances: an alternative to the use of antibiotic growth promoters in poultry production—a review. Journal of Applied Poultry Research. 2020.
[42] Rauw WM, Kanis E, Noordhuizen-Stassen EN, Grommers FJ. Undesirable side effects of selection for high production efficiency in farm animals: a review. Livestock production science. 1998; 56(1):15-33.
[43] Koenig, M., G. Hahn, K. Damme, M. Schmutz, 2012: Utilization of laying-type cockerels as "coquelets": Influence of genotype and diet characteristics on growth performance and carcass composition. Arch. Geflügelk. 76(3), 197-202.

[44] Giersberg MF, Kemper N. Rearing male layer chickens: A German perspective. Agriculture. 2018; 8(11):176.
[45] Rozenboim I, Ben Dor E. The use of reflectance spectroscopy for fertility detection in freshly laid egg and gender sorting in mid incubation period. Poult Sci. 2001;90(E-Suppl. 1):98.
[46] Yılmaz-Dikmen B, Dikmen S. A Morphometric Method of Sexing White Layer Eggs. Braz J Poultry Sci. 2013 Jul; 15(3): 203–10.
[47] Gohler D, Fischer B, Meissner S. *In-ovo* sexing of 14-day-old chicken embryos by pattern analysis in hyperspectral images (VIS/NIR spectra): A non-destructive method for layer lines with gender-specific down feather color. Poult Sci. 2017 Jan 1; 96(1): 1–4.
[48] Tran HT, Ferrell W, Butt TR. An estrogen sensor for poultry sex sorting. J Anim Sci. 2010 Apr; 88(4): 1358–64.
[49] Steiner G, Bartels T, Stelling A, Krautwald-Junghanns ME, Fuhrmann H, Sablinskas V, et al. Gender determination of fertilized unincubated chicken eggs by infrared spectroscopic imaging. Anal Bioanal Chem. 2011 Jul; 400(9): 2775–82.
[50] Porat N, Bogdanov K, Danielli A, Arie A, Samina I, Hadani A. Direct detection of chicken genomic DNA for gender determination by thymine-DNA glycosylase. British poultry science. 2011 Feb 1;52(1):58-65.
[51] Reithmayer, C., Danne, M., Mußhoff, O. (2021). Societal attitudes towards *in ovo* gender determination as an alternative to chick culling. Agribusiness, 37(2), 306-323.
[52] Eide AL, Glover JC. 1997. Developmental dynamics of functionally specific primary sensory afferent projections in the chicken embryo. Anat. Embryol. (Berl.) 195:237–250.
[53] Aleksandrowicz E, Herr I. Ethical euthanasia and short-term anesthesia of the chick embryo. ALTEX-Alternatives to animal experimentation. 2015 May 1;32(2):143-7.
[54] Sharma JM, Burmester BR. Resistance to Marek's disease at hatching in chickens vaccinated as embryos with the turkey herpesvirus. Avian Dis (1982) 26:134–49.
[55] Tako E, Ferket PR, Uni Z. Effects of *in ovo* feeding of carbohydrates and beta-hydroxy-beta-methylbutyrate on the development of the chicken intestine. Poultry Science. 2004;83(12):2023-8.
[56] Uni Z, Ferket PR, inventors; Yissum Research Development Co of Hebrew University of Jerusalem, North Carolina State University, assignee. Enhancement of development of oviparous species by *in ovo* feeding. United States patent US 6,592,878. 2003 Jul 15.
[57] Hargis PS, Pardue SL, Lee AM, Sandel GW. *In ovo* growth hormone alters the growth and adipose tissue development of chickens. Growth, development, and aging: GDA. 1989 Jan 1;53(3):93-9.
[58] Jochemsen P, Jeurissen SH. The localization and uptake of *in ovo* injected soluble and particulate substances in the chicken. Poultry Science. 2002 Dec 1;81(12):1811-7.
[59] Bhanja S1, Mandal AB, Goswami TK. Effect of *in ovo* injection of amino acids on growth, immune response, development of digestive organs and carcass yields of broiler. Indian Journal of Poultry Science. 2004;39(3):212-8.
[60] Uni Z, Ferket RP. Methods for early nutrition and their potential. World's Poultry Science Journal. 2004 Mar;60(1):101-11.
[61] Hajihosaini M, Mottaghitalab M. Effect of amino acid injection in broiler breeder eggs on hatchability and growth of hatched chicken. J. Agric. Sci. 2004;1(3):23-32.
[62] Mottaghitalab M, Razani K. Egg Treatment with Anti-aromatase: Effects on the chicks male: female ratio and their economic performance. Iranian Journal of Agricultural Science. 2005; 36:375-83.
[63] Burke WH, Henry MH. Gonadal development and growth of chickens and turkeys hatched from eggs injected with an aromatase inhibitor. Poultry science. 1999 Jul 1;78(7):1019-33.
[64] Shimada K, Yoshida K, Saito N. Effects of Aromatase Inhibitor on Sex Differentiation and Levels of P45017α and P_{450}aromMessenger Ribonucleic Acid of Gonads in Chicken Embryos. General and comparative endocrinology. 1996; 102(2):241-6.
[65] Mohammadrezaei M, Toghyani M, Eghbalsaied S, Gheisari A, Esmaeili M. Growth performance and sex differentiation in broiler chickens submitted to *in ovo* injection of fadrozole and insulin-like growth factor I. InProc. Nutr. Feed Technol. Conf., which city 2012 (pp. 1039-1042).
[66] Fuxjager MJ, Barske J, Du S, Day LB, Schlinger BA. Androgens regulate gene expression in avian skeletal muscles. PLoS One. 2012; 7(12):e51482.

[67] Matsushita S, Yamashita J, Iwasawa T, Tomita T, Ikeda M. Effects of *in ovo* exposure to imazalil and atrazine on sexual differentiation in chick gonads. Poultry science. 2006 Sep 1;85(9):1641-7.
[68] Yang X, Zheng J, Na R, Li J, Xu G, Qu L, Yang N. Degree of sex differentiation of genetic female chicken treated with different doses of an aromatase inhibitor. Sexual Development. 2008; 2(6):309-15.
[69] Aslam MA. Offspring sex ratio bias and sex related characteristics of eggs in chicken. Wageningen University; 2014.
[70] Wartenberg H, Lenz E, Schweikert HU. Sexual differentiation and the germ cell in sex reversed gonads after aromatase inhibition in the chicken embryo. Andrologia. 1992 Jan 2;24(1):1-6.
[71] Li WM, Feng YP, Zhao RX, Fan YZ, Affara NA, Wu JJ, Fang J, Tong Q, Wang C, Zhang SJ. Sex ratio bias in early-dead embryos of chickens collected during the first week of incubation. Poultry science. 2008; 87(11):2231-3.
[72] Lambeth LS, Cummins DM, Doran TJ, Sinclair AH, Smith CA. Overexpression of aromatase alone is sufficient for ovarian development in genetically male chicken embryos. PloS one. 2013 Jun 28;8(6):e68362.
[73] Mokarrami T, Navidshad B, Hedayat Evrigh N, Mirzaei Aghjehgheshlagh F. The Effect of *in ovo* Injection of Aromatase Inhibitors on the Performance of Broilers. Iranian Journal of Applied Animal Science. 2020; 10(1):113-8.
[74] Fazli N, Hassanabadi A, Mottaghitalab M, Hajati H. Manipulation of broiler chickens sex differentiation by *in ovo* injection of aromatase inhibitors, and garlic and tomato extracts. Poultry science. 2015; 94(11):2778-83.
[75] Jamshasb A, Mottaghitalab M. The Effect of In-ovo Injection of Tomato Extract on Sex Differentiation and Gonadal Structure of Broiler Chicks and Their Performance. Research On Animal Production (Scientific and Research). 2019; 10(25):86-95.
[76] Sarbozi FAA, Ansari-Pirsaraei Z, Biparva P, Dirandeh E. Effect of *in ovo* injection of Pine pollen extract on growth and sex differences of broiler chicks. Research On Animal Production (Scientific and Research) 2018; 8(18):66-75.
[77] Heidari HA, Navidshad B, Nikbin S, Mirzaei AF. Effect of *in ovo* injection of green tea extract and fadrozole hydrochloride on sex reversal and muscle structure of broiler chickens. Research On Animal Production (Scientific and Research). 2018; 9(22):18-25.

Hydroponics "Soilless Farming": The Future of Food and Agriculture – A Review

Roukaya Ghorbel *[1], *Jamel Chakchak* [2], *Hatice Basmacıoğlu Malayoğlu* [1], *Numan S. Çetin* [2]
[1]*Ege University, Agriculture Faculty, Department of Animal Science, Feeds and Animal Nutrition, Izmir, Turkey*
[2]*Ege University, Solar Energy Institute, Solar Energy Department, Izmir, Turkey*
** Corresponding author: roukayaghorbel@gmail.com*

Abstract

It is estimated that the global population will reach approximately 10 billion people by 2050 and 66% of the world population will live in urban areas. This growth in cities creates demand for fresh products to maintain a healthy population, a product that often exposed to a long journey to reach the consumer, not only losing quality and nutritive value in the process, but also requiring a significant cost of fossil fuel for transportation and storage. However, the world's agricultural land among being limited, is also facing major problems such as pollution, salinization and drought that do not favor crop production. The need for food security has paved the way for landless agriculture, becoming more popular in the urban area and becoming a part of urban farming. This article aims to examine hydroponic technologies to help expand the knowledge of their application in terms of science, origin, dynamics and farming systems. Among the benefits of soilless cultures; reservation of cultivated land for main crops; saving at least 90% of irrigation water; use of almost constant amount of recycled water; successfully growing almost every vegetable crops and having highest productivity compared to conventional agriculture. Therefore, it is an indispensable solution in areas where arable land is not available or in saline-prone areas, in short, wherever there is competition for land and water.

The purpose of this study is an overview of soilless farming systems, explaining the most widely used hydroponic system, the importance of water quality, nutrient content, grown crops and ultimately cost benefit in terms of economics.

Keywords: hydroponics; soilless culture; alternative; sustainable; agriculture

Introduction

Water scarcity, pollution and nutrient deficient soils present a major challenge worldwide and these are likely to deteriorate with increasing global populations particularly, in urban areas. By 2050 it is expected that the global population will expanse to approximately 10 billion people, and it is estimated that by this time, 66% of the world's population will be settled in urban areas [1]. For healthy population, this growth in population will be the reason behind a raising demand for fresh product, but this produce will be often exposed to travel a long way to reach the consumer, not only losing quality and nutrition along the way, but also requiring a significant fossil fuel cost for transportation and storage. Adding to this the required packaging and preservatives, which always have negative effects on environment.

Soilless systems present a significant alternative to soil cultivation in case of soil and/or water issues, and some of the most important problems are salinization and water shortage [2]. The three main soilless systems are liquid hydroponics, solid media culture and aeroponics. Hydroponics (Fig. 1) can further be divided into open and closed systems. The open system doesn't provide the recycling of the excess of nutrient solution, however in closed systems, the surplus flow of nutrients coming from the roots is collected and recycled back to the system (Fig. 4). Solid media culture systems (Fig. 2) can also be separated to open or closed systems, several substrates can be used for plants anchorage (i.e. coconut coir, vermiculite, perlite), as long as characterized by water/air holding capacity and easy drainage. Aeroponics (Fig. 3) enables the maximum utilization of space by growing plants with roots suspended in air sprayed every 2–3 minutes, plants get nutrients and water from the solution film that adheres on roots [3]. This diversity of techniques makes soilless culture adaptable to every situation, with a great applicable potential to provide food in areas characterized by soil and water availability issues [4].

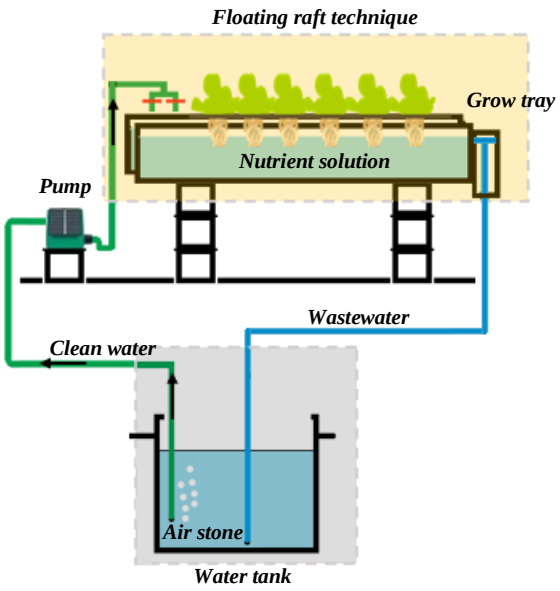

Figure 1. Scheme of the Hydroponics system

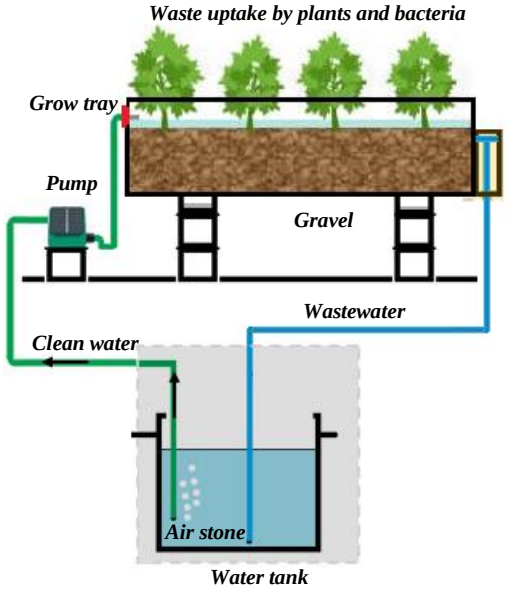

Figure 2. Scheme of the Solid media culture system

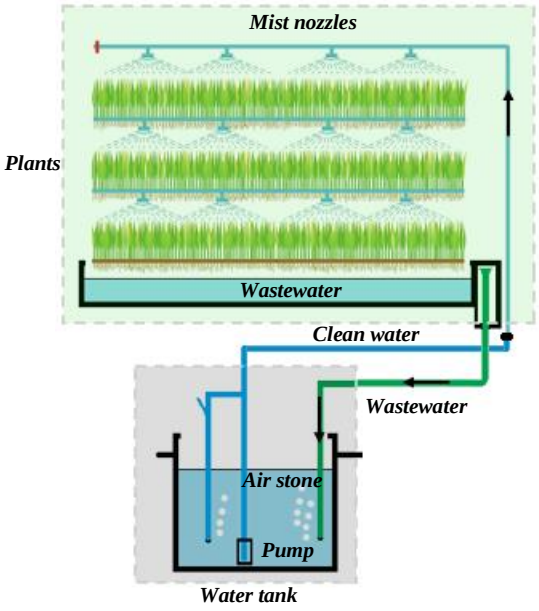

Figure 3. Scheme of the Aeroponics system

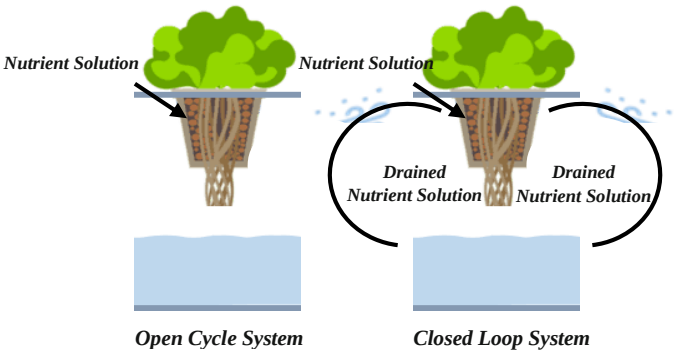

Figure 4. Scheme of open cycle and closed loop systems

A number of crops can be grown commercially in hydroponic, principally vegetables and fruits. Such as Fragaria ananassa (Strawberry), Lactuca sativa (Lettuce), Lycopersicon esculentum (Tomato), Phaseolus vulgaris (Green bean), Beta vulgaris (Beet), Cucumis sativus (Cucumbers), Cucumis melo (Melons), Allium cepa (Onion) and many others [5]. Accordingly, hydroponics can play a major role in providing essential dietary fiber, minerals and vitamins [6]. Even more, it could help in fulfilling the recommended minimum intake of fruits and vegetables per person. Actually, some types of food which are nowadays under-consumed worldwide [7], due to cultural lack in their cultivation and use [8], or due to absence of appropriate environmental requirements. Thus, hydroponics systems can enhance crop diversification and consumption attitude. In addition, significant reduction in water consumption is noticed in soilless culture compared to soil cultivation, with a considerable increase of water use efficiency [9], in terms of both yield and gross income [10]. In fact, no percolation losses occur when growing plants with roots directly in contact with the growing media. Moreover, water for soil leaching is in this case unneeded, such amount of water depends on several parameters: site specific estimation of total precipitation, irrigation, evapotranspiration, soil bulk density and porosity, solute characteristics and distribution [11].

Hydroponic Systems Designs and Technologies

Proceeding to create or use a hydroponic system to grow plants, there are hundreds of variations of hydroponic systems available to use. However, these main five types of hydroponic systems combine all variated systems.

Deep Flow Technique (DFT)

Deep flow technique (*DFT*), also known as deep water technique, is the cultivation of plants on floating or hanging support (rafts, panels, boards) in reservoirs filled with 10–20 cm of nutrient solution [12] (Fig. 1). In this kind of system water level, electrical conductivity (E.C.), pH, and dissolved oxygen levels needs to be continuously monitored. To maintain an actively aerated container and homogeneously mixed nutrients, the system, shown in Figure 1, includes an air compressor and air-stones. The plants float on top of the water using a raft, typically made of extruded polystyrene foam or low-density polyethylene, and the roots of the plant grow into the water and fertilizer solution. The DFT systems requires a large amount of water and nutrients to operate successfully, and the dissolved oxygen levels are not always homogenized. Also it is important to mention that it is easier to maintain a stable temperature of the fertilizer solution in a DFT system compared to an NFT system [13].

Nutrient Film Technique (NFT)

The NFT technique is often used and can be considered the classic hydroponic cultivation system, in this type of system the nutrient solution flows along and circulates in troughs with a 1–2 cm layer of water [14,15] (Fig. 5). The recirculation of the nutrient solution and the absence of substrate represent one of the main advantages of the NFT system. As an additional advantage this system has a great automation potential needed to save on labor costs (planting & harvesting) and to manage optimal plant density during crop cycle. On the other hand, the lack of substrate and low water levels makes the NFT vulnerable to pump failure due to e.g., clogging or lack of power supply. Temperature fluctuations in the nutrient solution can cause plant stress followed by diseases. NFT systems can use a Venturi device that supplies oxygen to the system by entraining ambient air bubbles into the water. The system's potential limitations are; potential pump failures (which quickly endanger the plants because of loss of water to the roots), lack of sufficient dissolve oxygen due to continuous recirculation of nutrient solution, unequal distributions of temperature, oxygen, and nutrients in the water caused by sloped planes, and tube clogging due to algal growth.

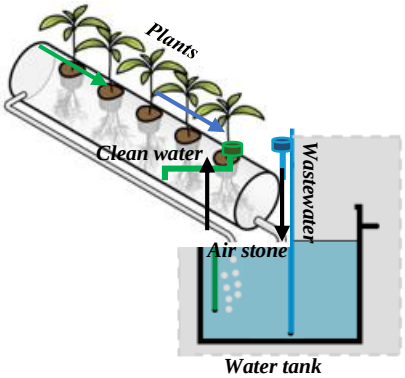

Figure 5. Illustration of NFT system

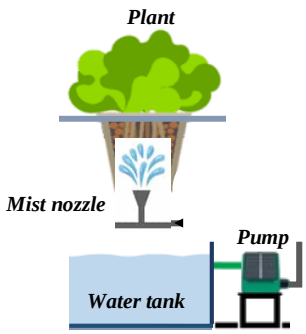

Figure 6. Illustration of the aeroponics technique

Aeroponic Systems

The aeroponic technique is specifically aimed at smaller horticultural species and has not yet been widely used due to the high investment and management costs. Plants are mainly supported by panels arranged horizontally or on inclined tops of growing boxes. These panels are supported by a structure made with inert materials (plastic, steel coated with plastic film, polystyrene boards), used to form closed boxes for the development of the suspended root system (Fig. 6). The plant's roots are suspended in air and sprayed directly by the nutritional solution with static sprinklers (nozzle).

Vertical wall systems

Vertical wall systems can be efficient in using growing space and can create an aesthetically pleasing living wall. This system is ideal for growing strawberries because of their shallow root systems [16]. The vertical walls maximize growing space per floor footprint, like it is shown in Fig. 7, allowing it to be useful in small unproductive areas.

Dutch bucket systems

The Dutch bucket system is a low-footprint type of drip system giving the grower the opportunity to arrange the system's layout according to the building's spacing and type of crop. Displayed in Fig. 8, the buckets are connected through an irrigation line that pumps water and nutrient solution from the system's reservoir. The system can be set to water the plants at certain times and durations. This system is ideal for crops like tomatoes, which grow best using cycled watering times rather than continuous water flows [17].

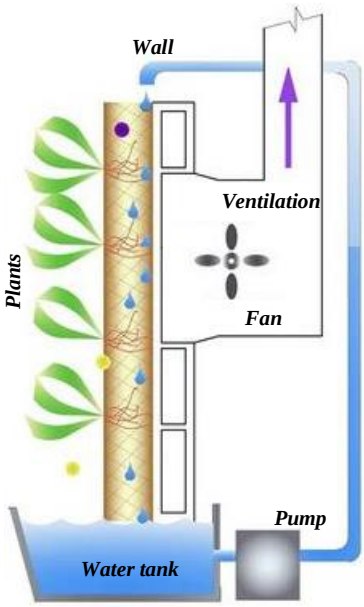

Figure 7. Vertical wall system diagram

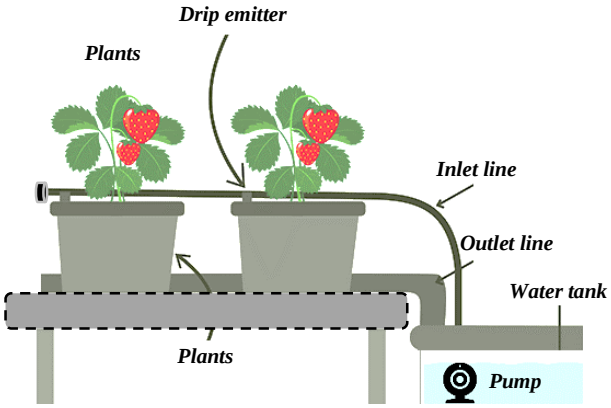

Figure 8. Dutch bucket system diagram

Nutrient Management

Essential Nutrients

In hydroponics, plants are grown outside the soil so required nutrients must be delivered directly through the watering solution to enhance the growth of the plants.

Nitrogen (N)

Nitrogen is primordial for plants because it allows the production of amino acids consequently proteins, enzymes and chlorophyll. Nitrate and ammonium are the main nitrogen forms used in fertilization. Nitrate is quickly absorbed by the roots; and can be accumulated inside the plant without toxic effects. However, ammonium can be absorbed only in low quantities and at high quantities can cause toxicity [18].

Phosphorus (P)

Phosphorus stimulates roots growth, the rapid development of buds and quantity of flower. Absorption of P is very easy and its accumulation present no damage to the plant. Phosphorus's main role is to help the formation of high-energy compounds necessary for plant metabolism [19].

Potassium (K)

Potassium is fundamental component for cell division and extension, protein synthesis, enzyme activation and photosynthesis. It actually transports other elements and carbohydrates between intra and

extra cellular environment, playing a major role in keeping an equilibrate osmotic potential of the cell and a regulated stomatal opening [20].

Calcium (Ca)

Calcium is needed for cell wall formation, cell division, cell extension and membrane permeability.ca helps raise the plant's resistance barrier against fungal and bacterial infections [21]. The absorption is very closely controlled by the water flow between roots and aerial parts.

Magnesium (Mg)

Magnesium is involved in the constitution of chlorophyll molecules. Its immobilization occurs at pH below 5.5 and it is always in competition with K and Ca. The observed yellow color between leaf veins and internal chlorosis of the basal leaves it may indicate Mg deficiency [22].

Sulphur (S)

Sulphur is required by the plant in quantities comparable to those of phosphorus, and for better absorption, its ratio with nitrogen must be 1:10 [23].

Iron (Fe)

Iron is very important micro-nutrients for the plant because it has a key role in some major biological processes like photosynthesis [24]. The optimal ratio of Fe–Mn is generally around 2:1 [25].

Chlorine (Cl)

Chlorine has been recently considered a micro-nutrient, even if its content in plants (0.2–2.0% dw) is quite high. It is easily absorbed and very mobile within the plants. It is involved in the photosynthetic process and the regulation of the stomata opening.

Sodium (Na)

Sodium, it can be toxic if absorbed in big quantity it can enter in antagonist activity and minimize the absorption of other ions. Similar to Cl, it is very important to monitor the concentration of Na in the nutrient solution [26].

Manganese (Mn)

Manganese get involved in the formation of many coenzymes, the extension of root cells and their resistance to pathogens. Its availability is controlled by the pH of the nutrient solution and by competition with other nutrients [27].

Boron (B)

Boron is essential for fruit setting and seed development. Its absorption methods are similar to Ca that's why they are always in competition. The optimal pH of the nutrient solution should be between 4.5 and 5.5 [28].

Zinc (Zn)

Zinc take an important role in some enzymatic reactions. PH and P content in the nutrient solution can strongly affect Its absorption [29].

Copper (Cu)

Copper is mainly implicated in respiratory and photosynthetic processes. pH values above 6.5 can affect negatively its absorption, whilst pH values lower than 5.5 may result in toxic effects [29].

Molybdenum (Mo)

Molybdenum is primordial in protein synthesis and in nitrogen metabolism. Contrary to other micro-nutrients, its availability is optimal at neutral pH values. Symptoms of deficiency shows as chlorosis and necrosis along the main rib of old leaves, whilst the young leaves appear deformed [29].

Water Quality and Nutrients

Supplied water's quality is enormously important in hydroponic and AP systems. For long-term recirculation, the chemical composition of nutrient solution can deteriorate that's why it should be frequently monitored and analyzed not only to avoid a deficiency in nutrient supply but also to avoid the accumulation of some toxic elements. De Kreij et al. [30] made an overview about the chemical needs for water quality in hydroponic systems. For example, if rainwater is used as watering solution, major attention has to be made for the amount of Zn especially when water collected from untreated gutters. For the case of tap water, Na, Ca, Mg, SO4 and HCO3 amounts may appear to be problematic. Furthermore, some water sources such as surface and bore hole water can be used and that can cause some issues because it may contain amounts of Na, Cl, K, Ca, Mg, SO4 and Fe and also microelements such as Mn, Zn, B and Cu. It should be taken into consideration too that all valves and pipes should be preferably made of synthetic materials such as PVC and PE, and are free from Ni or Cu parts.

Disinfection of Nutrient Solution

To minimize the risk of spreading soil-borne pathogens, disinfection of the circulating nutrient solution is required [34]. Heat treatment [35] was the first method used. Van Os [36] made an overview for the most important methods. Recirculating the nutrient solution opens possibilities to save on water and fertilizers [37]. But offer also some disadvantage such as an increased risk of root-borne pathogens propagation through all the system. To reduce this kind of risks, the nutrient solution must be controlled and treated before reuse.

Crops

A variety of crops can be planted on commercial level in hydroponic, principally fruits and vegetables.

Tomato crop

Always a favorite of gardeners, tomatoes are a popular hydroponic crop. But for its culture proper support is critical, because the plants will get heavy as fruit begins to develop. Tomatoes require heat and high light levels to grow vigorously and produce fruit [39].

Lettuce

Lettuce is a popular crop which can grow perfectly well in almost any gardening system, whether hydroponic, aquaponic, or traditional soil gardens. It takes up relatively little space, has a short (5-6 weeks from transplant or 9-11 weeks from seed) growing cycle, and has always high market demand [38].

Strawberries

Strawberries are one of the most popular grown crops, it is best if it is planted as rootstock rather than seed. Vegetative growth (runners) tends to be much faster than sexual reproduction (seeds), so you can cut the time from planting to production by months or years by using rootstock. Strawberries are vulnerable to pest and diseases that's why soilless culture is a great alternative.

Radishes

Radishes are one of the easiest vegetables to grow either in soil or hydroponics. It's better grown from seeds, and it will show seedlings within 3 – 7 days. Cool temperatures and minimum light will stimulate radishes' growth which as vegetable will make a good flavoring mix with other vegetables.

Cucumbers

Cucumbers are a common grown vegetable planted at home or in commercial greenhouses. If given sufficient needed conditions its characterized by rapid growth hence high yields. There are several types and sizes of cucumbers, including the thick-skinned American slicers, long thin-skinned seedless European, and the smooth-skinned Lebanese cucumbers. All can grow well in Hydroponics.

Peppers

Peppers are similar to tomatoes concerning hydroponic growing conditions; it both needs warm temperature and great amounts of lights. Recommended varieties for hydroponically growing are Jalapeno, Habanero for hot peppers; Mazurka, Cubico, Nairobi, Fellini for sweet peppers.

Costs and Benefits of Hydroponics

Unlike conventional farming, hydroponic system offers quiet important benefits. As well as the societal benefits of 'greening' urban areas and improve public spaces, hydroponic farming presents also the ability to move farming closer to population and to improve resource usage and growth efficiency [31]. A study about the yield and resource usage of lettuce farmers in Arizona showed that hydroponic farming system can decrease water usage by 13 ± 2.7 times and increase yield production by 11 ± 1.7 times compared to conventional agricultural systems [32]. Over an equal area, the water consumption for both methods was roughly comparable, but using hydroponic farming, characterized by vertical growing beds and fewer harvest cycles, resulted in raising yield and more efficiency. Being closer to urban population had reduced transport and CO2 emission but this savings are difficult to calculate precisely as it varies greatly from city to city depending on transport links, transport type, amount of imported food, and food consumption culture. Several estimations have been made, however. A study in Seoul, South Korea, for example, mentioned that if urban farming was set up in a 51.15 km2 area around Seoul, it can decrease CO2 emissions by 11.67 million kg annually, which is the equivalent CO2 emissions of 1155 people each year [33]. The major costs of installing and operating a small indoor hydroponic farm can be limited to water consumables (nutrients and grow plugs) and electricity costs (water pump, cooling, air flow and lighting).

Conclusion

Soilless agriculture is potentially one of the alternatives that can completely change the landscape of food sector, making a significant difference for the world. One of the most important benefit hydroponic system can provide is efficient water use to grow the same product compared to traditional agriculture. The water in a hydroponic system is re-circulated and has minimal losses, whereas water in typical farming practices suffers from evaporation and leakage into the soil. Since agricultural water consumption is a major contributor to the draining of world's freshwater sources, hydroponics provides a way to grow food and minimize water usage. Another noteworthy benefit of hydroponics is nutrient efficiency. Nutrients when operated in closed system, are protected from losses caused by leakage into the ground or runoff water as with field systems. This closed system aims to decrease the pollution of lakes and rivers, to enhance better water quality compared to land used for agriculture. Lastly, hydroponic systems can also be much more space efficient than typical farming methods and help grow plants in large cities lacking outside agricultural fields. As the global population continues to increase, there is more pressure on agricultural production methods to increase food production. Since there is often limited space available and open land farming methods can endanger surrounding water systems, hydroponics is a potential solution to food insecurity as well as water scarcity.

References

[1] United Nations. World urbanization prospects: the 2014 revision, highlights. Department of Economic and Social Affairs; 2014. https://doi.org/10.4054/DemRes.2005.12.9.

[2] Olympios, C.M., 1999. Overview of soilless culture: advantages, constraints and perspectives for its use in Mediterranean countries. Cah. Options Méditerranéennes 31, 307–324.

[3] Hussain, A., Iqbal, K., Aziem, S., Mahato, P., Negi, A.K., 2014. A review on the science of growing crops without soil (soilless culture) – a novel alternative for growing crops. Int. J. Agric. Crop Sci. 2227

[4] Sheikh, B.A., 2006. Hydroponics: key to sustain agriculture in water stressed and urban environment. Pakistan J. Agric. Agric. Eng. Vet. Sci. 22, 53–57.

[5] Hussain, A., Iqbal, K., Aziem, S., Mahato, P., Negi, A.K., 2014. A review on the science of growing crops without soil (soilless culture) – a novel alternative for growing crops. Int. J. Agric. Crop Sci. 2227.

[6] FAO, 2003. In: FAO Agricu (Ed.), Handling and Preservation of Fruits and Vegetables by Combined Methods for Rural Areas FAO Agricultural Services Bulletin 149. The Food and Agriculture Organization of the United Nations, Rome.
[7] WHO, FAO, 2003. Diet, Nutrition and the Prevention of Chronic Diseases Report of a Joint WHO/FAO Expert Consultation. Geneva.
[8] Orsini, F., Kahane, R., Nono-Womdim, R., Giaquinto, G., 2013. Urban agriculture in the developing world: a review. Agron. Sustain. Dev. 33, 695–720.
[9] Raviv, M., Lieth, J.H., 2008. Soilless Culture: Theory and Practice. Elsevier.
[10] Pardossi, A., Tognoni, F., Incrocci, L., 2004. Mediterranean greenhouse technology. Chron. Hortic. 44, 28–34.
[11] Baes, C.F., Sharp, R.D., 1983. A proposal for estimation of soil leaching and leaching constants for use in assessment models. J. Environ. Qual. 12, 17–28.
[12] Van Os EA, Gieling TH, Lieth JH (2008) Technical equipment in soilless production systems. In: Raviv, Lieth (eds) Soilless culture, theory and practice. Elsevier, Amsterdam, 57–207
[13] C. Maucieri, C. Nicoletto, E. van Os, D. Anseeuw, R. Van Havermaet, and R. Junge. Chapter 4: Hydroponic Technologies. Aquaponics Food Production Systems Combined Aquaculture and Hydroponic Production Technologies for the Future. Springer Open. ISBN 978-3-030-15943-6 (eBook). https://doi.org/10.1007/978-3-030-15943-6
[14] Cooper A (1979) The ABC of NFT. Grower Books, London.
[15] Van Os EA (2017) Recent advances in soilless culture in Europe. Acta Hortic 1176:1–8
[16] Halveland, J. (2020). Design of shallow-aero ebb and flow hydroponics and educational outreach for Tri Cycle Farms. Undergraduate thesis. University of Arkansas.
[17] Keane, R. (2019). Applying Ecosystem and Landscape Models in Natural Resource Management. CRC Press.
[18] Sonneveld C, Voogt W (2009) Plant nutrition of greenhouse crops. Springer, Dordrecht, p 403
[19] Le Bot J, Adamowicz S, Robin P (1998) Modelling plant nutrition of horticultural crops: a review. Sci Hortic 74:47–82
[20] Wang M, Zheng Q, Shen Q, Guo S (2013) The critical role of potassium in plant stress response. Int J Mol Sci 14:7370–7390
[21] Liu S, Hou Y, Chen X, Gao Y, Li H, Sun S (2014) Combination of fluconazole with non-antifungal agents: a promising approach to cope with resistant Candida albicans infections and insight into new antifungal agent discovery. Int J Antimicrob Agents 43:395–402
[22] Sonneveld C, Voogt W (2009) Plant nutrition of greenhouse crops. Springer, Dordrecht, p 403
[23] Muneer S, Lee BR, Kim KY, Park SH, Zhang Q, Kim TH (2014) Involvement of Sulphur nutrition in modulating iron deficiency responses in photosynthetic organelles of oilseed rape (Brassica napus L.). Photosynth Res 119:319–329
[24] Briat JF, Dubos C, Gaymard F (2015) Iron nutrition, biomass production, and plant product quality. Trends Plant Sci 20:33–40
[25] Heuvelink E, Kierkels T (2016) Iron is essential for photosynthesis and respiration: iron deficiency. In Greenhouses: the international magazine for greenhouse growers 5, 48–49
[26] Sonneveld C, Voogt W (2009) Plant nutrition of greenhouse crops. Springer, Dordrecht, p 403
[27] Uchida R (2000) Essential nutrients for plant growth: nutrient functions and deficiency symptoms. In: Silva JA, Uchida R (eds) Plant nutrient management in Hawaii's soils, approaches for tropical and subtropical agriculture. College of Tropical Agriculture and Human Resources, University of Hawaii at Manoa, Honolulu, 31–55
[28] Rooney CP, Zhao FJ, McGrath SP (2006) Soil factors controlling the expression of copper toxicity to plants in a wide range of European soils. Environ Toxicol Chem 25:726–732
[29] Gibson JL (2007) Nutrient deficiencies in bedding plants. Ball Publishing, Batavia
[30] De Kreij C, Voogt W, Baas R (1999) Nutrient solutions and water quality for soilless cultures, report 196. Research station for Floriculture and Glasshouse Vegetables, Naaldwijk, p 36
[31] Westphal. Urban greening and social benefits: a study of empowerment outcomes. J Arboric 2003;29(3).

[32] Barbosa, et al. Comparison of land, water, and energy requirements of lettuce grown using hydroponic vs. Conventional agricultural methods. Int J Environ Res Public Health 2015. https://doi.org/10.3390/ijerph120606879
[33] Lee, Lee, Lee. Landscape and Urban Planning Greenhouse gas emission reduction effect in the transportation sector by urban agriculture in Seoul, Korea. Landsc Urban Plann 2015
[34] Postma J, van Os EA, Bonants PJM (2008) Pathogen detection and management strategies in soilless plant growing systems. In: Raviv, Lieth (eds) Soilless culture, theory and practice. Elsevier, Amsterdam,425–458
[35] Runia WT, van Os EA, Bollen GJ (1988) Disinfection of drain water from soilless cultures by heat treatment. Neth J Agric Sci 36:231–238
[36] Van Os EA (2009) Comparison of some chemical and non-chemical treatments to disinfect a recirculating nutrient solution. Acta Hortic 843:229–234
[37] Van Os EA (1999) Closed soilless growing systems: a sustainable solution for Dutch greenhouse horticulture. Water Sci Technol 39:105–112
[38] Atzori, G., Guidi Nissim, W., Caparrotta, S., Masi, E., Azzarello, E., Pandolfi, C., Vignolini, P., Gonnelli, C., Mancuso, S., 2016. Potential and constraints of different seawater and freshwater blends as growing media for three vegetable crops. Agric. Water Manage. 176, 255–262. https://doi.org/10.1016/j.agwat.2016.06.016.
[39] Sgherri, C., Navari-Izzo, F., Pardossi, A., Soressi, G.P., Izzo, R., 2007. The influence of diluted seawater and ripening stage on the content of antioxidants in fruits of different tomato genotypes. J. Agric. Food Chem. 55, 2452–2458.

Marketing Channels of Mango Farmers in Mali

*Mohamed El Bechir Koita**, *Hakan Adanacıoğlu*
Ege University, Department of Agricultural Economics, Izmir, Turkey
**Corresponding author: koitamohamed66@gmail.com*

Abstract

Mango (Mangifera indica Linn) plays a central role as fruit crop among the horticultural fruits in Mali. Mali is among the largest mango producers in West Africa and among the fastest growing mango exporters in the world. The volume of mangoes produced is estimated at 575000 tons per year. Mango production is an important socio-economic activity in Mali, providing employment in rural areas and income through exportation. The study focused on marketing channels of mango famers in Mali. The secondary data were used to investigate marketing channels of mango in Mali. This paper consists of three parts. In the first part, the socio-economic characteristics of mango farmers in Mali were explained. In the second part, information about the development of Mango production and trade in Mali was given. In the third part, marketing channels of Mango farmers were examined. In general, it is difficult to say that Mango marketing channels operate effectively in Mali. The ineffectiveness of marketing channels occurs mostly at the local market level. It is important to strengthen the marketing infrastructure for Mango's marketing channels in Mali to be more effective. The government of Mali needs to implement a special incentive program, especially for wholesalers, who play an important role in increasing post-harvest losses. There is a need for financial support and training of wholesalers during the transportation, storage and processing of fresh mango. It is also important to extend these supports for mango producers.

Keywords: mango, farmers, marketing channels, Mali

Introduction

In Mali, where 80 percent of the population depends on agriculture as the primary source of income, more than 75 percent of Mali's inhabitants live in rural areas. Mali's agriculture is strongly dependent on a few major crops (such as cereals, rice, cotton), and livestock. The economy relies on two main export commodities, cotton and gold, representing 85 percent of the exports. Most small holders cotton growers have been striving to diversify their production to other crops, such as horticultural products, as complementary cash commodities in the dry season, given the excellent quality of the fruit and vegetables. As part of these practices of diversification to horticultural production by the smallholders, mangoes have been particularly favored in orchard development for the past thirty years in the South of the country, because of excellent agro-climatic conditions [1].

According to the Wikipedia data, in 2019, global production of mangoes was 56 million tons, led by India with 46% (26 million tons) of the world total. Almost half of the world's mangoes are cultivated in India alone, with the second-largest source being China. Other major mango-producing countries in total tonnage produced in 2020 are Thailand, Indonesia, Pakistan, Mexico, Brazil, Bangladesh, Nigeria, and the Philippines. The mango tree (Mangifera indica) so common in West Africa today is, in particularly in Mali, a recent introduction to and development in the area. Although the mango is, along with citruses, one of the most widespread fruits in French-speaking Africa, the mango tree is also a highly prized shade tree, employed either to line city streets, or in isolation or groves in yards, gardens and public places [2].It can be considered a fruit tree providing shade or as an ornamental tree providing fruits In Mali the agroecology and the relatively low cost of labor required by mango enterprises provide the country a comparative advantage in mango production. This advantage is not effectively used by different actors in the mango value chain. This is due to lack of appropriate infrastructure and competencies to overcome the technical, commercial, financial, and legal challenges that should be overcome in order to develop a viable activity. The mango is considered to be a high-contribution product for the Malian economy with a contribution of more than 21 billion CFA francs.

The mango from Mali is marketed mainly in the interior of the country, in Africa and in Europe, of which about a hundred varieties are available. However, only six of them (Kent, Keitt, Amélie, Tommy Atkins, Palmer and Valencia) are prized and exported in large quantities outside Mali through a form of contractualization and requirements in terms of quality, quantity and time[3] The mango intended for local consumption is sold on the local market without any processing.

The study focused on marketing channels of mango famers in Mali. The secondary data were used to investigate marketing channels of mango in Mali. This paper consists of three parts. In the first part, the socio-economic characteristics of mango farmers in Mali were explained. In the second part, information about the development of Mango production and trade in Mali was given. In the third part, marketing channels of Mango farmers were examined.

Methodology

This study has been prepared based on secondary data. There is no official database on both Mango and other agricultural products in Mali. For this reason, previous studies were used to obtain the data of this study. Previous studies include academic studies on mango as well as reports published by non-governmental organizations.

Socio-Economic Characteristics of Mango Farmers in Mali

In Mali, the age of mango producers is between 35 and 50 years at most. Hence, most mango production in Mali is partly handled by older producers. Also, among the actors involved in mango production in Mali, 90.6% are men. This means that this activity is largely carried out by men given the social status of women who cannot own a farm. The overall educational level of mango growers is quite low with some growers who have never been to school, and others have dropped out of school, and those who have received national language education. In addition, these producers have an average experience of 25 years in the mango production activity and have an average of 5 hectares of mango orchard [4].

Mango Production and Trade in Mali

In Mali, mango production is concentrated in three production basins namely the Sikasso basin with 70% of national production followed by the Koulikoro and Bamako basins which represent respectively 11 and 19% of national production. Production is generally ensured by small owners of small orchards, between 2 ha and 3 ha for the most part traditional, however, for less than 15 years, there have been large orchards in the Sikasso region ranging in size from 50 to 100 ha. [5]The dominant variety is Kent, followed by Keitte and Amelie.

Mango production area and production amount in Mali are shown in Table 1. Mango production area increased from 16713 hectares in 2015 to 44728 hectares in 2019. The amount of mango production increased from 517 592 tons in 2015 to 814920 hectares in 2019. In general, it is seen that Mango production in Mali has increased over the years[3].

Table 1. Mango production area and production amount by years in Mali

Years	Area harvested (ha)	Production (tons)
2015	16713	517592
2016	44619	808040
2017	44255	754892
2018	44728	813490
2019	44728	814920

Source: FAOSTAT database

Mali has tripled its mango exports in the last decade. Mali exported 7,200 tons of mango to Europe in 2018. Most of the exports to Europe were made to France and the Netherlands. However, Mali's largest export markets are Burkina Faso, Gabon, Ghana, Mauritania, Morocco, Niger and Senegal. Total mango export was 22,214 tons in 2018. Total mango exports are CFA 8.9 billion (€13.65 million) in value [6].

Marketing channels of Mango in Mali

In Mali, there are two marketing circuits for fresh mango, a circuit I which is the short circuit which mainly concerns the zones of production towards exports (Figure 1). These markets are located either at the village level or at the city level.

In addition to circuit, circuit II or long circuit which represents the export and marketing of fresh mango in Mali. This activity is partly carried out by collectors. These collectors are responsible for the purchase (collection) and packaging of mangoes for export. In this case, exporters maintain direct (producer-exporter) or indirect (producer-collector-exporter) relations with mango producers. In view of this analysis, we pay particular attention to the export circuit also called the long fresh mango marketing circuit. Here, we look at the transactions between the players identified in this study in order to make the link between the different export players [7].

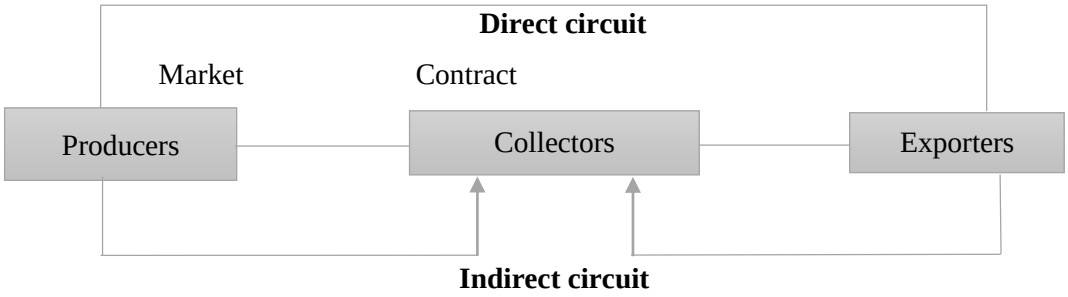

Figure 1. Fresh mango marketing channels in Mali

In local markets, mango trade is handled by retailers and wholesalers. In addition, there are many marketing channel members involved in Mango's trade. These include packaging service providers, exporters, transporters, wholesalers and customers. At the national level, it is stated that there are more than 20 mango exporters [6]

Activities for the processing of mango are generally carried out by agricultural processors and exporters. Intermediaries collect the mango from farms after harvest. The collected mangoes are then sold to exporters and agricultural processors. Mango is processed at a low rate. The processed products are turned into fruit juice, pureed or dried.[2]

Conclusion

In this study, marketing channels of mango producers in Mali were mainly examined. In general, it is difficult to say that Mango marketing channels operate effectively in Mali. The ineffectiveness of marketing channels occurs mostly at the local market level. It is seen that two main actors play a role in the marketing of Mango at the national local market level. These are retailers and wholesalers merchants. Wholesalers are the main source of supply for retailers. However, wholesalers do not have the necessary infrastructure to transport and store the fresh mango they purchase. This causes high post-harvest losses. It is claimed that almost half of the fresh mango disappears before reaching the final consumer due to post-harvest losses.

It is important to strengthen the marketing infrastructure for Mango's marketing channels in Mali to be more effective. The government of Mali needs to implement a special incentive program, especially for wholesalers, who play an important role in increasing post-harvest losses. There is a need for financial support and training of wholesalers during the transportation, storage and processing of fresh mango. It is also important to extend these supports for mango producers.

References

[1] Davies K, Menage N. Connecting farmers to markets, No. 60, 2009.
[2] Rey JY, Diallo TM, Vannière H, Didier C, Kéita S, Sangaré M. The mango in French-speaking West Africa, *Fruits*, 61(4): 281–289, 2006. doi: 10.1051/fruits:2006027.
[3] Diallo B, Coulibaly J, Diarisso T, Staatz J, Traore A, Teme B. Développement de la filière mangue au Mali: analyse des modèles de coordination et de partenariat entre les différents acteurs, 2019: 1-14.
[4] Ag I, Ag A, Ahmad S. Analyse des modes de coordination verticale dans la filière d'exportation de la mangue fraîche au Mali, 2020.
[5] Kergna AO, Dembélé D, Oluwole FA, *Innovation Opportunities in Mango production in Mali*, no. January. 2018.

[6] Danielou M. Mali: exporting mangoes to Europe., 2003 October, No:231.
[7] Haidara M. Etude nationale mangue. PACCIA II. Centre du Commerce International, 22, 2012.

Somali'de Yoksulluğun Azaltmasında Kadınların Tarımsal Faaliyetlerine Katılım Durumu : Hirshabelle Eyaleti Örneği

*Abdishakur İbrahim Abdi**, *Sevtap Gümüş*
Ege University, Ziraat Fakültesi, Tarım Ekonomisi Bölümü, İzmir, Türkiye
**İletişimden sorumlu yazar: abdishakur077@gmail.com*

Özet

Tarım, Somali'nin GSYİH'sinin % 65'sini, istihdamının % 45.8'sini ve ihracatının % 93'ünü sağlamaktadır. Kadın işgücünün en yoğun olduğu faaliyet alanlarının başında ise tarım sektörü gelmektedir. Ancak, kadınların tarımsal üretim faaliyetleri ve gıda güvenliğine önemli katkı sağlamalarına rağmen, birçok ülkede olduğu gibi, Somali'de de görünmez konumdadırlar. İşte bu çalışmada, Somali'de yoksulluğun önlenmesinde kadınların sosyo-ekonomik durumları ile tarımsal faaliyetlere katılım durumlarının incelenmesi amaçlanmıştır. Araştırmanın ana materyalini oransal örnek hacmi formülü kullanılarak yapılan hesaplama sonucunda 96 kadın ile yüzüyüze anketlerden elde edilen veriler oluşturmaktadır. Bu kapsamda, elde edilen veriler basit istatistiki yöntemler ile analiz edilmiştir. Çalışmada, farklı nitelikte çok sayıda bulgu elde edilmiş olup, görüşülen kadınların %22.8'sinin 31-40 yaş aralığında olması, %43.5'sinin okur-yazar olmaması, %77.2'sinin evli olması, %72.8'sinin tarımsal faaliyetlerin her aşamasına katılması ve farklı nitelikte sorunlarının olması, %27.2' sinin 10 yıldan daha az tarımla uğraşması, %38.0' inin kendi arazisinde ve %29.3' ünün 1 hektar ve daha az araziye sahip olması, %93.5'sinin ise herhangi bir tarımsal kooperatife üye olmaması elde elde edilen bulgulardan bazılarıdır.

Anahtar Kelimeler: Somali, yoksulluk, tarım, kadın, tarımsal faaliyetlere katılım

Giriş

Afrika'nın en doğu ucunda yer alan, Afrika boynuzu diye bilinen bölgede bulunan Somali'nin kuzey batısında Cibuti, güney batısında Kenya, Kuzeyinde Aden Körfezi ve Yemen doğusunda Hint Okyanusu, Batısında ise Etiyopya bulunmaktadır. Tarım, birçok Afrika ekonomisinin temel gıda ve geçim kaynağıdır ve özellikle sahra altı Afrika'da Gayri Safi Yurtiçi Hasılanın (GSYİH) büyük bir kısmını oluşturmaktadır (AGRA, 2013). Kırsal kesimde yaşayan kadınlar, özellikle tarımsal faaliyetlerde önemli bir rol oynamaktadır (FAO, 2011; Goebel, 2005; Singh and Vinay, 2013). Bu itibarla, Afrika ülkelerinin gıda talebi ihtiyacının karşılanması ve kapasitelerinin arttırılmasında, kadınların rollerinin tanınması ve toprak mülkiyet hakkına, kredi olanaklarına, yayım hizmetlerine ve kooperatiflere üyelik haklarının verilmesi gerekmektedir (Winrock, 2001). Bu yönüyle Somali' nin zengin doğal kaynaklara sahip olmasına rağmen, diğer nedenlerin yanısıra kaynaklarının tam ve etkin kullanılamaması nedeniyle yoksulluk ve yoksunluk yaygın olarak hüküm sürmektedir (Unicef, 2017). 2018 yılı verileri itibariyle; ülke toplam nüfusunun yarısından fazlasını kadınlar oluşturmaktadır. Birçok gelişmekte olan ülkede olduğu gibi ailelerde gelir genellikle erkeklerin sorumluluğunda, genellikle kadın ve çocuklar ekonomik olarak erkeklere bağımlı bulunmaktadır. Bir üretim faktörü olarak kadınların sosyal, kültürel ve ekonomik hayatın içinde olması, toplumların gelişmesinde önemli faktörlerden biri olarak kabul edilmektedir. Kadın işgücünün en yoğun olduğu faaliyet alanlarının başında ise tarım sektörü gelmektedir. Ancak, kadının işgücüne katılım oranını etkileyen ekonomik, sosyal, kültürel, toplumsal birçok faktör bulunmakta, bu faktörler kadınların yoksulluğu ve yoksunluğu üzerinde önemli rol oynamaktadır. Bilindiği üzere, kırsalda yaşayan kadınların tarımsal üretime katılma biçimleri toplumun kültürel yapısı ve ekonomik ve sosyal gelişme düzeyi ile yakından ilişkilidir. Bu kapsamda, toplumsal cinsiyet eşitsizliğinin görüldüğü ve kadınların istihdama katılımının çok sınırlı olduğu Somali gibi ülkelerde refah seviyesinin yükseltilmesi ve kalkınmanın sürdürülebilirliğinin sağlanabilmesi bakımından; kadınların tarım gibi temel geçim alanları içerisinde istihdam edilmesi büyük önem arz etmektedir. Bu doğrultuda, özellikle gelişmemiş ve gelişmekte olan ülke ekonomileri açısından kadınların işgücünde yer alması ve işgücünde yer almasını engelleyen faktörlerin önceden doğru bir şekilde belirlenip, bunlara yönelik tedbirler alınması ekonomik ve kültürel sosyal kalkınmanın sağlanması açısında oldukça önemlidir. Yapılan bazı araştırmalar, kadınların özellikle kırsal alanlarda tarımsal faaliyet ve gıda güvenliğinin sağlanmasında önemli bir rol oynadığını göstermektedir (Ahmed

et al., 2012; Bhat et al., 2012; FAO, 2011). Ancak, kadınların tarımsal üretim faaliyetleri ve gıda güvenliğine önemli katkı sağlamalarına rağmen, Somali'de de olduğu gibi görünmez konumdadırlar (Bhat et al., 2012; Farid et al., 2009; Singh and Vinay, 2013, Rahman, 2008). İşte bu çalışmada, Somali'de yoksulluğun önlenmesinde kadınların sosyo-ekonomik durumları ile tarımsal faaliyetlere katılım durumlarının incelenmesi amaçlanmıştır.

Materyal ve Yöntem

Bu araştırmanın ana materyalini, Somali Hirshabelle eyaletinde bulunan Jowhar ilçesinde tarımsal faaliyet yürüten kadınlar ile yapılan anketlerden elde edilen veriler oluşturmaktadır. Anket yoluyla toplanan orijinal verilerin yanında, bölgede bulunan konuyla ilişkili çeşitli kurum kuruluşlardan sağlanacak verilerile önceden yayınlanmış tezler, araştırmalar, makaleler, bildiriler, projeler vb. çalışmanın ikincil veri kaynaklarını oluşturmaktadır. Bu çalışmada Somali'de tarımsal üretimin yoğun olarak gerçekleştirildiği, oransal olarak yüksek bir paya sahip olan Hirshabelle eyeleti- Jowhar ilçesinde yürütülmüştür. Araştırmanın yürütüldüğü Hirshabelle eyaletinin Jowhar İlçesinin toplam nüfusu 47 000 kişi olup, toplam nüfusun 26 000 'i kadından oluşmaktadır. Araştırma kapsamında görüşülen kadın sayısı oransal örnek hacmi formülüyle hesaplanmıştır (Newbold, 1995).

$$n = \frac{N_P(1-p)}{(N-1)_\sigma^2 Px^{+p}(1-p)} \quad (1)$$

n= örnek hacmi
N= Seçilen bölgedeki toplam kadın sayısı
p: Oran (en yüksek örnek hacmine ulaşmak için %50 alınmıştır)
σPx^2 = oranın varyansı

Araştırmada maksimum örnek hacmine ulaşılmak istenmiştir. Bu amaçla p:0.50 ve (1-p):0.50 alınmıştır. Oransal örnek hacmi, %95 güven aralığı ve %10 hata payı kullanılarak belirlenmiştir. Oransal örnek hacmi formülü kullanılarak yapılan hesaplama sonucunda 96 anket yapılması uygun görülmüştür. Ancak koşullar nedeniyle 4 tane anket iptal edilmiştir.

Somali'ye Ait Bazı Sosyo-Ekonomik Göstergeler

Somali nüfusunun 1960 yılı sonrasında sürekli artığı gözlenmekte, 1960 yılında toplam nüfusu 2,755,972 kişi iken. 2019 yılında, ülke nüfusunun 15,442,905'e yükseldiği görülmektedir. 1960 yılında Kent nüfusu, toplam nüfusun %17'sini oluştururken kırsal nüfus, toplam nüfusun yaklaşık %83'sünü oluşturmaktadır. 2019 yılında ise kent nüfusu, toplam nüfusun yaklaşık %46'sını kırsal nüfus, toplam nüfusun %54'sünü oluşturmaktadır. Bu kapsamda, birçok ülkede olduğu gibi Somali'de de kırsal nüfus oranı zaman içerisinde azalma eğiliminde olup, ekonomisinin tarıma dayalı olması nedeniyle hala nüfusun büyük kısmı kırsal alanda yaşamaktadır (Tablo 1).

Tablo 1. Somali'de toplam nüfusun dağılımı (%)

Yıllar	Toplam nüfus sayısı	Kent nüfus sayısı	%	Kırsal nüfus sayısı	%
1960	2,755,972	477,114	17.31	2,278,858	82.7
1970	3,444,568	781,159	22.67	2,663,409	77.3
1980	6,281,134	1,681,020	26.8	4,600,114	73.2
1990	7,225,092	2,142,818	29.7	5,082,274	70.3
2000	8,872,254	2,949,758	33.2	5,922,496	66.8
2010	12,043,883	4,734,450	39.3	7,309,433	60.7
2019	15,442,905	7,034,861	45.6	8,408,044	54.4

Kaynak: World Bank, World Development indicators

2014-2019 yılları arasındaki nüfus artışı yüzdesi ve GSYİH artış hızı Tablo 2'de verilmiştir. Tabloda görüleceği üzere, Büyüme oranı %3.4 ile en yüksek 2015 yılında gerçekleşmiştir. Bunun nedeni ülke genelinde ki yağışların artmasıyla birlikte bitkisel üretimin ve meralardaki ot varlığının artmasıyla tarımsal üretimi olumlu yönde etkilemesidir. 2014-2019 yılları arasında ülkenin nüfus artışı ve GSYİH

artış hızı neredeyse aynı oranda arttığı görülmektedir. 2014-2019 yılları arasında ortalama nüfus artışı ve GSYİH artış hızı 2.7 oranı gerçekleştirmiştir.

Tablo 2. Yıllar itibariyle Somali'nin nüfus artışı hızı ve ekonomik büyümedeki gelişmeler (%)

Yıllar	Nüfus Artışı %	GSYİH Artış Hızı %
2014	2.7	2.3
2015	2.7	3.4
2016	2.8	2.9
2017	2.8	1.9
2018	2.8	2.8
2019	2.8	2.9

Kaynak: World Bank, World Development indicators

1980-2016 dönemi itibariyle Somali'nin Toplam GSYİH ve Kişi Başına Düşen GSYH ($) ise Tablo 3'te verilmiştir. Ülkelerin gelişmişlik düzeylerinin belirlenmesinde en önemli göstergelerden biri kişi başına düşen milli geliridir. Tablo' da görüldüğü üzere, 1980 yılında Somali'de kişi başına düşen yıllık gelir 96 dolar iken 2016 yılında bu sayının 513 dolara yükseldiği görülmektedir. Somali kişi başına düşen gayrisafi yurtiçi hasıla bakımından, Dünya Bankası verilerine göre, dünyanın en yoksul 5. ülkesi olarak ifade edilmektedir (World Bank,2016).

Tablo 3. Yıllar itibariyle Somali'nin toplam GSYİH ve kişi başına düşen GSYH ($)

Yıllar	GSYİH (Milyon $)	Kişi başına GSYİH ($)
1980	603	96.09
1985	876	131.8
1986	934	168.3
1987	1,023	147.1
1988	1,038	148.2
1989	1,092	153.1
2013	5,452	435
2014	6,528	505
2015	6,739	517
2016	6,887	513

Kaynak. World Bank, World Development indicators.
International Monetary Fund, Article IV Consultation and First Review under the Staff-Monitored Program-Press Release; Staff Report; and Statement by the Executive Director for Somalia, 2017.

Somali'nin kent ve kırsal alanlara yönelik okur-yazar olma durumu Tablo 4'te verilmiştir. Kırsal alanlarda kırsal nüfusun % 27'si okur-yazar iken, bu sayı kadınlar da % 23'e düşmektedir. Kentlerde bu oranlar sırasıyla % 64 e %58 dir. Somali'nin kırsal alan yetişkin okur-yazar oranı %27.5, kent yetişkin okur-yazar oranı %64.2, İDP kamplarında yaşayanların yetişkin okur yazarlığı %32.8 olurken göcebe olanların %12.1'dir. Somali de yetişkin okur-yazarlığının en düşük olduğu eyalet Hirshabelle'dir ve okur yazarlık oranının sadece % 20 olduğu görülmektedir (Tablo 4). Hirsebella eyaletinden sonra yetişkin okur-yazarlık oranları eyaletler itibariyle Güney Batı Eyaleti (% 26,4), Jubaland Eyaleti (% 29,3), Puntland Eyaleti (%42.9), Somaliland Eyaleti (%45.3) izlemekte ve yetişkin okur yazarlığının en yüksek olduğu Eyalet Galmuduğ olduğu görülmektedir.

Somali'de 2016 yılında altı yaş ve üstü nüfusun üçte birinden fazlası (yüzde 36,6) okula kayıtlı olduğu belirtilmiştir. Bu oran cinsiyete göre kadınların %35.0 iken erkekler ise %38.1'dir. Okulda kayıt olan öğrencilerin %34.2 kırsalda, %52.8 kentlerde, % 24.2 İDP kamplarda, %15.7 ise göcebe olduğu belirtmiştir (UNFP, 2016). Dünya Bankasının 2020 yılında yayınladığı rapor ile ülke genelinde okuma

yazma bilenlerin oranı %55 olduğu belirtilmiştir (Waheed, 2020). Afrikanin diğer ülkerde yetişkin okur yazar oranı, Kenya 2019 yılında %81.5, 2017 yılında Etopya %51.7, Uganda 2018 yılında %76.5, Güney Sudan ise 2018 yılı itibariyle %34.5'dir.

Tablo 4. Bölgelere göre okuryazar durumu

Okur yazar durumu	Kadın %	Erkek%	Toplam %
Kırsal okur-yazar durumu	23.8	31.3	27.5
Kentsel okur yazar durumu	58.1	70.5	64.2

Kaynak: Federal Government of Somalia Ministry of Education, Culture and Higher Education, 2017

Somali'de 1991 yılında başlayan iç savaş ülkedeki sağlık sisteminin yıkılmasına neden olmuştur. Somali'nin sağlık göstergeleri dünyanın en kötü ülkeleri arasında yer almaktadır. 2019 yılında 5 yaşın altındaki çocuklar için ölüm oranı 1000 doğumda tahmini 117'dir. Somali'de doğuşta beklenen yaşam süresi, 2010 yılında ortalama 54 iken 2018 yılında 57'ye yükselmiştir. Ülkede doğuşta beklenen yaşam süresi dünya ortalamasının çok altında kalmaktadır. Afrika Kalkınma Bankasının 2019 yılında yayınladığı raporda, Somali'ye komşu ülkelerin doğuşta beklenen yaşam süresine bakıldığında, Jibuti 63, Kenya 68, Etiyopya doğuşta beklenen yaşam süresi 66'dır. Yoksul ülkelerde insan ömrünün daha kısa olmasının nedeni, iç çatışma ve savaş gibi unsurlar dışında, önlenebilir hastalıklara karşı etkili bir tedavi sisteminin geliştirilememiş olması ve salgın hastalıkların yaygın oluşu, buna karşın sağlık kuruluşlarının yaygın olmaması gibi faktörler bulunmaktadır. Somali'de bebek ölüm oranı binde 79.7 iken Kenya'da 33.6, Benin'de 63.5, Mali'de 65.8, Sudan'da 43.7 Sierra leon'da 81.7, Rwanda'da ise 28.9 dr. Somali'de 2017 yılında 5 yaş altı ölüm oranı binde 127 olduğu Mali'de 106 olduğu, Nijerya'da 100 olduğu, Gana'da 49 olduğu Seirra Leone'da ise 111 olduğu belirlenmiştir (AfDB, 2019).

Somali-Hirshabelle Eyaleti Jowhar ilçesinde Kadınların Tarımsal Faaliyetlere Katılım Durumu

Görüşülen Kadınlara ilişkin Genel Bilgiler

Araştırmaya katılan kadınların yaş dağlımı incelediğinde; 8'sinin (%8.7) 20 yaş ve altında, 35'sinin (%38.0) 21-30 yaş aralığında, 21'sinin (%22.8) 31-40 yaş aralığında, 17'sinin (%18.5) 41-50 yaş aralığında, 11'sinin (%12.0) 51 ve üstü yaş aralığında olduğu görülmektedir (Tablo 5).

Tablo 5. Katılımcıların yaş grupları

Yaş Grubu	N	%
20 yaş ve alti	8	8.7
21-30	35	38
31-40	21	22.8
41-50	17	18.5
51 yaş ve üzeri	11	12
Toplam	92	100

Yapılan araştırmaya katılan kadınların eğitim durumları incelediğinde; 40'sinin (%43.5) okuryazar olmayan, 17'sinin (%18.5) okuryazar, 9'u (%9.8) ilkokul mezunu, 8'si (%8.7) ortaokul mezunu, 9'u (%9.8) lise mezunu, 9'u (%9.8) lisans öğrencisi olduğunu tespit edilmiştir. Bu oranlar, araştırmaya katılan kadınların büyük bir çoğunluğunun okuryazar olmadığını görülmektedir (Tablo 6).

Tablo 6. Katılımcıların eğitim grupları

Eğitim Durumu	N	%
Okur-yazar değil	40	43.5
Okur-yazar	17	18.5
İlkokul mezunu	9	9.8
Ortaokul mezunu	8	8.7
Lise mezunu	9	9.8
Lisans öğrencisi	9	9.8
Toplam	92	100

Yapılan araştırmada görüşülen kadınların medeni durumları incelediğinde; 16'si (%17.4) bekar, 5'I (%5.4) boşanmış veya dul, 71'i (%77.2) evlidir. Bu oranlar, yapılan araştırmaya katılan kadınların çoğu evli olduğunu göstermektedir (Tablo 7).

Tablo 7. Katılımcıların medeni durumu

Medeni durumu	n	%
Bekar	16	17.4
Evli	71	77.2
Eşinden boşanmış/dul	5	5.4
Toplam	92	100

Görüşülen Kadınların Tarımsal Faaliyetleri ve Çalışma Durumlarına İlişkin Genel Bilgiler

Yapılan araştırmaya katılan kadınların tarımda çalışma durumu incelediğinde; 67'sinin (%72.8) tarımda uğraştığı görülürken 25'sinin (%27.2) tarımda uğraşmadığı tespit edilmiştir. Tarımda uğraşmayan 25 kadının (%27.2) tarımsal arazisi olmadığı belirlenmiştir (tablo 8).

Tablo 8. Görüşülen kadınların tarımda çalışma durumu

Tarımda Çalışma Durumu	n	%
Çalışıyor	67	72.8
Çalışmıyor	25	27.2
Arazisi yok	25	27.2
Toplam	92	100

Görüşülen kadınların kaç yıldır tarımda uğraştıkları incelediğinde; 25'sinin (%27.2) 10 yıldır veya daha az tarımda uğraştığı, 22'sinin (%23.9) 11-20 yıl aralığında, 9'sunun (%9.8) 21-30 yıl aralığında, 7'sinin (%7.6) yıl aralığında, 4' ünün ise (%4.3) 41 yıl veya üstü tarımda uğraştıkları tespit edilmiştir (Tablo 9).

Tablo 9. Görüşülen kadınların tarımda çalışma süresi

Kadınların tarımda çalıştığı süre (yıl)	n	%
≤10	25	27.2
11-20	22	23.9
21-30	9	9.8
31-40	7	7.6
≥41	4	4.3
Toplam	67	72.8

Yapılan araştırmaya katılan kadınların sahip oldukları arazi büyüklüğü incelediğinde de, 27'sinin (29.3%) 1 hektar ve daha az araziye sahip olduğu, 19'sunun (20.7%) 2-4 hektara sahip olduğu, 1'sinin (1.1%) 5-7 hektara sahip olduğu, 2 sinin (2.2%) 8-10 hektara sahip olduğu, 1'inin ise, (1.1%) 11 hektar ve daha fazla araziye sahip olduğu saptanmıştır (Tablo 10).

Tablo 10. Katılımcıların arazi büyüklüğü

Arazi Büyüklüğü (hektar)	N	%
≤ 1	27	29.3
2-4	19	20.7
5-7	1	1.1
8-10	2	2.2
≥11	1	1.1
Toplam	50	50.4

Görüşülen kadınların tarımda günde kaç saat çalıştıkları incelediğinde; 10'unun (%10.9) 2 saat veya daha az çalıştığı, 21'sinin (%22.8) 3-4 saat, 24'ünün (%26.1) 5-6 saat çalıştığı, 12'sinin ise (%13.0) 7 saat veya üstünde çalıştığı görülmektedir. Yapılan araştırmaya katılan kadın tarımda haftada kaç gün çalıştıkları incelediğinde de; 10'unun (%10.9) 2-3, 24'ünün (%26.1) 4-5 gün, 33' ünün ise (%35.9) 6-7 gün çalıştığı görülmektedir (Tablo 11).

Tablo 11. Görüşülen kadınların tarımsal faaliyetlerde günlük ve haftalık çalışma süresi

Tarımsal Faaliyetlerde Günlük Çalışma Süresi	N	%
2 saatten daha az	10	10.9
3-4 saat arası	21	22.8
5-6 saat arası	24	26.1
7 saatten daha fazla	12	13
Tarımsal Faaliyetlerde Haftalık Çalışma Süresi		
1 gün	3	3.3
2-3 gün	7	7.6
4-5 gün	24	26.1
6-7 gün	33	35.9
Toplam	67	72.8

Yapılan araştırmaya katılan kadınların çalıştığı arazi incelediğinde; 26'sının (28.3) kendi mülk arazisinde, 9' unun (%9.8) ailesinin arazisinde, 6'sının (%6.5) kiraladığı arazide, 16'sinin (%17.4) başkasının arazisinde ücretli olarak çalıştığı, 1'inin de (%1.1) kendi arazisini kiralayıp aynı arazide başkasının tarım işçisi olarak çalıştığı, 9' unun (%9.8) hem kendi arazisi hem de başkasının tarım işçisi olarak çalıştığı görülmüştür (Tablo 12).

Tablo 12. Çalıştığı arazinin mülkiyet durumu

Çalıştığı Arazinin Mülkiyet Durumu	n	%
Kendi arazisinde çalışıyor	26	28.3
Ailesinin arazisinde çalışıyor	9	9.8
Kiraladığı arazide çalışıyor	6	6.5
Başkasının arazisinde ücretli olarak çalışıyor	16	17.4
Kendi arazisini kiralayıp, aynı arazide başkasının tarım işçisi olarak çalışıyor	1	1.1
Hem kendi arazisi hem de başkasının tarım işçisi olarak çalışıyor	9	9.8
Toplam	67	72.9

Tablo 13. Görüşülen kadınların tarım dışında çalışma durumu

Görüşülen Kadınların Tarım Dışında Çalışma Durumu	N	%
Çalışıyor	22	23.9
Çalışmıyor	45	48.9
Toplam	67	72.8
Görüşülen Kadınların Tarım Dışı Faaliyetleri	**N**	**%**
Esnaf	10	10.9
Temizlik işi	3	3.3
Öğretmen	1	1.1
Pazarcı	4	4.3
Restoran	2	2.2
Sağlık elemanı	1	1.1
Fotokopi işi	1	1.1
Toplam	22	23.9

Kadınların tarım dışında çalışma durumu incelediğinde; 22'sinin (%23.9) tarım dışında bir iş çalıştığı söylerken, 45'i (%48.9) tarım dışında herhangi bir işte çalışmadığı belirtmiştir. Görüşülen kadınların tarım dışında hangi işlerde çalıştıkları tablo' dan görülebilmektedir (Tablo 13).

Yapılan araştırmaya katılan kadınların çalıştığı tarımsal üretim alanları incelediğinde; 35'sinin (38.0) bitkisel üretimde, 4'ünün (%4.3) hayvansal üretimde, 28'sinin ise (%30.4) hem bitkisel hem de hayvansal üretiminde çalışmaktadır (Tablo 14).

Tablo 14. Görüşülen kadınların çalıştığı tarımsal faaliyet tipi

Tarımsal Faaliyet tipi	n	%
Bitkisel üretim	35	38
Hayvansal üretim	4	4.3
Bitkisel+Hayvansal	28	30.4
Toplam	67	72.8

Görüşülen kadınların bitkisel üretimde en fazla üretilen ürünleri incelediğinde; 9' unun (%9.8) mısır, 11'inin (%12.0) susam, 13'ünün (%14.1) sebze ve meyve, 3'ünün (%3.3) fasulye, 2'sinin (%2.2) yer fıstığı, 4'ünün (%4.3) prinç, 3'ünün (%3.3) tatlı patates, 4' ünün ise (%4.3) tüm ürünleri ürettiği tespit edilmiştir.

Tablo 15. Bitkisel üretimde en fazla üretilen ürünler

Bitkisel üretimde en fazla üretilen ürünler	n	%
Mısır	9	9.8
Susam	11	12
Karışık Meyve	13	14.1
Fasulye	3	3.3
Yer Fıstığı	2	2.2
Pirinç	4	4.3
Tatlı patates	3	3.3
Hepsi	4	4.3
Toplam	49	53.3

Yapılan araştırmaya katılan çifçilerin en fazla yaptığı tarımsal faaliyeti incelediğinde ise, toprak hazırlığı (%14.1), ekim veya dikim (%7.6) ve sulamanın (%3.3) sulamanın ilk sıralarda yer aldığı görülmektedir (Tablo 16).

Tablo 16. Bitkisel üretimde kadınların en fazla katıldığı tarımsal faaliyetler

Tarımsal Faaliyetler	n	%
Toprak hazırlığı	13	14.1
Ekim veya dikim	7	7.6
Sulama	3	3.3
Hasat	12	13
Ürün işleme	1	1.1
Ürün depolama	3	3.3
Taşıma	3	3.3
Pazarlama	2	2.2
Hepsi	23	25
Toplam	67	72.8

Araştırmaya katılan kadınların hayvan varlığı incelediğinde, küçükbaş hayvancılık ve kümes hayvancılığının yaygın olarak yapıldığı belirlenmiştir (Tablo 17).

Tablo 17. Görüşülen kadınların hayvan varlığı

Görüşülen Kadınların hayvan Varlığı	n	Minimum	Maximum	Ortalama
Deve	1	2	2	2
Kümes Hayvanı	7	9	42	24.14
Küçükbaş hayvan	16	11	24	18,24
Büyükbaş Hayvan	7	2	15	7.14

Yapılan araştırmaya katılan kadınların tarımda çalışma sistemi incelediğinde; ancak %3.3' ünün düzenli olarak çalıştığı, %23.9'unun iş bulduğu zaman çalıştığı tespit edilmiştir.

Çalışma yerlerine ulaşım durumunda ise, 21 kadın yürüyerek çalışma yerlerine ulaştığı söylerken 5 kadın ise traktörle çalışma yerlerine ulaştığı söylemiştir (Tablo 18).

Tablo 18. Kendi arazisi dışında çalışan tarım işçilerin çalışma durumu ve çalışma yerlerine ulaşım durumu

Kendi arazisi dışında çalışan tarım işçilerin çalışma durumu	N	%
Düzenli olarak çalışıyor	3	3.3
İş bulduğu zaman çalışıyor	23	25
Toplam	92	100
Çalışma yerlerine ulaşım durumu	N	%
Yürüyerek	21	22.8
Traktör	5	5.4
Toplam	26	28.3

Ücretli olarak tarımda çalışan kadınların ayda ortalama ne kadar gelir elde ettiği incelediğinde; 11 kadın 50 $ ve altında, 6 kadının 51-60 $ aralığında, 5 kadının 61-70 $ aralığında, 3 kadının 71 $ ve üzerinde gelir elde ettiği tespit edilmiştir (Tablo 19).

Tablo 19. Kendi arazisi dışında çalışan tarım işçilerin gelir düzeyi

Gelir ($/ay)	N	%
≤50	11	12
51-60	6	6.5
61-70	5	5.4
≥71	3	3.3
Toplam	25	27.2

Görüşülen kadınların herhangi bir kuruluş, dernek veya kooperatife üye olup olmadığı incelediğinde; 6'sının (%6.5) üye olduğu, 86'sının (%93.5) üye olmadığını söylemiştir. Yapılan araştırmada katılan kadınların hangi kooperatife üye oldukları incelediğinde; 1'sinin (%1.1) tarımsal kalkınma kooperatifne üye olduğu, 5'iının (%5.4) zararlardan korunma kooperatifine üye olduğu söylemiştir (Tablo 20).

Tablo 20. Görüşülen kadınların kooperatife üye olma durumu

Her hangi bir kuruluş, dernek veya kooperatife üyelik durumu	n	%
Evet	6	6.5
Hayır	86	93.5
Toplam	92	100
Evet ise		
Tarımsal kalkınma kooperatifi	1	1.1
Zararlardan korunma kooperatif	5	5.4
Toplam	6	6.5

Kadınların iş Yaşamı ve Tarımsal Faaliyetlere Katılımında Karşılaştıkları Sorunlar

Kadınların çalışma ve sosyal hayata katılımı ile karşılaştıkları sorunlar Tablo 21'de gösterilmiştir. Görüşülen kadınların Yaklaşık yarısı hiçbir sorunla karşılaşmadığını ifade ederken, 17 kadın kadınların erkeklerden daha düşük ücret ile çalışması, 6 kadın iş bulmanın zor olmasını, 5 kadının ise tarımsal desteklere kadınların erişimin az olmasını dile getirmiştir.

Tablo 21. Görüşülen kadınların çalışma ve sosyal hayata katılımı ile karşılaştıkları sorunlar

	n	%
Evdeki işlerin sadece kadınlar tarafından yapılması	2	2.2
Erkeklerden daha düşük ücret ile çalışılması	17	18.5
Çalışma saatlerinin erkeklerden daha fazla olması	1	1.1
Erken evlenme ile sorumlulukların artması	3	3.3
Çalışırken çocukların evde kalıyor olması	2	2.2
İş bulmanın kolay olmaması	6	6.5
Tarım eğitim atölyelerine kadınların fazla katılım sağlanmaması	2	2.2
Toplumun kadınların eğitimini önemsememesi	3	3.3
Yapılan desteklemelerin kadınlara erişimin az olması	5	5.4
Hiçbir sorun karşılamıyorum	47	51.1
Toplam	92	100

Kadınların Tarımsal Faaliyetlere Katılımını Kısıtlayan Faktörler

Yapılan araştırmaya katılan kadınların tarım faaliyetlerini gerçekleştirirken karşılaştıkları zorluklar tablo 4.4.1. de gösterilmiştir. %6.5 pay ile hasat kayıpları yüksek olması, %5.7' lik pay ile düşük ücretle çalışma, ve %5.4' lük pay ile de girdi fiyatlarının yüksek olması ilk üç sırada yer alan sorunlardır. Bu sorunları sırası ile, uygun olmayan çalışma koşulları, verimliliğin düşük olması,) sulama kanalların kötü olması, yol koşullarının kötü olması ve kullanılan teknolojinin son derece kısıtlı olduğu gibi sorunlar takip etmektedir. Tarım faaliyetlerini gerçekleştirirken diğer karşılaşılan sorunlardan ise pazarda ürünün değerine satamamak, risk ve belirsizlik, erozyon problemi, sağlık sorunun yaygın olması ve hastaneye erişememe, altyapı sorunları, doğal afetler olarak belirlenmiştir (Tablo 22).

Tablo 22. Tarım faaliyetlerde çalışan kadınların en çok karşılaştıkları zorluklar

Tarımda en çok karşılaşılan zorluklar	N	%
Hasat kayıplarının yüksek olması	17	6.50
Düşük ücretle çalışma	15	5.70
Girdiler fiyatlarının yüksek olması	14	5.40
Uygun olmayan çalışma koşulları	13	5.00
Düşük verimlilik	13	5.00
Sulama kanalların kötü olması	12	4.60
Yol koşullarının kötü olması	12	4.60
Kullanılan teknoloji son derece kısıtlı	10	3.80
Sel felaketi yüksek	10	3.80
Çiftçi eğitim ve yayım faaliyetleri sınırlı	9	3.40

Kadınların Tarımsal Faaliyetlere Etkin Katılımı için Vermiş Oldukları Öneriler

Görüşülen kadınların tarımsal faaliyetleri gerçekleştirirken bir kadın olarak hangi desteklere ihtiyaç duydukları incelendiğinde; 16 kadının (%7.8) girdi maliyetlerine yardım edilmesine ihtiyaç duyduğu, 15'inin (%7.3) pazarlama kanalların iyileştirilmesine, 11' er kadının (%5.3) ise, tarımsal arazi, finansman ve krediye ihtiyaç duyduğunu ifade etmiştir. Ayrıca, makine ve üretim ekipmanları, ile sulama kanallarının iyileştirilmesi, yem desteği ve tarımsal ücretlerin artırılması önerileri kadınların tarımsal faaliyetlere daha fazla etkin katılımını sağlayacağını düşünmektedirler (Tablo 23).

Tablo 23. Kadınların ihtiyaç duydukları destekler ile ilişkin bulgular

Görüşülen kadınların tarımla ilgili ihtiyaç duyduğu destekler	N	%
Girdi maliyetlerine destek	16	7.80
Pazarlama kanallarının iyileştirilmesi	15	7.30
Arazi desteği	11	5.30
Finansman ve kredi desteği	22	10.60
Tarımsal makine desteği	10	4.90
Sulama kanalları iyileştirilmeli	10	4.90
Üretim alet ve ekipmanları desteği	9	4.40
Yem desteği	9	4.40
Tarımsal ücretlerin artırılması	8	3.90

Kadınların Tarımsal Faaliyetlere Katılımını Artırmaya Dönük Öneriler

Yapılan araştırmaya katılan kadınların tarımsal faaliyetlere etkin katılımı için önerileri incelediğinde; topraksız kadınlara toprak verilmesi (%10.9), Üretim alet-ekipman desteği verilmesi ve pazarlama kanalarının iyileştirilmesi (%8.7), ile girdi desteği verilmesi, çiftçi kadınlara tarımsal eğitim sağlanması ve kadınlara yönelik okur yazarlık oranının yükletilmesi (%7.6) en çok dile getirdikleri konular arasındadır (Tablo 24).

Tablo 24. Kadınların tarımsal faaliyetlere etkin katılımı için vermiş oldukları öneriler

Kadınların tarımsal faaliyetlere etkin katılımı için vermiş oldukları öneriler	n	%
Topraksız kadınlara toprak verilmeli	10	10.9
Üretim alet-ekipman desteği verilmeli	8	8.7
Pazarlama kanaları iyileştirilmeli	8	8.7
Girdi desteği verilmeli	7	7.6
Çifçi kadınların tarımsal eğitim sağlanmalı	7	7.6
Kadınlara yönellik okur-yazar oranı artırılmalı	7	7.6
Sağlık problemlerinin iyileştirilmesine destek verilmeli	6	6.5
Çiftçi eğitim ve yayım faaliyetleri yaygınlaştırılmalı	5	5.4
Tarım dışı gelir kaynağına kavuşturulmalı	4	4.3
Eğitim atölyeleri artırılmalı	4	4.3

Somali'de Kadınların Tarımsal İş Yaşamına Dahil Edilmesinde Karşılaşılan Sorunlar ve Çözüm Önerileri

- Tarımsal üretimin her aşaması için verilen eğitim olanaklardan kadınların büyük ölçüde yararlanmaması ve erkeklerin öncelikli oldukları görülmektedir. Araştırmada elde edilen veriler doğrultusunda, kadınların büyük bir oranla (43.5%) okur-yazar olmadığı sonucuna varılmıştır. Bu kapsamda, okuma yazma beceresi kazandıran eğitim ve kurs olanakları geliştirilmelidir.
- Kadınların iş yaşamına dahil edilmesine yönelik olumsuz toplumsal yargılar bulunduğu gözlenmektedir. Kadınların çalışma yaşamında yer alması kadının kendisinin kararından çok, erkeklerin kararına bağlı olabilmektedir.
- Kadınların tarımsal iş yaşamına dahil edilmesinde karşılaşılan en önemli sorunlardan birisi de cinsiyete dayalı ücret eşitsizliğidir. Kadınların erkeklerden daha az üçret ile çalıştırılmasıdır.
- İşe alınma konusunda kadınlar, eşitsizliklere uğramaktadırlar. Erkeklere göre daha zor iş bulabilmekte ve daha zor işlerde çalışmaktadırlar.
- Kadınların özellikle tarımsal çalışma hayatına girmesini sağlayacak eğitim ve farkındalik faaliyetleri yapılmalıdır. Tarımsal faaliyetlerinin her aşamasında bulunan kadınlara yönelik yayım ve eğitim çalışmaları artırılmalıdır.

- Kadınların eğitime erişememesi, kırsal alanlarda eğitim ve eğiticilerin bulunmaması ile ilgili mevcut sorunlar çözülmelidir.
- Kadınların eğitim eksikliğinin giderilmesi sadece kadınların eğitim seviyesini yükseltmeyecek aynı zamanda kadınlarla erkekler arasındeki eşitsizliğini giderilmesine de katkıda bulunacaktır.
- Somali'de yoksulluğun önlenmesinde kadınların sosyo-ekonomik durumları ile tarımsal faaliyetlere katılım durumlarının incelenen bu çalışmada kadınların büyük bir çoğunluğunun (72.8%) tarımsal faaliyetlerine katıldığı görülmektedir. Çalışmadan elde edilen verilere göre kadınların çoğunluğunun (93.5%) kooperatife üye olmadığı tespit edilmiştir.
- Kooperatif, kırsal alanlarda üretimin artması, yoksulluğun azaltılması ve kadınların güçlendirilmesinin en önemli araçlardan biridir. Bu doğrultuda bölgede kadınlara yönelik kooperatifçilik konusunda eğitimler düzenlenmelidir.
- Bölgede kalkınmayı teşvik edecek unsurların başında altyapı gelmektedir. Köy yolları, kanalizasyon, içme suyu ve elektrik gibi altyapı hizmetleri daha da iyileştirilmesi de kadınların çalışma yaşamına yer almalarını artıracaktır.

Referanslar

[1] AfDB A. 2019, Indicators on Gender, Poverty, the Environment and Progress toward the Sustainable Development Goals in African Countries-2019. African Development Bank.
[2] Ahmed AE, Imam NA, Siddig KHA. 2012, Women as a Key to Agriculture and Food Security in Sudan: The Case Study of Northern Kordofan State. Journal of Agricultural Science and Technology.
[3] Alliance for a Green Revolution in Africa (AGRA), 2013, Africa Agriculture Status Report: Focus on Staple Crops.
[4] Barau A, Oladeji DO. 2017, Participation of urban women in agricultural production activities in the Sokoto Metropolis, Nigeria. Journal of Natural Resources and Development, 7(1), 84-90.
[5] Bhat AH, Bhat GM, Khan BA, Bhat AS. 2012, Analysis of Women Participation in Farm Activities in Rural Kashmi- Some major Findings. Journal of Arts, Science & Commerce.
[6] Dhruw B, Kaushal R, Bhagat R, Attri N. 2020, Tribal Women Participation In Agriculture And Allied Sectors In Gariaband District Of Chhattisgarh. International Journal of Research-Granthaalayah, 8(9), 334-344
[7] Dünya Bankasi. Rebuilding resilient and sustainable agriculture in Somalia; 2018
[8] Ergin G. 2009, "Türkiye'de Tarım Sektöründe Çalışan Kadın işgücü: "Malatya Örneği", İnönü Üniversitesi, Yayınlanmamış Yüksek Lisans Tezi. İnönü Üniversitesi, Malatya.
[9] FAO. 2014. AQUASTAT Country Profile – Somalia. Food and Agriculture Organization of the United Nations (FAO). Rome, Italy
[10] Farid KS, Mozumdar L, Kabir MS, Goswani UK. 2009, Nature and Extent of Rural Women's Participation in Agricultural and Non-Agricultural Activities. Agricultural Science Digest.
[11] Food and Agriculture Organisation (FAO), 2011, Women – Key to Food Security 2010-2011.
[12] Goebel A. 2005, Gender and Land Reform. The Zimbabwean Experience. London:
[13] Million, S. D. R., and Percent Quota. "FUND RELATIONS." (2017).
[14] Plan ESS. 2017, Federal government of Somalia ministry of education, culture and higher education. Somalia, Mogadishu: Ministry of Education, 1-179.
[15] Rahman SA. 2008, Women's involvement in agriculture in northern and southern Kaduna State, Nigeria. Journal of Gender Studies, 17(1), 17-26.
[16] Singh D, Vinay D. 2013, Gender Participation in Indian Agriculture: An Ergonomic.
[17] UNFPA, 2016, Educational Characteristics of the Somali People
[18] Unicef, 2017, Somali Poverty Profile 2016.
[19] Waheed HA. 2020, Concept Project Information Document (PID)-Somalia Education for Human Capital Development Project-P172434 (No. PIDC28113, pp. 1-0). The World Bank.
[20] Winrock, International Ethiopia, 2001, The Study of Appropriate Technologies Developed to Increase Women's Production and Productivity Ethiopia, Addis Ababa.
[21] World Bank, 2015, Somalia Economic Update.

The Importance of Gerbera as a Cut Flower and Advances of It in Scientific Research

Tuğçe Ünsal[1], Kübra Yazıcı[2]*
[1]Tokat Gaziosmanpaşa University, Graduate Education Institute, Horticulture Department, Tokat, Turkey
[2]Yozgat Bozok University, Faculty of Agriculture, Department of Landscape Architecture, Yozgat, Turkey
**Corresponding author: tugce_9526@outlook.com*

Abstract

Gerbera, a member of the Asteraceae family, has approximately 30 species known in nature. It has spread naturally in South Africa, Africa, Madagascar, and tropical Asia. The first scientific description of gerberas is J.D. Described by Hooker. It is also known as the Transvaal Daisy or Barberton Daisy. It is the second most produced cut flower after carnation as cut flower in our country. We can divide the scientific studies conducted on the gerbera plant into four groups. Studies in general; To produce 1st quality gerbera by providing the growth of plant height, flower diameter and flower stem with growth regulators, to obtain fast and many plants with tissue culture, to bring new products to the product range with breeding studies and to maintain the vitality of the plant in the process from harvest to consumer It is based on increasing the life of the vase and introducing new solutions to the market. This study was conducted to emphasize the importance of Gerbera as a cut flower and its developments in scientific research.

Keywords: Gerbera, cut flower, growth regulators, yield, quality

Introduction

Ornamental plants have entered human life as a symbol of beauty, goodness, respect and love in ancient times [1]. Flowers, which started to be used for aesthetic purposes years ago, are used for purposes such as urbanization, eliminating the longing for nature of people who are away from nature, making cities more livable environments, they draw attention as a commercial area. Also flowers play an important role in the economic development of many countries [2,3].

The ornamental plants sector was generally classified into four groups of activity: cut flowers, indoor ornamental plants, outdoor ornamental plants and natural flower bulbs (geophytes). It was very difficult to evaluate the countries at the level of ornamental plants production activity area due to different classification methods [4-6].

In Turkey, commercial cut flower cultivation first started in around Istanbul and in the 1940s, then it was spread to other regions. This type of aquaculture has become widespread due to its suitability for ecology and because it is a significant alternative in ornamental plants production [7]. According to the data of TUIK [8], the first three cut flowers are respectively carnation, gerbera and rose with the highest production amount and production area in Turkey. In Turkey, in gerbera production, Antalya (905 decares) ranks first, İzmir (73,161 decares) second and Tokat ranks third with 47 decares.

Gerbera sp.

Gerbera which is the family Asteraceae and there are approximately 30 species in nature (Figures 1 and 2). It grows naturally South Africa, Africa, Madagascar, and tropical Asia.

The first scientific description of the gerbera was given by J.D. It was made by Hooker in the Curtis Botanical Magazine in 1889. The described species, *Gerbera jamesonii*, is a South African species and is also known as Transvaal daisy or Barberton daisy [9].

Figure 1. *Gerbera* sp. [10]

- It has an herbaceous structure.
- They can withstand winter temperatures down to -7ºC.
- It is very sensitive to sudden changes in day and night temperatures.
- It is a long-lived plant.
- They bloom again in the spring.
- Gerbera flowers are examined in 3 groups according to their quality. 1 Quality; stem length is 50 cm or more, flower diameter is 12 cm. In addition, there should be no defects in the flowers. 2. Quality; Stem length is 35 cm or more, 3. Quality stalk length is 20 cm or more.

Seed propagation is not a preferred method in gerbera production as it opens and takes a long time to produce flowers More vegetative propagation methods are used and faster seedling production is achieved. The most used vegetative propagation techniques are used [11-13].

Figure 2. *Gerbera* sp. [10]

The Studies on Gerbera

Gerbera has an important place in the cut flower industry. For this reason, the studies are aimed at commercial development.

Scientific studies in this field can be grouped as follows:

1. Producing 1st quality gerberas by providing the development of plant height, flower diameter, and flower stem with growth regulators,
2. To obtain fast and many plants with ın Vıtro
3. Adding new products to the product range with improvement studies

4. Studies are carried out on the basis of increasing the vase life and introducing new solutions to the market in order to maintain the vitality of the plant in the process from harvest to consumer.

Some of these studies are given in Table 1.

Table 1. Studies on Gerbera

Author	Hormone used	Purpose of the study
Abd-Elkader et al. (2020) [14]	Some Amino Acids (glycine, arginine, asparagine, alanine, tryptophan and a mixture of all) 100 ppm doses and control (tap water)	The study was carried out to determine the effect of some Amino Acids on yield and quality in Gerbera. Number of leaves, rooting rate, fresh and dry weight, total leaf area, leaf area per plant and amount of chlorophyll (A, B and total), total carbohydrate, N, P, K contents in leaves were measured.
Chauhan et al. (2017) [15]	Three different doses of GA3 (50, 100, 150 ppm) were applied.	The aim of their study was to determine the effect of GA3 on growth and flower yield of Gerbera. The contents of cut flower fresh and dry weight, number of cut flowers per plant, number of cut flowers per square meter, plant height, first flower appearance and highest leaf number at flowering were measured.
Patra et al. (2015) [15]	Nine different doses of GA3 (0, 25, 50, 75, 100, 125, 150, 175, 200)	In the study, they examined the effect of GA3 on flowering and growth in Gerbera; The number of leaves per plant, stem length, number of flowers per plant, flower diameter were taken and recorded monthly.
Mehraj et al. (2013) [16]	150 ppm GA3 dose on four different days. (G0, no spray, G1; spray once after 15 days G2; spray twice after 15 and 30 days and G3; 15 after 30 and 45 days) applied to plants	The study was carried out to increase plant growth, flower production and gerbera flower quality; Number of leaves per plant, plant height, leaf area, chlorophyll, first flower bud formation date, number of flowers per plant, flower diameter parameters were examined.
Chauhan et al. (2014) [17]	Three different doses of GA3 (50, 100, 150 ppm) were applied.	The study was carried out to determine the effect on flowering and cut flower yield in Gerbera plant. The flowering duration, flower stem length, flower stem thickness, cut flower fresh weight, dry weight, number of cut flowers per plant, number of flowers per square meter and flower yield were examined.
Jadhao et al. (2010) [18]	4 different nitrogen (0, 10, 20, 30 g/m2) and 4 different GA3 (0, 50, 100, 150 ppm) doses were applied.	The study was carried out to determine the effects of different levels of GA3 and nitrogen on gerbera growth. The flowering and flower yield. plant height, number of leaves per plant, root formation per plant and number of flowering days were measured.
Sharifuz-zaman and Ara (2018a) [19]	6 different concentrations of GA3 (0, 50, 100, 150, 200, 250 ppm) were applied.	This study, which was carried out in order to increase the yield and quality of gerbera were examined the number of leaves per plant, plant spread, flowering date, chemical absorption per plant, stem length, number of flowers per plant, flowering time and vase life.
Sharifuz-zaman and Ara (2018b) [20]	T1: Control (soil), T2: Coconut shell, T3: Perlite, T4: Sawdust, T5: Coconut shell+ Perlite (1:1), T6: Coconut shell+ soil (1:1),	The effects of 7 different soilless agricultural cultures on yield and quality in gerbera were researched. The number of leaves, flowering days,

	T7: Coconut shell +Sawdust (1:1).	number of flowers, stem weight, stem diameter, vase life and flowering time were examined.
Khanaj and Noroozi-sharaf (2020) [21]	Different NO3- : NH4+ (100:0, 80:20, 60:40, 40:60) ratios were used.	The effects of different NO3-: NH4+ treatments on flower height, stem and disc diameter, flower number, flowering, fresh and dry weight, vase life, K, Ca, Mg contents of gerberas were researched.
Dalal et al. (2009) [22]	Three different doses of GA3 (50, 100, 150 ppm) were applied.	Results were recorded by looking at parameters such as growth, flowering, flower yield and quality.
Şirin (2011) [23]	Five different nutrient solution formulations (Hoagland and Arnon, Hewitt, Çolakoğlu-1, Steiner, Çolakoğlu-2) were used.	In the study, yield and quality parameters (cut flower yield, flower quality, plant growth, number of offspring, plant fresh weight) were examined.
Kılıç and Yaman (2020) [24]	Plant extracts of H. heterophyllum, H. perforatum and H. Scabrum which were St. John's Wort species were used at 0.50, 100, 150 ppm doses.	Vase life of flowers, proportional fresh weight and daily and total vase solution intake were researched to increase the vase life of the gerbera.
Kaya et al. (2019) [25]	Different doses of GA3 (125, 250, 500 ppm) and BA (100, 200, 400 ppm) were applied.	The aim of their study was to determine the effect of GA3 and Benzyladenine (BA) application on gerbera. The yield and quality components (multiplying ratio, flower stem length, flower diameter, vase life, flower stem diameter,) were examined.
Sangma et al. (2017) [26]	Control (T0) (water) GA3 50 (T1), 100 (T2), 150 (T3), 200 (T4) ppm) NAA (50 (T5), 100 (T6), 150 (T7), 200 (T8) ppm) was used as 9 different applications.	The study was carried out to research the effect of GA3 and NAA on yield, quality, and flowering in gerbera. The plant height, number of leaves per plant, first flower, flower diameter, stem length, stem circumference, number of flowers per plant, and number of cuttings, flowers per treatment, vase life, and number of absorbents per plant were examined.
Salem (2016) [27]	Six different doses of Benzyl Adenine (0, 50, 100, 150, 200 and 250 ppm) were applied.	The aim of the study was to determine the effect of Benzyl Adenine on growth, yield and flowering of Gerbera. The stem length, number of flowers per plant, flower diameter, stem diameter, number of absorbents per plant parameters were examined.
Danaee et al. (2011) [28]	6 different doses of GA3 (0, 50, 100, 150, 200, 300) and BA (0, 10, 25, 50, 100, 150) for 48 hours, then 2.5% ethyl alcohol and 3% ethanol were applied to plants. Vases containing sugar were placed.	The study was carried out to determine the effect of GA_3 on Gerbera and BA on increasing post-harvest quality and vase life, vase life, solution uptake, fresh weight, membrane stability and total soluble solids content were examined.
Yazıcı and Alkaç (2019) [29]	Different varieties and doses of GA3 150, 300, 450 and 600 ppm) were applied.	The aim of their study was to determine the effects on Gerbera; yield and quality components (multiplying ratio, flower stem length, flower diameter, vase life, flower stem diameter) were examined.
Ünsal (2021) [30]	Two different types (Ulaş and Transvaal), four BA (0, 200, 400 and 600 ppm) and four NAA (0,	The aim of the study was to determine the effects on Gerbera; yield and quality components (multiplying ratio, flower stem length, flower

	100, 200, 300) doses were applied.	diameter, vase life, flower stem diameter) were examined.
Emongor (2004) [31]	The doses of 0, 2.5, 5 or 7.5 mg L-1 GA3 were used freshly cut flower stalks of 'Ida Red' gerbera cultivar	The aim of study was to research the effect of gibberellic acid (GA3) on the postharvest quality and vase life of Gerbera cut flowers.
Abd-El-Hady (2020) [32]	Two rates of adenosine triphosphate (0.0 and 7.0 g/l) alone or combined with potassium nitrate at the dose of 2.5, 5.0, 7.5 and 10.0 g/pot,	The study was performed on vegetative growth, flowering and chemical constituents of gerbera (Gerbera jamesonii). The highest values of plant height, number of leaves per plant, leaf area, number of flowers per plant, flower diameter, stalk length as well as the contents of total chlorophyll, carbohydrates.
Farina et al. (1989) [33]	Three different doses of GA3 (50, 100, 150 ppm) were applied.	The aim of their study was to determine the effect of GA3 on growth and flower yield, the contents of cut flower fresh and dry.
Albino-Garduño (2007) [34]	Gerbera jamesonii cultivation (‘Amaretto’ and ‘Darling’ varieties), using the Steiner nutrient solution that contains 9 meq L− 1 of calcium (Ca2 +) plus two modified nutrient solutions with 6, and 12 meq Ca2 +· L− 1 on a red volcanic rock substrate known in Mexico as “tezontle”.	Results (the greatest dry mass weight, flower production, and quality of the inflorescence) related to high CO2 net assimilation rates.

Conclusion

In Turkey, the gerbera plant forms an important base of scientific studies in the field of ornamental plants. There are studies in the above-mentioned study areas, and new doses and different application methods are still being tested for product development. Prolonging the life of the vase, new solutions obtained with natural products attract attention as an important field of study. However, the ornamental plants sector is a newly developing and open sector in Turkey. Our product range is almost non-existent gerbera varieties on a national scale.

It is a fact that collaborative approaches are important in the cut flower sector as in all sectors. For this reason, effective studies such as research, education and practice should be increased and the farmers in the field should be included in these studies. Ornamental plants producer sub-unions report the production amount, production area, export and import inputs and outputs every year. These reports will be positively affected by activities such as increasing the product range, increasing efficiency and quality.

References

[1] Gençer B. Dünya’da kesme çiçek sektörü pazarlama organizasyonları ve tüketici eğilimleri. (Doktora Tezi), Namık Kemal Üniversitesi Fen Bilimleri Enstitüsi, Tekirdağ, 2014.
[2] Özyavuz M, Yazgan ME, Korkut AB, Barış E, Erkal S, Yılmaz R, Erken K, ve Gürsan K. Süs Bitkileri Üretimindeki Gelişmeler. Araştırma Makalesi, 2015.
[3] Korkut A, Yıldırım T, Görür G, Çakmak S, Türkiye’de Süs Bitkileri Tüketim Projeksiyonları ve Üretim Hedefleri”, IV. Türkiye Ziraat Mühendisliği Teknik Kongresi, Tarım Haftası’95 Kongre Kitabı, 1995, 2. Cilt, T.C. Ziraat Bankası Kültür Yayınları No:26, 697-714, Ankara.
[4] Anonim, www.wikipedia.org https://tr.wikipedia.org/ Erişim Tarihi: 16.04.2020.

[5] Karagüzel O, Korkut AB, Özkan B, Çelikel F.G, Titiz S. Süs bitkileri üretiminin bugünkü durumu, geliştirilme olanakları ve hedefleri. Kongresi, (11-15 Ocak 2010), TMMOB Ziraat Mühendisleri Odası, Cilt I, 539-558, Ankara.
[6] Süs Bitkileri Sektör Raporu SÜSBİR 2019.
[7] Yazgan M. E, Korkut A.B, Barıs E, Erkal S, Yılmaz R, Erken K, Gürsan K, Özyavuz M. Süs bitkileri üretiminde gelişmeler. Türkiye Ziraat Mühendisliği VI. Teknik Kongresi, (3-7 Ocak 2005), 589-607, Ankara, 2005.
[8] Türkiye İstatistik Kurumu (TÜİK), (2020): http://www.tuik.gov.tr/UstMenu.do?metod=temelist Yıllara Göre bitkisel üretim.
[9] Mendi Y. 2008. Gerbera Yetiştiriciliği Ders Notu, tps://silo.tips/download/gerbera-yettrcl
[10] https://ziraatyapma.blogspot.com/2012/10/gerbera-cicegi-yetistiriciligi.html
[11] Das P, Sıngh PKS. Gerbera. In: BOSE T.K., YADAV L.P. (eds), Commercial Flowers. Calcutta, Naya Prokash: 1989, 601–622.
[12] Nhut DT, Truong TTA, Nguyen TDH, Nguyen TD, Nguyen TH, Nguyen QT, Nguyen HV. Effect of genotype, explant size, position, and culture medium on shoot generation of Gerbera sp. by receptacle transverse thin cell layer culture Sci Hortic, 111 (2007), 146-151.
[13] Diker M, Şan B. Gerberanın (Gerbera Jamesonii Bolus) yaprak ve yaprak sapından in vitro sürgün rejenerasyonu. Süleyman Demirel Üniversitesi Ziraat Dergisi Araştırma Makalesi, 2016, 11(2), 104-111.
[14] Abd-Elkader H.H, Massoud H.Y, El-Baz TT, El-Arian MA. Effect of amino acids spray on growth, flowering and keepin quality of gerbera jamesonii l. as a pot plant. J. Of Plant Production. Mansoura Univ, 2020,11(2), 201-206.
[15] Chauhan RV, Kaval K, Vasova, NJ. Effect of GA3 on growth and yield of gerbera under protected condition. Trends in Biosciences, 2017, 10 (28), 5964-5965.
[16] Patra SK, Beura S, Shasani T.. Efficacy of GA3 on growth and flowering regulation of in vitro raised hybrid gerbera under shade. Net. Agric. Sci. Digest, 2015, 35 (3), 173-177.
[17] Mehraj H, Ona AF, Roni MZK, Jamal Uddin AFM, Taufique, T. 2013. The effect of spraying frequency of gibberellic acid on growth and flowering in gerbera. J. Expt. Biosci., 4 (2), 7-10.
[18] Chauhan RV, Kaval KP, Babarıya VJ, Pansuria PB, Savaliya AB. Effect of Giberallic Acid on Flowering and Cut Flower Yield İn Gerbera Under Protecred Condition. The Asian Journal of Horticulture, 2014, 404-407.
[19] Sharifuzzaman SM, Ara KA. Effect of Gibberellic Acid on growth, yield and quality of gerbera under polytunnel. Agricultural Research Council Farmgate Dhaka-1215, syf: 25-29,2018a.
[20] Sharifuzzaman SM, Ara KA. Effect of substrates on yield and quality of gerbera in soilless culture. Agricultural Research Council Farmgate Dhaka-1215, 32-39, 2018b.
[21] Khalaj MA, Amiri M, Sindhu SS. 2011. Response of different growing media on the growth and yield of gerbera in hydroponic open system. Indian J. Hort., 68(4), 583-586.
[22] Dalal SR, Somavanshi AV, Karale GD. Effect of GA_3 On Growth Flowering Yield and Quality of Gerbera Under Polyhouse Conditions. Internatonal Journal of Agricultural Sciences, 2009, 5(2), 355-356.
[23] Şirin, U. Effect of different nutrient solution formulations on yield and cut flower quality of gerbera *(Gerberea jamesonii)* Grown In Soilless Culture System. African Journal Of Agricultural Research, 2011, 6 (21), 4910-4919.
[24] Kılıç T, Yaman C. Bazı kantaron ekstraktlarının gerberanın vazo ömrüne Etkileri. Ege Üniversitesi Ziraat Fakültesi Dergisi, 2020, 57 (3), 425-432.
[25] Kaya AS, Aydınşakir K, Karagüzel, ÜÖ. 2019. Assesment of GA_3 and BA Application On Gerbera Cultivation in Soilless Culture. Internatonal Journal of Agriculture Envronment and Food Scences, 3 (1), 41-45.
[26] Sangma ZCN, Singh D, Fatmi U. Effect of growth regulators on growth, yield and flower quality of gerbera (Gerbera Jamesonii L.) cv. Pink Elegance Under Naturally Ventilated Polyhouse(NVPH). International Journal of Current Microbiology and Applied Sciences, 2017, 6 (10), 468-476.
[27] Selam RAA. Effect of Benzyl Adenine on Growth, Yield and Flowers of Gerbera *(Gerbera jamesonii).* Ridha, 2016, 5(3).

[28] Danaee E, Mostofi Y, Moradi P. Effect of GA_3 and BA On Postharvest Quality and Vase Life of Gerbera *(Gerbera jomesonii cv. Good Timing)* Cut Flowers. Hort. Environ Biotechnol, 2011, 52 (2), 140-144.
[29] Yazici K, Alkaç O S. The Effects of GA3 Applications on the Yield and Quality of Gerber Daisy Gerbera sp Cultivars in Erbaa Tokat Ecological Conditions. Gaziosmanpaşa Üniversitesi Ziraat Fakültesi Dergisi, 2019, 36(1), 45–54.
[30] Ünsal T. Bazı Gerbera (Gerbera Sp.) Çeşitlerinde Naftalen Asetik Asit ve Benzil Adenin Uygulamalarının Çiçek Kalitesi Üzerine Etkileri, 2021, Tokat Gaziomanpaşa Üni, Lisansüstü Eğitim Enst. Bahçe Bitkileri ABD. Y. Lisans Tezi.
[31] Emongor VE. Effect of gibelerllic acid on postharvest quality and vase life of gerbera cut flowers (Gerbera jamesonii). J. Agron. 2004, 3:191–195.
[32] Abd-El-Hady WMF. Effect of potassium nitrate and adenosine triphosphate on pre-and posthervest gerbera *(Gerbera jamessonii L.)* plants. Scientific J. Flowers & Ornamental Plants, 2020, 7(3), 337-348.
[33] Farina E, Volpi L. Effect of GA3 treatments on flowering of gerbera grown for winter production. Acta Horticulturae, 1989, 246: 159–163.
[34] Albino-Garduño R, Zavaleta-Mancera HA, Ruiz-Posadas LM, Sandoval-Villa M, Castillo-Morales A. Response of Gerbera to Calcium in Hydroponics, Journal of Plant Nutrition, 2007, 31(1): 91-101,

Investigations and Concerns about the Fate of Transgenic DNA and Protein in Livestock

*Jacob Matovu**, *Ahmet Alçiçek*
Ege University, Faculty of Agriculture, Department of Animal Science, Izmir, Turkey
**Corresponding author: matoisrael@gmail.com*

Abstract

The fate of transgenic DNA (tDNA) and protein from feed derived from Genetically Modified organisms (GMOs) in animals has been a major issue since their commercialization in 1996. Several studies have investigated the risks of horizontal gene transfer (HGT) of tDNA and protein to bacteria or animal cells/tissues, but some of the reported data are controversial. Previous reports showed that tDNA fragments or proteins derived from GM plants could not be detected in tissues, fluids, or edible products from livestock. Other researchers have shown that there is a possibility of small fragments entering animal tissues, fluids and organs. This motivated us to update our knowledge about these concerns.

Therefore, this review aimed to evaluate the probable transfer and accumulation of tDNA/proteins from transgenic feeds in animal samples (ruminant and non-ruminant) by evaluating the available experimental studies published scientifically. This study found that the tDNA/protein is not completely degraded during feed processing and digestion in Gastro-Intestinal Tract (GIT). In large ruminants (cattle), tDNA fragments/proteins were detected in GIT digesta, rumen fluid, and faeces. In small ruminants (goats), traces of tDNA/proteins were detected in GIT digesta, blood, milk, liver, kidney, heart and muscle. In pigs, they were detected in blood, spleen, liver, kidney, and GIT digesta. In poultry, traces were detected in blood, liver and GIT digesta but not in meat and eggs. Notwithstanding some studies that have shown transfer of tDNA/protein fragments in animal samples, we cannot rely on these few studies to give general evidence for transfer into tissues/fluids and organs of farm animals. However, this study clearly shows that transfer is possible. Therefore, intensive and authentic research should be conducted on GM plants before they are approved for commercial use, investigating issues such as the fate of tDNA or proteins and the effects of feeding GM feed to livestock.

Keywords: transgenic DNA/proteins, gene, genetically modified organisms, Bt Maize, PCR

Introduction

The worldwide increasing population led to the need to develop high producing crops that can be able to provide food for both the growing population and as feed to the animals. Most of these are genetically modified plants (GMP) and their importance in animal nutrition is increasing.

The effect of feeding GM feeds to animals on several occasions have shown no significant difference in animal performance compared to those fed non-GM feeds. However, the fate of transgenic DNA or proteins has been highlighted as an important topic of concern in the current debate about the use of GM plants as animal feeds along with human food products.

According to a statement by EFSA [1], tDNA or protein fractions have not been found in the animal in tissues, fluids, or edible products of farm animals. Hence very many of the GM plants have been widely used in animal feeding and nutrition. However, there is increasing concerns about the detection of tDNA in animal tissues and organs, which may lead to cases of antibiotic resistance genes, toxicity and allergenicity of GM plants, in addition to environmental concerns [2]. Therefore, these controversial findings motivated us to evaluate the recently published experimental studies, concerning the fate of tDNA or protein in the different animal species.

GMO Testing

Legislation enacted worldwide to regulate the presence of genetically modified organisms (GMOs) in crops, foods, and ingredients has necessitated the development of reliable and sensitive methods for GMO detection. Analytical methods and their standardization for GM ingredients in food and feed are essential for the implementation of labeling regulations [3]. Raw material (e.g., cereals) and processed products (e.g. food) derived from GM crops could therefore be identified by testing for the presence of introduced DNA or by detecting expressed novel proteins encoded by the genetic material [4].

Detection of GM Plants by DNA-based Methods

Although several techniques are available, the most commonly used are: Southern blot, Polymerase Chain Reaction (PCR) analyzes and microarray [5];[4]. PCR, which involves amplification of transgenic elements, is a widely used method for GM detection [6]. PCR-based GM detection methods range from screening methods to gene-specific methods to construct-specific methods and event-specific methods [7]. Numerous studies investigating the fate of transgenic DNA in the digestive tract of livestock have demonstrated the usefulness of PCR for the detection of GM material in complex samples [8].

The PCR method is widely employed for GM detection and quantification due to its high specificity, sensitivity robustness, and low-cost detection procedures [4]. However, due to the involvement of cumbersome and time-consuming electrophoretic analysis in conventional PCR and the use of sophisticated equipment, its application in GMO testing is limited to specialized laboratories with high availability of resources and expertise [7]. Another limitation is that there are not able to detect the corresponding exogenous target DNA or protein under severe heating conditions, including autoclaving or baking. PCR and immunoassay techniques were able to detect transgenic maize in low processed foods, but it was impossible to obtain good quality DNA or detect Cry proteins by PCR method in foods subjected to high heat treatments. Therefore, detection of exogenous DNA in GM ingredients of processed foods is challenging [6].

Detection of GM Plants by Protein-Based Methods

Protein-based detection methods measure the level of proteins expressed in plant tissues or the amount of protein present in products made from them. Immunoassays containing protein-specific antibodies are routinely used for protein analysis. Microtiter-plate-based, Enzyme-linked Immunosorbent Assays (ELISA) and Lateral Flow Strips (LFS) are the two most common assay formats for protein detection in agricultural biotechnology. LFS is primarily designed for qualitative assays, although some have been developed for quantitative measurements using a reader [3].

However, protein-based methods are not suitable for processed foods due to denaturation that occurs during processing. In addition, the higher cost of developing specific antibodies and the fact that antibodies cannot be easily synthesized compared to oligonucleotides limit the development of the method [4]. This means that in pellets containing GM materials, the fate of the transgene may not be well detected. Therefore, there is a need to standardize the methods used for GMO detection.

Digestion and Fate of Dietary DNA in Ruminants and Non-Ruminants

Issues such as the fate of the recombinant DNA and protein during processing, passage through the Gastrointestinal Tract (GIT), the potential for absorption of the digested DNA/protein and the ability of the absorbed DNA/protein fragments to be biologically viable are the aspects that need to be considered when investigating whether or not tDNA/protein fragments enter animal tissues, fluids or edible products [9].

One of the major concerns expressed by the scientific community and the public is the possibility that exogenous DNA in GM plants can be transferred to bacteria in the gastrointestinal tract of farm animals and food products of animal origin [10]. This is likely to lead to problems such as toxicity, allergenicity, antibiotic resistance and environmental concerns. Potential recipient bacteria for antibiotic resistance genes include bacteria that infect plants or reside on plant surfaces, soil bacteria, endosymbionts, and gastrointestinal bacteria from mammals that consume plant products [11].

Early studies, as reviewed by Tufarelli et al.,[12], showed that DNA delivered by GMOs is rapidly degraded by normal digestive processes, like normal plant DNA. Moreover, the amount of DNA in GM crops is small relative to the total plant DNA consumed by animals or humans. However, various studies have repeatedly shown that the tDNA can survive the various processing methods even with heat treatment. Also, they probably survive the GIT mechanical and enzymatic digestion processes, on the other hand, they can be completely degraded [13].

In a recent study by Nadal et al.,[14] in ruminants, low copy number genes, such as GMO-delivered genes, are unlikely to survive until reaching the proximal small intestine due to ruminal and intestinal DNase activity. On the other hand, in non-ruminants, DNA fragments have been seen throughout the GIT, although they consist of small fragments (400bp, up to 17900bp in rare cases) and detectability is

related to high DNA uptake. The passage of specifically small plant DNA fragments of the high-copy chloroplast Rubisco gene across the intestinal barrier is a natural process [8].

Through animal feeding studies, the fate of tDNA in various animals has been explored and these are summarized in Table 1. The table has shown that tDNA fragments and protein have been detected in the different parts of the GIT, digesta and some tissues/fluids or organs of the different animal species.

Table 1. Transfer and detection of tDNA/proteins in different animal samples

Authors	DNA source	Animal	Studied characteristics	Results
Sieradzki et al.,[15]	HT soybean and Bt maize	Calves	Fate of tDNA	Not detected in the blood, organs, tissues, eggs, excreta.
Paul et al.,[16]	Bt Maize	Dairy cow	To investigate the degradation of Cry1Ab protein	Detected in the GIT digesta and in feaces.
De Giacomo et al.,[17]	GM soybean and maize	Dairy cow	Carry-over of tDNA	Not detected in the milk samples.
Furgał-Dierzuk et al.,[18]	Bt Maize and HT soybean	Dairy cow	Fate of tDNA sequences	Not detected in milk.
Furgał-Dierzuk et al.,[19]	Bt Maize and HT soybean	Calf	Transfer of tDNA to tissues	Rumen fluid was detected positive, however, no tDNA in the blood, studied organs, intestinal content or meat.
Guertler et al.,[20]	Bt Maize	Dairy cow	Fate of cry1Ab DNA and recombinant protein	Milk, blood and urine samples were free of tDNA and protein. While as Cry1Ab protein were detected in feaces.
Bertheau et al.,[21]	Bt176 Maize	Dairy cow	Fate of tDNA or proteins	Not detected in blood.
Phipps et al.,[22]	Glufosinate tolerant maize	Dairy cow	Fate of tDNA	Not detected in milk.
Phipps et al.,[23]	Soybean meal (cp4epsps gene) and GM corn grain (cry1a[b] gene),	Dairy Cows	Transgenic DNA fate	Detected in the digesta and rumen fluid, but not in the milk.
Calsamiglia et al., [24]	Corn silages (2GM: herbicide tolerance: mepsps and insect resistance: cry1Ab)	Dairy Cows	Fate of tDNA and encoded protein Cry1Ab	No tDNA and Cry1Ab protein were detected in milk
Agodi et al.,[25]	Milk from Italian market focused on GM Bt maize and GM HT soybean	Cow milk	Fate of transgenic DNA	Samples demonstrated the presence of GM maize and soybean sequences, however concluded that there could possible contamination from feaces or air.
Einspanier et al., [26]	Bt176 Maize	Cows	Fate of recombinant protein CryIAb	Bt toxin detected in contents of the GIT and the protein found in faeces

Sieradzki et al.,[15]	HT soybean and Bt maize	Broilers, layers	Fate of tDNA	Not detected in the blood, organs, tissues, eggs, excreta
Deaville & Maddison,[27]	HT soybean and Bt maize	Broilers	Fate of Maize cry1a(b) gene and Soybean meal (CP4EPSPS gene)	tDNA detected in the gizzard Digesta, while as in blood and tissue tested negative.
Aeschbacher et al., [28]	Bt176 corn	Broilers and layers	Fate of recombinant plant DNA fragments such as bla or Cry1A(b)	Not detected in the muscle, liver, and spleen,
Řehout, et al.,[29]	HT soybean	Broilers	Fate of tDNA	Detected in blood
Nemeth et al.,[30]	Bt maize	Broilers	Fate of tDNA fragments	Not detected in the muscle
Świątkiewicz et al., [31]	Bt corn, HT soybean meal	Broilers	Fate of Maize Cry1A (b) and soybean epsps genes	Detected in crop and gizzard content, but not in the in duodenum, jejunum, ileum, and caecum digesta, excreta. Also, the blood, liver, spleen, and breast muscle tested negative.
Yonemochi et al., [32]	Event CBH 351-derived hybrid (SL), maize	Broilers	The Cry9C gene and Cry9C protein	Not detected in blood, liver and muscle
Řehout, et al., [33]	Bt maize, HT soybean meal	Broilers	Fate of Maize Cry1A (b) and soybean epsps genes	Fragments of soybean transgene were identified in liver. But no Maize transgene was detected in Liver. There is no gene detected in the kidneys.
Ma et al.,[34]	Phytase transgenic corn	Laying Hens	Fate of transgenic phyA2 gene DNA and protein	Not detected in blood, heart, liver, spleen, kidney, breast muscle, and eggs
Świątkiewicz et al.,[35]	Bt maize, HT soybean meal	Laying Hens	Fate of recombinant Cry1A(b) and CP4EPSPS genes	No fragments were detected in the digesta of jejunum, ileum and caeca, excreta, tissues (blood, liver, spleen, lungs) and in eggs.
Wang et al.,[36]	Transgenic silkworms	Male chickens	Fate of transgenic gene	Not detected in the digesta and tissues
Walsh et al.,[37]	Bt maize	Pig	Fate of the tDNA and protein	The cry1Abgene and protein were seen in the GIT digesta but not detected in the kidneys, liver, spleen, muscle, heart or blood.

Beagle et al.,[38]	An Escherichia coli glutamate dehydrogenase (gdhA) Corn	Pig	Digestive fate of the tDNA (gdhA)	Ileal and stomach ingesta tested positive. Not detected in the large intestine, white blood cells, plasma, liver, or muscle samples.
Jennings et al.,[39]	HT soybean	Pig	Detection of transgenic soyabean (CP4EPSPS) gene	No fragments detected in muscle of pigs
Walsh et al.,[40]	Bt maize	Pig	Fate of Cry1Ab gene and truncated Bt toxin.	The *cry1Ab* gene was detected in stomach and ileum content, Bt toxin fragments were detected at all sites in the GIT. No cry1Ab transgene or Bt proteins fragments in organs or blood
Broll et al.,[41]	GM potato	Piglets	Fate of tDNA	Not detected in any organ.
Świątkiewicz et al., [42]	Bt maize, HT soybean meal	Pig	Fate of transgenic DNA	Detected in stomach and duodenum content, but not in the intestinal digesta, blood and other examined organs
Yonemochi et al.,[43]	Event CBH 351-derived hybrid (SL), maize	Pig	The Fate of Cry9C gene or Cry9C protein	No traces in the blood, liver or muscles
Świątkiewicz et al.,[44]	Bt maize, HT soybean meal	Sows	Transfer of tDNA	tDNA not detected in blood
Buzoianu et al.,[45]	Bt maize	Pig	Fate of Cry1Ab gene	Transgenic material or Cry1Ab-specific antibodies were not detected
Mazza et al.,[46]	Bt maize	Pig	Fate of Cry1Ab gene	Detected in blood, liver, spleen and kidney
Sharma et al.,[47]	Roundup Ready Canola	Pig	Fate of CP4EPSPS transgene	Not detected in the spleen in pigs. Fragments detected in the liver and kidney and the porcine ceacal content
Sieradzki et al.,[15]	RR soybean or/and Bt maize	Pig	Fate of tDNA	Not detected in the blood, organs, tissues, eggs, excreta
Trabalza-Marinucci et al.,[48]	Bt176 maize	Sheep	Transfer of tDNA	No transgenic DNA was detected in tissues, blood, and ruminal fluid or ruminal bacteria
Alexander et al.,[49]	Glyphosate tolerant rapeseed	Sheep	Fate of tDNA	Not detectable in feces or blood, detected in Ruminal and duodenal fluids
Sharma et al.,[47]	Roundup Ready Canola	Sheep	Fate of CP4EPSPS transgene	Detected in the ovine ruminal or abomasal content and large intestinal content, not detected in visceral tissues (liver, kidney) of lambs

Tudisco et al.,[2]	HT soybean meal	Goats and kids	Fate of CP4EPSPS transgene	Goat's blood and milk, the CP4 EPSPS gene were detected. In the kids the gene fragment in liver, kidney, heart and muscle was detected.
Mastellone et al.,[50]	HT soybean	Kids Born from Goats Fed GMP	Detection of CP4EPSPS gene	Detected in liver, kidney and blood

RR: Roundup Ready, HT: herbicides tolerant

In broilers, plant genes were detected in the GIT digesta, liver and blood [27];[33]. Using the PCR method, fragments of Roundup Ready soybean were identified in 3 samples of broiler livers, as shown in Table 2.

Table 2. Results of detections of control genes and transgenes of Roundup Ready soybean and Bt maize MON810 in liver and kidney of broilers

	Number of positive samples		
Samples of kidney and liver	Positive samples (in all 3 repeats)	Positive samples (in 1 or 2 repeats)	Total
Soybean - control	1	17	18
Soybean - transgene	0	3	3
Maize - control	0	0	0
Maize - transgene	0	0	0

Adapted from Řehout et al., [33].

In pigs, fragments were detected in blood, liver, spleen, kidney and GIT digesta [46]; [47]; [38]; [42]; [40] (Table 1).

Table 3. Transgenic DNA detection in milk samples (A to N, different milk brands tested)

Milk samples	Type of milk	No. of sample analyzed	Cry1A	CP4EPSPS
A_1	Normal	5	1	3
A_2	Normal	3	1	0
A_3	Organic	4	1	2
B_1	Normal	3	0	1
B_2	For children	2	0	0
C_1	Normal	3	0	1
C_2	Normal	1	0	0
C_3	Organic	4	1	0
D_1	Normal	5	2	0
D_2	Normal	3	2	0
D_3	Normal	1	0	0
E	Normal	2	1	0
F	Normal	2	0	0
G_1	For children	2	0	0
G_2	For children	2	0	0

H	For children	3	1	0
I	Organic for children	3	1	0
L	Organic	3	1	0
M_1	Organic	3	1	0
M_2	Organic for children	3	1	0
N	For children	2	1	0
P	Sheep	1	0	0
Total		60	15	7
%			25.0	11.7

Adapted from Agodi et al.[25].

In dairy cows and calves, tDNA fragments and proteins have been detected in digesta, feces and rumen fluid (Table 1), indicating that the fragments can survive rumen digestion. In a study by Paul et al.,[16] in which dairy cows were fed diets containing (GM) maize MON810, concentrations of Cry1Ab protein were lowest in the abomasum (0.38 lg/g) and highest in the rumen (3.84 lg/g), indicating incomplete degradation by DNases in the rumen. In another study examining milk from cows fed GM soybeans and maize, sequences of GM soybeans and maize were found in the milk samples (Table 3). Of the 60 samples tested from different brands of milk, 25% were positive for GM maize sequences (Cry1A) and 11.7% for GM soybean sequences (CP4EPSPS) [25]. This study proved that the tDNA sequences can survive during the pasteurization process. However, the authors noted that the positive detection could be due to airborne or fecal contamination with tDNA sources, for instance with GM feed.

In small ruminants, tDNA gene sequences have been detected in liver, kidney, blood, heart, milk and GIT contents [47],[8], [2], [50] as shown in Table 1. In addition, kids fed with milk from mothers who had GM soybean in their diet showed fragments of tDNA gene sequences in their liver, kidney, heart and muscle [2], as shown in Table 4.

Table 4. Number of kids with organs in which DNA sequences were detected

	CONTROL						TREATED					
	Blood	Muscle	Kidney	Liver	Spleen	Heart	Blood	Muscle	Kidney	Liver	Spleen	Heart
Chlor	7	7	8	8	7	6	7	8	8	6	7	7
Lectine	4	4	5	5	3	3	4	4	5	5	2	4
35S	–	–	–	–	–	–	4	3	5	5	2	3
CP4 EPSPS	–	–	–	–	–	–	2	4	3	3	2	4

Adapted from Tudisco et al.,[2]

Conclusions

Based on our studies, it has been shown that the tDNA and protein can survive processing and GIT DNAses in different animal species, increasing the possibility of being absorbed into animal tissues and organs and even into animal products consumed by humans, such as milk and meat. Although very many studies have shown no health concerns in both animals and humans, more studies are needed on the effects of feeding GM feed to livestock, as few exist. In addition, potential processing methods that can help to fully degrade the tDNA and protein in GM feeds before they are fed to animals need to be developed to reduce the risks of absorption.

References

[1] EFSA. (2007). Statement on the fate of recombinant DNA or proteins in the meat, milk or eggs of animals fed with GM feed. EFSA J. 5(7):1–8.
[2] Tudisco R, Mastellone V, Cutrignelli MI, Lombardi P, Bovera F, Mirabella N, et al. (2010). Fate of transgenic DNA and evaluation of metabolic effects in goats fed genetically modified soybean and in their offsprings. Animal. 4(10):1662–71.
[3] Alarcon CM, Shan G, Layton DT, Bell TA, Whipkey S, Shillito RD. (2019). Application of DNA- and Protein-Based Detection Methods in Agricultural Biotechnology. J Agric Food Chem. 67(4):1019–28.
[4] Zhang D, Guo J. (2011). The Development and Standardization of Testing Methods for Genetically Modified Organisms and their Derived Products. J Integr Plant Biol. 53(7):539–51.
[5] Ahmed F. (2002). Detection of Genetically Modified Organisms in Feed. TRENDSin Biotechnol. 20(5):207–22.
[6] Wang X, Chen X, Xu J, Dai C, Shen W. (2015). Degradation and detection of transgenic Bacillus thuringiensis DNA and proteins in flour of three genetically modified rice events submitted to a set of thermal processes. Food Chem Toxicol. 84:89–98. Available from: http://dx.doi.org/10.1016/j.fct.2015.08.010
[7] Randhawa G, Singh M, Sood P. (2016). DNA-based methods for detection of genetically modified events in food and supply chain. Curr Sci. 110(6):1000–9.
[8] Alexander TW, Reuter T, Aulrich K, Sharma R, Okine EK, Dixon WT, et al. (2007). A review of the detection and fate of novel plant molecules derived from biotechnology in livestock production. Anim Feed Sci Technol. 133(1–2):31–62.
[9] EFSA. (2008). Safety and nutritional assessment of GM plants and derived food and feed : The role of animal feeding trials Safety and nutritional assessment of GM plants and derived food and feed : The role of animal feeding trials Report of the EFSA GMO Panel Working. Food Chem Toxicol. 46(S1):70.
[10] EFSA. (2013). Review of the strategies for the comprehensive food and feed safety and nutritional assessment of GM plants per se. EFSA Supporting publication EN- 480. ADAS UK Ltd. & Rothamsted Research. 2013. Available from: http://www.efsa.europa.eu/en/supporting/doc/480e.pdf.
[11] de Santis B, Stockhofe N, Wal JM, Weesendorp E, Lallès JP, van Dijk J, et al. (2018). Case studies on genetically modified organisms (GMOs): Potential risk scenarios and associated health indicators. Food Chem Toxicol. 117:36–65.
[12] Tufarelli V, Selvaggi M, Dario C, Laudadio V, Tufarelli V, Selvaggi M, et al. (2015). Genetically Modified Feeds in Poultry Diet: Safety, Performance, and Product Quality. Food Sci Nutr. 55(4):562–9.
[13] Salisu IB, Amin AB, Ali Q, Tijjani A, Ibrahim AA. (2019). Digestive fate of transgenic DNA and protein in livestock tissues fed genetically modified feed ingredients: A review. Niger J Anim Prod. 46(2):8–21.
[14] Nadal A, Giacomo M De, Einspanier R, Kleter G, Kok E, Dijk J Van, et al. (2018). Exposure of livestock to GM feeds : Detectability and measurement. Food Toxicol. 117:13–35.
[15] Sieradzki Z, Mazur M, Kwiatek K, Świątkiewicz S, Świątkiewicz M, Koreleski J, et al. (2013). Assessing the possibility of genetically modified DNA transfer from GM feed to broiler, laying hen, pig and calf tissues. Pol J Vet Sci. 16(3):435–41.
[16] Paul V, Guertler P, Wiedemann S, Meyer HHD. (2010). Degradation of Cry1Ab protein from genetically modified maize (MON810) in relation to total dietary feed proteins in dairy cow digestion. Transgenic Res. 19(4):683–9.
[17] De Giacomo M, Di Domenicantonio C, De Santis B, Debegnach F, Onori R, Brera C. (2016). Carry-over of DNA from genetically modified soyabean and maize to cow's milk. J Anim Feed Sci. 25(2):109–15.
[18] Furgał-Dierzuk I, Strzetelski J, Twardowska M, Kwiatek K, Mazur M. (2015). The effect of genetically modified feeds on productivity, milk composition, serum metabolite profiles and transfer of tDNA into milk of cows. J Anim Feed Sci. 24(1):19–30.
[19] Furgał-Dierzuk I, Strzetelski J, Kwiatek K, Twardowska M, Mazur M, Sieradzki Z, et al. (2014).

The effect of genetically modified maize (MON 810) and soyabean meal (Roundup Ready) on rearing performance and transfer of transgenic DNA to calf tissues. J Anim Feed Sci. 23(1):13–22.
[20] Guertler P, Paul V, Steinke K, Preißinger W, Albrecht C, Spiekers H, et al. (2010). Long-term feeding of genetically modified corn (MON810) — Fate of cry1Ab DNA and recombinant protein during the metabolism of the dairy cow. Livest Sci J. 131(2–3):250–9.
[21] Bertheau Y, Helbling JC, Fortabat MN, Makhzami S, Sotinel I, Audéon C, et al. (2009). Persistence of plant DNA sequences in the blood of dairy cows fed with genetically modified (Bt176) and conventional corn silage. J Agric Food Chem. 57(2):509–16.
[22] Phipps RH, Jones AK, Tingey AP, Abeyasekera S. (2005). Effect of corn silage from an herbicide-tolerant genetically modified variety on milk production and absence of transgenic DNA in milk. J Dairy Sci. 88(8):2870–8. Available from: http://dx.doi.org/10.3168/jds.S0022-0302(05)72968-4
[23] Phipps RH, Deaville ER, Maddison BC. (2003). Detection of transgenic and endogenous plant DNA in rumen fluid, duodenal digesta, milk, blood, and feces of lactating dairy cows. J Dairy Sci. 86(12):4070–8. Available from: http://dx.doi.org/10.3168/jds.S0022-0302(03)74019-3
[24] Calsamiglia S, Hernandez B, Hartnell GF, Phipps R. (2007). Effects of Corn Silage Derived from a Genetically Modified Variety Containing Two Transgenes on Feed Intake, Milk Production, and Composition, and the Absence of Detectable Transgenic Deoxyribonucleic Acid in Milk in Holstein Dairy Cows. J Dairy Sci. 90(10):4718–23. Available from: http://dx.doi.org/10.3168/jds.2007-0286
[25] Agodi A, Barchitta M, Grillo A, Sciacca S. (2006). Detection of genetically modified DNA sequences in milk from the Italian market. Int J Hyg Environ Health. 209(1):81–8.
[26] Einspanier R, Lutz B, Rief S, Berezina O, Zverlov V, Schwarz W, et al. (2004). Tracing residual recombinant feed molecules during digestion and rumen bacterial diversity in cattle fed transgene maize. Eur Food Res Technol. 218(3):269–73.
[27] Deaville ER, Maddison BC. (2005). Detection of Transgenic and Endogenous Plant DNA Fragments in the Blood, Tissues, and Digesta of Broilers. J Agric Food Chem. 53(26):10268–75.
[28] Aeschbacher K, Messikommer R, Meile L, Wenk C. (2005). Bt 176 Corn in Poultry Nutrition : Physiological Characteristics and Fate of Recombinant Plant DNA in Chickens. Poult Sci [Internet]. 84(3):385–94. Available from: http://dx.doi.org/10.1093/ps/84.3.385
[29] Řehout V, Hanusova L, Čítek J, Kadlec J, Hosnedlova B. (2008). Detection of DNA fragments from Roundup Ready soya in blood of broilers. J Agrobiol. 25(1):145-148.
[30] Nemeth A, Wurz A, Artim L, Charlton S, Dana G, Glenn K, et al. (2004). Sensitive PCR Analysis of Animal Tissue Samples for Fragments of Endogenous and Transgenic Plant DNA. J Agric Food Chem. 52(20):6129–35.
[31] Świątkiewicz SŚWIĄ, Twardowska M, Markowski JAN, Mazur MAŁG, Sieradzki Z, Kwiatek K. (2010). Fate of transgenic DNA from Bt corn and Roundup Ready soybean meal in broilers fed GMO feed. Bull Vet Inst Pulawy. 54:237–42.
[32] Yonemochi C, Fujisaki H, Harada C, Kusama T, Hanazumi M. (2002). Evaluation of transgenic event CBH 351 (StarLink) corn in broiler chicks. Anim Sci J. 73(3):221–8.
[33] Řehout V, Hanusová L, Kadlec J, Čítek J, Hosnedlová B. (2008). Detection of DNA fragments from roundup ready soya and Bt maize in organs of broilers. J Agrobiol. 25(1):141–4.
[34] Ma Q, Gao C, Zhang J, Zhao L, Hao W, Ji C. (2013). Detection of Transgenic and Endogenous Plant DNA Fragments and Proteins in the Digesta , Blood , Tissues , and Eggs of Laying Hens Fed with Phytase Transgenic. PLoS One. 8(4):1–10.
[35] Swiatkiewicz S, Koreleski J, Arczewska-Wlosek A, Swiatkiewicz, M., Twardowska M, Markowski J, Kwiatek K. (2011). Detection of transgenic DNA from Bt maize and herbicide tolerant soybean meal in tissues, eggs and digestive tract content of laying hens fed diets containing genetically modified plants. Ann Anim Sci. 11(3):413–24.
[36] Wang Y, Wang Z, Guo H, Huang J, Li X, Sun Q, et al. (2020). Potential of transferring transgenic DNA from silkworm to chicken. Int J Biol Macromol [Internet]. 142:311–9. Available from: https://doi.org/10.1016/j.ijbiomac.2019.09.102
[37] Walsh MC, Buzoianu SG, Gardiner GE, Rea MC, Gelencse E, Epstein MM, et al. (2011). Fate of Transgenic DNA from Orally Administered Bt MON810 Maize and Effects on Immune Response and Growth in Pigs. PLoS One. 6(11):e27177.

[38] Beagle JM, Apgar GA, Jones KL, Griswold KE, Radcliffe JS, Qiu X, et al. (2006). The digestive fate of Escherichia coli glutamate dehydrogenase deoxyribonucleic acid from transgenic corn in diets fed to weanling pigs. J Anim Sci. 84(3):597–607.
[39] Jennings JC, Kolwyck DC, Kays SB, Whetsell AJ, Surber JB, Cromwell GL, et al. (2003). Determining whether transgenic and endogenous plant DNA and transgenic protein are detectable in muscle from swine fed Roundup Ready soybean meal 1, 2, 3. J Anim Sci. 81(6):1447–55.
[40] Walsh MC, Buzoianu SG, Rea MC, O'Donovan O, Gelencsér E, Ujhelyi G, et al. (2012). Effects of feeding Bt MON810 maize to pigs for 110 days on peripheral immune response and digestive fate of the cry1Ab gene and truncated Bt toxin. PLoS One. 7(5):1–11.
[41] Broll H, Zagon J, Butschke A, Leffke A, Spiegelberg A, Böhme H, et al. (2005). The fate of DNA of transgenic inulin synthesizing potatoes in pigs. J Anim Feed Sci. 14(SUPPL. 1):337–40.
[42] Świątkiewicz M, Hanczakowska E, Twardowska M, Mazur M, Kwiatek K, Kozaczyński W, et al. (2011). Effect of genetically modified feeds on fattening results and transfer of transgenic DNA to swine tissues. Bull Vet Inst Pulawy. 55(1):121–5.
[43] Yonemochi C, Suga K, Harada C, Hanazumi M. (2010). Evaluation of transgenic event CBH 351 (StarLink) corn in pig. Anim Sci J. 81(1):94–101.
[44] Świątkiewicz M, Bednarek D, Markowski J, Hanczakowska E, Kwiatek K. (2013). Effect of feeding genetically modified maize and soybean meal to sows on their reproductive traits, haematological indices and offspring performance. Bull Vet Inst Pulawy. 57(3):413–8.
[45] Buzoianu SG, Walsh MC, Rea MC, Donovan OO, Gelencse E, Nagy A, et al. (2012). Effects of Feeding Bt Maize to Sows during Gestation and Lactation on Maternal and Offspring Immunity and Fate of Transgenic Material. PLoS One. 7(10):e47851.
[46] Mazza R, Soave M, Morlacchini M, Piva G, Marocco A, Cuore UCS, et al. (2005). Assessing the transfer of genetically modified DNA from feed to animal tissues. Transgenic Res. 14(5):775–84.
[47] Sharma R, Damgaard D, Alexander TW, Dugan ME, Aalhus JL, Stanford K, et al. (2006). Detection of Transgenic and Endogenous Plant DNA in Digesta and Tissues of Sheep and Pigs Fed Roundup Ready Canola Meal. J Agric Food Chem. 54(5):1699−1709.
[48] Trabalza-Marinucci M, Brandi G, Rondini C, Avellini L, Giammarini C, Costarelli S, et al. (2008). A three-year longitudinal study on the effects of a diet containing genetically modified Bt176 maize on the health status and performance of sheep. Livest Sci. 113(2–3):178–90.
[49] Alexander TW, Reuter T, Okine E, Sharma R, McAllister TA. (2006). Conventional and real-time polymerase chain reaction assessment of the fate of transgenic DNA in sheep fed Roundup Ready® rapeseed meal. Br J Nutr. 96(6):997–1005.
[50] Mastellone V, Tudisco R, Monastra G, Pero ME, Calabrò S, Lombardi P, et al. (2013). Gamma-Glutamyl Transferase Activity in Kids Born from Goats Fed Genetically Modified Soybean. Food Nutr Sci. 04(06):50–4.

Appendix

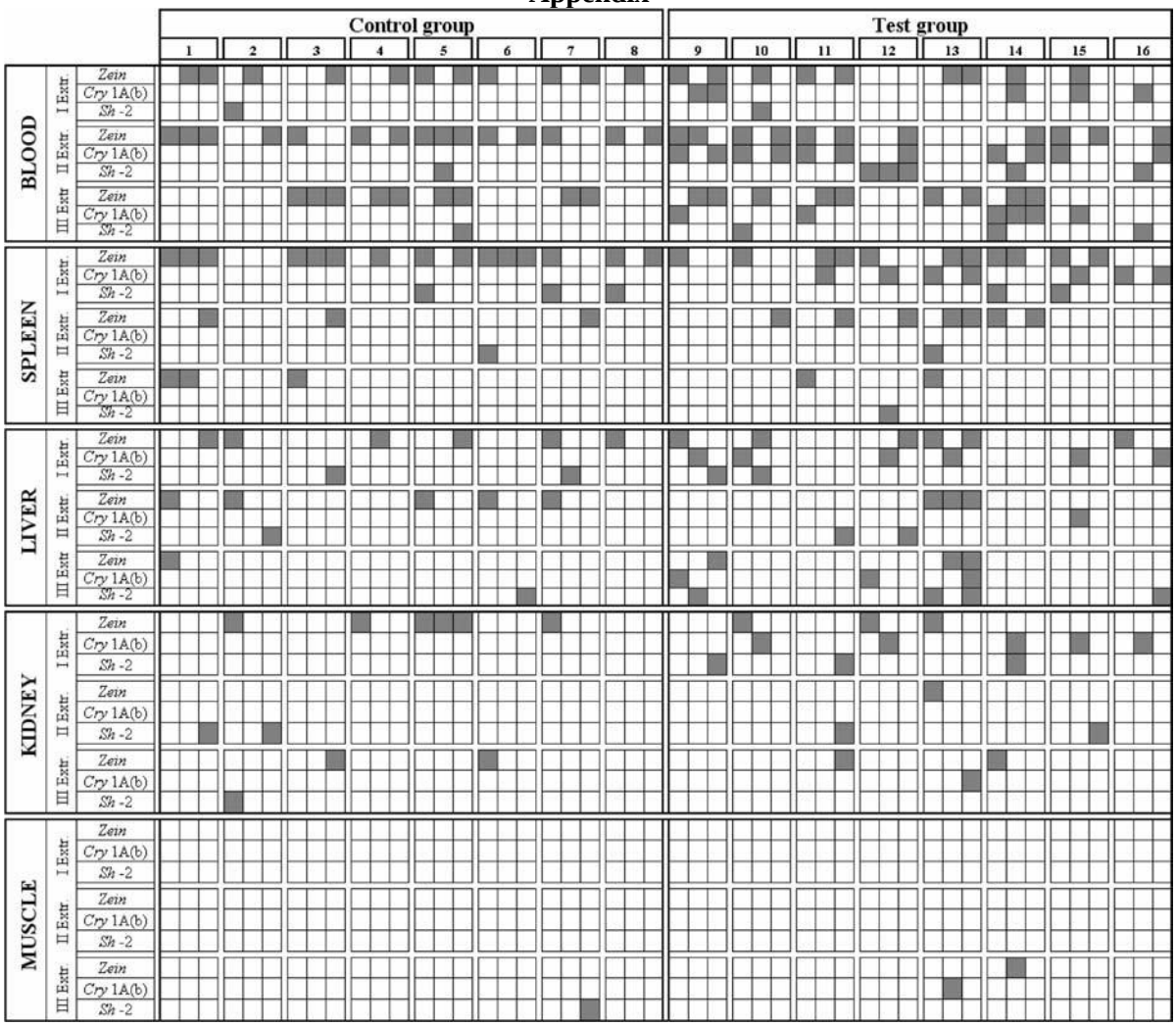

Adapted from Mazza et al.,[46]. Representation of the results obtained from PCR reactions performed on five tissues from piglets. A blank cell means a negative result in the PCR reaction while a grey cell means a positive result.

Tip 2 Diyabette Devamlı Egzersiz ve Safran Kullanımının İnsülin Direnci ve Glikozun Hücre İçine Alımına Etkisi

Raihana Halim[1], Zaynab Dahi[2], Nazar Mohammad Halim[3]*
[1]Kabil Üniversitesi, Biyokimya-Beslenme Bölümü, Eczacılık Fakültesi, 1001, Kabil, Afganistan
[2]Jowzjan Üniversitesi, Kimya Bölümü, Eğitim Fakültesi, 1901, Jowzjan, Afghanistan
[3]Kabil Üniversitesi, Kimya Bölümü, Fen Fakültesi, 1001, Kabil, Afganistan
**İletişimden sorumlu yazar: halimraihana@gmail.com*

Özet

Diyabet (Şeker Hastalığı) insülin hormonunun eksikliği veya etkisizliği sonucu oluşan, ömür boyu süren, yüksek kan glikoz seviyesi ile karakterize bir metabolik hastalıktır. İnsülin hormonu tamamen eksikse "Tip 1 diyabet (insüline bağımlı diyabet)", denmekte, genellikle çocuklarda ve gençlerde görülmektedir. "Tip 2 diyabet (insüline bağımlı olmayan diyabet)", tip 1 diyabetten farklı olarak, insülin hormonun miktarı yetersiz veya dokular insüline karşı direnç göstermektedir daha çok 35 yaş ve üzeri görülmektedir. Diyabetin en yaygın şekli olan tip 2 diyabet gelişiminde insülin direnci önemli bir rol oynar.2014 yılında yapılan çalışmaya göre diyabet hastalarının sayısı 422 milyon olduğu belirtmiştir. Bu rakam 2035'te 592 milyona çıkacağı tahmin edilmektedir. İlaç tedavisinin yanı sıra, diyabet sağlıklı beslenme ve fiziksel egzersizle kontrol edilebilmektedir. Eski çağlardan beri, bitkiler dünya çapında bir ayurveda tıbbı kaynağı olarak kullanılmıştır ve tıp babası Hipokrat "Gıda ilacınız olsun ve ilacınız yemeğiniz olsun" tavsiyesinde bulunmuştur. Safran (Crocus sativus L.) bitkisi dünyadaki en eski doğal ve farmasötik bitkilerden biri olarak bilinmektedir. Safran, 150'den fazla bileşen içermekte, biyolojik olarak aktif metabolitleri krosin, pikrokrosin ve safranaldır. Safran ağırlıklı olarak gıda, kozmetik ve boya endüstrilerinde kullanılmasının yanında, son zamanlardaki çalışmalar; antidepresan, antispazmodik, antidiyabetik, antikanser ve balgam söktürücü etkilerini göstermektedir. Yapılan birkaç araştırmada safranın insülin direnci üzerinde etkisi olduğu saptanmıştır. Safran tedavisi ile glikoz alımı hücreler tarafından önemli ölçüde uyarılmıştır. Ayrıca, safran ekstresi, doza bağımlı bir şekilde insülin sekresyonunu belirgin olarak arttırmıştır. Aynı şekilde, fiziksel egzersiz de, diyabetin önlenmesi ve tedavisinde önemli bir rol oynamakta ve glikozun hücre içine taşınmasını kolaylaştırmaktadır. Diyabet hastalarında, egzersizin glikoz seviyesi üzerinde etkisi birçok çalışmada araştırmacılar tarafından belirtilmiştir. Egzersiz yoğunluğu ile uyarılan insülin sekresyonundaki değişiklikler hakkında az bilgi bulunmaktadır. Birkaç çalışmada kadın ve erkek, obez ve orta yaşlarda olan diyabetik hastalar üzerinde denemeler gerçekleştirilmiştir. Katılımcıların insülin sekresyonlarındaki değişiklikleri, glikoz seviyeleri ve ortalama glikoz toleransları kaydedilmiştir. Bireyler orta şiddette egzersiz yaptıktan sonra anlamlı derecede düşük glikoz seviyeleri göstermişlerdir. Başka bir çalışmada, fiziksel egzersiz ile birlikte safran ekstresinin kullanımının etkisi araştırılmıştır. Bu yöntemi kullanarak, diyabetin kontrolü için daha etkili ve doğal bir yöntemin ortaya çıkabileceği düşünülmüştür. Özetle, bazı çalışmalarda elde edilen sonuçlara göre, kadınlar ve erkekler üzerinde akut yüksek yoğunluklu egzersizin, orta yoğunluklu egzersizden daha fazla kan glikozunun düşürdüğünü göstermiştir. Ayrıca, safranının devamlı egzersizle birleştirilmesinin diyabetik hastalar üzerinde güçlü bir törapatik faktör olduğu gösterilmiştir. Bu nedenle, diyabet hastalıklarına, devamlı egzersiz ve safran tüketiminin kombinasyonundan yararlanarak glikoz düzeylerini kontrol etmeleri tavsiye edilir. Bununla birlikte, moleküler düzeyde diyabetik parametreler üzerinde safranın spesifik bileşiklerinin uygun dozunu ve rolünü tanımlamak için daha fazla araştırma yapılması gerekmektedir.

Anahtar Kelimeler: Tip 2 diyabet, safran, egzersiz, insülin direnci

Giriş

Diabetes mellitus, pankreas tarafından insülin üretimindeki kalıtsal ve/veya edimsel eksiklikten veya üretilen insülinin etkisizliğinden kaynaklanan en yaygın bulaşıcı olmayan hastalıktır. Böyle bir eksiklik kandaki glikoz konsantrasyonlarının artmasına neden olur ve bu da vücudun birçok sistemine, özellikle kan damarlarına ve sinirlerine zarar verir. 1980 yılında 108 milyon olan diyabetli sayısı 2014 yılında 422 milyona yükselmiştir [1, 2]. İki yaygın tip diyabet vardır: Tip 1 diyabet otoimmün bir hastalıktır. Bu durumda pankreastaki insülin üreten hücreler yok edilir. Diyabetli kişilerin %10 kadarında tip 1

vardır. Genellikle çocuklarda ve genç erişkinlerde teşhis edilir (ancak her yaşta gelişebilir). Tip 2 diyabet, vücudun ya yeterince insülin üretmediği ya da vücut hücrelerinin insüline normal tepki vermediği tiptir. Bu diyabetin en yaygın türüdür. Tip 2 diyabet, tüm diyabet vakalarının% 90-95'ini oluşturur. Genellikle orta yaşlı ve yaşlı kişilerde görülmektedir. Tip 2 diyabet için diğer yaygın isimler arasında yetişkin başlangıçlı diyabet ve insüline dirençli diyabet bulunur. Diyabetin kendisi yüksek ölüm oranına sahip bir durum değildir (dünya genelinde 1,3 milyon ölüm), ancak diğer ölüm nedenleri için önemli bir risk faktörüdür ve yüksek atfedilebilir bir sakatlık yüküne sahiptir. Diyabet ayrıca kardiyovasküler hastalık, böbrek hastalığı ve körlük için önemli bir risk faktörüdür [3]. Son bulgular, iskelet kası lipidinin aşırı birikiminin insan obezitesinde ve tip 2 diabetes mellitusta (DM) insülin direnci ile ilişkili olduğunu göstermektedir. İnsüline dirençli iskelet kası, daha düşük oksidatif kapasite ve daha düşük emilim sonrası yağ asidi oksidasyonu oranları ile karakterizedir. Bu, kas içindeki lipid birikimi ile insülin direnci arasındaki ilişkinin, bir enerji substratı olarak lipidin oksidasyonu için daha düşük bir kapasiteden etkilenmesi olasılığını yükseltir. Lipid oksidasyon kapasitesi, aşırı kas lipid birikimi ile insülin direnci arasındaki ilişkinin önemli bir aracısı olabilir [4].

Diyabet tedavisinin amacı, diyabetin kronik komplikasyonlarını önlemek veya geciktirmek için glikoz, yağ ve tansiyonu düzenlemektir. Diyet, ilaç tedavisi ve egzersiz, diyabeti kontrol etmenin üç ana yöntemidir. Akarboz, miglitol ve vogliboz gibi anti-diyabetik ilaçlar hiperglisemiyi kontrol etmek için kullanılır. Bununla birlikte, bu anti-diyabetik ilaçlar, gastrointestinal yan etkilerle ilişkilidir [2]. Endüstriyel ilaçların yan etkileri nedeniyle, tıbbi bitkilerin kullanımı ve spor aktiviteleri gibi düşük komplikasyonlu tedavilere bariz bir ihtiyaç vardır [5].

In vitro ve in vivo çalışmalardan artan kanıtlar, meyve ve sebzelerden elde edilen fitokimyasalların obezite, diyabet, kanser, kardiyovasküler ve nörodejeneratif hastalıklar gibi bazı kronik durumlara karşı koruyucu bir etkiye sahip olduğunu göstermektedir. Fitokimyasallar, gıdalarda az miktarlarda oluşan ve biyoaktif etkileri olan besinsel olmayan kimyasal bileşiklerdir. Bu nedenle çeşitli hastalık ve rahatsızlıkları önlemek için meyve ve sebzeler açısından zengin bir diyet önerilmektedir. Bitkiler çok sayıda farklı biyoaktif bileşik üretebilir. Bütün gıdaların 5.000 ila 25.000 ayrı fitokimyasal içerdiği tahmin edilmektedir [1]. Egzersiz ise, insülin duyarlılığını ve lipid oksidasyonu kapasitesini artırır. Egzersiz ayrıca egzersiz sırasında kas içi TG depolarından yağ asidi oksidasyonunu artırır. Eğitimli dayanıklılık sporcularının iskelet kası önemli ölçüde insüline duyarlıdır ve yüksek lipid içeriğine sahip olmasına rağmen yüksek oksidatif kapasiteye sahiptir [4].

Tip2 Diyabet Üzerinde Fiziksel Aktivitesi Etkisi

Daha önce belirtiği gibi, aslında egzersiz diyet ve ilaç tedavisine ek olarak diyabet tedavisinin üç temel unsurundan biridir [6]. Dayanıklılık, direnç ve kombine egzersiz, diyabeti ve onun tehlikeli yan etkilerini kontrol etmede faydalıdır. Bir seans aerobik egzersiz, 24-72 saat boyunca insülin duyarlılığını artırmıştır. Egzersizin olumlu etkisi kilo kaybı, artmış GLUT4 (insüline bağımlı glikoz taşıyıcı), artmış kan akışı, azalmış hepatik glikoz üretimi ve normalleştirilmiş kan lipidleri ile ilgilidir. Uzun süreli direnç eğitimi, glikoz toleransı ve insülin duyarlılığı Egzersiz, vücudun insülin duyarlılığını artırmakta ve kan şekerini düzenlemektedir. Egzersiz, tansiyonun düzenlenmesinde de etkilidir, egzersiz vücut yağ kütlesini azaltarak kilo vermeye yardımcı olur, egzersiz enerjiyi artırır ve stresi azaltıp vücuttaki bağışıklığı geliştirmektedir [7]. Bir deneysel çalışmada, diyabetli kişilerde kan şekeri seviyelerini kontrol etmek için yüzme ve atletizm gibi aerobik sporlarda çalışan 70 erkek ve kadın, egzersizden önce ve sonra kan şekeri düzeylerini incelenip kan şekeri açısından test edilmiştir, bu da sağlıklı insanlarda hipoglisemi ve sabit kan şekeri seviyelerine neden olmuştur. Diyabetli bir kişi sadece yüksek kan şekerini önlemekle kalmaz, aynı zamanda fiziksel aktivite, ilaç ve günlük besin alımını dengeleyerek kan şekerinin düşmesini de önleyebilmektedir. Egzersiz sırasında, egzersizin aktivite düzeylerini artırmadaki rolü göz önüne alındığında, yağ hücrelerinde depolanan yağ asitleri kan yoluyla kalp, akciğer ve kas gibi organlara bu yağ asitlerini yakıt olarak kullanmak üzere taşınmaktadır ve diyabetin önlenmesi ve tedavisinde kilo kaybı görülebilir. Diyabetini kontrol eden çoğu insan düzenli egzersiz yapanlardır [8].

Akut egzersiz, yoğunluğa bağlı bir şekilde yağ ve hepatik insülin direncindeki değişikliklere göre pankreas insülin sekresyonunu azaltırken, orta ve yüksek yoğunluklu egzersiz, iskelet kası insülin direncindeki değişikliklere göre ayarlandığında insülin sekresyonunu arttırmıştır. Bununla birlikte, bu veriler, egzersiz yoğunluğunun, prediyabetli kişilerde glisemik kontrolü desteklemek için egzersizden

hemen sonraki dönemde glikoz düzenleyici dokular arasında benzersiz bir şekilde pankreatik insülin sekresyonunu ayarladığını göstermektedir [9]. Bir çalışmada, iskelet kası insülin direnci orta ve yüksek yoğunluklu egzersizden sonra kontrole göre azalmıştır. Hepatik insülin direnci, kontrol ile karşılaştırıldığında orta şiddette egzersiz sonrasında değişmedi. Adipoz insülin direnci de yüksek yoğunluklu egzersizden sonra önemli ölçüde arttı, ancak orta yoğunluklu egzersiz veya kontrolde değil [10]. Aerobik eğitim, lipid profillerinde ve insülin duyarlılığında iyileştirmelerle Tip 2 diyabeti tedavi etmek için en etkili egzersiz modu olarak tanıtılmıştır [11]. Tip 2 diyabetli daha yaşlı yetişkinlere, eklem hareket açıklığını artırmanın ve yaralanma riskini azaltmanın bir yolu olarak dengeyi koruyan veya iyileştiren egzersizler yapmaları tavsiye edilmektedir [12].

Stephens ve arkadaşları [13], aşırı kilolu insüline dirençli erişkinlerde egzersiz sonrası hemen beslenmenin iskelet kası insülin duyarlılığı üzerinde en büyük etkiye sahip olduğunu göstermiştir. Egzersizden hemen sonra beslenmenin, egzersiz yoğunluğuna dayalı bir şekilde insülin metabolizması üzerinde farklı etkileri olup olmadığı, özellikle prediyabetli yetişkinlerden oluşan bir klinik popülasyonda belirsizdir. Burada, yüksek yoğunluklu egzersizin, toparlanma döneminde orta yoğunluktaki egzersize göre insülin metabolizması üzerinde daha derin etkilere sahip olduğu görülmektedir ve bu kısmen gelişmiş glikoz toleransını açıklayabilir [14].

Önceki çalışmalar, egzersizden hemen sonra beslenmenin, egzersizden önce veya yaklaşık 3 saat sonra besin alımına kıyasla iskelet kası insülin duyarlılığını bir sonraki güne artırıp artırmadığını belirlemeye çalışmıştır [15]. Amerikan Spor Hekimliği Koleji (ACSM), Tip 2 diyabetli kişilerin haftada en az 150 dakika orta ila şiddetli aerobik egzersiz yapmalarını, haftada en az 3 gün boyunca ve aerobik aktivite nöbetleri arasında art arda 2 günden fazla olmayacak şekilde yaymalarını tavsiye etmiştir ve haftada en az 150 dakika orta ila şiddetli aerobik fiziksel aktivite ve/veya en az 90 dakika/hafta şiddetli aerobik egzersiz önerilmiştir [16]. Zanuso ve arkadaşları [9], egzersiz ve metabolik sonuçlar arasındaki karşılıklı ilişkilere ilişkin kanıtları belirlemek için literatürü eleştirel bir şekilde gözden geçirmiştir. Aerobik egzersizlerin etkilerinin iyi anlaşıldığı ve daha kuvvetli aerobik egzersiz programlarıyla yapılan müdahalelerin HbA1c'de daha fazla azalmaya ve insülin duyarlılığında daha fazla artışa neden olduğu sonucuna varıldı [9, 17].

Son sistematik çalışmalar, Tip 2 diyabetin tedavisinde ve önlenmesinde fiziksel aktivitenin etkinliğini değerlendirdi ve daha yüksek fiziksel aktivite seviyeleri ile daha düşük Tip 2 diyabet insidansı arasındaki ilişkiyi gösterdi. Hem aerobik hem de direnç egzersizlerinin azalmış Tip 2 diyabet riski ile ilişkili olduğu gösterilmiştir. Tip 2 diyabetli bireylerde haftada üç kez kombine eğitim, kan şekeri kontrolüne daha fazla fayda sağlayabilir. Misra ve arkadaşları [18] Asyalı Hintliler için günde 10-15 dakikalık direnç egzersizi ve işle ilgili aktivite içeren 60 dakikalık fiziksel aktivite önermiştir.

Gestasyonel şeker hastalığı olan 18-38 yaş arası kadınlar üzerinde yapılan bir araştırmanın sonuçları, egzersizin sonunda (30 dakika) kan şekeri seviyesinin dinlenmeye kıyasla her egzersiz koşulu için ve düşük yoğunluklu kıyasla orta düzeyde düşük olduğunu göstermiştir. Egzersizden 45 dakika sonra kan şekeri değerleri neredeyse aynı olmuştur. Düşük ve orta yoğunluklu egzersiz için kan şekeri eğrisinin altında kalan alan dinlenmeye göre anlamlı derecede daha düşüktü olmuştur. Üç koşul arasında, başlangıçtan 30 dakikalık seansa kadar insülin değişim eğimi, anlamlılığa yaklaşmıştır. Düşük ve orta yoğunluklu egzersiz sırasında dinlenme ile karşılaştırıldığında kan şekeri seviyesinde önemli düşüşler gözlenmiştir. Bu farklılıklar egzersizden 45 dakika sonra ortadan kalkmıştır. Devam eden araştırmalar, Gestasyonel diyabetli kadınlarda egzersizin kan şekeri ve insülin seviyeleri üzerindeki etkisinin daha fazla değerlendirilmesi için yüksek vücut kitle indeksi ve daha belirgin hiperglisemiye sahip kişileri incelemelidir [19].

Egzersizi ana öğünlerden önce kısa, yoğun 'egzersiz atıştırmalıkları' olarak dozlamak, insülin direnci olan bireylerde glisemik kontrolü iyileştirmek için zaman açısından verimli ve etkili bir yaklaşımdır. Plazma glikozunun egzersize bağlı olarak düşürülmesini önlemek için basit bir atıştırma stratejisinin kullanılmasıdır. Atıştırmalık ile egzersiz sırasında kalıcı insülin infüzyonu, egzersiz sonunda plazma glukozundaki artışları sınırlamada da etkili gibi görünmektedir [20, 21]. Bununla birlikte, aralıklarla küçük atıştırmalıklar, büyük atıştırmalıklardan daha iyidir. Büyük atıştırmalıklar, sürekli egzersizle anında düşen yüksek kan şekerine neden olduğundan, bu tür atıştırmalıklar önerilmez (Şekil 1) [22].

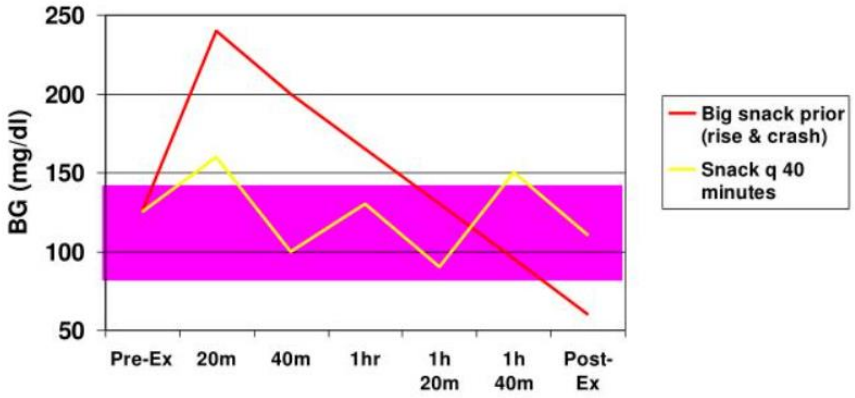

Şekil 1. Büyük ve küçük atıştırmalık, egzersiz ve zamanla ilişkisi [22]

Tip2 Diyabet üzerinde Safran Etkisi

Çoğu araştırmacı, ana etkili madde olarak krosetin olan safranın lipidler ve glisemik indeks üzerindeki etkisini araştırmışlardır [23, 24]. Son bilimsel bulgular, safran ve türevlerinin çeşitli in-vivo ve in-vitro modellerde hiperglisemiyi etkileyebileceğini, özellikle de krosin, krosetin ve safranalın önemli anti-diyabetik aktiviteye sahip olduğunu tekdüze bir şekilde göstermektedir. Safran ve bileşenlerinin (krosin, koketin ve safranal) modları için ana hipotezlerden biri, serbest radikal zincir reaksiyonları üzerindeki inhibitör etkidir. Safran bileşenleri, antioksidan gen ekspresyonunu modüle etti ve mitokondriyal antioksidan genleri yukarı regüle ederek, daha düşük bir mitokondriyal oksijen radikali oluşumuna yol açmıştır; deneyseller diyabetik modelde gelişmiş hiperglisemi, hiperlipidemi ve oksidatif stresten en azından kısmen sorumlu olabilmektedir [24, 25].

Safran ekstraktının hipoglisemik etkisi, periferik dokular tarafından glukoz alımının uyarılması, bağırsak glukoz emiliminin inhibisyonu, hem karaciğer hem de böbrekte insülinaz aktivitesinin inhibisyonu, endojen glukoz üretiminin inhibisyonu, renal glukoz reabsorpsiyonunun inhibisyonu gibi mekanizmalar tarafından uygulanması [26] veya insülin direncinin düzeltilmesi [27] Langerhans adacıklarının β hücrelerinin uyarılması, Langerhans β-hücre adacıklarının daha fazla insülin rejenerasyonu salması gibi görünmektedir [24, 28].

Diğer bazı araştırmalar, safranın insülin direnci üzerindeki etkisinden dolayı geleneksel tıpta diyabet tedavisinde kullanıldığını ortaya koymuştur. Ayrıca, krosetinin insülin duyarlılığını arttırdığını ve bozulmuş glukoz toleransı, yüksek fruktozlu diyete bağlı hiperinsülinemi ve farelerde deksametazon enjeksiyonu gibi insülin direnciyle ilgili anormallikleri iyileştirdiğini belirtmişlerdir [28]. Bir in vitro model çalışması, safranın glikoz alımını ve AMP ile aktive olan protein kinaz (AMPK)/asetil-CoA karboksilaz (ACC) ve mitojen ile aktive olan protein kinazların (MAPK'lar) fosforilasyonunu güçlü bir şekilde arttırdığını göstermiştir; AMPK, safranın iskelet kası hücrelerinde glikoz alımı ve insülin duyarlılığı üzerindeki etkilerinde önemli bir rol oynamaktadır [29, 30].

Milajerdi ve arkadaşlarının [31] araştırmasının sonuçlarına göre, safran hidroalkolik ekstresinin T2D hastalarında FBS serum konsantrasyonlarını azaltarak kan şekeri kontrolünü önemli ölçüde iyileştirebileceği söylenmelidir. Bununla birlikte, safran özütü, T2D hastalarında lipid serum konsantrasyonları ve kan basıncı üzerinde önemli bir etkiye sahip değildir. Bazı araştırmaların sonuçları, safran ekstraktının glisemik parametreler üzerindeki doza bağımlı olduğunu göstermiştir (Şekil 2 ve 3) [32].

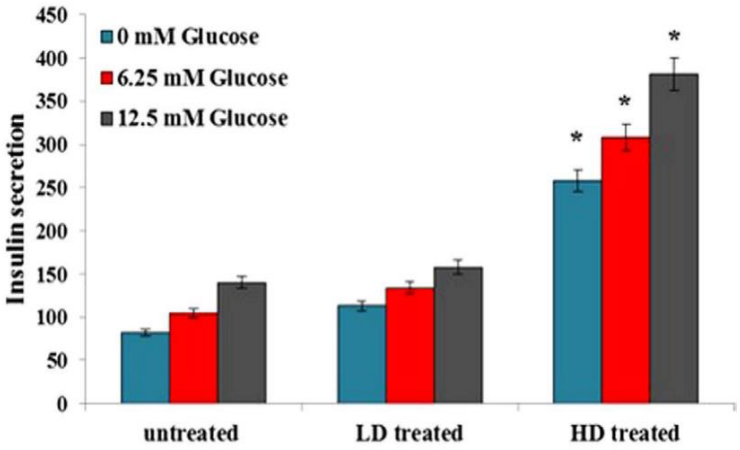

Şekil 2. Safran ekstraktının glukoz ile uyarılan insülin salınımı üzerindeki etkisi.
LD; düşük doz safran (200 µ g/ml), HD; yüksek doz safran (400 µ g/ml) [32]

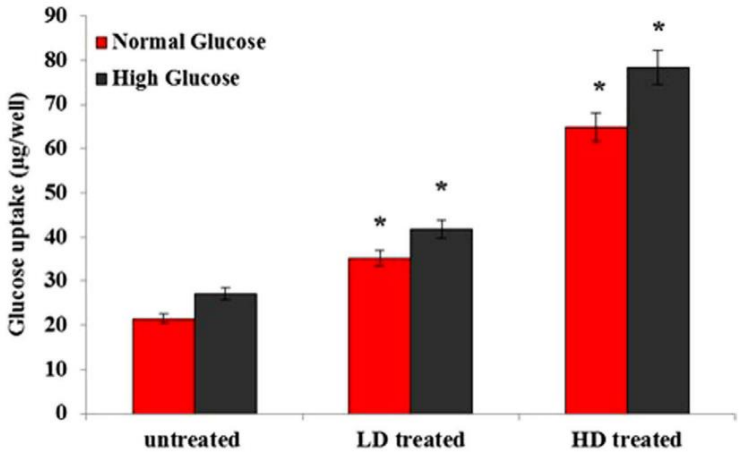

Şekil 3. Safran ekstraktının glukoz alımına etkisi.
LD; düşük doz safran (200 µ g/ml), HD; yüksek doz safran (400 µ g/ml) [32]

Tip2 Diyabet üzerinde Safran ile Egzersiz Etkisi

Streptozotosin ile indüklenen diyabetik farelerde safran ekstraktının bir kombinasyonunun ve iki haftalık eğitimin glisemik indeks üzerindeki etkisi araştırılmıştır. Sonuçlar, streptozotosin ile indüklenen diyabetik fareler safran ekstresi kombinasyonunun ve iki haftalık glisemik indeks üzerindeki etkisinin kan şekeri üzerinde önemli bir etkiye sahip olduğunu, ancak kan insülin duyarlılığı, insülin duyarlılığı ve insülin direnci üzerinde önemli bir etkisi olmadığını göstermiştir. Çalışmanın sonucuna göre, safran özü kullanımının ve aerobik egzersizin kan şekerini düşürmede etkili olabileceğini göstermiştir. Safran içerisindeki antioksidan bileşikler, glikoz alımında etkilidir ve ayrıca egzersiz, insülin benzeri bir etkiyle kan şekerini düşürmede rol oynayabilir [33].

Şirazi ve arkadaşları [5] tarafından yürütülen bir çalışmanın sonuçları, dört haftalık yüzme eğitiminin diyabetik farelerde açlık glikozunu azaltmada önemli bir etkisi olduğunu gösterdi. Dört hafta boyunca tek başına safran özü tüketirken, tek başına yüzmeye göre açlık glikozunu ve insülin direncini düşürmede daha büyük bir etkiye sahiptir. Ayrıca, tek başına yüzme antrenmanına kıyasla, yüzme antrenmanı ile birlikte safran özütü tüketimi ve tek başına safran özütü tüketimi, açlık glukozunu ve insülin direncini azaltmada daha büyük bir etkiye sahiptir.

Dehghan ve arkadaşları [32], safran ekstraktının RIN-5F hücreleri tarafından insülin salgılanmasını arttırdığını belirtti. Yüksek doz tedavide insülin sekresyonunun uyarılması anlamlıydı. Ek olarak safran, hiperglisemik ve normoglisemik koşullar altında L6 miyoblast hücrelerinde glikoz alımını önemli ölçüde uyarmıştır. İnsülin salgılanması ve glikoz emilimi, safran tarafından doza bağımlı bir şekilde uyarılmıştır, bu yüksek doz safranla tedavi edilen hücrelerde daha belirgin olmuştur. İn vivo çalışmanın

sonucu, diyabetik farelerde in vitro bulgularla birlikte altı haftalık direnç egzersizi ve/veya safran tedavisi sonrasında açlık glukozunun düştüğünü göstermiştir. Safranın antioksidan sonuçları ile ilgili olarak, insülin sekresyonu ve glukoz alımı üzerinde redoks aracılı mekanizmalar olarak hareket etme olasılığı vardır. Veriler ayrıca, safran ekstraktının altı haftalık tüketiminin diyabetik farelerde açlık glikozunu azalttığını göstermiştir. Ayrıca, direnç eğitimi ile birlikte safran takviyesi, açlık glikozunu azaltmada tek başına ekstrakt veya direnç eğitiminden daha etkili olmuştur. Altı haftalık direnç eğitiminin diyabetik farelerde insülin azalması üzerinde önemli bir etkisi olmamıştır, bu da diğer çeşitli çalışmaların bulgularıyla çelişkilidir [34, 35]. Direnç egzersizinin gelişmiş insülin direnci üzerindeki olumlu etkileri, kas hücrelerinde insülin reseptörünün güçlendirilmesi veya iskelet kası hücrelerinde glikoz taşıyıcı proteinlerin sayısının artması yoluyla elde edilebilir. Glikoz taşıyıcı proteinler ailesinden GLUT4, insüline duyarlıdır ve kas kasılması ve kaslardaki insülin yoluyla glikoz taşınmasına fayda sağlar. Bu nedenle, direnç egzersizi nedeniyle toplam kas kütlesindeki artış, insülin aracılığı ile artan bir glikoz alımına yol açar [32].

Sonuç ve Değerlendirme

Diyabet görülme sıklığı, kritik bir hastalığı temsil eden dünya çapında keskin bir şekilde artmaktadır [36]. Bazı araştırmalar, 30-40 dakikalık orta yoğunlukta yürüyüş gibi hem fiziksel aktivite protokollerinin hem de Tip2 diyabette günde 10.000 adıma ulaşmanın etkinliğini göstermiştir. Fiziksel aktivitedeki herhangi bir artış, Tip2 diyabette teşvik edilmeli ve olumlu şekilde pekiştirilmelidir. Fiziksel aktivite de uygun rehberlik ve desteğe sahip bireylerin ihtiyacına göre hedeflenmelidir [17]. Safran tüketimi ile kısa süreli egzersiz arasındaki etkileşimi, antioksidan sistemi güçlendirdiği ve kardiyorespiratuar fonksiyonu arttırdığı gösterilen bir dizi çalışma vardır. Başka çalışmalar, safran tüketimi ve uzun süreli direnç egzersizi ile gelişmiş vücut kompozisyonu, azalmış kardiyovasküler risk faktörleri ve kontrollü açlık glikozu arasındaki etkileşimi incelemiştir. Bir dizi başka çalışmanın sonuçları, safran tüketimi ile uzun süreli aerobik egzersiz arasındaki etkileşimin antioksidan sistemi güçlendirdiğini, kan şekerini iyileştirdiğini ve glisemik indeksi iyileştirdiğini göstermektedir [32]. Benzer çalışmalarda, ısırgan gibi bitkilerin ekstraktı fiziksel aktivite ile birlikte diyabet farelerin üzerinde etkili olmuştur [37].

Genel olarak safran tüketimi ve fiziksel aktivitenin etkileşimi vücudun organlarını teşvik ederek metabolizmayı düzenler. Araştırmaların çoğu, bu ikisinin korelasyon ve sinerjisinin nedenini, özellikle safran metabolitlerinin, en çok flavonoidlerin (krosetin ve krosin) yanı sıra polifenolik bileşiklerin varlığından ve safranın antioksidan savunma sisteminin artmasından söz etmiştir.

Özetle, geçmiş bulgular, bitkisel safran tüketiminin direnç egzersizi ile birlikte tüketilmesinin, in-vivo diyabetik parametreler üzerinde güçlü bir terapötik etkili faktör olduğunu göstermiştir. Bu nedenle, sağlık risk faktörlerini azaltmada direnç eğitimi ve eş zamanlı safran tüketiminin faydaları ile diyabet hastalarına hastalıklarını kontrol etmek ve yönetmek için bu faktörlerin kombinasyonundan yararlanmaları tavsiye edilir. Bununla birlikte, safranın spesifik bileşiklerinin moleküler düzeyde diyabetik parametreler üzerindeki uygun dozunu ve rolünü belirlemek için daha fazla araştırma yapılması garanti edilmektedir.

Kaynakça

[1] Agarwal P, Gupta R., Alpha-amylase inhibition can treat diabetes mellitus. Res. Rev. J. Med. Health Sci, 2016. 5(4): 1-8.
[2] Brown, A., et al., Evaluation of phenolic phytochemical enriched commercial plant extracts on the in vitro inhibition of α-glucosidase. Frontiers in nutrition, 2017. 4: 56.
[3] Pisoschi, A.M, Pop A. The role of antioxidants in the chemistry of oxidative stress: A review. European journal of medicinal chemistry, 2015. 97: 55-74.
[4] Goodpaster, B.H., et al., Skeletal muscle lipid content and insulin resistance: evidence for a paradox in endurance-trained athletes. The Journal of Clinical Endocrinology & Metabolism, 2001. 86(12): 5755-5761.
[5] Iman, A.S., H. Sayeedali, and K. Farideh, Interaction effects of hypoglycemia on aqueous extract of saffron and swimming training in streptozotocin-induced diabetic rats. 2017.
[6] Rokling-Andersen, M.H., et al., Effects of long-term exercise and diet intervention on plasma adipokine concentrations. The American journal of clinical nutrition, 2007. 86(5): 1293-1301.

[7] Sriwijitkamol, A., et al., Effect of acute exercise on AMPK signaling in skeletal muscle of subjects with type 2 diabetes: a time-course and dose-response study. Diabetes, 2007. 56(3): 836-48.
[8] Ahmadpoor, A., et al., The effect of exercise and physical activity on blood glucose. Pious inside the country, 2020.
[9] Zanuso, S., et al., Exercise for the management of type 2 diabetes: a review of the evidence. Acta Diabetol, 2010. 47(1): 15-22.
[10] O'Neill, H.M., AMPK and Exercise: Glucose Uptake and Insulin Sensitivity. Diabetes Metab J, 2013. 37(1): 1-21.
[11] Hills, A., et al., Resistance training for obese, type 2 diabetic adults: a review of the evidence. Obesity reviews, 2010. 11(10): 740-749.
[12] Thomas, D., E.J. Elliott, and G.A. Naughton, Exercise for type 2 diabetes mellitus. Cochrane database of systematic reviews, 2006(3).
[13] Stephens, B.R., et al., Effect of timing of energy and carbohydrate replacement on post-exercise insulin action. Applied Physiology, Nutrition, and Metabolism, 2007. 32(6): 1139-1147.
[14] Richter, E.A., et al., Enhanced muscle glucose metabolism after exercise: modulation by local factors. American Journal of Physiology-Endocrinology And Metabolism, 1984. 246(6): E476-E482.
[15] Malin, S.K., et al., Exercise Intensity Modulates Glucose-Stimulated Insulin Secretion when Adjusted for Adipose, Liver and Skeletal Muscle Insulin Resistance. PLoS One, 2016. 11(4): e0154063.
[16] Colberg, S.R., et al., Exercise and type 2 diabetes: the American College of Sports Medicine and the American Diabetes Association: joint position statement executive summary. Diabetes care, 2010. 33(12): 2692-2696.
[17] Guglani, R., S. Shenoy, and J.S. Sandhu, Role of Pedometer Based Walking in the Management of Type 2 Diabetes: A Review. Inter J Sci Res, 2014. 3: 449-452.
[18] Misra, A., et al., Consensus physical activity guidelines for Asian Indians. Diabetes technology & therapeutics, 2012. 14(1): 83-98.
[19] Avery, M. and A. Walker, Acute effect of exercise on blood glucose and insulin levels in women with gestational diabetes. Journal of Maternal-Fetal Medicine, 2001. 10(1): 52-58.
[20] Patel, N.S., et al., Mitigating reductions in glucose during exercise on closed-loop insulin delivery: the Ex-Snacks study. Diabetes technology & therapeutics, 2016. 18(12): 794-799.
[21] Francois, M.E., et al., 'Exercise snacks' before meals: a novel strategy to improve glycaemic control in individuals with insulin resistance. Diabetologia, 2014. 57(7): 1437-1445.
[22] Scheiner, G., Unleash Your Inner Exercise Expert! AADE in Practice, 2014. 2(3): 16-21.
[23] Arasteh, A., et al., Crocus sativus on serum glucose, insulin and cholesterol levels in healthy male rats. Journal of Medicinal Plants Research, 2010. 4(5): 397-402.
[24] Tahereh, F. and S. Saeed, The effect of saffron (Crocus sativus L.) and its ingredients on the management of diabetes mellitus and dislipidemia. African Journal of Pharmacy and Pharmacology, 2014. 8(20): 541-549.
[25] Aruoma, O.I., et al., Free radicals, antioxidants and diabetes: embryopathy, retinopathy, neuropathy, nephropathy and cardiovascular complications. Neuroembryology and Aging, 2006. 4(3): 117-137.
[26] Maghrani, M., J.B. Michel, and M. Eddouks, Hypoglycaemic activity of Retama raetam in rats. Phytotherapy Research: An International Journal Devoted to Pharmacological and Toxicological Evaluation of Natural Product Derivatives, 2005. 19(2): 125-128.
[27] Farkhondeh, T. and S. Samarghandian, The effect of saffron (Crocus sativus L.) and its ingredients on the management of diabetes mellitus and dislipidemia. African Journal of Pharmacy and Pharmacology, 2014. 8(20): 541-549.
[28] Elgazar, A.F., A.A. Rezq, and H.M. Bukhari, Anti-hyperglycemic effect of saffron extract in alloxan-induced diabetic rats. Eur J Biol Sci, 2013. 5(1): 14-22.
[29] Kang, C., et al., Saffron (Crocus sativus L.) increases glucose uptake and insulin sensitivity in muscle cells via multipathway mechanisms. Food Chem, 2012. 135(4): 2350-8.
[30] Kang, C., et al., Saffron (Crocus sativus L.) increases glucose uptake and insulin sensitivity in muscle cells via multipathway mechanisms. Food chemistry, 2012. 135(4): 2350-2358.

[31] Milajerdi, A., et al., The effect of saffron (Crocus sativus L.) hydroalcoholic extract on metabolic control in type 2 diabetes mellitus: A triple-blinded randomized clinical trial. J Res Med Sci, 2018. 23: 16.
[32] Dehghan, F., et al., Saffron with resistance exercise improves diabetic parameters through the GLUT4/AMPK pathway in-vitro and in-vivo. Sci Rep, 2016. 6: 25139.
[33] Nikpoursardaei, A., M.A. Azarbayjani, and M. Piri, The effect of a combination of saffron aqueous extract and two weeks of training on glycemic index in streptozotocin-induced diabetic rats. Pious inside the country, 2011.
[34] Dunstan, D.W., et al., High-intensity resistance training improves glycemic control in older patients with type 2 diabetes. Diabetes care, 2002. 25(10): 1729-1736.
[35] Dunstan, D.W., et al., Community center–based resistance training for the maintenance of glycemic control in adults with type 2 diabetes. Diabetes care, 2006. 29(12): 2586-2591.
[36] Samarghandian, S., M. Azimi-Nezhad, and T. Farkhondeh, Immunomodulatory and antioxidant effects of saffron aqueous extract (Crocus sativus L.) on streptozotocin-induced diabetes in rats. Indian heart journal, 2017. 69(2): 151-159.
[37] Norouzi, S., M. Rahmati, and R. Mirnsuri, The effect of six weeks of endurance training with nettle hydroalcoholic extract on neuropathic pain in male Wistar rats with diabetic neuropathy. Peshnehade, 2017.

Consumer Perception of Ready-To-Eat Fruits Sold in Ogun and Lagos, Nigeria During the Covid-19 Pandemic

Wasiu Ayodele Abibu[1], AbdulWasiu Sakariyau[2], Gafar Bamigbade[3], Amos Kolawole Oyebisi[4], Isqeel Ogunsola[5]*
[1]Dokuz Eylul University, Department of Biotechnology, The Graduate School of Natural and Applied Sciences, Izmir, Turkey
[2]Crescent University, Department of Microbiology, Abeokuta, Nigeria
[1,3,4]Federal University of Agriculture, Department of Microbiology, Abeokuta, Nigeria
[5]Federal University of Agriculture, Department of Statistics, Abeokuta, Nigeria
**Corresponding author: abibu@funaab.edu.ng*

Abstract

Covid-19 pandemic is a global health issue that adversely affected every sector of the world's economy. Fruits are known to be a source of vitamins providing the body with necessary defense against infections (inclusive of Coronaviruses). Nigerians prefer to buy ready-to-eat (RTE) fruits than whole fruits due to their high prices. Consumer perception of RTE fruits sold in Ogun and Lagos, Nigeria during the Covid-19 pandemic months in 2020 and within January and March 2021 via an online survey were compared. Ogun and Lagos states were selected because they represent major entry routes for land and air travel into Nigeria respectively. 500 respondents were obtained with 49.7% each as male and female respectively in Ogun state while Lagos had 49.5% and 50.5% of the male and female gender. In addition, the predominant age group that responded to the questionnaire falls within 21 – 30 with 49.7% in Ogun state and 54.1% in Lagos state. 96.1% of the respondents in Ogun state had a tertiary education while 99% was recorded to possess tertiary education in Lagos state. 34% respondents took RTE fruits 2- 3 times a week, 31.2% less than once a week while only 2.8% took RTE fruits 4 – 5 times a week. From the survey, 84% of the respondents were aware that fruits possess needed vitamins to fight infections while only 87.4% of the respondent were aware of fruit borne poisoning and have knowledge of fruit borne pathogens like *Staphylococcus aureus*, *Escherichia coli*, *Klebsiella spp*, *Pseudomonas aeruginosa*, *Penicillium spp*, *Aspergillus niger* and *Rhizopus stolonifer*. This study shows that fruit consumers neglected health consciousness in the purchase of RTE fruits in Ogun and Lagos in the first 3 months of 2021 compared to 2020. This negligence may result in a spike of another Covid-19 wave in Ogun and Lagos if the necessary food and health regulatory authorities fail to act timely. Also, the application of an effective hazard analysis and critical control point (HACCP) application reduces the chance of contamination of ready- to- eat fruits.

Keywords: fruits, ready to Eat, Covid-19, Coronavirus

Introduction

Fruits are important for the wellbeing of the body as they possess important macro and micronutrients, vitamins and fiber needed by man. The role of fruits in the prevention of diseases has been documented by Kalia and Gupta (2006) [1]. According to Muinde *et al* (2005) and Barro *et al* (2006), the possibility of illnesses and food borne outbreak arising from Ready to Eat fruits (RTE) fruits consumption were high due to poor hygienic practices by fruit handlers, numerous possible routes of contamination and non-involvement of food and health regulatory authorities in certifying the safety in consumption of RTE fruits [2-3].

Illnesses arising from consumption of fruits and foods keep increasing annually most especially in developing nations where advanced technology for food and fruit processing are lacking (FAO and WHO, 1983) [4]. RTE are fruits requiring little or no processing before being consumed. The concept of RTE foods is common in Africa particularly in Nigeria where fruits are being cut and nylon packed before being sold to consumers. Increasing rate of unemployment drove youths into the RTE fruit business coupled with increasing rise in cost of whole fruits. Most consumers of RTE fruits are the low and middle income earners of the population with little or no idea of fruit borne illnesses while individuals involved in RTE fruits business exhibit zero hygienic measures during fruits preparation. Oranusi and Olorunfemi (2011) researched on the Microbiological safety evaluation of street vended ready to eat fruits in a local market and a University cafeteria in Nigeria [5]. High coliform and fungal

counts were obtained from the study. Identified food borne pathogens from the study are Bacillus spp, *S. aureus*, Penicillium spp, *Aspergillus niger*, *E. coli*, Enterobacter, Salmonella, Klebsiella and Mucor spp. Afolabi *et al* (2015) also researched on Microbial safety of RTE fruits sold in Abeokuta, Nigeria. Identified microbial pathogens were the same to the findings of Oranusi and Olorunfemi (2011) [6]. Afolabi *et al* (2015) suggested the possibility of fruit disinfection in chlorinated water in order to reduce microbial contamination prior to cutting of fruits and packaging in polyethylene [6].

On the 30th of January 2020, the novel coronavirus, COVID-19, was declared by the WHO, as a Public Health Emergency of International Concern. It had spread to several countries and world governments alerted their citizens to the possibility of a global pandemic. Nigeria was no exception; mandatory quarantine was imposed on travelers arriving from China, while the Public Health Emergency Operation Centers in states were strengthened [7]. In addition, through the Nigeria Centre for Disease Control (NCDC) in collaboration with the Africa Centre for Disease Control (Africa CDC) and with the support of the World Health Organization (WHO) and Infection Control Network Africa (ICNA) training for the prevention and control of COVID-19 was initiated [8]. Alas, the pandemic had its way, on 27th of February 2020; The Federal Ministry of Health confirmed the nation's first coronavirus disease (COVID-19) case in Lagos State [9]. One year on, and COVID-19 has turned out to be the worst pandemic the world has faced in a long time. In Nigeria, as at April 2021, the numbers are thus: 1,870,915 tests, 164,633 confirmed cases, 7,929 active cases and 2,061 deaths [10]. However, the effect of COVID-19 stretch far beyond numbers, behavior, choices and lives of people affected.
Food and fruits have been implicated as vehicles in the transmission of food borne illnesses. Undoubtedly, food may act as a vehicle in the transmission of COVID-19. Although, no literature exist to back this claim, however, food and fruit handlers may make this possible via poor personnel handlings of fruits, surfaces and other packaging materials used for RTE fruits before final consumption by buyers (Yetka *et al*, 2020) [11] . This may be a possible route for an indirect COVID-19 transmission through RTE fruits. The present research studies Consumer perception of RTE fruits Sold in Lagos and Ogun States, Nigeria during the COVID-19 pandemic. Lagos and Ogun States were chosen for the research as they represent major air and land boarders to Nigeria.

Materials and Methods

Sample and Sampling Techniques

This study recruited a total of 500 participants using the snowball sampling technique. The participants were residence of Ogun and Lagos States of Nigeria.

Instrumentation

This study was an online survey and a self-structured web-based questionnaire was used for data collection. The questionnaire has five sections and consisted of 28 items in all sections. To ensure content validity of the instrument, the initial draft of the questionnaire was reviewed by a food safety expert and necessary corrections were made. The reliability of the instrument was also ensured through a trial test on a sample of 50 participants. Reliability test was done using Cronbach's alpha and a value of 0.791 was obtained.

Procedure for Data Collection

The survey was conducted online with the use of Google Forms. The link to the survey was shared via WhatsApp and Facebook. Consents of the prospective participants were sought in order to allow only residents of Ogun and Lagos States to participate in the survey. The participants were encouraged to take the survey once and they could share the survey link with their acquaintances.

Data Analysis

Data obtained were analysed using Statistical Package for Social Sciences (SPSS) version 21. Descriptive statistics (frequencies and percentages) were used to analyse the socio-demographic characteristics of the participants and the distribution. Analysis of Variance (ANOVA) was used to analyse parameters and the means were compared between the two states.

Results

Socio-Demographic Characteristics

Table 1 shows the socio-demographic characteristics of the participants. The total number of participants was 500. Half of the participants were female; most of the participants were in the age group 21-30 and 31-40 years. All the participants have at least secondary education while most of them have tertiary education in the two states. Quite a number of the participants were Civil servants and students while few were unemployed.

Table 1. Socio-demographic characteristics of the participants

		Location			
		Ogun State (N=306)		Lagos State (N=194)	
		Frequency	Percentage (%)	Frequency	Percentage (%)
Gender	Male	152	49.7	96	49.5
	Female	152	49.7	98	50.5
	Prefer not to say	2	0.6	0	0.0
	Total	306	100.0	194	100.0
Age Group	Below 20 years	32	10.5	12	6.1
	21 - 30 years	152	49.7	105	54.1
	31 - 40 years	76	24.8	51	26.2
	41 - 50 years	42	13.7	26	13.6
	Above 50 years	4	1.3	0	0.0
	Total	306	100.0	194	100.0
Level of Education	Primary Education	0	0.0	0	0.0
	Secondary Education	12	3.9	2	1.0
	Tertiary Education	294	96.1	192	99.0
	Total	306	100.0	194	100.0
Occupation	Civil servant	96	31.4	51	26.3
	Trader	20	6.5	20	10.4
	Artisan	31	10.2	28	14.4
	Medical and Health practitioner	30	9.8	18	9.3
	Student	61	19.9	36	18.5
	Unemployed	20	6.5	9	4.6
	Others	48	15.7	32	16.5
	Total	306	100.0	194	100.0

Shopping Preferences for RTE Fruits

All the participants indicated that they ate one or more RTE fruits before the COVID-19 pandemic. Most of them 344(68.8%) stated that they ate the selected RTE fruits at least once in a regular week while 156(31.2%) ate it less than once in a week (Table 2). The fruits were mostly purchased from street hawkers and vendors 320(64%) and fruit stalls 148(29.6%). More so, more than half of the participants 284(53.6%) claimed that the pandemic influenced their shopping preferences. People who purchased their fruits from street hawkers and vendors less than once in a week significantly increased from 178 (35.6%) before pandemic to 242(48.4%) during pandemic (Table 2).

Hygienic Measures on Consumption of RTE Fruits before and During Pandemic

Higher number of the respondents 436(87.2%) indicated that they do wash their hands before and after eating RTE fruits before the pandemic. However, the number increased to 466(93.2%) during the pandemic. There was also an increment in the number of respondents who wash/rinse their RTE fruits before consumption from 464(92.8%) before pandemic to 480(96.0%). Similar trend was recorded for

number of respondents who properly dispose wastes from RTE fruits from 482(96.4%) before pandemic to 490(98%) during pandemic (Table 3).

Table 2. Shopping preferences for RTE fruits

		Location					
		Ogun State (N=306)		Lagos State (N=194)		Total (N=500)	
		Frequency	Percentage (%)	Frequency	Percentage (%)	Frequency	Percentage (%)
In a regular week, how often do you eat the selected fruits before the COVID-19 pandemic?	Daily	14[a]	4.6	4[a]	2.1	18	3.6
	Once a week	90[a]	29.4	52[a]	26.8	142	28.4
	2 - 3 times a week	106[b]	34.6	64[a]	33.0	170	34
	4 -5 times a week	10[a]	3.3	4[a]	2.1	14	2.8
	Less than once a week	86[ab]	28.1	70[b]	36.1	156	31.2
	Total	306	100.0	194	100.0	500	100.0
Where do you purchase your RTE fruits before the COVID-19 pandemic?	Directly from farmers	10[a]	3.3	4[a]	2.1	14	2.8
	Fruit stalls	94[a]	30.7	54[b]	27.8	148	29.6
	Street hawkers & vendors	194[a]	63.4	126[a]	64.9	320	64
	Supermarket	8[a]	2.6	10[a]	5.2	18	3.6
	Total	306	100.0	194	100.0	500	100.0
Would you continue to purchase RTE fruits at the same place during this pandemic?	No	134	43.8	86	44.3	220	44
	Yes	172[a]	56.2	108[a]	55.7	280	56
	Total	306	100.0	194	100.0	500	100
Does COVID-19 pandemic influence your shopping preference for RTE fruits?	No	126	41.2	90	46.4	216	43.2
	Yes	180	58.8	104	53.6	284	56.8
	Total	306	100.0	194	100.0	500	100.0
Have you ever purchased RTE fruits from street hawkers and vendors in the last 15 months?	No	36	11.8	32	16.5	68	13.6
	Yes	270	88.2	162	83.5	432	86.4
	Total	306	100.0	194	100.0	500	100.0
In a regular week, how often do you buy RTE fruits from street hawkers and vendors before the pandemic?	2 - 3 times a week	92[b]	30.1	44[ab]	22.7	136	27.2
	4 - 5 times a week	12[a]	3.9	18[a]	9.3	30	6.0
	Daily	16	5.2	8	4.1	24	4.8
	Less than once a week	104[a]	34.0	74[a]	38.1	178	35.6
	Once a week	82[a]	26.8	50[a]	25.8	132	26.4
	Total	306	100.0	194	100.0	500	100.0
In a regular week, how often do you buy RTE fruits from street	2 - 3 times a week	62[b]	20.3	30[a]	15.5	92	18.4
	4 - 5 times a week	4	1.3	6	3.1	10	2.0

hawkers and vendors during the pandemic?	Daily	10	3.3	4	2.1	14	2.8
	Less than once a week	138[a]	45.1	104[b]	53.6	242	48.4
	Once a week	92[a]	30.1	50[ab]	25.8	142	28.4
	Total	306	100.0	194	100.0	500	100.0

Values with different superscript within a row are significantly different ($p < 0.05$)

Table 3. Hygienic measures on consumption of RTE fruits before and during Pandemic

		Ogun State (N=306)		Lagos State (N=194)			
		Frequency	Percentage (%)	Frequency	Percentage (%)	Frequency	Percentage (%)
Do you wash your hands before and after eating RTE fruits before the pandemic?	No	38	12.4	26	13.4	64	12.8
	Yes	268	87.6	168	86.6	436	87.2
	Total	306	100.0	194	100.0	500	100.0
Do you wash your hands before and after eating RTE fruits during the pandemic?	No	26	8.5	8	4.1	34	6.8
	Yes	280	91.5	186	95.9	466	93.2
	Total	306	100.0	194	100.0	500	100.0
Do you wash/rinse your RTE fruits before consumption before the pandemic?	No	18	5.9	18	9.3	36	7.2
	Yes	288	94.1	176	90.7	464	92.8
	Total	306	100.0	194	100.0	500	100.0
Do you wash/rinse your RTE fruits before consumption during the pandemic?	No	14	4.6	6	3.1	20	4.0
	Yes	292	95.4	188	96.9	480	96.0
	Total	306	100.0	194	100.0	500	100.0
Do you properly dispose wastes/leftovers from RTE fruits before the pandemic?	No	10	3.3	8	4.1	18	3.6
	Yes	296	96.7	186	95.9	482	96.4
	Total	306	100.0	194	100.0	500	100.0
Do you properly dispose wastes/leftovers from RTE fruits during the pandemic?	No	6	2.0	4	2.1	10	2.0
	Yes	300	98.0	190	97.9	490	98.0
	Total	306	100.0	194	100.0	500	100.0

Compared to the pre-pandemic period, there were significant differences in the practice of good hygienic measures such as hand washing before and after food eating RTE fruits, washing RTE fruits before consumption and proper disposal of RTE fruit wastes during the pandemic (Table 4).

Table 4. Mean scores of hygienic measures on consumption of RTE fruits before and during pandemic

	Location	N	Mean	Standard Deviation
Do you wash your hands before and after eating RTE fruits before the pandemic?	Ogun	306	1.12[a]	0.33
	Lagos	194	1.13[a]	0.34
	Total	500	1.12	0.33
Do you wash your hands before and after eating RTE fruits during the pandemic?	Ogun	306	1.08[b]	0.27
	Lagos	194	1.04[ab]	0.19
	Total	500	1.06	0.23
Do you wash/rinse your RTE fruits before consumption before the pandemic?	Ogun	306	1.05[a]	0.23
	Lagos	194	1.09[ab]	0.29
	Total	500	1.07	0.26
Do you wash/rinse your RTE fruits before consumption during the pandemic?	Ogun	306	1.04[ab]	0.20
	Lagos	194	1.03[a]	0.17
	Total	500	1.03	0.18
Do you properly dispose wastes/leftovers from RTE fruits before the pandemic?	Ogun	306	1.03[a]	0.17
	Lagos	194	1.04[a]	0.19
	Total	500	1.03	0.18
Do you properly dispose wastes/leftovers from RTE fruits during the pandemic?	Ogun	306	1.01[ab]	0.13
	Lagos	194	1.02[a]	0.14
	Total	500	1.01	0.13

Values with different superscript within a column are significantly different ($p < 0.05$).

Relevance of Fruits in the Control of COVID-19

Table 5 shows the awareness of the respondents on relevance of fruits in the control of COVID-19. Almost all the respondents 496(99.2%) agreed that regular consumption of fruits contributes to general wellness of the body. Similarly, all the respondents were aware that consumption of fruits helps to boost immunity and that fruits contain vitamins which help to fight against infections. More so, 450(90%) of them were also aware that consumption of fruits contributed to people's recovery from COVID-19 infection.

Table 5. Awareness on relevance of fruits in the control of COVID-19

		Location					
		Ogun State (N=306)		Lagos State (N=194)		Total (N=500)	
		Frequency	Percentage (%)	Frequency	Percentage (%)	Frequency	Percentage (%)
Regular consumption of fruits contributes to general wellness of the body	Strongly agree	246	80.4	178	91.8	424	84.8
	Agree	56	18.3	16	8.2	72	14.4
	Disagree	0	0.0	0	0.0	0	0.0
	Strongly disagree	4	1.3	0	0.0	4	0.8
	Total	306	100.0	194	100.0	500	100.0
Consumption of fruits helps to boost immunity	Strongly agree	260	85.0	172	88.7	432	86.4
	Agree	46	15.0	22	11.3	68	13.6
	Disagree	0	0.0	0	0.0	0	0.0
	Strongly disagree	0	0.0	0	0.0	0	0.0
	Total	306	100.0	194	100.0	500	100.0
Fruits contain vitamins which	Strongly agree	246	80.4	174	89.7	420	84.0
	Agree	60	19.6	20	10.3	80	16.0
	Disagree	0	0.0	0	0.0	0	0.0

help to fight against infections	Strongly disagree	0	0.0	0	0.0	0	0.0
	Total	306	100.0	194	100.0	500	100.0
Consumption of fruits contributed to people's recovery from COVID-19 infection	Strongly agree	118	38.6	72	37.1	190	38.0
	Agree	156	51.0	104	53.6	260	52.0
	Disagree	26	8.5	18	9.3	44	8.8
	Strongly disagree	6	2.0	0	0.0	6	1.2
	Total	306	100.0	194	100.0	500	100.0

Safety of RTE Fruits for Consumption

More than 90% of the respondents were aware that RTE fruits are easily contaminated by microorganisms and that consumption of fruits contaminated by microorganisms could lead to food-borne infections such as diarrhea (Table 6). Also, 437(87.4%) of the respondents were aware that RTE fruits spoil easily but many of them were unaware of the microorganisms that cause spoilage of RTE fruits. Few of them indicated that *Escherichia coli*, *Pseudomonas marginalis*, *Clostridium botulinum*, *Corynebacterium diphteriae*, *Aspergillus niger*, *Saccharomyces cerevisae*, *Rhizopus stolonifer*, and *Penicillium digitatum* causes spoilage of fruits. However, almost 75% of the respondents agreed that RTE fruits are safe for consumption.

Table 6. Awareness on safety of RTE fruits for consumption

		Location					
		Ogun State (N=306)		Lagos State (N=194)		Total (N=500)	
		Frequency	Percentage (%)	Frequency	Percentage (%)	Frequency	Percentage (%)
RTE fruits are easily contaminated by microorganisms	Strongly agree	106	34.6	70	36.1	176	35.2
	Agree	170	55.6	108	55.7	278	55.6
	Disagree	28	9.2	16	8.2	44	8.8
	Strongly disagree	2	0.7	0	0.0	2	0.4
	Total	306	100.0	194	100.0	500	100.0
Consumption of RTE fruits can lead to food poisoning and food-borne infections such as diarrhea	Strongly agree	80	26.1	60	30.9	140	28.0
	Agree	138	45.1	94	48.5	232	46.4
	Disagree	80	26.1	38	19.6	118	23.6
	Strongly disagree	8	2.6	2	1.0	10	2.0
	Total	306	100.0	194	100.0	500	100.0
RTE fruits spoil easily	Strongly agree	76	24.8	64	33.0	140	28.0
	Agree	190	62.1	102	52.6	292	58.4
	Disagree	40	13.1	28	14.4	68	13.6
	Strongly disagree	0	0.0	0	0.0	0	0.0
	Total	306	100.0	194	100.0	500	100.0
RTE fruits are unsafe for consumption	Strongly agree	12	3.9	10	5.2	22	4.4
	Agree	62	20.3	38	19.6	100	20.0
	Disagree	194	63.4	122	62.9	316	63.2
	Strongly disagree	38	12.4	24	12.4	62	12.4
	Total	306	100.0	194	100.0	500	100.0

Discussion

The main objective of this research was to evaluate the changes in the consumer perception of ready to eat fruits during the global COVID-19 pandemic in Lagos and Ogun states of Nigeria. Overall, most of the respondents from the two states posited that COVID-19 has a significant influence on their choice

and shopping of RTE fruits. It is worthy of note to state that amidst the overall influence, there was no difference in the magnitude at which consumers purchase fruits before and during the pandemic. Also, a significant increase was observed on washing of hands before and after consuming RTE fruits during the pandemic. It is also interesting we observed that highest number of respondents strongly agree that regular consumption of fruits contributes to general wellness of the body and helps to boost immunity. Most of the respondents in the two states also agree that fruits contribute to recovery from COVID-19 infection and that RTE fruits are easily contaminated by microorganisms, consumption of RTE fruits can result into food poisoning and food-borne infections and RTE fruits spoil easily.

The findings are in line with Janssen *et al*., 2021 [12] who in their study reported that there was a significant difference on the consumption of food before and during the pandemic. Food choices are undoubtedly dynamic but relatively stable and highly driven by many factors like age, religion, economic status and state of the nation. The findings is also in consonance with the work of Faour-Klingbeil *et al*., 2021 [13] who reported in their study that there were no substantial differences in the number of time consumers shopped for food before and during the pandemic. This may be as a result of many factors among which are the household needs, availability of storage and preservation facilities and chiefly economic situation of the consumers as well as assurance on the safety of the RTE fruits owing to the ravaging pandemic. For example, Jribi *et al*. (2020) [14] posited that 67% of the consumers in Tunisia trusted shopping in the supermarkets due to the proper implementation of the stores' safety measures such as social distancing and continuous cleaning and hygiene. Similar to our study, the authors posited that more than a third (39.8%) of the Tunisian consumers performed food shopping once a week, 31.0% two or three times a week, 15.0% daily, and 7.5% every 2 weeks, and 3.5% once a month. Also, only a small percentage of Tunisian consumers (2.1%) relied on food delivery or bought their foods online [14].

A comparison of the pre and during COVID-19 period revealed a significantly higher number of people were practicing hand washing before and after handling the fruits. Frequent hand washing remains the most campaigned and recommended practices for combating Covid-19, however only 8.8% increase in frequent hand washing before and after RTE fruits consumption were observed in the survey subjects. Also, a 3.2% increment was observed from the respondents who wash/rinse their RTE fruits before consumption during the pandemic. More so, the data generated reveal an increase of 1.6% in attitude related to the proper disposal of the RTE fruits wastes and leftovers during the pandemic in Lagos and Ogun states. Several information from international sources (Center for Food Safety & Applied Nutrition, 2020a, 2020b; WHO, 2020) [15-17] indicating the unavailability of reports that the COVID-19 virus can be transmitted via fruits from the store or RTE fruits from hawkers but with a focus that primary infection route is respiratory were televised on local television stations; however, indirect contact with contaminated surfaces and objects would had been reported to play a role in the transmission cycle (Al Hurra, 2020; Nesan; News, 2020; Nidaa al watan, 2020; R´epublique Tunisienne Minist`ere dela Sant´e, 2020). [18-21]. Hence, to reduce the potential risk of coming in contact with RTE fruits previously exposed to the COVID-19 virus, handling of RTE fruits should be followed by hand washing or using hand sanitizer [22]. There is no evidence that food is a route of transmission of SARSCoV-2. However, the coronavirus transmission to fresh fruits and vegetables through an infected person via sneezing or coughing directly on them suggested caution in washing FFV unless they are cooked [23].

The data generated also indicated that most of all the respondents 99.2% concur that fruits consumption contributes to general body wellness and contributes to immunity. Similarly, 90% of the respondents stated that consumption of fruits contributes to people recovery from COVID-19. This observed data could be traced to the awareness created on fruits containing certain vitamins and minerals which can boost immunity.

Conclusion

This study has contributed to the behavioural changes that came with COVID-19 pandemic. The COVID-19 pandemic has showed a significant dynamic in the consumption of RTE fruits in Nigeria, especially in Ogun and Lagos States. The data generated also revealed a notable perception of consumers in their precautionary measures to prevent the contamination of the RTE fruits with COVID-19 virus such as washing of hands before and after handling RTE fruits. However, as the COVID-19 pandemic

is still ravaging the world, it is essential to conduct a confirmatory research of our results in larger population studies.

References

[1] Kalia, RP. Gupta, Fruit Microbiology, in: Hui, YHJ, Cano, MP, Gusek, W, Sidhu, JW, Sinha, NK. (Eds.), Handbook of fruit and fruit processing, 1st Edition, Blackwell publishing, 2006, pp. 3-28
[2] Muinde, OK, Kuria, E. Hygienic and sanitary practices of vendors of street foods in Nairobi, Kenya, AJFAND. 2005; 5: 1-3.
[3] Barro, N, Iboudo, I, Traore, AS. Hygienic status assessment of dishwater, utensils, hands and pieces of money in street food vending sites in Ouagadougou, Burkina Faso, African Journal, Biotechnol. 2006; 5: 1107-1112.
[4] FAO/WHO. 1983. The role of food safety in health and development. Report of the Joint FAO/WHO Expert Committee on Food Safety. Geneva: World Health Organization.
[5] Oranusi, S and Olorunfemi, OJ. Microbiological safety evaluation of street vended ready-to-eat fruits sold in Ota, Ogun state, Nigeria. International Journal of Research in Biological Sciences. 2011; 1 (3): 27-32.
[6] Afolabi, OR, Oloyede, RA, Abibu, WA, Adeyanju, A. Microbial Safety of Polythene Packaged Sliced fruits sold in Abeokuta, South-West Nigeria. Journal of Natural Sciences Research. 2011; 5 (13): 16-21.
[7] https://ncdc.gov.ng/news/222/3rd-february-2020%7C-public-health-advisory-to-nigerians-on-novel-coronavirus-%28%233%29. Accessed 4th May, 2021.
[8] https://ncdc.gov.ng/news/226/nigeria-leads-training-on-infection-prevention-and-control-to-strengthen-coronavirus-preparedness-in-africa. Accessed 4th May, 2021.
[9] https://ncdc.gov.ng/news/227/first-case-of-corona-virus-disease-confirmed-in-nigeria. Accessed 4th May, 2021.
[10] https://covid19.ncdc.gov.ng/. Accessed 4th May, 2021.
[11] Yekta, R, Vahid-Dastjerdi, L, Norouzbeigi, S, Mortazavian, AM. Food Products as Potential Carriers of SARS-CoV-2. Food Control, 2020; 107754. doi:10.1016/j.foodcont.2020.107754.
[12] Janssen, M, Chang, BPI, Hristov, H, Pravst, I, Profeta, A, Millard, J. Changes in Food Consumption during the COVID-19 Pandemic: Analysis of Consumer Survey Data from the First Lockdown Period in Denmark, Germany, and Slovenia. Frontiers in Nutrition. 2021; 8:635859. doi: 10.3389/fnut.2021.635859.
[13] Faour-Klingbeil, D, Osaili, MT, Al-Nabulsi, AA, Jemni, M, Todd, ECD. An on-line survey of the behavioral changes in Lebanon, Jordan and Tunisia during the COVID-19 pandemic related to food shopping, food handling, and hygienic practices. Food Control. 2021; 25:1-10.
[14] Jribi, S, Ben Ismail, H, Doggui, D, Debbabi, H. COVID-19 virus outbreak lockdown: What impacts on household food wastage? Environ. Dev. Sustain. 2020; 22: 3939–3955.
[15] Center for Food Safety, & Applied Nutrition. Food safety and the coronavirus disease 2019 (COVID-19). FDA; FDA. https://www.fda.gov/food/food-safety-during-emergencies/food-safety-and-coronavirus-disease-2019-covid-19. 2020. Accessed 7th May, 2021.
[16] Center for Food Safety and Applied Nutrition. Shopping for food during the COVID-19 pandemic—information for consumers. FDA; FDA. https://www.fda.gov/food/food-safety-during-emergencies/shopping-food-during-covid-19-pandemic-information-consumers. 2020. Accessed 7th May, 2021.
[17] WHO. (2020). Q&A: Food safety and nutrition related to COVID-19 [the world health Organization]. https://www.who.int/westernpacific/news/q-a-detail/food-safety-and-nutrition. 2020. Accessed 7th May, 2021.
[18] Al Hurra. Sanitization of purchases. Important facts that will change your behavior in shopping. www.alHurra.com. https://rb.gy/zk6llu. 2020. Accessed 12th May, 2021
[19] News, N. Food and Drug Administration: Corona is not transmitted through food. Nesan News. http://nesannews.org/?id=144911. 2020. Accessed 7th May, 2021.
[20] Nidaa al watan. The World Health Organization: Corona is not transmitted via food. Nidaa El Watan. https://rb.gy/cgop17. 2020. Accessed 7th May, 2021.

[21] République Tunisienne, Ministère de la Santé. (2020). Adaptation du Plan de Riposte “2P2R COVID-19” pendant la phase d’ouverture des Frontieres. Observatoire national des maladies nouvelles et emergentes. R´epublique Tunisienne Minist`ere de la Sant´e. August 27, 2020 http://www.santetunisie.rns.tn/images/01_07_2020_procedures.pdf.
[22] Seymour, CW, MCcreary, EK, Stegenga, J. Sensible Medicine - Balancing Intervention and Inaction During the COVID-19 Pandemic. *JAMA*. 2020; 324 (18): 1827–1828. doi: 10.1001/jama.2020.20271.
[23] French National Academy of Medicine. (2020). Hygiene at home : A bulwark against COVID-19 to be protect from SARS-CoV-2. Bulletin de l’Academie Nationale de Medecine. https://doi.org/10.1016/j.banm.2020.05.020.

Sectional Ductility of Wide Beams

Ornela Lalaj Şen[1], Mehmet Çevik[2], Ali Haydar Kayhan[3]*
Izmir Katip Çelebi University, Department of Civil Engineering, Izmir, Turkey
Izmir Katip Çelebi University, Department of Mechanical Engineering, Izmir, Turkey
Pamukkale University, Department of Civil Engineering, Denizli, Turkey
**Corresponding author: lalaj.ornela@gmail.com*

Abstract

Wide beam structures are categorized as Limited Ductility Class in Turkey and elsewhere and considered not fit for construction in areas of high seismicity. One of the main reasons that wide beam structures are considered to possess limited ductility is the perceived low local ductility of the wide beams, due to the high reinforcement ratios.

Wide beams have small depths, which indeed require higher reinforcement ratios to produce the necessary moment capacities, as compared to normal beams. However, the low local ductility of the wide beams can be contested. This paper presents a database of more than 150 beam sections, some of which are normal and some of which are wide beams. The moment-rotation relationships were computed for all the sections, and the sectional ductility was calculated from the yield and ultimate rotations.

The relations between sectional ductility and other parameters such as section aspect ratio, longitudinal reinforcement ratio and transverse reinforcement ratio were investigated. An example of the relation between ductility and section properties, in this case section aspect ratio is shown. Both positive and negative ductility were calculated and plotted. It should be noted that beams with section ratio of 0.5 are conventional beams, while the rest are wide beams. The values of ductility vary for all beams, and conventional beams have a slightly wider spread.

While these parameters vary within the section database, the sectional ductility oscillates around 30, and no clear correlations could be established for any of the above-mentioned parameters. There were no significant differences between the average sectional ductility of conventional and wide beams. For this dataset, the mean positive ductility was 29.66 and 29.33 for conventional and wide beams respectively, and the mean negative ductility was 28.96 and 31.50 for conventional and wide beams, respectively.

Keywords: ductility, wide beams, aspect ratio, reinforcement ratio

Introduction

Wide and shallow beams are reinforced concrete (RC) beams that have limited depth, which is generally compensated by greater widths than normal beams. Such beams are thought to have limited sectional rotational ductility, due to the high reinforcement ratios that are needed to provide sufficient moment capacities in beams of limited depths.

In this study a large database of beam sections was analyzed analytically to obtain their moment-rotation curves. The ductility calculated from the moment-rotation curves was related to parameters that define the beam sections such as:

- Aspect ratio
- Longitudinal reinforcement ratio
- Transverse reinforcement ratio

Ductility is simply defined as the ratio of the ultimate deformation to the yield deformation, which can be displacement, deflection, rotation etc. There are various studies [1-3] carried out on the ductility analysis of RC beams. Performing tests on full-scale beam specimens would be appropriate from where the force-deformation behavior can be obtained. Some researchers also investigated the performance of wide beam RC frames [4-6]. Additionally, the force-deformation behavior of beams can also be obtained numerically by iterative calculations until crushing of concrete or rupture of steel occurs. However, there are a considerable number of packages that facilitate these calculations. The software XTRACT, which has section drawing capabilities, the ability to generate the plastic rotation capacity based on a code assumed plastic hinge length and the option to vary the post peak bilinearization of the idealized moment curvature response, was used in this study to obtain the numerical moment- rotation relationships of the

beam sections. The beam sections were modeled and meshed. The Mander model [7] was used to model the confined concrete. The moment-rotation relationships were obtained from multistep incremental analyses of the sections.

Methodology

The materials used for the design and subsequent analyzes are C30 and B420C. The beam depths are selected as 300 mm for wide beams and 500 mm for normal beams. The width/depth aspect ratio considered in the study varies from 05 to 2.33. Longitudinal and transverse reinforcement ratios are also considered. Figure 1 shows typical sections of normal and wide beams.

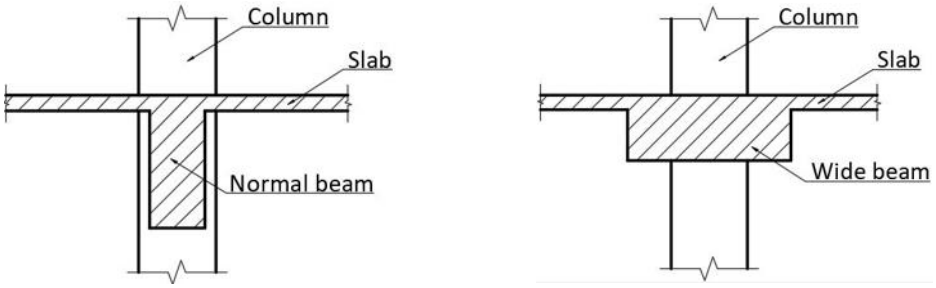

Figure 1. Typical sections of normal and wide beams

The normal beams which are considered as means of comparion have 250 mm by 500 mm rectangular sections. On the other hand, the depth of wide beams 300 mm, while their width varies between 300 mm and 700 mm.

Beams were designed according to Turkish Standards TS500 [8] and Turkish Building Earthquake Code TBEC2018 [9]. The normal beams were designed as high ductility class while the wide beams were designed as limited ductility class. The beams in this study were sections obtained from the complete design of 3D frames, therefore they had different amounts of top and bottom reinforcement, and different positive and negative moment capacities. The moment-rotation relationships, and consequently ductility, were calculated for both positive and negative moment loading directions.

Results of Analysis

In this section, the effects of longitudinal and transverse reinforcement on sectional ductility are presented in graphical form.

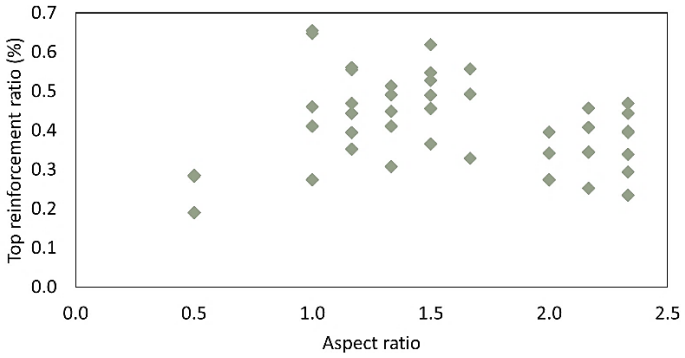

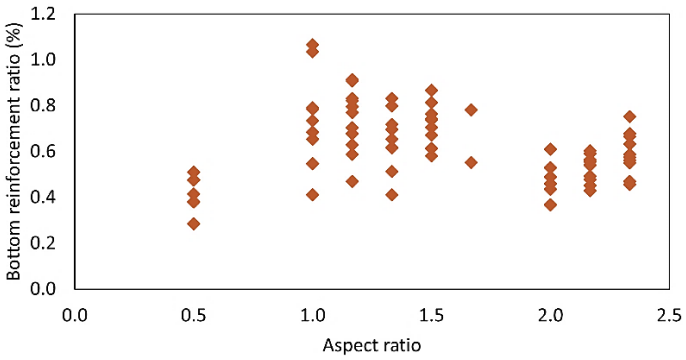

Figure 2. The variance of top and bottom reinforcement ratios with respect to aspect ratio

Figure 2 illustrates the variance of top and bottom reinforcement ratios with respect to aspect ratio. In this figure, all normal beams have an aspect ratio of 0.5 while the beams with aspect ratios of 1.00, 1.17, 1.33, 1.50, 1.67, 2.00, 2.17 and 2.33 are all wide beams. As observed from the graph, generally the normal beams have lower longitudinal reinforcement ratios than wide beams, both for top and bottom.

Figure 3 illustrates the variance of transverse reinforcement ratio with respect to aspect ratio. In some of the wide beams the transverse reinforcement ratio is similar or greater than the ratio of normal beams; however, in most of the cases wide beams have lower transverse reinforcement ratios than normal beams.

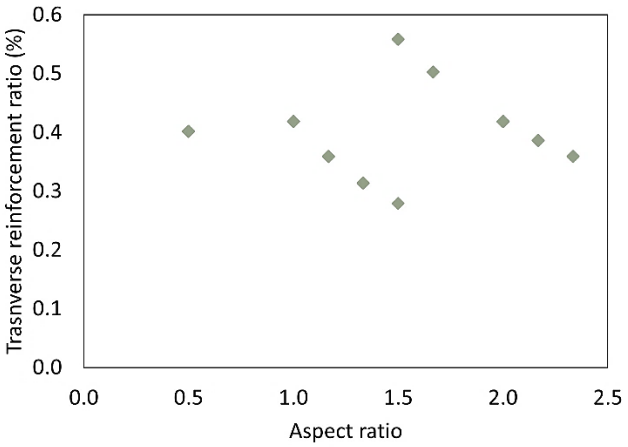

Figure 3. The variance of transverse reinforcement ratio with respect to aspect ratio

The effect of aspect ratio on sectional ductility is illustrated in Figure 4. The ductility of the beam sections considered for this purpose varies between 18 and 37; however, some data are extreme and not very often. On the other hand, most of the values of the ductility range between 25 and 35. This demonstrates that no correlation, such as linear or polynomial can be set between ductility and section aspect ratio. However, the values of ductility oscillate around 30.

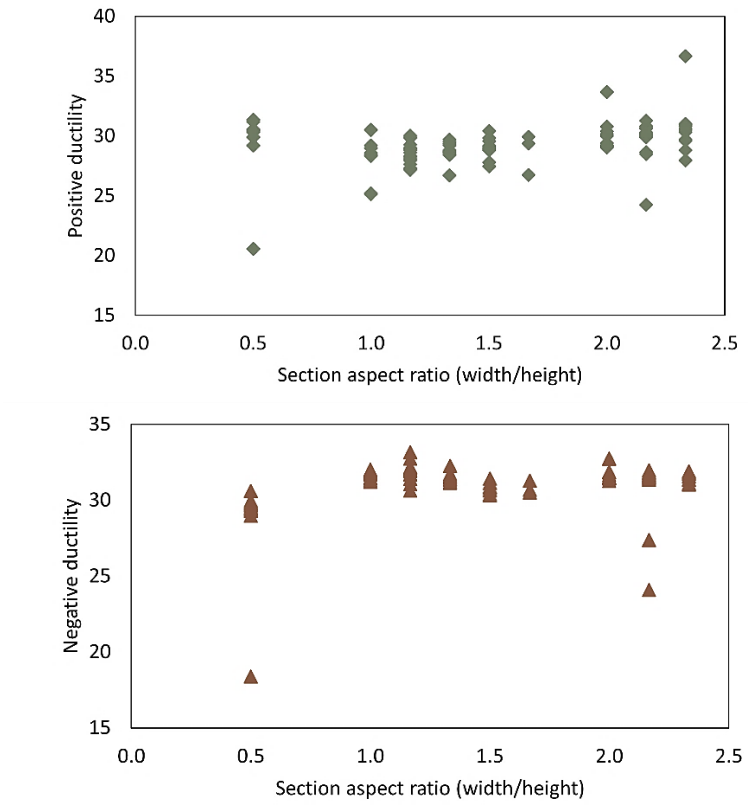

Figure 4. The effect of aspect ratio on sectional ductility

The effect of longitudinal reinforcement ratio on sectional ductility is illustrated in Figure 5. According tho the graphs, there does not seem to be any clear trend or correlation between the ductility and longitudinal reinforcement.

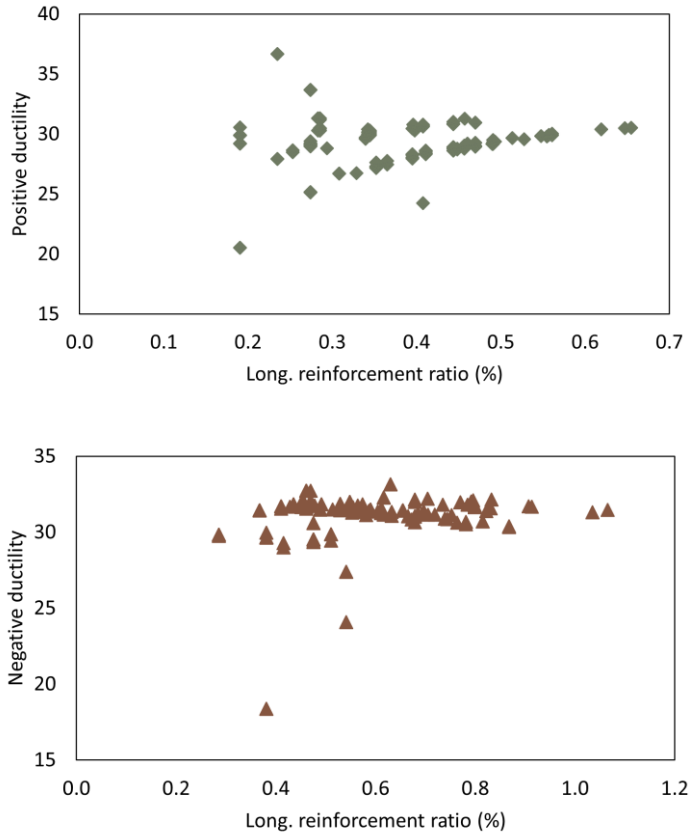

Figure 5. The effect of longitudinal reinforcement ratio on sectional ductility

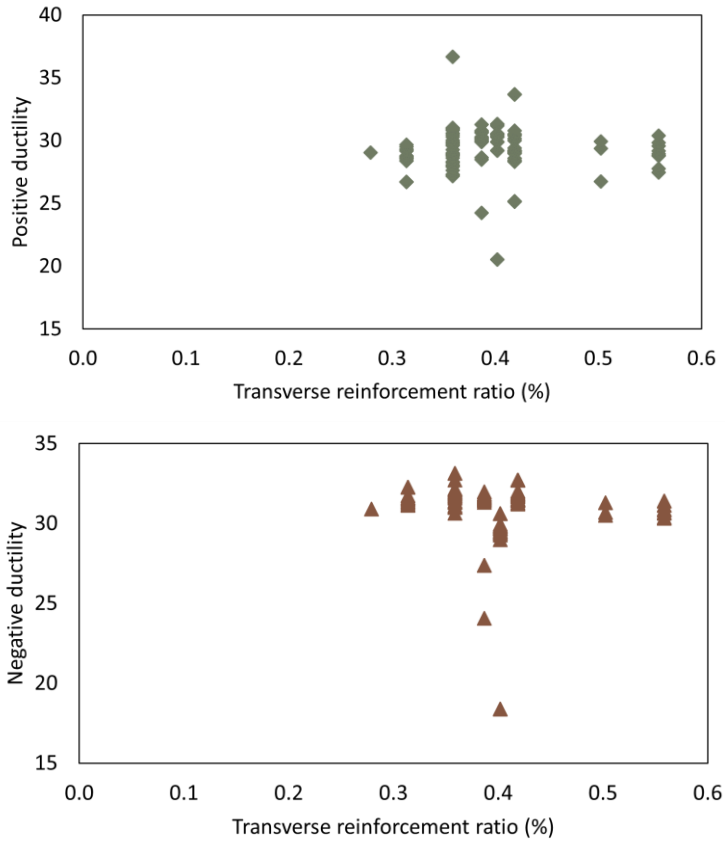

Figure 6. The effect of transverse reinforcement ratio on sectional ductility

The effect of transverse reinforcement ratio on sectional ductility is illustrated in Figure 6. There does not seem to be any clear trend or correlation between the ductility and longitudinal reinforcement. A scatter of points representing the relationship between transverse reinforcement and sectional ductility was observed from the graphs. Therefore, no clear correlation could be determined from this scatter either.

Finally, the ductility distribution is investigated. No strong correlations were observed when numerical ductility of beam sections were related to such parameters as aspect ratio, longitudinal reinforcement ratio and transverse reinforcement ratio. The sectional ductility obtained from numerical analysis of beam sections oscillated around 30, with most values seeming to be within the range of 25-35. There were some extreme values below 25 and above 35 as well, but they were limited. It was suggested that the ductility of the beam sections is a normal distribution instead. Figure 7 illustrates the positive and negative ductility distribution.

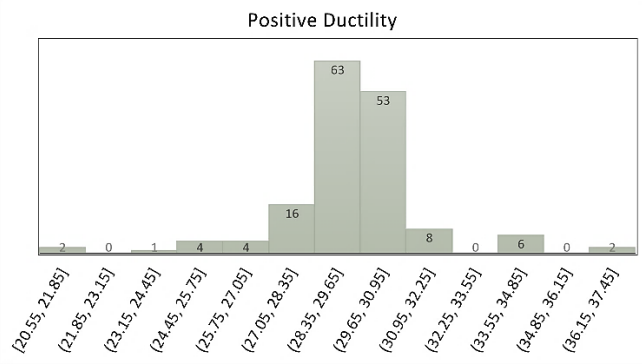

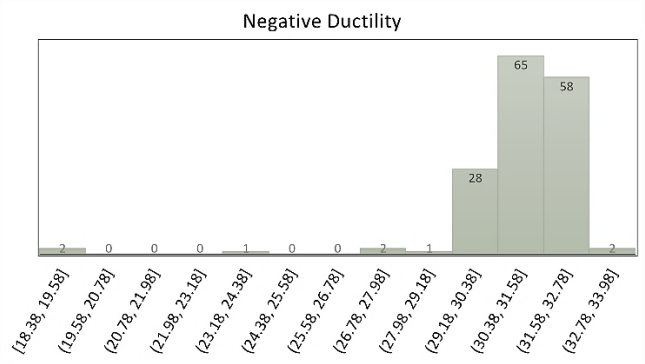

Figure 7. Ductility distribution

An observation of the average mean and variance of ductility distribution for the beams of the dataset is shown in Table 1. It can be noticed that the type of beams does not affect greatly the mean ductility, however it does affect the distribution. Normal beams have higher variance of ductility than wide beams, thus greater ranges and variation occur.

Table 1. Ductility distribution – Mean and variance

	Positive ductility		Negative ductility	
	Mean	CoV	Mean	CoV
All beams	29.39	0.07	30.99	0.06
Normal beams	29.66	0.08	28.96	0.09
Wide beams	29.33	0.06	31.50	0.03

Conclusion

In this study a database of 150 beams was investigated to draw relationships between section parameters such as aspect ratio and reinforcement ratios and sectional ductility computed numerically. All the beam sections were designed according to TS500 and TBEC2018. The normal beams were designed as high ductility class, while the wide beams were designed as limited ductility class.

An observation of the relationship between aspect ratio and ductility showed that there is no clear correlation between these two parameters. Some extreme values of ductility were obtained from the normal beams, and from the wide beams with the greatest aspect ratios. The rest of the ductility values fall mostly in a range between 25 and 35, and the aspect ratio, therefore the type of the beam does not considerably affect the value of ductility.

An observation of the relationship between reinforcement ratios and ductility also showed no clear correlation. Lower longitudinal reinforcement ratios were generally characterized by a greater scatter in the values of the ductility, while the ductility values corresponding to higher reinforcement ratios tended to converge towards 30-31. Lower longitudinal reinforcement ratios were mostly typical to normal beams, while wide beams mostly had higher reinforcement ratios.

The ductility sets can be assumed to be normal distributions from the shape of the histograms. When the means and variances of the ductility sets for all the beams, normal beams only and wide beam only were compared it was observed that the type of beam did not affect the mean ductility value. Variance of the ductility distributions was smaller for wide beams.

Wide beams were designed as limited ductility class and normal beams were designed as higher ductility class. Both types of beams displayed very similar levels of rotational ductility. While aspect ratio and reinforcement ratios affect the ductility of the sections, no clear correlations could be obtained. Adequate design procedures seem to be sufficient to provide adequate ductility to the beam sections, independent of their aspect ratio.

References

[1] Nogueira CG, Rodrigues ID. Ductility analysis of RC beams considering the concrete confinement effect produced by the shear reinforcement: a numerical approach. Latin American Journal of Solids and Structures 2017; 4(13): 2342-2372.
[2] Lee TK, Pan ADE. Estimating of relationship between tension reinforcement and ductility of reinforced concrete beams sections. Engineering Structures 2003; 25: 1057-1067.
[3] Arslan MH. Estimation of curvature and displacement ductility in reinforced concrete buildings. KSCE Journal of Civil Engineering 2012; 16: 759-770.
[4] Lalaj O, Çevik M. Comparison of stiffness and ductility of conventional and wide beam reinforced concrete frames. Proc. 4th International Conference on Earthquake and Seismology (4.ICEES) 2017, Eskişehir, Turkey.
[5] Fadwa I, Ali TA, Nazih E, Sara M. Reinforced concrete wide and conventional beam-column connections subjected to lateral load. Engineering Structures 2014; 76: 34-48.
[6] Lalaj O, Çevik M, Kayhan AH. Seismic demand on 4-story limited ductility class frames designed according to TBEC2018. Proc. 5th International Conference on Earthquake and Seismology (5.ICEES) 2019, Ankara, Turkey.
[7] Mander JB, Priestley MJN, Park R. Theoretical stress-strain model for confined concrete. ASCE Journal of Structural Engineering 1988; 114(8): 1804-1826.
[8] TS500 (2000) Design and Construction Guidelines for Reinforced Concrete Structures. Turkish Institute of Standards, Ankara.
[9] TBEC (2018) Turkish Building Earthquake Code (TBEC2018) (Turkish). Directory of Natural Disasters, Ministry of Environment and Urban Planning, Earthquake Research Department, Ankara.

The Effect of Compaction Temperatures and Numbers on the Air Void Level of Porous Asphalt Pavements

Ahmet Buğra İbiş[1], Burak Şengöz[2], Ali Topal[2], Derya Kaya Özdemir[2]*
[1]Dokuz Eylul University, The Graduate School of Natural and Applied Sciences, Izmir, Turkey
[2]Dokuz Eylul University, Department of Civil Engineering, Izmir, Turkey
**Corresponding author: ahmetbugra.ibis@gmail.com*

Abstract

Porous asphalt pavement is defined as an asphalt concrete that is designed with open gradation aggregate which helps in removing the water with an air void content of about 20% by creating drainage channels. Open gradation consists of large amounts of coarse aggregates and small amounts of fine aggregates. The water is drained due to this hollow structure, this air void content in the porous asphalt mixture which inevitably decreases with time is the main parameter affecting the service life as well as the structural and functional performance. Moreover, the reduction in air void content is one of the main reasons for the loss of permeability in porous asphalt pavements and this lead to the increase in pavement density under heavy traffic conditions. Each country has its own technical asphalt specification involving the required compaction energy and temperature. This study involves the effect of compaction temperatures and numbers on the air void in porous asphalt pavements prepared with 50/70 penetration grade bitumen. As a result of experimental studies, it has been observed that the reduced compaction temperature and the number of compaction (energy) increase the air void level in porous asphalt pavements.

Keywords: porous asphalt, air void, number of compaction

Introduction

Porous asphalt is designed with a higher percentage of air voids to allow water to seep from surfaces. It provides faster drainage than conventional asphalt pavements. Porous asphalt is characterized by high porosity, consequently a high macro roughness, a lower thermal conductivity, a strong permeability to water, and less contact points between the stones in comparison to the traditional dense graded mixes [1]. Normally, the recommended air void content is between 18% and 25% to provide adequate drainage during heavy rainfall [2]. On the other hand, temperature is an important factor in asphalt pavement construction [3]. The effect of temperature is very important especially during mixing, laying and compaction processes in the construction of a strong and durable coating [4]. This is because asphalt needs to be heated to achieve the required viscosity for better adhesion. Further compaction may fracture the aggregate in the mix, decrease pavement density and frustrate the purpose of compacting [5]. If asphalt mixtures are cooler than desirable temperature, a variation in mix temperature can cause poor mix compaction leading to non-uniform densities [6]. The severe decrease in density leads to a loss of fatigue life and serviceability of the pavement [7]. Too much compaction may cause micro-cracks in the sample. These micro-cracks disrupt the special structure of the porous asphalt pavement, causing the pores to become blocked and the permeability to decrease over time [8].

Materials and Experimental

In this study 50/70 base bitumen grade and limestone aggregate supplied by DERE ASFALT were used. Some conventional bitumen and aggregate experiments were carried out to determine the properties of materials. The physical properties of the base bitumen and aggregate used in this study were listed in Tables 1 and 2, respectively. All the material properties were in accordance to Karayolları Genel Müdürlüğü (KGM).

Table 1. Properties of the base bitumen

Test	Specification	Result	Specification Limit
Penetration (25 °C; 0.1mm)	TS EN 1426	57	50 – 70
Softening Point (°C)	TS EN 1427	49.8	46 – 54
Change of Mass (%)	TS EN 12670-1	-0.2	-0.5 - 0.5
Retained Penetration (%)	TS EN 12670-1	61	>50
Flash Point (°C)	TS EN ISO 2592	344	>230

Table 2. Properties of the limestone aggregate

Test	Specification	Result	Specification Limit
Bulk Specific gravity (coarse aggregate)	TS EN 1097-6	2.649	
Bulk Specific gravity (fine aggregate)	TS EN 1097-6	2.603	
Specific gravity (filler)		2.725	
Los Angeles abrasion (%)	TS EN 1097-2	24	Max 25
Sodium sulfate soundness (%)	TS EN 1367-2	1.54	Max 10
Water absorption (%)	TS EN 1097-6	1.3	< 2.0
Flakiness (%)	TS EN 933-3	3	< 15

Preparation of Porous Asphalt Samples

The samples of porous asphalt mixture were prepared using an Automatic Marshall Compactor with 4% binder content. The aggregates were dry sieved kept in an oven at 170 degrees for 24 hours. Two different compaction temperature and number respectively 120°C, 130°C and 40 blow, 50 blow and three different aggregate gradation were used. The aggregate gradations used are shown in Table 3. The compacted samples were then tested for volumetric properties (in terms of density and air void content) and mechanical performance Marshall Stability Test. The Marshall Stability Test was conducted to determine the optimum bitumen content according to the desired aggregate type and gradation to be used in the wearing course of bituminous mixtures that are directly exposed to traffic loads.

Table 3. Aggregate gradations

Sieve No	Specification Limit (KGM Type-2)	Gradation-1	Gradation-2	Gradation-3
3/4 in	100	100	100	100
1/2 in	90-100	95	95	90
3/8 in	63-77	70	70	63
No.4	11-35	25	20	11
No.10	10-20	15	15	10
No.80	5-10	7	7	5
No.200	3-7	4	4	3

Results and Discussion

The porous asphalt void ratio was calculated according to TS EN 12697-6 procedure D. The effect of different compaction number and temperature on different gradations is shown in Figures 1, 2 and 3.

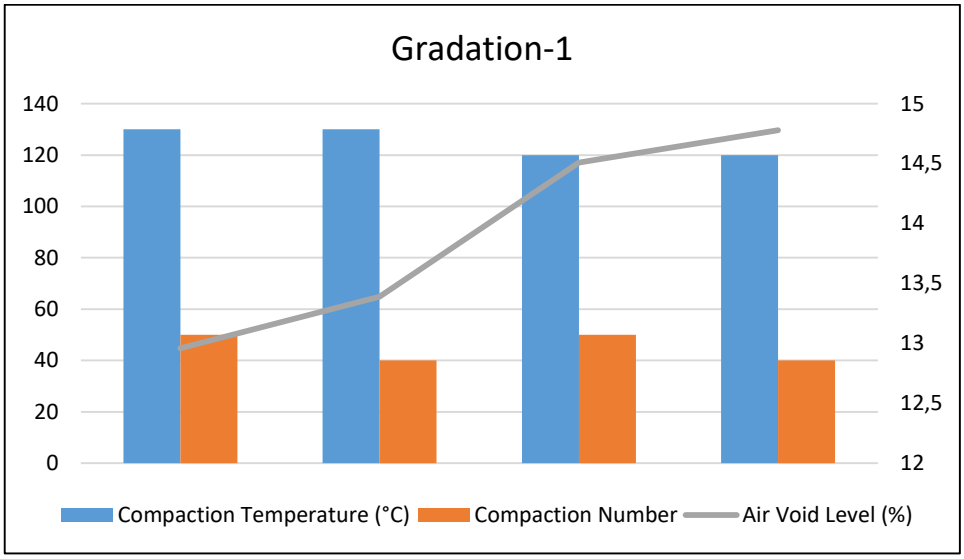

Figure 1. Gradation-1

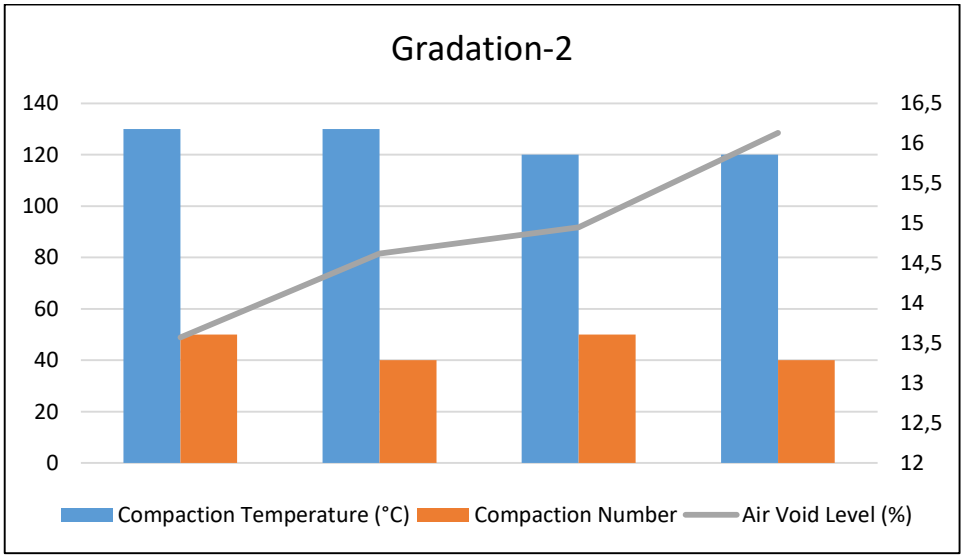

Figure 2. Gradation-2

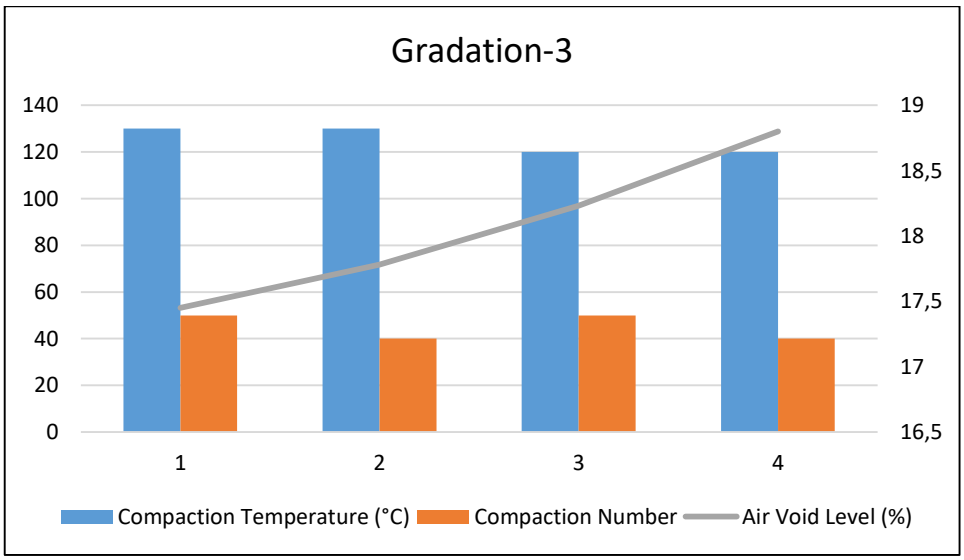

Figure 3. Gradation-3

In general when the examination is made for three different gradations, an increase in the void ratio occurs when the temperature is decreased and the number of compaction is increased. In fact, this is a result contrary to what is expected.

Stability values were measured by performing Marshall Stability Test on the produced porous asphalt samples. Relevant data are shown in Figures 4, 5 and 6.

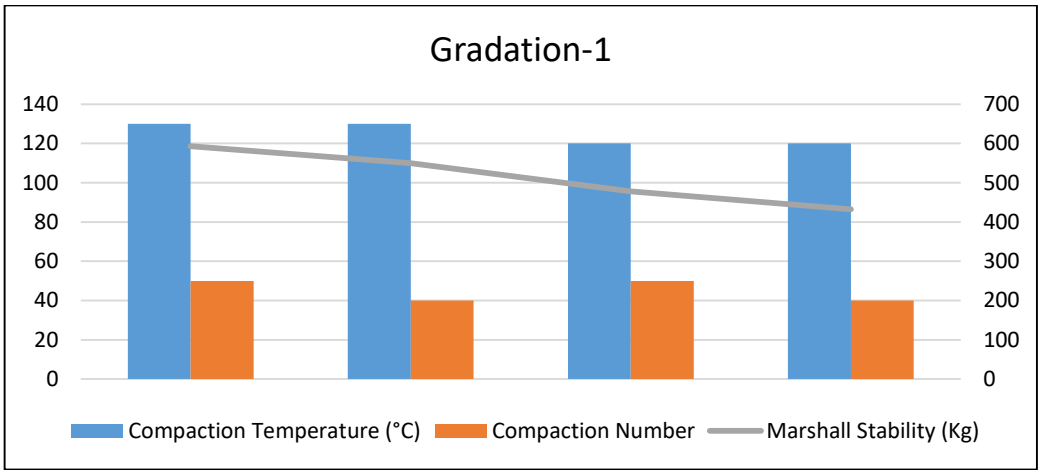

Figure 4. Marshall Stability for Gradation-1

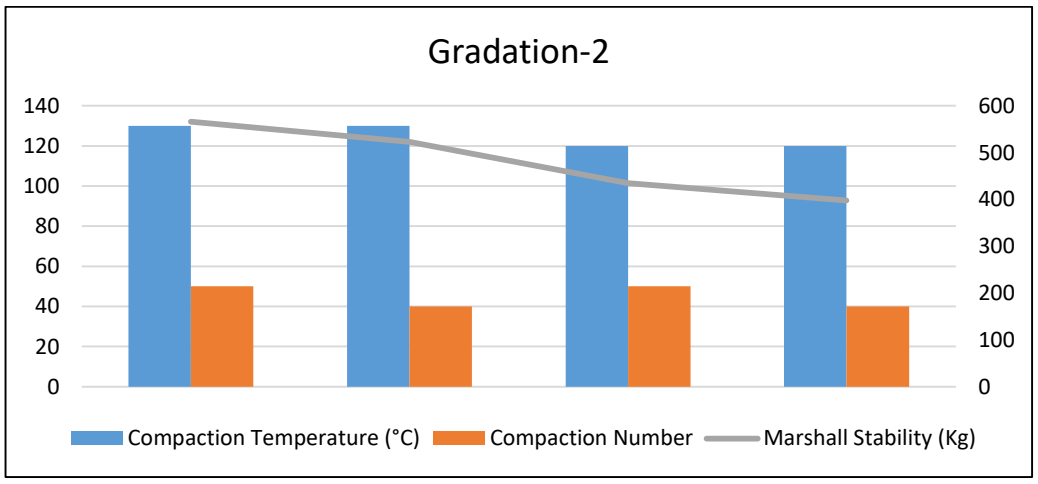

Figure 5. Marshall Stability for Gradation-2

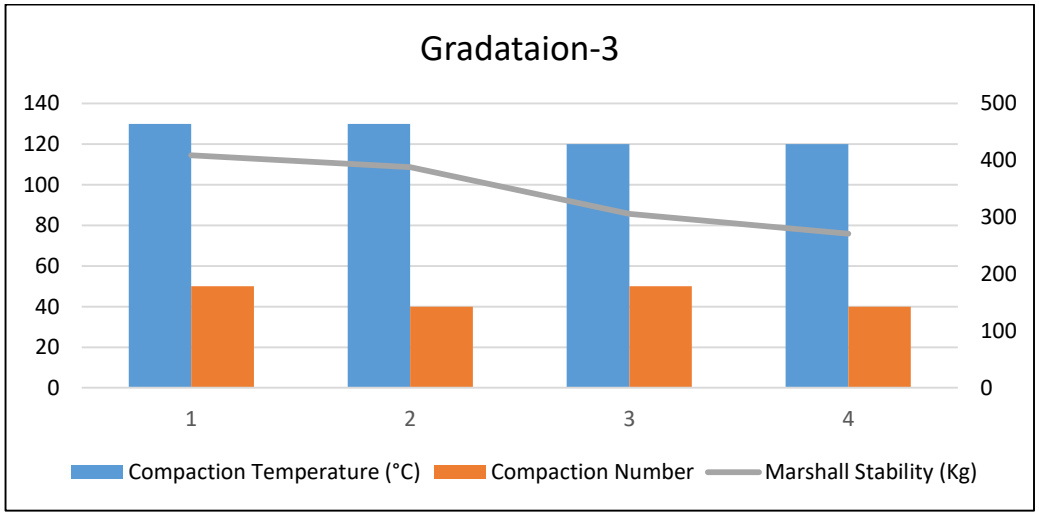

Figure 6. Marshall Stability for Gradation-3

When the stability results were examined, the gradation change had a negative effect on the stability values. It is seen that the decrease in temperature and number of compaction has a negative effect on the stability of the porous asphalt pavement.

Conclusion

Based on the obtained results, in experiments with three different gradations, the void ratio gave better results in type 3 gradation. The reason for this is that the selected gradation has less fine material than other gradations. That is, the cavities in the sample are filled with air instead of thin material. However, when the stability values are examined, there is a decrease in the stability values with the gradation change. In other words, decreasing the fine material in the sample and increasing the coarse aggregate ratio negatively affect the stability. When the temperature is kept constant and the number of compaction is increased, the void ratio decreases. When the number of compaction is kept constant and the temperature is increased, a decrease in the void ratio occurs as the compression amount of the sample will be greater. When the results for the stability value were examined, a result was directly proportional to the temperature and the number of compaction. In other words, the stability value increased when the temperature was kept constant and the number of compaction increased. Likewise, when the number of compaction was kept constant and the temperature was increased, the stability value increased.

References

[1] Hassan NA, Mahmud MZH, Adi N, Rahmat N, Hainin MR, Jaya RP. 2006 Effects of air voids content on the performance of porous asphalt mixtures.
[2] Kamar FHA, Sarif JN. 2009 *Proc. of 13th Conf. of the Road Eng. Ass. of Asia and Australasia (REAAA)* 9-07.
[3] Capitão SD, Picado-Santos LG, Martinho F. 2012 *Const. Build.*, 1016-1024.
[4] Vasconcelos KL, Bernucci LB, Chaves JM. 2012, *Proc. 5 th Euras.t and Eurobit.Congr.*
[5] Köster, H. Drainasphalt Beobachtungen des Verhaltens von hohlraumreichen Verschliessschichten 1991 VSS report Nr. 218.
[6] Bochove GG. Twinlay, a New Concept for Porous Apshalt, Proc. Eurasphalt & Eurobitume Congress, 1996, pp. E&E.7.187.
[7] Japan Highway Research Institute, Statistic data of Porous Asphalt on Japanese Highways. (Unpublished).
[8] Daines ME. Trials of porous asphalt and rolled asphalt on the A38 at Burton, Departmentof transport TRRL Report RR323, Transport and Road research Laboratory, Crowthorne, 1992.

Numerical Analysis of Flush End-Plate Beam-to-Column Connection using Mathematical Model and Finite Element Analysis

*Mohammad Haroon Ehsan**, *Mutlu Seçer*
Izmir Katip Çelebi University, Department of Civil Engineering, Izmir, Turkey
**Corresponding author: ehsan.haroon20@gmail.com*

Abstract

In the conventional analysis and design of steel structures, beam-to-column connections are generally assumed as entirely rigid or perfectly pinned. This assumption simplifies analysis and design steps and preferred extensively in structural engineering practice. However, experimental studies conducted in recent years have revealed that handling some of the beam-to-column connections as entirely rigid or perfectly pinned does not give realistic results. In fact, most of the connections used in current practice have some certain amount of stiffness which fall between the extreme cases of entirely rigid and perfectly pinned. In order to model the beam-to-column connections properly, several researchers have proposed various mathematical models based on experimental results. In these models, moment rotation relations of beam-to-column connections are defined according to the type of connection. In this study, moment-rotation behaviors of beam-to-column connections formed by flush end-plate are investigated using finite element analysis and a well-known practical mathematical model. Moreover, numerical analysis outcomes were compared with the test results of a reference study from the literature. This paper showed the importance of structural design parameters in determining moment-rotation relationship of flush end-plate type of beam-to-column connections and evaluated the efficiency of the practical numerical models.

Keywords: steel structures, semi-rigid connections, finite element method, flush end-plate connection

Introduction

End-plate connections are widely used in steel structures, which consist of two main types, extended and flush end-plate connections, [1–3]. Beam-to-column connections, including end-plate types, often significantly influence the behavior of steel frames, with deformation of the connection in combination with the P-delta effect contributing to excessive lateral drift in unbraced multistory frames [4]. For most connections under ambient conditions, the axial and shearing deformations are usually small compared to the rotational deformation and consequently the rotational deformation is the most important characteristic of the connection. This rotational deformation is customarily expressed as a function of the moment in the connection [1–3,5]. In the conventional analysis and design of steel structures, beam-to-column connections are generally assumed as entirely rigid or perfectly pinned. This assumption simplifies analysis and design steps and preferred extensively in structural engineering practice. However, the actual behavior of frame connections lies between these two extremes and is semi-rigid [4]. Thus, semi-rigid connections attained considerable attention in recent years in terms of modeling [5].

Various analytical and numerical methods have been developed to study of the semi-rigid characteristics of beam-to-column joints as well as their influence on the response of the structural elements [6,7]. In order to predict the moment-rotation behavior accurately, a large number of studies have been performed on endplate bolted joints considering experimental, numerical, and analytical approaches [8-14]. The types and details of the studied connections are numerous and innovative, and they concerned many parameters such as diameter and number of bolts, pretension force of bolts, thickness of endplate, beam and column dimensions, steel yield strength, stiffening type, and coefficient of friction between contacts surfaces.

The finite element analysis (FEA) of end-plate connections have been performed by Krishnamurthy [8–10]. Tarpy and Cardinal [11] carried out an elastic finite element study of unstiffened end-plate connections that was verified experimentally and they also proposed a design methodology for these joints. Maxwell et al. [12] developed a prediction equation for the ultimate moment of connections, as well as their moment-rotation (M–Θ) relationships, based on a FEA and on tests. Jenkins et al. [13] did FEA on flush end-plate connections and those extended on one side, then put forward a bilinear M–Θ

model for flush end-plate connections. Kukreti et al. [14] adopted two-dimensional FEA model to calculate 50 flush end-plate connections and verified the recommended M–Θ relationship for this type of connection based on regression analysis. Sherbourne and Bahaari used two-dimensional [15] and then three-dimensional [16] finite element analysis models to model end-plate connections. Adey et al. [17] indicated that the presence of stiffeners on the extended part of the endplate increased the flexural strength of the connection as well as its rotation and its energy dissipation capacity. Moreover, Ostrander [18] developed a test program for column-to-beam joints with flush end-plates, with or without stiffeners on the column web. Abidelah et al. [19] conducted an experimental and numerical study on stiffened or unstiffened end-plate bolted joints, of beam-to-column and beam-to-beam type, for the purpose of studying the stiffening effect. They also examined the effect of flexural stiffness of a bolt in a T-stub. Bai et al. [20] studied the prying effect in a joint with an extended endplate and then proposed an improved joint design taking into account this effect.

In order to model flush end-plate beam-to-column connection and evaluate the importance of structural design parameters in determining moment-rotation relationship, three-dimensional FEA models are applied to generate the effective moment–rotation response of the flush end-plate connections. FEA results are then evaluated with the experimental work and test results of Ostrander [18]. In addition, flush end-plate beam-to-column connections are examined with the help of a practical mathematical model.

Flush End-Plate Beam-to-Column Connection Model

Flush end-plate beam-to-column connections are selected from a reference study of Ostander [18]. In the reference [18], geometric and structural properties of flush end-plate beam-to-column connections were given in details and laboratory test results were presented in terms of moment-rotation relationship. The test setup of Ostander [18], includes two beam segments with equal lengths, which were symmetrically bolted to a stub column. The beam ends were simply supported and the stub column could move vertically. Therefore, an applied load on the center of the stub column generated a moment on the connection. Assembled specimens of Ostrander [18] test setup are presented with Fig. 1 for clarification. Dimensions that are given with Fig. 1 were common to all specimens [18].

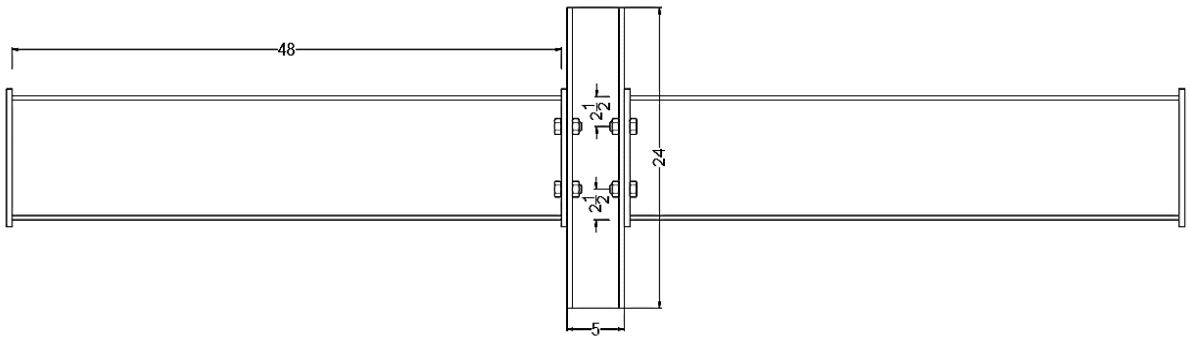

Figure 1. Assembled specimens Ostrander [18]

Geometries of Connection Models

Ostrander's [18] experiments include 24 test specimens of flush end-plate connections. In this study seven specimens that are representing various types of configurations are accounted and end plate thickness and stiffeners of the column web are the main parameters to be focused. Geometric properties of the seven connections which are analyzed in this study are presented in Table 1. Parameters that are given in In Table 1 can be summarized as; w is the element width, d is the element depth, t is the thickness of element, g is the horizontal bolt gage and p is the vertical bolt pitch.

Table 1. Test specimen number and geometric properties of the connections of Ostrander [18]

Test number	Beam section	Column section	End plate			Stiffener			Bolt	
			w(in.)	d(in.)	t(in.)	w(in.)	d(in.)	t(in.)	g(in.)	p(in.)
TEST 1	W10x21	W8x28	$6\frac{1}{2}$	11	1/2	-	-	-	$3\frac{1}{2}$	5
TEST 3	W10x21	W8x28	$6\frac{1}{2}$	11	3/8	-	-	-	$3\frac{1}{2}$	5
TEST 4	W10x21	W8x28	$6\frac{1}{2}$	11	1/4	-	-	-	$3\frac{1}{2}$	5
TEST 6	W10x21	W8x28	$6\frac{1}{2}$	11	3/8	3	$7\frac{1}{8}$	1/4	$3\frac{1}{2}$	5
TEST 7	W10x21	W8x28	$6\frac{1}{2}$	11	1/4	3	$7\frac{1}{8}$	1/4	$3\frac{1}{2}$	5
TEST 8	W10x21	W8x28	$6\frac{1}{2}$	11	1/4	3	$7\frac{1}{8}$	1/4	$3\frac{1}{2}$	5
TEST 11	W12x27	W8x40	$7\frac{1}{2}$	13	3/8	-	-	-	4	7

Material Properties

ASTM A36 steel was used for the beam, column and plate of the connection [18]. The yield stress and ultimate strength of the connections were taken from the mean value of coupon test result [18]. Bolt yield stress and ultimate strength are assumed based on the nominal properties of A325 bolts [24]. Effective material properties of connection assemblages are shown in Table 2.

Table 2. Material properties of connection components [18]

	Lab. Test result		
Materials	Yield stress (ksi)	Ultimate strength (ksi)	% Elongation in 2″
W10x21	41.3	66.9	35
W8x28	51.1	77.3	38.3
W12x27	58	78	37.3
W8x40	48.6	75	33.8
End plate 1/4″	46.5	71.2	34.3
End plate 3/8″	45.5	68.5	38.8
End plate 1/2″	45.4	70.3	39
Stiffener 1/4″	49.6	71.9	38
Stiffener 3/4″	32	58.5	45

Finite Element Modeling

Three-dimensional refined FEA models are used to generate the effective moment–rotation response of the connections. In this study, experimental work of Ostrander [18] about flush end-plate beam-to-column connection is considered and FEA model is prepared [21]. Afterwards, three-dimensional FEA are performed in order to examine the capability of the numerical models. Analysis results are then compared with the experimental response of the connections. Geometric details of all components that are used in flush end-plate connections are as same as those of the tested specimens given in Table 1. Due to the symmetry of the geometric details, loading and boundary conditions, only connection on one side of the cruciform arrangement was modeled to reduce computing time (Fig. 2). The hexagonal solid element C3D8 type with 8 nodes was used with reduced integration and hourglass control [22]. The mesh density was increased in critical zone of the connections (Fig. 2). The contact areas including bolt head and nut to components were modeled by implementing the penalty contact algorithm with finite-sliding scheme. The normal behavior that appears between two surface is defined as hard contact and the coefficient of friction was taken as 0.33 in the tangential direction [22].

Stress-strain relation of steel is represented by using a bilinear constitutive model. Isotropic hardening rule is applied for plastic deformation of steel [24]. ASTM A36 steel was used for the beam, column and plate. The yield stress and ultimate strength of the connections are taken from the mean value of coupon test results of the reference study [18]. Bolt yield stress and ultimate strength are assumed based on the nominal properties of A325 bolts [24].

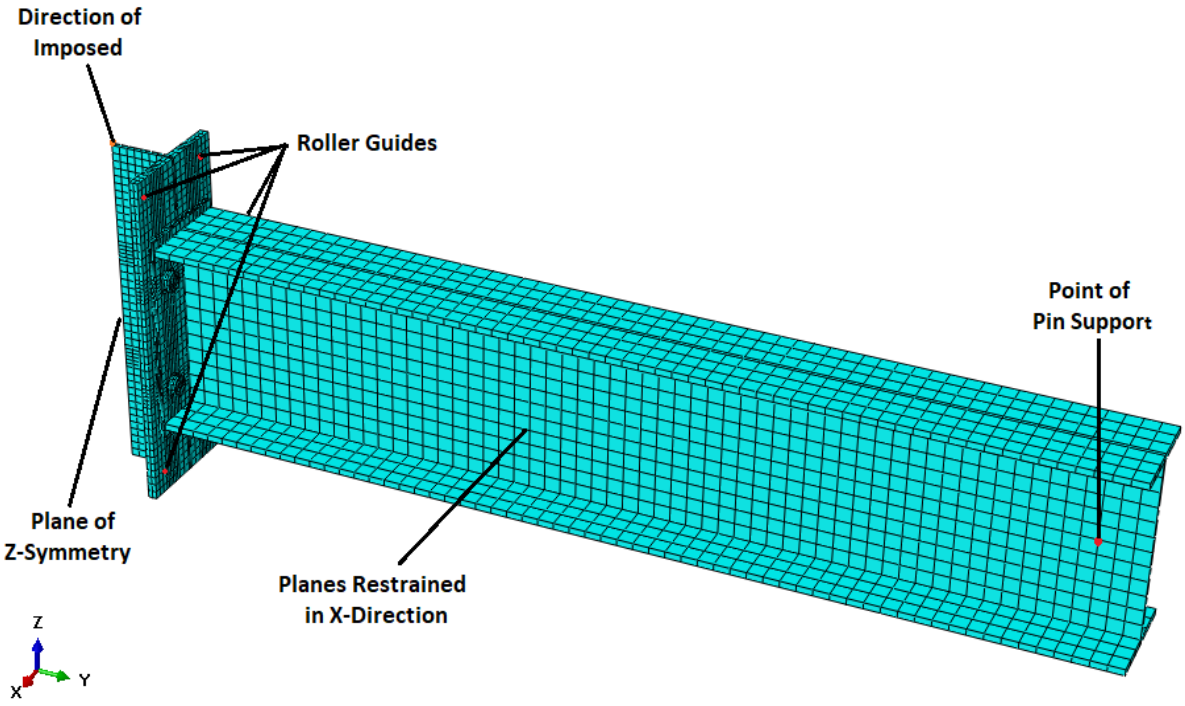

Figure 2. FE modeling of flush end-plate beam-to-column connection (TEST 11)

Boundary Conditions and Applied Loads

The boundary conditions defined on the model realistically reflect the experimental setup (Fig. 2). In order to disallow the local deformation under the concentrated force, the column top surface is coupled through coupling constraint to the load application point. Bolt pre-tension is applied as the first load case, and for this purpose a thermal gradient is applied on the bolt shanks to yield equivalent pretension force yields. A force of 133 kN (30000 psi) is applied to the 3/4 inches (19.1 mm) diameters bolts [23]. The 50 mm vertical displacement is applied on the nodes of the load application point. The resulting moment and relative rotations of the connections are evaluated respectively by Eq. (1) and Eq. (2):

$$M = P \cdot L \tag{1}$$

$$R = \frac{d_1 - d_2}{h} \tag{2}$$

where, M is applied connection moment, P is summation of the reactions of the applied displacements on the beam end nodes, L corresponds to the beam length, R is the relative rotation of the connection, h is the beam depth, d_1 and d_2 are the top and bottom flange horizontal displacements respectively.

After analyzing the flush end-plate beam-to-column connections, the deformed shape of connections are plotted and behavior is evaluated. The deformed shape of TEST 11 is shown in Fig. 3 at 0.03 rad.

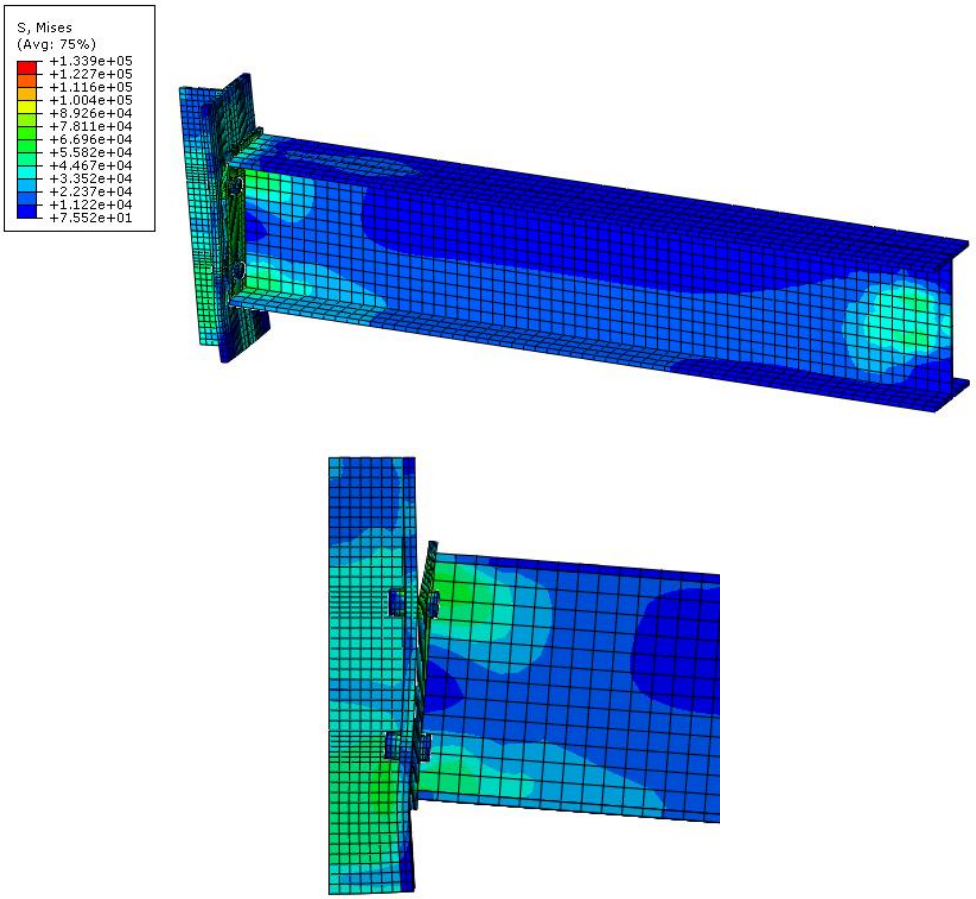

Figure 3. Deformed shape of TEST 11 connection at 0.03 rad

Finite element analysis results of flush end-plate beam-to-column connections

Finite element analysis results of flush end-plate beam-to-column connections are presented with Fig. 4 in comparison with the test results of Ostrander [18] and a mathematical model named as Power Model and described in [25]. It can be observed that the results obtained from finite element models have a good agreement with the test data Ostrander [18]. Differences between the numerical simulation and test results are probably the result of several causes such as; numerical modeling simplification, test specimen defects, residual stress and bolt pre-tension.

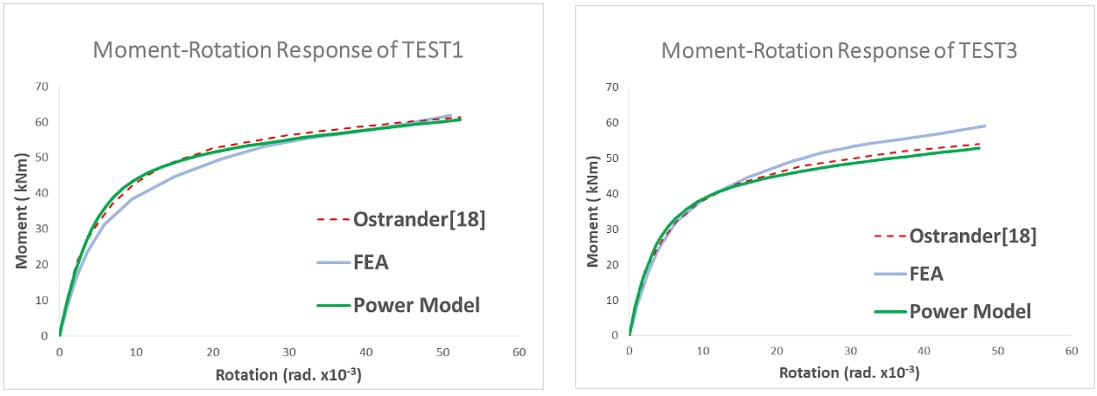

Figure 4. Comparisons of FEA results, mathematical model and experimental test result of Ostander [18] for flush end-plate beam-to-column connections

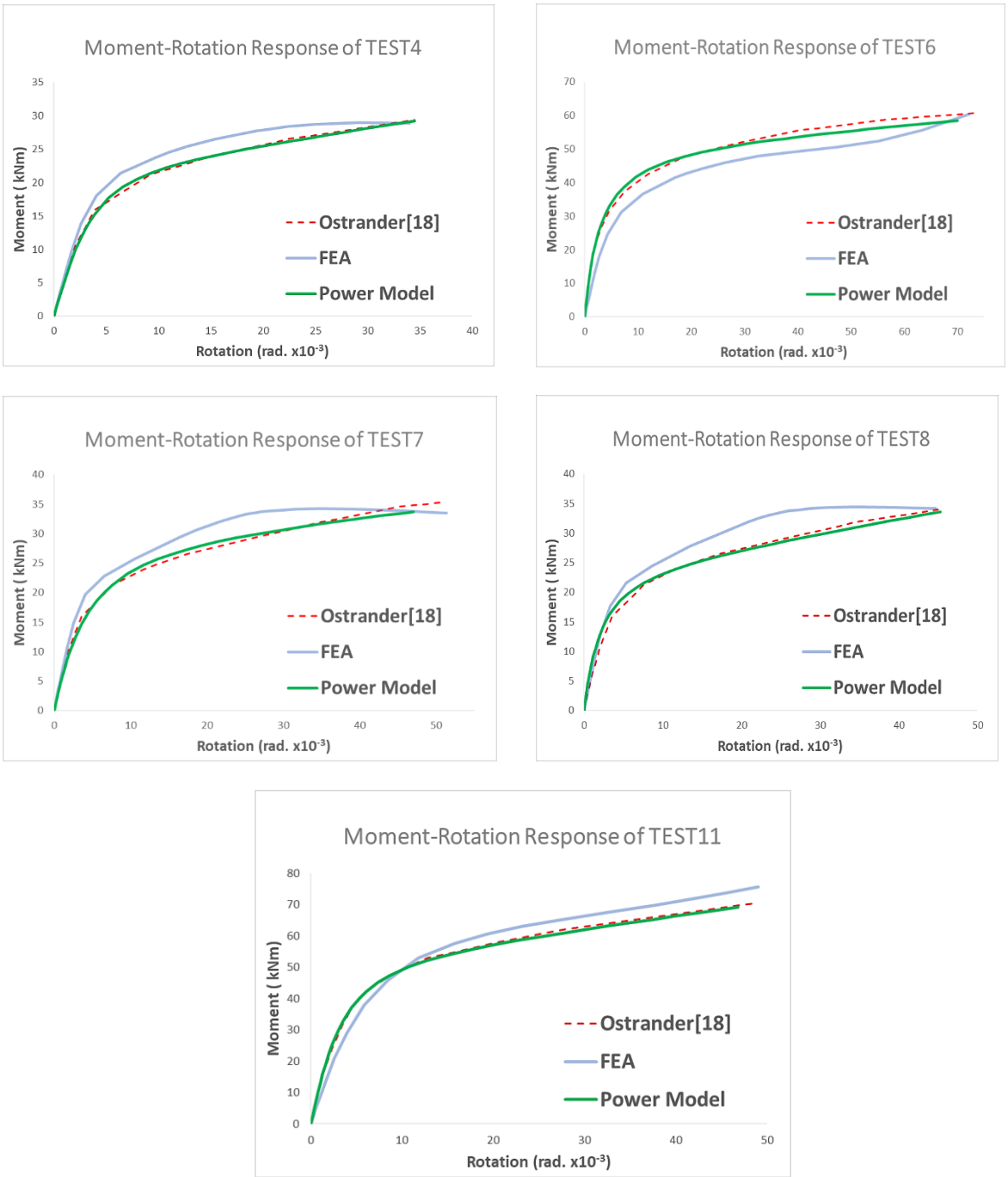

Figure 4. (continued)

Effect of Bolt Pretension Load

It is possible to extend the study of the connections beyond the experimental data having the prediction capability of the proposed modeling approach. A model is used to study the effect of bolt pretension on the response of the flush end-plate beam-to-column connection. A variation on the pretension load is modeled in order to monitor the effect of pretension. TEST 1 and TEST 3 of Ostander [18] are accounted and varying values of pretension is applied. The variation in pretension is limited with 100% (133 kN), 75% (100 kN), 50% (66.5 kN) and 25% (33.25 kN) and analysis results of the TEST 1 and TEST 3 connections are presented with Fig. 5 and Fig. 6, respectively.

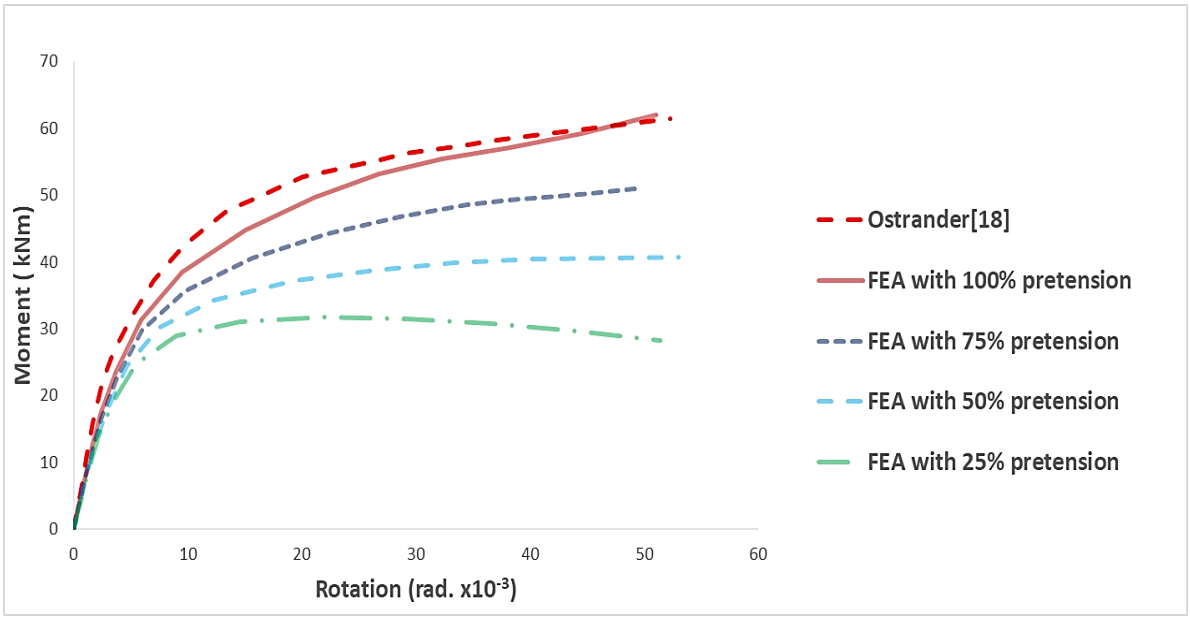

Figure 5. Moment-rotation response of TEST 1 connection with varying bolt pretension.

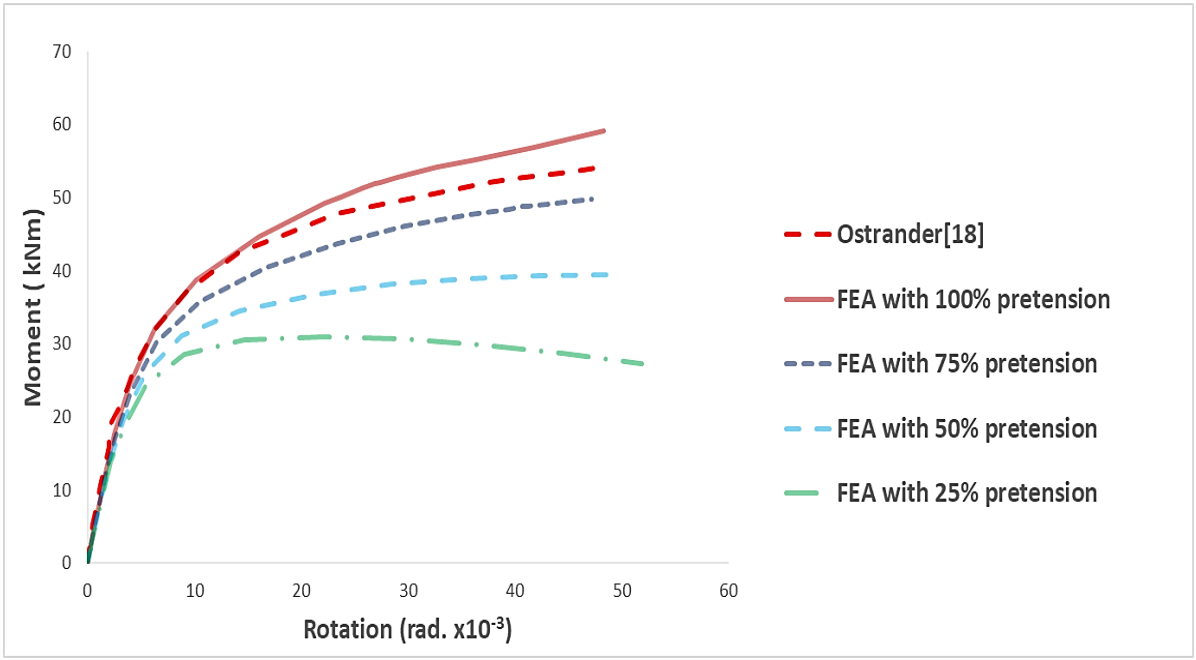

Figure 6. Moment-rotation response of TEST 3 connection with varying bolt pretension

Conclusion

In this study, the moment–rotation behaviors of bolted flush end-plate connections are investigated by using three-dimensional finite element model and a practical mathematical model. Numerical analysis results are compared with the test results of a reference study from the literature. Analysis results showed that the finite element analysis and mathematical model has a good agreement with the test data of the reference study. On the other hand, the effect of bolt pretension load on the response of flush end-plate connections is focused. Finite element analysis results reveal that pretension loads have significant effect on moment-rotation curve of flush end-plate type of connections.

References

[1] Trahair NS, Bradford MA, Nethercot DA, Gardner L. The behaviour and design of steel structures to EC3. 4th edn. British. London: Spon Press; 2007.
[2] Owens GW, Cheal BD. Structural steelwork connections. London: Butterworths; 1989.
[3] Kulak GL, Fisher JW, Struik JHA. Guide to design criteria for bolted and rivetted joints. 2nd edn. New York: John Wiley and Sons; 1987.
[4] Attiogbe E, Morris G. Moment–rotation functions for steel connections. Journal of Structural Engineering, ASCE 1991;117(6):1703–18.
[5] Chen WF, Lui FM. Stability design of steel frames. Boca Raton (FL): CRC Press; 1991.
[6] Chen WF. Practical analysis for semi-rigid frame design. Singapore: World Scientific; 2000.
[7] Lee SS, Moon TS. Moment–rotation model of semi-rigid connections with angles. Engineering Structures 2002; 24: 227–237.
[8] Krishnamurthy N, Graddy DE. Correlation between 2- and 3-dimensional finite element analyses of steel bolted end-plate connections. Computers and Structures 1976;6(4–5):381–9.
[9] Krishnamurthy N, Huang HT, Jeffrey PK, Avery LK. Analytical Mtheta curves for end-plate connections. Journal of the Structural Division, ASCE 1979;105(ST1):133–45.
[10] Krishnamurthy N. Modelling and prediction of steel bolted connection behavior. Computers and Structures 1980;11(1-2):75–82.
[11] Tarpy TS, Cardinal JW. Behaviour of semi-rigid beam-to-column endplate connections. In: Howlett JH, Jenkins WM, Stainsby R, editors. Joints in structural steelwork. London: Pentech Press; 1981. p. 2.3–2.25.
[12] Maxwell SM, Jenkins WM, Howlett JH. Theoretical approach to the analysis of connection behaviour. In: Howlett JH, Jenkins WM, Stainsby R, editors. Joints in structural steelwork. London: Pentech Press; 1981. 2.49–2.70.
[13] Jenkins WM, Tong GS, Prescott AT. Moment-transmitting end-plate connections in steel construction and a proposed basis for flush end-plate design. The Structural Engineer 1986;64A(5):121–36.
[14] Kukreti AR, Murray TM, Abolmaali A. End-plate connection moment–rotation relationship. Journal of Constructional Steel Research 1987;8:137–57.
[15] Bahaari MR, Sherbourne AN. Computer modelling of an extended endplate bolted connection. Computers and Structures 1994;52(5):879–93.
[16] Sherbourne AN, Bahaari MR. 3D simulation of end-plate bolted connections. Journal of Structural Engineering, ASCE 1994;120(11): 3122–36.
[17] B.Adey, G.Grondin, J.J.cheng, Cyclic loading of end plate moment connections, Can.J.Civ.Eng.27 (2000) 683-701.
[18] J.R. Ostrander, An Experimental Investigation of End-Plate Connections. M.S. Thesis, University of Saskatchewan, Saskatchewan, 1970.
[19] A.Abidelah, A. Bouchair, D. Kerdal, Experimental and analytical behavior of bolted end-plate connections eith or without stiffeners, J.Constr. Steel Res. 76 (2012) 13-27.
[20] R. Bai, S.L.Chan, J.P. Hao, Improved design of extended end-plate connection allowing for prying effects, J. Constr. Steel Res. 132 (2017) 97-107.
[21] ABAQUS, Analysis User's Manual. Version 6.12, ABAQUS, Inc., Dassault Systemes, USA, 2012.
[22] H. AlHendi, M. Mahmoud, M. celikag, Numerical study of top and seat angle with double web angle connection with high-strength steel, Journal of Constructional Steel Research, 174(2020), 106297.
[23] F.Danesh, A.Pirmoz, A.Saedi Daryan. Effect of shear force on the initial stiffness of top and seat angle connections with double web angles. Journal of Constructional Steel Research 63(2007), 1208-1218.
[24] Kishi N, Ahmed A, Yabuki N, Chen WF. Nonlinear finite element analyses of top and seat-angle with double web-angle connections. International Journal of Structural Engineering and Mechanics 2001;12:201–14.
[25] N.Kishi, M.Komuro, W.F.Chen. Four-Parameter Power Model For M-θ Curves of End-Plate connections. Connections in Steel Structures, V - Amsterdam, June 3-4, 2004.

Effect of Fly Ash on Compaction Behavior of Alluvial Soil

Abdulmuner Malikzada, Hasan Fırat Pulat, İnci Develioğlu*
Izmir Katip Çelebi University, Department of Civil Engineering, Izmir, Turkey
**Corresponding author: hfirat.pulat@ikcu.edu.tr*

Abstract

Low plasticity, high bearing capacity, low settlement, etc. are the preferred properties for most engineering projects. Alluvial soils are problematic soils because of low bearing capacity, high organic matter content, and high void ratio so they do not meet the preferred condition for engineering projects. It has been necessary to improve unsuitable materials to make them acceptable for construction. Fly ash (FA) has earlier been used for stabilizing roads due to its high content of calcium and silicate oxides which give puzzolanic properties and thus high compression strength. In this research, fundamental engineering properties, compaction behaviors of three types of (fine, medium, and coarse) alluvial deposits, and the effect of fly ash on compaction behavior of these alluvial soils are presented. Alluvial soil is taken from Çiğli, Balatçık (Izmir, Turkey). To determine geotechnical index properties; wet sieve analysis, plastic limit, liquid limit, specific gravity, standard compaction tests were conducted. In order to determine the effect of fly ash on compaction behavior of alluvial deposits, three different samples (fine < 0.425mm, medium < 2mm, and coarse < 4.75 mm) are prepared and 10%, 15%, 20% fly ash by dry weight of soil is mixed and standard proctor test is performed. As a result of laboratory tests, the liquid limit, plastic limit, and plasticity index values obtained as 38.3%, 25.7%, and 12.6%, respectively. The specific gravities for fine, medium, and coarse samples are 2.68, 2.67, and 2.66, respectively. According to the results of wet sieve analysis and consistency limit tests, it was stated that the soil contains large amounts of sand and clay. The washed sieve analysis and consistency limit tests results were evaluated according to USCS. The conducted test results have shown that maximum dry unit weight for fine, medium, and coarse soils are 16.9, 19.35, and 19.55 (kN/m3), and optimum moisture content for fine, medium, and coarse samples are 17, 11, 10.5% respectively. Generally, by increasing the content of FA, maximum dry unit weight decreased and optimum moisture content increased for all three types of alluvial soil. By increasing FA to 20%, maximum dry unit weight of medium and coarse soils decreases 1.5% and 2%, respectively.

Keywords: alluvial soil, fly ash, compaction behavior, soil stabilization

Introduction

It is evident that earth structures, such as embankments, highways, airport runways, dams, or reclamation appurtenance require soils with sufficiently good engineering properties: low plasticity, high bearing capacity, low settlement, etc. Since alluvial deposits are loose soils that do not fully complete their geological formation, they have high void ratio, low bearing capacity and high organic matter content. It has been necessary to improve unsuitable materials to make them acceptable for construction. Improvement of soil by altering its properties is known as soil stabilization. An increment in strength, a reduction in compressibility, improvement of the swelling or squeezing characteristics, and increasing the durability of soil are the main aims of soil stabilization [1].

The stabilization is achieved by the soil particles being glued more chemically than physically. Dealing with weak soil is one of the most major challenges in the construction industry. This situation probably might occur in road and highway construction or in geotechnical engineering. It is vital to find methods of soil improvement techniques so that demands can be met [2 -5].

Fly ash has earlier been used for stabilizing roads due to its high content of calcium and silicate oxides which give puzzolanic properties and thus high compression strength [6, 7]. The frost-thawing properties and the bearing capacity of road material have also been increased when fly ash is used [8 - 10].

Mahvash et al. [5] investigated the effect of class F fly ash on fine sand compaction and its suitability as a material for embankment through soil stabilization. They determined the optimum quantity of FA content for stabilization of this type of soil. This is achieved through particle size

distribution and compaction (standard proctor) tests. The sand was stabilized with three proportions of FA (5%, 10% and 15%) and constant cement content of 3% was used as an activator. Samples with FA contents of 10% and over produced results in consistence of the literature, higher OMC and lower MDD [5]. Ansary et al. [1] studied the effect of fly ash stabilization on geotechnical properties of Chittagong coastal soil. In this study unconfined compressive strength (q_u), compaction properties and flexural properties has been studied. Compaction apparatus was employed to determine the strength of the stabilized soils. The investigated admixture was fly ash with lime; the amount of lime was fixed at 3 %with the amount of fly ash 0, 6, 12 and 18 %. Compared with the untreated samples, the values of maximum dry density (γ_{max}) increased with fly ash content. Compared with the untreated sample, the values of γ_{max} increased up to 7.5% for both the soil with 18% fly ash. The values of w_{opt} reduced up to 15% and 10%, respectively [1]. Mir and Sridharan [11] investigated the volume change behavior of clayey soil – fly ash mixtures. In their study, the void ratio, the compression index, swelling potential, coefficient of consolidation, permeability, and preconsolidation pressure of clayey soil – fly ash specimens were investigated. The test results indicate a significant decrease in compressibility characteristics and swell potential of the treated soils. It was seen that 20% high-calcium fly ash content is the optimum quantity to improve the compressibility characteristics of clayey soil cured for 7 days against 60% for immediate tests.

In this study the effect of fly ash on compaction behavior of three different particle size (fine < 0.425 mm, medium < 2mm, and coarse < 4.75mm) alluvial deposits is studied. Firstly, fundamental engineering properties of those three different size alluvial soils are presented. Then, compaction behavior of alluvial soil by adding 10%, 15%, and 20% fly ash is investigated. To determine geotechnical index properties and compaction behavior; wet sieve analysis, plastic limit, liquid limit, specific gravity, standard compaction tests were conducted.

Materials and Methods

In this section, the materials used in the study and the methods applied are explained. Alluvial deposit was used as the soil sample, and fly ash was used as an additive. Laboratory tests have been carried out to determine the geotechnical index properties and compaction characteristics.

Alluvial deposits are those which are formed as a result of the deposition of sediments by rivers. They consist of clay, silt, sand, and gravel. Alluvial deposits have high void ratio because they have not completed their geological formation for this reason, they have low bearing capacity and liquefaction potential. So that they are defined as a problem in geotechnical engineering. Due to these properties, buildings that are constructed on alluvial soils cause high damage during earthquakes.

Alluvial soils that are used in this study were taken from Çiğli – Balatçık region (İzmir, Turkey). The samples were taken from a construction site where is located at İzmir Katip Celebi University. The samples were immediately coated with nylon bag to protect its natural properties and they were transferred to the soil mechanics laboratory and kept in airtight boxes.

Figure 1. General view of Çiğli-Balatçık

Lignite coal (20-50%) used in thermal power plants generating electrical energy and 10-15% of hard coal comes out as ash. This ash (75-85%) is removed from the boiler by flue gases and this ash is defined

as "thermal power plant fly ash". The thermal power plant fly ash used in this study was obtained from İzmir Kâtip Çelebi University, Civil Engineering Department, Construction Materials Laboratory. Maximum grain size of thermal power plant fly ash is 0.425 mm. The chemical properties of the thermal power plant fly ash used are shown in Table 1.

Table 1. Chemical composition of thermal power plant fly ash

Main compound	Amount (%)
SiO_2	43.3
Al_2O_3	24.1
P_2O_5	0.2
CaO	14.9
Na_2O	0.3
SO_3	4.1
TiO_2	0.9
Cr_2O_3	0.02
K_2O	2.6
MgO	3.1

Index Properties of Alluvial Deposits

All experiments were conducted according to the process given in the American Society for Testing and Materials (ASTM) and British Standards (BS). The specific gravities of alluvial soil samples were determined according to ASTM D854-14. In this experiment, a vacuum pump, air-free distilled water, pycnometer, and 20 g sample were used [12]. The liquid and plastic limits of soil sample were determined according to ASTM D4318 and BS1377-2[13, 14]. Wash sieve analysis was performed to determine the grain size distribution of all soil samples according to ASTM *Standard test method for particle size analysis of soils* [15, 16].

Compaction Test

The compaction properties of soil were defined using standard Proctor laboratory tests. There are three methods for the standard Proctor compaction test in ASTM D698. The soil is compacted in a cylindrical mold using a standard compaction energy. Three different samples (fine < 0.425mm, medium < 2mm, and coarse < 4.75 mm) are prepared, 10%, 15%, and 20% fly ash by dry weight of soil is mixed and standard proctor test is performed. In the Proctor test, the volume of the mold is 936.75 cm^3 and the soil (with all particles larger than 20 mm removed) is compacted by a rammer in existence of a 2.5 kg mass falling freely through 305 mm: the soil is compacted in three layers, each layer getting 25 blows with the rammer. After compaction, the bulk density and water content of the soil are defined, and the dry density is calculated. For a certain soil, the process is repeated at least five times, the water content of the sample being increased each time. The dry unit weight is plotted versus water content, and the curve of maximum dry unit weight against optimum moisture content is plotted [17].

Figure 2. Sample preparation of compaction test

Results and Discussions

In this section, the results obtained from the laboratory experiments and the interpretation of these results are included.

Results of Index Properties of Alluvial Deposits

The maximum dry unit weight, optimum moisture content, specific gravity, liquid limit, plastic limit, grain size distribution values are listed in Table 2. Grain size distribution curve is shown in Figure 3, it can be observed that fine soil has higher amount of silt and clay, while coarse soil has high amount of sand and gravel.

Table 2. Engineering properties of alluvial soil used

	Fine Soil	Medium Soil	Coarse Soil
Max. Dry Unit Weight (kN/m^3)	16.9	19.35	19.55
Opt. Moist. Content (%)	17	11	10.5
Specific Gravity	2.68	2.67	2.66
Liquid Limit (%)	38.3	38.3	38.3
Plastic Limit (%)	25.7	25.7	25.7
Plasticity Index	12.6	12.6	12.6
Grain Size	10%<4.75 mm 30%<2.0 mm 60%<0.425 mm	35 % < 4.75 mm 30%<2.0 mm 35%<0.425 mm	60 % < 4.75 mm 30%<2.0 mm 10%<0.425 mm

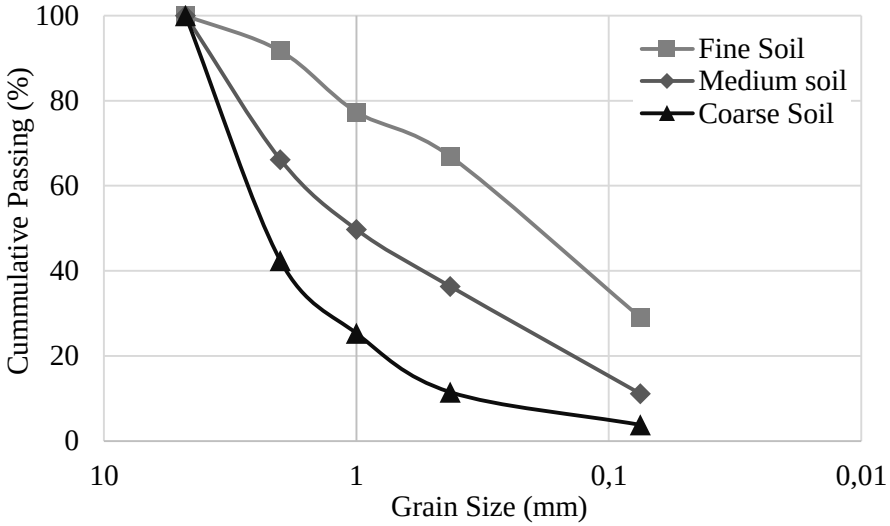

Figure 3. Grain size distribution curves of samples

The typical alluvial deposit behavior has been shown by basic physicochemical parameters. Also, the results were consistent with previous literature studies [5, 11].

Results of Compaction Characteristic of Alluvial Deposits

Standard proctor compaction experiments were carried out on fly ash treated fine, medium and coarse soils and untreated soils using a standard Proctor compaction effort of 592.8 kJ/m^3. Figure 4 shows the compaction curves of untreated fine, medium, and coarse soils. Figures 5, 6, and 7 show the compaction curves of FA treated fine, medium, and coarse soils, respectively. The effect of fly ash on the optimum moisture content and maximum dry unit weight for the fine, medium, and coarse soils are shown in Figures 8 and 9. Table 3 shows the variation of optimum moisture content and maximum dry unit weight by adding fly ash. There is an increase in maximum dry unit weight and decrease in optimum moisture content for 10% FA treated all soils, then there is a clear tendency that optimum moisture content increases while maximum dry unit weight decreases in 15% and 20% FA treated soils. The cause for the reduction in the optimum water content, especially in fine soil with 10% fly ash can be explained as follows: the cation exchange between additives and fine soil decreases the thickness of electric double layer and promotes the flocculation. The flocculation of the solid particles implies that the water additives soil mixtures can be compacted with lower water content, and the optimum water content is reduced. The decrease in the optimum water content indicates that alluvial soil can be stabilized by adding fly ash even for soils with low water content. The decrease of the maximum dry unit weight with the increase of the percentage of fly ash is mainly due to the lower specific gravity of the fly ash compared with alluvial soil, and the immediate formation of cemented products which reduce the density of the treated soil [18, 19].

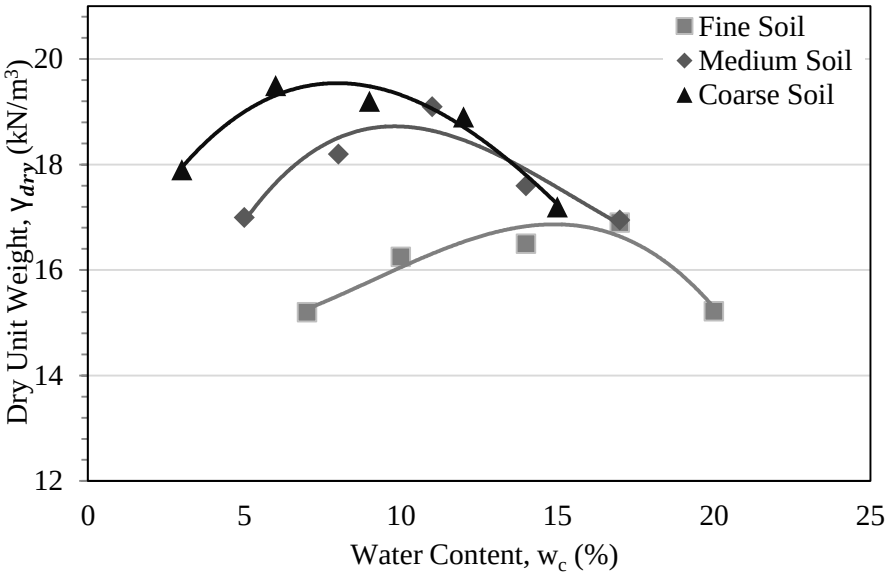

Figure 4. Compaction curves of fine, medium, and coarse soils

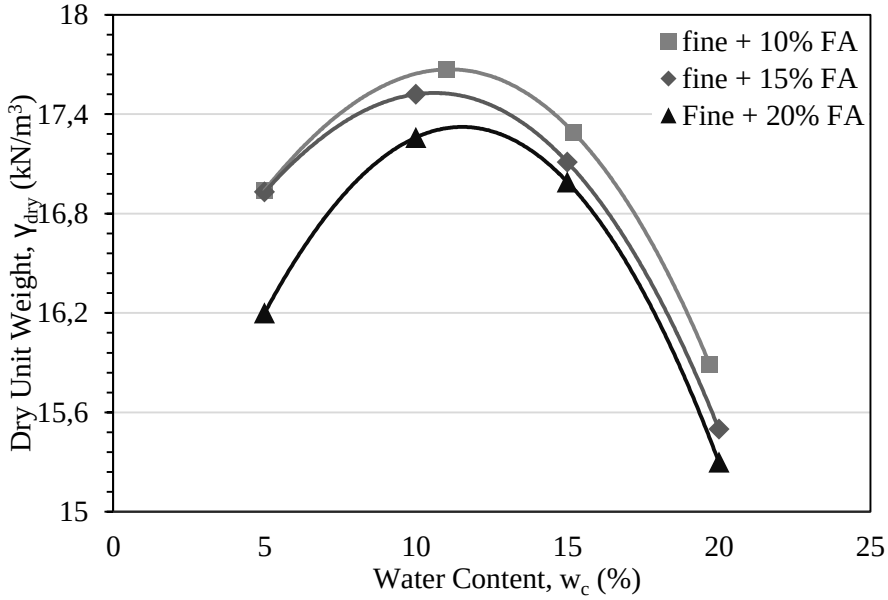

Figure 5. Compaction curves of fine soil treated with 10%, 15%, and 20% FA

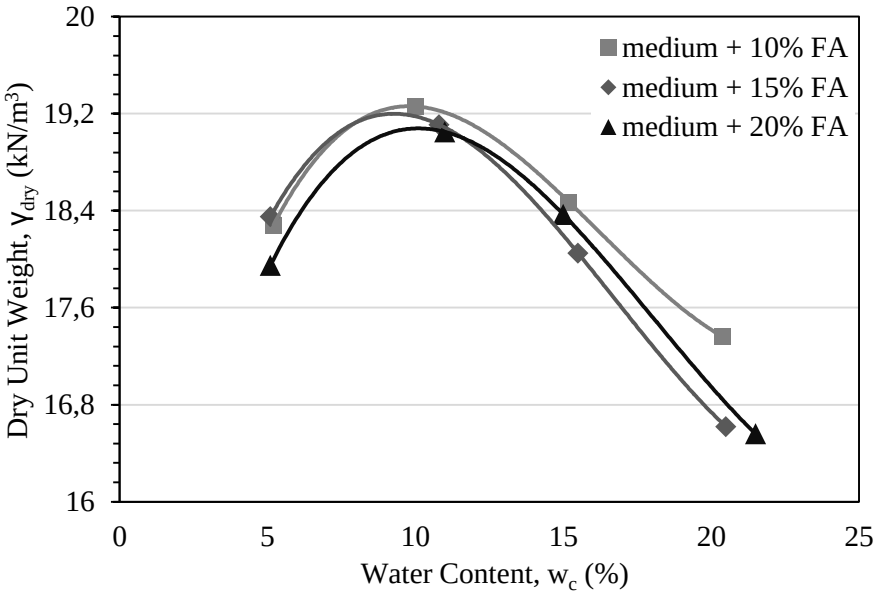

Figure 6. Compaction curves of medium soil treated with 10%, 15%, and 20% FA

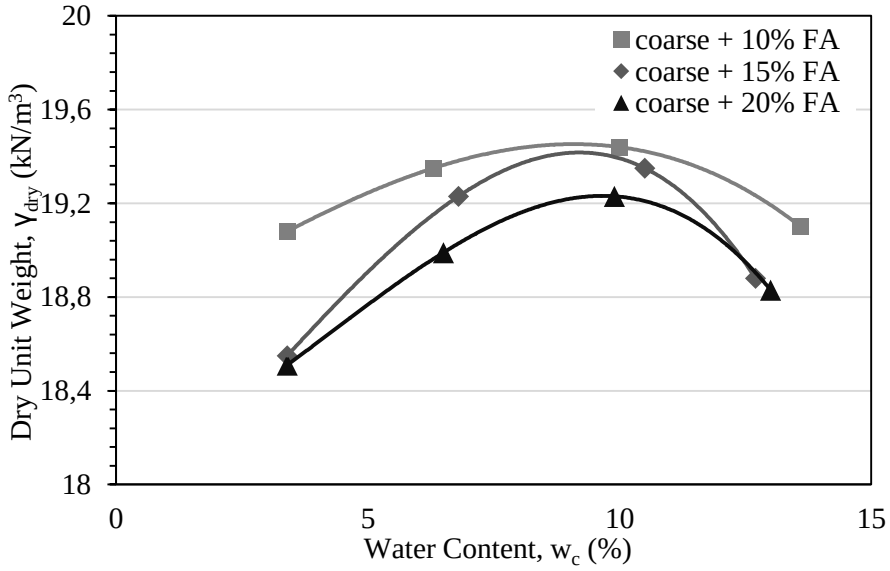

Figure 7. Compaction curves of coarse soil treated with 10%, 15%, and 20% FA.

It has been observed that the results obtained with the studies in the literature are consistent. Fsheng Zha et al. (2008) investigated the behavior of expansive soil stabilized with fly ash. Standard proctor tests were carried out on the fly ash treated soils. Their study shows, with an increase in fly ash content, the maximum dry unit weight and optimum moisture content decreased. By increasing the fly ash content to 15%, optimum moisture content and maximum dry unit weight decreased 7% and 4.3%, respectively.

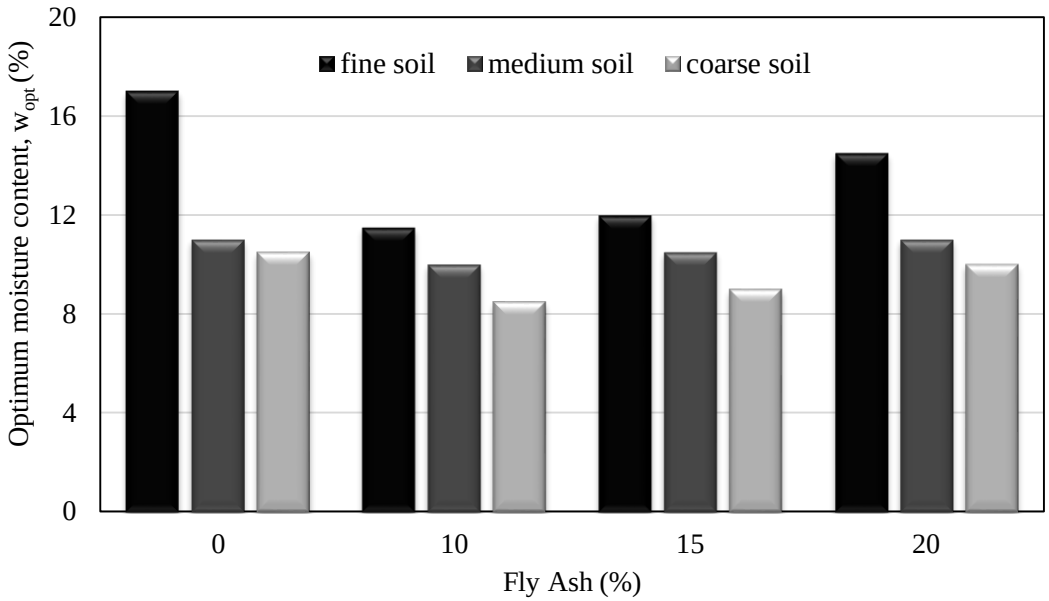

Figure 8. Optimum moisture content - FA content of fine, medium, and coarse soils treated with 10%, 15%, and 20% FA

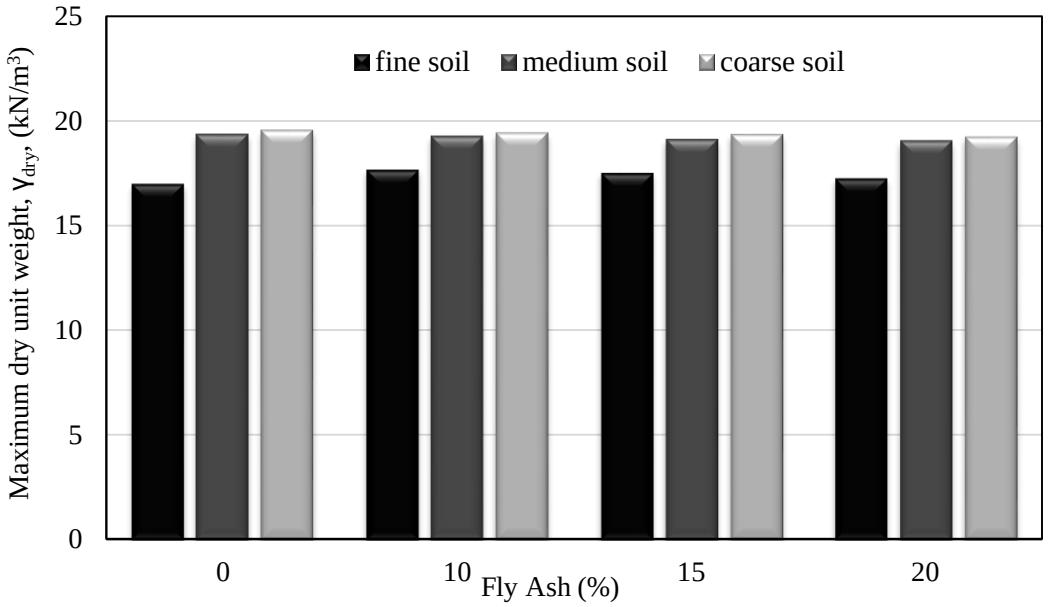

Figure 9. Maximum dry unit weight - FA content of fine, medium, and coarse soils treated with 10%, 15%, and 20% FA

Table 3. Variation of maximum dry unit weight and optimum moisture content

	Fine		Medium		Coarse	
FA (%)	$\gamma_{dy\ max}$ (kN/m^3)	w_{opt} (%)	$\gamma_{dy\ max}$ (kN/m^3)	w_{opt} (%)	$\gamma_{dy\ max}$ (kN/m^3)	w_{opt} (%)
0	16.9	17	19.35	11	19.55	10.5
10	17.67	11.5	19.26	10	19.44	8.5
15	17.52	12	19.11	10.5	19.35	9
20	17.26	14.5	19.05	11	19.23	10

Conclusion

Two parameters of alluvial deposits have been investigated in this study. The first parameter is the index properties of three different size (fine, medium, and coarse) alluvial soil. The second parameter is the compaction behavior of alluvial soils and effect of fly ash on compaction behavior of fine, medium, and coarse alluvial soils treated with 10%, 15%, and 20% flay ash. The following results were obtained:

1. Generally, by increasing the content of FA, maximum dry unit weight decreased and optimum moisture content increased for all three types of alluvial soil.
2. Maximum dry unit weight increases while there is a decrease in optimum moisture content of all three (fine, medium, and coarse) soils treated with 10% FA, this change is more obvious in fine soil with 4.5% increase in maximum dry unit weight and 32% decrease in optimum moisture content.
3. Maximum dry unit weight for fine, medium, and coarse untreated alluvial soil are 16.9, 19.35, and 19.55 (kN/m^3), respectively and optimum moisture content for fine, medium, and moarse are 17, 11, and 10.5%, respectively.
4. By increasing FA to 20%, maximum dry unit weight of medium and coarse soils decreases 1.5% and 2%, respectively.
5. While there was 4.5% increase in maximum dry unit weight of fine soil treated with 10% FA, it declined to 2% by increasing the content of FA to 20%.

References

[1] Ansary MA, Noor MA, Islam M. Effect of fly ash stabilization on geotechnical properties of Chittagong coastal soil. Geotechnical Symposium in Roma, 2006.
[2] Cristelo, N, Glendinning S, Fernandes L, Pinto AT. Effects of alkaline activated fly ash and Portland cement on soft soil stabilisation. Acta Geotech. 2013; 8(4): 395-405.
[3] Fauzi A, Nazmi WM, Fauzi UJ. Subgrade stabilization of Kuantan Clay using Fly Ash and bottom ash. The 8th international conference on geotechnical and transportation engineering, 2010.
[4] Senol A, Edil TB, Bin-Shafique MS, Acosta H, Benson CH. Soft subgrades stabilization by using various fly ashes. Resour. Conserv. Recy. 2006; 46(4):365–376.
[5] Mahvash S, López-Querol S, Bahadori-Jahromi A. Effect of class F fly ash on fine sand compaction through soil stabilization. Heliyon; 00274.
[6] Lahtinen P. Fly ash mixtures as flexible structural materials for low-volume roads. Finnra reports. 2001; 70.
[7] Mulder E.mixture of fly ashes as road base construction material. Waste Management. 1996; 16(1–3): 15-20.
[8] Tuncan A, Tuncan M, Koyuncu H. Use of petroleum-contaminated drilling wastes as sub-base material for road construction. Waste Management and Research. 200; 18(5): 489-505.
[9] Zhou H, Smith DW, Sego DC. Characterization and use of pulp mill fly ash and lime by-products as road construction amendments. Canadian Journal of Civil Engineering.2000; 27(3): 581-593.
[10] Mácsik J, Svedberg B.ogsbilvägsrenovering av Ehnsjövägen, Hallstavik. Värmeforsk Rapport 968, Stockholm in Swedish with English summary, 2006.
[11] Mir BA and Sridharan A. Volume change behavior of clayey soil-fly ash mixtures. International Journal of Geotechnical Engineering. 2014; 8(1).
[12] ASTM (2014) D 854 – 14: Standard Test Methods for Specific Gravity of Soil Solids by Water Pycnometer. ASTM International, West Conshohocken, PA, USA.
[13] ASTM (2010) D4318-10e1: Standard test methods for liquid limit, plastic limit, and plasticity index of soils, ASTM International, West Conshohocken, PA, USA.
[14] *Methods of test for soils for civil engineering purposes*, 2016. British Standard Institution, London, UK.
[15] ASTM (2007) D 422 – 63: Standard Test Method for Particle-Size Analysis of Soils (Withdrawn 2016). ASTM International, West Conshohocken, PA, USA.
[16] ASTM (2011) D 2487 – 11: Standard Practice for Classification of Soils for Engineering Purposes (Unified Soil Classification System). ASTM International, West Conshohocken, PA, USA.

[17] ASTM (2012) D 698 – 12: Standard Test Method for Laboratory Compaction Characteristics of Soil Using Standard Effort (12 400 ft-lbf/ft3 (600 kN-m/m3))1. ASTM International, West Conshohocken, PA, USA.
[18] Bell FG. Lime stabilization of clay minerals and soils. Eng Geol. 1996; 42: 223-237.
[19] Lees G, Abdelkader MO, Hamdani SK. Effect of the clay fraction on some mechanical properties of lime–soil mixtures. J Inst Highw Eng. 1982; 11: 3-9.
[20] Zha F, Liu S, Du Y, Cui K. Behavior of expansive soils stabilized with fly ash. Natural Hazards 2018; 47(3): 509–523.

Homojen Dolgu Baraj Yıkılması Üzerine Deneysel Bir Çalışma

Ebru Taşkaya[1], Gökçen Bombar[2], Gökmen Tayfur[3]*
[1,2]İzmir Kâtip Çelebi Üniversitesi, İnşaat Mühendisliği Bölümü, İzmir, Türkiye
[3]İzmir Yüksek Teknoloji Enstitüsü, İnşaat Mühendisliği Bölümü, İzmir, Türkiye
**İletişimden sorumlu yazar: ebruutsky@gmail.com*

Özet

Baraj yıkılması sonucu oluşacak taşkın hareketinin belirlenmesi, baraj mansabında herhangi bir yerleşim yeri olması durumunda, tehlikenin saptanması açısından önemli ve gerekli bir çalışmadır. Taşkın hareketi sonucu oluşan suyun hareketinin yanında aynı zamanda sediment taşınımı da toprak dolgu barajlar için incelenmesi gereken önemli bir konudur. Yapılan bu çalışmada homojen yapılı toprak dolgu baraj yıkılma problemi deneysel olarak ele alınmıştır. Dikdörtgen kesitli açık kanalda toprak dolgu barajın su aşması ile yıkılması sonucu taşkın dalgasının mansap boyunca yayılması ve taşkın sonucu mansap boyunca yayılan sediment taşınımı incelenmiştir. Baraj gövdesinde medyan dane çapı D_{50} = 0,441 mm olan malzeme kullanılmıştır. Toprak dolgu baraj gövdesini 20×20 cm'lik tahta plaka üzerine 1,5 kg ağırlığın yaklaşık 20 cm yükseklikten 10 kez düşürülmesi ile sıkıştırılmıştır. İki katman halinde bir katman 10 cm, diğer katman 14 cm kalınlığındaki sediment serilmiş ve sıkıştırılarak baraj kret genişliği 58 cm, baraj genişliği 106 cm, baraj yüksekliği 24 cm olarak şekilde baraj gövdesi hazırlanmıştır. Kanal boyunca 2 adet kamera ile sedimentin alansal yayılımı belirlenmiştir. Deney sonunda alınan ölçümler ile yıkılma sonrası sediment derinlik profili elde edilmiştir. Sediment maximum yayılma uzunluğu 631 cm, maximum yayılma genişliği ise 139 cm ölçülmüştür. Maksimum sediment kalınlığı ise en yüksek 20,8 mm ölçülmüştür.

Anahtar Kelimeler: baraj yıkılması, sediment taşınımı, taşkın dalgası ve sediment yayılımı

Giriş

Barajlar, eski zamanlardan beri su ihtiyacını karşılamak amacıyla büyük nehirler üzerine kurulan akışı engelleyerek, suyu rezervuarında tutan önemli su yapılarıdır. Barajların inşaa edilme amaçları arasında elektrik üretimi, taşkın önleme, tarım alanlarının sulanması, sanayi, şehir şebekelerine içme suyu sağlanması ve su ürünleri üretimi bulunmaktadır. Bol yağış alan yerlerde inşa edilen barajlar, taşkınla gelen yüksek hacimli fazla suyun baraj haznesinde depolanarak kontrolünü sağlamak amacıyla da kullanılmaktadırlar. Barajlar rezervuarlarında yüksek hacimli su depoladıklarından dolayı sağlam inşa edilmesi gereken yapılardır. Fakat doğal afetler sebebiyle veya yapısal sorunlar nedeniyle barajların yıkılma ihtimali vardır. Bu durum can kaybı ve maddi hasar ile sonuçlanabilir. Baraj yıkılması sonucunda oluşan taşkının şiddeti, aşırı yağışlar sonucu oluşan taşkınlara göre çok daha büyüktür. Bu yüzden olası bir taşkında, baraj mansabında taşkına maruz kalacak alanların belirlenmesi, bölgede yaşayan insanları erken uyarmak ve tahliye etmek için acil durum planı hazırlamak olası zararları en aza indirmeye yardımcı olacaktır.

Baraj yıkılma sebepleri farklılık gösterebilir; üstten aşma, iç erozyondan kaynaklı borulanma yüzünden veya yapısal sepeplerden dolayı, gibi. Uluslararası Büyük Barajlar Komisyonu'nun (International Commission on Large Dams, ICOLD) 1973 yılında sunduğu raporda tüm baraj yıkılmalarının %38'i dolusavak kapasitesinin yetersizliğinden suyun üstten aşmasından dolayı olduğunu açıklamıştır. Barajların %33'ü baraj gövdesinde meydana gelen borulanma yada sızma yüzünden yıkılmaktadır. %23'lük kısmın yıkılma nedeni olarak temel problemleri, şev kaymaları, zemin sıvılaşması veya rezervuarlarda toprak kaymaları sonucu oluşan büyük taşkın dalgaları olduğu gösterilmektedir. Costa'nın 1985 yılında yayınlamış olduğu çalışmada, baraj yıkılmalarının yaklaşık %34'ü suyun üstten aşması, %30'u temel kusurları, % 28'inin de borulanma yüzünden olmaktadır [1].

Suyun baraj mansap yüzünde kret üstünden aşarak barajın erozyonuna sebep olma durumuna üstten aşma denir. Zhang ve ark.'nın yayınlamış çalışmasında 593 tane toprak dolgu barajın yıkılma sebeplerini incelemişler ve toprak dolgu barajların %36,4'ü üstten aşma yüzünden yıkılmış olduğunu görmüştür [2]. ABD'de 1889 yılında South Fork Barajı'nın gövdesinde suyun üstten aşması sonucu yıkılmasıyla 2200 kişinin ölümüne sebep olmuş, Hindistan'da 1974 yılında yıkılan Machhu II Barajı yine barajın üstten su aşması sebebiyle 2000 kişinin ölümüne neden olmuştur [1].

Baraj yıkılması sonucu rezervuarda bulunan büyük kütleli suyu oluşturan taşkın dalgasının yayılımını ve hidrodinamik özeliklerini anlamak mühendislik alanındaki çalışmalar arasında önem arz etmektedir. Taşkın dalgası ile yıkalan enkaz halindeki baraj gövdesini oluşturan malzemeler, tabandaki katı maddeler ve sediment, taşınarak mansap bölgesindeki vadide oyulmalar ve yığılmalar meydana getirir.

Cao ve ark.'nın yapmış olduğu çalışmada taşkın dalgası sebebiyle yıkılan barajlardaki hareketli tabanı gözlemlemiş ve morfolojik gelişimini tahmin etmeye çalışmışlardır [3]. Sığ su hidrodinamiğine göre teorik bir model geliştirmişler ve bu denklemi numerik olarak çözmüşlerdir. Elde ettikleri sonuca göre baraj yıkılmasından sonra, mansap bölgesinde ağırlıklı olarak taşkın dalgası yatak formları bulmuşlar, ayrıca baraj yıkılmasının başında sediment erozyonundan kaynaklı barajın mansabında oluşan ve daha sonra yok olan hidrolik sıçramanın oluştuğunu gözlemlemişlerdir. Ayrıca Wu ve Wang'da benzer bir taşkın dalgası nedeni ile baraj yıkılımını sonucunda oluşan yatak formlarını bir boyutlu olarak incelemiştir [4]. Cao ve ark.'nın geliştirmiş olduğu modeli kabul etmişler ve sediment taşınımına etki eden faktörleri, akımın yatak değişimi üzerindeki etkisini değerlendirerek sığ su denklemini kullanmışlarıdır. Sediment taşınımını belirlemek için Van Rijn formüllerini modifiye edip kullanmışlardır. İki deneysel durumda için simülasyonlar ve ölçümler arasında tutarlılık oldukça yüksek bulunmuştur.

Barajların yıkılması sonucu oluşan taşkın dalgasının hidrodinamik üzerine yapılan modellemeler literatürde yer almaktadır, fakat barajlarda baraj yıkılması ile sedimentin hareketi ve yayılımı hakkında yapılmış çalışmalar oran olarak daha azdır. Bu çalışmada, toprak dolgu barajların yıkılması deneysel olarak ele alınmış, barajlarının yıkılması sonucu taşkın dalgası ile birlikte barajın mansabına doğru hareket eden sedimentin yayılımı incelenmiştir.

Metodoloji

Deney, İzmir Kâtip Çelebi Üniversitesi, Hidrolik Laboratuvarında bulunan, 18 m uzunluğunda, 2 m genişliğinde beton kanalda yapılmıştır. Boyutları Şekil 1'de verilen homojen olarak inşa edilen baraj gövdesi kanalın 3,0 m ile 4,06 m kesitleri arasındadır.

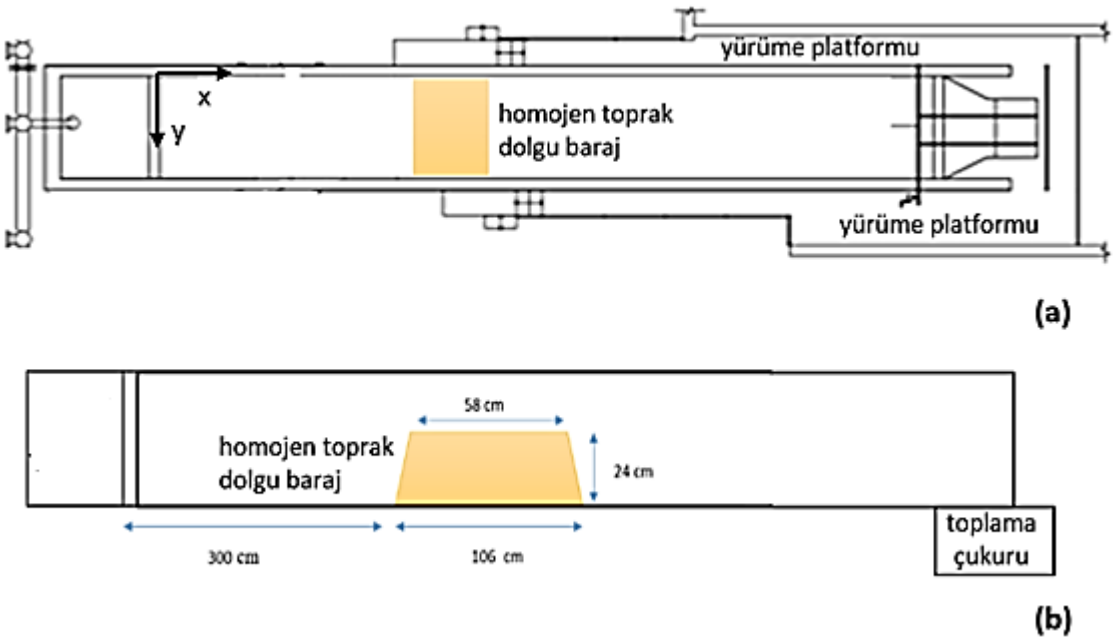

Şekil 1. Deney düzeneği (a) plan ve (b) kesit görünümü

Gövdede kullanılan malzemenin medyan dane çapı D_{50} = 0,441 mm olup toplam 461,22 kg sediment kullanılmıştır. Malzemenin dane çapı dağılımı Şekil 2'de verilmiştir.

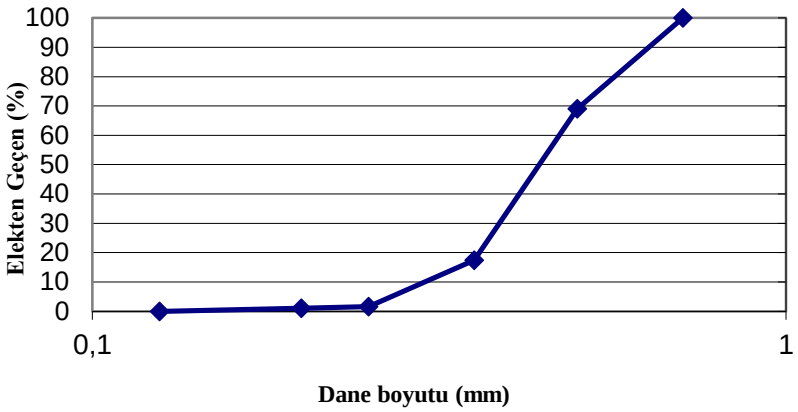

Şekil 2. Dane çapı dağılımı

Gövde inşaatı iki katman halinde oluşturulmuştur. İlk katman 10 cm yüksekliğinde serilmiştir. Toprak dolgu baraj gövdesini 20×20 cm'lik tahta plaka üzerine 1,5 kg'lık ağırlık yaklaşık 20 cm yükseklikten 10 kez düşürülmesi ile yaklaşık 2 cm sıkıştırılmıştır (Şekil 3). Daha sonra 14 cm yüksekliğindeki ikinci katman 14 cm olarak serilmiş ve aynı yöntem kullanılarak yaklaşık 2-2,5 cm sıkıştırılmıştır. İnşa işlemi tamamlandıktan sonra baraj kret genişliği 58 cm, baraj genişliği 200 cm, baraj uzunluğu 106 cm, baraj yüksekliği 24 cm olarak şekilde baraj gövdesi hazırlanmıştır.

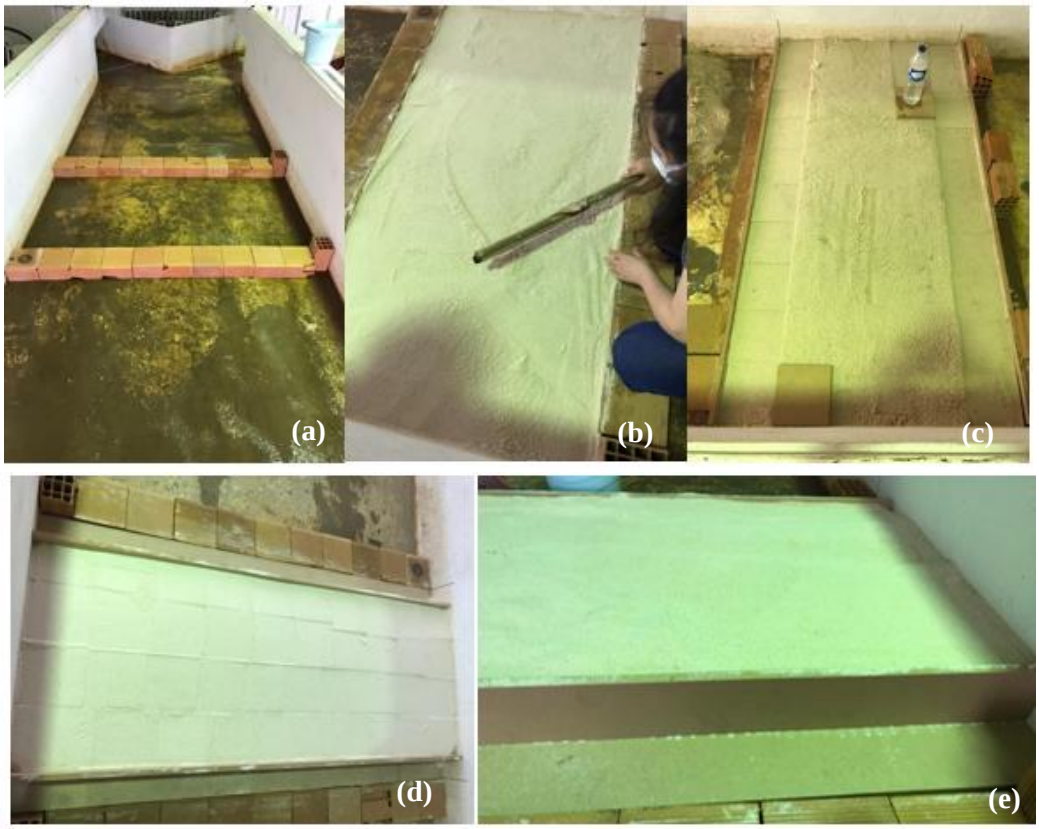

Şekil 3. (a)-(e) Deney hazırlık aşamaları

Baraj membasındaki hazneye su doldurulurken barajın zarar görmesini engellemek için baraj memba yüzü plastik örtü ile korunmuştur. Barajın memba tarafında tutulan su hacmi 2,68 m^3'dir. Memba su seviyesi kret kotu seviyesine geldiğinde örtü memba tarafından çekilmiş ve deney başlatılmıştır. Biri memba diğeri mansap kısımlarına yerleştirilen 2 adet kamera ile memba ve mansap bölgesinde sedimentin alansal yayılımını gözlemlemek için kayıt alınmıştır.

Deney sonunda kumpas kullanılarak alınan ölçümler ile yıkılma sonrası sediment derinlik profili elde edilmiştir.

Deneysel Sonuçlar

Yıkılma başladıktan sonra barajın sol sahilinde yıkılma gözlenmiş ve baraj gövdesindeki sediment bu bölgeden ayrılarak mansaba taşınmıştır. Yaklaşık 6 dakika içerisinde yıkılımı tamamlanmıştır. Barajın yıkılma aşamaları Şekil 4.'da verilmiştir. Şekil 4'te 1 numaralı fotoğraf baraj membasına serilen plastik örtünün kaldırılmadan önceki hali, 2 numaralı fotoğraf suyun üstten aşma durumunu göstermektedir. Baraj gövdesindeki erozyonun başlama bölgesi 3 numaralı fotoğrafta gösterilirken, 4, 5, 6 numaralı fotoğraflar baraj gövdesindeki sedimentin kanal tabanında yayılımının zamanla değişimini gösterilmektedir. 7 numaralı fotoğraf deney sonunda oluşan tabandaki sedimentin yayılımını göstermektedir.

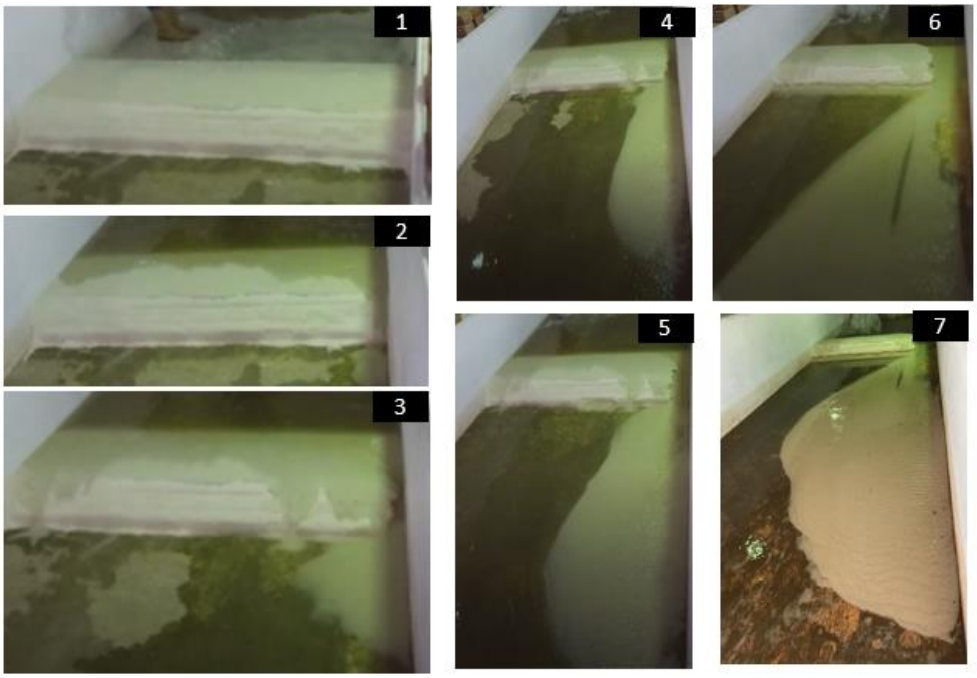

Şekil 4. Deney esnasındaki sediment yayılımı (1-7),

Karşılaştırma amaçlı deney başında ve sonunda sediment durumu Şekil 5'te sunulmuştur. Sediment yayılma uzunluğu 6,31 m, yayılma genişliği ise x = 4,28 m'de y =1,39 cm'dir.

Şekil 5. (a) Barajın deney başlangıç ve (b) - (c) bitişindeki durumu

Deney sonunda, kanal içerisindeki su yeteri kadar drene olduktan sonra kumpas yardımı ile sediment yükseklikleri okunup not edilmiştir. Ölçümler x ekseninde 0,25 m aralıkla, y ekseninde 0,10 m aralıkla alınmıştır. Sediment yükseklikleri kullanılarak taban topografyası çıkarılmış ve Şekil 6'da verilmiştir. Taban ortalama yüksekliği yaklaşık 10 cm olup maksimum sediment yüksekliği x = 4,31 m'de, y = 0,5 m'de iken z = 23,4 mm olarak ölçülmüştür.

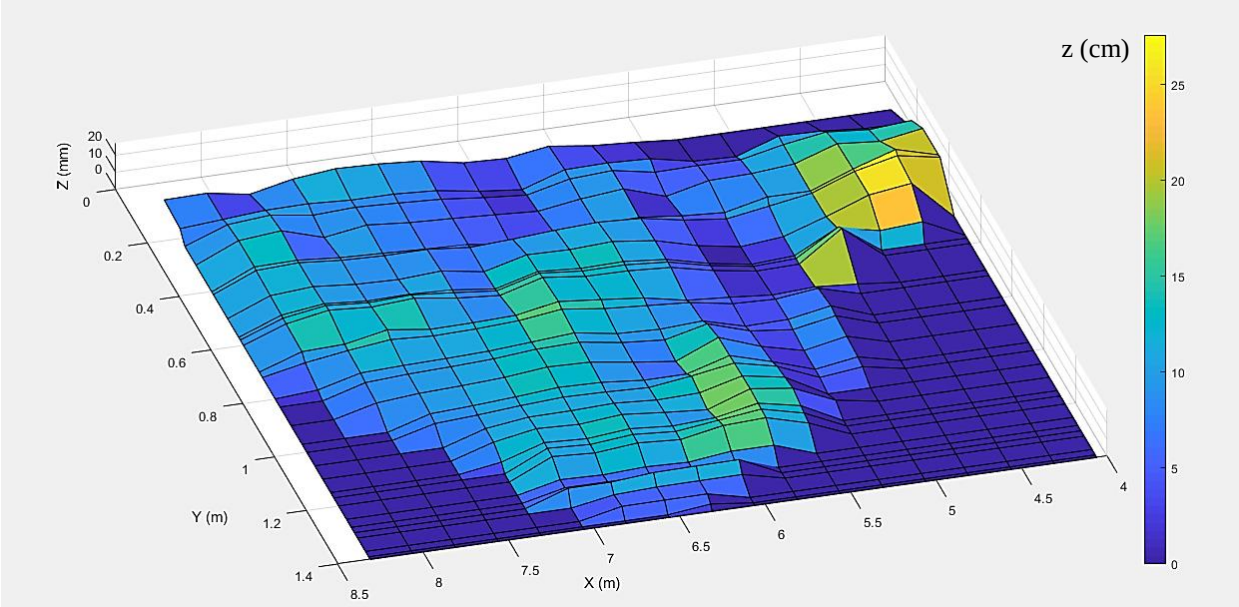

Şekil 6. Taban topografyası

Sonuçlar

Ülkemizde ve dünyada çeşitli amaçlar için barajlar inşa edilmekte veya planlanmaktadır. Barajlar yıkılmaları sonucu ciddi can ve mal kayıplarına sebep olduğundan baraj projeleri hazırlanırken aynı zamanda yıkım senaryoları için de planlamalar yapılmalıdır. Baraj yıkılması sırasında oluşan taşkın dalgasının özellikleri ve yıkım gücünün modellemesi ile toprak dolgu barajlar için sediment taşınımın modellenmeside büyük önem arz etmektedir. Bu çalışma kapsamında homojen tipli toprak dolgu barajın üstten aşma sebebiyle yıkılması durumunda baraj gövdesini oluşturan malzemenin yayılması üzerine deneysel bir inceleme gerçekleştirilmiştir. Benzer şekilde farklı deney senaryoları ile elde edilen veriler karşılaştırılarak daha kapsamlı ve büyük çalışmalar yapılarak mevcut toprak dolgu barajların yıkılma senaryoları ile baraj mansabındaki yerleşim bölgelerine kaç metre yükseklikte, uzunlukta, genişlikte sediment taşınacağı modelleme çalışmaları ile belirlenebilmesi ve yerleşim yerleri daha önceden planlanarak önlemler alınabilmesi mümkündür.

Teşekürler

Bu çalışma, TÜBİTAK tarafından finanse edilen 1001 araştırma programının 119M959 proje numaralı "TOPRAK DOLGU BARAJ YIKILMASI SONUCU OLUŞAN SEDİMENT TAŞINIMININ DENEYSEL VE SAYISAL MODEL İLE ARAŞTIRILMASI—GERÇEK BARAJLARA CBS ORTAMINDA UYGULANMASI" projesinin bir parçasıdır.

Kaynakça

[1] Costa JE. Floods from Dam Failures; Open File Report 85-560. US Geological Survey: Denver, CO, USA, 54, 1985
[2] Zhang LM, Xu Y, Jia JS.Analysis of earth dam failures: A database approach. Georisk 2009; 3(3): 184-189.
[3] Cao Z, Pender G, Wallis S, Carling P. Computational dam-break hydraulics over erodible sediment bed. J. Hydraul. Eng. 2004; 130(7): 689–703
[4] Wu W, Wang SS. One-dimensional modeling of dam-break flow over movable beds. Journal of Hydraulic Engineering, ASCE 2007.

Simetrik Akarsu Kavşaklarında Farklı Mansap Derinliklerinin Su Yüzeyi Profiline Etkisi

Cihan Canıbek[1], Gökçen Bombar[2], Antônio Heleno Cardoso[3]*
[1,2]İzmir Katip Çelebi Üniv., İnşaat Mühendisliği Bölümü, İzmir, Türkiye
[3] Universidade de Lisboa, Ceris, Instituto Superior Tecnico, Portugal
**İletişimden sorumlu yazar: cihancanibek@hotmail.com*

Özet

İki veya daha fazla akarsuyun birleşerek kavşak noktası oluşturmaları, açık kanal hidroliği alanında sık karşılaşılan bir durumdur. Kavşaklar, hidrolik açıdan önemli kontrol noktalarıdır. Kavşak içinde memba ve mansap derinliklerinin bilinmesi oluşacak yük kaybının hesaplanabilmesi açısından önem arz etmektedir.

İzmir Kâtip Çelebi Üniversitesi Hidrolik Laboratuvarı'nda bulunan deney düzeneği üzerinde gerçekleştirilmiş bu çalışmada, yan kollardan gelen debi sabit tutularak mansap derinliği değiştirilerek yan kollar ve ana kanal boyunca akım derinlikleri ölçülmüştür. Simetrik 90° açıyla birleşen yan kolların genişliği 1 m, ana kanalın genişliği ise 2 m olup yan kollar ile ana kanalın taban kotları eşit olacak şekilde düzenlenmiştir. Akım derinlikleri, limnimetre vasıtasıyla ölçülmüş olup önce taban kotları ölçülmüş, daha sonra su yüzey kotları ölçülmüştür. Ölçümler, ana kanalda, her 50 cm'de bir, yan kollarda ise her 25 cm'de bir yapılmıştır. Çalışmada, ana kanalda Froude sayıları 1'den küçük olup akım, nehir rejiminde olmuştur.

Bu çalışmada sağ kolun debisi 29,61 l/s, sol kolun debisi 20 l/s olup ana kanaldaki toplam debi 49,61 l/s'dir. Mansap kısmında bulunan kapak vasıtasıyla mansap akım derinliği ayarlanmıştır. Gerçekleştirilen deneylerde mansap akım derinliği sırasıyla 9,3 cm 12,60 cm ve 15,35 cm olacak şekilde ayarlanmıştır. Bu koşullarda kavşak birleşim noktasında derinlik sırasıyla, 9,8 cm, 12,8 cm ve 15,75 cm olmuştur.

Her 3 deneyde de ana kanalda H2 profili gözlenmiş ve kavşak birleşim noktasındaki derinlik mansap derinliğinden daha fazla olmuştur. Yan kol ve ana kanal debileri arasındaki oran ile akım derinlikleri arasındaki ilişki literatür ışığında incelenmiştir.

Deneylerde taban eğimi 0 ve $y>ycr$ olup çalışmalar nehir rejiminde yapıldığından *H2* profili gözlemlenmiştir. Su yüzey profillerinde eğimler birbirine paralellik göstermiştir. Mansaptaki derinliğinin artması, su seviyesi ortalamasını artırmıştır.

Anahtar Kelimeler: simetrik akarsu kavşağı, akım derinliği, su yüzeyi profili

Giriş

Akarsu Kavşakları; iki veya daha fazla akarsuyun birleştikleri yer olarak tanımlanmaktadır. Açık kanal hidroliği alanında sık karşılaşılan bir fenomen olup hidrolik açıdan önemli kontrol noktalarıdır. Kavşak civarında akım derinliklerinin bilinmesi daha sonradan akarsu kavşağı civarında yapılması planlanan yapıların tasarımı açısından önem arz etmektedir. Günümüzde bu alandaki araştırmalar devam etmektedir. Kavşaklar, simetrik yapıda olabileceği gibi asimetrik yapıda da olabilmektedir. Simetrik akarsu kavşaklarında iki yan kol birleşerek ana kanalı oluşturur. Ana kanal ile yan kolun birleşmesi ile toplam debi artar ve akarsu, ana kanal istikametinde yoluna devam eder (Şekil 1).

Şekil 0. Akarsu Kavşağı - Negro ve Solimoes Nehirlerinin Birleşimi, Brezilya [1]

Çalışmanın Amacı

Bu çalışmanın amacı 90° açı ile birleşen simetrik akarsu kavşaklarında, taban kotunun eşit olması durumunda, mansap akım derinliği ile yan kollardan gelen farklı debi ve debi oranlarının, kavşak civarında oluşan akım derinliğine etkisinin incelenmesi ve bu alanda literatürdeki boşluğun doldurulmasıdır. Yine simetrik akarsu kavşaklarında, taban eşitliği durumunda, yan kollardan gelen farklı debiler ve debi oranları ile mansap akım derinliğinin, su yüzeyi profili üzerine etkisinin belirlenmesi hedeflenmiştir.

Akarsu kavşaklarında akım derinliklerinin incelenebilmesi ve su yüzeyi profilinin belirlenebilmesi açısından fiziksel modeller ve deneyler önem taşımaktadır. Çalışmamızda mansap derinliği ve yan kollardan gelen debiler değiştirilerek farklı koşullar altında kavşak içi ve yakınındaki akım derinlikleri ölçülmüş ve yük kayıpları elde edilmiştir.

Açık Kanal Kavşaklarında Akım Karakteristiği

Açık kanal kavşaklarında akım karakteristiği şu temel unsurlardan meydana gelmektedir. Kavşağın hemen mansabında bir ayrılma bölgesi oluşur. Ayrılma bölgesi, ana kanaldaki akımın daralmasına sebep olur ve bu kısım daralan bölge olarak adlandırılır. Kavşağın hemen membaya bakan tarafında yan koldan gelen debiye bağlı olarak yerinin değiştiği gözlemlenebilen bir durgunluk noktası oluşmaktadır. İki veya daha fazla akımın birleşmesi, kayma düzlemi oluşturur. Mansaptan membaya doğru akım derinliğinde artış gözlemlenir. Ayrılma bölgesi; yan koldan gelen akımın yaratmış olduğu momentumun, ana kanalı kavşağın mansap köşesinden ayırması sebebiyle oluşur (Şekil 2).

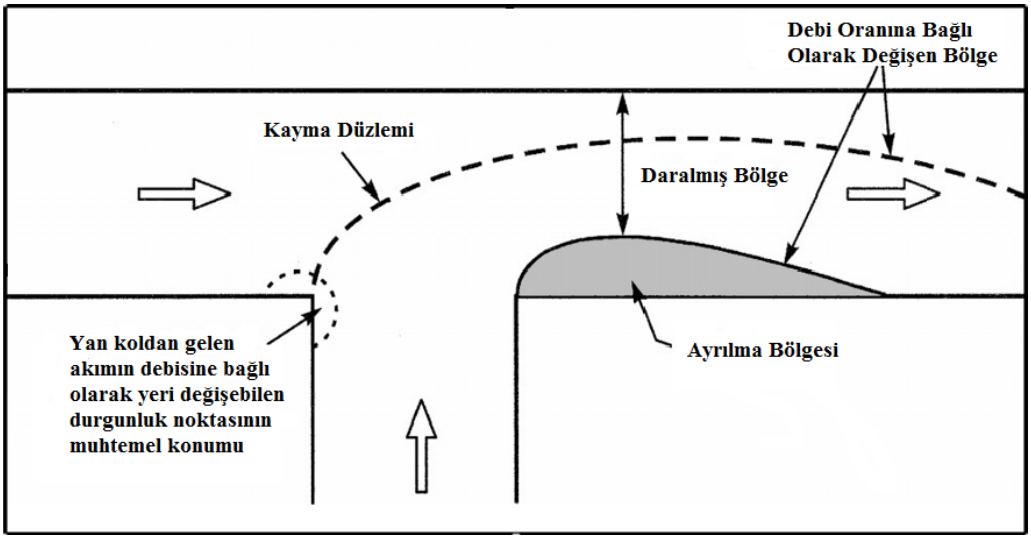

Şekil 2. Açık Kanal Kavşaklarında Akım Karakteristiği [2]

Genel olarak durgunluk bölgesinde basıncın ve akım derinliğinin arttığı, akım hızlarının ve kayma gerilmelerinin azaldığı gözlenmektedir. Ana kanaldan gelen akım, yan koldan gelen akımı önüne katarak ana kanaldan gelen akımın yönüne doğru saptırır. Kavşağın mansap kısmında ve ana kanal kenarında ayrılma bölgesi oluşur. Ayrılma bölgesi sürekli olarak kendi etrafında dönen çevrintilerden oluşmaktadır. Ayrılma bölgesinin uzunluğu ve genişliği, yan koldan gelen akımın debisine bağlı olarak değişmektedir. Akarsu tabanında, ayrılma bölgesinin genişliği ve uzunluğu, su yüzeyine oranla azalmış olsa da varlığını korumaktadır. Ayrılma bölgesinin belli bir genişliği bulunduğundan, ana koldan gelen akım bu bölgeden geçerken daralmış olur. Akımın daralması, bu bölgeden geçmekte olan akımın hızının artmasına sebep olur. Ana kanal ve yan koldan gelen akımın birleşmesi ile toplam debi ve hız artar [2].

Akarsu kavşaklarındaki akım yapısı, Best [3]'nin öncülüğünde ortaya konan kavramsal modelin ardından, hassas ve güvenilir hız ölçüm cihazlarının kullanılmaya başlanmasıyla derinlik kazanmıştır.

Açık Kanal Hidroliği Alanında Yapılan Bazı Çalışmalar

İlk olarak Taylor (1944) memba ve mansap arasında bulunan derinlik oranları üzerine çalışmalarını yoğunlaştırarak açık kanal kavşak akımlarını ele almıştır. Bu çalışmaların sonucunda derinlik oranlarının hesabında kullanılacak bir denklem elde etmiştir. Taylor'un çalışması, açık kanal kavşaklarının kuramsal tarifinin yapılmasına duyulan ihtiyacın saptanması açısından önemlidir (Şekil 2). Weber, Schumate ve Mawer (2001) [2].

Best vd. [3] tarafından yapılan çalışmalarda, ana kanal 0,12 m, yan kol 0,08 m genişliklerinde olup aralarındaki açı 30° olarak ayarlanmıştır. Model, 3,5 m uzunluğunda olup genişliği 0,30 m, uzunluğu 10 m olan devir daim kanalına yerleştirilmiştir. Böylece akım derinliğini kontrol etmek adına kavşaktan mansaba yeterli mesafe kalmıştır (Şekil 3).

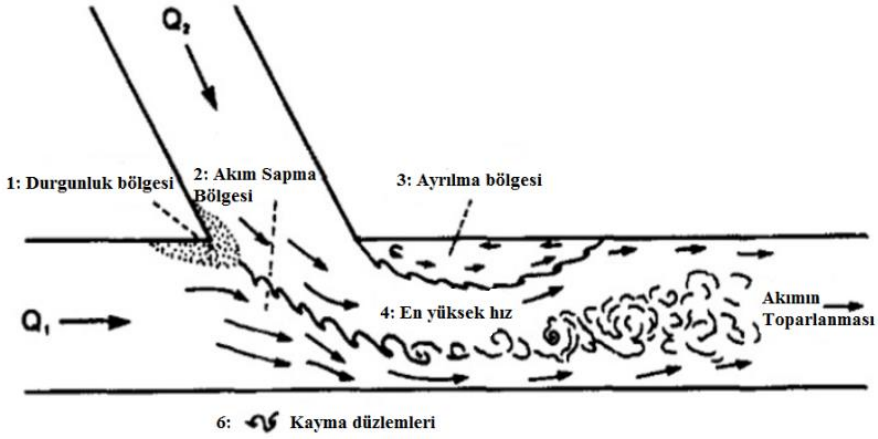

Şekil 3. Kanal ve Akarsu Kavşaklarındaki Akarsu Yapısı

Best'e [3] göre Kavşak; Şekil 3'te belirtilen durgunluk bölgesi (stagnation zone), akımın sapması (flow deflection), akım ayrılma bölgesi (flow seperation zone), maksimum hız (maximum velocity), akımın toparlanması (flow recovery) ve kayma düzlemleri (shear layers) gibi karakteristik unsurlardan oluşmaktadır.

Durgunluk bölgesinde; basınç ve akım derinliği artmakta olup akım hızı ve kayma gerilmesi azalmaktadır. Yan koldan gelen akımın, ana kanaldaki akım ile birleşmesiyle akım yönünde sapma oluşmuştur. Ayrılma bölgesinde kavşağın mansabında ana kanal kenarında kendi etrafında dönen çevrintiler meydana gelmiş ve yukarı yönde düşey hızların önemli ölçüde belirginleştiği gözlenmiştir. Düşey hızlar, bir nevi su perdesi oluşturmuş ve ana kanaldaki akımın bu bölgeye girmesini engellemiş, böylece karışma noktasının mansabındaki akımın akmakta olduğu kesit aslında daha da daralmış ve daha büyük hızlara sebep olmuştur. Ana kanal ve yan koldaki debinin birleşmesi ile toplam debi ve hız artmıştır. Kesitsel ortalama hız daha da artmıştır. Sağ ve sol kısımdaki akım hızlarının farklılığından kaynaklanan çevrintiler oluşmuştur. Mansaba doğru ilerledikçe akarsuyun artık yeni bir genişlikte ve debide akmaya devam ettiği görülmüştür.

Best'in [3] yapmış olduğu çalışmada olduğu gibi çalışmamızda da her iki yan koldan gelen debinin birleşmesiyle toplam debi ve hız artmıştır. Ayrılma bölgesi oluşmuştur. Ana ve yan kollardan gelen debi ve debi oranları farklı olmuştur.

Mevcut modeller, öncelikle kavşakların membasında su seviyelerindeki yükselmeye ve kuramsal ve deneysel faktörler vasıtasıyla ayrılma bölgesinin boyutları üzerine odaklanmıştır. Tümüyle nehir rejimindeki akımlarda, birleşimlerde su seviyelerinin yükselmesi üzerine ilk çalışma Taylor tarafından yürütülmüştür (1944). Bu çalışmada eşit genişlikte ve taban eğiminin sıfır olduğu karışımlar için şu varsayımlarda bulunulmuştur; (1) Sürtünme gerilmeleri ihmal edilmiştir. (2) Basınç dağılımları hidrostatiktir. (3) *AB* ve *BC* düzlemlerindeki su seviyeleri eşittir. (4) *BC* ve *CD* düzlemlerindeki basınç eşittir. (5) bütün en kesitlerdeki hızlar üniform şekilde dağılmaktadır. Süreklilik ve momentum denklemlerinin basitleştirilerek *ABCDFGA* açık sisteminde uygulanmasıyla bahsi geçen varsayımlar da göz önünde bulundurularak denklem elde edilmiştir Coelho (2015) [4].

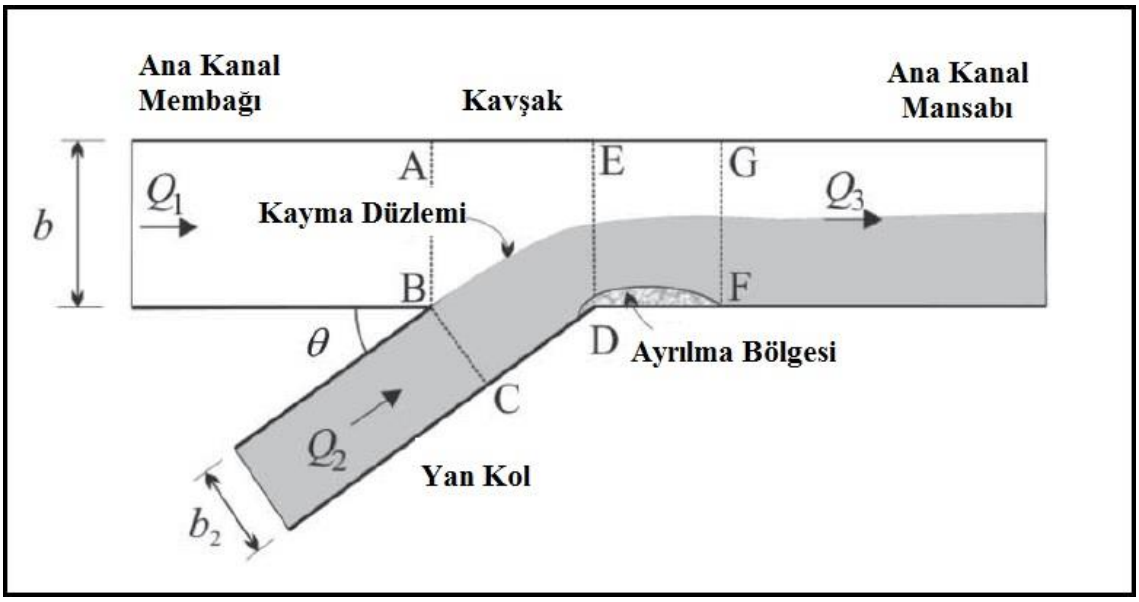

Şekil 4. Kavşaktaki Akış Dinamiğinin Genel Şematiği [4]

Taylor'un çalışmasında kullanılan deney düzeneği, birleşen kolların genişliğinin eşit olması, yatak eğiminin sıfır olması, nehir rejiminde akımlar üzerinde çalışılması, ayılma bölgesi oluşması gibi unsurlar bakımından çalışmamızla paralellik göstermiştir.

Deney Düzeneği, Cihazlar, Deneysel Yöntem

Deneyler, İzmir Katip Çelebi Üniversitesi-İnşaat Mühendisliği Bölümü, Hidrolik Ana Bilim Dalı için tahsis edilmiş olan Hidrolik Laboratuvarında gerçekleştirilmiştir. Deney düzeneğini oluşturan kısımlar aşağıda açıklanmış ve Şekil 5'te plan görünümü verilmiştir. Yan kollar arasında bulunan açı,

90° olarak ayarlanmış, yan kol ve ana kanal genişlikleri sırasıyla 1 m ve 2 m olacak şekilde ayarlanmış ve bu parametreler sabit tutulmuştur. Mansap akım derinliği ile yan kollardan gelen debiler değiştirilerek yan kollarda, ana kanalda ve kavşak civarında bazı önemli noktalarda oluşan akım derinlikleri ölçülmüştür. Sağ yan kol, *T1* simgesi ile gösterilmiş olup sol yan kol *T2* şeklinde gösterilmiştir. Sağ yan koldaki debi $Q_{t1,}$ sol yan koldaki debi Q_{t2} ve toplam debi $Q_{p\text{-}c}$ olarak gösterilmiştir. Deney düzeneğinin tabanı yatay olup yan kollar ile ana kanal arasında seviye farkı bulunmamaktadır. 2 adet santrifüj pompa vasıtasıyla, yan kolların memba yönünden istenen büyüklükte debiler sağlanmıştır.

Deney düzeneğinde ana kanalın mansap yönü, koordinat sistemine göre x ekseninde pozitif yönü göstermektedir. Kavşak birleşim noktası y ekseninde sıfır noktasıdır. Buna bağlı olarak kanal tabanından su yüzeyine doğru hareket edildikçe, z aksında pozitif yönde ilerlenmiş olacaktır (Şekil 5).

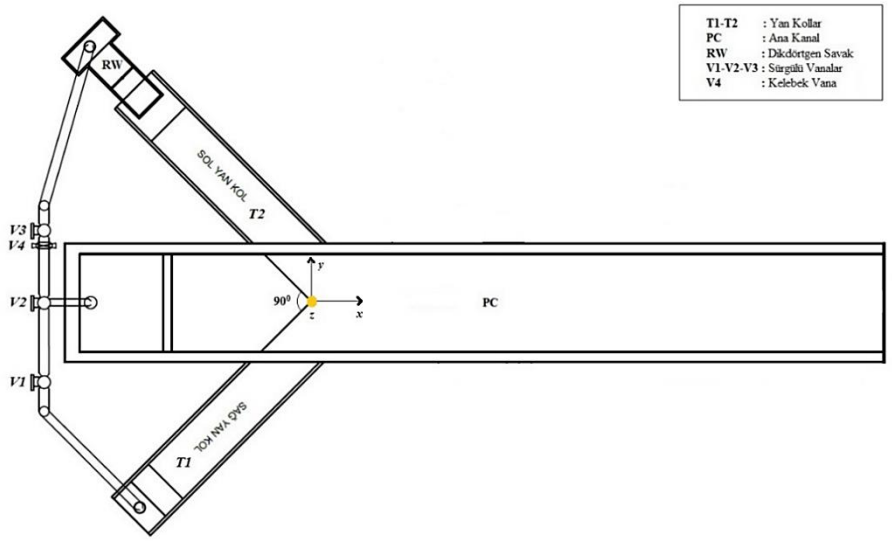

Şekil 5. Deney Düzeneğinin Plan Görünümü

Ölçümler, ana kanalda, kavşaktan itibaren mansap noktasına kadar her 50 cm'de bir, yan kollarda ise membadan kavşak noktasına kadar her 25 cm'de bir yapılmıştır. Yan kollarda ölçüm yapabilmek maksadıyla yan kolların membasından başlayacak şekilde, *y* düzleminde orta noktalarından ip çekilerek ana kanal karşı duvarında sabitlenmiştir. Çekilen ipler, kavşak noktasında kesişmiş olup bu şekilde elde edilen doğrusal hat sayesinde yan kollarda ölçümler gerçekleştirilebilmiştir (Şekil 6).

Yan kolların kesişim noktası, *x, y* ve *z* eksenlerinde 0 noktası olarak kabul edilmiştir. İplerin kesişim noktasında *y* ekseninde 25 cm'de bir olmak üzere toplam 6 noktada daha ölçüm yapılmıştır. Bu bilgiler ışığında her deney seti için toplam 70 noktada ölçüm yapılmıştır (Şekil 7).

Şekil 6. İplerin Kesişim Noktası

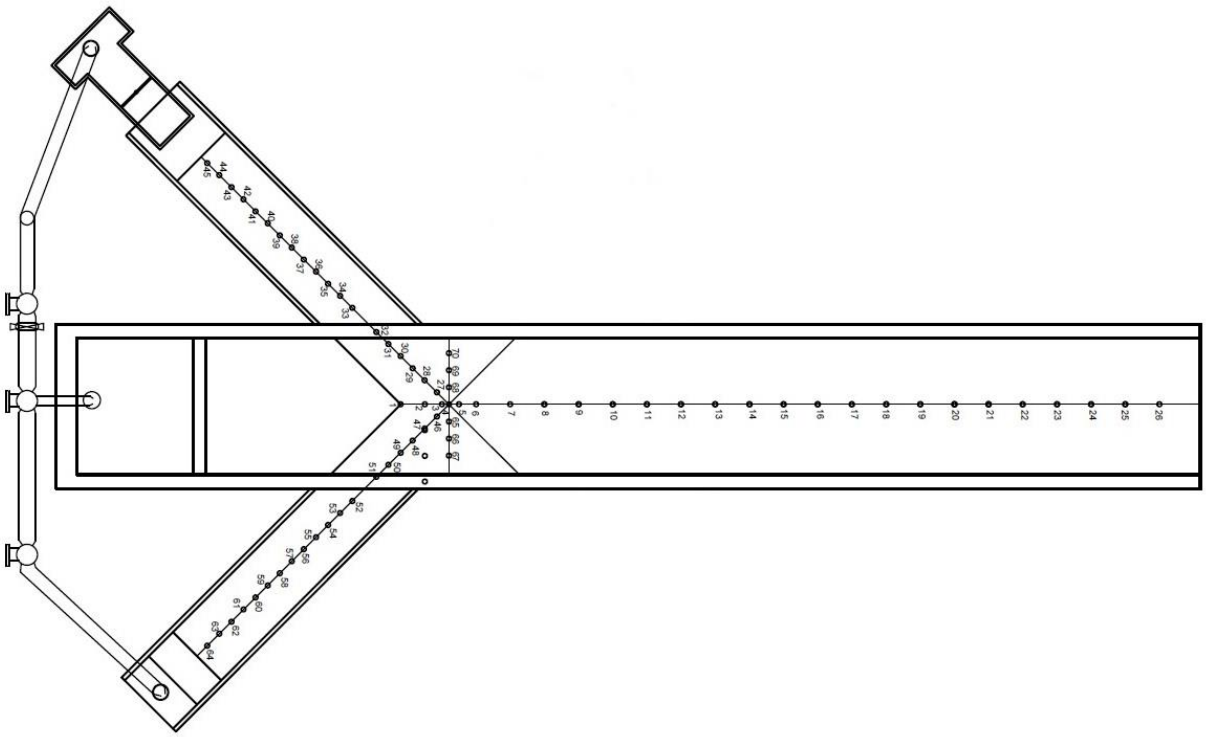

Şekil 7. Deney Düzeneğinin Ölçüm Şeması

Deneyler sırasında ihtiyaç duyulan su, ana kanala bağlı olan ve bodrum katta bulunan su deposu vasıtasıyla sağlanmıştır. Deneyler esnasında kanal mansabından dökülen su, önce metal yapı elemanlarıyla etrafı kapatılmış olan su dönüş haznesine ulaşmakta, daha sonra metal borular vasıtasıyla bodrum katta bulunan su deposuna ulaşmaktadır. Su deposuna bağlı durumdaki iki adet kelebek vana sayesinde depodan su çıkışı kontrol edilmekte, vanalara yakın olacak şekilde konumlandırılmış olan 2 adet santrifüj pompa vasıtasıyla bodrum kattan, zemin katta bulunan ana kanalın sağ ve sol yan kollarına

su akışı sağlanmaktadır. Böylelikle deney setleri sırasında ihtiyaç duyulan su, devir daim yaptırılarak sağlanmış olmaktadır (Şekil 8).

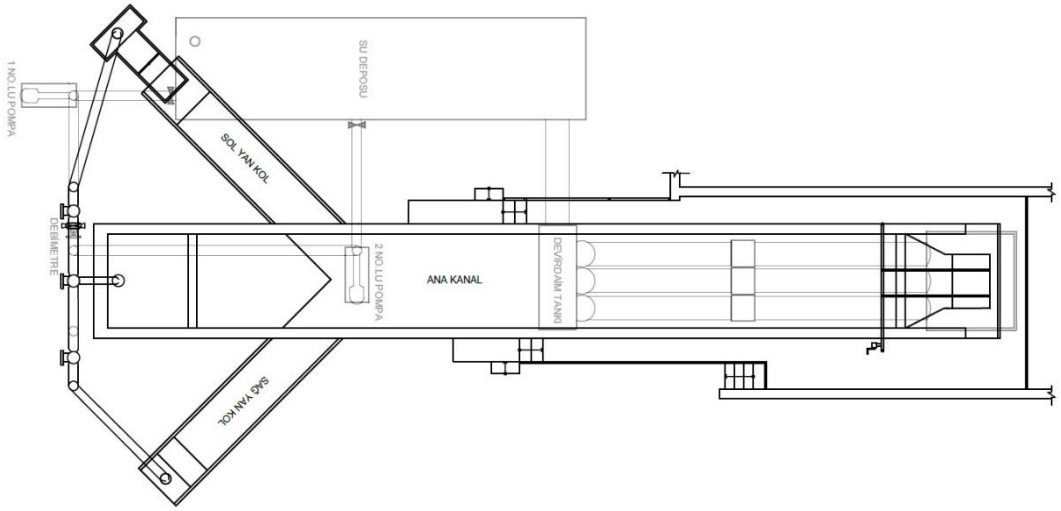

Şekil 8. Deney Düzeneği - Bodrum ve Zemin Kat Planı

Sol yan kol için istenen debinin ayarlanabilmesi maksadıyla sol yan kolun membasına dikdörtgen kesitli savak yerleştirilmiştir. Savak yüksekliği, önce durgun haldeyken ölçülmüş daha sonra üzerinden akan suyun yüksekliği ölçülmüştür. Bu savaktan akan suyun yüksekliği *h* ile savağa gelen suyun debisi *Q* arasındaki ilişkiyi ortaya koyan Rehbock formülü (Denklem 1) kullanılarak kalibrasyon yapılmış ve böylelikle istenen debi elde edilmiştir. Bunu yapabilmek için öncelikle savaktan akan suyun yüksekliği, savağın orta noktasına sabitlenen kumpas vasıtasıyla ölçülmüş, istenen debinin elde edilebilmesi maksadıyla *h* yüksekliği, sürgülü vana vasıtasıyla gerektiği şekilde ayarlanmıştır (Şekil 9).

$$Q = C_d \frac{2}{3} \sqrt{2gB} H^{3/2} \tag{1}$$

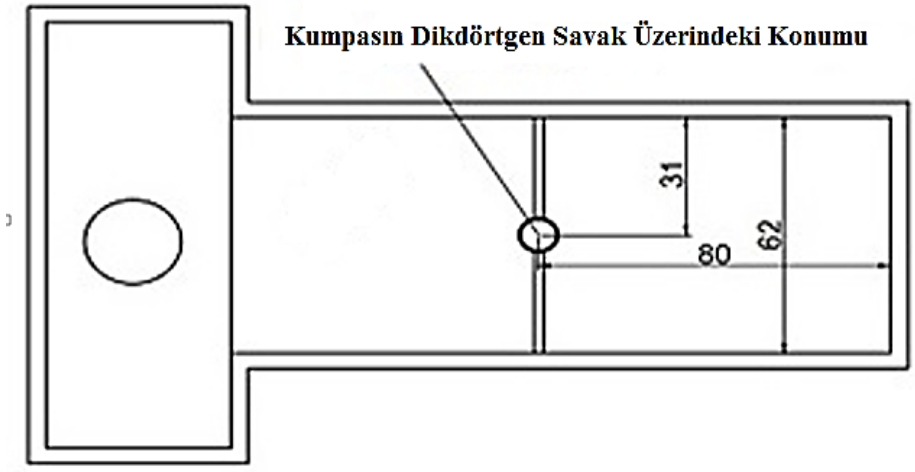

Şekil 9. Dikdörtgen Kesitli Savak ve Kumpasın Plan Görünümü

Deneyler

Bu çalışma kapsamında yapmış olduğumuz deneylerden 3 tanesi ele alınmıştır. Seçilen bu 3 deneyde mansap akım derinliği ayarlanarak kavşak birleşim noktasında elde edilen derinlikler tabloda gösterilmiştir (Tablo 1).

Tablo 1. Deneysel veriler

Deneyler	Sağ Kol Debisi (l/s)	Sol Kol Debisi (l/s)	Kavşak Derinliği(cm)	Mansap Derinliği (cm)
Deney 1	29,61	20	9,8	9,3
Deney 2	29,61	20	12,8	12,60
Deney 3	29,61	20	15,75	15,35

Her 3 deneyde de ana kanalda H2 profili gözlenmiş ve kavşak birleşim noktasındaki derinlik, mansap derinliğinden daha fazla olmuştur. Yan kol ve ana kanal debileri arasındaki oran ile akım derinlikleri arasındaki ilişki literatür ışığında incelenmiştir.

Sayısal Çalışma

Deney sonuçları, enerji ve süreklilik denklemleriyle birleştirilerek, elde edilen değerlere bağlı olarak su ve taban yüzeyi profilleri oluşturulmuştur. Su yüzeyi profili, direkt adım yöntemiyle (derinlikten mesafeye) hesaplanmıştır. Direkt adım yönteminde, kanalda seçilen derinliklerde ara mesafeler hesaplanır. Bu hesapta deneme yanılma yöntemi ile *x* mesafeleri belirlenmiştir.

Seçilen dikdörtgen en kesitli bir kanalda *b* kanal taban genişliğini, *y* yüksekliği, $v^2/2g$ ifadesi enerji çizgisini ifade etmektedir. h_1 yük kaybıdır (Şekil 10). Bu parametreler direkt adım yönteminde kullanılmış olan parametrelerdendir. Hesaplamalarda sağ ve sol kollardan verilen debiler, toplam debi, kanal taban genişliği, kanal taban pürüzlülük katsayısı, alan, ıslak çevre, hidrolik yarıçap, (Denklem 2) hız, enerji denklemi (Denklem 3), Manning denklemi (Denklem 4) kullanılarak *x* mesafeleri belirlenmiştir. Bu denklemler direkt adım yönteminde kullanılmış olan denklemlerdir.

Deney düzeneğinin tabanı betondur. Kanal tabanındaki pürüzlülük değerini belirlemek üzere Manning denklemi kullanılmış, grafikte farklı katsayılar için çizimler kıyaslanmış ve en uygun pürüzlülük değeri her bir deney için $n = 0{,}015$ olarak bulunmuştur.

Enerji Denklemi

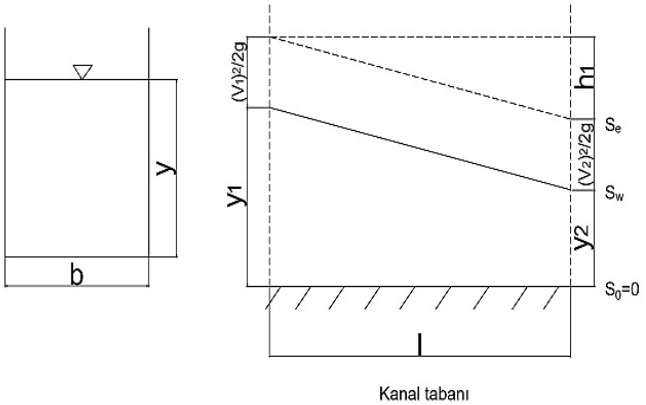

Şekil 10. Su Yüzey Profili

Denklem 2'de gösterilen ifadelerden *A* seçilen en kesitin alanını, *U* ıslak çevreyi, *R* hidrolik yarıçapı, *E* enerji çizgisini temsil etmektedir.

$$A = b.y\,, \quad U = b + 2y \quad R = \frac{A}{U} = \frac{b.y}{b+2y}, \qquad E = y + \frac{V^2}{2g} \tag{2}$$

İki nokta arasında Enerji denklemi Denklem 3'te ifade edilmiştir.

$$y_1 + \frac{{V_1}^2}{2g} = y_2 + \frac{{V_2}^2}{2g} + h_1 \tag{3}$$

Manning Denklemi

Denklemlerde değerler yerine yazılmış, Excel'de tablolar oluşturulmuş ve buna bağlı olarak su yüzeyi profilleri oluşturulmuştur. Çalışmada direkt adım yöntemi kullanılmıştır. Manning denkleminden yararlanılmıştır.

$$V = \frac{1}{n} R^{\frac{2}{3}} S_e^{\frac{1}{2}} \quad S_e = \frac{n^2 V^2}{R^{\frac{4}{3}}} \quad \bar{s}_e = \frac{1}{2}\left(S_{e_1} + S_{e_1}\right) \tag{4}$$

Manning denklemi kullanılarak enerji çizgisinin eğiminin aritmetik ortalama değeri bulunmuştur. Bulunan bu değerler, her iki adımın x noktaları arasındaki ilişkinin kurulabilmesini sağlamıştır (Denklem 5).

$$y_0 > y > y_{cr} \; için \; \Delta x = \frac{\Delta E}{S_0 - \bar{S}_E} \qquad x_2 = x_1 + \frac{E_2 - E_1}{S_0 - \bar{S}_E} \tag{5}$$

1.Deney için RMSE, yani kök ortalama kare hatası 0,18 olmuş, 2. deney için RMSE 0,138 olmuş, 3.Deney için 0,14 olmuştur. Kanal taban pürüzlülük katsayısı her deneyde en uygun olarak n = 0,015 olmuştur.

Deney sonuçlarına istinaden elde edilen su yüzeyi profilleri aşağıda gösterilmiştir.

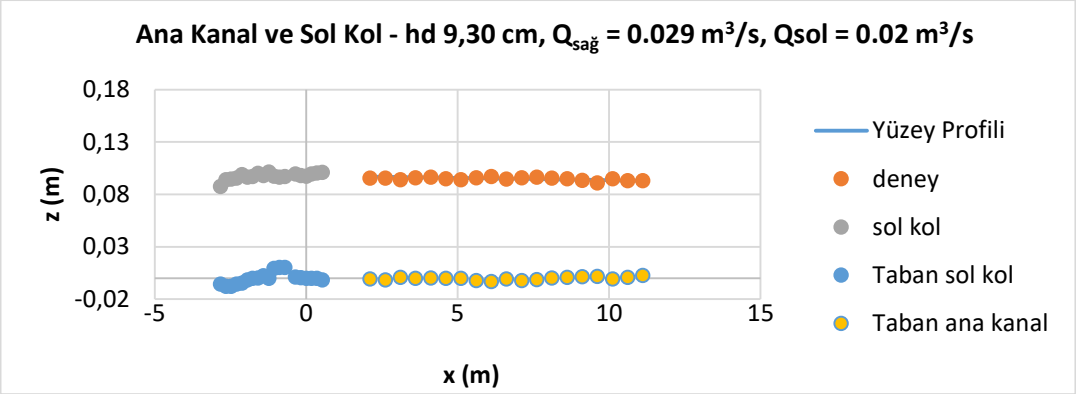

Şekil 11. Deney 1 Ana kanal ve sol kol - Yüzey profili

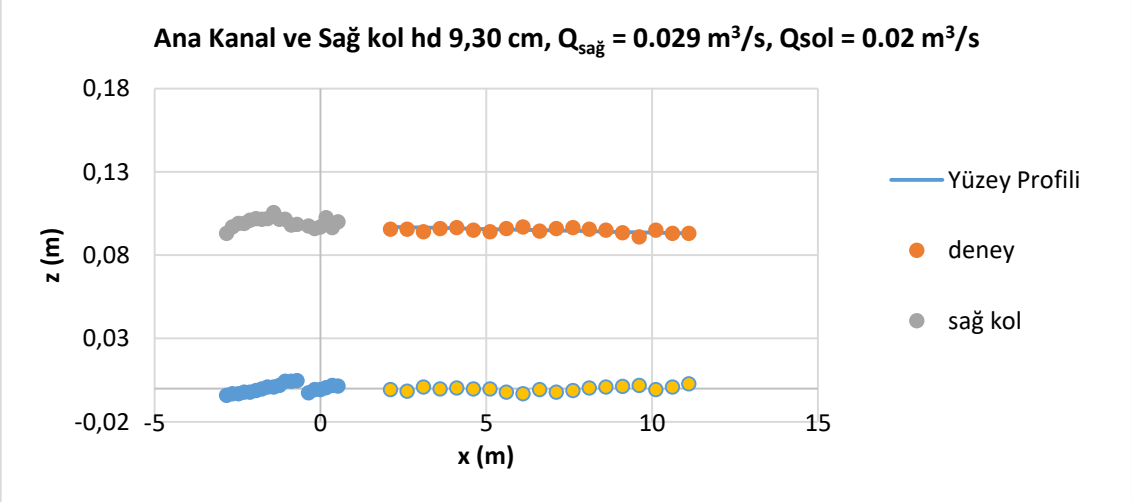

Şekil 12. Deney 1 Ana kanal ve sağ kol – Yüzey profili

Şekil 13. Deney 1 - Kanal görünümü

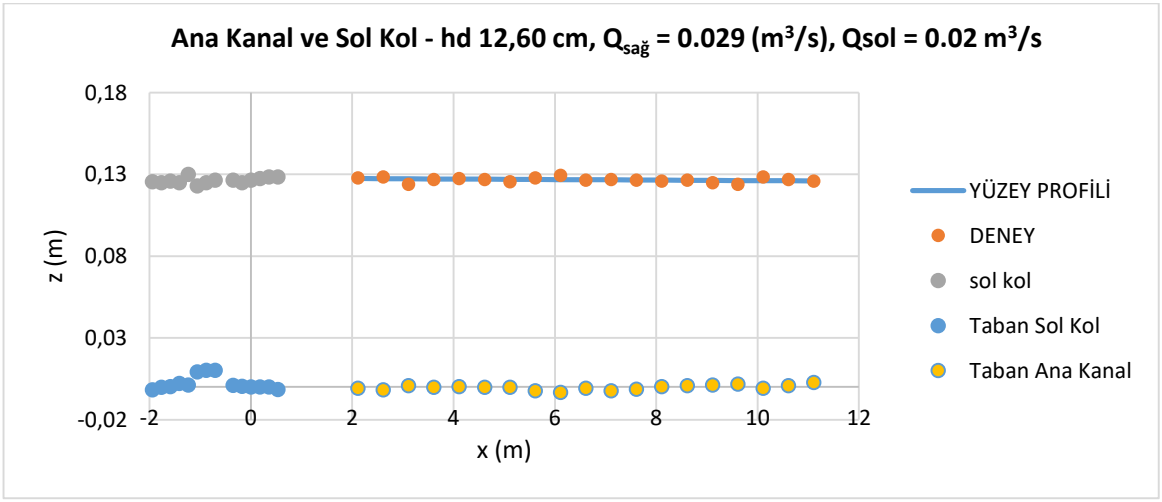

Şekil 14. Deney 1 - Ana kanal ve sol kol - Yüzey profili

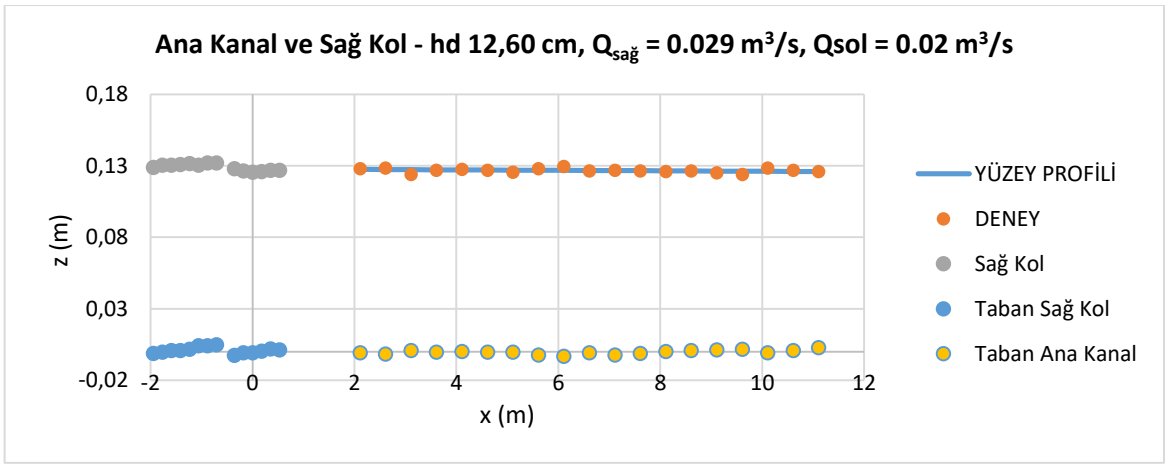

Şekil 15. Deney 1 - Ana kanal ve sağ kol - Yüzey profili

Şekil 16. Deney 2 - Kanal görünümü

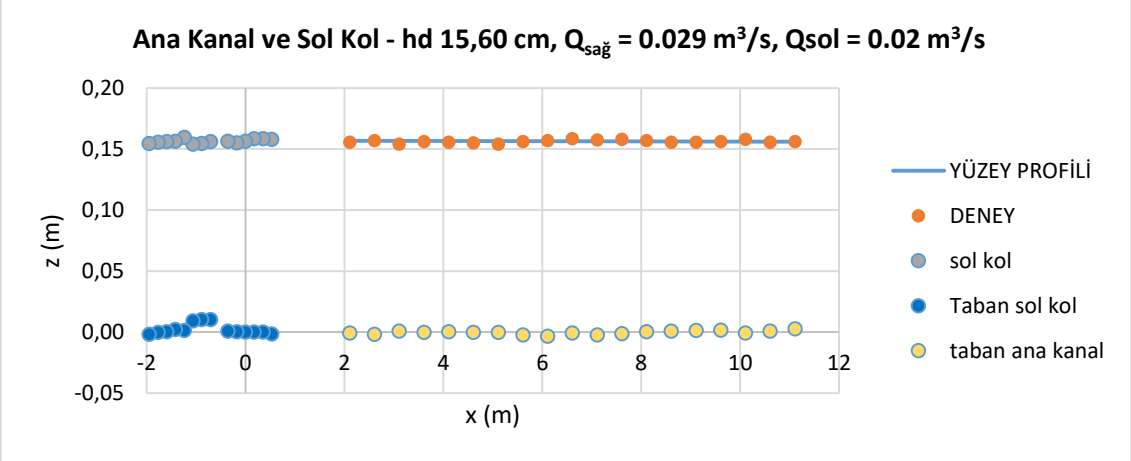

Şekil 17. Deney 3 - Ana kanal ve sol kol - Yüzey profili

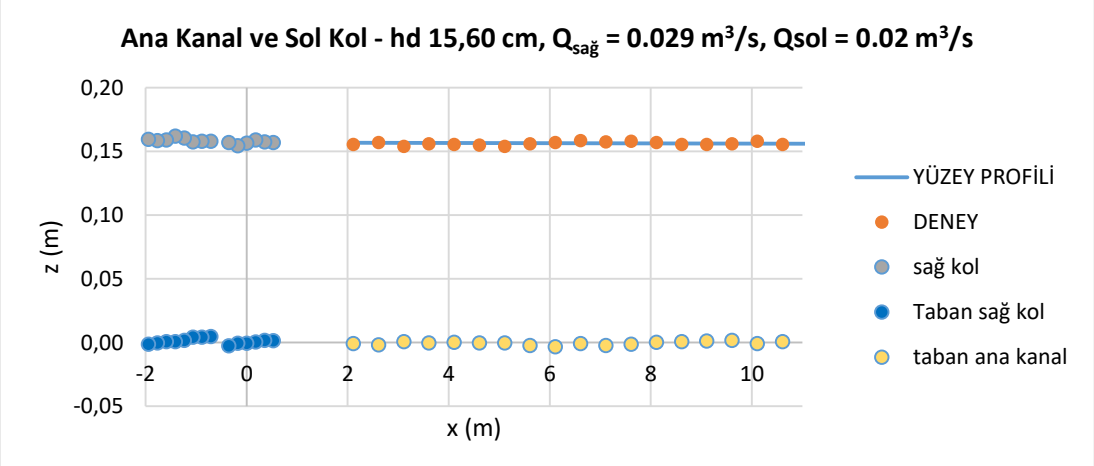

Şekil 18. Deney 3 - Ana kanal ve sağ kol - Yüzey profili

Şekil 19. Deney 3 - Kanal görünümü

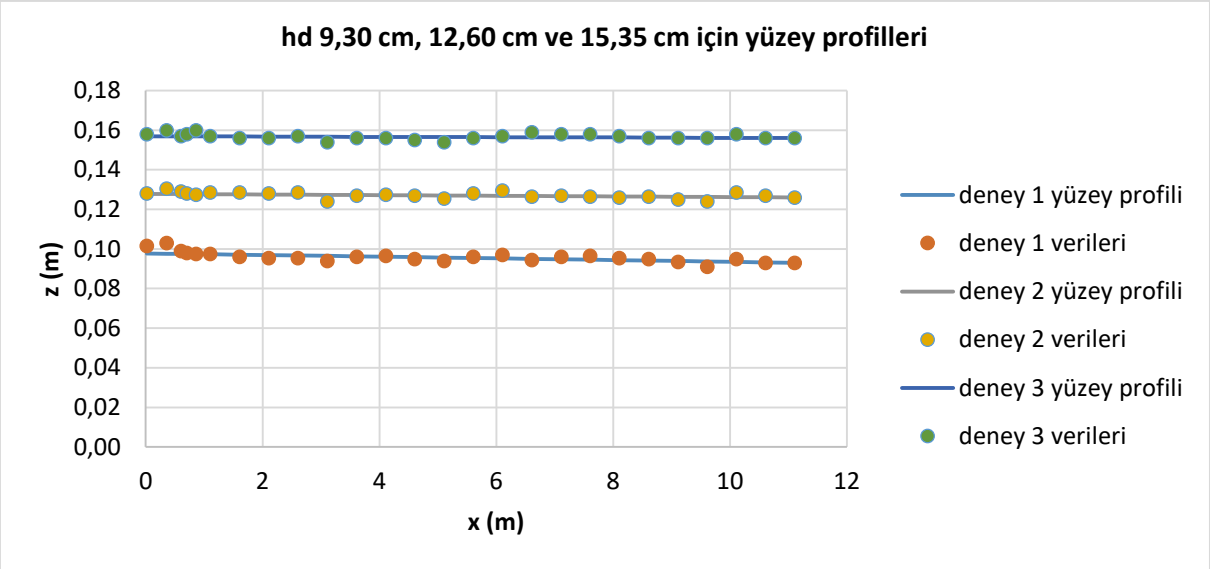

Şekil 20. Sonuçların karşılaştırılması

Sonuçlar

1. deney için RMSE, yani kök ortalama kare hatası 0,18 olmuş, 2. deney için RMSE 0,138 olmuş, 3. deney için 0,14 olmuştur.

Mansap yüksekliği için en uygun taban pürüzlülük katsayısı deneylerden her biri için n=0,015 olmuştur. Taban eğimi *0* ve $y>y_{cr}$ olup çalışmalar nehir rejiminde yapıldığından *H2* profili gözlemlenmiştir. Su yüzey profillerinde eğimler birbirine paralellik göstermiştir. Mansaptaki derinliğinin artması, genel su seviyesi ortalamasını artırmıştır.

Teşekkür

Bu çalışma 2017-T2L-FEBE-0041 nolu proje kapsamında yapılmıştır.

Kaynaklar

[1] Akarsu Kavşağı - Negro ve Solimoes Nehirlerinin Birleşimi, Brezilya (2011, Şubat)
[2] Larry J. Weber, Member ASCE, Eric D. Schumate and Nicola Mawer (2001) "Experiments on flow at a 90° open channel junction" J. Hydraul. Eng., 2001, 127(5): 340-350
[3] Best J. Flow dynamics at river confluences: Implications for sediment transport and bed morphology. Recent Development in Fluvial Sedimentology, SEPM 1987, Spec. Publ. 39, F.G. Etheridge, R.M. Flores, and M.D. Harvey, eds.
[4] Marcia Maria Lara Pinto Coelho. Experimental determination of free surface levels at open channel junctions. Journal of Hydraulic Research 2015; 53(3).

Eşit Debili Akarsu Kavşağında Taban Kotu Eşitsizliği Durumunda Mansap Akım Derinliğinin Su Yüzeyi Profiline Etkisi

Mustafa Eyhan [1], Gökçen Bombar[2], António Heleno Cardoso[3]*
[1,2]İzmir Kâtip Çelebi Üniv., İnşaat Mühendisliği Bölümü, İzmir, Türkiye
[3] Universidade de Lisboa, Ceris, Instituto Superior Tecnico, Portugal
**İletişimden sorumlu yazar: mustafa_eyhan@hotmail.com*

Özet

Bu çalışmada, akarsu kavşaklarında taban kotlarının eşitsizliği durumunda akım derinlikleri deneysel olarak araştırılmıştır. Deneyler, İzmir Kâtip Çelebi Üniversitesi İnşaat Mühendisliği Bölümü Hidrolik Laboratuvarı'nda, mevcut dikdörtgen kesitli 2 m genişliğindeki ana kanal ve birbiri ile 90°'lik açı ile bağlanan, her birinin genişliği 1 m olan 2 yan koldan oluşan akarsu kavşağı deney düzeneği üzerinde gerçekleştirilmiştir. Yan kolların taban kotları ana kanal taban kotundan 12 cm yüksekte bulunmaktadır. Deneylerde genişlikler ve kavşak açısı sabit tutulup, mansap derinliği ve yan kollardan gelen debiler değiştirilerek, farklı koşullar altında, akım derinlikleri kanal ekseninde akım yönünde 50 cm aralıklar ile, yan kollarda ise 25 cm aralıklar ile ölçülmüş ve buna bağlı olarak su yüzeyi profilleri oluşturulmuştur. Yapılan tüm çalışmalarda akım nehir rejimindedir.

Yapılan deneylerde her iki yan koldaki debi 20 l/s, toplam debi 40 l/s ve buna bağlı olarak belirlenen mansap derinlikleri 8,15- 15, 35- 18,30 cm'dir. Bu mansap yüksekliklerine bağlı olarak kavşak birleşiminde okunan yükseklik değerleri sırasıyla 8,90 – 15,90 – 18,50 cm'dir.

Bu veriler ışığında simetrik akarsu kavşaklarının rehabilitasyonu, bu kavşakların etrafına inşa edilecek olan su yapılarının tasarım parametrelerinin belirlenmesi adına tasarım esaslarının belirlenmesi amaçlanmıştır. Ayrıca bu çalışma ile ana kanal ve yan kol debileri arasındaki oranın akım derinliklerine etkisi mevcut literatür ışığında incelenmiştir.

Anahtar Kelimeler: akarsu kavşağı, taban kotu eşitsizliği, su yüzeyi profili

Giriş

Akarsular, doğal bir yatak içerisinde akan su kütleleri olarak tanımlanmaktadır. Akarsu kavşağı, iki akarsuyun birbirine karıştığı, birinin ötekine eklendiği yer olarak tanımlanmaktadır.

Şekil 1. Akarsu kavşağı

Bu çalışmada, akarsu kavşaklarında taban kotlarının eşitsizliği durumunda yan kollardan gelen aynı debiler ve farklı mansap akım derinliklerinin su yüzeyi profili üzerine etkisinin belirlenmesi amaçlanmıştır. Bu çalışma ile elde edilen sonuçlar simetrik akarsu kavşaklarının etrafına inşa edilecek olan su yapılarının tasarım parametrelerinin belirlenmesi sırasında kullanılabilecektir.

Literatür İncelemesi

Çalışmada tipik akarsu kavşağını modellemiştir. Bu modellemeye göre akarsu kavşağı; durgunluk bölgesi, akımın sapması, akım ayrılma bölgesi, maksimum hız, akımın eski haline geri gelmesi ve kayma tabakaları gibi bölgelere ayrılmaktadır. [2]

Durgunluk bölgesinde; basınç ve akım derinliği artmakta, akım hızı ve kayma gerilmesi azalmış, akım yönünde sapma yan koldan gelen akımın, ana kanaldaki akım ile birleşmesiyle oluşmuş, ayrılma bölgesinde kavşağın mansabında ana kanal kenarında kendi etrafında dönen çevrintiler meydana gelmiş ve yukarı yönde düşey hızlar önemli ölçüde artmış, ana kanal ve yan koldaki debinin birleşmesi ile toplam debi ve hız artmış, sağ ve sol kısımdaki akım hızlarının farklılığından kaynaklanan çevrintiler oluşmuş, mansaba doğru ilerledikçe akarsuyun artık yeni bir genişlikte ve debide akmaya devam ettiği görülmüştür. [2]

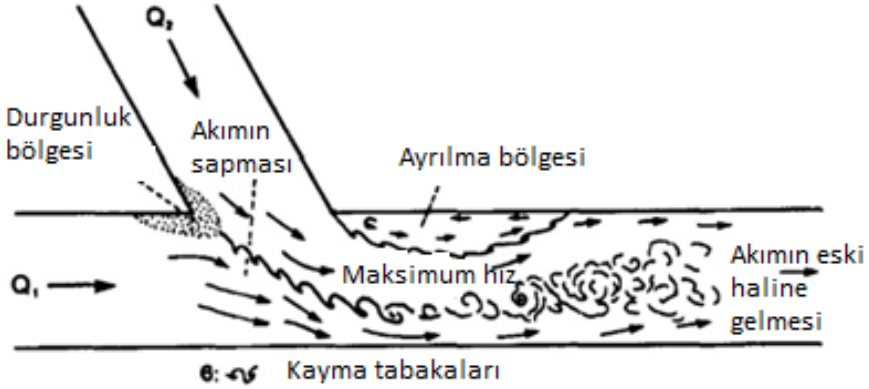

Şekil 2. Kanal ve akarsu kavşaklarındaki akarsu yapısı [2]

Bu çalışma farklı debi oranları ile kanallardan gelen nehir veya sel rejimlerine göre kanal mansabında oluşan rejimlere bağlı olarak birleşim bölgelerindeki su yüksekliği değişimlerini belirlemek ve daha önceki çalışmalar ile kıyaslamalar yapmak amacıyla yapılmıştır. Bu çalışmada, kavşağa gelmekte olan farklı debiler dikkate alınmış, akım derinliklerini değerlendirmek üzere deneyler gerçekleştirilmiştir. [3]

Kavşak açılarının etkisini belirlemek için 30° ve 60° derece açılara sahip iki adet fiziksel model kullanılmış, çalışmada taban eğimi ayarlanabilmekte, genişlik 30 cm, derinlik 50 cm, debiler akım ölçerler ile ölçülmüş, yan kol girişlerinde bulunan ayarlanabilir kapaklar aracılığı ile kanallardan sel veya nehir rejimi gönderilmiş, buna bağlı olarak ana kanal mansabında oluşan sel veya nehir rejimlerine göre toplamda 36 adet deney yapılmış ve deneyler tip 1, 2, 3 olacak şekilde sınıflandırılmıştır. Tip 1 akımlarında membalar nehir rejiminde, mansap akım rejimi de nehir rejiminde elde edilmiştir. Tip 2 akımında, membalar sel ya da rejiminde mansap ise nehir rejiminde, Tip 3 akımlarında ise membalar sel ya da rejiminde mansap ise sel rejiminde elde edilmiştir. Ayrıca önceki yapılan çalışmalar ile kıyaslamalar yapılmış, 2 ve 4 noktalarındaki (Şekil 3) su yükseklerinin eşit olması varsayımına göre sonuçlardaki farklar yorumlanmıştır. [3]

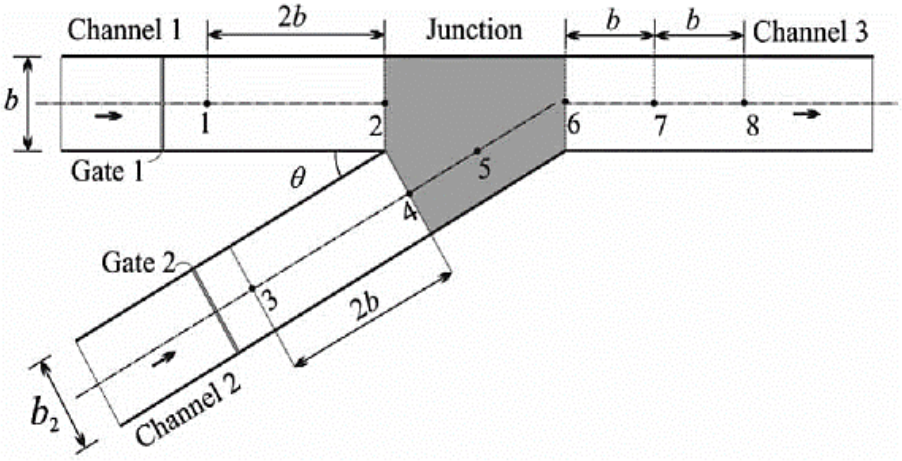

Şekil 3. Çalışmanın şematiği [3]

Elde edilen verilere göre; mansap akımı nehir rejiminde olduğunda, kavşağın membasında en kesitlerde su seviyesinin eşit olduğu varsayımının doğrulandığı belirtilmiş, ayrıca; mansap akımının sel rejiminde olduğu durumlarda dahi, mansapta nehir rejimi akımlarına sahip olan birleşimlerde, su seviyelerindeki yükselmelerin tahmin edilebilmesi için klasik kuramsal modellerin kullanılabileceği belirtilmiş, diğer çalışmalarla kıyaslandığında sonuçlarda çok büyük sapmalar olmadığı belirtilmiştir.

Yapılan çalışma ile bu çalışmanın benzerliği tip 1 akımlarında nehir rejimleri kullanılmış ve mansap bölgesinde de nehir rejimi elde edilmiştir.

Nehir rejiminde akım; kritik eğimden daha düz (kritik altı veya yumuşak) eğimlerde teşekkül eder ve nispeten büyük derinlikler ve düşük hızlarda gerçekleşir, sel rejiminde akım ise kritik eğimden daha dik (kritik üstü veya dik) eğimlerde teşekkül eder, nispeten küçük derinlikler ve büyük hızlarda gerçekleşir. Bu tür akımlara dik akarsularda sıkça rastlanmaktadır. [5]

Sel rejimi memba kontrollü olmaktadır. Bunun için deneysel çalışmada memba girişine hareket ettirililebilir kapak konmakta ve kapak açılıp kapatılarak sel rejimi elde edilmektedir.

Deneysel Çalışma

Bu çalışmada, eşit debili akarsu kavşağında taban kotu eşitsizliği durumunda mansap akım derinliğinin su yüzeyi profiline etkisi derinlikleri deneysel olarak araştırılmıştır. Deneyler, İzmir Katip Çelebi Üniversitesi İnşaat Mühendisliği Bölümü Hidrolik Laboratuvarı'nda gerçekleştirilmiştir.

Bu çalışma kapsamında sabit parametreler; yan kollar arasındaki açı α=90^0, yan kol ve ana kanal genişliği (B_t=1 m ve $B_{p\text{-}c}$=2 m) ve her iki koldaki taban eşitsizliğidir (Δz = 12 cm). Bu çalışma kapsamındaki değişken ise mansap su derinliğidir.

Bu parametrelere bağlı olarak yan kollardan gelen debiler için 3'er adet mansap derinliği belirlenmiştir. Deneyler sırasında yan kollar ve ana kanal boyunca su yüzeyi profili çıkartılmış ve fotoğraflanmıştır.

Bu çalışma kapsamındaki en önemli çıktı kavşakta oluşacak su yüzeyi profilinin taban eşitsizliği durumunda mansaptaki farklı derinlikler ile ne şekilde değiştiği konusuna açıklık getirmek olmuştur. Deney düzeneğinde T1-T2 yan kolları, RW dikdörtgen savağı, V1-V2-V3 sürgülü vanaları, V4 kelebek vanayı, Kavşak mansabını temsil edecek ana kanal olarak 12 m uzunluğunda, 2 m genişliğinde dikdörtgen kesitli kanal kullanılmıştır. Yan kollar 3,96 m uzunluğunda, 1 m genişliğindedir. Simetrik yan kollar birbirine 90^0'lik açı ile bağlanmaktadır. (Şekil 4.)

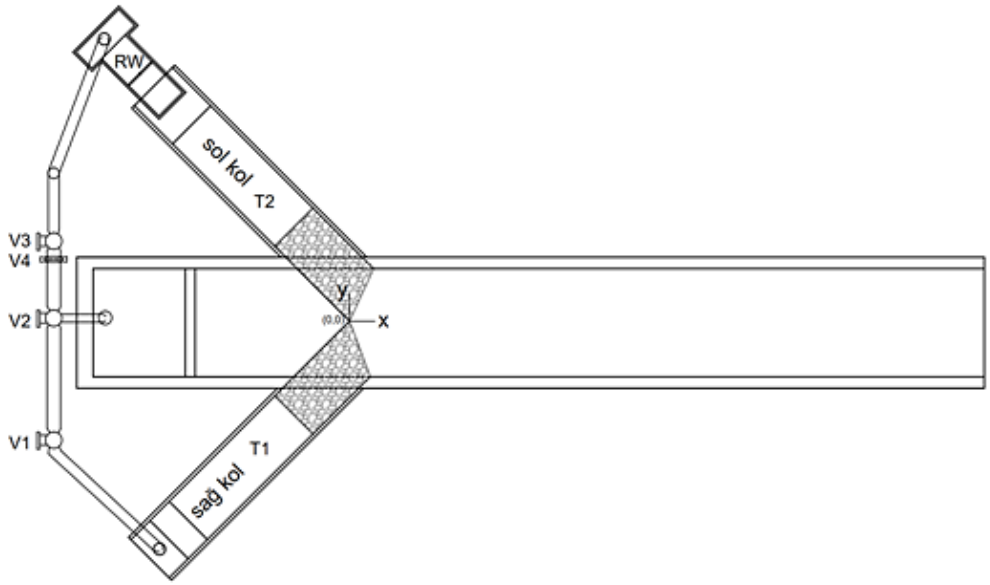

Şekil 4. Deney düzeneğinin plan görünümü

Çalışma kapsamında seçilen debiler her iki kolda da 20 l/s, mansap akım derinlikleri sırasıyla; 8,15-15,35 - 18,30 cm'dir. Çalışmada 70 noktada ölçüm yapılmıştır.

Bu çalışma kapsamında ilk önce, 12 cm olarak belirlenmiş olan taban kotu eşitsizliğini sağlamak amacıyla yan kolların mansap bölgelerinden memba bölgelerine doğru 120 cm boyunca çeşitli

büyüklükteki taşlarla ve parke taşlarıyla kot yükseltmesi yapılmıştır. Ana kanal ve yan kollardaki kot farkı 2 yan kolda da aynıdır.

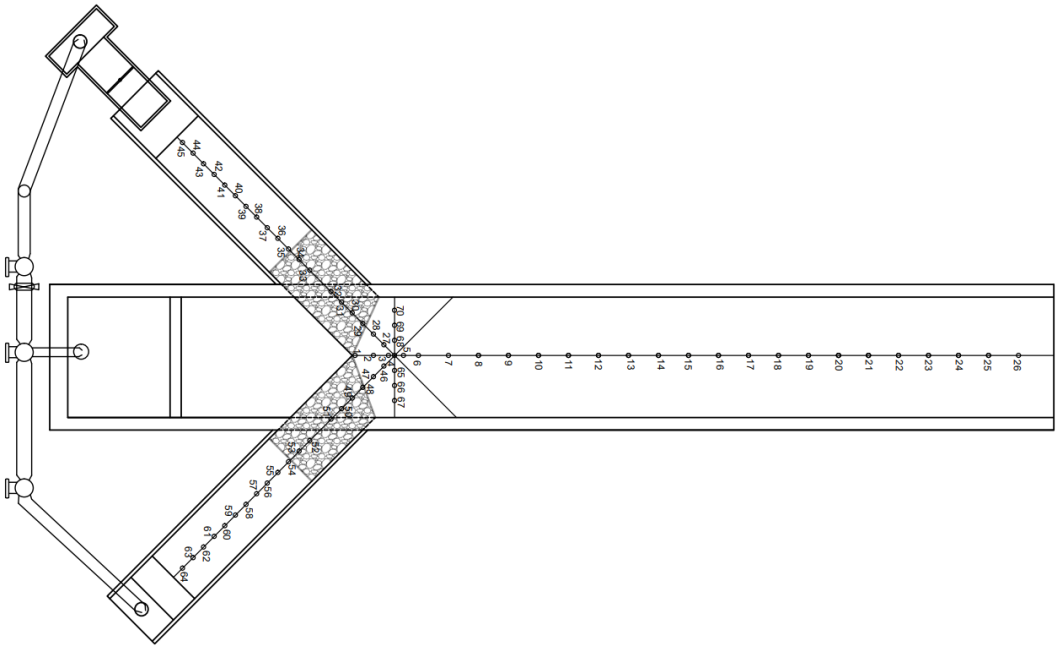

Şekil 5. Deney ölçüm noktalarının görünümü

Şekil 6. Deney düzeneği laboratuvar görünümü

Yan kollarda ve ana kanalda yapılacak ölçümlerin yerlerini belirlemek ve her ölçümde aynı noktada ölçüm yapmak adına, yan kol orta bölgelerine aks ipi yardımıyla ip çekilmiş, ana kanaldaki ölçümler için ise ana kanal duvarı üzerine kağıt metreler yapıştırılarak, hem ip üzerinde hem de cetvel üzerinde ölçüm yapılacak yerler işaretlenmiştir. Deney çalışmasında, sağ yan kola (T1) santrifüj pompası yardımıyla gelen su hattında debimetre cihazı bağlıdır. Bilgisayara bağlı olan pompadan manuel ayar ile istenilen debi alınmış, debimetre okuma ekranından anlık debi kontrolleri sağlanmıştır.

Diğer yan kolda (T2) herhangi bir debimetre cihazı bulunmamaktadır. Bu yüzden buraya gelen debiyi belirlemek adına dikdörtgen savak kullanılmıştır. Bu savağa gelen debinin hesabı için savak üzerine, savak orta noktasına su yüksekliğini ölçmek adına kumpas aleti sabitlenmiştir. Kumpas aleti sabitlenirken, savak taşmayacak şekilde tam dolu iken, kumpas ucu açık halde su yüzüne temas ettirilerek referans yükseklik belirlenmiştir. Kullanılan kumpasın maksimum yükseklik değeri 15 cm'dir. Daha sonra santrifüj pompası yardımıyla gelen su hat üzerinde bulunan sürgülü vana yardımıyla istenilen debi oranındaki yükseklik elde edilene kadar manuel çevirme yaparak debi sabitlenmiştir. Buradaki yükseklik değeri ilk baştaki kumpas açık haldeki 15 cm'lik değerden çıkarılarak elde edilen

değerdir. Bu yükseklik değeri Rehbock'un dikdörtgen savak formülüne göre hesaplanmıştır. Daha güvenilir okuma yapılması amacıyla kumpas ucu törpülenerek daha sivri hale getirilmiştir.

Kullanılan savak formulü:

$$Q = c_d \frac{2}{3}\sqrt{2gB}H^{3/2} \quad (1)$$

Bu formüle ait C_d katsayısı:

$$c_d = 0{,}602 + 0{,}083\ \frac{H}{P} \quad (2)$$

Çalışmada; deneysel veriler kullanılmış, enerji ve süreklilik denklemleri yardımıyla elde edilen değerler ile tablolar oluşturulmuştur. Ayrıca su yüzeyi profili direkt adım yöntemiyle (derinlikten mesafeye) de hesaplanmış ve su yüzeyi profili oluşturulmuştur. Direk adım yönteminde, kanalın seçilen derinliklerde ara mesafeler hesaplanmıştır. Bu yöntem prizmatik kanallara uygulanabilmektedir. Bu hesapta deneme yanılma yöntemi ile x mesafeleri belirlenmiştir ve buna bağlı olarak su yüzeyi profilleri oluşturulmuştur.

Enerji denklemi:

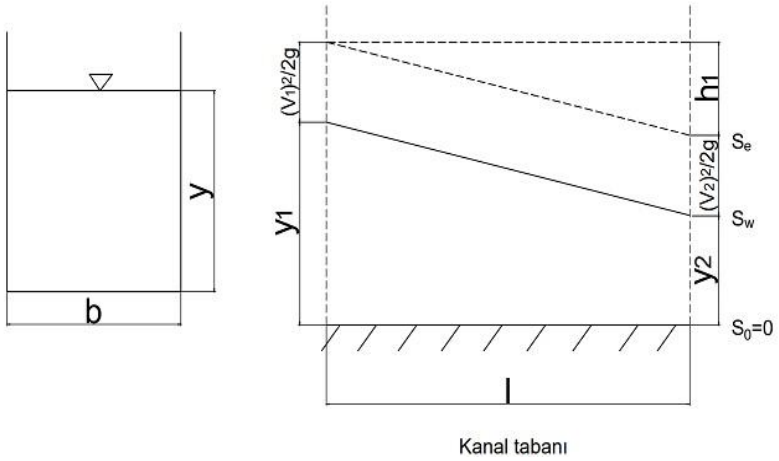

Şekil 7. Tipik dikdörtgen geometrili açık kanal kesiti ve enerji çizgisi

$$A = b.y \quad U = b + 2y \quad R = \frac{A}{U} = \frac{b.y}{b+2y} \quad (3)$$

Enerji denklemi yazıldığında; $E = y + \frac{V^2}{2g} \Rightarrow y_1 + \frac{{V_1}^2}{2g} = y_2 + \frac{{V_2}^2}{2g} + h_1$ (4)

Deneysel çalışmada kanal zemini betondur ve taban eğimi 0'dır. Fakat kanal tabanındaki pürüzlülük değeri için Manning denklemi kullanılmış, grafikte farklı katsayılar için deney ve direkt adım yöntemindeki grafikler kıyaslanmış ve en uygun pürüzlülük değeri her bir deney için n=0,015 olarak bulunmuştur.

Manning denklemi:

$$V = \frac{1}{n}R^{\frac{2}{3}}S_e{}^{\frac{1}{2}} \quad S_e = \frac{n^2V^2}{R^{\frac{4}{3}}} \quad \bar{S_e} = \frac{1}{2}(S_{e_1} + S_{e_2}) \quad (5)$$

$y_0 > y > y_{cr}$ *için* $\Delta x = \frac{\Delta E}{S_{0-}\ \bar{S_e}} \Rightarrow x_2 = x_1 + \frac{E_2 - E_1}{S_{0-}\ \bar{S_e}}$ (6)

Tablo 1. Deneysel veriler

No	Q_{T1} (l/s)	Q_{T2} (l/s)	Q_{p-c} (l/s)	U_{p-c} (m/s)	Q_{T1}/Q_{p-c}	Q_{T2}/Q_{p-c}	Q_{T1}/Q_{T2}	Fr_{p-c}	h_{mansap} (cm)	h_{savak} (cm)	B (m)	A (m^2)
1	20,0	20,0	40,00	0,245	0,50	0,50	1,00	0,274	8,15	6,25	2	0,163
2	20,0	20,0	40,00	0,130	0,50	0,50	1,00	0,106	15,35	6,25	2	0,307
3	20,0	20,0	40,00	0,109	0,50	0,50	1,00	0,082	18,30	6,25	2	0,366

Su yüzeyi profilleri, bir açık kanal akımında akım boyunca elde edilecek akım derinliklerinin grafiği olarak açıklanabilir. Başka birdeyişle akım yolu boyunca akım derinliklerinin grafiği, akımın su yüzeyi profilini verir. Su yüzünün akım yolu boyunca kanal tabanından yüksekliğini gösteren bu profil kanal boyunca akım en kesitinin belirlenmesini sağladığı gibi, sıvı ağırlığı, kayma kuvveti ve atalet etkileri arasındaki dinamik dengeyi de yansıtır [6].

Açık kanal akımlarında 12 farklı tipte su yüzeyi profili oluşmaktadır (Şekil 8). Su yüzeyi profillerini sınıflandırmada harf ve rakamdan oluşan bir kodlama kullanılır. Harf, kanal taban eğiminin tipini, sayı ise üniform ve kritik derinliğe göre su derinliğinin bulunduğu bölgeyi tanımlar. [4]

Yapılan çalışma Tablo 1'deki veriler ışığında, Şekil 8'deki su yüzeyi profilleri görseline göre incelendiğinde H2 profilinde olduğu görülmüştür. ($S_0=0$, $y>y_c$)

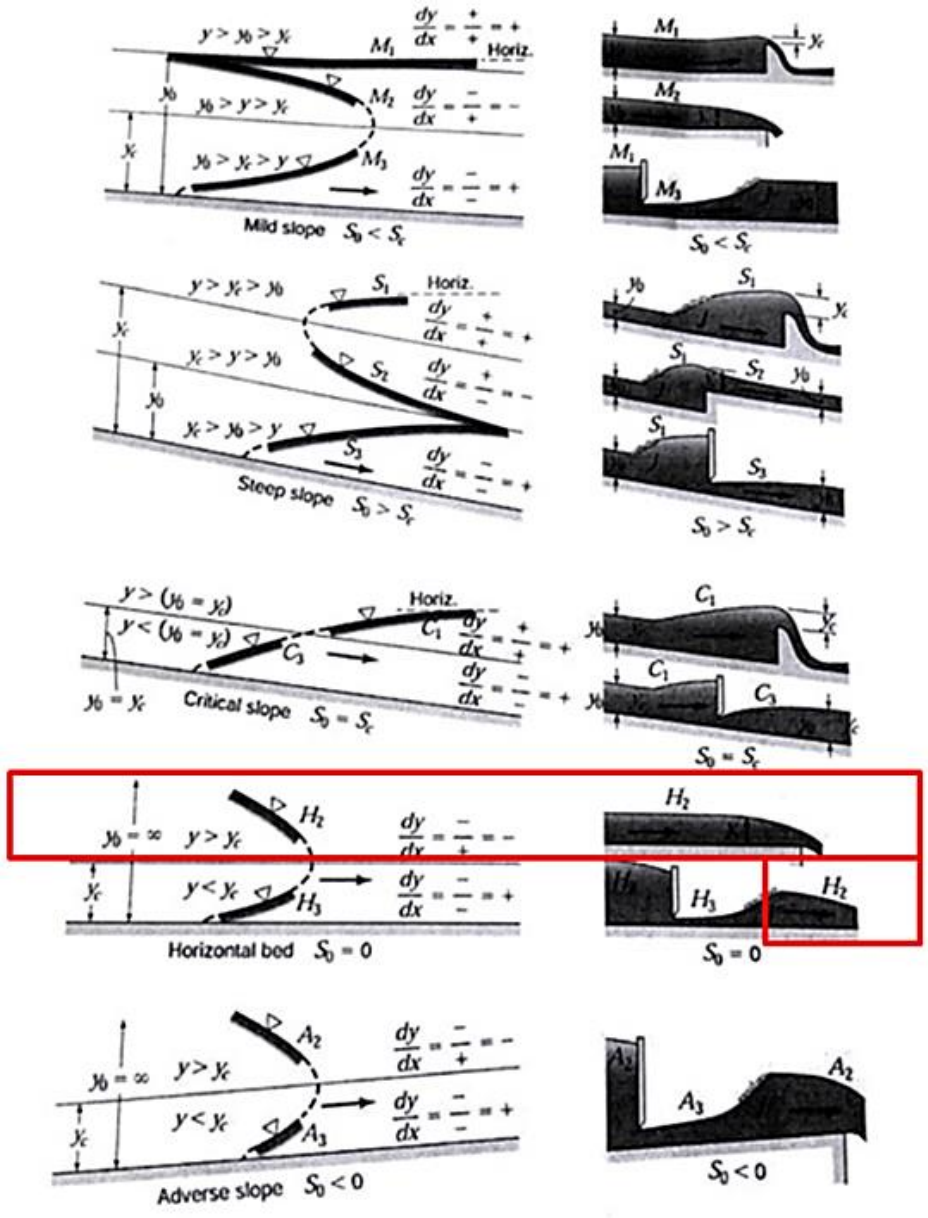

Eğim Tipi	Eğim Notasyonu	Froude Sayısı	Yüzey Profili Tipi
$S_0 < S_C$	Küçük (yumuşak) <Eğim	$F_r < 1$	M_1
		$F_r < 1$	M_2
		$F_r > 1$	M_3
$S_0 = S_C$	Kritik Eğim	$F_r < 1$	C_1
		$F_r > 1$	C_2
$S_0 > S_C$	Büyük (Sert) Eğim	$F_r < 1$	S_1
		$F_r > 1$	S_2
		$F_r > 1$	S_3
$S_0 = 0$	Yatay	$F_r < 1$	H_2
		$F_r > 1$	H_3
$S_0 < 0$	Ters Eğim	$F_r < 1$	A_2
		$F_r > 1$	A_3

Şekil 8. Su yüzeyi profilleri ve tipleri (mild: yumuşak eğim, steep: sert eğim, critical: kritik eğim, horizontal: yatay eğim, adverse: sert eğim [4]

Bir yüzey profili; eğer akım derinliği hem kritik hem de normal derinliğin üzerindeyse (y>yc ve y>y0) 1 ile, eğer akım derinliği bu ikisi arasındaysa (y0> y>yc) 2 ile ve eğer akım derinliği hem kritik hem de normal derinliğin altındaysa (y<yc ve y<y0) 3 ile gösterilir. Görüldüğü üzere, belirli bir kanal eğimi tipi için üç farklı profil mümkündür. Ancak yatay ve ters eğimli kanallarda akım asla üniform olmadığı için normal derinlik tanımlaması yapılmaz ve 1 tipinde akım görülmez. Ayrıca kritik eğimli kanallarda, normal ve kritik derinlikler özdeş olduğundan 2 tipindeki akım oluşmamaktadır. Bir bölgesinde eğimler kabarma eğrisi (pozitif eğim), iki bölgesindeki eğimler alçalma eğrisi (negatif eğim), olarak isimlendirilir. [6]

Çalışma sonucunda elde edilen grafikler Şekil 9-10-11'da verilmiştir.

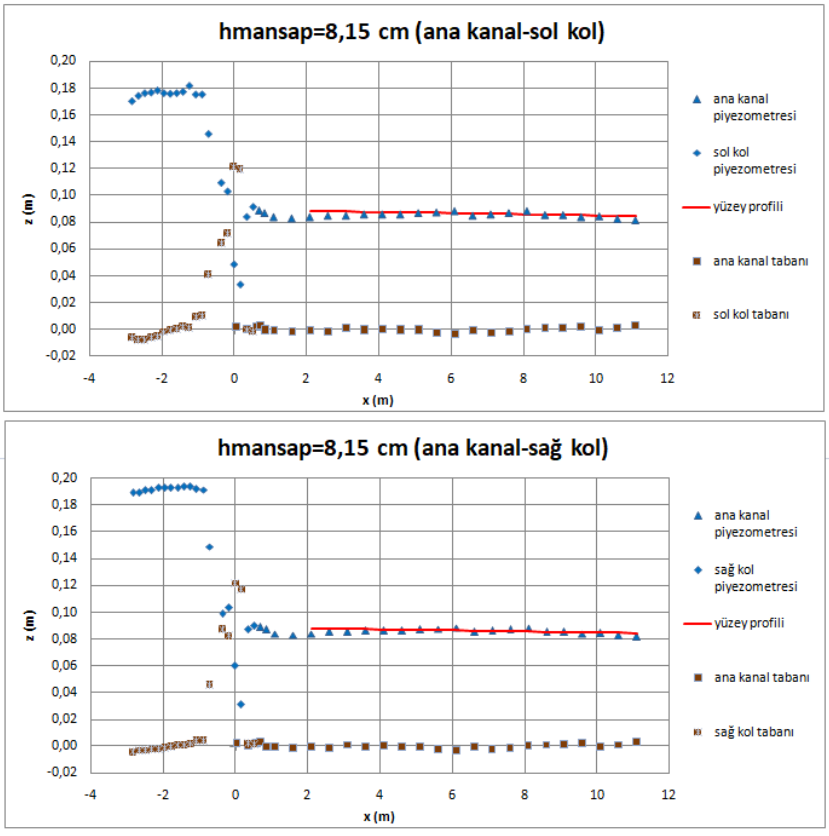

Şekil 9. Su yüzeyi ve taban profili grafiği hmansap: 8,15 cm

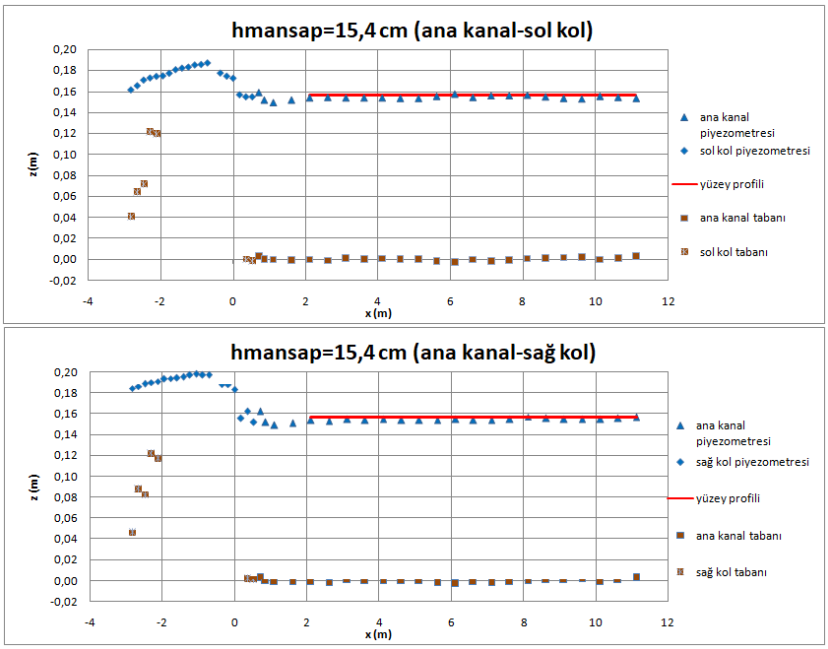

Şekil 10. Su yüzeyi ve taban profili grafiği hmansap : 15,40 cm

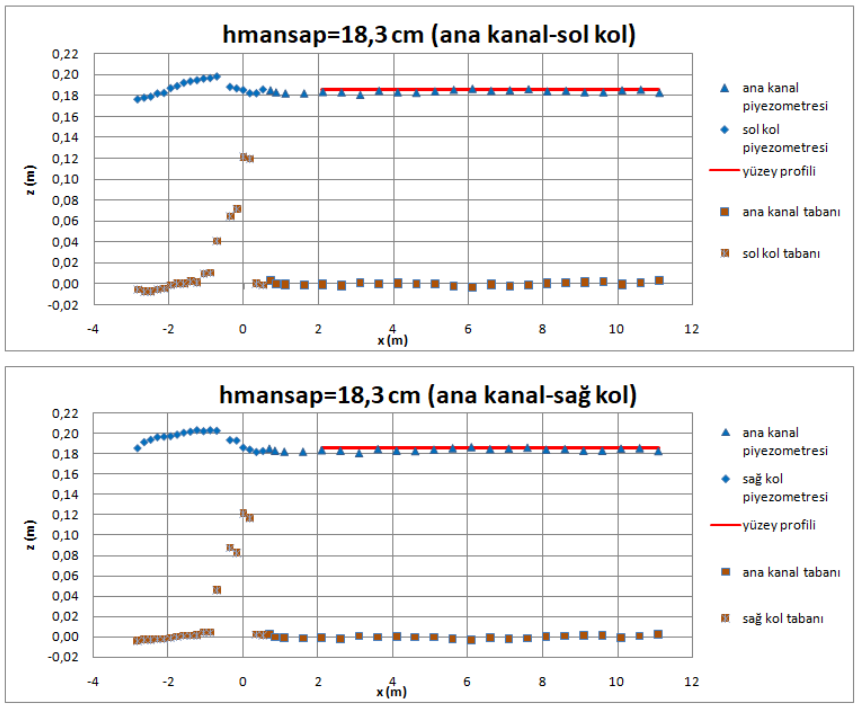

Şekil 11. Su yüzeyi ve taban profili grafiği hmansap : 18,30 cm

Çalışma sonucunda 3 farklı mansap yüksekliği için ana kanal su yüzeyi profillerinin görünümü Şekil 12'de görüldüğü gibidir.

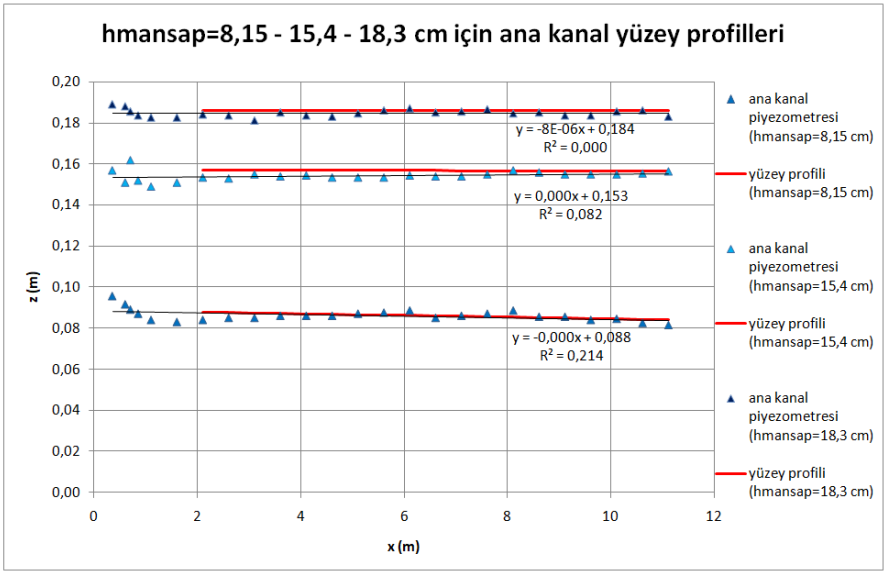

Şekil 12. Ana kanal su yüzeyi profilleri

Çalışma sonucunda deneysel sonuçlar ve direkt adım yönteminde hesaplanan değerlerdeki sapma değerleri; ortalama kare hata (MSE), kök ortalama kare hata (RMSE) ve ortalama mutlak hata (MAE) değerleri Tablo 2'de verilmiştir.

Tablo 2. Deneysel çalışma ve direkt adım yöntemi arasındaki sapmalar

	MSE (cm)	RMSE (cm)	MAE (cm)
8,15	0,0376	0,1939	0,1508
15,4	0,0582	0,2412	0,2109
18,3	0,0098	0,0988	0,1666

Sonuçlar

Yapılan çalışma ile aynı debi değerine sahip simetrik akarsu kavşağında su yüzeyi profilinin laboratuvar ortamındaki veriler ışığında yaklaşık hangi profilde olacağının tahmini açısından önemli bulgulara sahiptir.

Çalışmada 2 yan koldaki Froude sayılarına bakıldığında nehir rejiminde akım ile çalışma yapılmış ve ana kanal mansabında da nehir rejimi elde edilmiştir.

Yapılan çalışmada taban eğimi 0 ve y>ycr olduğundan ve çalışmalar nehir rejiminde yapıldığından H2 profili gözlemlenmiştir.

Deney düzeneği tabanında en uygun taban pürüzlülük katsayısı farklı mansap yükseklikleri için n=0,015 olarak bulunmuştur.

Referenslar

[1] Simetrik Akarsu Kavşağı. http://3.bp.blogspot.com/_KV-lA7YaO9U/SSGqh-4EhXI/AAAAAAAAC6o/cwyQO1ZMcws/s1600-h/IMG_7254.JPG.

[2] Best J., (1987), Flow dynamics at river confluences: Implications for sediment transport and bed morphology". Recent Development in Fluvial Sedimentology, SEPM Spec. Publ. 39, F.G. Etheridge, R.M. Flores, and M.D. Harvey, eds.

[3] Coelho M., Experimental determination of free surface levels at open channel junction, Journal of Hydraulic Research Vol. 53, No.3 (2015).

[4] Kaçmaz A., Açık kanal su yüzü profil hesabının Newton Raphson ile çözümü ve bilgisayar programı geliştirilmesi, Yüksek Lisans Tezi (2018).

[5] Ö. Yüksek, KTÜ MF İnşaat Müh. Bölümü Ders Notu (2017).

[6] Çengel YA, Cimbala, JM. Akışkanlar Mekaniği Temelleri ve Uygulamaları, Çeviri: T. Engin, H.R. Öz, H. Küçük, Ş. Çeşmeci, Güven Kitapevi, İzmir (2012).

Simetrik Akarsu Kavşağında Tek Yan Koldaki Taban Eşitsizliğinin Su Yüzeyi Profiline Etkisi

Zehra Büyüker[1], Gökçen Bombar[2], Antônio Heleno Cardoso[3]*
[1,2]İzmir Kâtip Çelebi Üniversitesi, İnşaat Mühendisliği Bölümü, İzmir, Türkiye
[3] Universidade de Lisboa, Instituto Superior Tecnico, Portugal
**İletişimden sorumlu yazar: zehra.buyuker@ikcu.edu.tr*

Özet

İki ya da daha fazla akarsuyun birleşmesiyle oluşan akarsu kavşakları, akış ağlarında sıklıkla karşılaşılan bir oluşum olup, kollardaki su seviyesinin yükselmesi gibi akış koşullarının değişmesi ve buna bağlı olarak taşkın hasarlarına ve ekonomik kayıplara neden olabileceğinden incelenmesi gereken bir konudur. Bu kapsamda, İzmir Kâtip Çelebi Üniversitesi'nde mevcut dikdörtgen kesitli birbirine 90° açıyla bağlanan 1 m genişliğinde simetrik iki yan kola sahip ve 2 m genişliğinde ve 18 m uzunluğunda açık kanaldan oluşan simetrik akarsu kavşağı üzerinde deneyler gerçekleştirilmiştir. Yan kollardan birinde taban eşitsizliği 12 cm'lik bir yükselti ile sağlanmıştır. Deneylerde sağ kol debisi 15 l/s, taban eşitsizliğine sahip sol kol debisi 20 l/s'dir. Mansap derinlikleri 15 cm ve 25 cm olacak şekilde mansap kapağı ayarlanmış ve akım derinlikleri ölçümü kanal eksenlerinde, akım yönünde ana kanalda kavşaktan mansaba kadar 50 cm, yan kollarda membadan kavşağa kadar 25 cm arayla yapılmıştır. Çalışmada, yan kollardaki ve ana kanaldaki su seviyeleri mevcut raylı sistem üzerine monte edilmiş limnimetre yardımıyla elde edilmiştir. Her iki deney için su yüzeyi profili elde edilmiştir. Elde edilen deneysel sonuçlar uniform olmayan akım tiplerinden H2 tipi için su yüzeyi profili sayısal olarak çözülmüş ve karşılaştırılmıştır. Sayısal ve deneysel sonuçların akarsu kavşağı mansabında uyum içinde olduğu görülmüştür.

Anahtar Kelimeler: simetrik akarsu kavşağı, taban eşitsizliği, su yüzeyi profili

Giriş

İki ya da daha fazla akarsuyun birleşmesiyle oluşan akarsu kavşakları, akış ağlarında sıklıkla karşılaşılan bir oluşum olup, kollardaki su seviyesinin yükselmesi gibi akış koşullarının değişmesi ve buna bağlı olarak taşkın hasarlarına ve ekonomik kayıplara neden olabileceğinden incelenmesi gereken bir konudur. Ayrıca ana akım ve yan kanalların tabanlarındaki uyumsuzluk çoğu nehir birleşimlerinin ortak bir özelliğidir ve taban kotlarındaki bu farklılık kavşaklardaki akış dinamiğini etkilemektedir [1].

Akarsu kavşaklarının hidrodinamiği üzerine ilk çalışmalar Taylor [2] ile Webber ve Greated [3] tarafından tek boyutlu akım varsayımı ile yapılmıştır. Bu çalışmalarda farklı birleşme açıları uygulanarak memba ve mansap derinlikleri arasındaki ilişki ve kavşakta oluşan enerji kaybı araştırılmıştır. Tek boyutlu modellerde kütle ve momentumun korunumundan faydalanılmış ve pürüzlülük ihmal edilmiştir. Kavşak içinde gerçekte akım üç boyutlu olduğundan bu modellerde ampirik düzeltme katsayısı kullanılması gerekmektedir.

Best, sabit tabanlı asimetrik bir kavşakta gerçekleştirilen deneylerin sonuçlarına dayanan kavramsal bir hidrodinamik model geliştirmiştir [4]. Bu model farklı özelliklere sahip altı bölgeden oluşmaktadır (Şekil 1).

İki akımın birleşmesi, akım derinliğinin ve buna bağlı olarak basıncın artmasına ve akım hızıyla kayma gerilmesinin azalmasına sebep olur. Buna ek olarak akımda bir sapma meydana gelir. Durgunluk bölgesi olarak adlandırılan birleşmenin memba köşesinde oluşan bu bölge tüm bu olaylarla ilişkilidir.

Sapma bölgesi, yan koldan gelen akımın ana kanaldaki akımı ana kanalın dışına doğru ittiği bölgedir.

Ayrılma bölgesi, yan koldan gelen akımın ana kanal akımında meydana getirdiği yön değişikliğinden kaynaklı ana kanalın iç kısmında kavşağın mansabında oluşan bölgedir. Bu bölge yön değişiminin neden olduğu çevrintiler ile ilişkilidir.

Ayrılma bölgesi ve ana kanalın dışı arasında akım maksimum hız ve ivmeye ulaşır. Ayrılma bölgesi nedeniyle etkin akım kesitinin azalması ve akım sapması sebebiyle ana kanalın dış yarısında akım yoğunluğunun artmasıyla oluşan bu bölge hızlanma bölgesi olarak adlandırılmaktadır. Akımın hızlanması kayma gerilmesini arttırmaktadır.

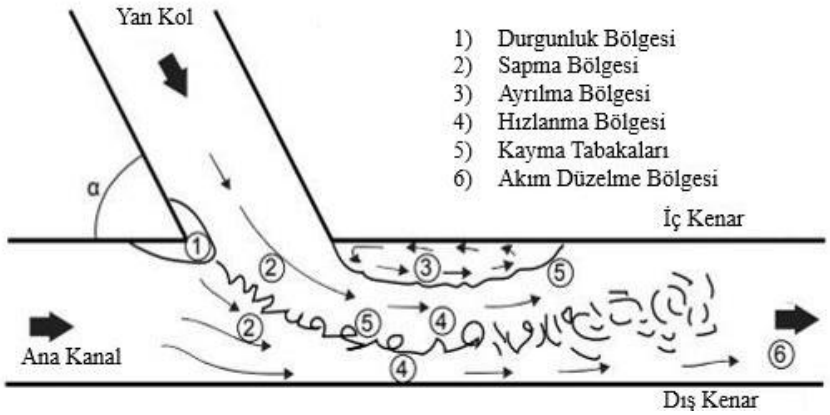

Şekil 1. Açık Kanal Kavşağındaki Hidrodinamik Bölgeler (Best, 1987)

Güçlü hız gradyanları, biri ayrılma bölgesi ve bu bölgeyi çevreleyen akım arasında oluşan, diğeri yan koldan gelen akım ile ana kanal akımını ayıran iki kayma tabakası oluşturur. İkincisi dış kayma tabakası olarak adlandırılır, yüksek türbülans ve kayma gerilmesi ile karakterize edilir.
Son olarak, birleşme sonrası akımın kavşak etkisinden kurtulduğu akım düzelme bölgesi gözlenir.

Coelho yatay tabanlı asimetrik bir kavşakta farklı birleşim açısının (30°- 60°) ve değişen akım koşullarının kanaldaki su seviyesine etkisini incelemiştir [5]. Deneysel çalışmada kanal boyunca belirlenen 8 noktada ölçümler yapılmıştır (Şekil 2). Çalışma kapsamında, kavşaktaki maksimum akım derinliği değeri ile mansaptaki kritik derinlik değeri karşılaştırılarak kavşak çalışmalarında yaygın olarak benimsenen eşit su seviyesi varsayımı değerlendirilmiştir. Ayrıca birleşen akımlardan herhangi birinin ya da her ikisinin de sel rejiminde ve mansaptaki akımın nehir rejiminde olması koşullarında elde edilen akım derinlikleri, Taylor'ın geliştirmiş olduğu modelden elde edilen akım derinlikleriyle karşılaştırılmıştır. Çalışma sonucunda ölçümler ve model arasındaki maksimum ortalama sapma değeri %6 olarak elde edilmiştir.

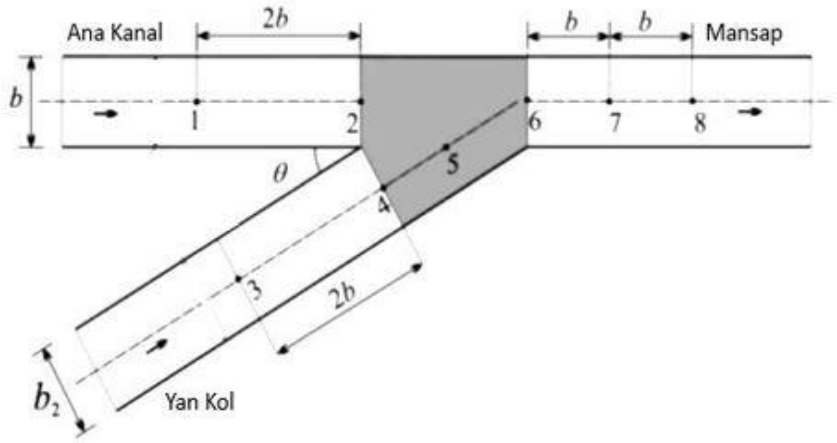

Şekil 2. Değerlendirilen açık kanal kavşağının şeması [5]

Literatürdeki çalışmalara bakıldığında asimetrik akarsu kavşaklarının hidrodinamiğiyle ilgili birçok çalışma mevcutken simetrik akarsu kavşaklarının su yüzeyi profilinin incelenmesi konusunda yeteri kadar çalışmanın olmadığı görülmüştür.

Bu çalışma kapsamında simetrik akarsu kavşağında kollarından birinde taban kotu uyumsuzluğuna sebep olan bir eşik olması durumunda oluşan su yüzeyi profili, sayısal analizle elde edilen su yüzeyi profiliyle karşılaştırılmıştır. Karşılaştırma için doğrudan adım metoduyla elde edilen su yüzeyi profilinden yararlanılmıştır.

Uniform Olmayan Açık Kanal Akımlarında Su Yüzeyi Profili

Açık kanallarda akım derinliği zamana göre değişmezken konuma göre değişiyorsa kararlı üniform olmayan akım meydana gelmektedir. Akım derinliğinin değişmesine bağlı olarak üniform olmayan

akımlarda taban eğimi (S_o) ve serbest sıvı yüzeyi eğimi (S) birbirine eşit değildir. Bu nedenle su yüzeyi profilinin elde edilebilmesi için değişen akım derinliklerinin akım yolu boyunca hesaplanması ve grafiğinin elde edilmesi önem arz etmektedir [6]. Bu amaçla su yüzeyi diferansiyel denklemi kullanılmaktadır.

Tedrici değişen akımlarda bir kanal kesitindeki toplam enerjinin denklemi;

$$H = \frac{V^2}{2g} + h + z \tag{1}$$

şeklinde ifade edilmektedir. Burada *H* toplam enerji, *v* ortalama akım hızı, *h* sıvı yüksekliği, *z* geometrik yükseklik.

Bu denklemin x'e göre türevi alınıp, $dH/dx=-S$, $dz/dx=-S_0$, $Q^2B/gA^2=F_r^2$ yazılarak gerekli düzeltmeler yapıldığında;

$$\frac{dh}{dx} = \frac{S_0 - S}{1 - F_r^2} \tag{2}$$

Su yüzeyi diferansiyel denklemi elde edilir. Burada Q debiyi, B kanal genişliğini, A en kesit alanını, Fr Froude sayısını ifade etmektedir.

Açık kanal akımlarında taban eğimine (hafif, sert, kritik, yatay ve ters) ve akım derinliğine bağlı olarak 12 farklı su yüzeyi profili oluşmaktadır.

Bu çalışmadaki kanal yatay ve akım nehir rejiminde olduğundan ölçümler H2 tipi su yüzeyi profili ile karşılaştırılmıştır.

Bu çalışma kapsamında, su yüzeyi profili hesabında doğrudan adım metodu kullanılmıştır. Bu yöntemde derinlikleri bilinen iki kesit arasındaki mesafe hesaplanmaktadır (derinlikten-mesafeye). Çözüm mansaptan membaya doğru yapılmıştır. İki kesit arasındaki mesafe;

$$\Delta x = \frac{H_1 - H_2}{S_0 - \bar{S}} \tag{3}$$

denklemiyle elde edilir.

Deney Düzeneği

İzmir Kâtip Çelebi Üniversitesi'ndeki mevcut betonarme dikdörtgen kesitli birbirine 90° açıyla bağlanan 1 m genişliğinde simetrik iki yan kola sahip. 2 m genişliğinde ve 18 m uzunluğunda yatay açık kanaldan oluşan simetrik akarsu kavşağı üzerinde deneyler gerçekleştirilmiştir (Şekil 3). Simetrik akarsu kavşağına sahip açık kanalın yan kollarından sol kol üzerinde 12 cm taban kotu eşitsizliği bir eşik ile sağlanmıştır.

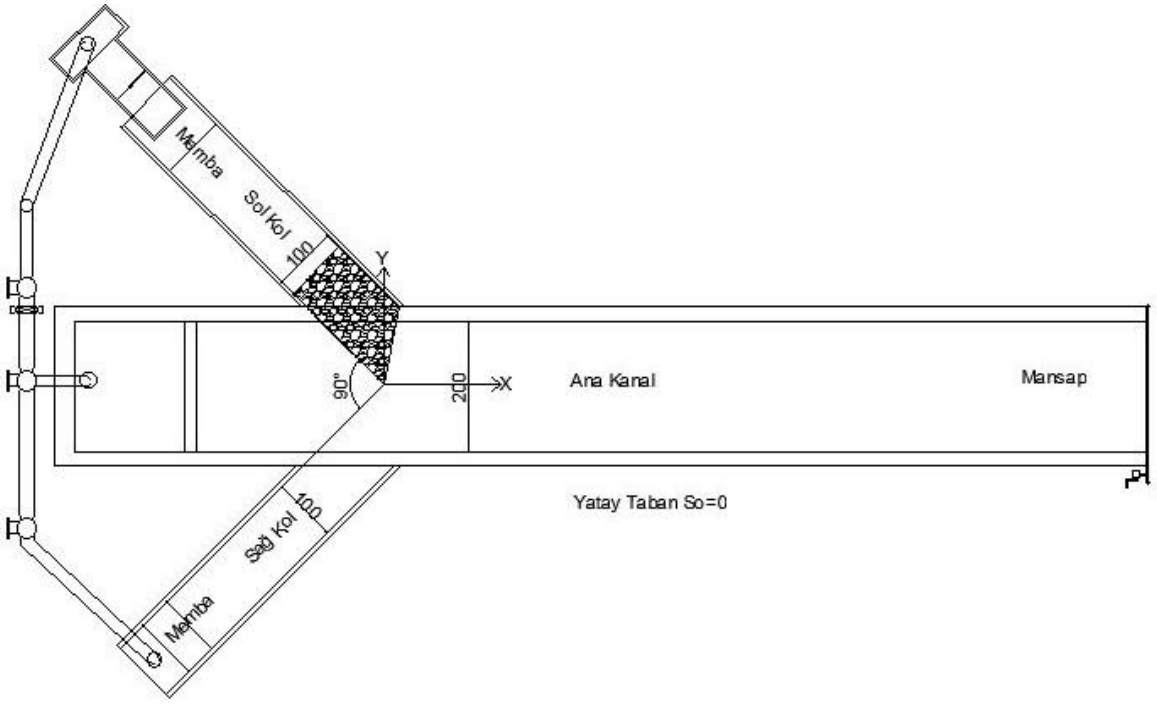

Şekil 3. Deney düzeneği

Deneylerde sağ kol debisi 15 l/s, taban eşitsizliğine sahip sol kol debisi 20 l/s'dir. Sağ koldaki debi elektromanyetik debimetre ile ölçülmüştür. Sol koldaki debi dikdörtgen kesitli dolu savak ile elde edilmiştir. Burada debi denklem (4) ile verilen Rehbock bağıntısı kullanılarak hesaplanmıştır (Şekil 4).

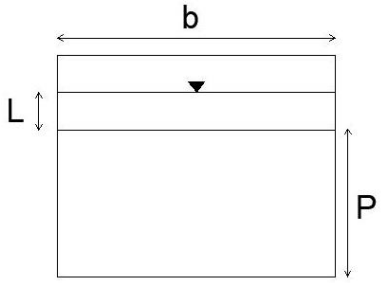

Şekil 4. Savağın karşıdan görünümü

$$Q = C_d \frac{2}{3}\sqrt{2g} b L^{3/2} \quad (4a)$$

$$C_d = 0{,}602 + 0{,}083 L/P \quad (4b)$$

Burada Q debi, b savak genişliği, C_d debi katsayısı, P savak yüksekliği, L savağın üstünde kalan su derinliğidir.

Deney boyunca sağ koldaki debi kaydedilmiş, sol koldaki su yükü olan H limnimetre ile kontrol edilip kaydedilmiştir (Şekil 5).

Mansap derinlikleri Şekil 6'da verilen mansap kapağı ile ayarlanmış, ilk deneyde mansap derinliği 15 cm ve ikinci deneyde 25 cm tutulmuştur.

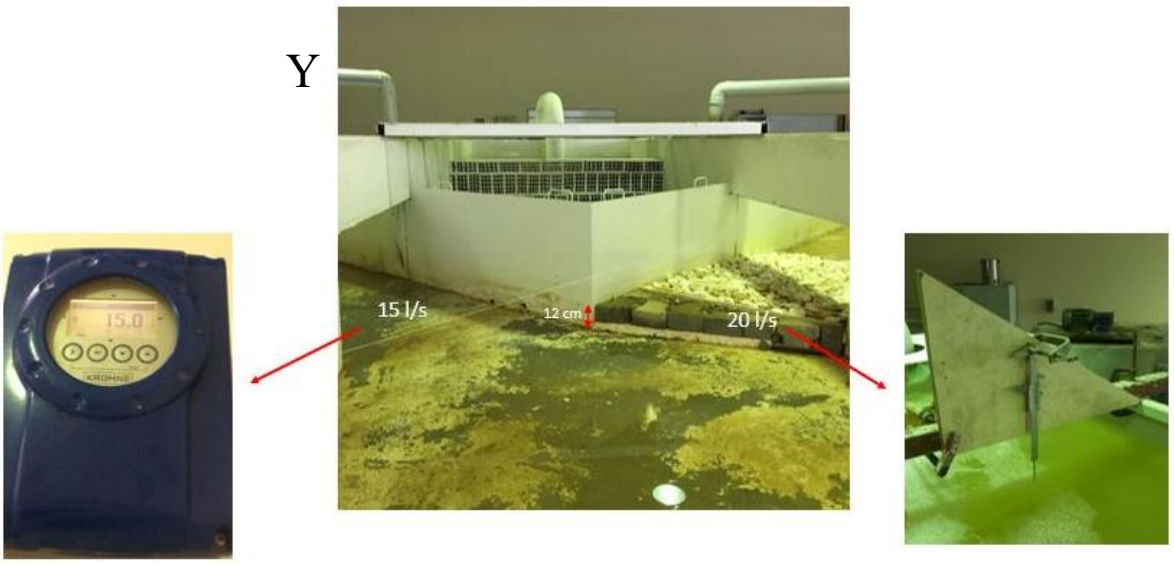

Şekil 5. Akarsu kavşağı, debimetre ve dikdörtgen savak

Şekil 6. Mansap kapağı

Akım derinlikleri ölçümü kanal eksenlerinde, akım yönünde ana kanalda kavşaktan mansaba kadar 50cm, yan kollarda membadan kavşağa kadar 25 cm arayla toplam 64 noktada yapılmıştır (Şekil 7).

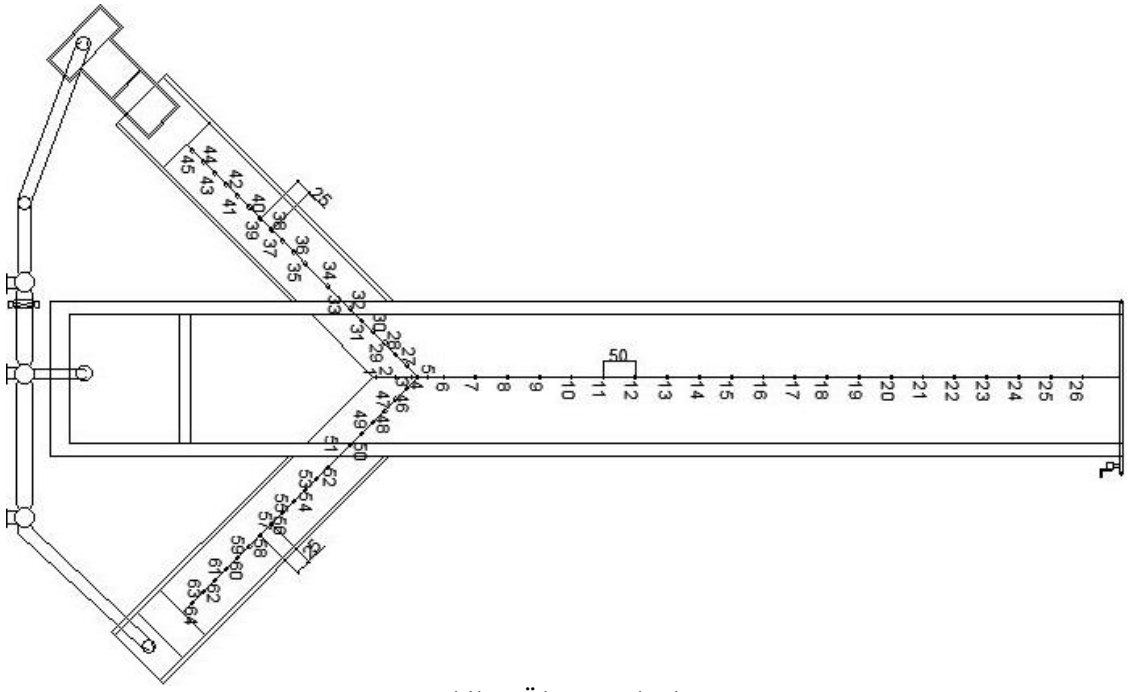

Şekil 7. Ölçüm noktaları

Çalışmada, yan kollardaki ve ana kanaldaki su seviyeleri mevcut raylı sistem üzerine monte edilmiş limnimetre yardımıyla elde edilmiştir (Şekil 8).

Şekil 8. Ana kanal üzerinde limnimetre

Deneysel Bulgular

Bu kısımda 15 cm ve 25 cm mansap derinliği için elde edilen akım derinlikleri ve su yüzeyi profilleri sunulmuştur.

Mansap derinliği 15 cm iken yapılan ilk deneyde elde edilen sol kol ve ana kanaldaki akım derinlikleriyle sayısal analiz su yüzeyi kotu Şekil 9a'da gösterilmektedir. Sağ kol ve ana kanaldaki akım derinlikleri ise Şekil 9b'de sunulmuştur.

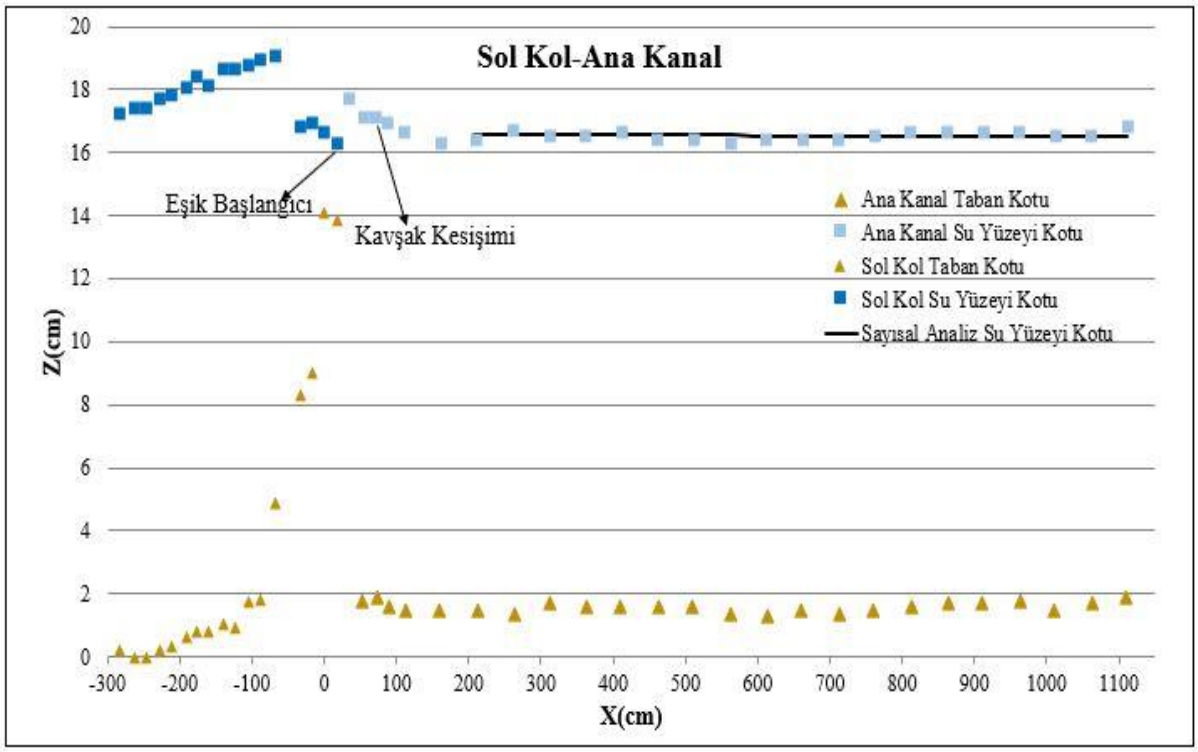

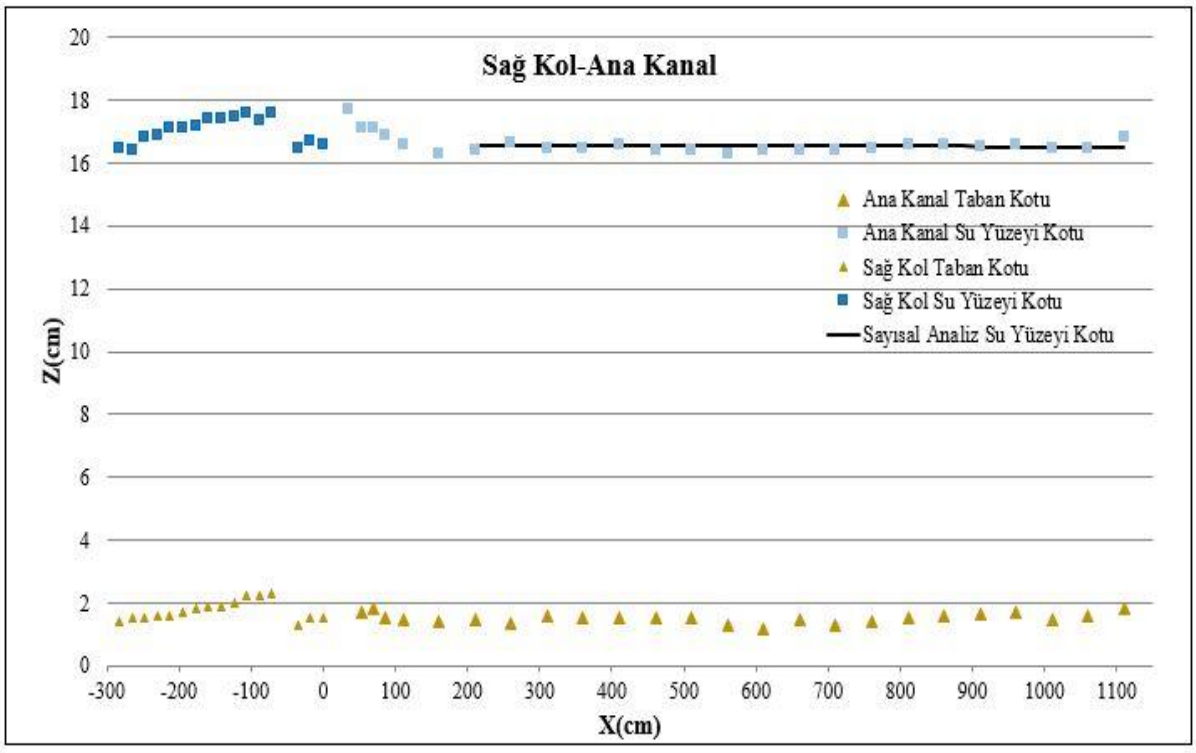

Şekil 9. (a) 15 cm mansap derinliği için sağ kol ana kanal su derinlikleri, (b) 15 cm mansap derinliği için sol kol ana kanal su derinlikleri

Mansap derinliği 25 cm iken yapılan deneyde elde edilen sol kol ve ana kanaldaki akım derinlikleriyle sayısal analiz su yüzeyi kotu Şekil 10a'da gösterilmektedir. Sağ kol ve ana kanaldaki akım derinlikleri ise Şekil 10b'de sunulmuştur.

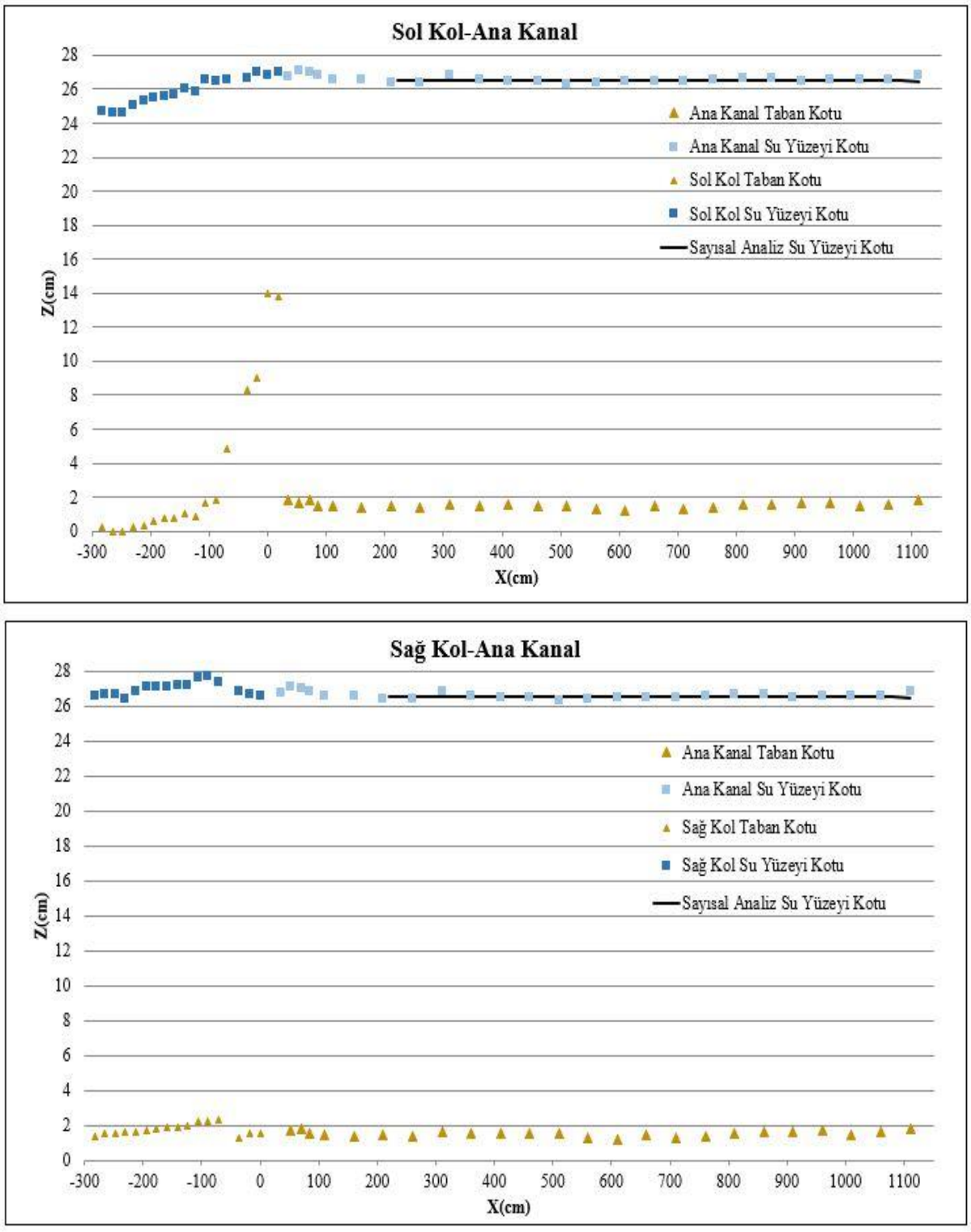

Şekil 10. (a) 25 cm mansap derinligi için sag kol ana kanal su derinlikleri, (b) 25 cm mansap derinligi için sol kol ana kanal su derinlikleri

15cm ve 25 cm mansap derinliği için sol kol ve ana kanaldaki akım derinlikleriyle sayısal analiz su yüzeyi kotu karşılaştırması Şekil 11a'da sunulmuştur. Benzer karşılaştırma sağ kol için yapılmış ve Şekil 11b'de verilmiştir.

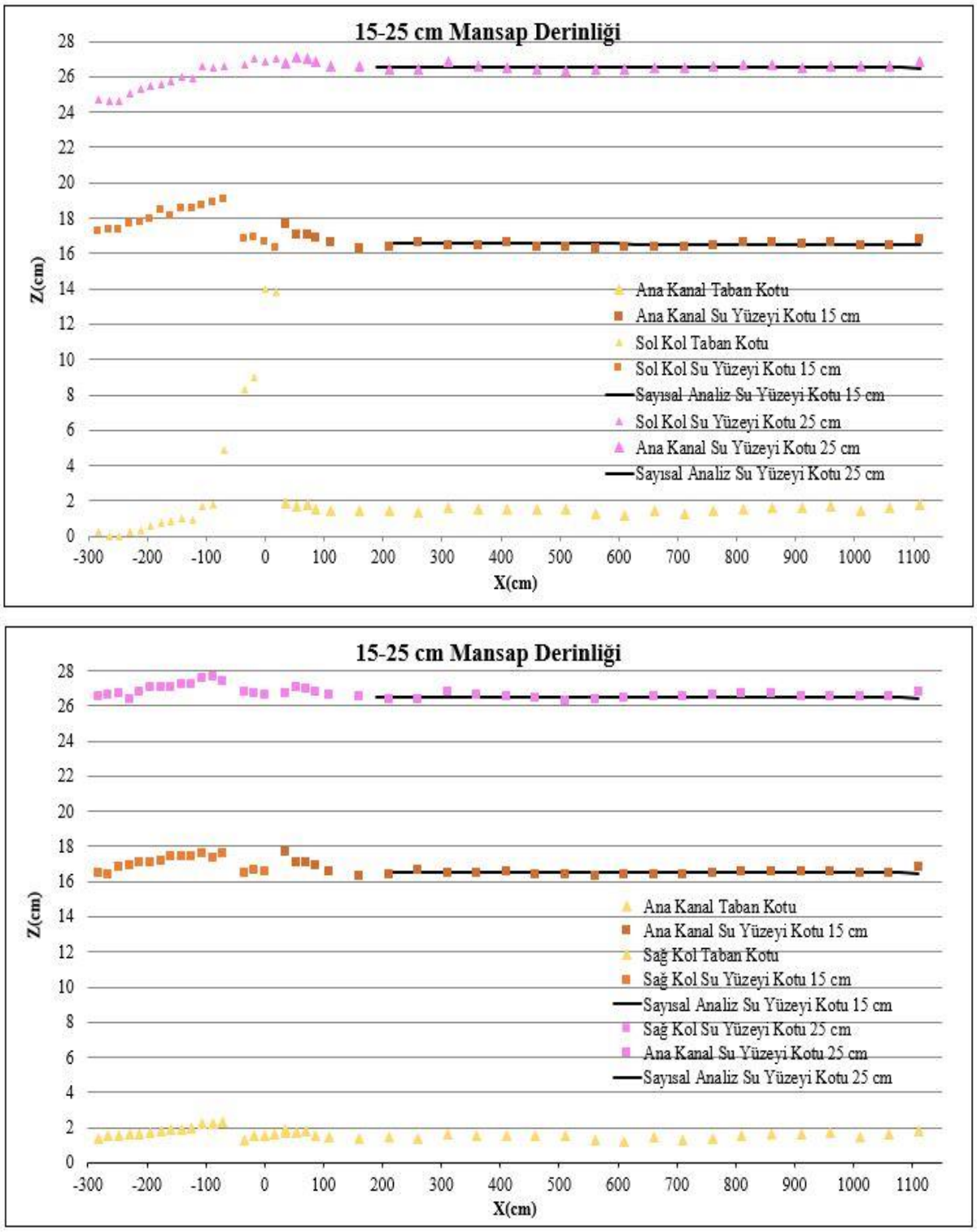

Şekil 11. 15-25 cm mansap derinliği için (a) Sol kol ana kanal su derinlikleri, (b) Sağ kol ana kanal su derinlikleri

Deneysel bulguların ve sayısal analiz sonucu elde edilen su yüzeyi profilinin kavşak bölgesindeki ikincil akımlardan dolayı ana kanalın *x* yönünde ikinci metresinden itibaren örtüştüğü görülmüştür.

Sonuç

Sürtünme katsayısı (n) 0,015 kabul edilerek 15 cm mansap derinliği için su yüzeyi profili elde edildiğinde ortalama karekök sapması (RMSE) 0,1486 ve ortalama mutlak hata (MAE) 0,0883 olarak hesaplanmıştır.

Sürtünme katsayısı (n) 0,015 kabul edilerek 25 cm mansap derinliği için su yüzeyi profili elde edildiğinde ortalama karekök sapması (RMSE) 0,1832 ve ortalama mutlak hata (MAE) 0,1145 olarak hesaplanmıştır.

Sürtünme katsayısı (n) 0,02 kabul edilerek 15 cm mansap derinliği için su yüzeyi profili elde edildiğinde ortalama karekök sapması (RMSE) 0,1517 ve ortalama mutlak hata (MAE) 0,0917 olarak hesaplanmıştır.

Sürtünme katsayısı (n) 0,02 kabul edilerek 25 cm mansap derinliği için su yüzeyi profili elde edildiğinde ortalama karekök sapması (RMSE) 0,1835 ve ortalama mutlak hata (MAE) 0,115 olarak hesaplanmıştır.

n değeri büyüdükçe RMSE ve MAE değerlerinin arttığı görülmüştür.

Referanslar

[1] Biron P, Best JL, Roy AG. Effects of bed discordance on flow dynamics at open channel confluences. Journel of Hydraulic Engineering 1996 Dec (Vol 122).

[2] Taylor E H. Flow characteristics at rectangular open-channel junctions. American Society of Civil Engineers1 70 : 119–121).

[3] Webber NB, Greated CA. An investigation of flow behaviour at the junction of rectangular channels. Proceedings of Institute of Civil Engineers 34 : 321–334).

[4] Best JL. Flow dynamics at river channel confluences: Implications for sediment transport and bed morphology. In F G Ethridge, R M Flores, and M D Harvey (Eds.). Recent Developments in Fluvial Sedimentology 1987 (pp. 27–35). SEPM (Society for Sedimentary Geology).

[5] Coelho MMLP. Experimental determination of free surface levels at open-channel junctions. Journal of Hydraulic Research. 2015 ; 53(3): 394-399.

[6] Kaçmaz A. Açık Kanal Su Yüzü Profil Hesabının Newton Raphson ile Çözümü ve Bilgisayar Programı Geliştirilmesi. Yüksek Lisans Tezi. 2018.

Bilgisayarlı Tomografi Görüntülerini Kullanarak Covid-19 Hastalığının Derin Öğrenme Teknikleriyle Tespiti

*Muhammed Alperen Horoz**, *Seda Arslan Tuncer*
Fırat Üniversitesi, Yazılım Mühendisliği Bölümü, Elazığ, Türkiye
**İletişimden sorumlu yazar: 191137101@firat.edu.tr*

Özet

Covid-19, beta-koronavirüs ailesi içerisinde yer alan, insanlarda basit bir soğuk algınlığından ağır akut solunum hastalıklarına kadar ilerleyebilen bir hastalıktır. Tansiyon, diyabet gibi kronik hastalıklarda ve 60 yaş üzerindeki insanlarda öldürücü etkisi daha fazladır. Bu nedenle tanının ve tedavinin acil olarak yapılması önem taşır. Covid-19 tanısında aktif olarak PCR (Polymerase Chain Reaction) testi kullanılmaktadır. Covid-19 tanısı için bilgisayarlı tomografi (BT), ultrason görüntüleme, laboratuvar testleri gibi birçok yöntem kullanılabilir. Bunun yanı sıra hekimler şüpheli hastanın BT görüntülerini tanıya yardımcı olması amacıyla kullanmaktadır. BT görüntüleri hızlı elde edilebilir ve Covid-19 hastalığının akciğerlerde yarattığı enfeksiyon BT ile görülebilir. BT bilgisayar destekli uygulamalarda sıkça kullanılmaktadır. Bilgisayar destekli uygulamalar hekimlere tanı ve tedavide destek veren sistemlerdir. Geliştirilen bu uygulamaların insan yanılgısından uzak, objektif olması tanıdaki güvenilirliği arttırır ve hata oranını ciddi oranlarda düşürür.

Derin öğrenme, sistemin otomatik olarak öğrendiği ve sınıflandırma için gerekli olan özellikleri çok sayıda girdi verisi katmanının işlenmesinden keşfettiği temsili öğrenmeye dayanan bir makine öğrenme tekniğidir. Derin öğrenme birçok bilgisayar destekli biyomedikal yazılımda kullanılmaktadır.

Bu çalışmada, BT verileri kullanılarak Covid-19 hastalığını derin öğrenme teknikleri ile tespit etmek amaçlanmıştır. Veri seti 118 Covid-19 tanılı hasta ve 100 sağlıklı bireyden oluşmaktadır. Çalışmada, 751 adet Covid-19 tanılı hastaya ve 628 sağlıklı bireye ait BT görüntüsü kullanılmıştır. Elde edilen toplam 1379 BT verisi %70 eğitim ve %30 test verisi olarak bölünmüştür. Bu veriler AlexNet, GoogleNet, VGG-16, VGG-19 gibi derin öğrenme modelleri ve önerilen derin öğrenme modeli kullanılarak sınıflandırılmıştır. Önerilen model dışında kullanılan ağlar ImageNet verisi ile eğitilmiştir. Eğitilen bu ağlar kullanılırken, önceden eğitilmiş ağırlıklarla başlanmış daha sonra kendi eğitim verimiz ile tüm ağ eğitilmiş ve ağırlıklar güncellenmiştir. Önerilen modelde veriler 100x100 boyutlarında ağlara girdi olarak verilmiştir. Önerilen modelde veriler 3 kanallı renkli görüntü olarak değil, 2 kanallı gri görüntüler olarak kullanılmıştır. 8 katmandan oluşan modelimizde, 256x256 boyutunda olan filtreler tam bağlantılı katman ve çıkış katmanı dışındaki tüm katmanlarda kullanılmıştır. Modelde 5 evrişim ve havuzlama katmanı, 1 tam bağlantılı katman bulunmaktadır. Buna ek olarak tam bağlantılı katmandan önce özellik haritalarının özellik vektörüne dönüştürüldüğü ve daha sonra tam bağlantılı katmana bağlandığı bir katman bulunmaktadır. Daha sonra çıkış katmanı ile ağ sonlandırılmıştır. Yapılan çalışma sonucunda AlexNet ile %80,39, GoogleNet ile %93,90, VGG-16 ile %93,75 ve VGG-19 ile %88,38 sınıflandırma doğruluğu elde etmiştir. Önerilen ağ diğer ağ modellerine göre %95,64 doğruluk elde ederek daha yüksek sınıflandırma doğruluğu göstermiştir. Bunun yanı sıra çalışmada önerilen model %98,94 hassaslık değerine sahip olurken, AlexNet ile %64,89, GoogleNet ile %92,89, VGG-16 ile %93,78, VGG-19 ile %81,33 hassaslık değerlerine ulaşılmıştır. Ayrıca önerilen model %92,89 özgüllük değerine sahip olurken, AlexNet %98,94, GoogleNet %95,21, VGG-16 %94,15, VGG-19 ise %96,81 özgüllük değerine ulaşmıştır. Gerçekleştirilen bu çalışmanın Covid-19 salgınında tanıya yardımcı olacağı, ayrıca yapay zekâ yardımı ile sağlık çalışanlarının iş yükünü azaltacağı ve maliyeti düşüreceği düşünülmektedir.

Anahtar Kelimeler: Covid-19, pandemi, derin öğrenme, sınıflandırma, yapay zekâ

Giriş

Koronavirüs salgını ilk olarak 2019 yılının aralık ayında Çin tarafından raporlanmıştır. Hastalık 31 Ocak 2020 yılına kadar Çin'de 9720 kişiyi ve diğer 19 ülkede 106 kişiyi enfekte etmiştir [1].

Dünya Sağlık Örgütü ise geçici olarak Şiddetli Akut Sendromlu Koronavirüs 2 (SARS-Cov-2) olarak adlandırılsa da daha sonra bu hastalığı Koronavirüs Hastalığı 2019 (Covid-19) olarak adlandırmıştır [2,3]. Koronavirüs, insanlarda basit bir soğuk algınlığından ağır akut solunum

hastalıklarına kadar uzanabilen ve bulaşıcılığı günden güne artan bir hastalıktır [4]. Tansiyon, diyabet gibi kronik hastalıklarda ve 60 yaş üzerindeki insanlarda öldürücü etkisi daha fazladır [4,5]. Hastalığın teşhisinde ve tedavisinde geç kalınması, yanlış sonuçlanan testler, hastalığının oldukça bulaşıcı olması vb. durumlar göz önünde bulundurulduğunda teşhisin, teşhisten sonra enfekte olan kişinin toplumdan izole edilmesinin ve tedavinin oldukça hızlı olması gerekir [6]. Covid-19 hastalığı basit olarak hızlı tanı kitleri ile teşhis edilebilir. Güvenilirliği oldukça düşük olan bu testlerin PCR testi ile teyit edilmesi gerekir. PCR testi ise virüs RNA'sını tanıyan ve sürüntü testi de denilen tanı yöntemidir [7]. Bununla birlikte hekimler şüpheli hastanın BT'sine bakıp, kesin tanı koyabilmektedir. Bunun sebebi Covid-19 hastalığında akciğer enfeksiyonu yüksek ölçüde görüldüğünden X-Ray ve BT gibi görüntüleme teknikleriyle hastalığı teşhis etmek mümkündür [8,9].

Hastalığın yayılma hızı, öldürücülüğü ve sağlık personellerinin pandemi sürecindeki iş yükü gibi etkenler göz önünde bulundurulduğunda Covid-19 teşhisinde insan ve yöntem hatalarından uzaklaşarak, hastalığın teşhisinde uzmanlara karar verme sürecinde yardımcı olacak bilgisayar destekli sistemlere ihtiyaç vardır [10]. Bu ihtiyaç bilgisayar bilimleri ve tıp alanlarını birleştirerek otomatik, hızlı, güvenilir tanı sistemleri olarak ön plana çıkmaktadır. Covid-19 hastalığında da BT görüntüleri ile yapay zekâ sistemleri kullanılarak hastalık teşhisine bilgisayar destekli sistemler literatüre kazandırılmıştır. Bu çalışmalardan bazıları şu şekildedir:

Wang ve arkadaşları BT video görüntüleri üzerinde ihtiyaç duyulan kesitleri 395*223 ile 636*533 piksel boyutlarında elde etmişlerdir. Toplamda 44 Covid-19 hastasından 195 kesit ve Covid-19 olmayan 50 hastadan 258 kesit seçilmiştir. Bu kesitlerden 236'sı sistemi eğitmek için kullanılırken, 217'si doğrulama için kullanılmıştır. Model olarak tipik Inseption modelini M-Inseption olarak değiştirip, önceden eğitilmiş ağırlıklarla ince ayar yapılmıştır. Bu ince ayar modelin son bağlanma noktasında yer almaktadır. Son olarak sınıflandırma katmanından önce özelliklerin boyutunu düşürüp, CNN ağının sınıflandırma aşamasına giriş olarak verilmiştir. İki farklı doğrulama verisinde sırasıyla %82,9 ve %73,1 doğrulama elde etmişlerdir [11].

Wang ve arkadaşları Covid-19 hastalığı ile ilgili iki adet veri seti elde etmişlerdir. Bu veri setlerinden ilki BT Epidermal Büyüme Faktörü Reseptörü (BT-EBFR) ile ilgili 4106 adet veriden oluşurken, bir diğeri Covid-19 veri kümesi 1266 veriden oluşmuştur. BT-EBFR veri kümesi prognostik analiz için yeni önerilen Covid-19NET ağını eğitmek için kullanılmıştır. Prognostik analizi Covid-19 hastalarının akciğer özelliklerini öğrenmek amacıyla yapmışlardır. Covid-19 veri setini ise daha önce ImageNet verisi kullanılarak eğitilmiş ve VESSEL12 verisi ile ince ayar yapılmış DenseNet121-FPN modelinde kullanmışlardır [12].

Ardakani ve arkadaşları kullandıkları verilere demografik değişikliklere bakmaksızın Covid-19 ve grip semptomları gösteren bütün denekleri çalışmaya dâhil etmişlerdir. Semptomu olan hastaları sürüntü örnekleri alarak RT-PCR testine tabi tutup hastalığı olmayan bütün denekleri veri seti dışında bırakmışlardır. Semptomlar başladığı günden itibaren 3 ile 6 gün ile sonra görüntüleme çalışmaları yapmışlardır. Uzman bir Radyolog ile akciğerde bulunan Covid-19 kaynaklı enfeksiyonlu bölgeleri etiketlemişlerdir. Daha sonra CNN mimarisinde bulunan 10 adet modelde bu verileri kullanmışlardır. Bu modeller; AlexNet, VGG-16, VGG-19, SqueezeNet, GoogleNet, MobileNetV2, ResNet-18, ResNet-50, ResNet-101 ve Xception'dur [13].

Jaiswal ve arkadaşları Kaggle'da bulunan SARS-CoV-2 BT taramalarını deneysel amaçla kullanmışlardır. Veri kümesi, 1262'si SARS-CoV-2 enfeksiyonu için pozitif ve geri kalan 1230'u SARS-CoV-2 enfeksiyonu, olan toplam 2492 BT taramasından oluşmaktadır. Hâlihazırda eğitilmiş VGG19, Inception ResNet, Resnet 152V2, DenseNet ağları verilerin %68'i ile yeniden eğitilmiş, %17'si doğrulama için kullanılmış ve %15'i test için kullanılmıştır [14].

Gozes ve arkadaşları yaptıkları çalışmada 4 farklı veri seti kullanılmıştır. Bunlardan ikisi sınıflandırma amaçlı eğitim ve test için kullanılırken, diğer ikisi akciğer enfeksiyonunun segmentasyonu amacıyla eğitim ve test olarak kullanılmıştır. Bütün veriler bilgisayarlı BT görüntüsüdür.

Sınıflandırma için toplamda 1865 veri ve toplam 1.725.320.270 kesit kullanılmıştır. Segmentasyon aşamasında ise toplamda 6.150 kesit kullanılmıştır. Görüntülerin boyutları 224x224 olarak seçilmiştir. Sınıflandırma için ResNet-50 kullanılmıştır. Segmentasyon aşamasında ise ImageNet verisi ile önceden eğitilmiş U-Net ağı kullanılmıştır [15].

Ying ve arkadaşları veri setlerini 88 hasta, 100 zatürre hastası ve 86 sağlıklı denekten oluşturmuşlardır. Geliştirdikleri ağ (DRE-Net), her bir görüntüden en iyi K ayrıntılarını çıkarmak için

Özellik Piramit Ağı 14'ün eklendiği önceden eğitilmiş ResNet5013 üzerine somut olarak oluşturulmuştur. Hem zatürre ve Covid-19 hastası arasındaki sınıflandırma yapılmış, aynı zamanda sağlıklı veriler kullanılarak direk teşhis yazılımı da gerçekleştirilmiştir. Bunları yaparken Transfer Öğrenme ağlarından daha fazla başarı elde etmişlerdir [16].

Zheng ve arkadaşları klinik olarak Covid-19 tanısı konmuş 313 hastayı ve Covid-19 bulunmayan 229 hasta dâhil olmak üzere 540 hastayı çalışmalarına dâhil etmişlerdir. İlk olarak U-Net ağı ile segmentasyon uygulayıp, daha sonra segmente edilmiş verileri kendilerinin geliştirdikleri DeCovNet ağına giriş olarak verip, sonuca ulaşmışlardır [17].

Bu çalışma BT kullanarak, derin öğrenme modelleri ile Covid-19 tanısı koymayı amaçlamaktadır. Kullanılan bir veri seti üzerinde derin öğrenme teknikleri kullanılarak akciğerde meydana gelen Covid-19 sebepli enfeksiyonu temel alarak Covid-19 hastalığının tanısı gerçekleştirilmektedir.

Materyal

Çalışmada kullanılan veriler Elazığ Fethi Sekin Şehir Hastanesi'nden elde edilmiştir. Veri seti akciğer tomografisi görüntülerinden oluşmaktadır. Veri setine 118 Covid-19 hastasının tomografi görüntülerinden ortalama 6 kesit kullanılarak, toplamda 751 adet akciğer tomografisi kesiti dahil edilmiştir. Bunda ek olarak, 100 sağlıklı bireyin tomografi görüntülerinden ortalama 6 kesit kullanılarak, toplamda 628 adet akciğer tomografisi kesiti dahil edilmiştir. Sonuç olarak veri setine toplamda 1379 akciğer tomografisi dahil edilmiştir. Veri setine ait sınıf tablosu Tablo 1'de verilmiştir.

Tablo 1. Veri kümesi

	Denek Sayısı	Deneklerden Alınan Ortalama BT Sayısı	Deneklerden Alınan Toplam BT Sayısı	Toplam Veri
Covid-19 Pozitif	100	6	628	1379
Covid-19 Negatif	118	6	751	

Metot

Çalışma COVID-19 hastası ve sağlıklı bireylerin verileri kullanılarak derin öğrenme ile sınıflandırma yaklaşımı üzerine kurulmuştur. 1379 BT verisi %70 eğitim ve %30 test verisi olarak bölünmüştür. Buna göre, 966 BT görüntüsü eğitim için 413 BT görüntüsü test için ayrılmıştır. Bu veriler AlexNet, GoogleNet, VGG-16, VGG-19 gibi derin öğrenme modelleri ve Önerilen derin öğrenme modeli kullanılarak sınıflandırılmıştır. Önerilen model dışında kullanılan ağlar ImageNet verisi ile eğitilmiştir. Eğitilen bu ağlar kullanılırken, önceden eğitilmiş ağırlıklarla başlanmış, daha sonra kendi eğitim verimiz ile tüm ağ eğitilmiş ve ağırlıklar güncellenmiştir. Sınıflandırma işleminden sonra, ağlara ait performanslar değerlendirilmiştir. Bu değerlendirme sonucunda oluşturulan veri setinde en yüksek doğruluk değerine oluşan ağ belirlenmiştir. Şekil 1'de çalışmaya ait süreç tasarımı verilmiştir.

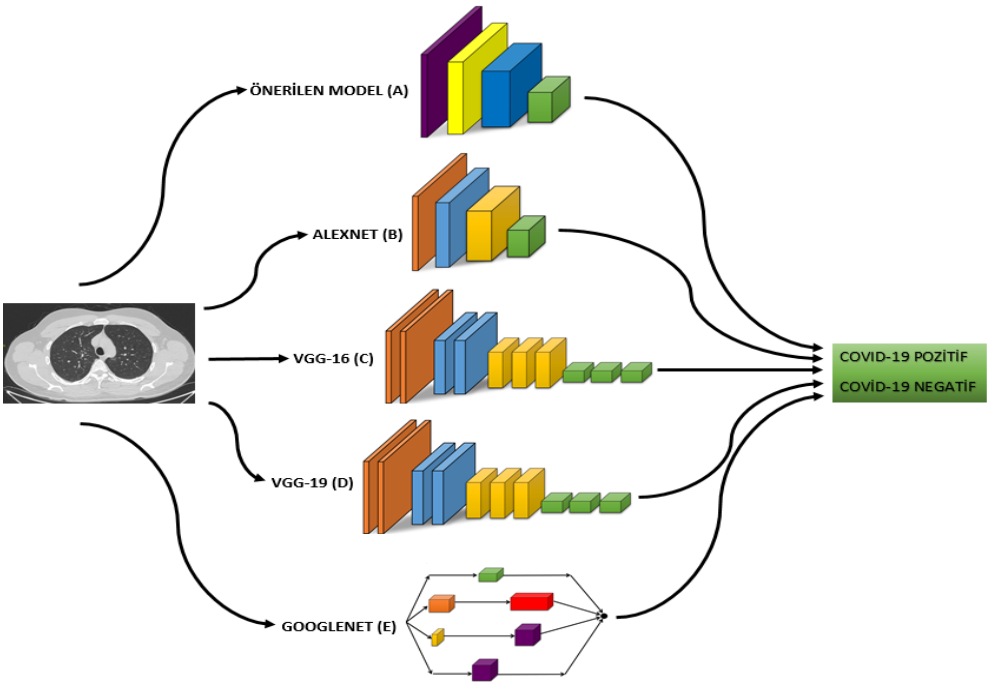

Şekil 1. Çalışmaya ait süreç tasarımı

Önerilen modelde veriler 2 kanallı gri görüntülere çevrilip, 100x100 olarak yeniden boyutlandırılmış, 8 katmandan oluşan sıralı ağımıza giriş olarak verilmiştir. 256x256 boyutunda olan filtreler tam bağlantılı katman ve çıkış katmanı dışında tüm katmanlarda kullanılmıştır. Modelde 5 evrişim ve havuzlama katmanı, 1 tam bağlantılı katman bulunmaktadır. Buna ek olarak tam bağlantılı katmandan önce özellik haritalarının özellik vektörüne dönüşütürüldüğü ve daha sonra tam bağlantılı katmana bağlandığı bir katman bulunmaktadır. Daha sonra çıkış katmanı ile ağ sonlandırılmıştır. Tam bağlantılı katmanda aktivasyon fonksiyonu olarak sigmoid, diğer katmanlarda relu kullanılmıştır.

2012 yılında evrişimli derin ağların tekrar popüler hale gelmesini sağlayan AlexNet, Alex Krizhevsky, Ilya Sutskever and Geoffrey Hinton tarafından geliştirilmiştir. Temel olarak birbirini takip eden evrişim ve pooling katmanlarından oluşmaktadır. 8 katmanlı derinliğe sahip olan AlexNet ile yaklaşık 60 milyon parametre hesaplanmaktadır. Buna ek olarak 5 evrişim katmanı ve 3 tam bağlantılı katmandan oluşur. Aktivasyon fonksiyonu olarak ReLU (Rectified Linear Unit), pooling katmanlarında ise da max-pooling kullanmaktadır [18].

GoogleNet, diğer ağlara göre yapısal olarak farklı bir mimari sayılabilir. Inception ağlar olarakta adlandırılan bu ağ, her birine inception adı verilen modüllerden oluşmaktadır. Evrişim ve pooling işlemleri her modül sonunda yapılmaktadır. Üç adet evişim işleminden sonra 9 adet modülü tamamlayıp, son olarak tam bağlantılı katman ile sona erer. GoogleNet 22 katman derinliğe sahiptir [19].

En basit mimariye sahip ağlardan biri olan VGG-16 ağı, bu özelliğine karşın derin bir ağdır. Her adımında girdi boyutları yarıya indirilirken, kullanılan filtre boyutları 2 katına çıkarılır.

Diğer modellere göre en önemli farkı mimarideki 5 evrişimli bloğun katmanlarının 2'li ya da 3'li kullanılmasıdır. Her evrişim katmanından sonra filtreler hesaplanır. Bu ağda yaklaşık 128 milyon parametre kullanılmaktadır. Son aşamada, yani tam bağlantı katmanında 7x7x512=4096 nöronlu bir öznitelik vektörüne dönüştürülür [20].

VGG 19, 5 evrişimli blok katmanı ve 3 tam bağlı katmanda sona eren 16 evrişim katmanından meydana gelen ve ReLU aktivasyon fonksiyonlarıyla tanımlı bir derin öğrenme modelidir. Toplamda 24 ana katmandan oluşan bu ağda filtreler 3x3 boyutunda olup, parametre sayısını azaltmak için kullanılır. VGG-19 ağı yaklaşık 138 milyon parametre içermektedir [21].

Bilinen ve bu çalışmada kullanılan 4 ağ modeli ImageNet verisi ile eğitilmiştir. Eğitilen bu ağlar kullanılırken, önceden eğitilmiş ağırlıklarla başlanmış, daha sonra kendi eğitim verimiz ile tüm ağ eğitilmiş ve ağırlıklar güncellenmiştir. Mimarilerinde bir değişiklik yapılmadan yalnızca ağların ağırlıkları değişime şart tutulmuştur.

Deneysel Sonuçlar

Çalışmada toplam 1379 bilgisayarlı tomografi kesiti veri seti olarak kullanılmıştır. Bu veriler önerilen modelde ve iyi bilinen, daha önce büyük görüntü verileriyle eğitilmiş ağlarda sınıflandırılmıştır. Modellere ait doğruluk değeri aşağıda verilen Denklem 1'e göre, hassaslık değeri Denklem 2'ye göre, özgüllük değeri Denklem 3'e göre, F1 skoru Denklem 4'e göre hesaplanmıştır. Modellere ait performans ölçütleri aşağıdaki yöntemlere göre hesaplanmıştır. Yöntemlerde yer alan TP doğru tahmin edilen pozitif vakaları, TN doğru tahmin edilen negatif vakaları, FP yanlış tahmin edilen pozitif vakaları ve FN yanlış tahmin edilen negatif vakaları temsil etmektedir. Çalışmada kullanılan tekniklerin başarımları Tablo 2'de gösterilmiştir. Buna ek modellere ait karmaşıklık matrisleri Şekil 2,3,4,5 ve Şekil 6'da gösterilmiştir.

$$Doğruluk = \frac{N_{TN}+N_{TP}}{N_{TN}+N_{FN}+N_{TP}+N_{FP}} \quad (1)$$

$$Hassaslık = \frac{N_{TP}}{N_{TP}+N_{FN}} \quad (2)$$

$$Özgüllük = \frac{N_{TN}}{N_{TN}+N_{FP}} \quad (3)$$

$$F1\ Skoru = 2 \times \frac{N_{TP}}{N_{TP}+N_{FP}+N_{FN}} \quad (4)$$

Tablo 2. Deneysel Sonuçlar

Model	Doğruluk	Hassaslık	Özgüllük	F1 Skoru
Önerilen Model	**0.9561**	**0.9864**	0.9289	**0.9538**
AlexNet	0.8039	0.6489	**0.9894**	0.7828
GoogleNet	0.9390	0.9289	0.9521	0.9436
VGG-16	0.9375	0.9378	0.9415	0.9441
VGG-19	0.8838	0.8133	0.9681	0.8841

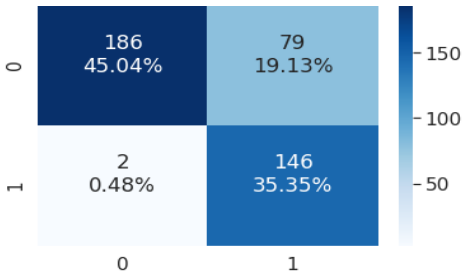

Şekil 2. Önerilen Modele ait karmaşıklık matrisi

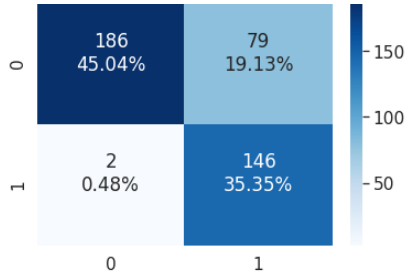

Şekil 3. AlexNet ağına ait karmaşıklık matrisi

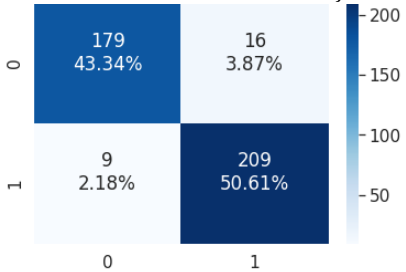

Şekil 4. GoogleNet ağına ait karmaşıklık matrisi

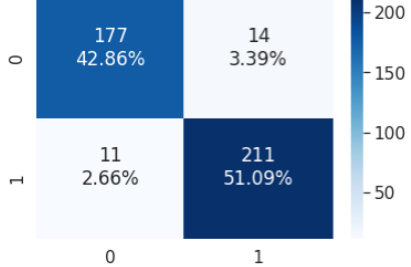

Şekil 5. VGG-16 ağına ait karmaşıklık matrisi

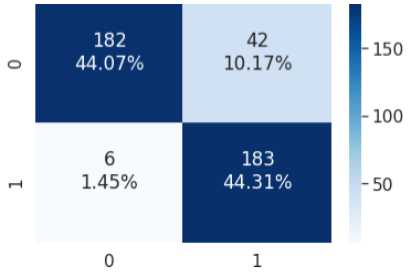

Şekil 6. VGG-19 ağına ait karmaşıklık matrisi

Gerçekleştirilen uygulamada akciğer görüntüleri kullanılarak yapılan sınıflandırma işlemi sonucunda en yüksek doğruluk oranı %95,61 olarak önerilen model ile elde edilmiştir. Bunun dışında AlexNet ile %80,39, GoogleNet ile %93,90, VGG-16 ile %93,75 ve VGG-19 ile %88,38 sınıflandırma doğruluğu elde etmiştir. Başarımları ve diğer sonuçları göz önüne bulundurduğumuzda yapılan çalışmanın performansının diğer modellere göre daha iyi sonuç verdiği görülmektedir.

Sonuçlar

Bu çalışmada, BT verileri kullanılarak Covid-19 tanısı derin öğrenme teknikleri kullanılarak konulmuştur. Çalışmada önerilen model ile literatür de kullanılan AlexNet, Google Net ve VGG-16 gibi modellerden daha yüksek doğruluk elde edilmiştir. Bununla birlikte kullanılan veri üzerinde AlexNet, Google Net ve VGG-16 ağlarında da %90 üzerinde başarı elde etmiştir. Çalışma önemli iş gücü ve kaynaklara ihtiyaç duymadığından, COVID-19 tanısında hekime yardımcı bir kaynak olarak kullanılabileceği kanaatine varılmıştır.

Referanslar

[1] Who.int. [cited 2021 Apr 14]. Available from: https://www.who.int/docs/default-source/coronaviruse/situation-reports/20200131-sitrep-1-ncov.pdf
[2] Lu R, Zhao X, Li J, Niu P, Yang B, Wu H, et al. Genomic characterisation and epidemiology of 2019 novel coronavirus: implications for virus origins and receptor binding. Lancet. 2020;395(10224):565–74.
[3] Zhou P, Yang X-L, Wang X-G, Hu B, Zhang L, Zhang W, et al. A pneumonia outbreak associated with a new coronavirus of probable bat origin. Nature. 2020;579(7798):270–3.
[4] Liu J, Zheng X, Tong Q, Li W, Wang B, Sutter K, et al. Overlapping and discrete aspects of the pathology and pathogenesis of the emerging human pathogenic coronaviruses SARS-CoV, MERS-CoV, and 2019-nCoV. J Med Virol. 2020;92(5):491–4.
[5] Li Q, Guan X, Wu P, Wang X, Zhou L, Tong Y, et al. Early transmission dynamics in Wuhan, China, of novel Coronavirus-infected pneumonia. N Engl J Med. 2020;382(13):1199–207.
[6] Beigel JH, Tomashek KM, Dodd LE. Remdesivir for the treatment of covid-19 - preliminary report. Reply. N Engl J Med. 2020;383(10):994.
[7] Binnicker MJ. Emergence of a novel Coronavirus disease (COVID-19) and the importance of diagnostic testing: Why partnership between clinical laboratories, public health agencies, and industry is essential to control the outbreak. Clin Chem. 2020;66(5):664–6.
[8] Pan Y, Guan H, Zhou S, Wang Y, Li Q, Zhu T, et al. Initial CT findings and temporal changes in patients with the novel coronavirus pneumonia (2019-nCoV): a study of 63 patients in Wuhan, China. Eur Radiol. 2020;30(6):3306–9.
[9] Clinicians use lung ultrasound to quickly triage coronavirus patients [Internet]. Radiologybusiness.com. [cited 2021 Apr 14]. Available from: https://www.radiologybusiness.com/topics/care-delivery/ultrasound-coronavirus-covid-19-x-ray-ct-scan-radiology
[10] Vaishya R, Javaid M, Khan IH, Haleem A. Artificial Intelligence (AI) applications for COVID-19 pandemic. Diabetes Metab Syndr. 2020;14(4):337–9.

[11] Wang S, Kang B, Ma J, Zeng X, Xiao M, Guo J, et al. A deep learning algorithm using CT images to screen for Corona virus disease (COVID-19). Eur Radiol [Internet]. 2021; Available from: http://dx.doi.org/10.1007/s00330-021-07715-1
[12] Wang S, Zha Y, Li W, Wu Q, Li X, Niu M, et al. A fully automatic deep learning system for COVID-19 diagnostic and prognostic analysis. Eur Respir J. 2020;56(2):2000775.
[13] Ardakani AA, Kanafi AR, Acharya UR, Khadem N, Mohammadi A. Application of deep learning technique to manage COVID-19 in routine clinical practice using CT images: Results of 10 convolutional neural networks. Comput Biol Med. 2020;121(103795):103795.
[14] Jaiswal A, Gianchandani N, Singh D, Kumar V, Kaur M. Classification of the COVID-19 infected patients using DenseNet201 based deep transfer learning. J Biomol Struct Dyn. 2020;1–8.
[15] Gozes O, Frid-Adar M, Sagie N, Zhang H, Ji W, Greenspan H. Coronavirus detection and analysis on chest CT with deep learning [Internet]. arXiv [eess.IV]. 2020. Available from: http://arxiv.org/abs/2004.02640
[16] Song Y, Zheng S, Li L, Zhang X, Zhang X, Huang Z, et al. Deep learning Enables Accurate Diagnosis of Novel Coronavirus (COVID-19) with CT images. IEEE/ACM Trans Comput Biol Bioinform. 2021;PP:1–1.
[17] Zheng C, Deng X, Fu Q, Zhou Q, Feng J, Ma H, et al. Deep learning-based detection for COVID-19 from chest CT using weak label [Internet]. bioRxiv. 2020. Available from: http://dx.doi.org/10.1101/2020.03.12.20027185
[18] Krizhevsky A, Sutskever I, Hinton GE. ImageNet classification with deep convolutional neural networks. Commun ACM. 2017;60(6):84–90.
[19] Szegedy C, Liu W, Jia Y, Sermanet P, Reed S, Anguelov D, et al. Going deeper with convolutions. In: 2015 IEEE Conference on Computer Vision and Pattern Recognition (CVPR). IEEE; 2015.
[20] Simonyan K, Zisserman A. Very deep convolutional networks for large-scale image recognition [Internet]. arXiv [cs.CV]. 2014. Available from: http://arxiv.org/abs/1409.1556
[21] Mateen M, Wen J, Nasrullah, Song S, Huang Z. Fundus image classification using VGG-19 architecture with PCA and SVD. Symmetry (Basel). 2018;11(1):1.

Lesion Detection on Skin Images Using Improved U-Net

*Elif Işılay Ünlü**, *Ahmet Çınar*
Fırat University, Department of Computer Engineering, Elazığ, 23119, Türkiye
**Corresponding author: eiunlu@firat.edu.tr*

Abstract

One of the most prevalent cancers in humans is skin cancer. The deadliest form of skin cancer is malignant melanoma and the incidence rate has increased rapidly in recent years. In the treatment of melanoma, early diagnosis is very critical. It is difficult and time consuming to automatically detect melanoma from images taken from dermoscopy devices. Computer-aided systems are needed, therefore. In this paper, a deep learning-based method for melanoma segmentation and classification with color images taken from dermoscopy devices is proposed. This technique uses ISIC 2017 International Skin Imaging Collaboration.

In this paper, for segmentation and classification measures, 1317 skin images taken from the ISIC archive were used. The approach is based on the architecture of Preprocessing, U-Net and VGGNet. Operations such as mean subtraction, image normalization, image cropping, and scaling are implemented in the preprocessing phase. It is intended to make pictures of the skin more convenient before segmentation. The training precision rate and jaccard similarity coefficient reached 93% as a result of segmentation with these results, and the dice coefficient reached 79%. The accuracy rate is 85.5% as a result of the classification in the two-class dataset in the pre-trained VGG16 network. The accuracy rate of dataset classification obtained with cross-validation is 95.86%.

Keywords: deep learning, image segmentation, image classification, melanoma, U-Net, VGGNet

Introduction

The need for more computer-aided systems has contributed to increased health concerns and forms of illnesses. Cancer cases are among the most significant of these diseases. Cancer is one of the leading causes of death in many countries in recent years. In the treatment of cancer disorders, early diagnosis is of high significance. Skin cancer is another significant kind of cancer that needs early diagnosis. Skin cancer is more common than breast, prostate, and colon cancer cases [1]. Melanoma is a deadly type of skin cancer. According to studies conducted in 2015, almost 160,000 people are diagnosed with melanoma every year and 48,000 people die from the disease [2].

In the detection of melanoma, examination of color images from dermoscopy equipments plays a significant role. However, changes in the appearance of melanoma and similarities with other benign tumors may cause wrong decisions among expert dermatologists. Using deep learning methods, structures that human perception cannot recognize can be detected and early diagnosis can be made in patient treatment [3].

Deep learning is an algorithm that is inspired by the brain and named artificial neural networks, one of the sub-branches of machine learning. Deep learning techniques are rooted in neural networks, where 'deep' refers to multiple layers layered on top of each other. A deep learning architecture is comprised of stack layers, each of which is expected to subtract from higher-level representations, ie features. For example, an image consists of pixels, and a deep model learns the edges of a picture, object parts, and objects from layers. Deep learning approaches are used in classification tasks, natural language processing, image processing, speech recognition, and are much more powerful than shallow architectures [4].

Deep learning algorithms have become a rapidly preferred methodology to analyze medical images, especially in convolution networks. Deep learning methods in the medical field in general; Its use for image classification, object detection, segmentation, recording and other tasks has become increasingly common. Image segmentation is the classification of each pixel on the image, creating a map of all the object areas on the image. Segmentation divides an image into various meaningful regions containing identical attributes for each pixel. Similar brightness may be present in the image, and this brightness may reflect objects in different areas of the image. Segmentation can be used to identify, classify, and diagnose object particles with the same brightness within the image [5].

As convolutional neural networks improve, classification and segmentation processes produce more efficient outcomes. Studies using different models and architectures in the literature are discussed.

Many studies have been conducted on the detection of melanoma from images since the 2000s. In the first studies, k-nearest neighbor (kNN), support vector machines (SVM) etc. classical machine learning methods were used. Divided 5393 different images into three classes: healthy, diseased, and diseased [6]. As a result of this research, they were able to reach 87% sensitivity and 92% specificity with the kNN classifier.

Celebi et al. performed binary classification as healthy and diseased using support vector machines (Support Vector Machine-SVM) after operations such as border detection and color removal for lesion segmentation. In this study, which was carried out using classical methods, an accuracy value of approximately 92% was reached [7].

Kawahara et al. have applied deep learning to 10 different skin diseases. The proposed solution achieved a favorable precision of 85.8% for 5 classes, with major increases of 60% precision for low-represented classes. The system achieved an accuracy of 81.8% in all 10 datasets of 1300 images collected from a regular (non-dermoscopic) camera [8].

Codella et al. performed a melanoma classification by extracting features in dermoscopic images with deep learning methods and classical machine learning methods, and an accuracy value of 93% was achieved [9].

Esteva et al. suggested a system using a single CNN to identify skin lesions by directly inputting pixels and disease tags. A dataset of 12932 clinical images and 2,032 different diseases has been used to train CNN. The proposed approach has been tested against at least 21 dermatologist information. In the 3-classification task, CNN reached 72.1% total accuracy and 65.56% and 66.0% precision in a subgroup of two dermatologist validation sets. In the second task, the classification with 9 classes, CNN reached 55.4% accuracy, while dermatologists achieved 53.3% and 55.0% accuracy [10].

Dandi et al. suggested a system for lesion quality detection. For these two tasks, they used a U-Net model consisting of three architectures. For the lesion segmentation task, they used 192 U-Net models with different architectures. Lesion feature detection was evaluated as five separate binary classification problems. Each feature has been identified by a classifier that integrates 60 U-Net models. In the given verification set, they were able to reach the threshold of 0.820 in task 1, Jaccard index in task 2, and 0.432 in task 2 [11].

Nasr-Esfahania et al. proposed a new class of fully convolutional networks with new dense pool layers for segmentation of lesion sites on non-dermoscopic images. Based on the Dermquest dataset, the dice score achieved in segmentation of skin lesions is 91.6% and outperforms the most advanced algorithms [12].

A new approach consisting of two steps based on very deep CNNs was proposed by Lequan to resolve automatic melanoma detection difficulties in dermoscopic images: segmentation and classification. They obtained 0.949 accuracy, 0.897 dice, 0.829 jaccard scores [13].

Li and Shen proposed two different deep learning methods for tasks such as lesion segmentation, feature extraction, and lesion classification. These methods were tested on the ISIC 2017 dataset. For different tasks, accuracy values of 0.753, 0.848, and 0.912 were obtained [14].

Yuan, Chao, and Lo used deep convolution-deconvolution neural networks (CDNN) for segmentation of skin lesions on dermoscopic images. And they obtained an average of 0.784 Jaccard indices in the dataset [15].

Tang et. al. suggested a U-Net based skin lesion segmentation method. In the application results, they obtained 93.03% and 86.93% Dice coefficient, 89.40% 79.26% Jaccard index values for two different datasets [16].

Unlu and Cinar, proposed a study on the classification of skin images. They performed binary and multiple classifications using the AlexNet model. They achieved an average of 81% accuracy, best 86% on average [17].

In the second part of the paper, the developed model is introduced. The dataset used for the developed method and preprocessing stages are mentioned. The architecture used in the segmentation and classification of skin images is explained with a deep learning-based system and interpreted together with the application results. The outcomes obtained and the studies planned for the future are listed in the last section.

Material and Method

In this paper, deep learning methods that give successful results are used. First with colored skin images taken from dermoscopy devices using U-Net, which is one of the conventional neural network models, lesion segmentation is performed. Then with VGGNet, classification is completed. In the Application Results section, the results are interpreted in detail with tables and graphics. In this section, dataset, preprocessing, the structure of the developed model, and CNN layers used in the developed model are examined. An overview of the proposed method is as in Figure 1.

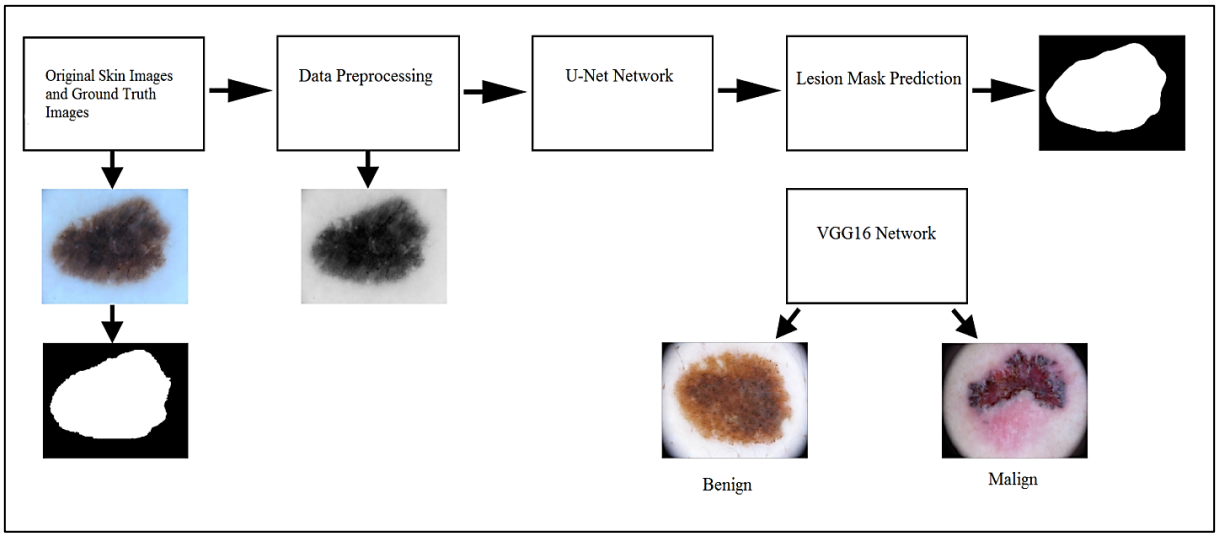

Figure 7. General view of the proposed method

Dataset

The ISIC (International Skin Imaging Collaboration) publicly accessible archive was used as a dataset in this paper [18]. 1317 skin images taken from the ISIC archive were used for segmentation and classification steps. Of these, 920 are grouped for training, 268 for testing, and 129 for validation. Images are labelled as benign or malignant and have a binary image mask in the image to label the lesion. The distribution of the images in the dataset is as in Table 1. Some examples of the original images are as in Figure 2.

Table 1. The distribution of dataset

Dataset Category	Malign	Benign
Train	153	767
Test	70	198
Validation	25	104

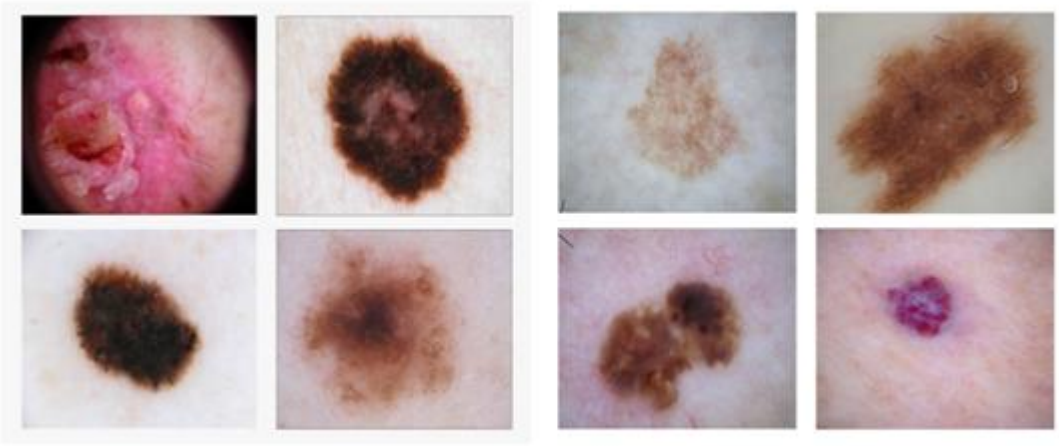

a. *Melanoma* b. *Non-melanoma*

Figure 8. a. Diseased images, b. Healthy images [18]

Preprocessing

Some preprocessing techniques are applied to the images before the segmentation step. These; Mean subtraction: A mean subtraction is applied to the image properties to center the RGB values cloud to approximately zero from the input data across each dimension of the image. The average subtraction calculation of an RGB image is as given in equations 1,2 and 3.

$$Rnorm(x,y) = R(x,y) - Rmean(x,y) \quad (1)$$

$$Gnorm(x,y) = G(x,y) - Gmean(x,y) \quad (2)$$

$$Bnorm(x,y) = B(x,y) - Bmean(x,y) \quad (3)$$

Image normalization: It is obtained by dividing each RGB size of the input images by standard deviation, normalizing the values normalized from the original 0 and 255-pixel values to 1 and 0. The linear normalization of a digital image is performed

$$Output_{channel} = 255 * \frac{(Input_{channel} - min)}{(\max - \min)} \quad (4)$$

Image cropping and resizing: To be approved by the architecture, the input images are preprocessed, but the image is dimensioned as required and resized to the original image as 64x80 pixels for U-Net and 224x224 pixels for VGG-16. Image examples before and after the preprocessing are as in Figure 3.

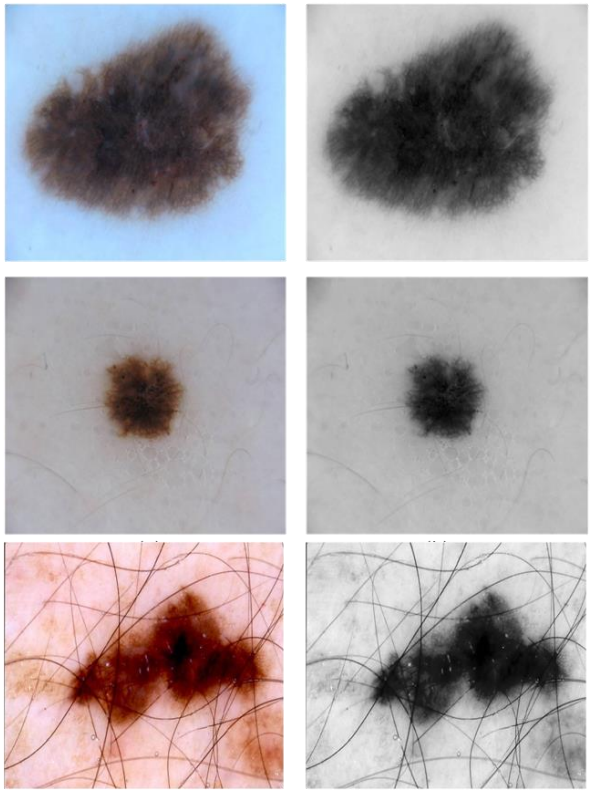

Figure 9. Original skin images b. Preprocessed skin images

Developed Model

U-Net Architecture

In the segmentation step of the developed system, the data are trained using one of the U-Net deep learning models. The structure of the developed model is given in Figure 4. The architecture of the U-Net is based on a Completely Convolutional Network (FCN) and has been updated to enhance medical imaging segmentation. There are two major differences from FCN. The U-net is symmetric and a concatenation operator instead of the complete operator applies the skip connections between the sub-sampling and the sampling path. Because of its symmetric nature, there are many feature maps that allow the transmission of information on the sampling path of the network. It consists of a downsampling path (left side) and an expanding sampling path (right side). The downsampling path is a typical convolutional network. It consists of 4 blocks and each block contains 2 3x3 convolution layers + activation functions (with batch normalization) and one 2x2 maximum pooling layer. The number of feature maps is doubled in each pooling process. The purpose of this downsampling path is to get the content of the input image for the segmentation process. This contextual data is then transferred via skip links to the sampling path. The expansion / upsampling path consists of 4 blocks. These blocks include the stride 2 deconvolution layer, the feature map from the lower sampling path, the 3x3 convolution layer + activation function (by batch normalization) steps. U-Net obtains the general information required to predict a good segmentation map by combining the information in the last sampling path with the information in the sampling path [19].

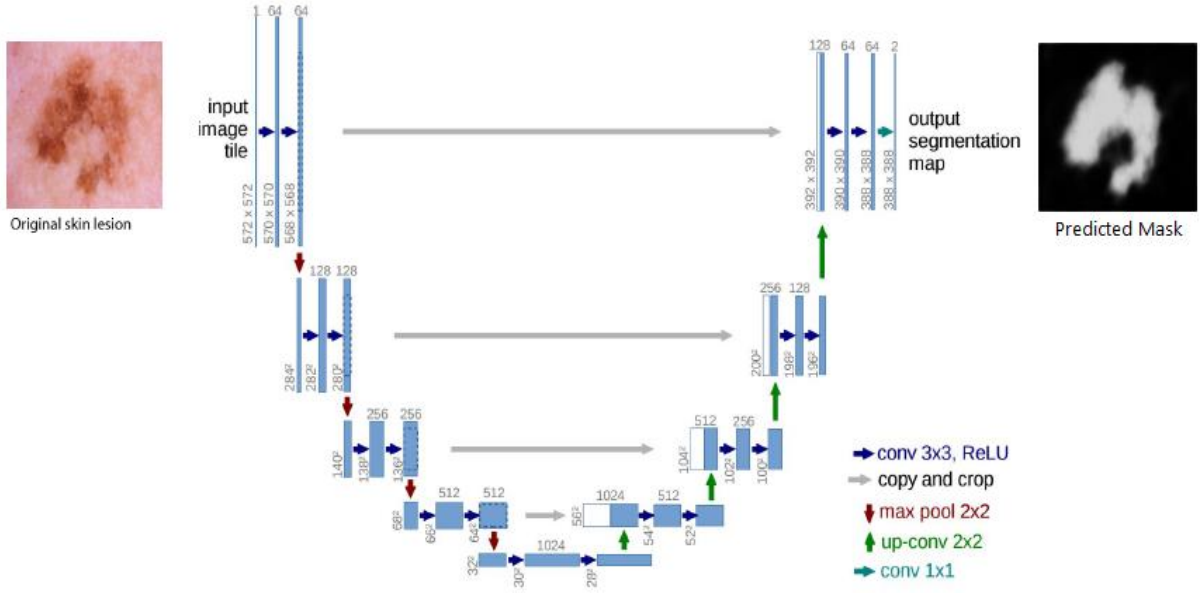

Figure 10. U-Net Architecture

VGGNet Architecture

The developed method uses VGGNet convolutional neural network architecture and transfer learning in the classification step. The proposed method model starts with weights from the VGG-16 trained in a larger dataset (like ImageNet), a process known as transference learning. The advantage of using transfer learning is that the model is pre-trained. Thus, the features required for classification are already learned. The benefit of training only to the top layers of the network is that it realizes the removal of more specific features. Therefore, the first four layers in the original VGG-16 architecture are initialized with weights used in the ImageNet dataset. With the weights registered during the extraction of features, the fifth and final convolution layers block is started. VGGNet is a widely used architecture for convolutional neural networks [20]. The structure of this model is as in Figure 5 and Table 2. It has two different structures, VGG-16 and VGG-19. In the VGG16 model, the input of the first convolution layer is a fixed size 224 x 224 RGB image. The image is passed through a convoluted layer stack with 3 x 3 filters. There are five maximum pooling layers after the convolution layers. Max-pooling is performed on a 2×2 pixel window, with stride 2. Three Fully Connected (FC) layers, each with 4096 channels, come last. The last layer is the softmax layer. Flattened linearization (ReLU) is used as the activation function in all layers.

$$Softmax: \sigma(x)_i = \frac{e^{x_i}}{\sum_{j=1}^{k} e^{x_j}}, i = 1,2,\dots,k \quad (5)$$

$$ReLU: f(x) = \begin{cases} 0, & x < 0 \\ x, & x \geq 0 \end{cases} \quad (6)$$

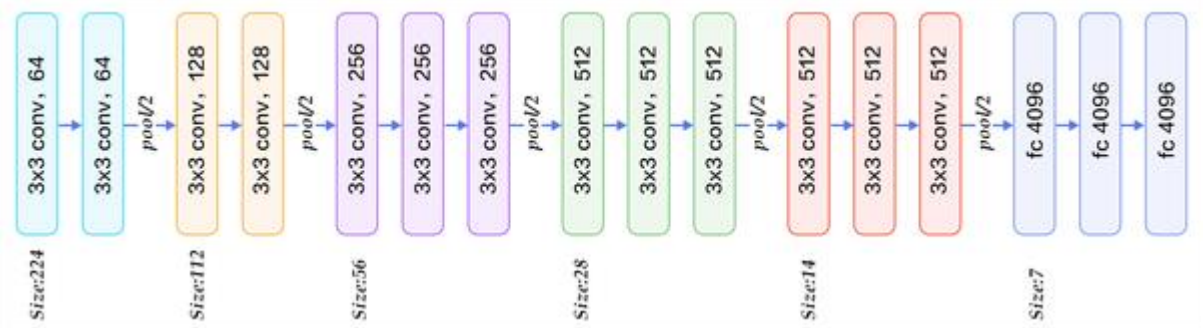

Figure 11. VGG16 architecture

Table 3. VGG16 layers

	Layer	Feature Map	Size	Kernel size	Stride	Activation
Input	Image	1	224 x 224 x 3	-	-	-
1	2 X Convolution	64	224 x 224 x64	3 x3	1	relu
	Max Pooling	64	112 x 112 x 64	3 x3	2	relu
3	2 x Convolution	128	112 x 112 x128	3 x3	1	relu
	Max Pooling	128	56 x 56 x 128	3 x3	2	relu
5	2 X Convolution	256	56 x 56 x 256	3 x3	1	relu
	Max Pooling	256	28 x 28 x 256	3 x3	2	relu
7	3 X Convolution	512	28 x 28 x 512	3 x3	1	relu
	Max Pooling	512	14 x 14 x 512	3 x3	2	relu
10	3 X Convolution	512	14 x 14 x 512	3 x3	1	relu
	Max Pooling	512	7 x 7 x 512	3 x3	2	relu
13	FC	-	25088	-	-	relu
14	FC	-	4096	-	-	relu
15	FC	-	4096	-	-	relu
Output	FC	-	1000	-	-	Softmax

Application and Results

In this paper, it is aimed to segmentation and classify skin lesion images. The dataset for the segmentation process is organized into training, training masks and test folders. Binary mask images obtained from specialist dermatologists are given as ground truth files. The preprocessed skin images are trained with 32 batch sizes for 200 epochs in the U-Net network. Original skin images and the estimated masks obtained as a result of the model are given in Figure 6. The segmentation results are obtained by a calculation between the binary mask and the ground truth mask automatically generated for each test mask. Some of the metrics used in the evaluation stage of the segmentation and their definitions are as follows:

Accuracy calculates the number of accurate estimates and divides by the total number of samples, as given in equation (7).

$$\text{Accuracy} = \frac{\text{TP+TN}}{\text{TP+TN+FP+FN}} \tag{7}$$

The Dice coefficient is calculated as in equation (8) by comparing the predicted segmentation (X) image corresponding to the ground truth (Y) image, in pixels.

$$Dice\ Coefficient = \frac{2 * |X \cap Y|}{|X| + |Y|} \tag{8}$$

The Jaccard similarity coefficient compares predictions (A) with ground truth data (B) to see which examples are common and which are different, as given in equation (9).

$$Jaccard\ index\ (A, B) = \frac{|A \cap B|}{|A \cup B|} \tag{9}$$

The average and best evaluation metrics obtained as a result of segmentation of the skin images are as in Table 3.

Table 4. Segmentation results

	Accuracy	Dice Coefficient	Jaccard index
Average	0.76	0.70	0.80
Best	0.93	0.79	0.93

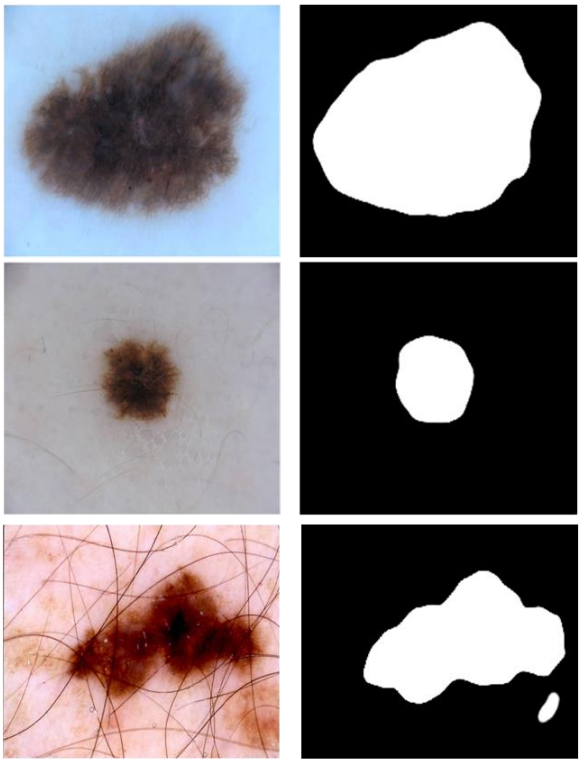

(a) (b)

Figure 12. a. Original Skin Images b. Predicted Masks

Classification is made by making fine-tuning to the pre-trained VGG16 network in the two-class dataset. As a result of the classification, the accuracy rate of the test data is 85% and the loss rate is 0.47. Accuracy and loss rates graphs are as in Figure 7. In addition to accuracy and loss rates, evaluation metrics such as precision and sensitivity are obtained.

These are a simple but useful way to measure the quality of estimates. If we briefly define these metrics:

Precision is the criterion indicating success in a situation that is positively predicted. The equation is calculated by the formula in (10).

$$Precision = \frac{\mathrm{TP}}{\mathrm{TP+FP}} \tag{10}$$

Sensitivity shows how successfully positive states are predicted. Equality is calculated by the formula given in (11).

$$Sensitivity = \frac{\mathrm{TP}}{\mathrm{TP+FN}} \tag{11}$$

The metrics obtained as a result of classification are as in Table 4.

Table 5. Classification results

Accuracy	Loss	Precision	Sensitivity
0.855435	0.478412	0.8423	0.8243

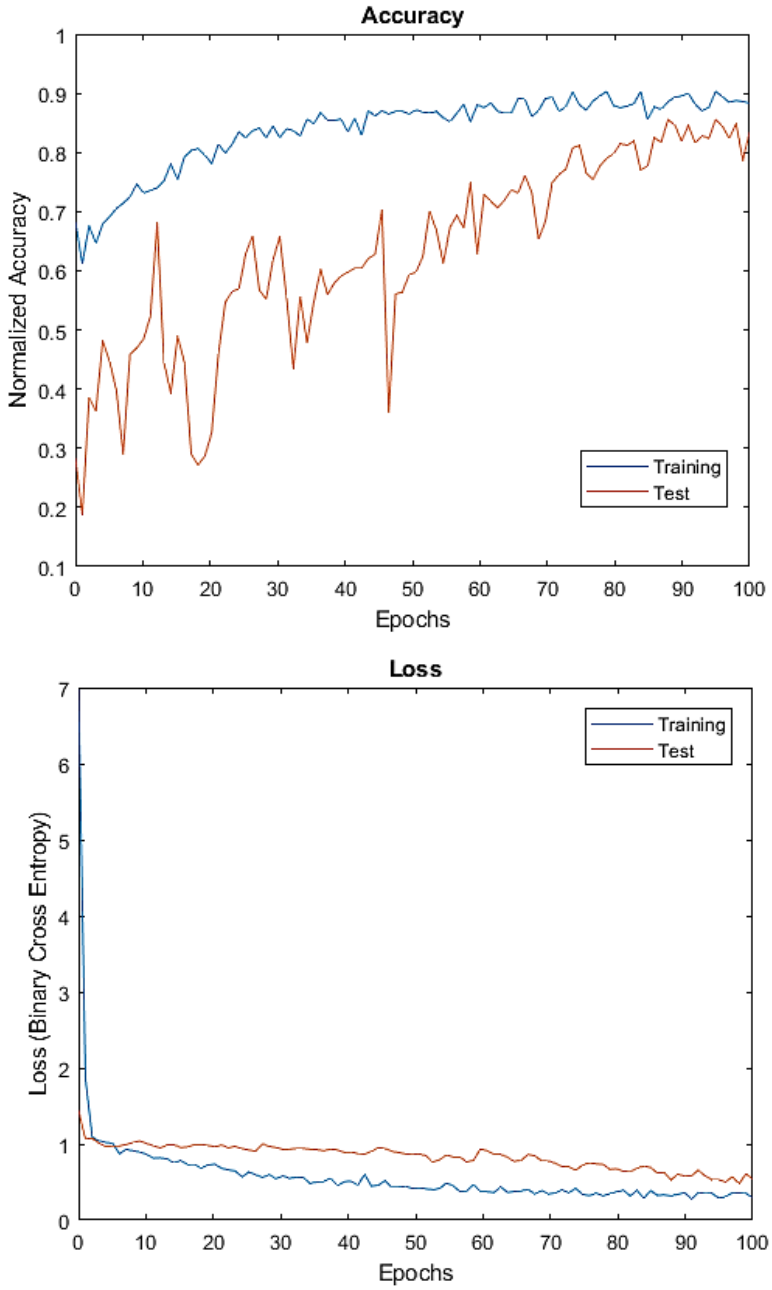

Figure 13. Accuracy and loss rates

With the verification dataset, the confusion matrix is obtained to evaluate the success of the model. For machine learning classification problems with two or more classes, the complexity matrix is a performance measure. It shows the performance of each classification model in the validation set. It is a table with 4 different combinations for predicted and real values. Estimates and actual values of the target quality are compared [21]. These 4 combinations are TP (True Positive), TN (True Negative), FP (False Positive), and FN (False Negative).

TP: It is a positive prediction of a situation that normally exists positively.

TN: The existing situation is negative and the forecast is negative. In other words, the wrong situation was correctly predicted incorrectly.

FP: The existing situation is negative but it is estimated as positive.

FN: The existing situation is positive but it is estimated as negative.

Using the confusion matrix, we can estimate how many of the images we provided as verification belong to the malignant class and how many of them belong to the benign class. The result of the

confusion matrix is as in Figure 8. It correctly classified 21 out of 25 images given as malignant. 95 of 104 images given as benign are correctly classified. This shows that our model has good classification performance.

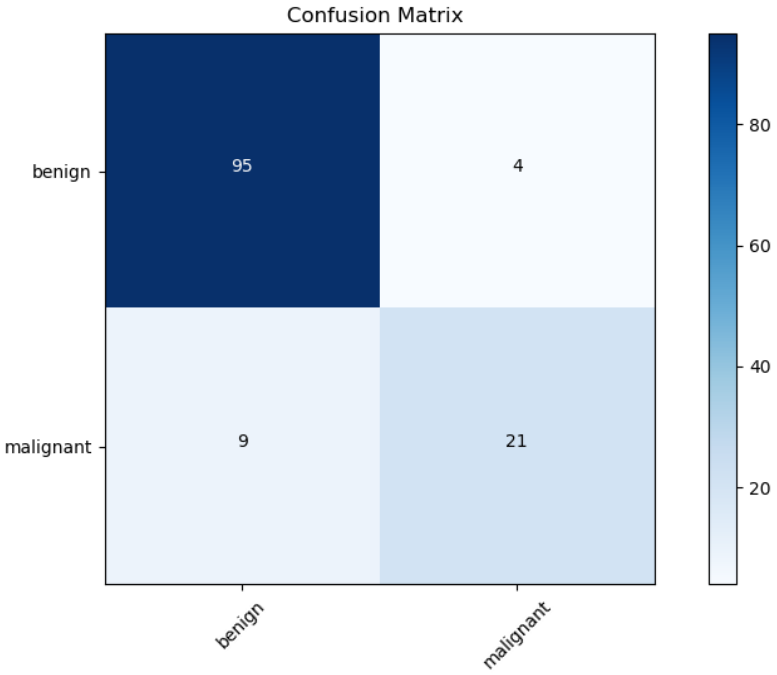

Figure 14. Confusion matrix

The goal of grouping the dataset as training and testing in deep learning is to prevent overfitting and evaluate the model's output on the dataset that it hasn't seen before The Cross-validation technique is used to minimize the errors caused by the distribution of the dataset during the training and testing phase. When the dataset is randomly divided into 'k' classes, cross-validation or 'k-fold cross-validation' is. One of these groups is used as a test set and the rest as a training set [22].

A new test dataset was obtained by selecting a different number of images first from the training data, which was previously set as 70% of the dataset, and then a different number of images. A new test dataset was obtained from the training data, which was set as 70% of the dataset, by first selecting five images and then a different number of images. While the accuracy value of this new dataset is 95%, the loss rate is 0.17. The result of the confusion matrix is as in Figure 9. Some of the metrics obtained are as in Table 5. Accuracy and loss rate graphs are given in Figure 10. Some studies used in the segmentation and classification of melanoma are examined in Table 6.

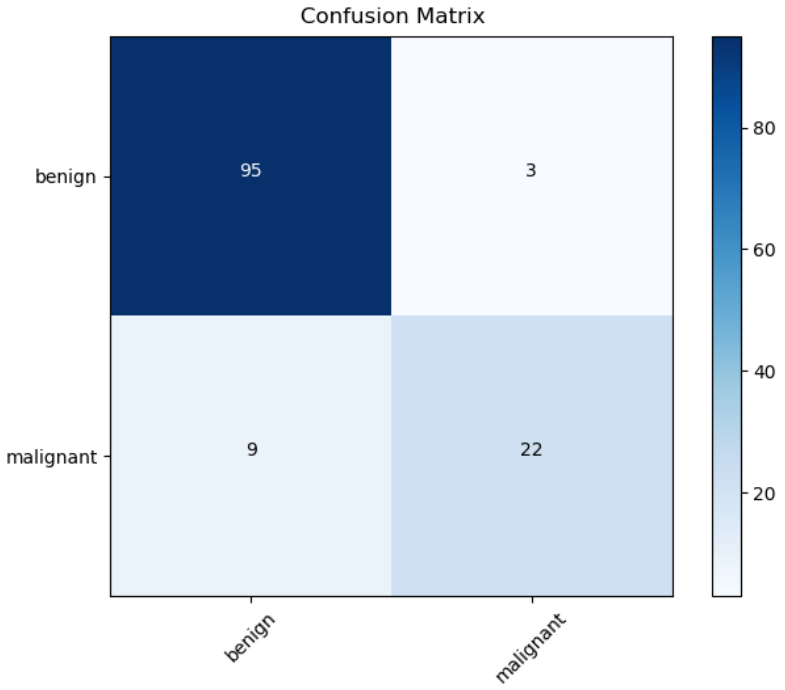

Figure 15. Confusion matrix

Table 6. Second Group Data Set Classification Results

Accuracy	Loss	Precision	Sensitivity
0.958696	0.173723	0.88	0.7096

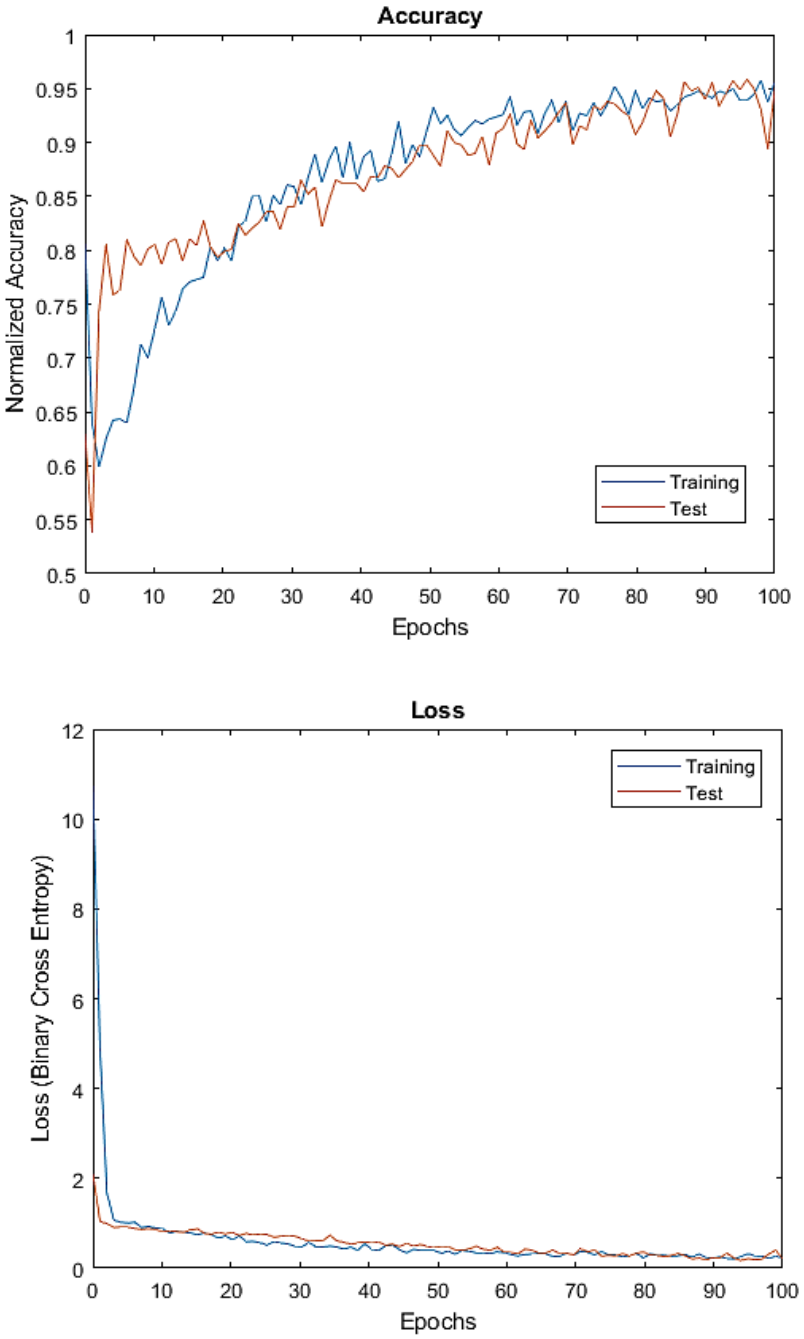

Figure 16. Accuracy and loss rates

As can be seen from the graphs, education and test success continued to increase very closely, and on the one hand, the loss rate decreased in parallel with the success rate. This shows that although the number of data is low, the model learned better than the previous one.

Table 7. Studies on skin lesion segmentation and classification

References	Method	Acc.	Dice	Jaccard
Ganster et al.	kNN, SVM	87%	-	-
Celebi et al.	SVM Border Detection	92%	-	-
Kawahara et al.	CNN	85.8%	-	-
Codella et al.	Deep Learning Sparse coding SVM	73.9%	93.1% -	-
Esteva et al.	CDNN	55.4%	72,1% -	-
Chen	U-Net Vgg-UNet	-	-	0.82 0.43
Nasr-Esfahani et al.	DFCN	-	91.6	-
Yu et al.	FCRN	94.9%	0.897	0.829
Li and Shen	FCRN CNN	84.8%	75.3% - 91.2%	-
Yuan et al.	CDNN	-	-	0.784
Tang et al.	U-Net	- -	0.93 0.86	0.89 0.79
Unlu and Cinar	AlexNet	85% ,81%	-	-
Proposed Method	U-Net VGGNet	93%	0.79 95%,85%	0.93

Conclusion

Automated analysis of dermoscopic images can help dermatologists in clinical decision making and even help patients evaluate skin lesions outside the hospital. To perform an automated analysis of dermoscopic images, the separation of skin lesions from the normal region is usually the first step. In this paper, a method with a deep network architecture has been proposed to determine the lesion site from skin images. U-Net architecture is used for lesion determination. As a result of segmentation applied to images that have been pre-processed, a good jacquard similarity coefficient was obtained. Even better results have been obtained that are quite similar to the ground truth images. As can be seen in Figure 6, even better results have been obtained that are quite similar to ground truth images.

As a result of the classification performed in the pre-trained VGG16 network, the accuracy rate of the test data is 85.5% and the loss rate is 0.47. By applying the cross-validation technique, images that the model has not seen before were given and reclassification was performed. 95.86% accuracy and approximately 0.17 loss rate were achieved. Figure 7 and Figure 10 show the accuracy and loss function curves.

Findings obtained as a result of this study show that deep learning structures can be an important tool for the diagnosis of melanoma. It is think that the performance of the system will increase by further expanding the dataset used, increasing the class labels and trying different classification, and segmentation methods.

References

[1] Cancer facts and figures 2016 , http://www.cancer.org/acs/groups/content/@research/documents /document/acspc-047079.pdf
[2] Lancet T. "Melanoma research gathers momentum", The Lancet, vol. 385, no. 9985, pp. 2323; 2015.
[3] Xu H, Hwang TH. "Automatic Skin Lesion Segmentation Using Deep Fully Convolutional Networks";2018
[4] Bengio Y. "Learning deep architectures for AI. Foundations and trends, in Machine Learning", Dept. IRO, Universite de Montreal, 2(1): 1-127; 2009.
[5] Jayasumana S. Semantic Image Segmentation with Deep Learning.
[6] Ganster H, Pinz P,Rohrer R, Wildling E, Binder M and Kittler H. Automated melanoma recognition, IEEE transactions on medical imaging, 20, no. 3, pp. 233-239;2001.
[7] Celebi ME, Kingravi HA, Uddin B, Iyatomi H, Aslandogan YA, Stoecker WV and Moss RHA methodological approach to the classification of dermoscopy images, Computerized Medical Imaging and Graphics, 31, no. 6, pp. 362-373; 2007.
[8] Kawahara J, BenTaieb A and Hamarneh G. Deep features to classify skin lesions. *IEEE* 13th International Symposium on Biomedical Imaging, Prague, Czech Republic; 13-16 April 2016.
[9] Codella, N, Cai, J, Abedini M, Garnavi R, Halpern A, and Smith JR. Deep learning sparse coding and svm for melanoma recognition in dermoscopy images, International Workshop on Machine Learning in Medical Imaging, pp. 118-126;2015.
[10] Esteva A, Kuprel B, Roberto A, Novoa, Justin, K., Susan, M., Swetter, Helen M., Blau, and Sebastian, T. Dermatologist-level classification of skin cancer with deep neural Networks. Research letter, 542, pp.115-118; 2017.
[11] Dandi, C, Xu M, Chao C, Jingyuan C, Zhuoran X and Fei W. U-Net Ensemble for Skin Lesion Analysis towards Melanoma Detection; 2018.
[12] Nasr-Esfahani, E, Rafiei S, Jafari MH, Karimi N, Wrobel J.S, Soroushmehr SM and Najarian K. Dense Fully Convolutional Network for Skin Lesion Segmentation. pp.1-9;2017.
[13] Lequan, Y, Hao C, Qi D, Jing Q and Pheng-Ann H. Automated Melanoma Recognition in Dermoscopy Images via Very Deep Residual Networks, IEEE Transactions on Medical Imaging, 36(4); 2017.
[14] Li Y, Shen L. "Skin Lesion Analysis towards Melanoma Detection Using Deep Learning Network", Sensors; Feb 2018.
[15] Yuan Y, Chao M and Lo YC. "Automatic skin lesion segmentation with fully convolutional-deconvolutional Networks" IEEE Journal of Biomedical and Health Informatics; 2018.
[16] Tang P, Liang Q, Yan X, Xiang S,Sun W, Zhang D, Coppola G. "Efficient skin lesion segmentation using separable-Unet with stochastic weight averaging" ELSEIVER Computer Methods and Programs in Biomedicine, 178 , 289–301;2019.
[17] Unlu EI, Cinar A. Classification of skin ımages with respect to melanoma and non-melanoma using the deep neural network. IOSR Journal of Engineering (IOSRJEN) 8(12): 35-40;2018.
[18] International Skin Imaging Collaboration,https://www.isic-archive.com.
[19] Ronneberger O, Fischer P and Brox T. U-Net: Convolutional Networks for Biomedical Image Segmentation, Medical Image Computing and Computer-Assisted Intervention (MICCAI), Springer, Lncs, 9351: 234—241; 2015.
[20] Simonyan K and Zisserman A. Very deep convolutional networks for large-scale image recognition, Conference Paper at ICLR. In arXiv preprint arXiv:1409.1556; 2014.
[21] Understanding Confusion Matrix,https://towardsdatascience.com/understanding-confusion-matrix-a9ad42dcfd62.
[22] Hold-out vs. Cross-validation in Machine Learning https://medium.com/@eijaz/holdout-vs-cross validation-in-machine-learning-7637112d3f8f .

Heart Sounds Classification Using Hybrid CNN Architecture

*Mohammed Mansur Abubakar** , *Taner Tuncer*
Fırat University, Department of Computer Engineering, Elazig, Turkey
**Corresponding author: ttuncer@firat.edu.tr*

Abstract

In this paper, we propose a hybrid model for diagnosing heart conditions by analyzing heart sounds and signals. The Hybrid CNN (Convolutional Neural Network) model is trained to classify distinguishable pathological heart sounds into three classes; normal, murmur, and extrasystole. Scalogram images of heart sounds were obtained by applying wavelet transform to heart sound signals. Images are inputs for Resnet50 and Resnet101 CNN models. The feature vectors of these architectures in the fc1000 layer are combined. Relief feature selection algorithm was applied to the obtained feature vector, and then the classification was performed with the support vector machine algorithm. Training the proposed model resulted in accuracy of 92.75%, thus, making it the best performing model in comparison to other models in this paper.

Keywords: cardiovascular disease, classification, CNN, heart sounds, relief algorithm

Introduction

Cardiac abnormalities are regarded as one of the life most threatening abnormalities today. As reports from the World Health Organization (WHO) indicates, cardiovascular (heart) diseases are the root cause of the majority of death globally. It is estimated that about 17.9 million people died from cardiovascular diseases (CVD) in 2016 [1]. This represents about 31% of all deaths worldwide with 85% of them related to heart attack and stroke [2]. Most heartbeat abnormalities are reflected in heart sounds. These sounds are listened to and interpreted by doctors using a stethoscope. This method is simple and inexpensive. In addition, by recording heart sounds, sounds can be converted into phonocardiogram graphics. This chart is then used by doctors for disease diagnosis. The accuracy of the diagnosis in these methods depends largely on the expertise of the physician. In recent years, systems that can automatically classify heart sounds and assist doctors have been developed.

Li et. al. combined a traditional feature engineering method with deep learning algorithms to automatically classify normal and abnormal heart sounds [3]. Krishnan et al. proposed deep neural network architectures such as one-dimensional convolutional neural network (1D-CNN) and Forward Feeding Neural Network (F-NN) for classification of the undivided phonocardiogram (PCG) signal. The performance of the model was determined using the Receiver Operating Characteristic (ROC) plot, which produces an Area Under Curve (AUC) value of 0.857 [4]. Li et. al. proposed a one-dimensional convolutional neural network (CNN) model that divides heart sound signals into normal and abnormal directly independent of the ECG. The proposed 1D CNN has a classification accuracy rate of 99.01% [5]. Noman et. al. proposed a framework for automatic heart sound classification based on deep convolutional neural networks (CNNs). In the study, 2D-CNN, which takes heart sounds as input to two-dimensional time-frequency feature maps based on both 1D-CNN and Mel-frequency cepstral coefficients, was designed. The best classification scores with 89.22% accuracy and 89.94% sensitivity were obtained by Ensemble CNN with a specificity of 91.55% and a modified accuracy of 88.82% in the test set with 2D-CNN alone [6].

In this paper, we propose a Resnet50 and Resnet101-based hybrid CNN model for the classification of normal, murmur, and extrasystole heart sounds. First of all, heart sounds have been transformed into scalogram images. Feature vectors of the images have been obtained from Resnet50 and Resnet101 and these feature vectors have been combined. Finally, the classification has been carried out by applying the feature selection algorithm to the feature vector.

Data

The data used for this experiment was gotten from the Peter J Bentley online repository. The data has been gathered from two sources: from the general public via the iStethoscope Pro iPhone app and from a clinic trial in hospitals using the digital stethoscope called the DigiScope. The lengths of the audio

heart sounds vary between 1 and 10s. The heart sound training data set used in this study consists of 3 categories: extrasystole, murmur and normal. Table 1 shows the amount of data in each class. Figure 1 shows the scalogram image of each class.

Table 1. The amount of data in each class

Categories	Number of files
Extrasystole	46
Murmur	100
Normal	200
Total	346

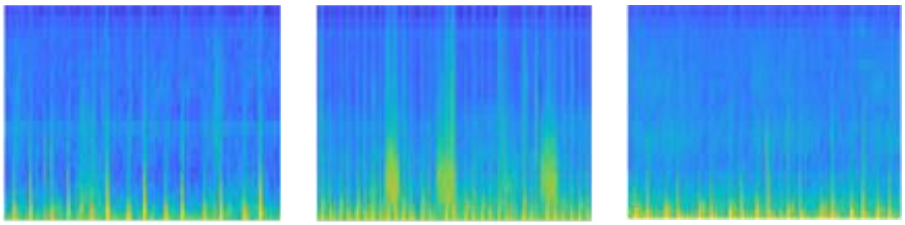

Extrasystole Murmur Normal

Figure 1. Sample scalogram images of heart sounds

The Proposed System

In this paper, a Hybrid CNN model based on the Resnet50 and Resnet101 architectures is presented for the classification of heart sounds (Figure 2). It takes the scalogram images obtained from model heart sounds as an input. Feature vector of each image is obtained from Fc1000 layers and feature vectors are combined. By applying the relief feature selection algorithm to the obtained feature vector, the features that maximize the success of the classification are determined. Finally, this feature vector has been classified using SVM. Figure 2 shows the Hybrid CNN model proposed in this paper.

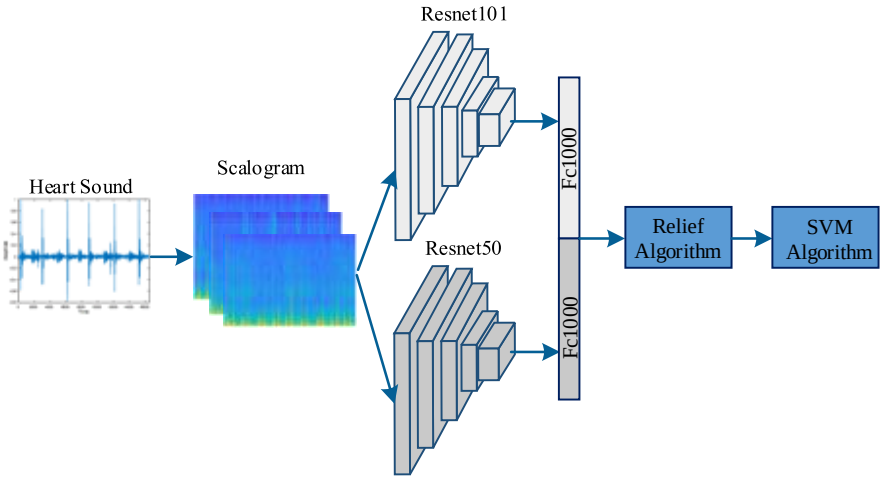

Figure 2. The proposed method

The following process is applied for the Hybrid CNN method proposed for classifying heart sounds in a total of 346 wav format.

Step 1: Convert the wav file format to time series. Figure 3 shows an example heart sound signal.

Step 2: Time-frequency representations of the signals are generated. These representations are called scalograms. A scalogram is the absolute value of the continuous wavelet transform (CWT) coefficients of a signal.

Step 3: Scalogram images are the inputs of Resnet50 and Resnet101 models.

Step 4: The new feature vector is created by combining the feature vectors obtained from the fc1000 layer of both models.

Step 5: Select feature vectors using relief algorithm and classify with Support Vector Machine (SVM).

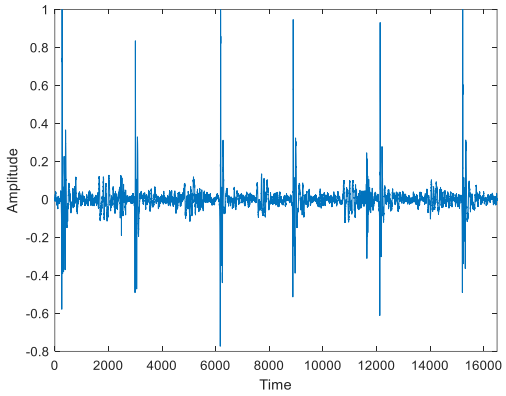

Figure 3. Heart sound signal

The classification performance of the proposed method is evaluated according to the Accuracy, Precision, Sensitivity, Specificity and F1 score parameters (Table 2) and compared with the pre-trained models Resnet50 and Resnet101. It is shown in the results that the developed model could assist doctors in diagnosing heart disease and making clinical decisions effectively.

Table 2. Performance Metrics

Accuracy	$\boldsymbol{\frac{TP+TN}{TP+FP+FN+TN}}$
Precision	$\frac{TP}{TP+FP}$
Sensitivity	$\frac{TP}{TP+FN}$
Specificity	$\frac{TN}{TN+FP}$
F1 Score	$2*\frac{(Sensitivity*Precision)}{(Sensitivity+Precision)}$

Results

The data set was randomly generated for training, validation, and testing, respectively, 70%, 10%, and 20%. 1x1000 size feature vectors were obtained from FC1000 layer of Resnet50 and Resnet101 models used in the model given in Figure 2. The new feature vectors with 1x2000 dimensions were combined and given to the Relief feature selection algorithm. Then, the properties that maximize the classification accuracy are determined and classified. . Thus, the classification according to Resnet50 and Resnet101 has been increased correctly. Figure 4 confusion matrices Table 3 shows the value of the classification parameters. The number of features for which the highest accuracy value was obtained with the proposed method was determined to be 315 (Figure 5). The Overall accuracy of the proposed method was determined to be 92.75%.

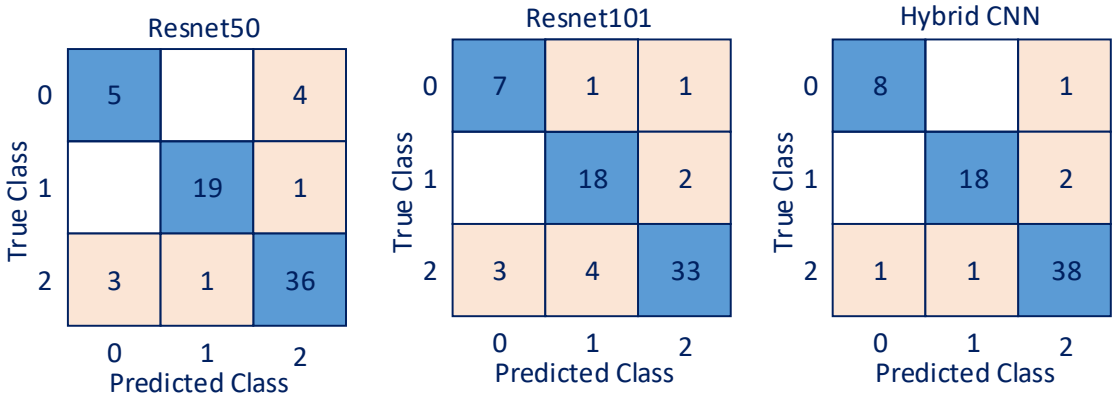

Figure 4. Confusion matrices

Table 3. Performance parameter values obtained

Methods	Accuracy	Precision	Sensitivity	Specificity	F1
ReliefF + SVM	92.75%	92.0%	92.3%	96.0%	92.1%
Resnet50	86.9%	80.2%	81.8%	91.9%	81.0%
Resnet101	84.0%	80.0%	83.4%	91.0%	81.7%

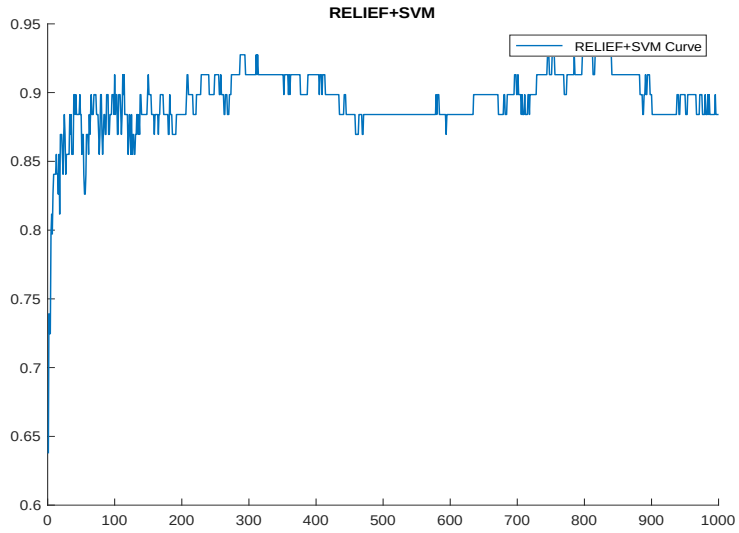

Figure 0. Accuracy variation of the proposed method according to the features used

Conclusion

In this paper, we utilized CNN for extracting features from time-frequency representations of the signals which are generated from heart audio sounds. The heartbeat sounds used in this study were a mix of recording gotten from a digital stethoscope and mobile phone app. The proposed hybrid method outperformed the other pre-trained CNN models overserved in this research with an accuracy level of 92.75%. The experiments reveal that our state-of-the-art hybrid method could be deployed to assist doctors in diagnosing heart conditions at an early stage while aiding clinicians in taking decisions efficiently and effectively.

References

[1] WHO, "cardiovascular diseases (CVDs) – fact sheet," 2017.Available: http://www.who.int /mediacentre/factsheets/fs317/en/? [Accessed 27 March 2021].

[2] WHO CVD Risk Chart Working Group, "World Health Organization cardiovascular disease risk charts: revised models to estimate risk in 21 global regions" The Lancet Global Health, vol. 7, no. 10, 1332-1345, 2019.

[3] Li F., Tang H., Shang S., Mathiak K., Cong F., "Classification of Heart Sounds Using Convolutional Neural Network", Applied. Sciences. Vol.10, 3956, 2020.

[4] Krishnan P.T., Balasubramanian P., Umapathy S., "Automated heart sound classification system from unsegmented phonocardiogram (PCG) using deep neural network". Phys Eng Sci Med vol.43, 505–515, 2020.

[5] Li F., Liu M., Zhao Y., et al., "Feature extraction and classification of heart sound using 1D convolutional neural networks". EURASIP J. Adv. Signal Process. 2019, 59 (2019).

[6] Noman F., Ting C., Salleh S., Ombao H., "Short-segment Heart Sound Classification Using an Ensemble of Deep Convolutional Neural Networks,"2019 IEEE International Conference on Acoustics, Speech and Signal Processing (ICASSP), 2019, 1318-1322.

Knime ile CRISP-DM Veri Bilimi Yöntemi Uygulaması

*Hilal Çelik**, *Ahmet Çınar*
Fırat Üniversitesi, Bilgisayar Mühendisliği Bölümü, Elazığ, Türkiye
**İletişimden sorumlu yazar: hilalcelikh@gmail.com*

Özet

Bu çalışma işsizlik sonucu bir bireyin ruhsal rahtsızlıklar sonucunda ruhsal hastalık geçirip geçirmemesi üzerine yapılan bir veri bilimi çalışmasıdır. Bir bireyin geliri, işsiz kalma süreci, yaşı gibi sistemi etkileyen faktörler hastalığı etkilemektedir. Burada veriden bilgiye ulaşırken önce tutarsız, gürültülü ve gereksiz verilerden veri seti arındırılarak veriden bilgiye ulaşılırken Crisp-dm veri bilimi yöntemi adımları izlenerek makine öğrenmesi algoritmalarından Karar Ağacı kullanıldı. Açık kaynak kodlu Knime platformu üzerinde çalışılmıştır.

Anahtar Kelimeler: makine öğrenmesi, crisp-dm, veri bilimi, Knime

Giriş

Küreselleşen dünyada ruhsal hastalıkları etkileyen faktör sayısı attıkça hastalığın önemi de benzer şekilde artıyor. Bireylerin ruh sağlığı yaşadığı toplumdaki trafik, hava kirliliği, eğitim düzeyi, yaşı, gelir düzeyi gibi iç ve diş etkenlerden etkilenmektedir. İnsan yaşamının olumsuz etkilendiği dönemlerde en çok ortaya çıkabilecek problemlerden biri kaygıdır. Kaygı ve kaygı temelli belirtiler yanında karamsarlık, mutsuzluk ve üzüntü gibi negatif durumları deneyimlenmektedir [1]. Günümüz toplumlarında kaygıya yol açan nedenlerden birisi de işsizliktir. Meşguliyet sözcüğüne dayanan çalışmak sadece gelir elde etmek değil, kişinin özgüvenin artırarak kendini gerçekleştirmesini, içinde bulunduğu grupla daha sıkı ilişkiler geliştirerek toplumsal aidiyet hissetmesini sağlayan bir yaşam biçimidir. Bunun tam tersine işsizlik, bireyin yaşam standardını düşüren, ekonomik sonuçlarının yanında sosyal ve psikolojik sonuçlara sebep olur [2].

Veri bilimi yöntemlerinden CRISP-DM 6 adımları; Problem i tanımlama, verinin anlaşılması ve toplanması, veri ön işleme, model oluşturma, değerlendirme, gerçekleme aşamalarından [3]. Makine öğrenmesi algoritmalarından Kara Ağacı algoritmasından faydalanılarak bu çalışma gerçekleştirilmiştir.

Bu anlatılanlar doğrultusunda bireylerin işsiz kaldıklarında ruhsal bir hastalık ile karşılaşıp karşılaşmayacağı öngörebilmek konusunda ciddi katkılar sağlayabilir.

Veri Bilimine Giriş

Veri; ham(işlenmemiş) bilgilere denir. Veriler her zaman hayatımızda işlenmeye hazır ve işe yarar halde değildir. Veri işlenmeye hazır hale getirilinceye kadar birçok aşamadan geçer. Bu aşamalar sonunda işlenmeye hazır hala gelen veri artık üzerinde çalışıp anlamlı ve işe yarar sonuçlar elde edilmesi mümkündür. Veriyi işlenmeye hazır hale getirmek için veri bilimi yöntemleri kullanılır. Veri işlenirken kullanılan birçok veri bilimi yöntemi vardır. Veri bilimi yöntemi seçilirken üzerinde çalışılan projenin optimum verimle sonuçlanmasını sağlayan veri bilimi yöntemi seçilmelidir.

Veri Bilimi Yöntemleri

Bu çalışmada en çok kullanılan veri bilimi yöntemlerinden CRISP-DM' kullanılmıştır. Şekil 1 görüldüğü üzere bazı adımlar arasında döngüler mümkündür ve bunların proje yönetimi açısından önemi büyüktür. Temel olarak 6 adımdan oluşan bu veri bilimi yönteminde projeye başlarken öncelikle problemin tanınması ve ikinci olarak verinin tanınması veya probleme uygun verinin toplanması şeklinde iki temel adımla başlar. Üçüncü adım verinin hazırlanması evresine geçilir. Bu aşamada veri üzerinde kirli ve eksik veri gibi veriler üzerinde çalışılır. Dördüncü adımda modelin inşasına geçilir ve beşinci adımda ise modellerin sonuçları değerlendirilir ve gerekirse iyileştirmeler yapılır. Altıncı ve son adım ise raporlama adımı; modelin analist ve son kullanıcılara sunulduğu ve değerlendirme sonucu alınan adımdır. Eğer bu aşama sonucunda istenilen derecede bir başarı oranı elde edildiyse ya da değerlendirme olumlu geçtiyse proje sonlandırılır ve üretime geçilir [3].

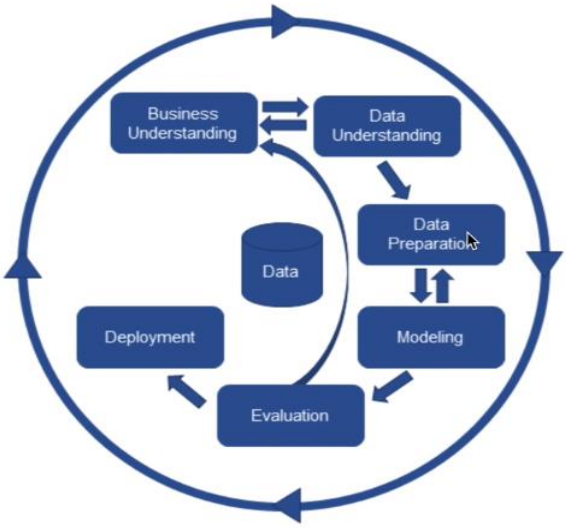

Şekil 1. CRISP-DM döngüsü

KNIME

Genel olarak "Uçtan Uca Veri Bilimi" olarak bilinir. Verinin görselleştirilmesi, makine öğrenmesi algoritması, birliktelik kurak çıkarımı gibi veri madenciliği araçlarının uygulanmasında kolaylık sağlayan açık kaynak kodlu veri madenciliği yazılımıdır. Düğümlerden (node) oluşan bir çalışma akışından oluşur.

Knime'nin kendi platform internet sitesinden indirilerek exe dosyasının çalıştırılması ile birkaç adımlık kurulum aşamalarının sonunda Knime kullanıma hazır hale gelir.

Problemi ve Veriyi Tanımak

Veri madenciliğinin veriden bilgiye ulaşma serüveninde problem ve veri arasında tutarlı bir ilişki olmalıdır. Veri setimiz çözmeye çalıştığımız problemimize uygun olmalıdır. Bu çalışmada kullandığımız veri seti www.kaggle.com üzerinden edinilebilen "Unemployment and Mental Illness Survey" veri setidir.

Problemi Tanımak

Bir projeye başlarken ilk yapılaması gereken şey problemin ne olduğunu anlamak esastır. "Bu projenin ihtiyacı ve hedefi nedir? Hedef kitlenin ihtiyaçları nelerdir?" gibi soruların cevapları aranır. Burada problem işsiz kalan bir bireyin karşılaşabileceği sorunlardan panik atak geçirip geçiremeyeceği üzerinedir. CRISP-DM veri bilimi yönteminin 1. adımı burada uygulayarak projenin hedeflerini ve ihtiyaçlarını karar verilir. Kullandığımız veri setinden yola çıkarak hedefimizi belirlemeye çalışıyoruz. Burada hedefimiz; işsiz bir insanın ruhsal bir hastalık geçirip geçirmeyeceğine anlamaya çalışmaktır.

Veriyi Tanımak

CRISP-DM veri bilimi yönteminin 2. adımı veriyi tanımaktır. Verilerini tanımaya çalıştığımız bu veri setinde veri kolonları bize yol gösterecektir. "Unemployment and Mental Illness Survey" veri seti ruhsal hastalık ve işsizlik arasındaki bağıntı üzerine yapılan bir ankettir. Veri setindeki verileri incelediğimizde belli bir grup işsiz kişinin sahip olduğu özellikler verilmiştir.

CSV dosyamızı Knime'ye yükleyerek çalışma akışına ilk düğümler ekleyerek projeyı başlatıyoruz. Kullanacağımız veri setimiz uygun düğüm seçimi yapılmalıdır. "Unemployment and Mental Illness Survey" veri seti bir CSV dosyası olduğu için "CSV Reader" düğümü seçilir.

Veriyi Hazırlama

CRISP-DM veri bilimi yönteminin 3.adımı veriyi işlenmeye hazır hale getirmektir. Veri setimizin eksiklikleri giderilmesidir. "Hangi kolonlar üzerinde çalışılacak? Eksik verilere ne gibi işlemler uygulanacak?" gibi sorunların çözümü CRISP-DM veri biliminin 3. adımında gerçekleştirilir.

Verinin işlenmesi, eksik verilerin bulunması ve eksik veriye nasıl bir uygulama yapılacağına karar verilir. Eksik veri sabit bir değer mi almalı yoksa bulunduğu kolonun ortak değerini mi almalı ya da kullanılmayan kolonlar veri setinden çıkarılmalı gibi kararlar verilir ve uygulanır. Knime'nin bize sunduğu düğümlerden "Column Filter" ve "Missing Value" düğümleri 3. adımda kullanılır. "Colon Filter" düğümü; veri setinde işimize yaramayan ve veri setinin anlaşılmasını zorlaştıran kolonlar çıkartılabilir. Örneğin kişilerin e-mail adresi çıkartılması veri kalabalığını önler. Çünkü kişilerin email adresine bakarak kişinin ruhsal hastalığı üzerine çıkarımda bulunulamaz. Bu düşüncemizden dolayı "Colon Filter" düğümü yardımıyla "Email Address" kolonunu veri setimizden ayırıyoruz. Veri setinde olmayan verilere eksik veri (missng value) denir. Knime da eksik veriler "?" ile gösterilir. Verimizin string ve integer olması durumlarında knime farklı alternatifler sunar. Knime'nin eksik veriler için sunduğu en basit çözüm yolu "ignore missing value" seçeneğidir. Örneğin; bu veri setinde "Annual income" kolonunda eksik veriler var. Bu verilere ne yapılacağına karar verilmelidir. Basit olarak "ignore missing value" seçilerek gözardı edilebir yani bu eksik veri olan satırlar dikkate alınmaz.

Model Oluşturma

CRISP-DM veri bilimi yönteminin 4. Adımı olan modelleme adımına geçtiğimiz bu aşamada makine öğrenmesi algoritmalarından "Karar Ağacı Makine Öğrenme Sınıflandırma Algoritması" kullanılacaktır.

Makine Öğrenmesi

Bilinenin aksine makineler insanlar gibi düşünmez, aslında insanların öğrettiği daha doğrusu eğittiği gibi düşünür. Veriyi eğitmek; veriyi bir serüvenin içine sokmak demektir. Veriyi eğiterek veriden amacımıza hizmet edecek bilgiyi elde ettiğimiz bu serüvenin sonunda henüz gerçekleşmemiş bir durum üzerinde çıkarımlarda bulunmaya çalışıyoruz.

Karar Ağacı Makine Öğrenme Sınıflandırma Algoritması

Verinin içerdiği ortak özelliklere göre ayrıştırılması ile sınıflandırma esasına dayanan karar ağacı yöntemi temel olarak entropiye dayalı algoritmalardan ID3 ve C4.5 algoritmaları ile çalışır. Karar ağaçları her bir nitelik bir düğümü temsil eden akış şemalarına benzeyen yapılardır. Tıpkı gerçek dünyadaki ağaçlar gibi "dallar", "yapraklar" ve "kök" ten oluşmaktadır. Karar ağaçlarında en üst yapı kök alt yapılar ise yapraklardır. Kök ve yaprak arasında karar almayı sağlayan yapıyı dallar oluşturur. C4.5 ID3'ün daha gelişmiş hali gibidir. ID3 algoritması ağaç üzeriden entropiye yani benzerlik ölçüsüne dayalı çalışırken C4.5 ise entropi değerleri birer oran olarak tutulur. Karar ağacımızı oluştururken bu iki algoritmanın farkı C4.5 ağaç yapısında budama işlemi yapılabilir [4].

Eğitim ve Test Verisi

Veri madenciliğinde makine öğrenmesinin temeli verinin eğitilmesi esasına dayanır. Makine öğrenmesi daha önce de bahsettiğimiz gibi makineler insanlar gibi düşünmez, insanların öğrettiği daha doğrusu eğittiği gibi düşünen bir yapay zekadır. Bu yapay zekayı oluşturulurken veri setini eğitim ve test verisi olarak ikiye ayrılır. Veri seti ayrılırken dikkat edilmesi gereken en önemli nokta veri setini ayırma türüdür. Veriyi seti ikiye ayrılırken, veri setinin ilk yarısı ve ikinci yarısı olarak ikiye ayırma yapılması pek kullanışlı olmayabilir. Örneğin; şehirlerde suç olması durumunun incelendiği bir projede şehirler alfabetik olarak sıralanmış ise veriyi üstten başlayarak ikiye bölme işlemi yapmak doğruluk oranımızı düşürme olasılığı yükselir. Burada en çok tercih edilen ayırma türü randomly(rasgele) ayırma türüdür. Eğitim verisi veri setinin tamamı olarak seçilebileceği gibi veri setinin belli bir bölümünden de seçilebilir. Veri setimizin ikinci bölümü; test veri seti bölümdür. Yapay zekamızın eğitim veri seti ile karşılaştırma yaparak bir çıkarımda bulunmasını sağlayan veri setine "Test veri seti" denir.

Knime'de veri setimizi eğitim ve test veri seti olarak ikiye ayırmayı sağlayan "Partitioning" ve "X Partitioning" düğümleri vardır. Biz bu çalışmamızda randomly ayırma türü olanağı sağlayan "Partitioning" düğümünü kullanacağız. Burada veri setimizin %70'lik kısmı "Eğitim veri seti" ve %30'luk kısmı test veri olarak randomly ayrılmıştır. Knime'de düğümler bağlanması şekil 2'de gösterilmiştir.

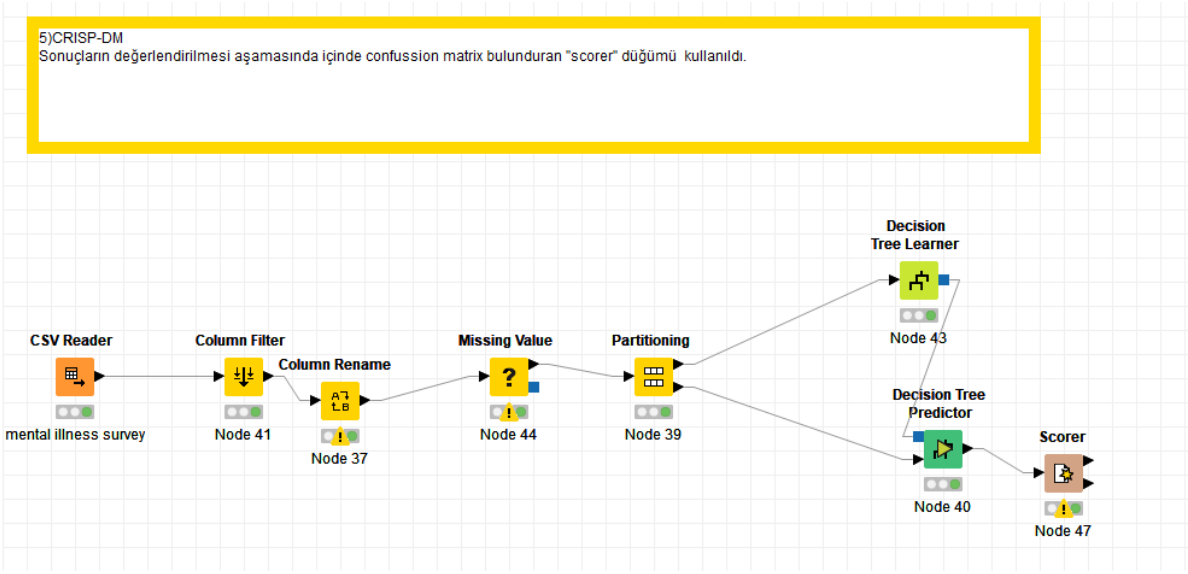

Şekil 2. Knime'de düğümlerin eklenmesi

Projenin Değerlendirilmesi

CRISP-DM veri bilimi yöteminin 5. adımında kullandığımız yöntemin değerlendirilmesi gerekiyor. "Karar Ağacı Makine Öğrenme Alğoritması" çalıştırılarak projenin değerlendirme adımı gerçekleştirilir. Biz burada veri setini daha kolay yorumlamamıza imkân sağlayacağını düşündüğümüz içinde "Confusion Matrix" bulunduran "Scorer" düğümünü kullandık.

Veri setinden rastgele seçtiğimiz, veri setinin %70'lik bölümünden oluşan eğitim verisinden seçtiğimiz "panic attack" kolonu ile veri setinin %30'luk kısmı olan test verisinden seçtiğimiz "Prediction (panic attack)" ile karşılaştırma yapılacaktır. Burada karşılastırma sonucu için confusion matrix kullanılacaktır.

Confusion matrix tablosunda görüldüğü gibi hasta olanlardan 8'ini doğru ve 9'unu hasta değil olarak yanlış olarak tahmin edilmiş. Hasta olmayanların 74'unu doğru 5'ini yanlış tahmin ediyor. Programımız %85,417 oranında doğru çalışmaktadır.

Değerlendirme aşaması olumsuz sonuçlanması durumunda, örneğin; %85,417 oranında doğruluk azımsana bilir. Bu gibi durumlarda CRISP-DM veri bilimi yöteminin 1. adımına geri dönülerek işlem adımları baştan yapılır. Değerlendirme aşaması olumlu geçmesi durumunda CRISP-DM veri bilimi yönteminin 6. ve son adımı olan dağıtım ve projeye son verme adımına geçilir.

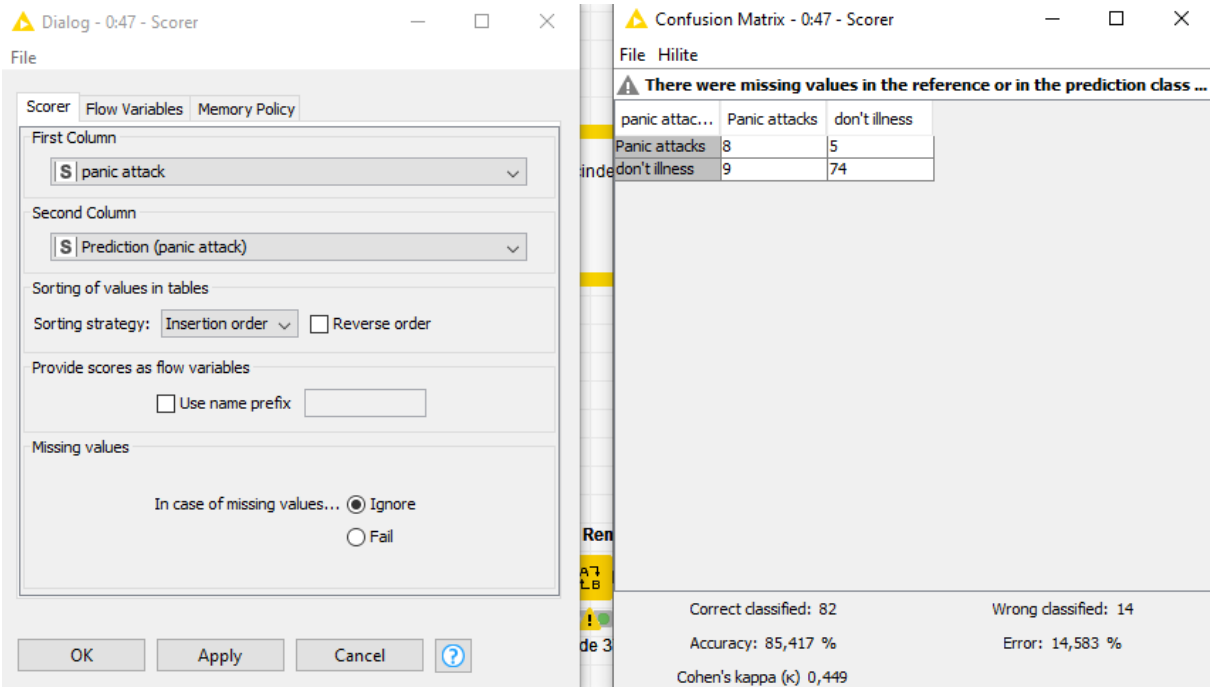

Şekil 3. Confusion Matrix sonuç gösterimi

Projeye Son Verme

Proje üzerinde uzun ve zorlu adımlar tamamlanarak CRISP-DM'IN 6. ve son adımı olan dağıtım ve projeye son verme adımına ulaşılır. Projemiz bu aşamada artık analist ve son kullanıcıya sunulmaya hazırdır.

Sonuç

Küreselleşen dünyada farklı sebeplerden işsiz kalan bir bireylerin sayısındaki artış, işsizlik oranlarının yükseldiği bugünlerde işsizlik sonucu ortaya çıkan olumsuz sonuçları ruhsal açıdan büyük oranda etkilediği görülmüştür.

Referanslar

[1] Kandemir M, Atak H, Stres ve Stresle İlişkili Belirtilerle Başa Çıkma; 2020.
[2] Adak N, Sosyal bir problem olarak işsizlik ve sonuçlar; 2020.
[3] Şeker SE, CRISP-DM: Endüstriler Arası Standart İşleme – Veri Madenciliği için (Cross Industry Standard Processing – Data Mining); 2018.
[4] Çalış A, Kayapınar S, Çetinyokuş T, Veri madenciliğinde karar ağacı algoritmaları ile bilgisayar ve internet güvenliği üzerine bir uygulama; 2014.

Karar Ağacı Algoritması ile E-ticaret Uygulaması

*Hilal Çelik**, *Ahmet Çınar*
Fırat Üniversitesi, Bilgisayar Mühendisliği Bölümü, Elazığ, Türkiye
**İletişimden sorumlu yazar: hilalcelikh@gmail.com*

Özet

İnternet kullanımının büyük bir ivme ile arttığı son yıllarda internet sadece bir araştırma ve veri depolama ortamı olmaktan ziyade birer alış veriş merkezi haline dönüştü. E-ticaret olarak adlandırılan bu kavram iş dünyası pazarına farklı bir boyut kazandırdı. Özellikle sosyal medya siteleri son zamanlarda birden fazla e- ticarete dönüşmüştür. Gelişen e-ticaret dünyasında doğru müşteri kitlesine daha yüksek doğruluk payıyla ulaşmaya çalıştığımız bu çalışmada amaç sisteme yeni giriş yapan bir müşteriye eldeki mevcut ürünün satışı yapılabilir mi? Bu çalışma Knime platformu üzerinde KDD veri bilimi yöntemi adımları takip edilerek makine öğrenmesi algoritmalarından karar ağaçları kullanılmış ve öğrenme tiplerinden gözetimli öğrenme ile gerçekleştirildi.

Bu çalışmanın scorer sonucu olarak %93,487 bir doğruluk payı elde edildi. Bu çalışmada veri setin üzerinde daha kolay çalışabilmek için Knime'nin düğümlerinden olan Rule Engine vasıtasıyla sözcük türünde aynı tür veriler sayısal veriye dönüştürülerek hem veri setinin daha kolay yorumlanması sağlanmış hem de veri seti üzerinde çalışılırken zamandan kazanç sağlanmıştır.

Anahtar Kelimeler: makine öğrenmesi, karar ağacı, Knime, gözetimli öğrenme

Giriş

Hızlı ve kolay alış veriş imkanı sunan e-ticaret sayesinde müşteriler mağazaya gitmeden, satıcı ile muhatap olmadan istediği ürünü alabildiğinden cazip gelmektedir. Satıcı açısından ise daha fazla müşteriye çok daha kısa sürede ulaşabildiğinden tercih edilmektedir. Eğer küçük bir müşteri potansiyeliniz varsa her müşteriye ciddi bir reklam ihtiyacınız olmayabilir. Fakat müşteri kitleniz büyükse doğru müşteri kitlesine ulaşmak zaman ve masraflardan tasarruf etmeyi sağlar. Doğru müşteri kitlesine doğru reklamın yapılması hem müşteri hem de satıcı için kazanç sağlar. Müşteri açısından alakasız reklamlarda muhatap olmadan alış verişini daha hızlı yapabilecektir ve hatta reklam sayesinde hızlı karar verebilecek. Satıcı açısından ise her reklamı her müşteriye yapmaktansa doğru müşteriye doğru reklam sayesinde veri trafiğini hafifletecek ve satış oranını arttırabilecek.

Veri Bilimine Giriş

Veri; ham(işlenmemiş) bilgilere denir. Veriler her zaman hayatımızda işlenmeye hazır ve işe yarar halde değildir. Veri işlenmeye hazır hale getirilinceye kadar birçok aşamadan geçer. Bu aşamalar sonunda işlenmeye hazır hala gelen veri artık üzerinde çalışıp anlamlı ve işe yarar sonuçlar elde edilmesi mümkündür. Veriden bilgiye ulaşırken işlenecek verinin türüne göre öğrenme yapılır.

Öğrenme Türleri

Verilerden anlamlı ve işe yarar bilgilere ulaşma esnasında her veri kedine benzeyen diğer veriler ile aynı yerde bulunmalıdır. Bu sayede verilere daha kolay ulaşılır ve daha kolay işlenir. Veriler işlenirken önce bir sistem oluşturulur. Bu sistem önce problemi ve problemin çözümüne giden yolu öğrenmesi gerekir. Oluşturulan sistemin bulduğu bu çözüm yolunu karşılaştığı yeni problemlerde uygulayabilir olmalı. Sistem oluşturulurken ilk aşamada sistem eğitilir. Bu eğitim işi iki şekilde yapılabilir [1].

Gözetimli Öğrenme (Supervised Learning)

Gözetimli öğrenmede sisteme sürekli bilgi sağlanır. Sistemde hangi sınıfların var olduğu ve bu sınıfların hangi kolon bilgisine sahip olduğu, hangi veri hangi sınıfa dahildir önceden bilinir. Gerçek hayattan örnek verirsek sürekli geometri sorusu çözen bir kişi sınava girdiğinde daha önceki tecrübelerinden yola çıkarak soru hakkında yorum yapması ve öğrendiği çözüm yöntemini yeni karşılaştığı soru üzerinde kullanması gözetimli öğrenmeye bir örnektir. Bu çalışmada gözetimli öğrenme yöntemi kullanılmıştır. Kullandığımız veri setinde sınıflar ve hangi verinin hangi sınıfa dahil olduğu bellidir [2]. Bu çalışmada Gözetimli Öğrenme (Supervised Learning) yöntemi kullanılmıştır.

Gözetimsiz Öğrenme (Unsupervised Learning)

Gözetimsiz öğrenmede sisteme gelecek veri hakkında sistem hangi verinin geleceği bilgisine önceden sahibi değildir. Sistemde kaç sınıf olduğu, gelen verilerin hangi sınıfta dahil olduğu bilgisi belli değildir. Sınıf sayısı ve verilerin hangi sınıfa dahil edileceğini makine kendisi öğrenmeye çalışarak karar verir. Gözetimsiz öğrenmeye verebileceğimiz en iyi bir örnek olarak mantık sorularıdır. Daha önce karşılaşmadığımız ilk bakışta ne sorusu olduğunu anlamakta zorluk çektiğimiz ama biraz düşündükten sonra matematik bilgisi ile çözülebileceğine karar vermek gibi [2].

Veri Bilimi Yöntemi Seçilmesi

Veriyi işlenmeye hazır hale getirmek için veri bilimi yöntemleri kullanılır. Veri işlenirken kullanılan birçok veri bilimi yöntemi vardır. Veri bilimi yöntemi seçilirken üzerinde çalışılan projenin optimum verimle sonuçlanmasını sağlayan veri bilimi yöntemi seçilmelidir. Veri ham halden işlenmeye hazır hale getirilmeye çalışılırken kullanılan veri bilimi yöntemlerinden sık kullanılandan bazıları CRISP-DM, SEMMA ve KDD'dır. Bu çalışmada KDD veri bilimi yöntemi kullanılmıştır.

KDD (Knowledge and Data Discovery)

KDD (Knowledge and Data Discovery); adında belli oluğu gibi "bilgi" ve "veri keşfi" olarak tanımlanmaktadır. KDD veri bilimi yönteminin SEMMA ve CRISP-DM veri bilimi yöntemlerinden farkı, SEMMA VE CRISP-DM dairesel iken KDD'nın doğrusal olmasıdır. Veriden bilgiye ulaşmayı sağlayan bu veri bilimi yöntemi Şekil 1'de görülen 6 adımdan oluşur [3].

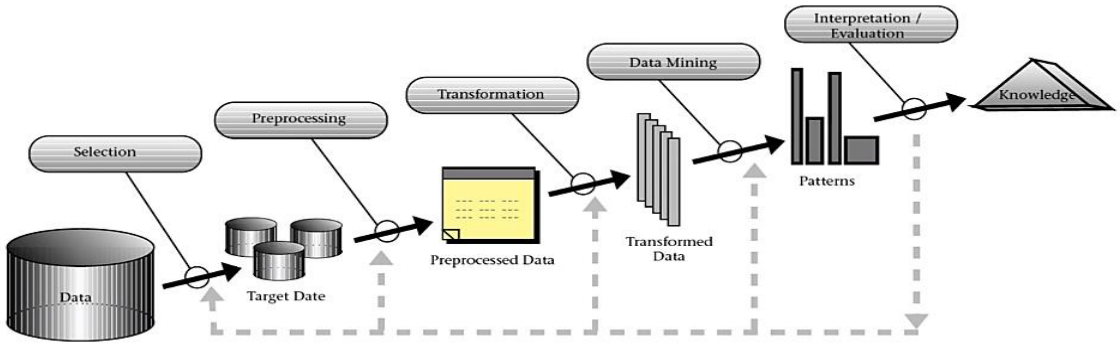

Şekil 1. KDD döngüsü [3]

KDD veri bilimi yöntem adımları; seçim, ön işleme, dönüştürme, veri madenciliği, değerlendirme ve bilgiden oluşmaktadır.

Seçim

Üzerinde keşfin gerçekleştirileceği değişkenlerin veya veri örneklerinin alt kümesinin bulunduğu veri seti seçilir. Bu çalışmada kullanılan veri seti www.kaggle.com sitesinden elde "Social_Network_Ads.csv"'dir.

Ön İşleme

Bu aşama tutarlı veriler elde etmek için hedef veri temizliği ve ön işlemeden oluşur. Tutarsız, kirli ve eksik veriler üzerinde çalışılır.

Dönüştürme

Boyut azaltma veya dönüştürme kullanılarak verilerin dönüştürülmesinden oluşur [4]. Örneğin; veri setinin cinsiyet kolonunda kadınlar için "kadın" ve erkekler için "erkek" yazılı olan bir kolonun dönüşüm aşamasında kadınlar 1 ve erkekler 0 olarak değiştirilerek veri setindeki sözel veriler sayısal verilere dönüştürülebilir [3].

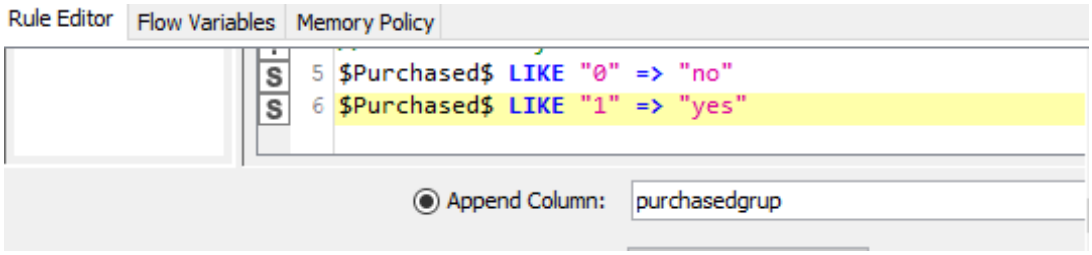

Şekil 2. Rule Engine

Bu çalışmada Şekil 2'de görüldüğü gibi Knime "Rule Engine" düğümünden faydalanılarak satın alma sonucu veri setinde eğer müşteri ürünü aldıysa "1" almadıysa "0" olarak barındırmaktadır. Bizim veri setimizde satın almayı "yes" ve satın almamayı "no" olarak tutmak kolaylık sağladığından dönüştürme yapıldı.

Veri Madenciliği

Bu aşamada projeye uygun istatistiksel modeller veya makine öğrenmesi modelleri geliştirilir [3]. Bu çalışmada makine öğrenmesi algoritması olarak karar ağacı kullanılmıştır. Şekil 3'de kara ağacının ilk adımda yaptığını işlem gösterilmiştir. Bu karar ağacı toplamda 280 veriden 182 kişiyi "no" yani satın almayan 98 kişiyi "yes" yani satın alan olarak tutmaktadır. Kararın ilk adımında cinsiyete bağlı bir kara verilmiştir. Bu kadınların %35,4 ve erkelerin %35,6'sının ürün satın aldığını yani kadınların erkeklere oranla daha fazla ürün satın aldığı yorumu yapılabilir

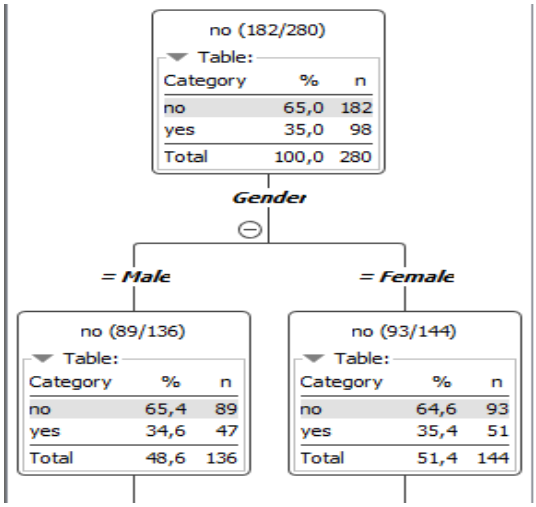

Şekil 3. Karar ağacı ilk adımı

Değerlendirme

Bu aşamada bir önceki adımda geliştirilen model değerlendirilir [3].

Şekil 4'de yapılan çalışmanın karmaşıklık matrisi sonucu verilmiştir. Bu sonuca göre Decission Tree Learner veri setinin % 30'u üzerinde yaptığı tahminden elde ettiği sonuç gösterilmiştir. Buradan sonuçla 112 kişiyi doğru ve 8 kişiyi yanlış tahmin etmiştir.

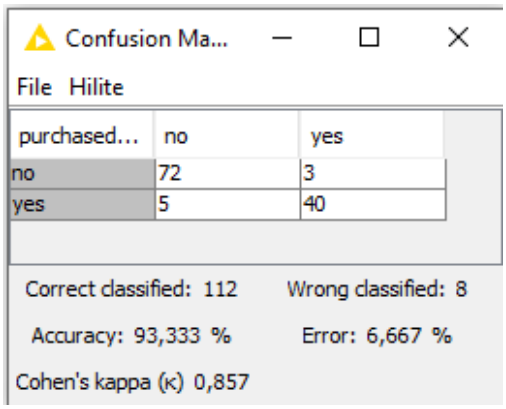

Şekil 4. Karmaşıklık matrisi

Bilgi

Son adımda artık veriden bilgiye ulaşıldığı adımdır. Bu adımda elde edilen model test edildikten sonra benzer bir durumlar bu model üzerinde çalıştırılabilir.

Knime

Genel olarak "Uçtan Uca Veri Bilimi" olarak bilinir. Verinin görselleştirilmesi, makine ögrenmesi algoritması, birliktelik kurak çıkarımı gibi veri madenciliği araçlarının uygulanmasında kolaylık sağlayan açık kaynak kodlu veri madenciliği yazılımıdır. Düğümlerden (node) oluşan bir çalışma akışından oluşur. Bu çalışmada kullanılan Knime düğümleri Şekil 5'te gösterilmiştir.

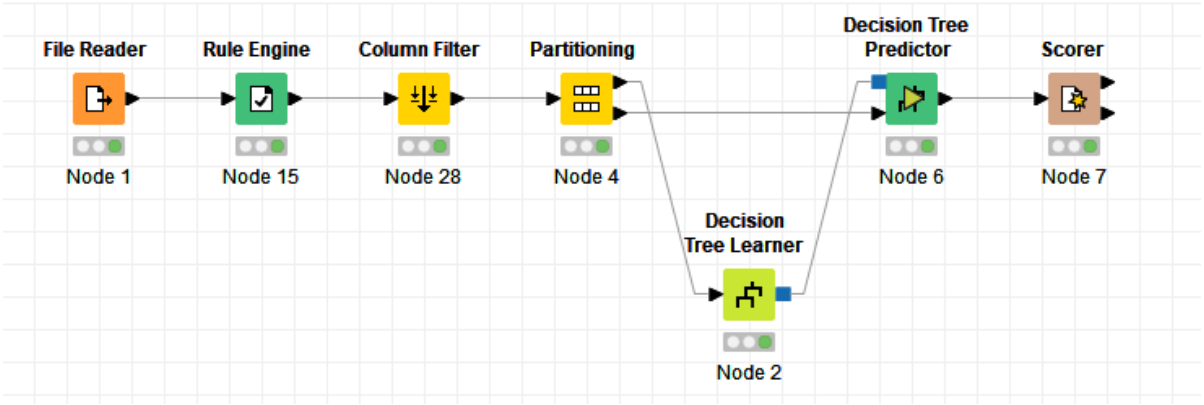

Şekil 5. Knime'de düğümlerin bağlanması

Sonuç

Veriden bilgiye ulaşırken verinin geçirdiği evreler adım adım anlatılmıştır. Veri işlemede açık kaynak kodlu Knime platformu üzerinde kullanılması gereken düğümler açıklanmıştır. Makine öğrenmesi algoritmasından faydalanılarak doğru müşteri kitlesine ulaşmayı hedefleyen çalışmamızda sonuç %93,33 oranında başarı sağlamıştır. Reklam yapılması düşünülen doğru hedef kitlene büyük oranda ulaşılmaya çalışılmıştır.

Referanslar

[1] Han J, Kamber M. Data Mining Concepts and Techniques, published by Morgan Kauffman, 2nd ed.; 2006.
[2] Mohammed M, Khan MB, Bashier M. Machine Learning Algorithms and Applications Bashier Mohammed Bashier; 2016
[3] Şeker SE. CRISP-DM: Endüstriler Arası Standart İşleme–Veri Madenciliği için (Cross Industry Standard Processing – Data Mining) 2018.
[4] Azevedo A, Santos MF. KDD, Semma and CRISP-DM: A parallel overview. IADIS European Conference on Data Mining 2008, Amsterdam, The Netherlands, 2008: 182-185.

Rural Electrification with Solar Powered Mini-Grids and Stand-Alone Solar System Installations: Case of Somalia

*Abdiaziz Hussein Abdi**, *Hasan Zorlu*
Erciyes University, Department of Electrical and Electronic Engineering, Kayseri, Turkey
**Corresponding author: abziizhs@gmail.com*

Abstract

Access to electricity still remains a distant dream in many parts of sub-Saharan Africa. In the energy sector, Somalia is one of the most underdeveloped in the region. Especially in rural areas, the rate of electrification is the lowest with the high cost of power, for electricity generation, Somalia depends on imported petroleum products, and cooking relies on biomass resources, and only a small fraction of the population has safe, reliable, and affordable energy services. Generally, the population in rural areas is composed of a high percentage of poor households and low population density. For this reason, there are not attractive economic benefits for electricity supply utilities or private investors to offer electricity services to these villages. So, this work presented technical and economic challenges for introducing solar-powered mini-grid and stand-alone solar system installations in Somalia's rural areas. Solar-powered mini-grid and stand-alone solar system have been considered for supplying an electrical load in a rural area.to design an off-grid system a well-known freeware HOMER modeling tool has been used. To supply electricity directly to the load solar energy is considered as the primary source and when excess generation happens a battery bank is considered for electrical storage. During the design of this power system the community's load has been suggested for lighting, fan, school, and health clinic equipment load, television, radio, and the simulation and optimization of the system were done based on the electrical load, sources of climatic data, the economics of the power components and other parameters. Finally, a solar-powered mini-grid is developed for a collection of communities and a standalone solar system for clustered buildings is also developed. For further research, the limitations, availability, and areas have also been identified.

Keywords: rural electrificatıon, HOMER model, mini gird, solar, standalone solar system

Introduction

More than 1.3 billion people worldwide still do not have access to electricity, and more than 95% of them they are located in sub-Saharan Africa and developing Asia, and about 2.6 billion people rely on traditional (like diesel and others) energy. This causes air pollution and has serious potential health effects. When used on a conventional stove. According to the latest report, 84% of the total The Somalia population lives without electricity. Our country is trying to meet the current energy demand; problems in the coming years associated with it, it will increase significantly in the coming decades to meet the growth need. Population and economy, changing lifestyles and evolving consumption, current pressure on the limited natural resources resource. These challenges become particularly critical. In countries experiencing accelerated transformation and rapid economic growth, or a country where a large part of the population does not have access to modern energy. Global energy Demand is expected to increase by more than a third in the period to 2035 and Electricity demand is expected to increase by 70% [1].

According to a report in Somalia, only 16% of the population in Somalia has access to electricity and one of the highest electricity costs worldwide those with access to electricity mostly live in rural areas, have the lowest electrification rate in the region and the world [2].

However, it is to use renewable energy such as solar powered generation to provide modern energy, economical and environmentally friendly electrical energy to those in need. Rural areas can be electrified using renewable technologies such as a solar photovoltaic. In this study, a Rural Electrification with Solar Powered Mini-Grids and Stand-Alone Solar System Installations, which will replace the existing conventional diesel generator electricity source, is designed and modeled.

Case Study

Initially, the target village for this study is Laas Geel (Dacar-budhuq); it is located in the north-western part of the Horn of Africa, about 50 km outside the capital Hargeisa Somaliland / Somalia. It’s

a rural area with a historical background one of the most important rock art sites in the Horn of Africa. In this village there are 100 households, to be precise 560 peoples living. The geographical location of the Laas Geel village, Maroodi jeex, Somalia at Latitude: 9° 35' 59.99" N and Longitude: 44° 06' 60.00" E with an altitude of 950 meters above sea level makes it a relatively sun-rich region as in Somalia gets an annual solar irradiance on average per year about 2,900 to 3,100 hours of sunlight the total daily radiation of Somalia is one of the highest in the world (RCREEE in 2015). This implies that electrifying this rural village with solar energy systems would be very efficient. The monthly average radiation of Laas Geel was taken from HOMER, this software uses NASA satellite data and by entering the latitude (9 35' N) and longitude (44° 06' E) of this location in Homer's solar input window; see Figure 1. The average monthly radiation of the location shows the solar radiation steady availability in the whole year and 6.4 kW h/m2/day is the yearly solar average radiation. Therefore, this solar radiation qualifies that solar-powered mini-grids and standalone solar home systems are the considerable alternative sources to electrify this rural area.

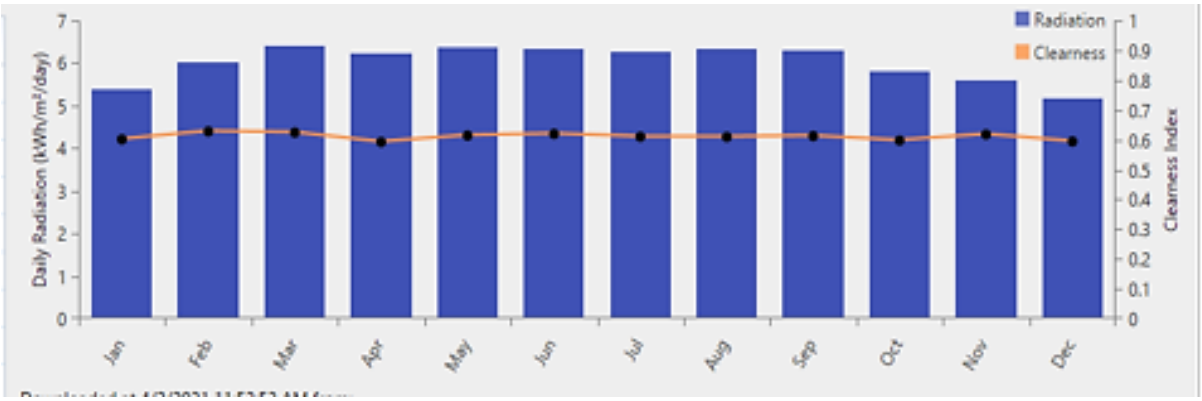

Figure1. Monthly average solar global horizontal irradiance (GH) data of Laas Geel

Electrical Load Estimation

General considerations

In our design, the major phase is to determine or estimate daily load demand of the village and one household as sample. So, the design approach of array sizing calculations is based on the location climatic data, system parameters and their efficiency, the valued output performance of PV modules, and so on. The daily electrical load of a usual rural village in sub-Saharan Africa requires a elementary load, such as lamps, radio, a TV set, refrigeration systems for vaccine, and water pumping. In this study, the electrical power energy of the village can be generally dived into three major classes like domestic, public center, and other public uses. One of the significant data sets is the load profile in each hour to design a standalone solar power system for the township. So, for analysis, four load profiles have been considered, namely:

- Loads in the night (household/domestic), for example, indoor lighting, a TV set, and street lighting.
- Load in the daytime, for example, pumping of the water
- Continuous load demand, for example, freezing
- Adjustable load demands, for example, radio

Collecting load data from the users is important in order to set the load profile of the village or the township. Unfortunately, always the customer in the rural don't understand or they know about energy consumption and costs [3].

Mainly in rural areas, the choice of the system voltage can be either direct current (DC) or alternating current (AC) dependent on a number of restrictions.

Table 1 shows the total load of the village.

Table 1. Total load of the village

Categories	Number of domestics	Required power (kW)	Total power (kW)	Power used per day kW/h/day	Total power kwh/day
Residential	100	1.728	172.8	13.94	1394
Medical center	1	1.125	1.125	17.5	17.5
Primary school	1	2.73	2.73	12.36	12.36
Administration post	1	0.585	0.585	3.87	3.87
Commercial	2	2.336	4.672	49.62	99.24
Mosque	1	0.93	0.93	2.760	2.760
Control room	1	0.344	0.344	5.520	5.520
Public use	1	1.120	1.120	7.920	7.920
Total	108		184.306		1543.17

Figure 2 shows the daily load including peak load and annual average load.

Figure 2. Daily load curve of the village

HOMER Modeling

System configuration

The system consists of PV panels for the conversion of sunlight to electric energy, inverter for the conversion of direct current to alternating current for powering of the AC loads. Also, it contains battery for electricity storage**.** Here, the modeling principles are analyzed mathematically, and the concept is then developed using model HOMER software analysis. In the simulation, solar and the storage batteries are considered. After simulations, different combinations were created and the most appropriate design was selected by evaluating environmental factors such as CO2 emissions and the potential of resources, and cost. All components are connected to the AC line. Components that generate AC electricity can be connected directly to the AC line, or an AC / DC converter may be required for a fixed component bonding topology.

Simulation: This system compares the load demand and energy supply in 1 hour out of 8,760 hours. During this time, it decides to use the incoming load or to run batteries.

Optimization: The purpose of optimization is to determine the optimum system according to the variables decided by the designer. HOMER software; The PV cell size may include variables such as the battery quantity.

Sensitivity analysis: The optimization process is repeated after the sensitive parametric variables are specified as an input in the software. Sensitivity variables; climatic data variations and components can be fuel cost, interest rate, capacity shortage, sensitive reserves to be processed, and other factors. HOMER performs multiple optimizations using various precision inputs to see how sensitive the power system is. Incoming sensitivity results can also be displayed in the form of charts and graphs [4].

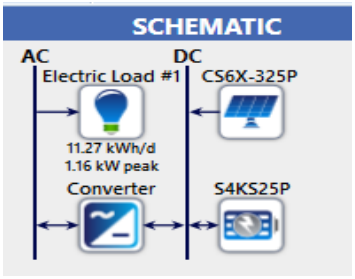

Figure 3. Display of sensitivity results

Sizing of Mini grid PV and Stand-Alone solar Power Systems

Sizing the system means when we are computing the size of the Mini-grid photo voltaic array and the battery storage that is essential to supply the critical loads. An irradiation profile and an approximation or record of the load demand calculations are required for the application. It's important to size the system because oversized PV/battery is expensive to install while undersized of the system cannot deliver the required power and this can lead to the battery excessive discharge, higher operating costs, and shortened battery life. For this reasons system sizing accurately is important and the aims of sizing are: at the design location based on the climate data to regulate the finest corresponding among the Mini-grid PV array's size and the storage system size or the battery to maintenance the design load and also correct the efficient equivalent of the components in the other hand system sizing provides the battery cycling environment this allows the battery to get good service environment. In practice, if a solar power system is under or over-sized it is often hard to tell and the effect to detect will not be easy [5]. An over-sizing of PV Mini-grid will lead to increase system costs, while if there is an under-sized of the system, the system will not supply the power required and it leads that the batteries will be undercharge, and also to an unacceptable failures of the system. If the system is not sized well the system will face some problems for example components in the system may not match each other, there can be extreme load demand according to the design load, degradation, and unsuitable battery or array. Because of these difficulties system sizing and designing is important so HOMER software is used for sizing systems correctly as you can see above in system configuration. These soft wares have the benefits like, the climatic data for the last years which can be used for the simulation as input data, the data of solar irradiation in the location, and also the size of solar panel and the size of the battery storage are available in this software [6].

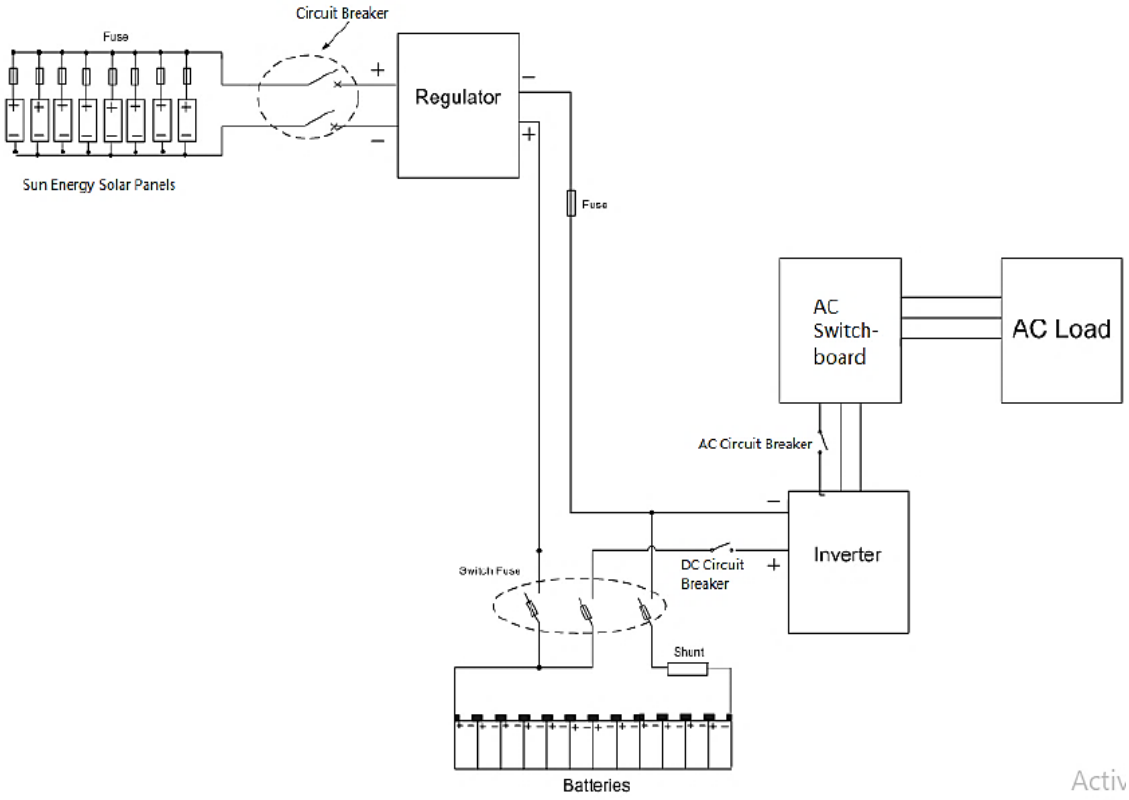

Figure 4. Standalone solar system circuit diagram [6]

Array size and Total Panel Requirements Calculation**:**

$$\text{Array load} = \frac{\text{total daily load(kW/day)}}{\text{battery efficiency} \times \text{charge regulator efficiency}} \quad (1)$$

Note: All calculations are taken randomly

$$\text{Array load} = \frac{500}{0.8 \times 0.9} = 700KW/day \quad (2)$$

$$\text{Array size} = \frac{\text{array load(kWh)}}{\text{No.of peak hours} \times \text{mismatch factor}} \quad (3)$$

$$\text{Array size} = \frac{700}{4.2 \times 0.85} = 200\text{kW/day} \quad (4)$$

The array which can deliver 200kWp/day will be required.

$$\text{No. of series modules} = \frac{\text{no.minal system voltage (V)}}{\text{no.minal module voltage(V)}} \quad (5)$$

$$\text{No. of series modules} = \frac{220}{12} = 18 \quad (6)$$

$$\text{No. of parallel modules} = \frac{\text{daily load demand(WH)}}{\text{module daily output(WH)}} \quad (7)$$

$$\text{No. of series modules} = \frac{\text{daily load(Ah)}}{\text{battery charging efficiency} \times \text{module} \times \text{derating}} \quad (8)$$

$$\text{No. of series modules} = \frac{500000/220(\text{Ah})}{0.8\times0.85\times17.43} = 200 \quad (9)$$

$$\text{Total number of series and parallel panels} = 18\ series \times 200 parallel = 3600 \quad (10)$$

Sizing of Battery

The bank of batteries is selected based upon the connected load and the availability of batteries in the market.

$$\text{Battery capacity} = \frac{\text{daily load(Ah)}\times\text{reserve days}}{\text{max allowable depth of discharge(DOD)} \times \text{temperature derate} \times \text{rate factor}} \quad (11)$$

$$\text{No. of Series Batteries} = \frac{Nominal\ System\ Voltage}{\text{Nominal battery voltage}} \quad (12)$$

$$\text{No. of parallel Batteries} = \frac{battery\ bank\ capacity}{battery\ indivisual\ capacity} \quad (13)$$

Solar powered Mini grid for Remote Rural Areas:

Solar powered mini grids have a significant impact in rural areas, it can combine two or more renewable energy resources and can meet up the power requirement while this study is based on just a Solar system this can just DC because it is less costly than AC grids station which includes those expensive Transformers and reactors.

By comparing DC grids with the AC grids, DC have many benefits over AC ones, just with the one condition that load must not be far away from the grid station.

1. DC systems have nothing to do with the synchronization, so it is easy to integrate more renewable energy resources.
2. They have high productivity and high reliability.
3. Less expensive than AC grids
4. Safe and easy to control.

Generally, utilities like to use solar power, in renewable energy case, as they are abundant in nature and also, they are environment friendly, no consumption of fuel and are less expensive [7].

Economic Analysis

Solar-based systems are regularly measured by way of a clean energy resolution that is approachable to the environment, though, solar-based systems are initially expensive and have financial issues. The solar-based system may pay back its venture and have additional earnings if there is actual design and operation. According to other types of generations, some of the solar-based systems have lower costs. Economic analysis is important in order to decide the cost and value of solar systems like solar-powered mini-grid and stand-alone solar home systems. Initial cost comprises the phase of design, devices, installation and engineering of the solar-based system. Shortly we can summarize the economic expenses like initial costs, repair costs, maintenance costs, and replacement costs. According to the results that we found from the HOMER software the initial cost of the system is **$**53**,**781 and net present cost is **$4,792** and also the values of equipment are obtained from sellers or manufacturer and also the components used in the thesis were estimates taken from international assessments from well-known online solar PV inquiry companies such as Genentech Media Inc, Solar Server (an online portal to solar energy), and Solar buzz (solar market research and analysis). The following two pictures show cost summary of the system.

Simulation Result, Discussion and Conclusion

HOMER Software displays the optimization results are generated in two forms; an overall form in which the top ranked system configurations are listed according to their net present cost (NPC) and in a categorized form where only the least cost system configuration is considered for each system type. Figures 5 and 6 are part of simulation results which shows that using this method of electrification is good and appropriate remote areas in Somalia.

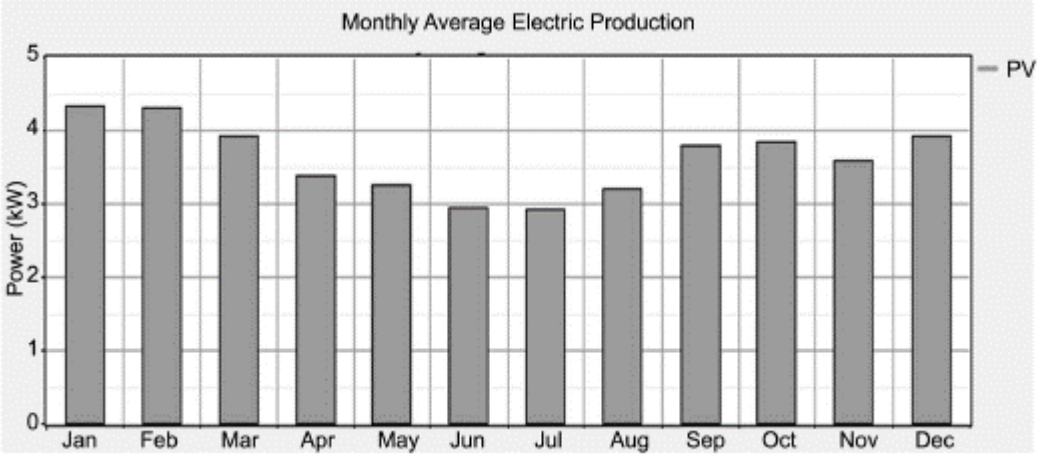

Figure 5. Monthly average electric production

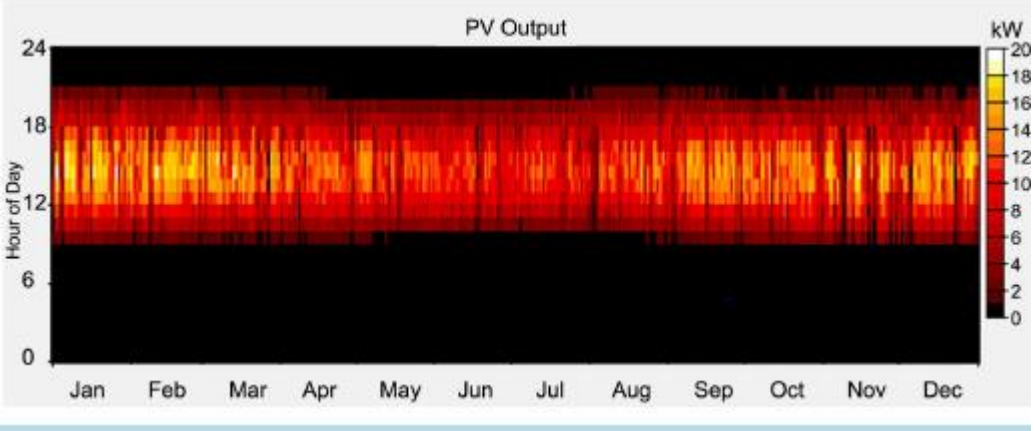

Figure 6. PV output of the system

The draft procedure developed touches on some very important issues to be considered in the design of the regional- scale mini-grid connected solar PV systems using a solar field. Notable among these design steps are the assessment of the solar radiation data for the location, the identification and assessment of the size of the field used, selection of solar PV system components and finally, designing the layout of the mini-grid connected PV system [8]. According to our simulation results this systems is suitable for rural electrification in Somalia also this system is economical and we recommend to implement this study for electrification in whole the country.

This section lists the main contributions of the work: A detailed HOMER economic software model of Solar Mini-Grids and Standalone Solar Systems to be used for rural electrification. Case study of solar-powered mini-grid and stand-alone solar home system which can apple applicable for rural areas in same the proposed system or mini-grid could be a useful technology for less developing countries. Future research should also examine the following topics: More accurate data on the cost of renewable energy components should be obtained. A computer with a high processing power for optimization, especially for the analysis of cases that require high precision.

References

[1] Connor R. The United Nations World Water Development Report, United Nations Educational, Scientific and Cultural Organization, Paris, 2014.
[2] World Energy Outlook (WEO, 2017), Electricity Access Database [Online]. Available: https://www.iea.org/publications/freepublications/publication/WEO2017SpecialReport_EnergyAccessOutlook.pdf
[3] "Energy and the challenge of sustainability" (PDF). “United Nations Development Programmed and World Energy Council”, September 2000. Retrieved August 2015.
[4] Habibullah M. Rüzgâr-Fotovoltaik-Biyogaz Hibrit Güç Sistemlerinin Akıllı Mikro Şebekelerde Kullanımının Kontrol ve Dizaynı, 2016. Yüksek Lisans Tezi, Ege Üniversitesi, Fen Bilimleri Enstitüsü.
[5] African Development Bank, Somalia Energy Sector Needs Assessment and Investment Programme, African Dev. Bank, 2015, [Online]. Available: https://www.afdb.org/fileadmin/uploads/afdb/Documents/Generic-Documents/Final_Somalia_Energy_Sector_Needs_Assessment_FGS__AfDB_November_2015.pdf
[6] Khatib T. (2010). A review of designing, installing and evaluating standalone photovoltaic power systems. Journal of Applied Sciences (Faisalabad), 10(13), 1212-1228.
[7] Thomas DR, Urpelainen J. Early electrification and the quality of service: Evidence from rural India, Energy Sustain. Dev., 44, 11–20, 2018, doi: 10.1016/j.esd.2018.02.004.
[8] Vernet A, Khayesi JNO, George V, George G, Bahaj AS. How does energy matter? Rural electrification, entrepreneurship, and community development in Kenya,” Energy Policy, 2018 126 : 88–98, 2019. doi:10.1016/j.enpol.2018.11.012.

Fotovoltaik Güç Sistemlerinde Maksimum Güç Noktası İzleyicisinin Verimliliği

Hande Demiröz[1], Numan Sabit Çetin[2], Fırat Salmanoğlu[3]*
[1]Ege Üniversitesi, Güneş Enerjisi Enstitüsü, Enerji Teknolojisi Bölümü, İzmir, Türkiye
[2,3]Ege Üniversitesi, Güneş Enerjisi Enstitüsü, İzmir, Türkiye
**İletişimden sorumlu yazar: 91190000919@ogrenci.ege.edu.tr*

Özet

Günümüzde yenilenebilir enerji kaynakları hızlı bir gelişim göstermektedir. Bu kaynaklardan biri olan güneş enerjisi, sınırsız, çevreye zarar vermeyen ve gürültüsü olmayan bir kaynak olması gibi avantajları sebebiyle elektrik enerjisi üretiminde önemli bir yere sahiptir. Ancak, güneş enerjisi sistemlerinin ilk yatırım maliyeti ve verimliliği açısından dezavantajları olduğu da bilinmektedir. Tüm bu bilgiler ışığında, güneş enerjisi sistemlerinden en fazla verimi elde etmek için maksimum güç noktası izleyicisi sistemleri geliştirilmiştir. Bu sistemler, güneş ışınlarının panel yüzeyi ile yaptığı açı ve panel sıcaklığına bağlı olarak değişmektedir. Bir başka deyişle, güneş enerjisi sistemlerinin çalışması her zaman maksimum gücü vermemektedir. Sistemin beslediği yüke, ihtiyacı olan gücü sürekli olarak verebilmek için maksimum güç noktası izleyicisi sistemleri kullanılmaktadır. Bu çalışmada, Matlab/Simulink ortamında değiştir ve gözle yöntemini kullanarak maksimum güç noktası izleyicisi algoritmasının verimlilik üzerine olan etkisini incelenmek için bir sistem tasarlanmıştır. Ayrıca, sistem verimliliği, maksimum güç noktası izleyicisi olmayan fotovoltaik bir sistem ile karşılaştırılmıştır.

Anahtar Kelimeler: fotovoltaik, DA-DA çevirici, maksimum güç noktası izleyicisi

Giriş

Dünyada doğal enerji kaynakları içerisindeki en önemlisi olarak bilinen Güneş, elektrik enerjisi üretiminde alternatif bir kaynak olarak kullanılmaktadır. Bu kaynak fotovoltaik sistemler kullanılarak istenilen güç hesaplamaları doğrultusunda tasarlanmaktadır. Fotovoltaik sistemlerde kullanılan paneller doğru akım (DA) olarak gerilim üretmektedir. Üretilen bu gerilim ile gerek DA ile çalışan ekipmanlar gerek AA (Alternatif Akım) ile çalışan ekipmanlar transformatör kullanılarak beslenebilmektedir. Ancak, üretilen elektrik enerjisinin uzak mesafelere aktarılması bir problem olduğu için depolama sistemleri üzerine çalışmalar başlamıştır. Bu durum içerisinde ise fotovoltaik sistemlerin kurum maliyeti yükselmiştir. Bu sebepten ötürü, çeşitli teknikler kullanılarak panellerin verimliliği üzerine çalışmalar başlamıştır. Buna ek olarak ise üretilen elektrik enerjisinin en verimli şekilde kullanılması ve depolanması için maksimum güç noktası izleyicisi (MPPT) tasarımları geliştirilmeye başlamıştır [1].

Bu çalışmada, öncelikle fotovoltaik sistemlerin ve panellerin elektriksel yapısı ve davranışı incelenmiştir. Bir başka deyişle, gerilim, akım ve güç değerleri açısından panellerin karakteristikleri göz önünde bulundurulmuştur. Sonrasında, MPPT modülleri içerisinde kullanılan DA-DA çeviricilerin çeşitleri olan yükselten (boost), azaltan (buck) ve azaltan-yükselten (buck-boost) çeviriciler incelenmiştir. Sonraki bölümde ise MPPT yöntemleri olan değiştir ve gözle, artan iletkenlik, kısmi açık-devre gerilim, kısmi kısa-devre akım ve bulanık mantık yöntemleri detaylı olarak ele alınmıştır. Uygulama kısmında ise Matlab/Simulink ortamında kurulan DA-DA Azaltan dönüştürücü devresi ile akü grubunun şarj edilmesi ve Değiştir ve Gözle MPPT yöntemi kullanılarak sistem verimliliği hesaplanmıştır. Ayrıca, bu devre MPPT olmadan kurulmuş ve sistemlerin elektriksel parametreleri karşılaştırılmıştır [2].

Fotovoltaik Sistemler

Fotovoltaik sistemler, güneş ışınlarını kullanarak elektrik üreten sistemler olarak tanımlanmaktadır. Bu sistemin en temel birimi güneş pili, seri ve paralel olarak bağlanarak panelin istenilen güçte olmasını sağlamaktadır. Benzer şekilde ise Şekil 1'de gösterildiği gibi paneller seri ve paralel bağlanarak fotovoltaik sistemler istenilen güçte tasarlanmaktadır [3].

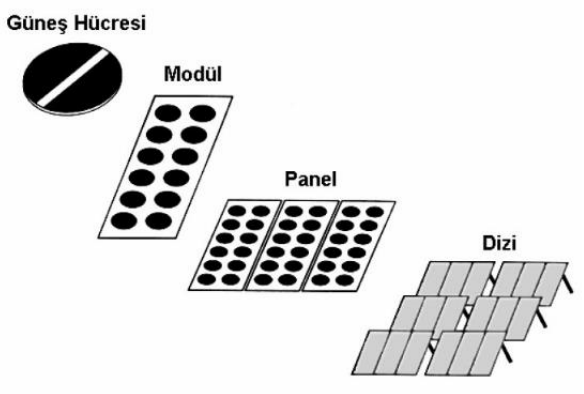

Şekil 1. Fotovoltaik paneller [3]

Fotovoltaik sistemlerin çıkışı lineer olmayan bir akım ve gerilim grafiğine sahip olduğu bilinmektedir. Bunun sebebi ise üretilen elektrik enerjisinin güneşin mevsimsel olarak hareketine bağlı olarak ışınım değerine bağlı olarak değişmesi olarak bilinmektedir. Bu durumdan ötürü, panellerden elde edilen gücün maksimum olması sistem verimliliği açısından önemli bir rol oynamaktadır. Ancak, panellerden elde edilecek gücün maksimum olması, beslenecek sisteme aktarılacak gücün maksimum olacağını göstermemektedir. Fotovoltaik panele ait Şekil 2'de akım ve gerilim, Şekil 3'de güç ve gerilim grafikleri verilmektedir. Bu grafiklerden, panelin çıkış gücünün geniş bir çalışma alanına sahip olduğu görülmektedir. Buna ek olarak, Şekil 4'de fotovoltaik panelin maksimum güç noktaları gösterilmektedir. Bu grafikten çıkan sonuç ise panelin elektriksel olarak geniş bir çalışma aralığına sahip olmasına rağmen panel gücünün maksimum olduğu noktalar sınırlıdır. Tüm bu bilgiler ışığında, fotovoltaik panelin üretmiş olduğu elektrik enerjisi, direk olarak ihtiyaç duyulan sisteme bağlandığında sadece maksimum güç noktalarında çalışabilecektir [4].

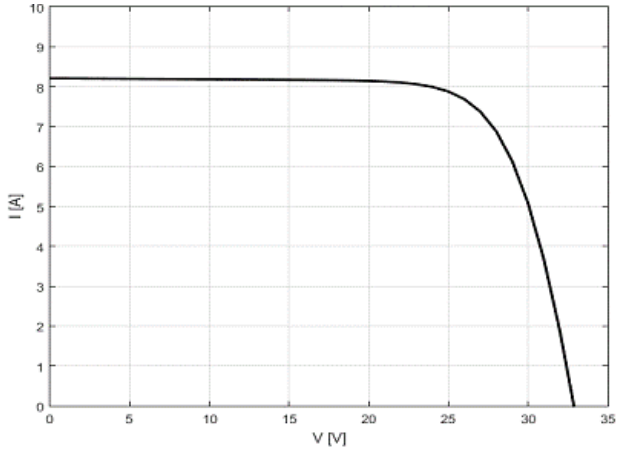

Şekil 2. Fotovoltaik panelin akım ve gerilim eğrisi [4]

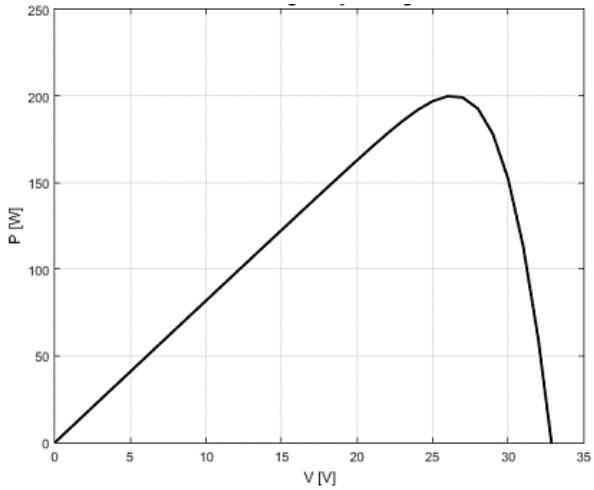

Şekil 3. Fotovoltaik panelin gerilim ve güç eğrisi [4]

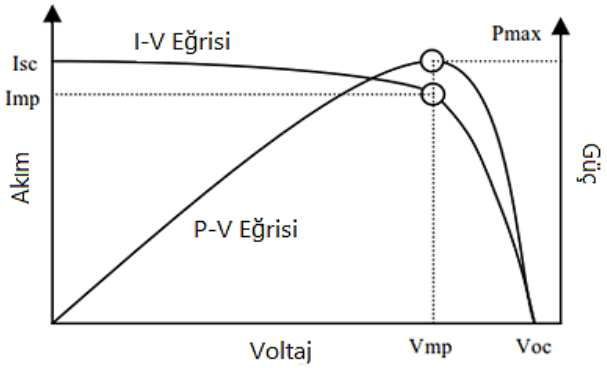

Şekil 4. Fotovoltaik panelin maksimum güç noktaları [4]

DA-DA Dönüştürücüler

DA-DA dönüştürücüler, doğru akıma sahip gerilim ve akımı hem yüksek hem de düşük doğru akıma dönüştüren elektronik devreler olarak bilinmektedir. Fotovoltaik sistemlerde MPPT modülleri ile kullanılan dönüştürücüler, panelden gelen elektrik enerjisini ihtiyaç duyulan sisteme yani yüke aktarılmasını sağlayan bir devre olarak rol oynamaktadır. Bir başka deyişle, fotovoltaik sistemlerden elde edilen elektrik enerjisinin yüke aktarılırken maksimum güç ile gerçekleşmesini sağlamaktadır [5].

Günümüzde DA-DA dönüştürücülerde anahtarlamalı özellikleri ön plana çıkmaktadır. Bu özelliği sebebi ile otomotiv, uçak ve elektronik cihazların birçoğunda güç kaynağı olarak kullanılmaktadır. Dönüştürücüler kullanım alanlarına göre çeşitlilik göstermektedir. Bu dönüştürücülerden bazıları; azaltan(buck), yükselten(boost), azaltan-yükselten(buck-boost), flyback, forward, push-pull, half bridge ve full bridge olarak sıralanmaktadır. Bu çalışma içerisinde ise azaltan(buck), yükselten(boost) ve azaltan-yükselten(buck-boost) dönüştürücüler üstünde durulmaktadır [6].

Azaltan (Buck) Dönüştürücüler

Azaltan dönüştürücüler, giriş geriliminin çıkış geriliminden düşük olmasının istendiği yerlerde kullanılmaktadır. Dönüştürücü içerisinde kullanılan yarı iletken anahtar enerji girişi ile bobin arasına seri bir şekilde bağlanmaktadır. Bundan ötürü giriş akımı süreksiz, bobin ve kapasitörün yüke direk olarak bağlı olmasından ötürü ise çıkış akımı sürekli olmaktadır [7].

Şekil 5'de bu tip dönüştürücüye ait temel bir devre görülmektedir. L bobini ve C kapasitörü, çıkış gerilimini filtrelemektedir. Devrede kullanılan R direnci, yük olarak gösterilmektedir. D diyotu ise genellikle serbest geçiş diyotu olarak tanımlanmakta ve geri dönüş akım ve gerilimini engellemektedir.

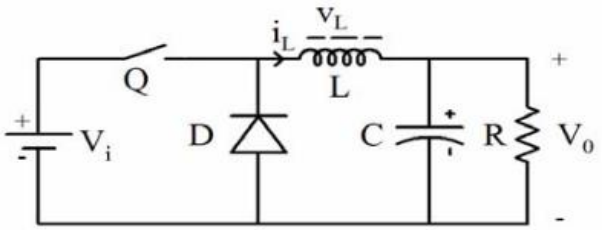

Şekil 5. Azaltan dönüştürücü [7]

Azaltan dönüştürücüde kullanılan bobin sürekli ve süreksiz akım olarak iki farklı mod içerisinde çalışmaktadır. Sürekli akım modunda, bobinden devamlı olarak akım geçmektedir. Süreksiz akım modunda ise bobin belirlenen periyot aralığında çalışmaktadır. Periyot başında bobin üzerinden geçen akım sıfır değerinden başlayarak yükselmektedir. Periyot sonuna gelmeden önce ise sıfır değerine geri dönmektedir. Şekil 6'da bu moda ait gerilim ve zaman grafiği gösterilmektedir [8].

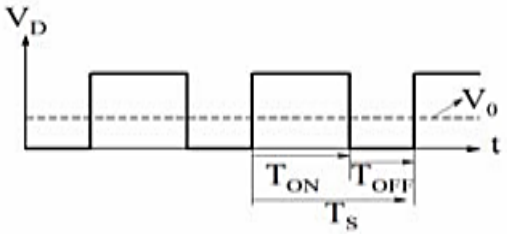

Şekil 6. Süreksiz modda çalışma gerilim grafiği [8]

Maksimum Güç Noktası İzleyicisi (MPPT)

Fotovoltaik sistemlerde MPPT kullanılmasının temel amacı, panellerden elde edilecek olan enerjisinin ve gücün maksimum olmasını sağlamaktır. Bu amacın etkili bir şekilde gerçekleşmesi için belirli bir sıcaklık ve ışınım değeri altında panellerin çıkış gerilimi ve akımının karar verilmesi gerekmektedir. Şekil 7'de MPPT kullanılan bir fotovoltaik sistemin genel blok şeması gösterilmektedir [9].

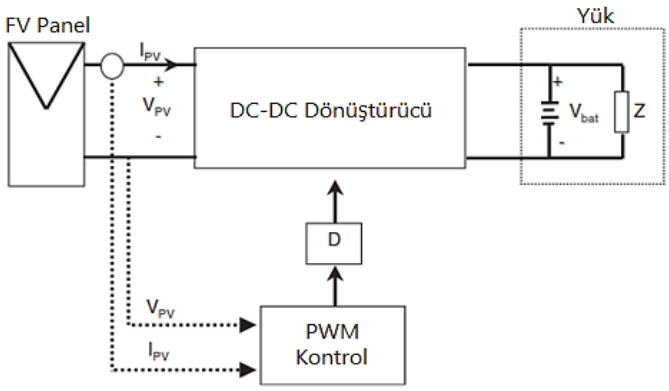

Şekil 7. MPPT kullanılan FV sistemin genel blok şeması [9]

Fotovoltaik panellerde maksimum güç noktası, farklı güneş ışınım değerlerine değişiklik göstermektedir. Fotovoltaik sistemler, bu noktalar belirlenerek tasarlanmaktadır. Bu değerleri gösteren grafik Şekil 8'de verilmektedir.

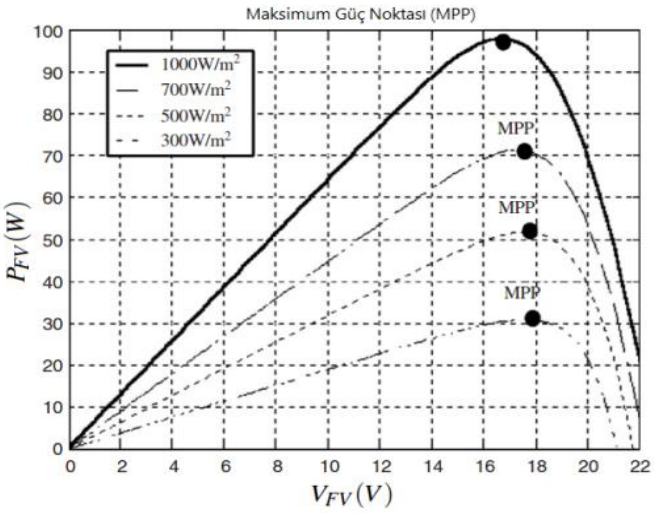

Şekil 8. Farklı ışınım değerlerinde maksimum güç noktasının değişimi [9]

Maksimum Güç Noktası İzleyicisi (MPPT) Yöntemleri

Yenilenebilir enerji kaynaklarında ağırlıklı olarak kullanılan MPPT modüller, beslenecek yükün yapısına göre çeşitlilik göstermektedir. Bir başka deyişle, MPPT çeşitliliği sistem içerisinde kullanım yöntemlerine göre farklılık göstermektedir. Farklı MPPT yöntemleri kullanılarak DA-DA dönüştürücüler kontrol edilmektedir [10]. MPPT yöntemlerinden en yaygın olarak kullanılanları sırası ile değiştir ve gözle, artan iletkenlik, kısmi açık-devre gerilim, kısmi kısa-devre akım ve bulanık mantık yöntemleri olarak bilinmektedir.

Değiştir ve Gözle Yöntemi

Değiştir ve gözle yöntemi, uygulanabilirliğinin kolay olması ve sonuçlarının anlaşılabilir olması açısından MPPT çalışmalarında en çok kullanılan yöntem olarak bilinmektedir. Bu yöntem ile fotovoltaik panelin maksimum güç noktası, akımın ve gerilimin değiştirilerek ortaya çıkan sonuçların analiz edilmesi ile elde edilmektedir. Örneğin, akım veya gerilim belirlenen bir yönde değiştirilmesi ile gücün arttığı gözlemlendiğinde, akım veya gerilim benzer şekilde değiştirilmeye devam edilmektedir. Ancak, gücün azaldığı gözlemlendiğinde ise ters yönde akım veya gerilim değiştirilmektedir [12].

Tablo 1. Değiştir ve Gözle yönteminin değişim durumları [12]

Değişim	Güçteki Değişim	Sonraki Değişim
Pozitif	Pozitif	Pozitif
Pozitif	Negatif	Negatif
Negatif	Pozitif	Negatif
Negatif	Negatif	Pozitif

Tablo 1'de söz konusu değişimin yönleri ve güç değerlerindeki değişimler gösterilmektedir. Tablo 1'de verilen değişiklikler panellerden elde edilen güç maksimum noktasına ulaşana kadar devam ettirilmektedir. Maksimum güç noktasına ulaşıldığında ise analizler bu nokta aralığında osilasyon yapmaktadır. Osilasyonun azalması için ise yapılan değişiklikleri daha küçük oranlarda yapılması gerekmektedir. Ancak, değişiklik oranı azaldıkça net bir maksimum güç noktası değerine ulaşılması zaman almakta ve bu durum bir problem olarak ortaya çıkmaktadır. Söz konusu problemi ortadan kaldırmak için bu yöntem içerisinde uygulanacak değişimlerin oranı, maksimum güç noktasından uzak değerlerde bulunduğunda büyük, yakın olduğunda ise küçük olarak alınması yöntemi uygulanmaktadır [13].

Tüm bunlara ek olarak, değiştir ve gözle yönteminin tek bir dezavantajı bulunmaktadır. Bu durum ise panelin anlık ışınım değişimlerine maruz kaldığında doğru olmayan veriler üretmesi olarak bilinmektedir. Söz konusu durum ile ilgili Şekil 9'da anlık ışınım değişimi ile panelin gücünün değişimi

gösterilmektedir. Bu şekil detaylı olarak incelendiğinde, sistem A noktasında çalıştığında, pozitif yönde bir değişiklik uygulanırsa sistem B noktasına ulaşacaktır. Bu durumda, gücün düştüğü gözlemlenerek negatif yönde bir değişiklik uygulanması uygun olacaktır. Tam bu noktada, ışınımda bir çevrim süresinden daha az bir süre içerisinde bir artış oluştuğunda, sistem C noktasına ulaşacaktır. Bu durumda, panelin gücünde bir artış olduğu gözlemlenmiş olacak ve bir sonraki değişim pozitif olarak uygulanacaktır. Sonuç olarak ise ışınım değişimi analizleri yanıltarak maksimum güç noktasından uzak bir değere varılmasını sağlayacaktır [14].

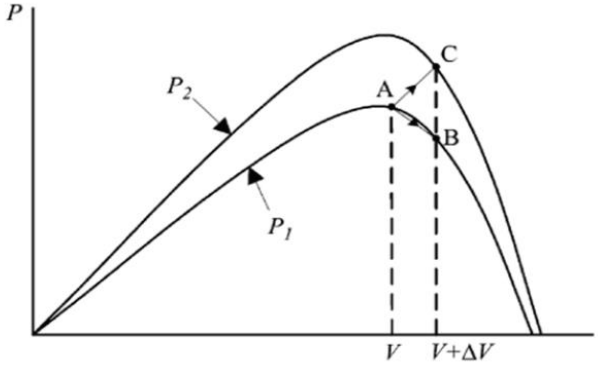

Şekil 9. Anlık ışınım değişimi ile gücün değişimi [14]

Artan İletkenlik Yöntemi

MPPT yöntemlerinden bir diğeri ise artan iletkenlik olarak bilinmektedir. Bu yöntem, panelin güç ve gerilim grafiğindeki eğimin analizine dayanmaktadır. Bu eğimin değerine göre sistemin sahip olacağı maksimum güç noktası değerine karar verilmekte ve panelin geriliminde değişiklikler yapılmaktadır. Tablo 2'de artan iletkenlik yönteminde panelin çalışma geriliminin eğimindeki değişimine bağlı olan durumu verilmektedir [13].

Tablo 2. Artan İletkenlik Yönteminde değişim durumları [13]

Eğim	Sistemin çalışma gerilimi
$dP/dV = 0$	Maksimum güç noktasında
$dP/dV > 0$	Maksimum güç noktasının solunda
$dP/dV < 0$	Maksimum güç noktasının sağında

Artan iletkenlik yöntemi ile değiştir ve gözle yönteminin çalışma şekli benzerlik göstermektedir. Ancak, artan iletkenlik yönteminde analiz edilen eğim sonucunda maksimum güç noktasının bulunması güneş ışınım değişiklikleri göz önünde bulundurulduğunda, değiştir ve gözle yöntemine kıyasla daha iyi sonuçlar ortaya çıkarmaktadır. Şekil 18'de artan iletkenlik yöntemine ait örnek bir grafik verilmiştir [11]

Kısmi Açık-Devre Gerilim Yöntemi

Kısmi açık devre gerilim yönteminde, fotovoltaik sistemlerde bulunan panelin açık devre gerilimi V_{OC} ile maksimum güç noktasındaki gerilim V_{MPP} arasındaki ilişki, k_1 olarak tanımlanan panel karakteristiğine bağlı olarak farklılık gösteren ışınım ve sıcaklık değeri ile değişmektedir. Yapılan araştırmalar sonucunda, k_1 değeri 0,71 ile 0,78 arasında değiştiği belirlenmiştir [12]. Lineer olan bu eşitlik aşağıda gösterilmektedir.

$$V_{MPP} \approx k_1 V_{OC} \quad (1)$$

Artan iletkenlik yönteminde k_1 değeri bulunduktan sonra fotovoltaik sistem içerisindeki panelin uçlarının yükten anlık olarak ayrılmasıyla V_{OC} ve V_{MPP} değerleri hesaplanabilmektedir. Bu yöntemin dezavantajı ise panelin yükten anlık olarak ayrılması sebebiyle enerji kaybının ortaya çıkması olarak bilinmektedir [15].

Kısmi Kısa-Devre Akım Yöntemi

Kısmi kısa devre akım yönteminde, fotovoltaik sistemlerde bulunan panelin kısa devre akımı I_{SC} ile maksimum güç noktasındaki akım I_{MPP} arasındaki ilişki, k_2 olarak tanımlanan panel karakteristiğine bağlı olarak farklılık gösteren ışınım ve sıcaklık değeri ile değişmektedir. k_2 fotovoltaik panelin karakteristiğine bağlı olan bir sabit olarak tanımlanmaktadır. Bu ilişki aşağıdaki denklem ile ifade edilmektedir [15].

$$I_{MPP} \approx k_2 \, I_{SC} \tag{2}$$

Bu yöntemin dezavantajı ise sistem normal şartlar altında çalışırken I_{SC} akımının ölçülmesi olarak bilinmektedir. Bu akımın ölçülebilmesi için sisteme ek olarak şalter konulması gerekmektedir. Bu durum ise sistem içerisinde kullanılacak olan malzeme sayısını yani maliyeti arttırmaktadır [15].

Uygulama

Bu çalışmanın uygulama kısmında kullanılan fotovoltaik panelin özellikleri Tablo 3'de verilmiştir.

Tablo 3. Panelin Elektriksel Karakteristiği

Panelin Elektriksel Karakteristiği	
Panelin Gücü (W)	250
Kısa Devre Akımı (A)	8,75
Açık Devre Gerilimi (V)	36,6
Maksimum Noktasındaki Gerilimi (V)	30,9
Maksimum Noktasındaki Akımı (I)	8,1

Fotovoltaik panellerden oluşan sistem, 4 seri ve 2 paralel bağlantı yapılarak toplamda 8 panel kullanılarak 2kW güç üretecek şekilde kurulmuştur. Sistemin sıcaklığı 25°C olarak sabitlenmiştir. MPPT devresi içerisinde akülerin kolaylıkla ve etkili bir şekilde şarj edilebilmesi için azaltan dönüştürücü tipi kullanılmıştır. Devre şeması ve elektriksel parametreleri aşağıdaki gibidir.

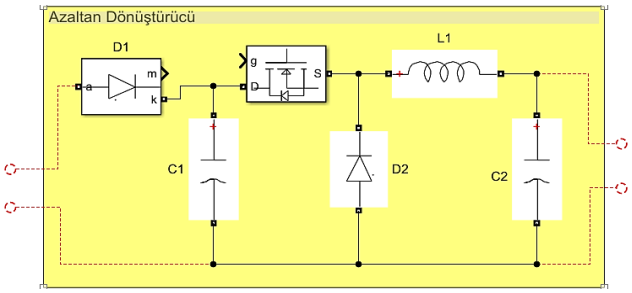

Şekil 10. Azaltan Dönüştürücü Devresi

Tablo 4. DA DA Dönüştürücünün Elektriksel Karakteristiği

DA DA Dönüştürücünün Elektriksel Karakteristiği	
C1(μF)	1000
C2(μF)	1000
L(mH)	10
R1 (Ω)	0,02
D1(V)	0,5
D2(V)	0,5
Frekans (Hz)	1000

MPPT sistemlerinde en önemli nokta, kontrol teknikleri tanımlanan yöntemler olarak bilinmektedir. Bu yöntemlerden ise ticari amaçlı olarak en çok kullanılanı, değiştir ve gözle yöntemidir. Bu yöntem içerisinde kullanılan algoritmada amaç, sistemin verimliliğini test etmektir. Sistem verimliliği ise,

fotovoltaik panellerden oluşan sisteminden MPPT devresi kullanılarak elde edilen gücünün, fotovoltaik panellerin belirlenen çalışma şartları altında üretebileceği maksimum güce oranı olarak bilinmektedir [22].

Bu çalışmada, MPPT devresinin verimliliğinin ölçülmesi için değiştir ve gözle yöntemi kullanılmıştır. Bu izleyicide, güneş ışınım değeri 100W/m^2 başlatılarak ve her 1 saniyede 100W/m^2 arttırılarak 100W/m^2 ile 1000W/m^2 arasında değiştirilmiştir. Ayrıca, analiz yapılırken mevsimsel ya da günlük hava durumundaki değişiklikler göz önünde bulundurularak 1000W/m^2 olan güneş ışınım değeri 8. saniyede 500W/m^2'ye düşürülmüş, 12. saniyede ise 1000W/m^2 yükseltilmiştir. Toplam analiz süresi ise 20 saniye olarak alınmıştır.

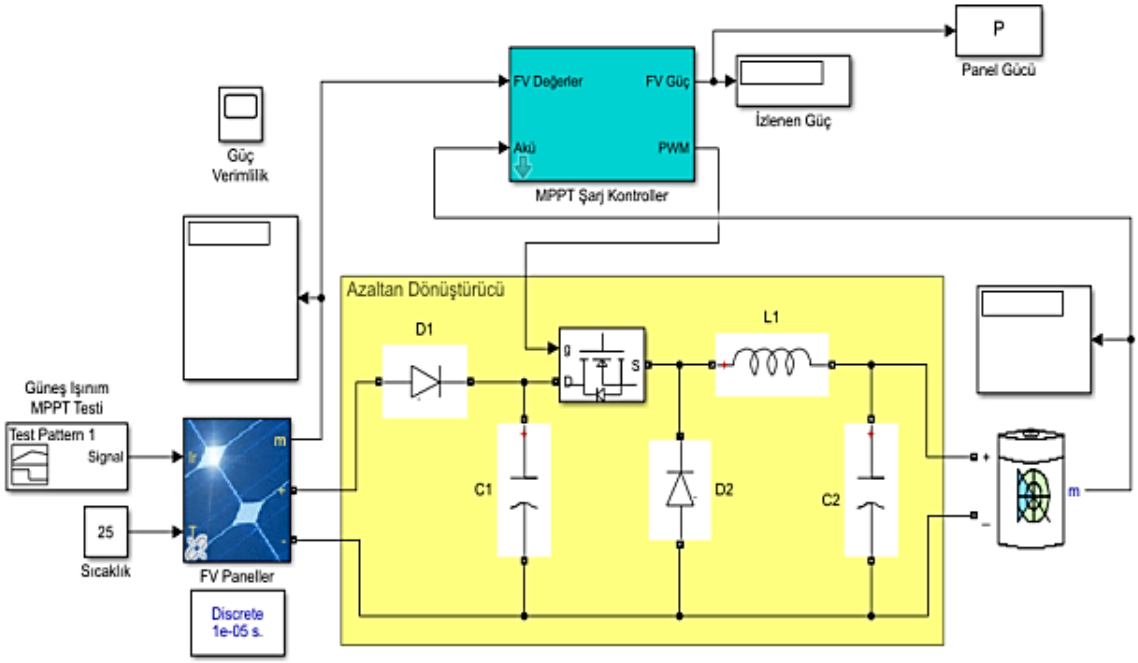

Şekil 11. MPPT'li FV Sistemin Devresi

MPPT'li devre kullanılarak güneş ışınım değerlerine göre değişiklik gösteren panellerin güç ve zaman grafiği Şekil 12'de, izlenen gücün zamana göre değişimini gösteren grafik ise Şekil 13'de verilmiştir.

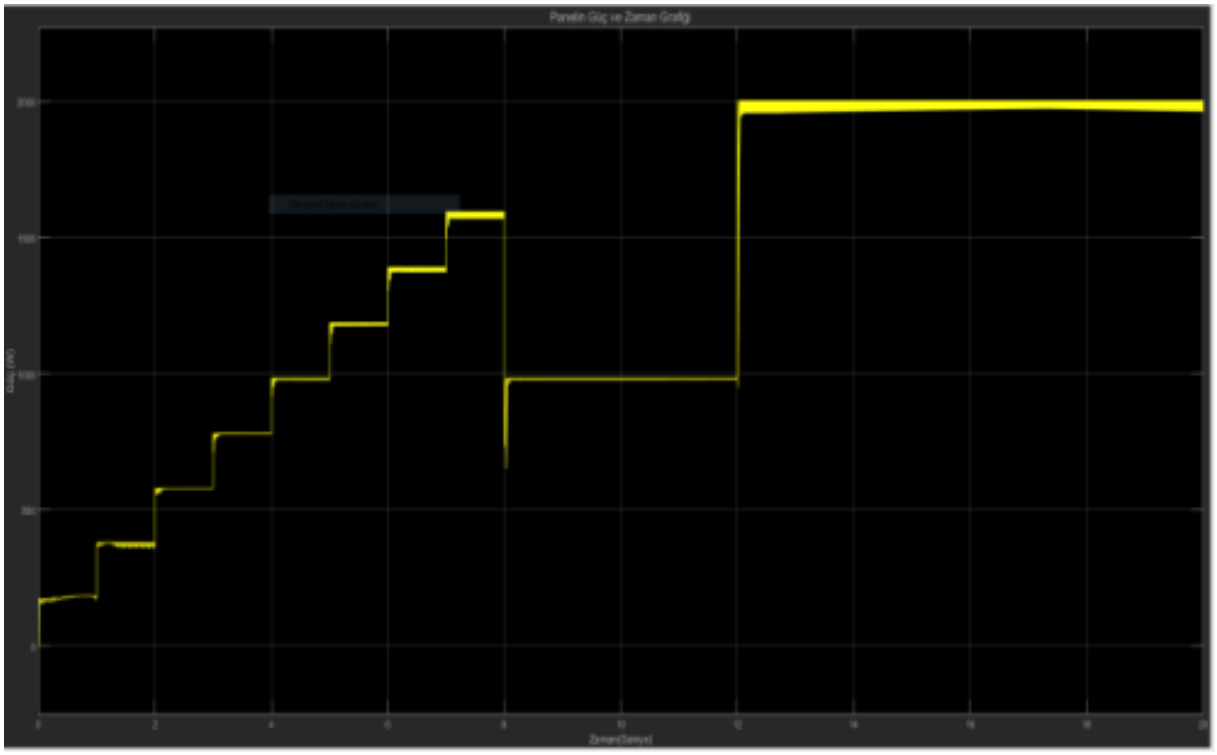

Şekil 12. Panellerin güç ve zaman grafiği

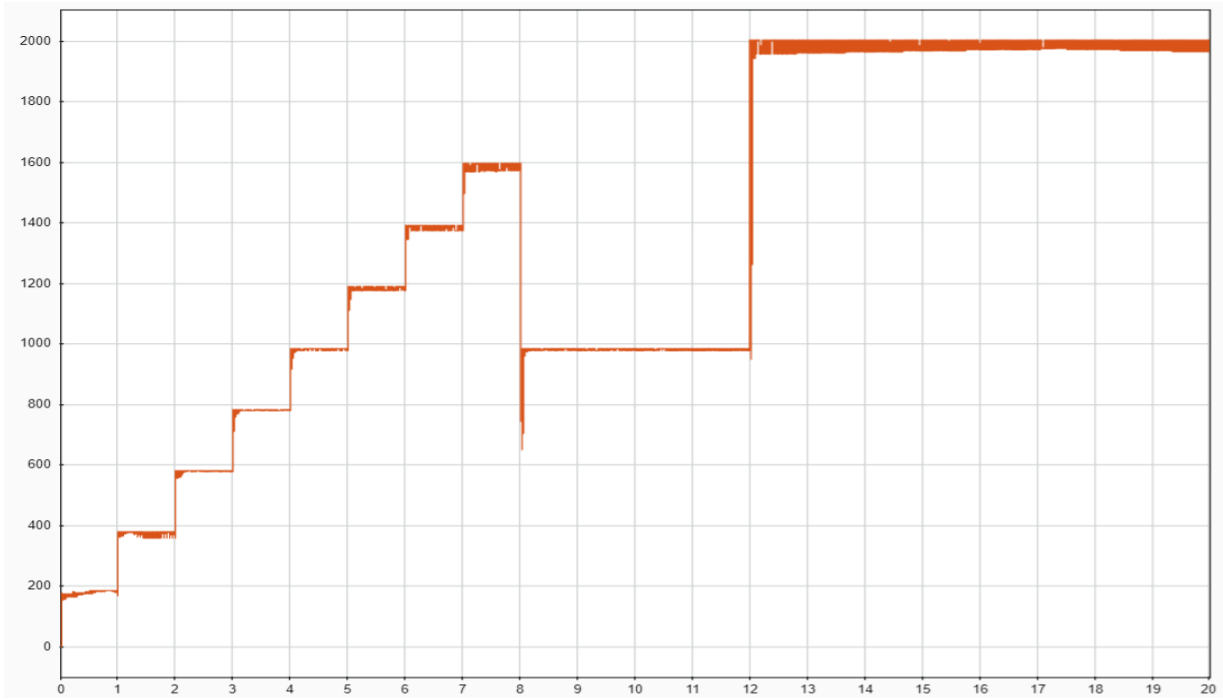

Şekil 13. İzlenen güç ve zaman grafiği

Panellerin 20 saniyelik analiz süresi içerisindeki gerilim grafiği Şekil 14'de, akım grafiği ise Şekil 15'te gösterilmiştir.

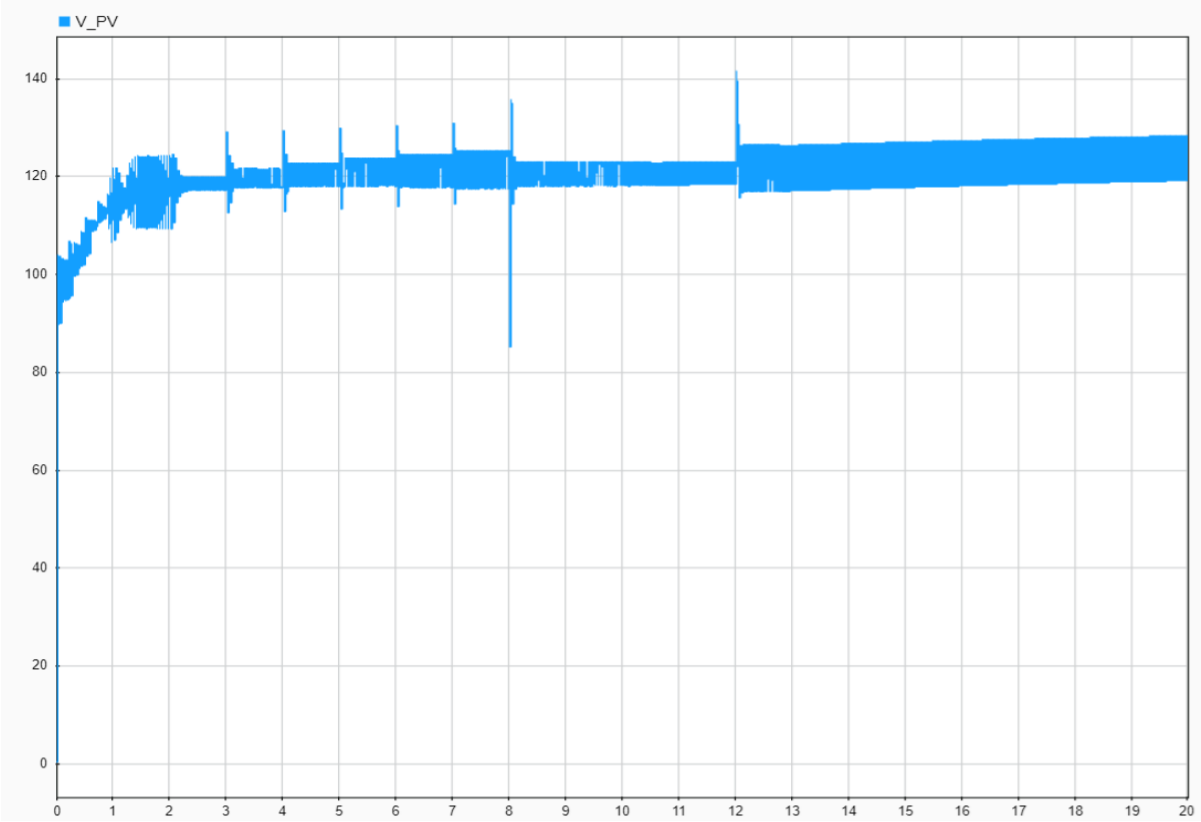

Şekil 14. Gerilim ve zaman grafiği

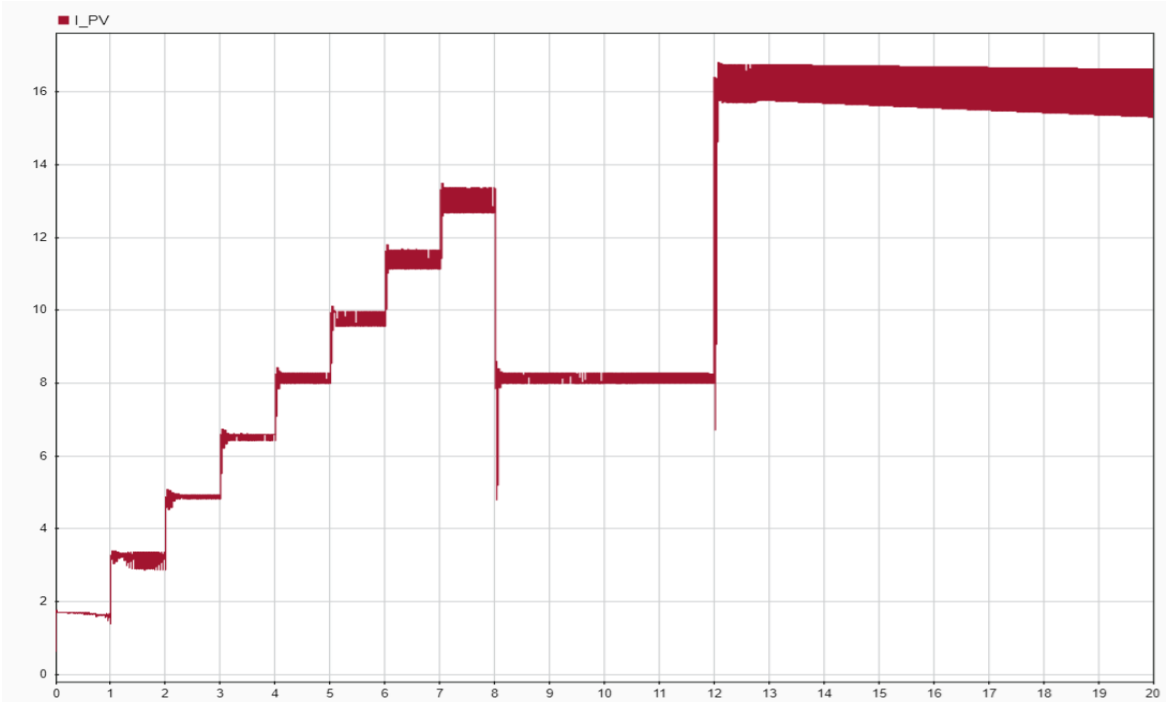

Şekil 15. Akım ve zaman grafiği

MPPT'li olarak kurulan fotovoltaik sistemin verimi ise Şekil 16'da gösterilmektedir. 100W/m^2'lik güneş ışınımında %97,5 olarak hesaplanan sistem verimliliği, 1000 W/m^2 ulaştığında ise %99 değerine ulaştığı gözlemlenmiştir.

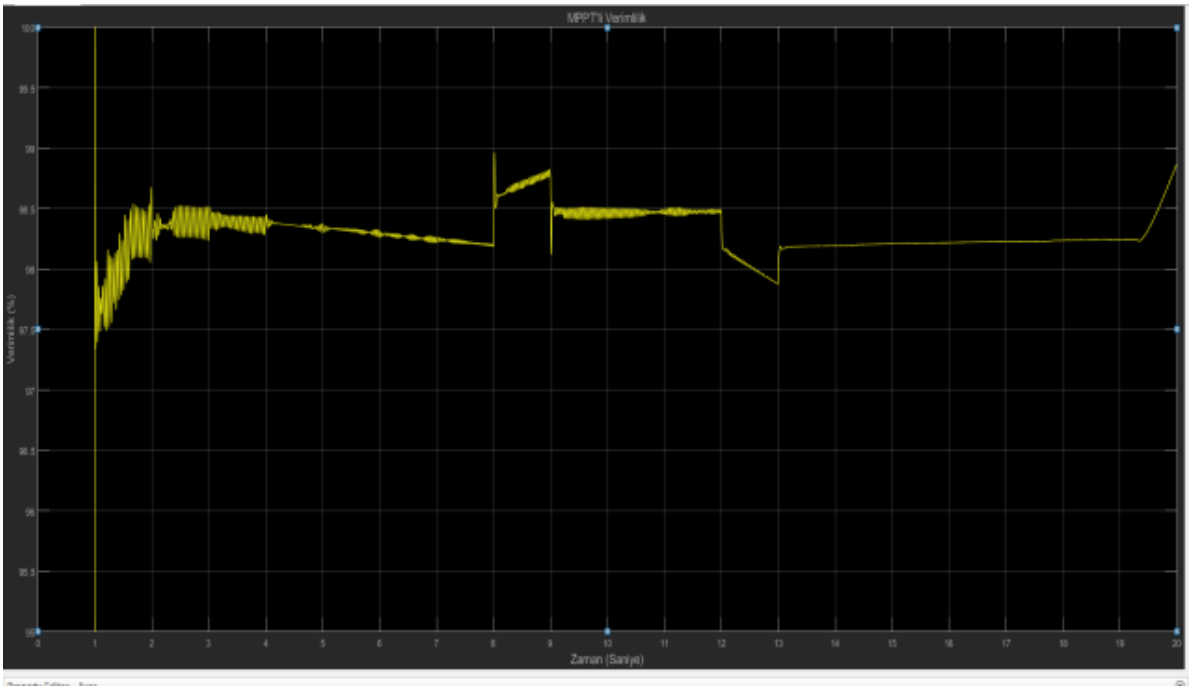

Şekil 16. MPPT'li FV sistemin verimliliği

MPPT'siz olarak kurulan sistemdeki panellerin güneş ışınım değerlerine göre değişiklik gösteren güç ve zaman grafiği Şekil 17'de, izlenen gücün zamana göre değişimini gösteren grafik ise Şekil 18'de verilmiştir.

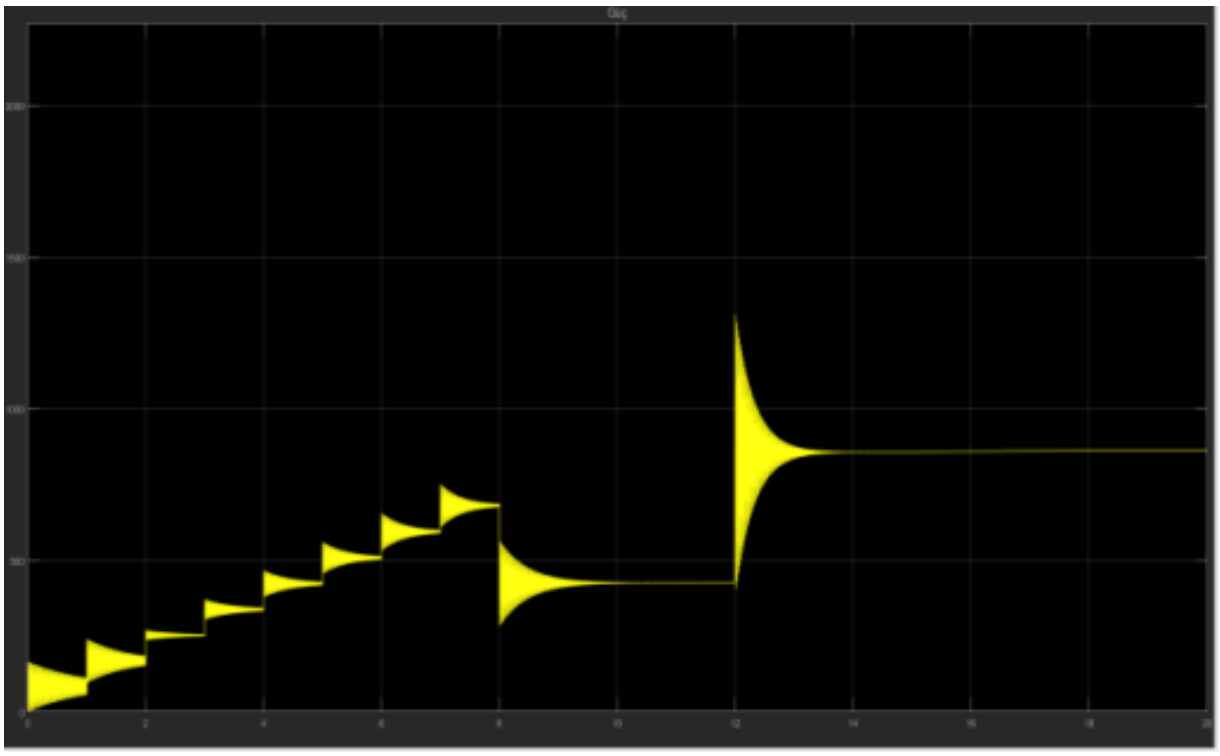

Şekil 17. Panellerin güç ve zaman grafiği

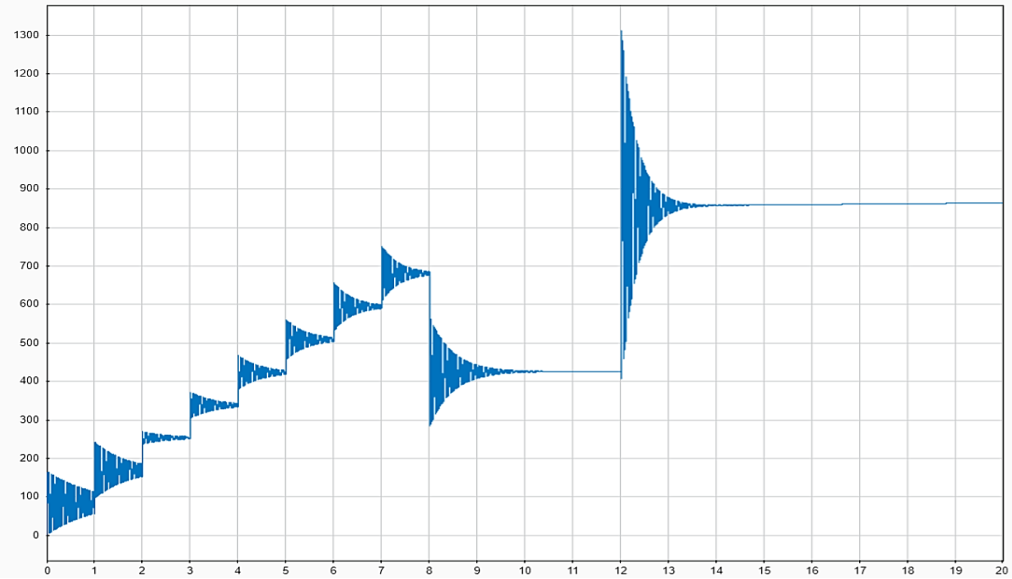

Şekil 18. İzlenen güç ve zaman grafiği

Panellerin 20 saniyelik analiz süresi içerisindeki gerilim grafiği Şekil 19'da, akım grafiği ise Şekil 20'de gösterilmiştir.

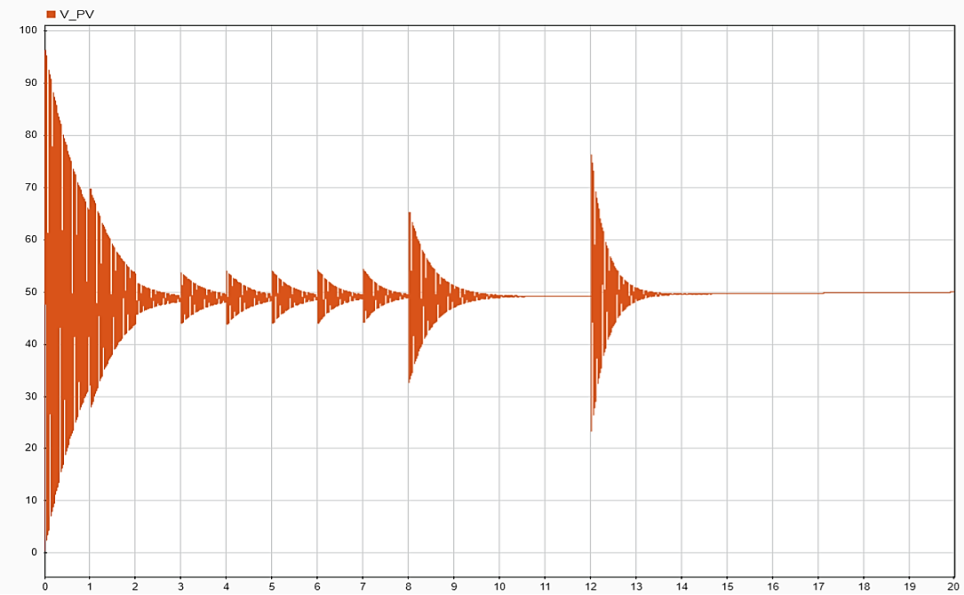

Şekil 19. Gerilim ve zaman grafiği

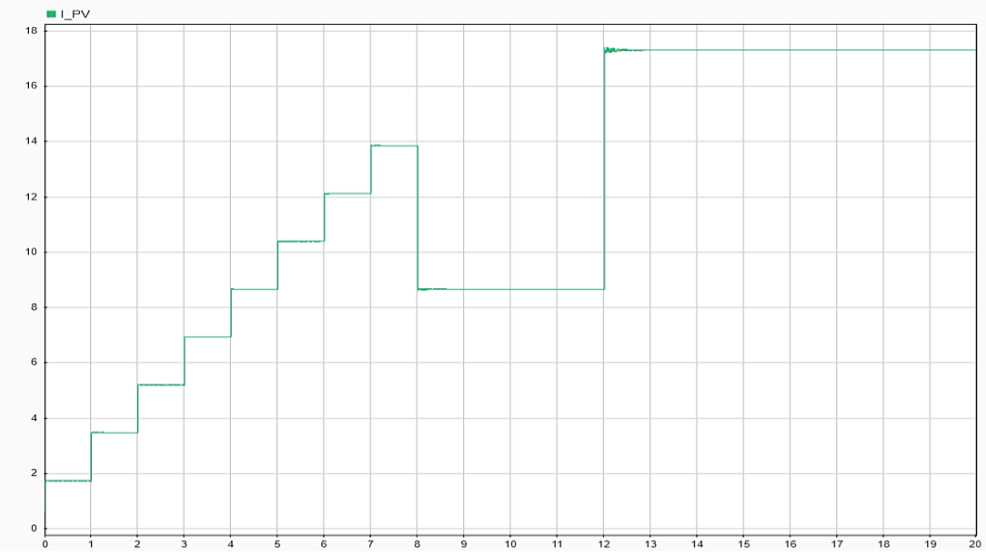

Şekil 20. Akım ve zaman grafiği

MPPT'siz olarak kurulan fotovoltaik sistemin verimi ise Şekil 21'de gösterilmektedir. Sistem verimliliği güneş ışınım değeri değiştikçe 2 saniyeden fazla olarak bir salınım göstermektedir. Buda kararsız bir yapıda verimlilik değeri ortaya çıkarmaktadır.

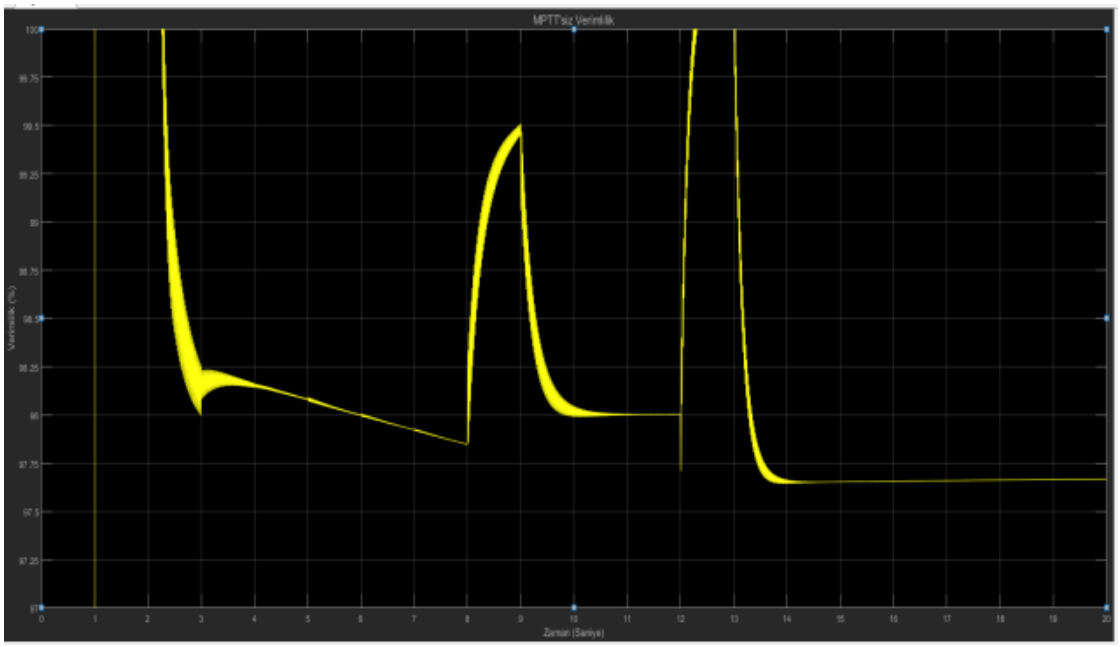

Şekil 21. MPPT'siz FV sistemin verimliliği

Bulguların Karşılaştırılması

Çalışmanın bu kısmında, MPPT'li ve MPPT'siz olarak kurulan sistemler karşılaştırılmıştır. MPPT devresine sahip sistemin maksimum gücü 2kW değerine kadar çıkabilmektedir. Ancak, MPPT devresi olmayan sistemde ise maksimum güç 800W olarak görülmüştür.

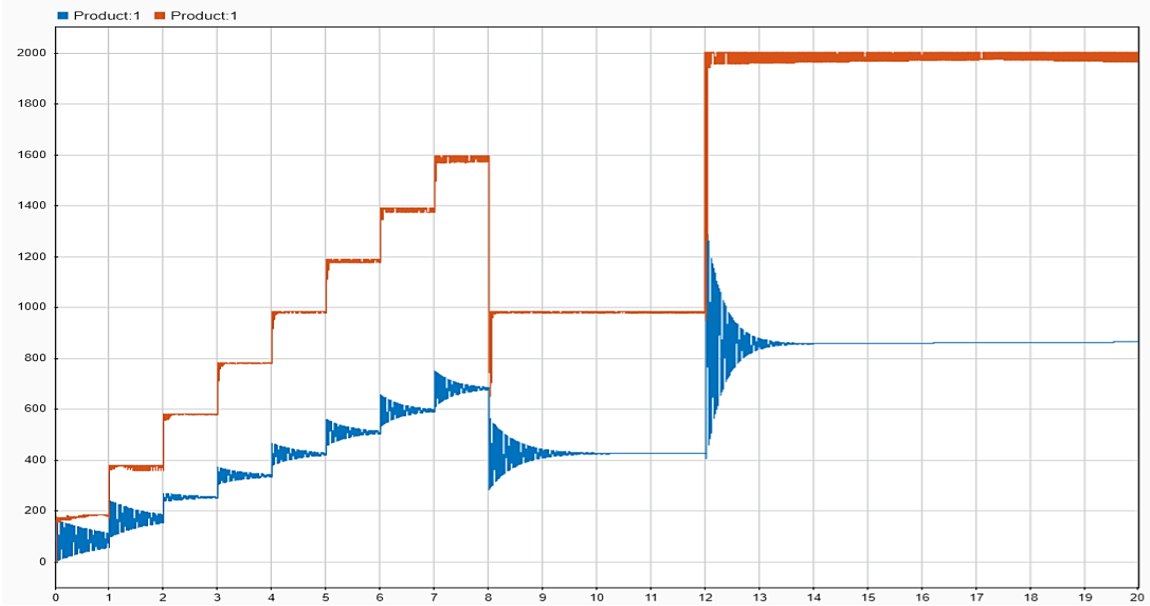

Şekil 22. İzlenen güç ve zaman grafiklerinin karşılaştırılması

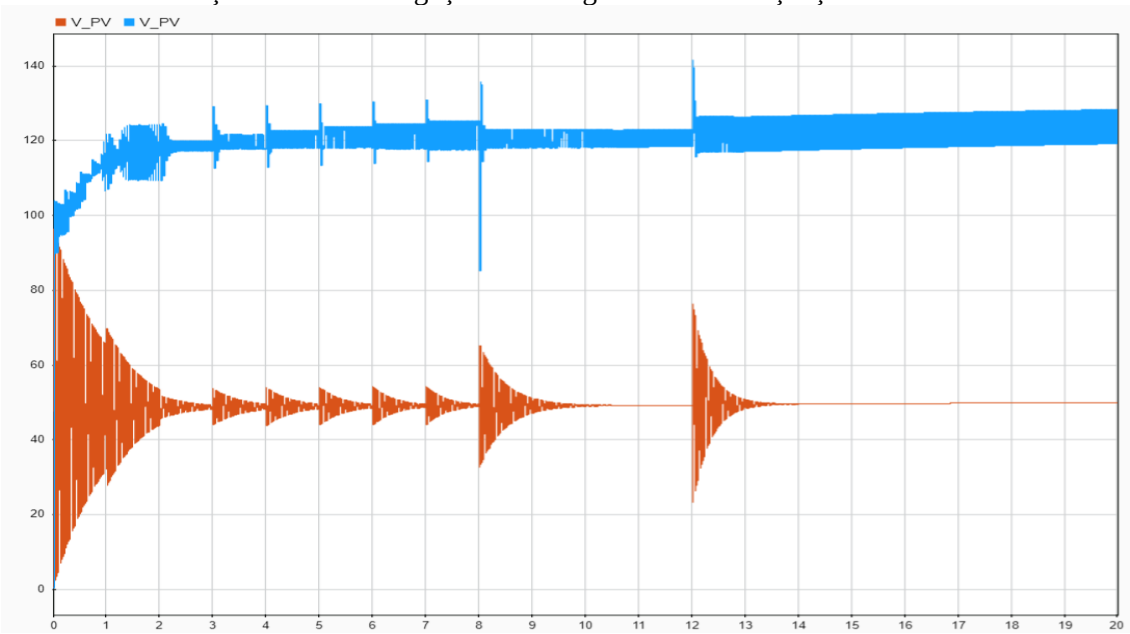

Şekil 23. Gerilim ve zaman grafiklerinin karşılaştırılması

Benzer şekilde, her iki sistemin gerilim açısından karşılaştırılması yapıldığında, MPPT'li sistemdeki gerilim 100V'dan başlayıp 120V aralığında devam etmektedir. MPPT'siz sistemdeki gerilim ise ortalama 50V değerinde ve dalgalı bir şekilde gözlemlenmiştir.

Sonuç

Bu çalışmada, fotovoltaik panellerin maksimum güç noktasında istikrarlı bir şekilde çalışmasını sağlamak için MATLAB/Simulink ortamında devreler kurulmuştur. Tasarlanan bu devrelerde, farklı güneş ışınımları altında fotovoltaik panellerden elde edilen gücün MPPT modülü kullanarak ve kullanmayarak sistemin verimliliğinin karşılaştırılması yapılmıştır. Her iki devre için elde edilen gerilim değerleri karşılaştırıldığında, MPPT modülü kullanılarak kurulan devrenin, MPPT modülü kullanılmadan kurulan devreye kıyasla yaklaşık olarak 80V civarında daha fazla bir değer elde edebildiği görülmüştür. Benzer şekilde, her iki devreden elde edilen güç değerleri kıyaslandığında, MPPT modülü olan sistemin aynı güneş ışınımı değerinde 1200W civarında daha fazla güç elde ettiği görülmüştür. Son olarak sistemlerin verimliliğine bakıldığında, MPPT modülüne sahip sistemin aynı güneş ışınım değerinde yaklaşık olarak %3 daha fazla verimlilik elde ettiği hesaplanmıştır. Buna ek

olarak, MPPT modülü olmayan sistemlerin verimliliğin güneş ışınım değerinin ani olarak değişmesi ile minimum %2, maksimum % 20 oranından dalgalandığı görülmüştür. Sonuç olarak fotovoltaik sistemlerde MPPT modülü kullanıldığında, verimin artacağı ve sürekli olacağı görülmektedir.

Referanslar

[1] Dimroth F, Baur C, Bett AW, Meusel M, Strobl G. (2005). 3-6 junction photovoltaic cells for space and terrestrial concentrator applications. In *Conference Record of the Thirty-first IEEE Photovoltaic Specialists Conference, 2005.* (525-529). IEEE.

[2] Mulligan, W. P., Rose, D. H., Cudzinovic, M. J., De Ceuster, D. M., McIntosh, K. R., Smith, D. D., Swanson, R. M. (2004). Manufacture of solar cells with 21% efficiency. *Proc. 19th EPVSEC, 387*.

[3] Batman MA. (2001). *Elektrik Üretimi İçin Güneş Pillerinin Kullanımında Verimi Arttırıcı Yeni Bir Yöntem* (Doctoral dissertation, Fen Bilimleri Enstitüsü).

[4] Larbes C, Cheikh SA, Obeidi T, Zerguerras A. (2009). Genetic algorithms optimized fuzzy logic control for the maximum power point tracking in photovoltaic system. *Renewable energy*, *34*(10), 2093-2100.

[5] Karanjkar, D. S., Chatterji, S., Shimi, S. L., Kumar, A. (2013). An improved current feedback based maximum power point tracking controller for solar photo-voltaic system. In *2013 Annual International Conference on Emerging Research Areas and 2013 International Conference on Microelectronics, Communications and Renewable Energy* (pp. 1-6). IEEE.

[6] Evran F. (2019). Azaltan ve Yükselten DA-DA Dönüştürücüleri için Tek Çevrim Denetleyici Tasarımı. *Düzce Üniversitesi Bilim ve Teknoloji Dergisi*, *7*(1), 757-768.

[7] Veerachary, M. (2005). Modelling and analysis of cascade step-down converters. *IEE Proceedings-Electric Power Applications*, *152*(1), 41-50.

[8] Ürgün, S., Erfidan, T., Çoruh, N. DA-DA Buck Dönüştürücü Tasarımı ve Gerçeklenmesi Design and Implementation of DC-DC Buck Converter.

[9] Larbes, C., Cheikh, S. A., Obeidi, T., Zerguerras, A. (2009). Genetic algorithms optimized fuzzy logic control for the maximum power point tracking in photovoltaic system. *Renewable energy*, *34*(10), 2093-2100.

[10] Deveci, O., Kasnakoğlu, C. (2014). Bir Fotovoltaik Sistemden Değişken Güneş Işınım Değerlerinde Maksimum Güç ve Sabit DA Gerilim Elde Edilebilmesine Yönelik DA/DA Dönüstürücü ve Kontrolcü Tasarımı. *DA Dönüştürücü ve Kontrolcü Tasarımı*, 187-193.

[11] Nedumgatt, J. J., Jayakrishnan, K. B., Umashankar, S., Vijayakumar, D., Kothari, D. P. (2011, December). Perturb and observe MPPT algorithm for solar PV systems-modeling and simulation. In *2011 Annual IEEE India Conference* (1-6). IEEE.

[12] Esram, T., Chapman, P. L. (2007). Comparison of photovoltaic array maximum power point tracking techniques. *IEEE Transactions on energy conversion*, *22*(2), 439-449.

[13] Xiao, W., Dunford, W. G. (2004, June). A modified adaptive hill climbing MPPT method for photovoltaic power systems. In *2004 IEEE 35th annual power electronics specialists conference (IEEE Cat. No. 04CH37551) 3*, 1957-1963. IEEE.

[14] Ort, M. İ. (2016). *Fv Sistemlerde Güneşi Takip Eden Sistem Tasarımı Ve Mppt Kontrolü İle Enerjinin Yüke Maksimum Olarak Aktarılması* (Doctoral dissertation, Fen Bilimleri Enstitüsü).

[15] Özçelik, M. A., Yılmaz, A. S. (2014). Solar Enerji Dönüşümünde, Maximum Güç Noktası İzleyicisinin Etkisi ve Kablosuz Enerji İletimine Uygulaması Effect of Maximum Power Point Tracking in Solar Energy Conversion and Its Application of Wireless Power Transmission.

Detection of Covid 19 from the Lungs X-ray Images by Using the Deep Learning Techniques

Muhammed Üsame Abdullah[1], Ahmet Alkan[1], Hanadi Abdullah Omaish[2]*
[1]Kahramanmaras Sütçü İmam Univ., Dept of Electrical & Electronics Engineering, Kahramanmaraş, Turkey
[2]Gaziantep Univ., Department of Civil Engineering, Gaziantep, Turkey
**Corresponding author: ousalab@gmail.com*

Abstract

The corona epidemic spreads frighteningly and rapidly in all countries of the world, forcing humanity to an abnormal life. Failure to fully control the epidemic and to find adequate and effective vaccines endangers human life. Fighting against the epidemic becomes important, as all these measures could not be taken in the near future. For this reason, it is important to detect whether the person caught the virus expressed in thousands of people is covid or not and to take the necessary measures.

For this purpose, an artificial intelligence-based study has been proposed that will speed up the diagnosis of the pandemic by saving labor and expense. In the study, X-Ray images were processed with the most up-to-date deep image processing techniques, and an objective decision support system was created, independent of the doctor's expertise. The proposed system can classify x-ray images as Normal, Covid -19 and Viral Pneumonia using pre-trained deep learning networks (AlexNet, GoogleNet, ResNet8 and ResNet50). The overall accuracies of the networks (AlexNet, GoogleNet, ResNet8 and ResNet50) were 95.7%, 94.5%, 95.4%, 97.4% respectively.

It is easy to diagnose in the advanced stages of the disease. As with most diseases, early diagnosis is important in covid-19. With the proposed system based on deep learning, an especially useful tool has been created in combating the pandemic by determining the disease at an early stage. The proposed system can also be used in areas with shortage of health personnel such as rural and remote areas.

Keywords: Covid-19 pandemic, deep learning, transfer learning, X-ray images

Introduction

COVID-19 is the disease caused by a new coronavirus called SARS-CoV-2. WHO first learned of this new virus on 31 December 2019, following a report of a cluster of cases of 'viral pneumonia' in Wuhan, Republic of China.

After this date, this disease turned into an epidemic that affected most countries of the world, so that all countries of the world were forced to full lockdown to limit the spread of this epidemic. This epidemic affects all age groups, but it has a great impact on people with chronic diseases, especially those related to the respiratory system. So, there are several studies in the literature from many countries around the world. These studies include artificial intelligence-based diagnosis of COVID-19 with the help of radiographs / radiographic images. Some researchers focus on using deep learning with transfer learning for detecting of COVID-19 from chest X-ray images or CT images, and other researchers focus on using IOT devices for helping in diagnosis of COVID-19, The use of deep learning models requires a large data set from reliable sources [1].

Tulin Ozturk et al. (2020) used the DarkNet model in their study as a classifier for the YOLO and they implemented 17 convolutional layers and introduced different filtering on each layer. Their dataset consists of x-ray images of the lungs divided to 125 Covid-19, 500 Pneumonia, and 500 No-Findings, their system can be employed via the cloud to immediately screen patients [2]. Ali Ardakani et al., (2020) used the Convolutional neural networks (AlexNet, VGG-16, VGG-19, SqueezeNet, GoogleNet, MobileNet-V2, ResNet-18, ResNet-50, ResNet-101, and Xception) in their study for the recognizing of the infection COVID-19 from the non-COVID-19, and their dataset consists of 1020 Computed tomography (CT) slices from 108 patients with laboratory proven COVID-19 and 86 patients with other a typical and viral pneumonia diseases (the non-COVID-19 group) [3]. Mesut Togaçar et al., (2020) used the deep learning models (MobileNetV2+SVM, SqueezeNet+SVM) in their study and

SVM as a classifier, their dataset consists of x-ray images of the lungs, the total number of images of the dataset is 458 divided into three groups Covid-19, Pneumonia, and Normal [4]. nCOVnet model was used in Panwar et al's (2020) study, this method is based on deep learning neural network, Panwar

dataset consists of 192 X-Ray images of COVID-19 and 142 images of normal X-rays, this dataset was taken from open-source compiled by Cohen et al [5,6]. CoroNet model was used in Asif's research, this model depends on Xception architecture pre-trained on the ImageNet dataset and trained end-to-end on their dataset, while their dataset was collected from the open-source Github repository by Joseph et al and from the Kaggle repository, Asif dataset's consist of the chest X-ray images divided into four groups 310 images normal,330 images Pneumonia Bacterial,327 images Pneumonia Viral, and 284 images Covid-19 [7,8]. VGG-16 is a convolutional neural network that was used in their research, Luca dataset consists of 250 X-ray images Covid-19, 2753 X-ray images other, and 3520 images healthy, they were obtained from the open-source Github repository by Joseph et al and from the Kaggle repository[8] [9].Ferhat Ucar et al., (2020) proposed method based on the SqueezeNet ,this network from deep learning model .The authors manage the training process of the SqueezeNet while performing a Bayes optimization with the validation phase [10].AytaçAltan et al., (2020) used a hybrid model consisting of 2D curvelet transform, chaotic salp swarm algorithm, and deep learning technique (EfficientNet-B0), this method for recognition of COVID-19 disease from X-ray images, their data set consisting of 1609 normal images, 263 COVID-19 positive images, and 1614 viral pneumonia images [11].

Data Set

In this study the dataset was used from Kaggle and GitHub sites, where this dataset consist of 2953 X-ray images for lungs, this dataset divided into three categories 267 images for covid-19, 1341 X-ray images for Normal health, and 1345 X-ray images for Viral Pneumonia (see Fig. 1).

Figure 1. Samples of the dataset

Computational Set-Up

MATLAB 2019B with Deep Learning Toolbox and transfer Learning algorithm are employed in the current study, this is illustrated in Fig. 2.

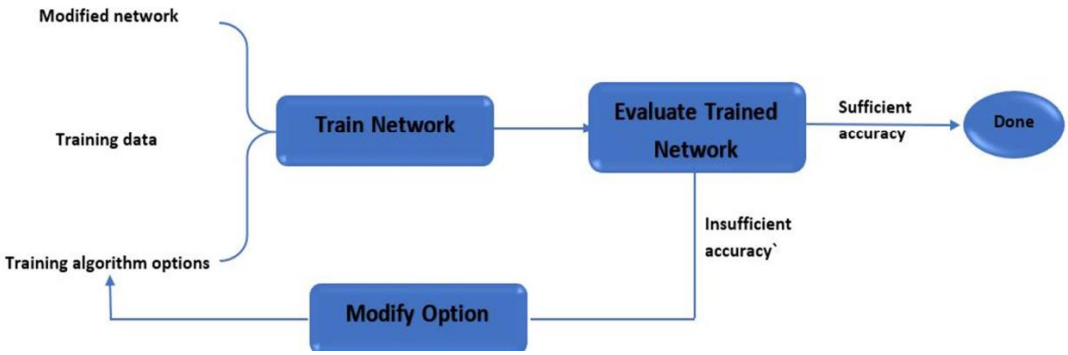

Figure 2. Workflow of Transfer Learning

Where AlexNet+TL, GoogleNet+TL, ResNet+TL, and ResNet 50+TL were used in the current study. All of those networks are pre-trained networks.

In this study, we have used a computer with CPU i7/7th, 16GB RAM, and GTX1050 4GB. These features enable the use of the GPU/CUDA to accelerate the processing in the training and the testing stages. The NVIDIA CUDA Deep Neural Network library (cuDNN) is a GPU accelerated library of primitives for deep neural networks. cuDNN provides highly tuned implementations for standard

routines such as forward and backward convolution, pooling, normalization, and activation layers[1]. Where MATLAB allows the use of NVIDIA graphics processing units to accelerate the process required by deep learning and other computationally intensive analysis units using CUDA and Parallel Computing Toolbox. Fig. 3 illustrates the architecture of using GPU with CUDA code.

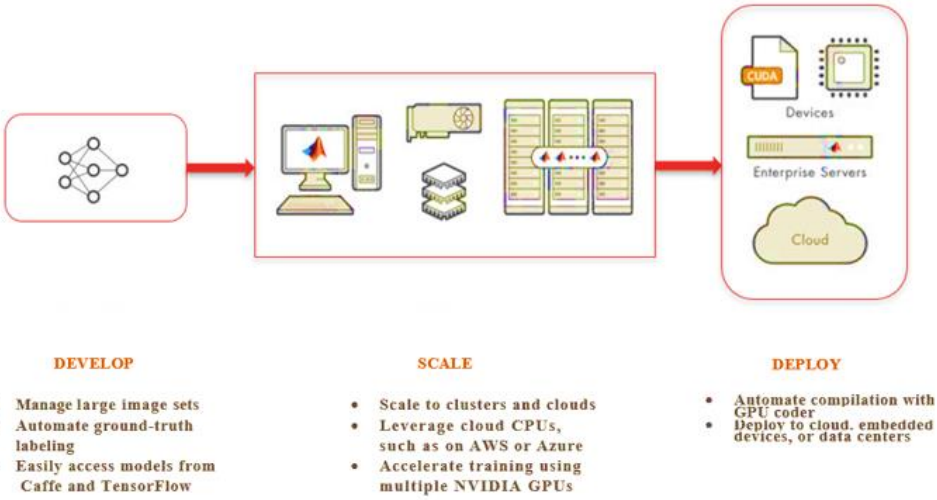

Figure 3. GPU pathway

Method

In the current study, four pre-trained networks (AlexNet + TL, GoogleNet + TL, ResNet18 +TL and ResNet50 + TL) were used to compare the accuracy of four model networks. ROC-AUC curves of four pre-trained networks + TL will be given in the experiments.

AlexNet

AlexNet is a deep convolutional neural network that was trained on a large dataset (Image Net) to classify the 1. 2 million high-resolution images with 1000 various classes [12]. It is beneficial that we use the pre-trained AlexNet architecture to build the network where the input layer refers to the input images of a size of 227×227×3 pixels Table 1 shows the Layers of the Alexnet architecture.

Table 1. Layers of the Alexnet architecture

N°	Name	Type	Description
1	Data	Image Input	227x227x3 images with 'zerocenter' normalization
2	conv1	Convolution	96 11x11x3 convolutions with stride [4 4] and padding [0 0 0 0]
3	relu1	ReLU	ReLU
4	norm1	Cross Channel Normalization	cross channel normalization with 5 channels per element
5	pool1	Max Pooling	3x3 max pooling with stride [2 2] and padding [0 0 0 0]
6	conv2	Grouped Convolution	2 groups of 128 5x5x48 convolutions with stride [1 1] and padding [2 2 2 2]
7	relu2	ReLU	ReLU
8	norm2	Cross Channel Normalization	cross channel normalization with 5 channels per element
9	pool2	Max Pooling	3x3 max pooling with stride [2 2] and padding [0 0 0 0]
10	conv3	Convolution	384 3x3x256 convolutions with stride [1 1] and padding [1 1 1 1]
11	relu3	ReLU	ReLU
12	conv4	Grouped Convolution	2 groups of 192 3x3x192 convolutions with stride [1 1] and padding [1 1 1 1]
13	relu4	ReLU	ReLU

[1] https://developer.nvidia.com/cudnn

14	conv5	Grouped Convolution	2 groups of 128 3x3x192 convolutions with stride [1 1] and padding [1 1 1 1]
15	relu5	ReLU	ReLU
16	pool5	Max Pooling	3x3 max pooling with stride [2 2] and padding [0 0 0 0]
17	fc6	Fully Connected	4096 fully connected layer
18	relu6	ReLU	ReLU
19	drop6	Dropout	50% dropout
20	fc7	Fully Connected	4096 fully connected layer
21	relu7	ReLU	ReLU
22	drop7	Dropout	50% dropout
23	fc8	Fully Connected	1000 fully connected layer
24	prob	SoftMax	SoftMax
25	output	Classification Output	crossentropyex with 'tench' and 999 other classes

GoogleNet

This pre-trained network is a convolutional neural network that is trained on more than a million images. This network contains 18 layers and can classify images into 1000 object categories, where the input layer refers to the input images of a size of 224*224*3 pixels. Fig. 4 shows the GoogleNet architecture [13].

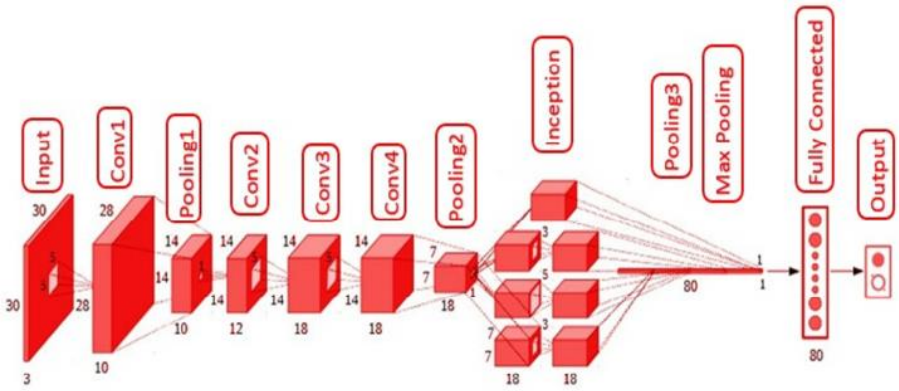

Figure 4. GoogleNet Architecture

ResNet 18

This pre-trained network is also a convolutional neural network that is trained on more than a million images‡. It contains 18 layers and can classify images into 1000 object categories, where the input layer includes the images of a size of 224*224*3 pixels (see Table 2) for the ResNet-18 architecture [14].

Table 2. ResNet-18 Architecture

Layer Name	**Output Size**	**ResNet-18**
conv1	112x112x64	7x7, 64, stride 2 3x3 max pool, stride 2
conv2x	56x56x64	$\begin{bmatrix} 3 \times 3.64 \\ 3 \times 3.64 \end{bmatrix} \times 2$
conv3x	28x28x128	$\begin{bmatrix} 3 \times 3.128 \\ 3 \times 3.128 \end{bmatrix} \times 2$
conv4x	14x 14 x 256	$\begin{bmatrix} 3 \times 3.256 \\ 3 \times 3.256 \end{bmatrix} \times 2$

conv5x	7x7x512	$\begin{bmatrix} 3 \times 3.512 \\ 3 \times 3.512 \end{bmatrix} \times 2$
Average pool	1x1x512	7x7 average pool
Fully connected	1000	512x1000 fully connection
SoftMax	1000	

ResNet 50

ResNet-50 is a convolutional neural network that is 50 layers deep. You can load a pretrained version of the network trained on more than a million images from the ImageNet database[1].The pretrained network can classify images into 1000 object categories, . As a result, the network has learned rich feature representations for a wide range of images. The network has an image input size of 224-by-224 Fig. 5 shows the ResNet 50 architecture.

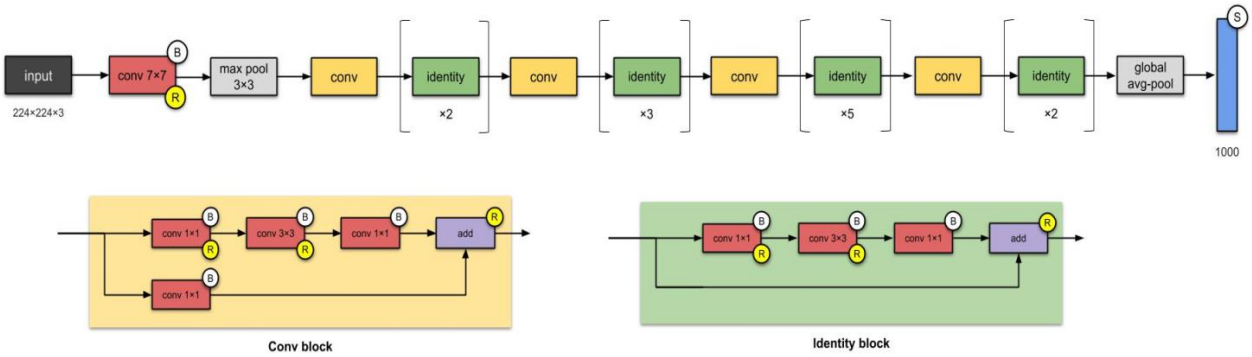

Figure 5. ResNet 50 architecture

Results and discussion

The prepared dataset images were applied to AlexNet+TL, GoogleNet+TL, ResNet 18, and ResNet 50+TL. For these operations, transfer learning (TL) was applied to four trained deep learning architectures (AlexNet, GoogleNet, ResNet 18, and ResNet 50) to get better parameterization of these architectures. features extracted from training images were used to train the model. At this stage, all the legacy network parameters were replaced with our new data (where this dataset consists of 2953 X-ray images for lungs, this dataset divided into three categories ,267 images for covid-19, 1341 X-ray images for Normal health, and 1345 X-ray images for Viral Pneumonia). We can see the results of the current study from confusion matrices, those results shown in Figures 6 to 9 respectively.

[1] https://image-net.org/challenges/LSVRC/2016/index.php

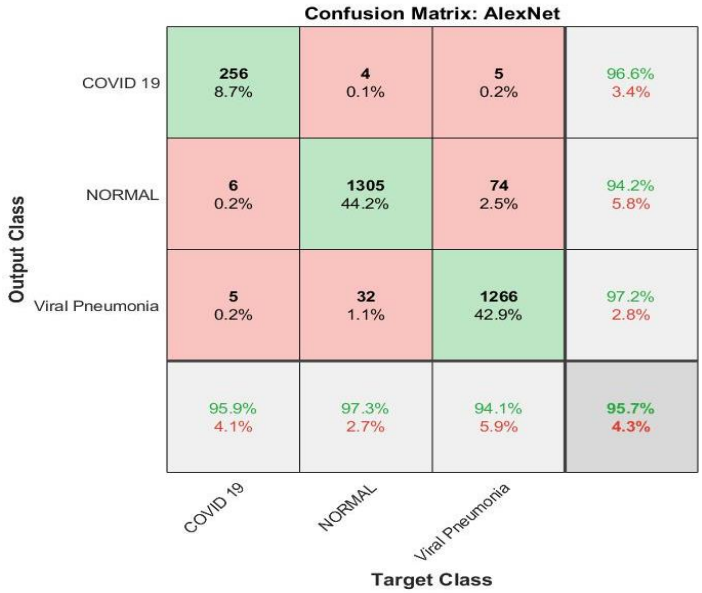

Figure 6. Confusion matrix for AlexNet+TL

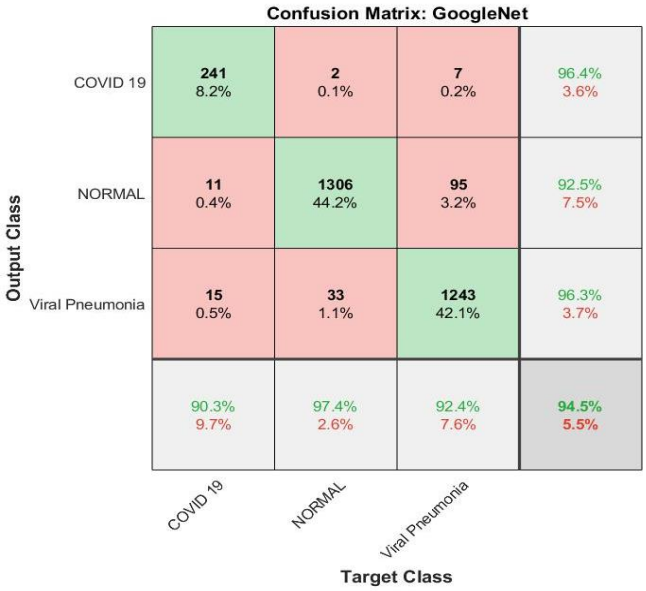

Figure 7. Confusion matrix for GoogleNet+TL

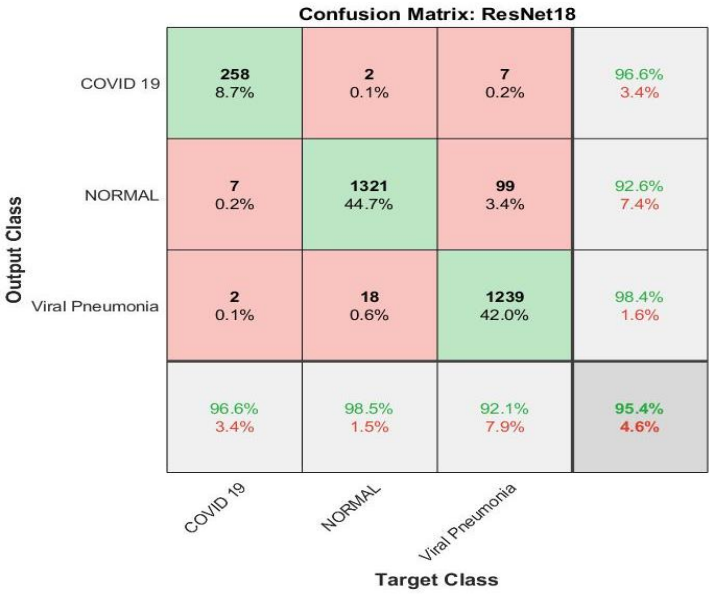

Figure 8. Confusion matrix for ResNet 18+TL

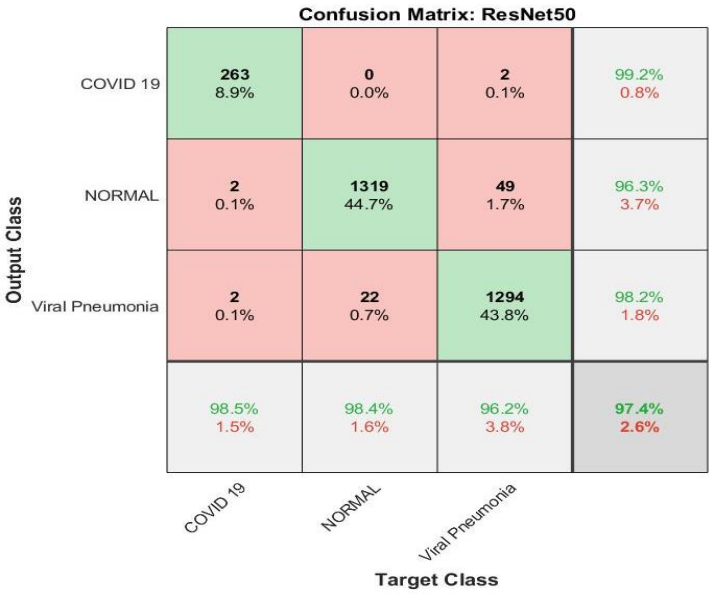

Figure 9. Confusion matrix for ResNet 50+TL

From those figures, it is clear from the confusion matrices that the best overall accuracy recorded by ResNet50 was 97.4%, then AlexNet was 95.7%, then ResNet 18 was 95.4 %, then GoogleNet was 94.5%.

Conclusion and future work

The use of smart technology in all fields of our life is increasing every day depending on technological developments, especially artificial intelligence, from those fields which developed based on artificial intelligence, is the health field. In this study, we developed a deep learning-based experimental system for automated detection of COVID-19 pandemic, Viral Pneumonia, and Normal lung health. Four various deep learning networks are employed. The highest results rate is achieved by using the ResNet 50+TL algorithm with a rate of 97. 4% accuracy. This system can detect/recognize COVID-19 automatically and rapidly, and hence our proposed system will be helpful for the doctors and scientists that study in practice.

For future projects, we plan to expand this research to connect directly with the large data in hospitals by using the internet of things, for creating a full system to detected/recognized COVID-19 and diseases of the lungs based on an online data set which updated frequently.

References

[1] Sufian A, Ghosh A, Sadiq AS, Smarandache F. A Survey on Deep Transfer Learning and Edge Computing for Mitigating the COVID-19 Pandemic. Journal of Systems Architecture.2020;101830. doi:10.1016/j.sysarc.2020.101830 .

[2] Ozturk T, Talo M, Yildirim EA, Baloglu UB, Yildirim O, Rajendra AU. Automated detection of COVID-19 cases using deep neural networks with X-ray images. Computers in Biology and Medicine.2020; 103792. doi:10.1016/j.compbiomed.2020.103792 .

[3] Ardakani AA, Kanafi AR, Acharya UR, Khadem N, Mohammadi A. Application of deep learning technique to manage COVID-19 in routine clinical practice using CT images: Results of 10 convolutional neural networks. Computers in Biology and Medicine.2020; 103795. doi:10.1016/j.compbiomed.2020.103795 .

[4] Toğaçar M, Ergen B, Cömert Z. COVID-19 detection using deep learning models to exploit Social Mimic Optimization and structured chest X-ray images using fuzzy color and stacking approaches. Computers in Biology and Medicine.2020;121, 103805. doi:10.1016/j.compbiomed.2020.103805 .

[5] Panwar H, Gupta PK, Siddiqui MK, Morales MR, Singh V. Application of Deep Learning for Fast Detection of COVID-19 in X-Rays using nCOVnet. Chaos, Solitons & Fractals.2020; 109944. doi:10.1016/j.chaos.2020.109944 .

[6] Cohen JP, Morrison P, Dao L. Covid-19 image data collection. arXiv preprint arXiv. 2020; 2003115972020 .

[7] Khan AI, Shah JL, Bhat MM. CoroNet: A Deep Neural Network for Detection and Diagnosis of COVID-19 from Chest X-ray Images. Computer Methods and Programs in Biomedicine.2020; 105581. doi:10.1016/j.cmpb.2020.105581.

[8] Cohen JP, Morrison P, and Dao L. COVID-19 image data collection, arXiv: 2003. 11597 , 2020; https://github.com/ieee8023/covid-chestxray-dataset .

[9] Brunese L, Mercaldo, F, Reginelli A, Santone A. Explainable Deep Learning for Pulmonary Disease and Coronavirus COVID-19 Detection from X-rays. Computer Methods and Programs in Biomedicine.2020; 105608. doi:10.1016/j.cmpb.2020.105608.

[10] Ucar F, Korkmaz D. COVIDiagnosis-Net: Deep Bayes-SqueezeNet based Diagnostic of the Coronavirus Disease 2019 (COVID-19) from X-Ray Images. J Medical Hypotheses.2020; 109761. doi:10.1016/j.mehy.2020.109761.

[11] Altan A, Karasu S. Recognition of COVID-19 disease from X-ray images by hybrid model consisting of 2D curvelet transform, chaotic salp swarm algorithm and deep learning technique. Chaos, Solitons & Fractals.2020; 110071. doi:10.1016/j.chaos.2020.110071

[12] *Krizhevsky A , Sutskever I, Hinton GE.* ImageNet classification with deep convolutional neural networks . *Communications of the* Association for Computing Machinery.*2017; 60 (6): 84–90.* doi*:*10.1145/3065386.

[13] Bengio Y. Deep learning of representations for unsupervised and transfer learning. In: Proceedings of International conference of Machine learning Workshop on Unsupervised and Transfer Learning.2012; 17-36.

[14] Guo Z, Chen Q, Wu G, Xu Y, Shibasaki R et al. Village Building Identification Based on Ensemble Convolutional Neural Networks. Sensors Journal 17.2017; (11): 2487-2508. doi: 10.3390/s17112487.

A Review of Solidity and Rotor Size Effects on Water-Pumping Windmills

*Omar Abdulkareem Qasim**, *Ahmet Samancı*
Necmettin Erbakan University, Department of Energy Systems Engineering, Konya, Turkey
**Corresponding author: oh95er@gmail.com*

Abstract

The windmill is one of the important applications of wind energy and it is one of the best and the easiest ways to manipulate this wind power and use it for water pumping. The best feature of windmills is their high solidity, which gives high torque at the starting. Therefore, they will be able to lunch at low wind speeds like 2 m/s which gives a great possibility of utilizing, especially in the agricultural countries. This feature has been the focus of attention of researchers and developers over the long years. There are several factors affected by it, the most prominent of which is the number of blades and the diameter of the rotor. Some researchers have tested with different models of different diameters and others did on different numbers of blades. The challenge is how to find a model with an ideal number of blades and diameter that can give us the highest torque value under low wind conditions. In this paper, the multi-bladed horizontal axis wind turbines, which are used for water pumping, are discussed. Besides, the literature review is described, which presented the basic design requirements for windmill rotors as solidity, diameter, and tip speed ratio, also information given about materials that used in manufacture. The investigations of this paper are focused on the effect of the number of blades to reach the main goal and the best performance at located wind speeds.

Keywords: multi-bladed windmill, wind energy, Horizontal axis wind turbine, solidity, tip speed ratio

Nomenclature

A = Area, area of swept by turbine blades
σ = Solidity
C_P = Coefficient of power
C_Q = Coefficient of torque
T = Torque
λ = Tip speed ratio
ω = Blade tip velocity
R = Radius
V = Wind speed
BET = blade element theory
OJF = Open jet facility
Ø = Rotor diameter
N = Number of blades
R_s = Capital cost
S = Solid rotor area

Introduction

Wind energy has been in use since the old period. Mechanical power was commonly provided from this energy for water pumping and grain grinding until around the early 20th century. In ancient days back to 3500 BC, wind energy was used to produce aerodynamic push to meet incredibly low energy demands to drive boats [1]. Little is known about windmills' early history. They appear to have been developed in Persia, now in Iran, or in Mesopotamia, which is today in Iraq. Certain windmills appeared in China for the first time. The first windmill in China was built and it was a vertical windmill axis with long curved strips of metal-like blades [2]. The windmill has a rather durable design with simple and cheap components. The device is easy to use and requires minimal servicing. The invention of steam turbines. The windmills use in Europe is decreased because of the invention of steam engines and the focus on the production of wind pumps was moved to the USA and Australia. In the United States by the 1880s there were built around six million wind pumps, and most of these pumps are no longer operating due to various competition from other water pumping facilities, but an estimated one million

wind pumps continue to be used worldwide. The "oil crisis" has led to the re-examination of wind energy and encouraged industrialized countries to start major research programs, with a view to modern wind turbines producing large-scale electricity [3,4]. Wind power has been the most common power technology for many countries worldwide. In 2010 a 22.5% growth was shown in the report of Global Wind Energy Council, adding 35,802 MW to 194,390 MW of total installations [5]. The uses of wind pumping include community and domestic water sources, equine watering, irrigation, drainage, and salt cups [6]. The study, its applications, economics, and potential on the state of the art in the field of wind pumping were made by Smulders [7], Smulders, and de Jongh [8]. Mohsen and Akash have written on the possibility of using wind energy for water pumping in different locations in Jordan [9]. Al-Suleimani and Rao investigated the efficiency of pumps with an average velocity at various wind speeds and monthly water production and compared the findings with the manufacturer's design standards [10]. Hammad has shown that photovoltaic wind pumping mechanical systems are cheaper economically than the diesel water pumping system in Jordan [11]. In a given water pumping scenario, Bragg and Schmidt proposed an optimal procedure for selecting pumps and windmills [12]. Elamouri presented perspectives of wind mechanical pumping in eight synoptic sites distributed in the Tunisian south. The wind resource analysis, based on meteorological data recorded for five years, showed that the south of the country has a good wind potential. The annual mean wind speed is between 2.7 and 5.08 m/s [32]. Liu employed numerical simulation to optimize the geometry parameters, the optimization values of those parameters are determined. The pressure rise of the optimization multiphase pump is increased by 12.8 KPa in comparison to the base pump. Results showed that the distributions of gas volume fraction (GVF) and the pressure became more uniform after optimization, which improves the transporting performance of the multiphase pump [40]

Multi Bladed Windmills

The windmill is a device that converts kinetic energy to mechanical power and use this power for pumping water for various irrigation uses and they are one of the earliest ways to harness wind energy to pump water, also wind turbines do the same thing in addition to electricity generation, but to use wind turbine for water pumping, the average wind velocity must be greater than 5 m/s so that they can be replaced with windmills which has the ability to lunch under low wind speed conditions since there is a much greater share of the swept field occupied by the rotor blades[13]. Most of the windmills for water-pumping applications are horizontal-axis and have multi-bladed rotors that can provide the high starting torque necessary to initiate the operation of a water pump, in Fig. 1 a windmill water pumping machine schematic is shown [14].

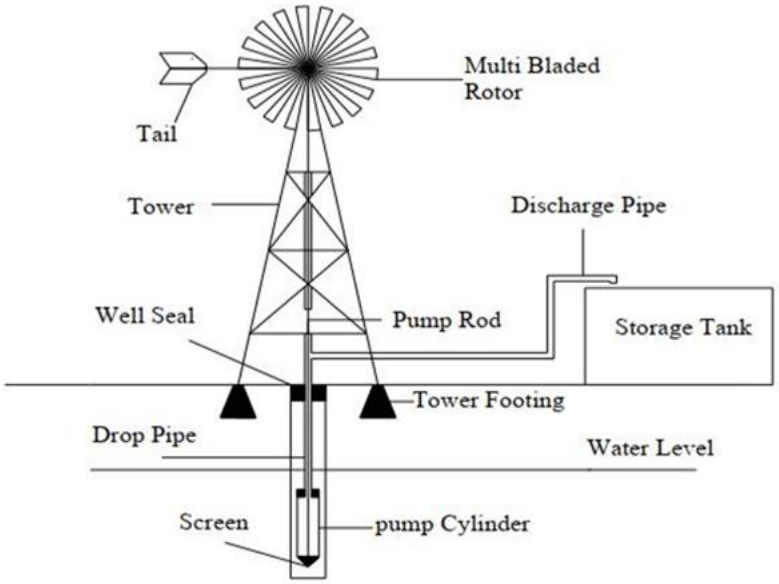

Figure 1. Schematic diagram of windmill water pumping system [14]

Farm and dutch types of windmills shown in Fig. 2 are ones that have excellent power and starting torque ranged between 0.15 and 0.25, but the starting torques of modern propeller turbines are low and power coefficients are low between 0.40 and 0.50[13]. Rotor concepts and power coefficients are shown in Fig.3.

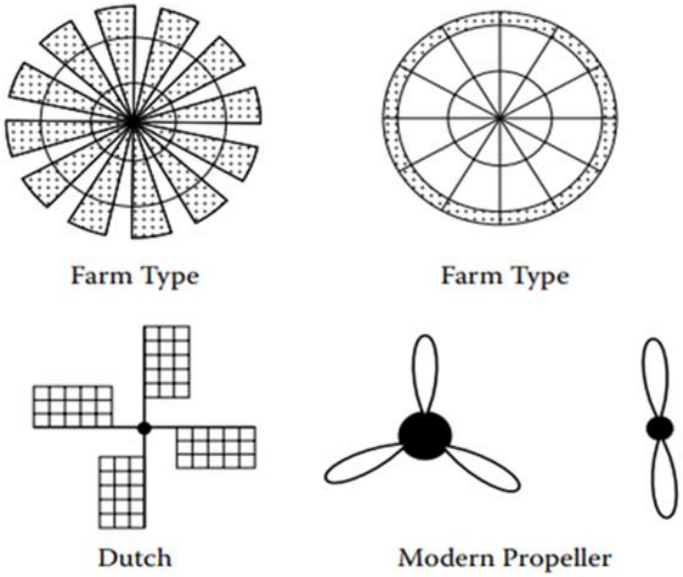

Figure 2. Different types of wind turbines [13]

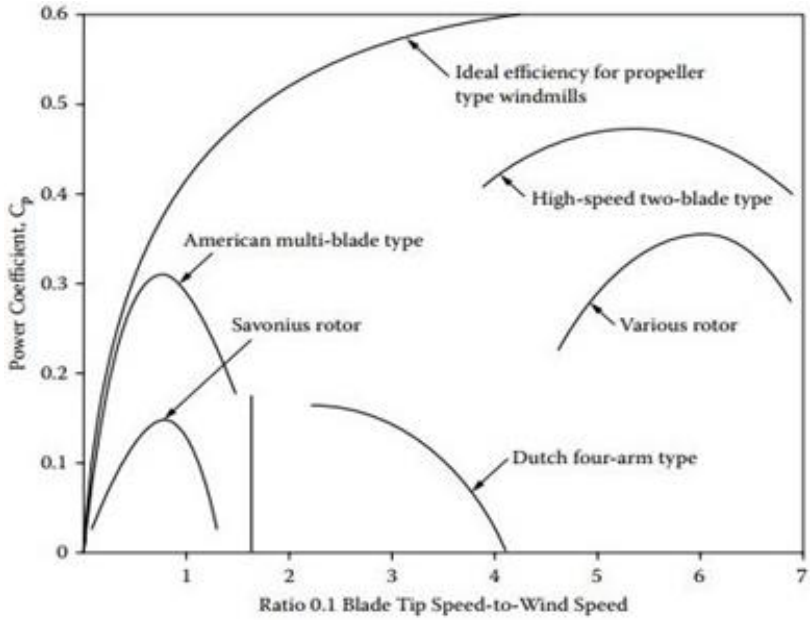

Figure 3. The C_p as a function of λ for different wind machines designs [15]

Basic Design Requirements of Multi-Bladed Windmills

There are three general important basics in designing a windmill, High torque (T), High solidity (σ) and relatively low tip speed ratio (λ), low rpm ω. In order to get a high starting torque which is required for starting a reciprocating water pump, a windmill must have a high solidity and low tip speed by increasing the number of blades or designing a multi-bladed one [2,13,14].

Effect of Number of Blades

Significant factors involved in the determination of the number of blades are Impact on the coefficient of power (C_P), design of tip speed ratio, and reducing the gyroscopic fatigue using yaw rate.

We can define solidity as a ratio between the actual blade areas to the swept area of the rotor (A), also high solidity makes the rotor starting easily, due to increasing the interaction area with the wind. Increased solidity can also increase the torque for a given rotational speed, thus increasing the power output. Kentfield [16] described that High solidity windmill produces much higher torque at a low-tip speed ratio relative to the modern one. Rector and Visser [17] tested a six-bladed design on an open test site and demonstrated that increased blade numbers potentially give the advantage of lower rotor speed variations in turbulent wind flow conditions due to increased rotor inertia. Duquette et al [18] tested the effect on the efficiency of the rotor solidity and the number of blades was at the test site in this analysis, they tested separate rotors, with the same diameter of 510 mm, under controlled conditions in a wind tunnel. They found that raising the number of blades from 3 to 12, while retaining a constant strength of 10%, decreased aerodynamic efficiency, due to low Reynolds number effects, although wind tunnel blockage impacted results. Sarkis and Pinilla [19] tested two different designed 10-bladed rotor types, each with a rotor diameter of 300 mm, in the second rotor type, which was based on the aerodynamic principle of the rotor relative to the first, substantial increase in aerodynamic performance has been made. Aized et al [2] used a 16-bladed rotor model in this investigation the numerical method which was designed on a solid edge as shown in Fig. 4, the radial length of each blade and rotor diameter were (1.2 m – 3m) respectively. He tested the model at different wind speeds varies between (2.5m/s-5 m/s) wind speed and given results estimated that For wind speed of 3.5 m/s, a windmill having 10 ft diameter can deliver about 250 GPH of water for use in irrigation, livestock and domestic purpose, also results showed that increased wind speeds increase the water flow and mechanical power.

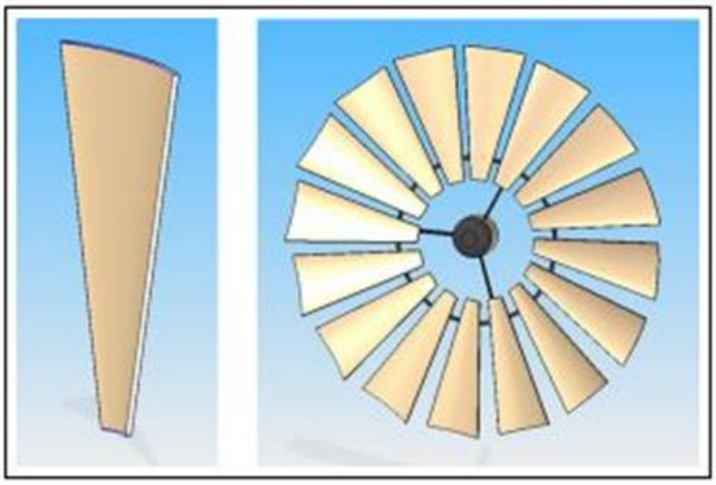

Figure 4. Aized's 16-bladed rotor model was designed on a solid edge [2]

Fagbenro et al [20] studied high solidity effects on a revolving arc-bladed windmill rotor. Their computational analysis found that the solidity did affect lift and drag coefficients and estimated that increasing the solidity decreases the lift, but increases the lift-to-drag ratio, which is the usual factor of the blade element performance of the wind turbine. Also, the angle at which maximum Lift: Drag occurs increases in solidity with huge ramifications for enhancing windmill performance. Purohit and kandpal [21] showed in their study costs of 5 different wind turbine pumps manufactured in India were compared and the most suitable model at low speeds was determined. Table 1 shows compared models in the study, where Cut_i & Cut_o represent the cut in and cut out wind speed (V) in (m/s) respectively.

Table 11. Design features of windmill pump that compared by Purohit and kandpal [21]

Model No	Ø (m)	Type	N	S (m^2)	V (m/s)			(R_s)
					Cut_i	rated	Cut_o	
GM - 11	3	Geared	18	4.55	22.2	33.3		74100
SICO	3	Geared	18	5.17	22.2	5.00	23.89	113400
AV - 45	4.5	Geared	18	7.63	1.8	2.8	10	98489
AV – 55	5.5	Geared	24	10.70	1.5	3.0	10	130675

APOLY – 12-PU-500	5	Geared	12	6.19	2.5	5.0	10.0	45000

Note: US$1 = Rs. 45.42 on October 2003

John et al [22] tested a 3,6,12 and 24 bladed model of the windmill with a diameter of 0.68m for each model. The investigation was made in two different test sizes wind tunnels, one of them had a high blockage of 36.3%, and the other with negligible 4.5% blockage. It has been found that Blade Element Theory (BET) is correct except for low tip speed ratios, where it under-predicts the torque, mostly due to the high torque solidity. The study indicates that high blockage has a large effect on rotor output. A comparison of measured and predicted torque and power coefficients of every model is shown in Table 2, where the (OJF) is the open jet facility and the (C_Q) represents the coefficient of torque.

Table 12. Comparison between torque and the power coefficients for models that were tested [22]

Rotor parameters	N = 3		N = 6		N = 12		N = 24	
	OJF	BET	OJF	BET	OJF	BET	OJF	BET
$C_{P,max}$	0.097	0.095	0.165	0.161	0.219	0.228	0.252	0.247
λ_{opt}	1.207	1.4	1.168	1.3	1.099	1.1	1.008	0.9
$C_{Q,max}$	0.075	0.069	0.141	0.126	0.2196	0.207	0.350	0.299
λ_{run}	2.317	2.2	2.244	2	2.197	1.9	2.058	1.9

Keawsuntia [23] tested a windmill model with 12 blades and 1m diameter, curvature plate ratio of 0.07, the chord length of 0.112 m, the length of 0.3 m, the blade setting angle of 30 degrees, 1 mm nominal thickness of aluminum, wind velocity inside wind tunnel was 3 m/s. A comparison between mathematical and experimental results was made and shown in Fig. 5. The maximum power coefficient is approximately 0.296 at a rate of tip speed of 1.18 and a mathematical model had a similar power coefficient with the experimental physical model.

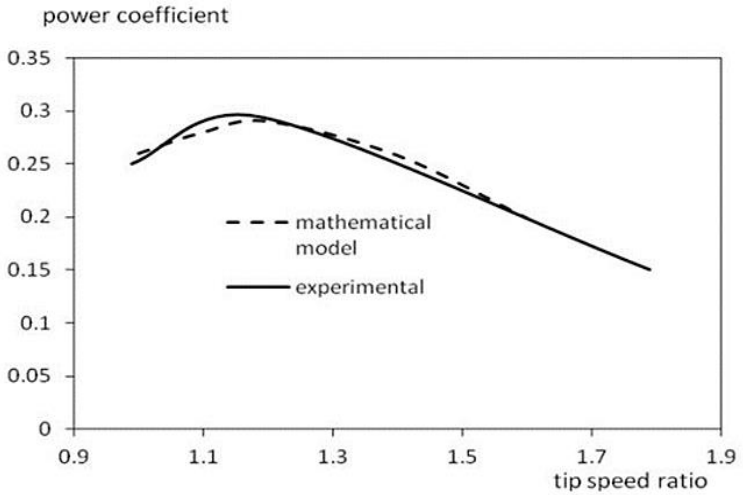

Figure 5. Comparison between mathematical and experimental results [23]

Diameter of Rotor

The scale of windmill rotor which is in use at the present ranges varies between 2 to 10 meters in diameter, in particular multi-bladed types [24,25]. The large size of the windmill rotor diameter about 10 meters is usually used for sprinkler irrigation and it is coupled to centrifugal pumps, but small sizes of rotor diameter are used to small size farm irrigation, domestic water supply, and watering livestock and piston pumps couples to this size [23]. As we know, increasing rotor size could give a better performance but at the same time, we must consider the increase in cost as well as the increase in weight. Through our review of previous experiments carried out by researchers from various countries, we noticed that the values of the rotor diameter ranges vary between 1 and 10 meters, which may be appropriate for the wind speed that is sufficient to rotate the rotor. Table 3 shows rotor diameter values for the previous studies.

Table 13. Rotor diameter and operated wind speeds values for previous studies

Author's Name	Year	N	Ø (m)	V (m/s)
Aized et al [2]	2019	16	3	3.5
Awad [26]	2019	24	2.5	3.5
Prabkeao & tantropiwat [27]	2018	30	4.2	2
Adinoyi et al [28]	2017	3	2.14	1.8-2.1
Hendiriana et al [29]	2015	6	7.5	4
Keawsuntia [23]	2013	12	1	3
Peillon et al [30]	2013	8	2.2	2.77
Sun et al [31]	2011	3	6	3
Benfarhat et al [33]	2005	8	2.5	3
Purohit &kandpal [21]	2004	12-18-2	3 - 5	3.33 - 5
Harries [34]	2002	12	6-12	5
Wegrif [35]	1984	6-12-24	6	3-5

Tip Speed Ratio

We can define Tip Speed Ratio (λ) as the ratio of blade tip velocity (ω) rad/s, at radius (R) m to the speed of the wind (V) m/s and it is numerically represented as:

$$\lambda = \frac{\omega R}{V} \tag{1}$$

The relationship above shows that the value of λ is zero when the windmill is stationary, also when the value of λ equals 1 this means that the blade tips are moving at the same speed as the wind and the efficiency of turbines reaches the maximum value. According to Le Gourière [35] relationship between λ and power coefficient Cp is shown for the American multi-bladed windmill Fig.6.

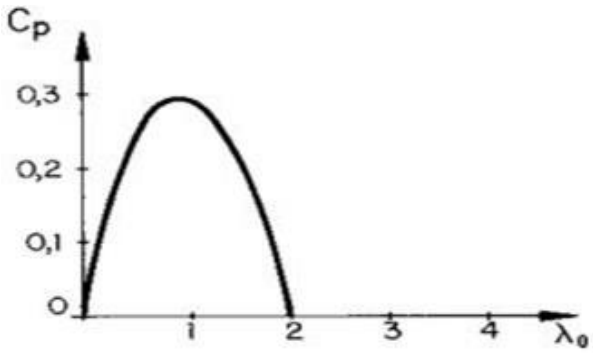

Figure 6. Relationship between λ and C_p for American multi-bladed windmill [35]

The relationship shown above can changes by using different models. Aized et al [2] calculated the relationship between power coefficient and tip speed ratio for his 16-bladed model and compared the results with Eschenbach W [39] and it's shown in Fig. 7. If the top speed is high, it requires a short choral length, which decreases the dimensions of the blade and the material used, but it also has an aerodynamic centrifugal frictional loss. Piston pumps operated at high torque values which can be reached with decreasing λ values [2].

The rotors with tip speed ratio ranges (1-2) have high torque, low rpm. They include multi-bladed windmills and rotors which are better for water pumping. They have low efficiency because of rotational wake due to relatively high torque of windmill. They have high solidity and contains 12, 16, 18 or 24 blades mounted on hub. Besides, there simple design, large, curved blades. Also, the have low noise due to low rotation and less sliding Parts. Finally, low frictional and hydraulic losses in pipes due to low rotational and pump speed.

The rotors with tip speed ratio up to 10 have low torque high rpm. 2–3 bladed wind turbines are suitable for utilization in the electricity generation. They have high efficiency up to 40% relative to Betz

limit. They have low solidity (usually 2 or 3 blades). The design considerations are very crucial, where thin aerofoil blades are used. They have relatively high noise. The frictional losses are increased as rotational speed increased [2].

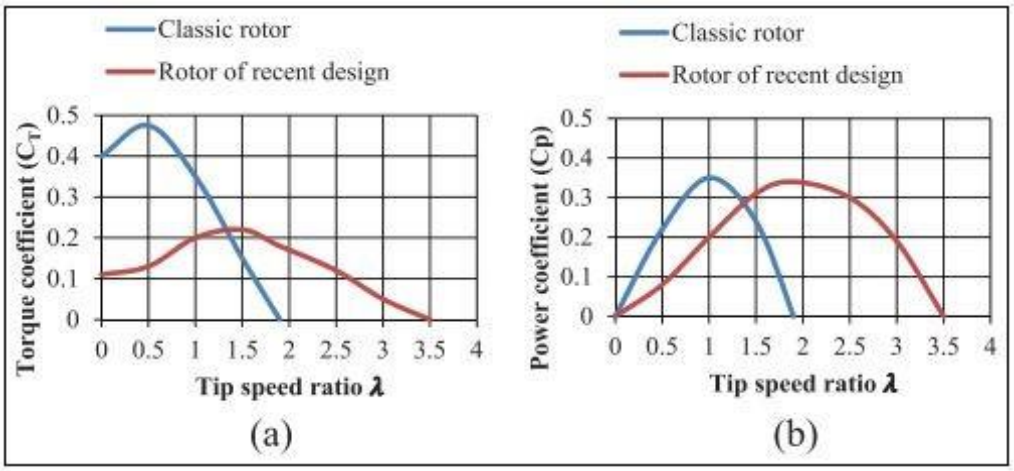

Figure 7. Dimensionless (a) torque-speed and (b) power-speed characteristic of wind rotors [2,39]

Material Selection

The most common materials used in manufacturing windmill rotors are Wood, Aluminum Extrusions, and Molded Plastic. Wood is simple to work, easily feasible, and with strong mechanical qualities, which can be classified as one of the most durable materials. Wood can be used simply with hand tools. Lightweight about 1/3 the density of aluminum. Good strength properties. Paints & stain coatings can be employed but they have poor formability [36].

Aluminum alloys also can be used for the manufacturing of rotors since they have good mechanical properties. Lightweight about which is about 1/3 of that for copper or steel. They can be easily formed and extruded in a wide variety of complex shapes including multi-void hollows. Mechanical and chemical prefinishes can be applied besides, also the anodic coatings, paints, and electroplated finishes can be applied.

Plastic molding is one of the good choices for the manufacturing of the rotors since this operation can be applied for mass production. Very lightweight of the products (rotors) about 60% of the weight of aluminum. High range of the tensile strength which varies from (0.08 to 8) of aluminum extrusions for glass-filled compounds. Easily molded into different desired shapes and the Colors can be integrated with the plastic materials [37].

Conclusion

From our literature review research of wind energy and windmill water pumping technologies, we estimated that using green energy has more benefits than other fossil types, starting from economic advantages and take by the way decreasing gas emissions. Windmills are devices that can transfer the kinetic energy of wind to mechanical power and use it for water pumping to provide water for livestock or irrigation. The design of these windmills has some basic requirements which we touched on some of them in this review as solidity or number of blades effects, tip speed ratio, and rotor diameter, also a comparison between some common materials that used in manufacturing was shown, most important notes and the most important results of our study can be summarized as follows:

- Wind pumps can perform well at low wind speeds.
- When the tip speed ratio is equal to 1 the wind and the performance of the turbines are equal to the highest or maximum value.
- In order to get a high starting torque, the windmill must have a high solidity and low tip speed by rising the number of blades.
- Increasing the number of blades decreases aerodynamic efficiency.
- At high wind speeds wind pump gives high mechanical power and water flow rate but overall efficiency decreases.

- Increasing the solidity decreases the lift but increases the lift-to-drag ratio.
- Increasing rotor size could give a better performance but increases the costs.
- The diameter of the rotor ranges between 1 and 10 meters, which may be suitable for the wind speed that is necessary to rotate the rotor.
- The selection material of rotor blades depends on shape design and the number of blades that are necessary to estimates the cost.

References

[1] Perez R, Schlemmer J, Moore K, et al. Satellite-derived resource assessment in Afghanistan & Pakistan in support of the USAID South Asia regional initiative. Final report. NREL subcontract # AEJ65517201, 2007. Golden, CO: National Renewable Energy Laboratory.
[2] Design and analysis of wind pump for wind conditions in Pakistan Tauseef Aized, Syed Muhammad Sohail Rehman, Sajid Kamran, Ali Hussain Kazim and Syed Ubaid ur Rehman. Advances in Mechanical Engineering 2019, Vol. 11(9) 1–18
[3] Wind-powered Water Pumping in Asia and The Pacific. (1991). Economic and Social Commission for Asia and Pacific, United Nations, New York.
[4] Investigation and Analysis of Wind Pumping System for Irrigation in Bangladesh by Sultan Ahmmed. A Doctor of philosophy in mechanical engineering thesis. Bangladesh University of engineering and technology, Dhaka February 2002.
[5] Global wind energy Council (GWEC), /http://www.gwec.net/index. php?id=180S; 2011 [accessed 27.03.11].
[6] Smulders PT. Wind water pumping: the forgotten option. Energy for Sustainable Development 1996; 5:8–13 II.
[7] Smulders PT. Wind energy for water pumping in developing countries. In: Proceedings of the 6th EWEC conference, Rome; 1986. 1, p. 99–105.
[8] 8- Smulders PT, de Jongh J. Wind water pumping: status, prospects and barriers. Renewable Energy 1994;5(1):587–94.
[9] Mohsen MS, Akash BA. Potentials of wind energy development for water pumping in Jordan. Renewable Energy 1998;14(1–4):441–6
[10] Al-Suleimani Z, Rao NR. Wind-powered electric water-pumping systeminstalled in a remote location. Applied Energy 2000;65:339–47.
[11] Hammad M. Photovoltaic, wind and diesel: a cost comparative study of water pumping options in Jordan. Energy Policy 1995;23(8):723–6
[12] Bragg GM, Schmidt WL. Performance matching and optimization of wind powered water pumping systems. Energy Conversion and Management 1979;19:33–9
[13] Wind Turbine Technology, A.R. Jha, Ph.D. CRC Press Taylor & Francis Group 6000 Broken Sound Parkway NW, Suite 300 Boca Raton, FL 33487-2742.
[14] Feasibility study of a wind powered water pumping system for rural Ethiopia Misrak Girma, , Marta Molina and Abebayehu Assefa AIMS Energy, 3 (4): 851–868. DOI: 10.3934/energy.2015.4.851.
[15] Johnson, G. L., 1985, Wind Energy Systems, Prentice-Hall, Englewood Cliffs, New Jerse
[16] 16- Kentfield, J., 1996, The Fundamentals of Wind-Driven Water Pumpers, Gordon and Breach, Amsterdam.
[17] Rector MC and Visser KD (2006) Solidity, blade number, and pitch angle effects on a one kilowatt HAWT. In: AIAA-2006-0608, 44th.
[18] Duquette MM, Swanson J and Visser KD (2003) Solidity and blade number effects on a fixed pitch, 50W horizontal axis wind turbine.Wind Engineering 27(4): 299–316
[19] Sarkis N and Pinilla AE (2006) Experimental study on a model of a commercial windpumping rotor. Wind Engineering 30(6): 511–520.
[20] Fagbenro K, Mohamed M and Wood D 2014 Computational modeling of the aerodynamics of windmill blades at high solidity Energy Sust. Dev. 22 13-20.
[21] Pallav Purohit, Tara C. Kandpal, Techno-economic evaluation of water pumping windmills in India, Int. J. Global Energy Issues, Vol. 21, No. 3, 2004

[22] Itoje H John, Jerson R P Vaz and David Wood, Aerodynamic performance and blockage investigation of a cambered multi-bladed windmill, Journal of Physics: Conference Series 1618 (2020) 042003
[23] Yuttachai Keawsuntia, A Study on Water Pumping by Using a Small Multi-Blades Windmill for Used in a Remote Area, Advanced Materials Research Vols 724-725 (2013) pp 527-530
[24] Chilcott RE. Wind Powered Water Lifting Devices for Small Scale Irrigation. FAO/DANIDA, Workshop on Water Lifting Devices in Asia and Near East, (1979)
[25] Harrtmut Bossel, Low Cost Windmill for Developing Countries Multivane Type. VITA, USA, (1977)
[26] Ahmad S. Awad, Practical Design And Testing Of Wind Driven Water Pumping Systems, International Journal of Mechanical Engineering and Technology (IJMET) Volume 10, Issue 03, March 2019, pp. 1419-1430.
[27] Chamlong Prabkeao and Akapot Tantrapiwat, Study on wind energy potential for agricultural water pumping system in the middle part of Thailand, MATEC Web of Conferences 192, 03058 (2018).
[28] Odesola IF, L.G.Adinoyi, Development of Wind Powered Water Pump, International Journal of Engineering Science and Computing, April 2017, Volume 7 Issue No.4.
[29] Dena Hendriana, Tommy Firmansyah, Joga Dharma Setiawan and Dodi Garinto, Design and Optimization of Low Speed Horizontal-Axis Wind Turbine Using Openfoam, ARPN Journal of Engineering and Applied Sciences, VOL. 10, NO 21, NOVEMBER, 2015.
[30] Peillo´ n M, Sa´ nchez R, Tarquis AM, et al. The use of wind pumps for greenhouse microirrigation: a case study for tomato in Cuba. Agr Water Manage 2013; 120: 107–114.
[31] Xiaojing Sun, Wanli Zhou, Diangui Huang, and Guoqing Wu, Preliminary Study on Thematching Characteristics Between Wind Wheel and Pumping Wind-Powered Water Pumping System, journal of renewable and sustainable energy 3,023109,(2011)
[32] Elamouri, Mustapha & Ben Amar, Fathi. (2016). Wind pumping assessment as source of renewable energy Wind pumping assessment as source of renewable energy.
[33] Benfarhat K, Terki F, Goutali I. Determination of The Loads Acting on The Pump Rod of a Water Pumping Windmill, Rev. Energ. Ren. Vol. 8 (2005) 73 – 80.
[34] Mike Harries, Disseminating Wind Pumps in Rural Kenya—Meeting Rural Water Needs Using Locally Manufactured Wind Pumps, Energy Policy 30 (2002) 1087–1094.
[35] Wegereef E. Scale model of the ITDG 6meter rotor wind tunnel tests for different bade setting angles. Report of Twente University of Technology, Netherlands, windmill group.Report WM 076, 1984.
[36] Le Gourière D., L'Énergie Éolienne – Théorie, conception et calcul practique des installations, 2nd edition, Eyrolles, Paris, 1982.
[37] Mario Alejandro Rosato, Small Wind Turbines for Electricity and Irrigation Design and Construction, CRC Press Taylor & Francis Group 6000 Broken Sound Parkway NW, Suite 300 Boca Raton, FL 33487-2742.
[38] Ronak D Gandhi, Pramod kothmire, Debarshi Sharma, Bhushan kumbhare, Shubham Choukade, Design and Development of Windmill Operated Water Pump, International Journal of Engineering and Technical Research (IJETR) ISSN: 2321-0869 (O) 2454-4698 (P), Volume-3, Issue-12, December 2015.
[39] Eschenbach W. Wind systems for pumping water: a training manual. Washington, DC: Peace Corps. Information.Collection and Exchange, 1984.
[40] Ming L, Lei T and Shuliang C. Design method of controllable blade angle and orthogonal optimization of pressure rise for a multiphase pump. Energies 2018; 11: 1048–1068.

Numerical Solution of Dirichlet Boundary Value Problems using Mesh Adaptive Direct Search Optimization

Muhammad Jalil Ahmad[1], Korhan Günel[2]*
[1]Aydın Adnan Menderes University, The Graduate School of Natural and Applied Sciences, Dept. of Mathematics, Aydın, Turkey
[2]Aydın Adnan Menderes University, Faculty of Arts & Sciences, Dept. of Mathematics, Aydın, Turkey
**Corresponding author: jalilahmad82@hotmail.com*

Abstract

This study gives a different numerical approach for solving second order differential equation with a Dirichlet boundary condition. Mesh Adaptive Direct Search (MADS) algorithm is adopted to train the feed forward neural network used in this approach. As MADS is a derivative-free optimization algorithm, it helps us to reduce the time-consuming workload in the training stage.

The results obtained from this approach are also compared with Generalized Pattern Search (GPS) algorithm.

Keywords: ordinary differential equation, Dirichlet boundary value problems, derivative-free optimization, direct search algorithm, mesh adaptive direct search

Introduction

Differential equations are considered as an important tool for mathematical modeling of a real-world problem. Most of these problems have nonlinear characteristics and despite of knowing the existence of a single solution, it is difficult to find analytical solution for these problems. Numerical methods are used in these situations to get an approximate solution. The mains issue in using numerical methods is that the approximate solutions are obtained only at the quadrature nodes which are generated via discretization or meshing procedure on the problem domain. At other points, the numerical solution can only be derived using interpolation methods which results causes increase in cumulative error. Alternatively, Lee and Kang (1990) show that the neural networks are capable of solving differential equations numerically [6]. Since then, researchers around the world are trying to develop neural networks with different topologies for solving different types of differential equations with various conditions. The detailed literature review can be found in [4].

In this study, we put forward Mesh Adaptive Direct Search (MADS) algorithm to train the neural network to get numerical solutions of Second order Dirichlet Boundary Value Problems for ordinary differential equations. The procedure is explained below.

In order to get numerical solution for Boundary Value Problem (BVP) using feed-forward neural network, we need to transform BVP to an optimization problem. After this we can use MADS algorithm to train neural network. At the end, the results will be compared to Generalized Pattern Search (GPS) algorithm [2].

Eq. (2) is used to transform the Dirichlet Boundary Value Problem given in Eq. (1) to an optimization problem.

$$\begin{cases} y'' = f(t, y, y'), a \le t \le b \\ y(a) = A \\ y(b) = B \end{cases} \tag{1}$$

$$y_T = \frac{(t-b)A-(t-a)B}{a-b} + (t-a)(t-b)Net(t, \vec{p}) \tag{2}$$

where y_t is the trial solution defined in Eq. (2). The trial solution satisfies the boundary conditions, and it depends on the neural network solution in Eq. (3). t represents the network input, and $\vec{p} \in \mathbb{R}^{3m+1}$ is the vector of arbitrary parameters of the neural network such that m is the total number of the neurons of the network

$$Net(t, \vec{p}) = \sum_{i=1}^{m} \alpha_i \sigma(\omega_i t + \beta_{1,i}) + \beta_2 \tag{3}$$

where ω_i values represent the weights of the connection between the input layer and the hidden layer, and α_i values represent the weights of the connection between the hidden layer and the output layer for $i = 1, 2, \cdots, m$. Similarly, $\beta_{1,i}$ values are the bias values of the neurons in the hidden layer for $i = 1, 2, \cdots, m$, and β_2 is the bias for the output of the network. In Eq. (3), σ is sigmoid function acting as an activation function. $\vec{p} = \vec{p}(\vec{\alpha}, \vec{\beta}, \vec{\omega})$ are unknown parameters of the neural network. To train the network, we prefer to use MADS algorithm as a derivative free optimization method. The network inputs, in training stage, are obtained via the discretization of the interval $[a, b]$ using $t_j = a + j.h$ where $h > 0$ is the step size for $j = 1, 2, \cdots, n$. After training stage, the network gives the numerical solutions of the boundary value problem given in Eq. (1) on whole of the interval $[a, b]$.

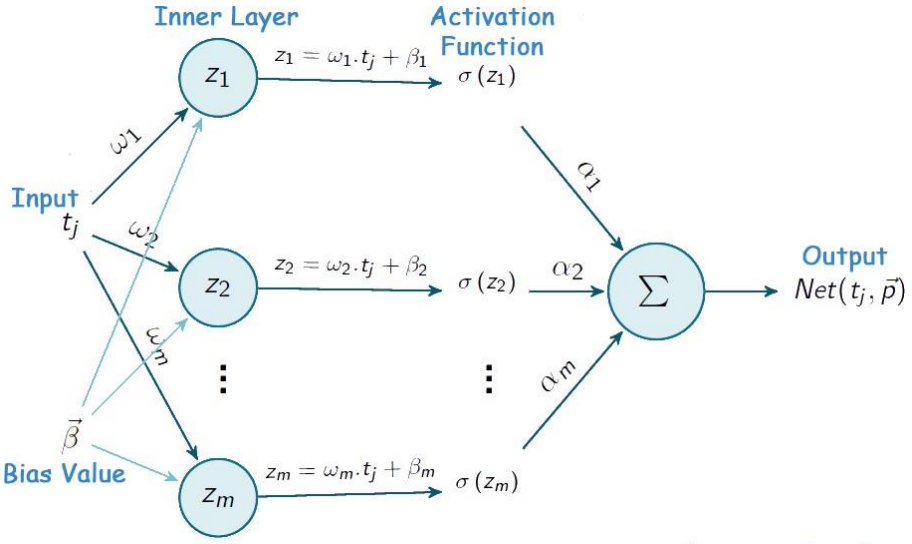

Figure 1. Topological structure of Feed-Forward Neural Network

This is the major difference from the classical numerical methods for solving differential equations. In the classical methods, the numerical solutions are only obtained at the discretization points.

In the beginning, the output of the neural network is calculated for arbitrary parameters $\vec{p} = \vec{p}(\vec{\alpha}, \vec{\beta}, \vec{\omega})$. Which will result in different output values than the expected one. Backpropagation algorithm is used to minimize this error.

$$E = \frac{1}{n}\sum_{i=1}^{n}\left(\frac{\partial^2 y_t(x_i)}{\partial {x_i}^2} - f\left(t_i, y_t(t_i), {y'}_t(t_i)\right)\right)^2 \quad (4)$$

Method

First of all, let's look at some important definitions which we need to understand the algorithm easily.

Definition No. 1:

Let $D \subset \mathbb{R}^n$. The positive span of D, denoted $pspan(D)$, is the set of all nonnegative linear combinations of vectors in D:

$$pspan(D) = \left\{\sum_{i=1}^{m} \lambda_i \boldsymbol{d}^i : \lambda_i \geq 0, \boldsymbol{d}^i \in D, m \in \mathbb{N}\right\} \subseteq \mathbb{R}^n$$

The set D is a positive spanning set for $\mathbb{R}^n$ if and only if $pspan(D) = \mathbb{R}^n$ [1]

Definition No. 2:

A set D is positive linearly independent if and only if $\mathbf{d} \notin pspan(D \backslash \{\mathbf{d}\})$ for all $\forall \boldsymbol{d} \in D$. [1]

Definition No. 3:

A set D is a positive basis of $\mathbb{R}^n$ if and only if it is a positive spanning set of $\mathbb{R}^n$ and is positive linearly independent. [3]

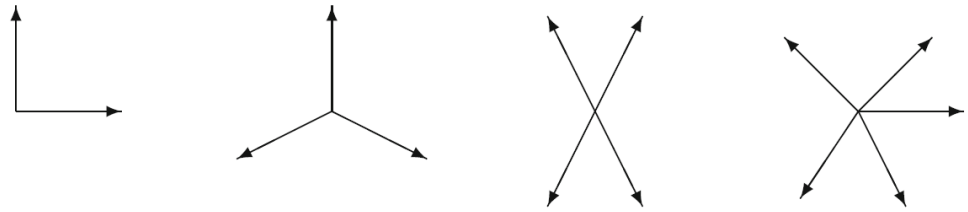

Figure 2. A basis, two positive bases, and a positive spanning set of $\mathbb{R}^2$ [1].

There are four sets of vectors in $\mathbb{R}^2$ in Figure 2. It is clear that the set of vectors in a) are not a positive spanning set. Hence, a) is not a positive basis of $\mathbb{R}^2$. Sets b), c), and d), all are positive spanning sets however only b) and c) are positive basis. Four vectors of d) can be obtained using a positives combination of the remaining vector. So, d) is not a positive basis.

Definition No. 4:

Let $\boldsymbol{G} \in \mathbb{R}^{n\times n}$ be invertible and $\boldsymbol{Z} \in \mathbb{Z}^{n\times p}$be such that the columns of $\mathbf{Z}$ form a positive spanning set for $\mathbb{R}^n$. Define $\boldsymbol{D} = \boldsymbol{GZ}$. The mesh generated by D centred at the incumbent solution $\boldsymbol{x^k} \in \mathbb{R}^n$of coarseness $\delta^k > 0$ is defined by

$$M^k = \left\{ \boldsymbol{x^k} + \delta^k D\boldsymbol{y} : \boldsymbol{x^k} \in \mathbb{R}^n, \boldsymbol{y} \in \mathbb{N}^p, \delta^k > 0 \right\} \subseteq \mathbb{R}^n \quad [1]$$

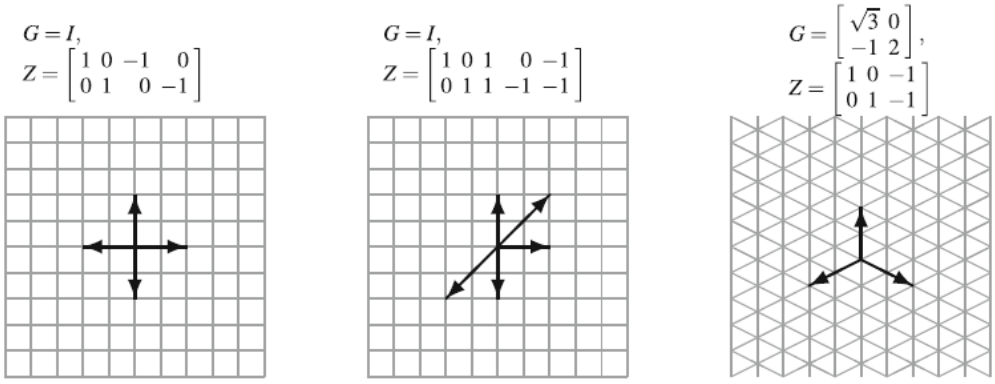

Figure 3. Examples of search sets and meshes in $\mathbb{R}^2$ with $\delta^k = \frac{1}{2}$ obtained by the directions $D = GZ$; the mesh points are at the intersections of the lines and the arrows represent the directions in D [1].

Now, we can present the GPS algorithm for unconstrained minimization,

$$\min(x): \{f(x): x \in \mathbb{R}^n\}$$

Algorithm No. 1:

0. Initialization:

$\Delta^0 \in (0, \infty)$	Δ: initial mesh size parameter
$D = GZ$	D: positive spanning matrix
$\tau \in (0,1),\ \tau \in Q$	τ: mesh size adjustment parameter
$\epsilon_{stop} \in [0, \infty)$	stopping tolerance
$k \leftarrow 0$	iteration counter

1. Search:

if $f(t) < f(x^k)$for some t in a finite subset S^k of the mesh M^k set $x^k + 1 \leftarrow t$ and $\delta^{k+1} \leftarrow \tau^{-1}\,\delta^k$and go to 3 otherwise go to 2

2. Poll

select a positive spanning set $D^k \subseteq D$ if $f(t) < f(x^k)$ for some $t \in P^k = \{x^k + \delta^k d : d \in D_\Delta^k\}$ set $x^{k+1} \leftarrow t$ and $\delta^{k+1} \leftarrow \tau^{-1}\delta^k$ otherwise x^k is a mesh local optimizer set $x^{k+1} \leftarrow x^k$ and $\delta^{k+1} \leftarrow \tau\,\delta^k$

3. Termination

if $\Delta^{k+1} \geq \epsilon_{stop}$ increment $k \leftarrow k + 1$ and go to 1
otherwise stop

Each iteration of the GPS algorithm is divided into two main steps. First step is called search step which is free to apply any strategy to select candidate mesh points at which f will be evaluated. The only condition is to select a finite number of mesh points. If the search step fails in finding a feasible improved mesh point, then the second step must be invoked which is known as poll step. At this stage the function is evaluated at neighboring mesh points around x^k. If the poll step also fails in finding a feasible improved mesh point, then x^k is said to be a mesh local optimizer. The mesh is then refined and x^{k+1} is set to x^k. If either the search or poll step succeeds in finding an improved mesh point, then the mesh size parameter is increased, and the next iterate is the improved point on the mesh.

Each iteration has two possible outcomes, leading to different parameter update rules. If a new incumbent solution is found, then the mesh size parameter δ^{k+1} is increased. If no new incumbent solution is found, then δ^{k+1} is decreased.

Definition No. 5:

Let $\boldsymbol{G} \in \mathbb{R}^{n\times n}$ be invertible and $\boldsymbol{Z} \in \mathbb{Z}^{n\times p}$ be such that the columns of $\boldsymbol{Z}$ form a positive spanning set for $\mathbb{R}^n$. Define $\boldsymbol{D} = \boldsymbol{GZ}$. Select a mesh size parameter $\delta^k > 0$ and let Δ^k be such that $\delta^k \leq \Delta^k$. The frame of extent Δ^k generated by $\boldsymbol{D}$, centred at the incumbent solution $\boldsymbol{x^k} \in \mathbb{R}^n$, is defined by

$$F^k = \left\{ x \in M^k : \left| x - \boldsymbol{x^k} \right|_\infty \leq b\Delta^k \right\}$$

and where Δ^k is called the frame size parameter. [1]

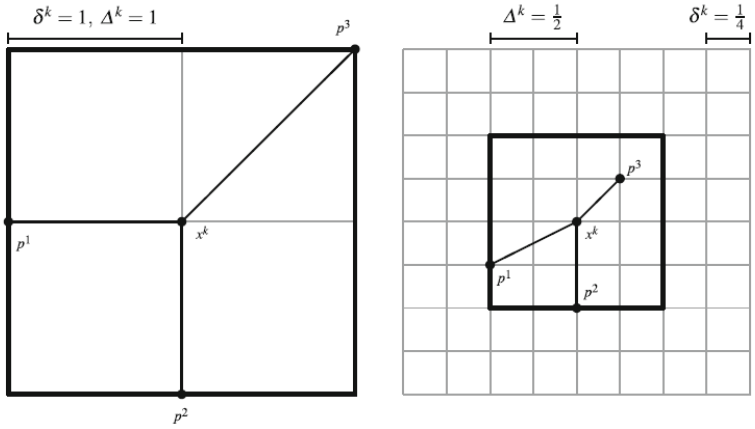

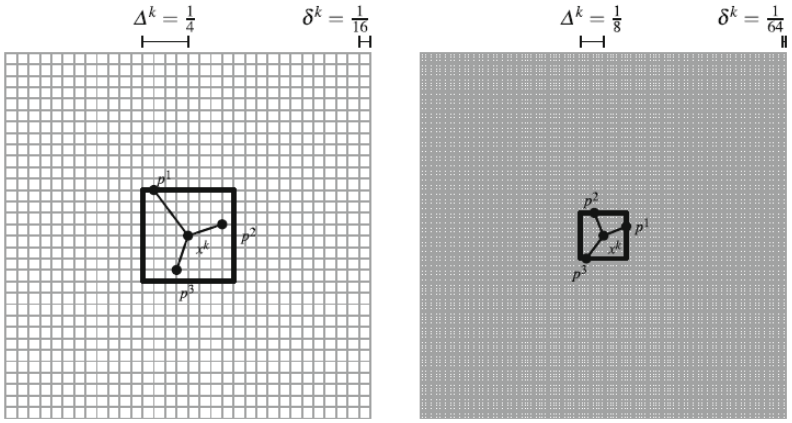

Figure 4 Example of meshes and frames in $\mathbb{R}^2$ for different values of δ^k *and* Δ^k [1]

Now, we present an advancement on the GPS algorithm, the Mesh Adaptive Direct Search (MADS) algorithm. The MADS algorithm will also address the limitation in the GPS algorithm of only proving that a finite list of directional derivatives is nonnegative. This shortcoming is because the initialization stage of the GPS algorithm requires a finite positive spanning set from which all future positive bases will be selected, effectively forcing the algorithm to only consider a finite list of potential polling directions. The MADS algorithm will generalize the GPS algorithm by allowing an infinite set of polling directions, while improving the convergence results.

The MADS is a direct search method for solving the constrained optimization problems. [5]

$$\min f$$

where $f: \mathbb{R}^n \to \mathbb{R}$ is called the objective function and n is the dimension.

Algorithm No. 2:

0. Initialization:

$\Delta^0 \in (0, \infty)$	Δ: initial mesh size parameter
$D = GZ$	D: positive spanning matrix
$\tau \in (0,1)$, $\tau \in Q$	τ: mesh size adjustment parameter
$\epsilon_{stop} \in [0, \infty)$	stopping tolerance
$k \leftarrow 0$	iteration counter

1. Parameter Update

set the mesh size parameter to $\delta^k = \min\left\{\delta^k, (\delta^k)^2\right\}$

2. Search:

if $f_\Omega(t) < f_\Omega(x^k)$ for some t in a finite subset S^k of the mesh M^k set $x^k + 1 \leftarrow t$ and $\delta^{k+1} \leftarrow \tau^{-1}\, \delta^k$ and go to 3 otherwise go to 4

3. Poll

select a positive spanning set D_Δ^k such that $P^k = \{x^k + \delta^k d : d \in D_\Delta^k\}$ is a subset of the frame F^k of the extent Δ^k if $f_\Omega(t) < f_\Omega(x^k)$ for some $t \in P^k$ set $x^{k+1} \leftarrow t$ and $\delta^{k+1} \leftarrow \tau^{-1}\, \delta^k$ otherwise set $x^{k+1} \leftarrow x^k$ and $\delta^{k+1} \leftarrow \tau\, \delta^k$

4. Termination

if $\Delta^{k+1} \geq \epsilon_{stop}$ increment $k \leftarrow k + 1$ and go to 1 otherwise stop

Experiments

Example

Consider the following BVP:

$$\begin{cases} y''(t) = \frac{-2x}{1+t^2}y'(t) + y(t) + \frac{2}{1+t^2} - \log(1+t^2) \\ y(0) = 0 \\ y(1) = \log(2) \end{cases} \quad (5)$$

The exact solution of this equation is given in Eq. 6

$$y = \log(1+x^2) \quad (6)$$

The trial solution for this problem can be derived from Eq. (2)

Results

Table 1 shows the results obtained from Mesh Adaptive Direct Search Algorithm for training set. These results are also compared with analytics results and numerical results obtained from GPS algorithm. Then absolute error is calculated.

Table 1. MADS & GPS numerical solutions for training set

i	t_i	Analytic Solution	MADS Solution	Absolute Error	GPS Solution	Absolute Error
1	0.000	0.000	0.000	0.000	0.000	0.000
2	0.040	1.599×10^{-03}	2.008×10^{-03}	4.095×10^{-04}	4.138×10^{-03}	2.539×10^{-04}
3	0.080	6.380×10^{-03}	7.328×10^{-03}	9.480×10^{-04}	1.145×10^{-03}	5.072×10^{-04}
4	0.120	1.430×10^{-02}	1.580×10^{-02}	1.507×10^{-03}	2.183×10^{-02}	7.536×10^{-03}
5	0.160	2.528×10^{-02}	2.729×10^{-02}	2.008×10^{-03}	3.516×10^{-02}	9.881×10^{-03}
6	0.200	3.922×10^{-02}	4.162×10^{-02}	2.396×10^{-03}	5.129×10^{-02}	1.207×10^{-03}
7	0.240	5.600×10^{-02}	5.864×10^{-02}	2.641×10^{-03}	7.007×10^{-02}	1.407×10^{-03}
8	0.280	7.548×10^{-02}	7.821×10^{-02}	2.733×10^{-03}	9.134×10^{-02}	1.586×10^{-03}
9	0.320	9.749×10^{-02}	1.002×10^{-01}	2.678×10^{-03}	1.149×10^{-01}	1.741×10^{-03}
10	0.360	1.219×10^{-01}	1.244×10^{-01}	2.493×10^{-03}	1.406×10^{-01}	1.872×10^{-03}
11	0.400	1.484×10^{-01}	1.506×10^{-01}	2.205×10^{-03}	1.682×10^{-01}	1.975×10^{-03}
12	0.440	1.770×10^{-01}	1.788×10^{-01}	1.846×10^{-03}	1.975×10^{-01}	2.050×10^{-03}
13	0.480	2.073×10^{-01}	2.088×10^{-01}	1.450×10^{-03}	2.283×10^{-01}	2.095×10^{-03}
14	0.520	2.393×10^{-01}	2.404×10^{-01}	1.050×10^{-03}	2.604×10^{-01}	2.109×10^{-03}
15	0.560	2.728×10^{-01}	2.734×10^{-01}	6.745×10^{-04}	2.937×10^{-01}	2.090×10^{-04}
16	0.600	3.075×10^{-01}	3.078×10^{-01}	3.490×10^{-04}	3.279×10^{-01}	2.037×10^{-04}
17	0.640	3.433×10^{-01}	3.434×10^{-01}	9.130×10^{-05}	3.628×10^{-01}	1.950×10^{-05}
18	0.680	3.801×10^{-01}	3.800×10^{-01}	8.792×10^{-05}	3.984×10^{-01}	1.829×10^{-05}
19	0.720	40177×10^{-01}	4.175×10^{-01}	1.858×10^{-04}	4.344×10^{-01}	1.676×10^{-04}
20	0.760	4.559×10^{-01}	4.557×10^{-01}	2.076×10^{-04}	4.708×10^{-01}	1.491×10^{-04}
21	0.800	4.947×10^{-01}	4.945×10^{-01}	1.667×10^{-04}	5.075×10^{-01}	1.280×10^{-04}
22	0.840	5.339×10^{-01}	5.338×10^{-01}	8.424×10^{-05}	5.444×10^{-01}	1.045×10^{-05}
23	0.880	5.735×10^{-01}	5.735×10^{-01}	1.157×10^{-05}	5.841×10^{-01}	7.918×10^{-05}
24	0.920	6.132×10^{-01}	6.133×10^{-01}	8.570×10^{-05}	6.185×10^{-01}	5.279×10^{-05}
25	0.960	6.532×10^{-01}	6.533×10^{-01}	9.723×10^{-05}	6.558×10^{-01}	2.609×10^{-05}
26	0.100	6.931×10^{-01}	6.931×10^{-01}	0.000	6.931×10^{-01}	0.000

Table 2 shows the results obtained from Mesh Adaptive Direct Search Algorithm for test set. These results are also compared with analytics results and numerical results obtained from GPS algorithm. Then absolute error is calculated.

Table 2. MADS & GPS numerical solutions for test set

i	t_i	Analytic Solution	MADS Solution	Absolute Error	GPS Solution	Absolute Error
1	0.760	4.581×10^{-01}	4.579×10^{-01}	2.068×10^{-04}	4.729×10^{-01}	1.480×10^{-02}
2	0.980	6.771×10^{-01}	6.772×10^{-01}	5.509×10^{-05}	6.782×10^{-01}	1.030×10^{-03}
3	0.230	5.272×10^{-02}	5.533×10^{-02}	2.608×10^{-03}	6.644×10^{-02}	1.372×10^{-02}
4	0.160	2.484×10^{-02}	2.683×10^{-02}	1.992×10^{-03}	3.464×10^{-02}	9.802×10^{-03}

Figure 5 shows the analytical solution and the numerical solution for the test and training set obtained from MADS BVP given in Eq. 5. Clearly MADS is efficient in solving the BVP given in Eq. 5.

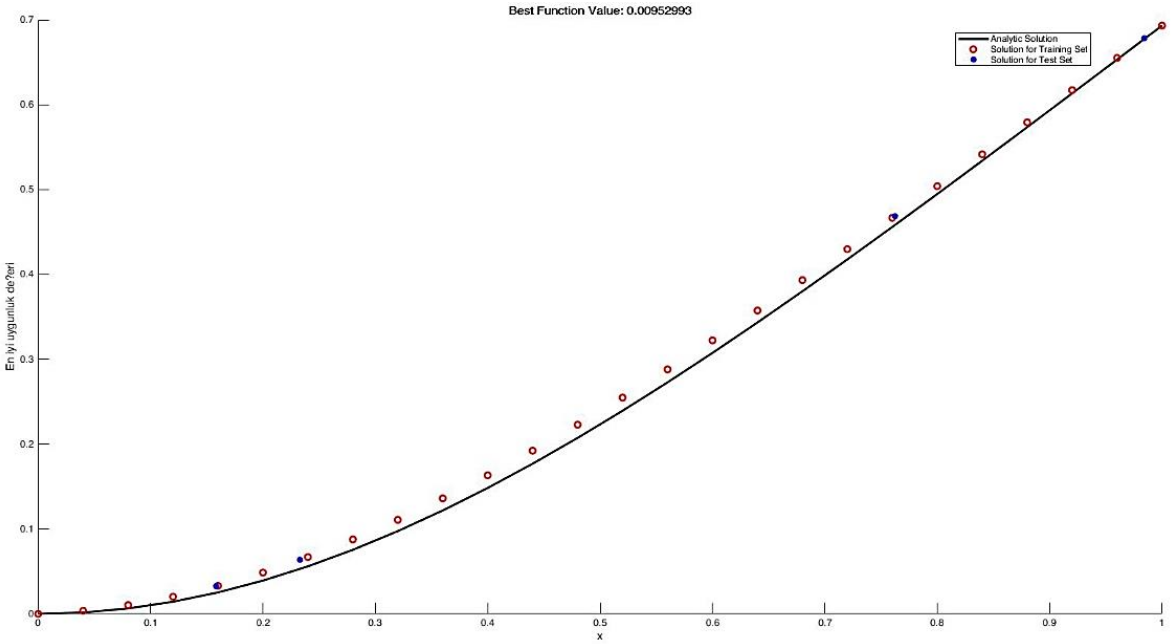

Figure 5 (a). Comparison of analytical solution and numerical solution obtained from MADS

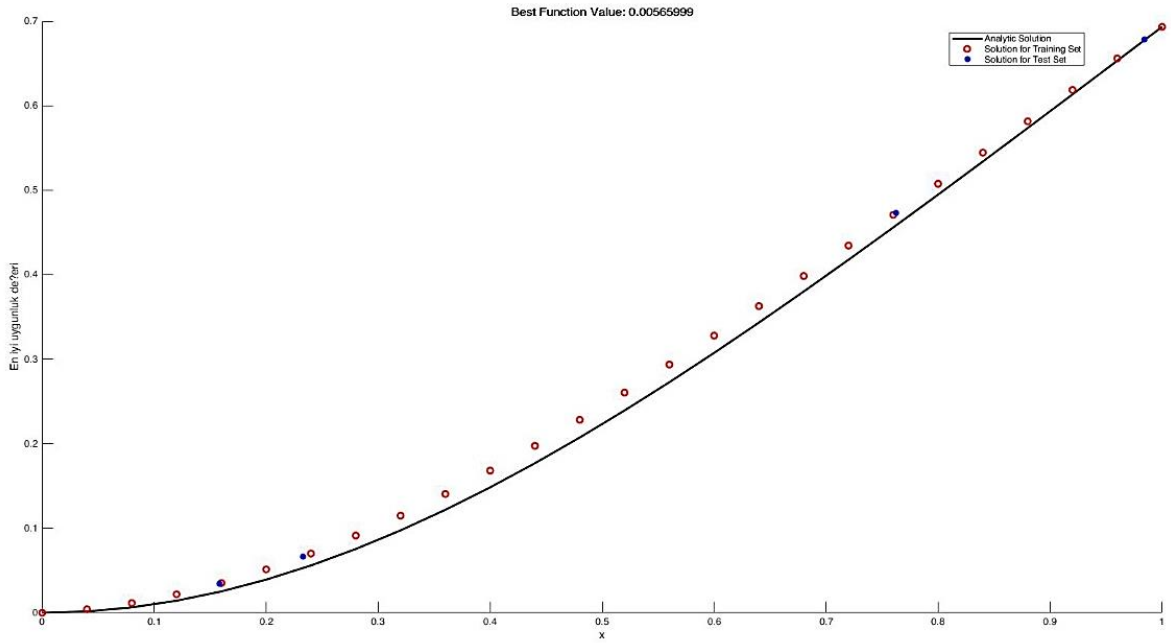

Figure 5 (b). Comparison of analytical solution and numerical solution obtained from GPS

Conclusions

In the study a Dirichlet Boundary Value Problem is solved using a Feed-Forward Neural Network, which is trained by Mesh Adaptive Direct Search optimization method which is upgraded from Generalized Pattern Search algorithm. The results show that MADS gives better results as compared to GPS hence it is preferred to train the neural network for solving BVP numerically. In our future work, MADS will be used to train the neural network to get numerical solution for some of the mathematical epidemiology models i.e., SI (Susceptible-Infected), SIS (Susceptible-Infected- Susceptible) & SIR (Susceptible-Infected-Recovered).

References

[1] Audet C, Hare W. Derivative-Free and Blackbox Optimization. Switzerland: Springer; 2017.
[2] Audet, Charles, and J. E. Dennis Jr. Analysis of Generalized Pattern Searches. SIAM Journal on Optimization. Volume 13, Number 3, 2003, pp. 889–903
[3] Charles Audet and J. E. Dennis, Jr. (2006). Mesh Adaptive Direct Search Algorithms for Constrained Optimization. SIAM Journal on Optimization. 17:1, 188-217.
[4] Gör I. Diferansiyel denklemlerin yapay sinir ağları ile nümerik çözümleri (en: Numerical solutions of differential equations by artificial neural networks), Phd. Thesis, Aydın Adnan Menderes University, Graduate School of Natural and Applied Sciences, Dept. of Mathematics, 2020.
[5] Hooke, R.; Jeeves, T.A. (1961). "Direct search" solution of numerical and statistical problems". Journal of the ACM. 8 (2): 212{229. doi:10.1145/321062.321069.
[6] Lee H, Kang IS. 1990. Neural algorithms for solving differential equations. Journal of Computational Physics, 91(1): 110-131.

Equi Integrity Partitions in Graphs

*Derya Doğan Durgun**, *Eray Sam*
Manisa Celal Bayar University, Department of Mathematics, Turkey
**Corresponding author: derya.dogan@cbu.edu.tr*

Abstract

In this paper some definitions and theorems of equi integrity defined by Sundareswaran and Swaminathan are given. Equi integrity partition of transformation graphs of paths and cycles are calculated where n>3.

Keywords: vulnerability, graph theory, integrity, equi integrity, partitions, transformation

Introduction

The Graph theory was admitted in 1736 when the mathematician Leonhard Euler was asked about the famous Konigsberg Bridge problem. In the solution of this problem, Euler modeled the land pieces as the vertex and the bridges as the edge then graph has been occured. According to this, the graph G consists of the vertices set V(G) and the edges set E(G).

The vulnerability of a graph is a determination that includes certain properties of the graph not to be damaged after the removal of a number of vertices or edges. One measure of vulnerability to vertex removal is integrity. C.A. Barefoot [2], et. al. introduced us to the integrity parameter, which is a very useful measure of vulnerability, and it is defined as folllows $I(G) = min\{|S| + m(G-S): S \subset V(G)\}$, where $m(G-S)$ denotes the order of the largest component in $G-S$. The integrity of the set S is defined as $|S| + m(G-S)$ and is denoted by I_S, where $m(G-S)$ denotes the order of maximum component in $G-S$. In 2012 Sundareswaran and Swaminathan[1] defined equi integrity of a graph.A partition of $V(G)$ into subsets $V_1, V_2, \dots, V_t$ such that I_{V_i} , 1≤ i ≤ t is a constant is called equi-integrity partition of G.The maximum cardinality of such a partition is called equi-integrity partition number of G and is denoted by $EI(G)$.

In this study, the equi integrity partitions in graphs parameter has been investigated and the equi integrity value of the transformation graphs of some graphs is computed.

Equi-Integrity Partitions of Graphs

Definition 2.1. [2] A set of vertices S in a graph G is an I-set of G if $|S| + m(G-S) = I(G)$.

Definition 2.2. [2] For a subset S of $V(G)$, let $I_S = |S| + m(G-S)$, where $m(G-S)$ denotes the order of the largest component in $G-S$.

Definition 2.3. [1] A partition of $V(G)$ into subsets $V_1, V_2, \dots, V_t$ such that I_{V_i}, 1≤ i ≤ t is a constant is called equi-integrity partition of G. The maximum cardinality of such a partition is called equi-integrity partition number of G and is denoted by $EI(G)$.

Example 2.1:

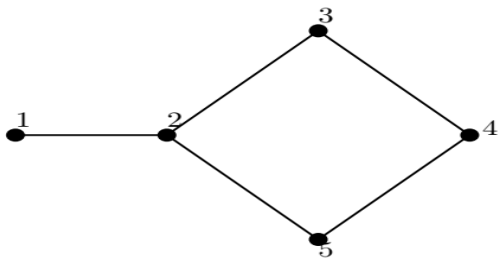

Figure 1. Connected Graph

$$V_1 = \{1,2\}\ for\ I_{V_1} = 2 + 3 = 5$$
$$V_2 = \{3\}\ for\ I_{V_2} = 1 + 4 = 5$$
$$V_3 = \{4\}\ for\ I_{V_3} = 1 + 4 = 5$$

$$V_4 = \{5\}\ for\ I_{V_4} = 1 + 4 = 5$$
$$\{V_1, V_2, V_3, V_4\}\ for\ EI(G) = 4.$$

Remark 2.1. Since $V(G)$ itself is an equi-integrity partition of G, the existence of EI-partition is guaranteed.

Theorem 2.1. [1] Let G be a nontrivial connected graph with order n. Then $EI(G) = n$ if and only if G has no cut vertex.

Proof. Suppose G is a nontrivial connected graph without cut vertex. Then $EI(G) = n$. Conversely, suppose G is a nontrivial connected graph. Then G has at least two vertices which are not cut vertices. For such a vertex say u, $I_u = n$. If G has a cut vertex say v. Then $I_v = 1 + m(G - v) < 1 + n - 1 = n$, a contradiction.

Example 2.2:

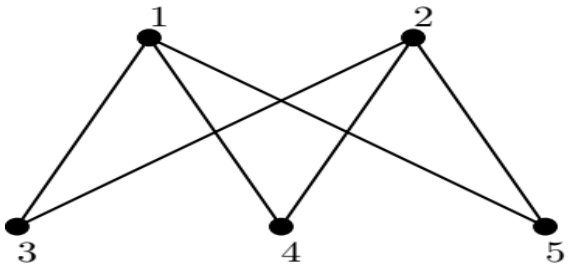

Figure 2. Bipartite Complete Graph

$$V_1 = \{1\}\ for\ I_{V_1} = 1 + 4 = 5$$
$$V_2 = \{2\}\ for\ I_{V_2} = 1 + 4 = 5$$
$$V_3 = \{3\}\ for\ I_{V_3} = 1 + 4 = 5$$
$$V_4 = \{4\}\ for\ I_{V_4} = 1 + 4 = 5$$
$$V_5 = \{5\}\ for\ I_{V_5} = 1 + 4 = 5$$
$$\{V_1, V_2, V_3, V_4, V_5\} = \{\{1\}, \{2\}, \{3\}, \{4\}, \{5\}\}\ for\ EI(G) = 5.$$

Remark 2.2. It can be easily shown that:

$$EI(K_n) = n, EI(K_{m,n}) = m + n, EI(W_{1,n}) = n + 1, EI(C_n) = n.$$

Theorem 2.2. [1] EI(P_n) = $\left\lceil \frac{n}{2} \right\rceil$.

Proof. Let $V(P_n) = \{v_1, v_2, \dots, v_n\}$.

If n is odd and $n = 2k + 1$, then $\{\{v_1, v_{k+1}\}, \{v_2, v_{k+3}\}, \dots, \{v_k, v_{2k+1}\}, \{v_{k+2}\}\}$ is a EI-partition with $I_{V_i} = k + 2$, for all i, $1 \le i \le k + 1$. Therefore, $EI(P_n) \ge \frac{n+1}{2}$. Suppose $EI(P_n) > \frac{n+1}{2} = k + 1$. Then any maximum EI-partition has at least three singletons have same integrity. Therefore, $EI(P_n) = \frac{n+1}{2}$.

If n is even and $n = 2k$, then $\{\{v_1, v_{k+1}\}, \{v_2, v_{k+2}\}, \dots, \{v_k, v_{2k}\}\}$ is a EI-partition with $I_{V_i} = k + 1$, for all i,$1 \le i \le k$. Therefore, $EI(P_n) \ge \frac{n}{2}$. Suppose $EI(P_n) > \frac{n}{2} = k$. Then any maximum EI-partition has at least two singletons.If there are three or more singletons, we get a contradiction. Therefore, any maximum EI- partition contains exactly two singletons and remaining are doubletons.It can be easily verified that in such a partition, the set may not have equal integrity. Therefore, $EI(P_n) \le \frac{n}{2}$. Therefore,$EI(P_n) = \left\lceil \frac{n}{2} \right\rceil$.

Theorem 2.3. [1] $EI(K_{1,n}) = 2$.

Proof. Let $V(K_{1,n}) = \{u, u_1, u_2, \dots, u_n\}$ and u be the vertex of degree n. Let $\{V_1, V_2, \dots, V_t\}$ be a maximum EI- partition of $V(K_{1,n})$. Suppose $u \in V_1$. Let $I_{V_1} = i + 2$, where $|V_1| = i + 1$. For any V_j,

$2 \le j \le t$, $I_{V_j} = n+1$. Since $I_{V_1} = I_{V_j}$ therefore, $i = n-1$ and hence $|V_1| = n$. Hence $t = 2$. Therefore, $|V_2| = 1$.

Definition 2.4. [3] Let $G = (V, E)$ be a graph and x, y, z be three variables taking values $+$ or $-$ .The transformation graph G^{xyz} is a graph whose vertex set is $V(G) \cup E(G)$, and for $\alpha, \beta \in V(G^{xyz})$, α and β are adjacent in G^{xyz} if and only if

1-) $\alpha, \beta \in V(G)$ α, β are adjacent in G if $x = +$ and α and β are not adjacent in G if $x = -$,

2-) $\alpha, \beta \in E(G)$ α, β are adjacent in G if $y = +$ and α and β are not adjacent in G if $y = -$,

3-) $\alpha \in V(G)$ and $\beta \in E(G)$ α, β are incident in G if $z = +$ and α and β are not incident in G if $z = -$.

The following theorems are obtained by investigate all values of x, y, z.

Theorem 2.4. $EI\left(P_n^{xyz}\right) = 2n-1, for\ n > 3$.

Proof. P_n^{xyz} has no cut vertex for $n > 3$ and $\left|V(P_n^{xyz})\right| = |V(P_n)| + |E(P_n)| = n + n - 1 = 2n - 1$ and according to Theorem 2.1. $EI\left(P_n^{xyz}\right) = 2n-1$.

Example 2.3: $EI(P_5^{+\,-\,+}) =?$

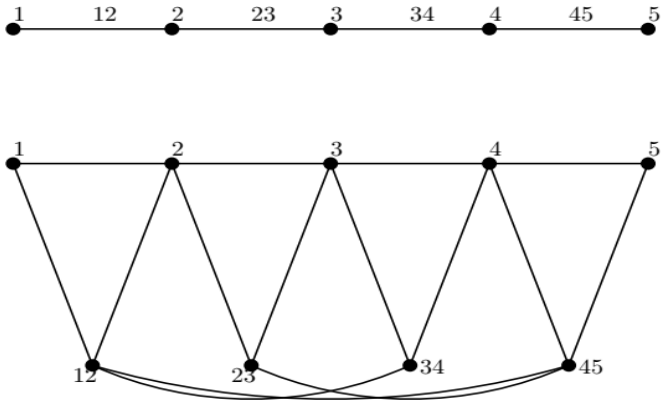

Figure 3. $P_5^{+\,-\,+}$ Transformation Graph

$$I_1 = I_2 = I_3 = I_4 = I_5 = I_{12} = I_{23} = I_{34} = I_{45}$$
$$\{\{1\},\{2\},\{3\},\{4\},\{5\},\{12\},\{23\},\{34\},\{45\}\} \text{ for } EI(P_5^{+\,-\,+}) = 9.$$

Theorem 2.5. $EI\left(C_n^{xyz}\right) = 2n\,, for\ n > 3$.

Proof. C_n^{xyz} has no cut vertex for $n > 3$ and $\left|V(C_n^{xyz})\right| = |V(C_n)| + |E(C_n)| = n + n = 2n$ and according to Theorem 2.1. $EI\left(C_n^{xyz}\right) = 2n$.

Example 2.4: $EI(C_6^{+\,+\,-}) =?$

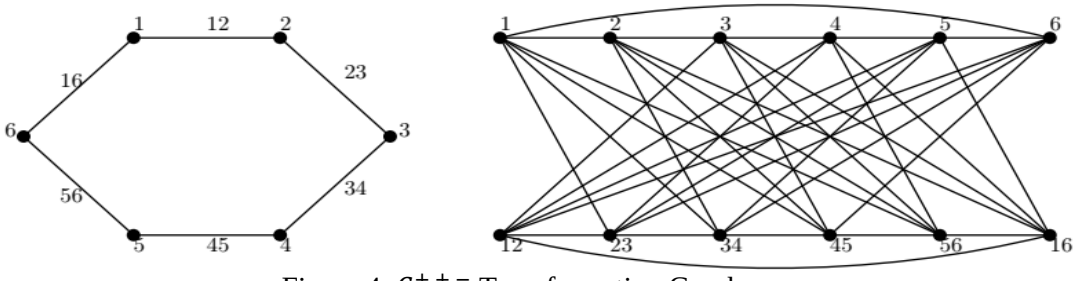

Figure 4. $C_6^{+\,+\,-}$ Transformation Graph

$$I_1 = I_2 = I_3 = I_4 = I_5 = I_6 = I_{12} = I_{23} = I_{34} = I_{45} = I_{56} = I_{16}$$
$$\{\{1\},\{2\},\{3\},\{4\},\{5\},\{6\},\{12\},\{23\},\{34\},\{45\},\{56\},\{16\}\}$$
$$EI(C_6^{+\,+\,-}) = 12.$$

Conclusion

A network allows sharing of files data, etc. This parameter shows us that in case of any problems, the communication can continue easily if there exist other subnetworks with the same integrity.

References

[1] Sundareswaran R, Swaminathan V. (2012) Equi integraty partitions in graphs, Bulletin of International Mathematical Virtual Institute, 2(2012), 93-100
[2] Barefoot CA, Entringer R, Swart HC. Vulnerability in graphs-a comparative survey, J.Combin.Math.Combin.Comput. 1(1987), 13-22
[3] Baoyindureng W, Jixiang M. Basic Properties of Total Transformation Graphs, Journal of Mathematical Study, 2001, (34), 109-116
[4] Goddard WD. On the vulnerability of graphs, Ph.D thesis University of Natal, Durban, South Africa,1989
[5] Bagga KS, Beineke LW, Goddard WD, Lipman MJ, Pippert RE. A survey of integrity, Discrete Appl. Math., 37-38(1992),13-28
[6] Chartrand G, Kapoor SF, McKee TA, Oellerman OR. The Mean Integrity of a Graph, Recent studies in Graph Theory, Vishwa International Publications, (1989), 70-80.

Statistical Approximation Properties of Some Positive Linear Operators

*Faruk Özger**
Ege University, Faculty of Agriculture, Department of Animal Science, Izmir, Turkey
**Corresponding author: farukozger@gmail.com*

Abstract

Statistical convergence is an important concept in functional analysis. In this work, we give a short survey about statistical convergence and statistical convergence of some positive linear operators to approximate functions.

Keywords: convergence of operators, approximation results, statistical convergence

Introduction

In this short paper, we study on statistical approximation properties and estimate rate of weighted A −statistical convergence for some know operators in literature. We also use weighted A −statistical convergence to prove a Voronovskaja-type approximation theorem.

Weighted mean matrix method is used to present some statistical approximation properties in terms of Korovkin-type statistical approximation theorem. Statistical convergence concept was first introduced by Fast [1] and Steinhaus [2]. We also refer to [3,4, 5] to see some examples of statistical approximation. Natural density of K_n is denoted by:

$$\delta(K) = \lim_n \frac{1}{n}|K_n| \tag{1}$$

provided that limit exists, where $K_n = \{k \leq n : k \in K\}$, $K \subseteq \mathbb{N}_0 := \mathbb{N} \cup \{0\}$ and vertical bars denote cardinality of the enclosed set. A sequence $x = (x_n)$ of numbers is called statistically convergent to a number L, denoted by $st\text{-}\lim_n x = L$, if, for each $\epsilon > 0$,

$$\delta\{n : n \in \mathbb{N} \text{ and } |x_n - L| \geqq \epsilon\} = 0. \tag{2}$$

A −transform of x denoted by $Ax := \{(Ax)_n\}$ is defined as:

$$(Ax)_n = \sum_{k=0}^{\infty} a_{nk} x_k \tag{3}$$

for a given non-negative infinite summability matrix

$$A = (a_{nk}), n, k \in \mathbb{N}. \tag{4}$$

It is provided defined series converges for every $n \in \mathbb{N}_0$. If

$$\lim_n (Ax)_n = L \tag{5}$$

whenever $\lim_n x_n = L$, we say that A is a regular method. Then sequence $x = (x_n)$ is said to be A −statistically convergent to L, denoted by $st_A\text{-}\lim x = L$, provided that for each $\epsilon > 0$,

$$lim_{n\to\infty} \sum_{k:|x_k - L| \geqq \epsilon} a_{nk} = 0. \tag{6}$$

A −statistical convergence becomes ordinary statistical convergence which was introduced in [6] if we take $A = (C_1)$, the Cesaro matrix of order one, and it becomes classical convergence if we take $A = I$, the identity matrix. We know that every convergent sequence is statistically convergent to the same limit but not conversely.

An extended form of A −statistical convergence has been introduced by Mohiuddine et al. [9], namely, weighted A −statistical convergence using a non-negative weighted regular matrix. A new

characterization in terms of weighted regular matrix has been given and a Korovkin type approximation theorem through statistically weighted A −summable sequences of real or complex numbers has been proved too.

Assume that $q = (q_n)$ is a sequence of non-negative numbers so that $q_0 > 0$ and

$$Q_n = \sum_{k=0}^{n} q_k \to \infty \tag{7}$$

as $n \to \infty$. Then $x = (x_n)$ is called weighted A −statistically convergent to L, if, for every $\varepsilon > 0$,

$$\lim_{n\to\infty} \frac{1}{Q_n} \sum_{k=0}^{n} q_k \sum_{l:|x_l - L| \geqq \epsilon} a_{kl} = 0. \tag{8}$$

An extended form of A −statistical convergence has been introduced by Mohiuddine et al. [9], namely, weighted A −statistical convergence using a non-negative weighted regular matrix. A new characterization in terms of weighted regular matrix has been given and a Korovkin type approximation theorem through statistically weighted A −summable sequences of real or complex numbers has been proved too.

Assume that $q = (q_n)$ is a sequence of non-negative numbers so that $q_0 > 0$ and

$$Q_n = \sum_{k=0}^{n} q_k \to \infty \tag{9}$$

as $n \to \infty$. Then $x = (x_n)$ is called weighted A −statistically convergent to L, if, for every $\varepsilon > 0$,

$$\lim_{n\to\infty} \frac{1}{Q_n} \sum_{k=0}^{n} q_k \sum_{l:|x_l - L| \geqq \epsilon} a_{kl} = 0. \tag{10}$$

This relation is denoted by $S_A^{\tilde{N}} - \lim x = L$ in this case. It is clear that weighted A −statistical convergence generalizes A −statistical convergence, which we recover by putting $q_n = 1$ for all $n \in \mathbb{N}$. Bernstein basis of degree n on $x \in [0,1]$ is defined in [7] by:

$$b_{n,i}(x) = \binom{n}{i} x^i (1-x)^{n-i} \qquad i = 0, \dots, n. \tag{11}$$

Many researchers have studied on Bernstein operators and tried to obtain certain generalizations. In [8], following new polynomials were defined for certain geometric problems:

$$\tilde{b}_{n,0}(\lambda; x) = b_{n,0}(x) - \frac{\lambda}{n+1} b_{n+1,1}(x), \tag{12}$$

$$\tilde{b}_{n,i}(\lambda; x) = b_{n,i}(x) + \lambda\left(\frac{n-2i+1}{n^2-1} b_{n+1,i}(x) - \frac{n-2i-1}{n^2-1} b_{n+1,i+1}(x)\right), i = 1,2 \dots, n-1, \tag{13}$$

$$\tilde{b}_{n,n}(\lambda; x) = b_{n,n}(x) - \frac{\lambda}{n+1} b_{n+1,n}(x), \tag{14}$$

where shape parameters $\lambda \in [-1,1]$.

In 2018, Cai et al. have introduced a new type λ −Bernstein operators [9]:

$$B_{n,\lambda}(f; x) = \sum_{i=0}^{n} f\left(\frac{i}{n}\right) \tilde{b}_{n,i}(\lambda; x) \tag{15}$$

where shape parameters $\lambda \in [-1,1]$ and $\tilde{b}_{n,i}(\lambda; x)$ is defined above.

Lemma 1 [9, Lemma 2.1] We have following equalities for λ −Bernstein operators:

$$B_{n,\lambda}(1; x) = 1; \tag{16}$$

$$B_{n,\lambda}(t; x) = x + \frac{1 - 2x + x^{n+1} - (1-x)^{n+1}}{n(n-1)} \lambda; \tag{17}$$

$$B_{n,\lambda}(t^2;x) = x^2 + \frac{x(1-x)}{n} + \left[\frac{2x-4x^2+2x^{n+1}}{n(n-1)} + \frac{x^{n+1}+(1-x)^{n+1}-1}{n^2(n-1)}\right]\lambda; \quad (18)$$

$$B_{n,\lambda}(t^3;x) = x^3 + \frac{3x^2(1-x)}{n} + \frac{2x^3-3x^2+x}{n^2} + \left[\frac{6x^{n+1}-6x^3}{n^2} + \frac{3x^2-3x^{n+1}}{n(n-1)} + \frac{9x^{n+1}-9x^2}{n^2(n-1)} + \frac{4x^{n+1}-4x}{n^3(n-1)} + \frac{1-x^{n+1}+(1-x)^{n+1}}{n^3(n^2-1)}\right]\lambda; \quad (19)$$

$$B_{n,\lambda}(t^4;x) = x^4 + \frac{6x^3(1-x)}{n} + \frac{7x^2-18x^3+11x^4}{n^2} + \frac{x-7x^2+12x^3-6x^4}{n^3} + \left[\frac{6x^2-2x^3-8x^4+4x^{n+1}}{n^2} + \frac{17x^{n+1}+16x^4-32x^3-x^2}{n^3} + \frac{x-x^{n+1}}{n^4} + \frac{7x^2-7x^{n+1}}{n^2(n-1)} + \frac{x-23x^2+22x^{n+1}}{n^3(n-1)} + \frac{(1-x)^{n+1}+x-1}{n^4(n-1)}\right]\lambda. \quad (20)$$

The following result for λ −Bernstein operators was obtained in [10].

Theorem 1 [10] Let $A = (a_{nk})$ be a weighted non-negative regular summability matrix for $n, k \in \mathbb{N}$ and $q = (q_n)$ be a sequence of non-negative numbers such that $q_0 > 0$ and,

$$Q_n = \sum_{k=0}^{n} q_k \to \infty \text{ as } n \to \infty. \quad (21)$$

For any $f \in C[0,1]$, we have:

$$S_A^{\tilde{N}} - \lim_{n\to\infty} \| B_{n,\lambda}(f;x) - f(x) \|_{C[0,1]} = 0. \quad (22)$$

Let $A = (a_{nk})$ be a weighted non-negative regular summability matrix and let $q = (q_n)$ be a sequence of non-negative numbers such that $q_0 > 0$ and,

$$Q_n = \sum_{k=0}^{n} q_k \to \infty \text{ as } n \to \infty. \quad (23)$$

Also let (u_n) be a positive non-decreasing sequence. We say that a sequence $x = (x_n)$ is weighted A −statistically convergent to L with the rate $o(u_n)$ if:

$$\lim_{n\to\infty} \frac{1}{u_n Q_n} \sum_{k=0}^{n} q_k \sum_{l:|x_l - L| \geq \epsilon} a_{kl} = 0. \quad (24)$$

In this case, we write:

$$[stat_A, q_n] - o(u_n) = x_n - L. \quad (25)$$

Theorem 2 [10] Let $A = (a_{nk})$ be a weighted non-negative regular summability matrix. Assume that following condition yields:

$$w(f, ß_n) = [stat_A, q_n] - o(u_n) \text{ on } [0,1], \quad (26)$$

where

$$ß_n = \| B_{n,\lambda}((s-x)^2;x) \|_{C[0,1]}^{1/2}. \quad (27)$$

Then for every bounded $f \in C[0,1]$ we have:

$$\| B_{n,\lambda}(f;x) - f(x) \|_{C[0,1]} = [stat_A, q_n] - o(u_n). \quad (28)$$

[10]. We also prove a Voronovskaja-type approximation theorem by $B_{n,\lambda}(f;x)$ family of linear operators using the notion of weighted A −statistical convergence.

Theorem 3 [10] Let $A = (a_{nk})$ be a weighted non-negative regular summability matrix and let (x_n) be a sequence of real numbers such that $S_A^{\tilde{N}} - limx_n = 0$. Also let $\Omega_{n,\lambda}(f;x)$ be a sequence of positive linear operators acting from $C_B[0,1]$ into $C[0,1]$ defined by:

$$\Omega_{n,\lambda}(f;x) = (1+x_n)B_{n,\lambda}(f;x). \tag{29}$$

Then for every $f \in C_B[0,1]$, and $f', f'' \in C_B[0,1]$ we have:

$$S_A^{\widetilde{N}} - \lim_{n\to\infty} n\{\Omega_{n,\lambda}(f;x) - f(x)\} = \frac{f''(x)}{2}x(1-x). \tag{30}$$

For further detail about statistical convergence of λ −Bernstein type operators we refer to [10, 11, 12].

References

[1] H. Fast, Sur la convergence statistique, Colloq. Math., 2, (1951), 241-244.
[2] H. Steinhaus, Sur la ordinaire et la convergence asymptotique, Colloq. Math., (1951), 2, 73-74.
[3] M. Mursaleen, V. Karakaya, M. Ertürk, F. Gürsoy, Weighted statistical convergence and its application to Korovkin type approximation theorem, Appl. Math. Comput., (2012), 218, 9132-9137.
[4] S. A. Mohiuddine Statistical weighted A-summability with application to Korovkin's type approximation theorem, J. Inequal. Appl., (2016), 2016:101.
[5] S. Orhan, K. Demirci, Statistical A-summation process and Korovkin type approximation theorem on modular spaces, Positivity, 18, (2014), 669-686.
[6] A. D. Gadjiev, C. Orhan, Some approximation properties via statistical convergence, Rocky Mountain J. Math., (2002), 32, 129-138.
[7] S. N. Bernstein, Demonstration du theoreme de Weierstrass fondee sur le calcul des probabilites, Communications of the Kharkov Mathematical Society (1912), 13(2), 1-2.
[8] Z. Ye, X. Long, X-M. Zeng, Adjustment algorithms for Bezier curve and surface, International Conference on Computer Science and Education, (2010), 1712-1716
[9] Q-B. Cai, B-Y. Lian, G. Zhou, Approximation properties of λ-Bernstein operators, J. Ineq. and App., (2018), 2018:61.
[10] F. Özger, Applications of Generalized Weighted Statistical Convergence to Approximation Theorems for Functions of One and Two Variables, Numerical Functional Analysis and Optimization, 41:16, 1990-2006, 2020.
[11] F. Özger, Weighted statistical approximation properties of univariate and bivariate λ-Kantorovich operators. Filomat, 2019, 33.11: 3473-3486.
[12] F. Özger, On new Bézier bases with Schurer polynomials and corresponding results in approximation theory. Communications Faculty of Sciences University of Ankara Series A1 Mathematics and Statistics, 2020, 69.1: 376-393.

Modeling and Optimization of 3D Printed PLA Material for Maximum Flexural Strength Using Multiple Nonlinear Neuro Regression Analysis

*Melih Savran**, *Asil Ayaz*, *Tuğrul Uslu*
Izmir Katip Çelebi University, Department of Mechanical Engineering, Izmir, Turkey
**Corresponding author: melih.savran@ikcu.edu.tr /mlhsvrn@gmail.com*

Abstract

Fused deposition modelling (FDM) is a growing additive manufacturing method to produce complex objects without geometrical limitations. In addition, mechanical strength, dimensional accuracy, product development cycle time, and surface properties can be improved depending on the application of the best settings of design variables. There are various printing parameters which influence the mechanical properties and quality of FDM parts.

In this study, appropriate printing parameters were determined to obtain desired quality on mechanical properties and dimensional accuracy. Then full factorial design was employed to form experiment set including process parameters. Multiple nonlinear neuro-regression analysis was used for modeling of FDM process. The present study aims at optimization of the FDM process parameters including infill pattern, infill density and build orientation on flexural strength and strain for polylactide (PLA) material. In this regard, optimization algorithms Differential Evolution and Nelder Mead were used to find the best design or elite designs. Third-order polynomial model and hybrid model including polynomial and logarithmic terms were employed as an objective function to define physical phenomena regarding flexural strength and strain, respectively. It was found that (i) maximum flexural strength as 99.66 MPa using a cubic pattern, flat orientation, and 90 % infill density, (ii) minimum ultimate strain as 1.102 % for gyroid pattern, flat orientation, and 47 % infill density.

Keywords: fused deposition modeling, optimization, flexural strength, multiple non-linear regression

Introduction

Historically, precise manufacturing in prototyping and in low quantities have been a challenge. Recent advances in computer aided manufacturing (CAM) technologies made it possible to eliminate some of the challenges such as die design, post-processing and ensuring precision. More recently, a special case of CAM, Fused Deposition Modelling (FDM) is entered in literature. FDM is rapidly growing additive manufacturing method enabling manufacturing of objects with complex geometries. In recent years, open-source hardware became an integral part of FDM 3d printing with many hobbyists and researchers contributing to 3d printing technology. Open-source hardware refers to the design specifications of a physical object which are licensed in such a way that said object can be studied, modified, created, and distributed by anyone. By the help of projects such as RepRap [1] that embraces open-source hardware, FDM 3d printing technology becomes more popular and affordable with each passing day.

In most cases, FDM works by depositing material on a build plate slice by slice, with each one deposited over previous one. Before manufacturing the parts, an array of commands must be generated for desired parts to be produced by the FDM device. This array of commands is generally transferred to the device by a G-code file and generated by special programs called as slicers. These programs may be supplied by manufacturer of FDM device, or an existing third-party and general-purpose slicer software can be configured to be compatible with desired FDM device. In preparation of G-code files by slicers, many manufacturing parameters can be set depending on slicer software and FDM device. In this study, FDM process parameters including infill pattern, infill density and build orientation were optimized for maximum flexural strength and minimum strain for polylactide (PLA) material.

Rao, Rajiv and Geethika [2] have conducted analysis of variance (ANOVA) methodology on full factorial design of experiments on FDM process parameters layer thickness, extruder temperature and infill pattern to optimize tensile strength of FDM parts. Torres et al. [3] optimized mechanical properties of PLA FDM parts by ANOVA, regression analysis. By tuning FDM process parameters of layer thickness, infill density and heat treatment time applied to the parts. Lee and friends [4] optimized

elasticity of acrylonitrile butadiene styrene (ABS) FDM parts with respect to layer thickness, raster width and print velocity by utilizing ANOVA and S/N ratio methods. Ning et al. [5] have investigated the effects of carbon fiber filler on mechanical properties such as tensile strength, flexural strength and toughness of ABS FDM material. Alafaghani and friends [6] found that dimensional accuracy and mechanical properties of FDM parts greatly affected by FDM process parameters including build orientation, extrusion temperature and layer height compared to infill patterns. Rajpurohit and Dave [7] optimized ultimate tensile strength and strain of PLA FDM parts using ANOVA methodology. Fernandes et al. [8] applied ANOVA methodology to optimize mechanical properties such as elongation, elasticity modulus, yield strength and ultimate tensile strength of PLA FDM parts.

As can be seen from literature, 3D printing technology is popular in both research and manufacturing. As 3d printing technology have become more affordable, it will become to appear in more applications where fast prototyping and low volume manufacturing are important qualities.

Materials and Methods

In the present study, flexural behavior of PLA material is investigated. PLA material is taken from Tinylab Company. The path followed throughout the study is given in Figure 1. Firstly, full factorial design was employed to form experiment set including process parameters and then specimens were produced using fused deposition modeling process. Secondly, flexural tests were carried out according to "ASTM D790" standards on "Shimadzu AGS-X" test machine with a 5 kN force transducer capacity. During 3-point bending tests, the loading speed of the machine was 2 mm / min for each specimen. The tests were repeated at least three times for each type of material produced to increase the sensitivity of the tests. Test results were determined according to the average values, taking into account the standard deviations. Thirdly, data selection and neuro regression modeling were considered to develop a mathematical model that gives the relationship between independent variables and the dependent variable. Finally, non-traditional optimization methods: Modified Differential Evolution (MDE) and Modified Nelder Mead (NMM) methods were used to solve the optimization problems.

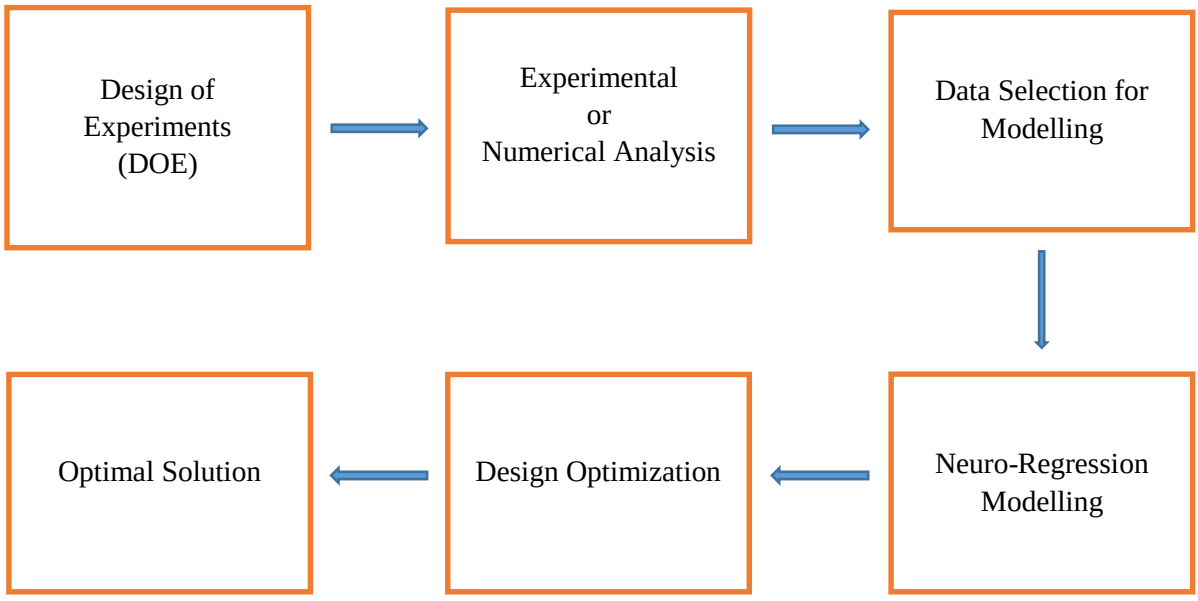

Figure 1. Flow diagram of design process [9]

Table 1. Full factorial design

Trial	Infill Pattern "x_1"	Infill Density (%) "x_2"	Building Orientation "x_3"	Infill Pattern "x_1"	Infill Density (%) "x_2"	Building Orientation "x_3"
1	1	30	1	Cubic	30	Flat
2	2	90	1	Gyroid	90	Flat
3	1	60	3	Cubic	60	Upright
4	2	60	3	Gyroid	60	Upright
5	2	30	3	Gyroid	30	Upright
6	2	30	2	Gyroid	30	Edge
7	1	90	1	Cubic	90	Flat
8	1	90	3	Cubic	90	Upright
9	2	60	2	Gyroid	60	Edge
10	1	60	2	Cubic	60	Edge
11	2	30	1	Gyroid	30	Flat
12	1	90	2	Cubic	90	Edge
13	1	30	2	Cubic	30	Edge
14	2	60	1	Gyroid	60	Flat
15	2	90	2	Gyroid	90	Edge
16	2	90	3	Gyroid	90	Upright
17	1	30	3	Cubic	30	Upright
18	1	60	1	Cubic	60	Flat

Regression Analysis and Optimization

Regression analysis is one of the statistical methods that are used to express mathematically the relationship between the data obtained from experimental or numerical methods, consisting of dependent and independent variables. In the literature, there are many types of linear and nonlinear regression models. The linear regression model is the simplest form in the modeling, and it includes a linear relationship between independent and dependent parameters. In complex problems where the relationship between parameters cannot be expressed linearly, a nonlinear regression model consisting of advanced mathematical functions might be essential to many engineering processes.

There are many different goodness-of-fit indexes used to test the reliability of the mathematical model obtained as a result of the regression analysis. Among these, Coefficient of determination (R^2) stands out, which is preferred as an evaluation criterion for many different study areas and problem types. R^2 consists of two parameters that show the relationship between predicted-observed and observed-mean values and are named as the sum of square error and the total sum of square, respectively. The fact that the R^2 value is close to 1 indicates that the proposed mathematical model very well defines the phenomena.

$$SSE = \sum_{i=1}^{n}(x_i - \hat{x}_i)^2 \quad (1)$$

$$SST = \sum_{i=1}^{n}(x_i - x_{mean})^2 \quad (2)$$

where $x_i, , x_{mean,}$ $\hat{x}_i$ and n show observed, mean, predicted values and the number of rows, respectively.

$$R^2 = 1 - \frac{SSE}{SST} \quad (3)$$

In the scope of this study, non-traditional optimization methods Differential Evolution and Nelder Mead which do not need to derivative information were used to solve the optimization problems.

Differential Evolution is a type of stochastic optimization method that maximizes or minimizes the design problem iteratively. Although it permits alternative and convergent global optimum solutions, it is not assured to find the global optimum. It includes initialization, mutation, crossover, and selection steps [10].

Nelder-Mead is an optimization method and enables to achieve minimum or maximum response of objective function for the unconstrained optimization problem. Even though this method is not a global optimization algorithm, it can give reasonable results for problems that do not have many local minima in practical use [10].

Problem Definition

In the present study, the effect of design parameters i) infill pattern, ii) infill density and iii) building orientation on the strength and strain of 3 D printed PLA material subjected flexural loading are investigated. Single objective optimization approach is preferred to determine the optimum value of design variables: x_1, x_2 and x_3. Two different problems are defined which objectives maximization of flexural strength and minimization of percentage strain. Single objective optimization approach has been used for these two optimization problems. Detailed explanation about the problems are given as follow:

Single Objective Problems

Strength Problem

Find

$\{x_1 \in \{1,2\} \wedge x_2 \in [30, 90] \wedge x_3 \in [1, 3]: \{x_1, x_2, x_3\}\}$

Maximizing

$UFS(x_1, x_2, x_3)$

Constraints

$1 \leq x_1 \leq 2, 30 \leq x_2 \leq 90, 1 \leq x_3 \leq 3 \quad \{x_1, x_2, x_3\} \in$ Integers

Design variables

x_1, x_2, x_3

Strain Problem

Find

$\{x_1 \in \{1,2\} \wedge x_2 \in [30, 90] \wedge x_3 \in [1, 3]: \{x_1, x_2, x_3\}\}$

Minimizing

$ST(x_1, x_2, x_3)$

Constraints

$1 \leq x1 \leq 2, 30 \leq x2 \leq 90, 1 \leq x3 \leq 3 \quad \{x_1, x_2, x3\} \in$ Integers

Design variables

x_1, x_2, x_3

where $x_1, x_2,$ and x_3 represent infill pattern, infill density and building orientation, respectively. Ultimate flexural strength (UFS) and strain in flexural loading (ST) are an objective function.

Results and Discussion

In this section, results of ultimate flexural strength and strain for 3d printed PLA material were given. First step, experiment set was formed using full factorial design of experiment method. Second step, specimens were produced using the fused deposition modeling method and then subjected to the bending test to determine their strength and strain values. Lastly, neuro-regression approach has been utilized to model the flexural behavior of PLA material. In this step, the data are divided into two parts as 20% and 80% of it. Nonlinear regression model is constituted using 80% of the data, and the 20% ones are used for testing. The training and testing data with the corresponding ultimate flexural strength and percentage strain values are given in Table 2. Since the numerical values of the inputs are needed in the modelling process, infill pattern and building orientation are expressed as numerical values in Table 2. For infill pattern, the values “1” and “2” show cubic pattern and gyroid pattern, respectively. For building orientation, the values “1”, “2” and “3” denote flat, edge and upright orientation, respectively. The experimental results in Table 2 shows that the highest strength value obtained as 102 MPa when used a cubic infill pattern, flat orientation, and 90% infill density. PLA sample produced by using the gyroid pattern in the edge orientation with a 30 % infill density showed the lowest strength

value (27 MPa) among the experimental results. In contrast to strength, strain must be minimum under flexural loading for the best design. According to experimental results, input parameters: infill pattern (x_1), infill density (x_2), and building orientation (x_3) must be selected as cubic (x_1 =1), 90 % (x_2=90) and flat orientation to obtain lowest ultimate strain, respectively. As can be clearly seen from the experimental results, the values obtained for the design variables are different from each other in maximum strength design and minimum strain design. Therefore, it is necessary to suggest separate designs where maximum strength is objective or minimum strain is objective.

Table 2. Training, testing data and experimental results

	Trial	Infill Pattern "x_1"	Infill Density (%) "x_2"	Building Orientation "x_3"	Flexural Strength (MPa)	Strain (%)
Training	1	1	30	1	61.427	2.689
	2	2	90	1	68.090	3.569
	3	1	60	3	64.694	3.054
	4	2	60	3	55.840	1.781
	5	2	30	3	44.235	2.861
	6	2	30	2	27.851	1.475
	7	1	90	1	102.25	3.297
	8	1	90	3	86.716	3.517
	9	2	60	2	42.459	1.472
	10	1	60	2	32.866	3.185
	11	2	30	1	52.022	1.349
	12	1	90	2	32.631	1.380
	13	1	30	2	32.432	3.208
	14	2	60	1	66.533	1.378
Testing	15	2	90	2	40.768	3.346
	16	2	90	3	76.747	3.537
	17	1	30	3	51.759	3.342
	18	1	60	1	80.355	2.862

The regression analysis has been used in the mathematical modeling phase of the experimental results. The strength and strain behavior of PLA materials under flexural load have been expressed with separate models. Table 3 denotes the proposed mathematical models for strength and strain problems and the goodness of fit parameters used to evaluate their performance. The fact that the R^2 value is close to 1 indicates that the proposed mathematical model very well defines the phenomena.

Table 3. Strength and strain model and their goodness of fit parameters

Mathematical Model	R^2 train	R^2adjusted	R^2 test
$UFS = -535.4 + 311.7x_1 + 183.3x_1^2 - 132.6x_1^3 + 197.8x_2 - 273.5x_1x_2 + 91.23x_1^2x_2 - 0.2318x_2^2 - 0.005871x_1x_2^2 + 0.001275x_2^3 + 32.1x_3 - 52.33x_1x_3 + 39.13x_1^2x_3 - 2.577x_2x_3 + 0.2152x_1x_2x_3 + 0.005032x_2^2x_3 - 5.769x_3^2 - 18.2x_1x_3^2 + 0.4214x_2x_3^2 +$	0.98	0.98	0.95
$ST = 1.2 + 0.72x_1 + 0.35{x_1}^2 + 0.16{x_1}^3 + 0.078{x_1}^4 + 0.022x_2 - 0.019x_1x_2 - 0.022{x_1}^2x_2 - 0.014{x_1}^3x_2 + 0.00024{x_2}^2 + 0.000077x_1{x_2}^2 + 0.000012{x_1}^2{x_2}^2 + 0.43x_3 - 0.65x_1x_3 - 0.68{x_1}^2x_3 - 0.43{x_1}^3x_3 - 0.014x_2x_3 + 0.041x_1x_2x_3 + 0.04{x_1}^2x_2x_3 - 0.00069{x_2}^2x_3 + 0.000051x_1{x_2}^2x_3 - 0.000014{x_2}^3x_3 + 0.0086{x_3}^2 + 0.19x_1{x_3}^2 + 0.17{x_1}^2{x_3}^2 - 0.0064x_2{x_3}^2 - 0.044x_1x_2{x_3}^2 + 0.00081{x_2}^2{x_3}^2 - 0.05{x_3}^3 + 0.29x_1{x_3}^3 - 0.0016x_2{x_3}^3 - 0.031{x_3}^4 + 1.7\mathrm{Log}[x_1] +$	0.99	0.97	0.90

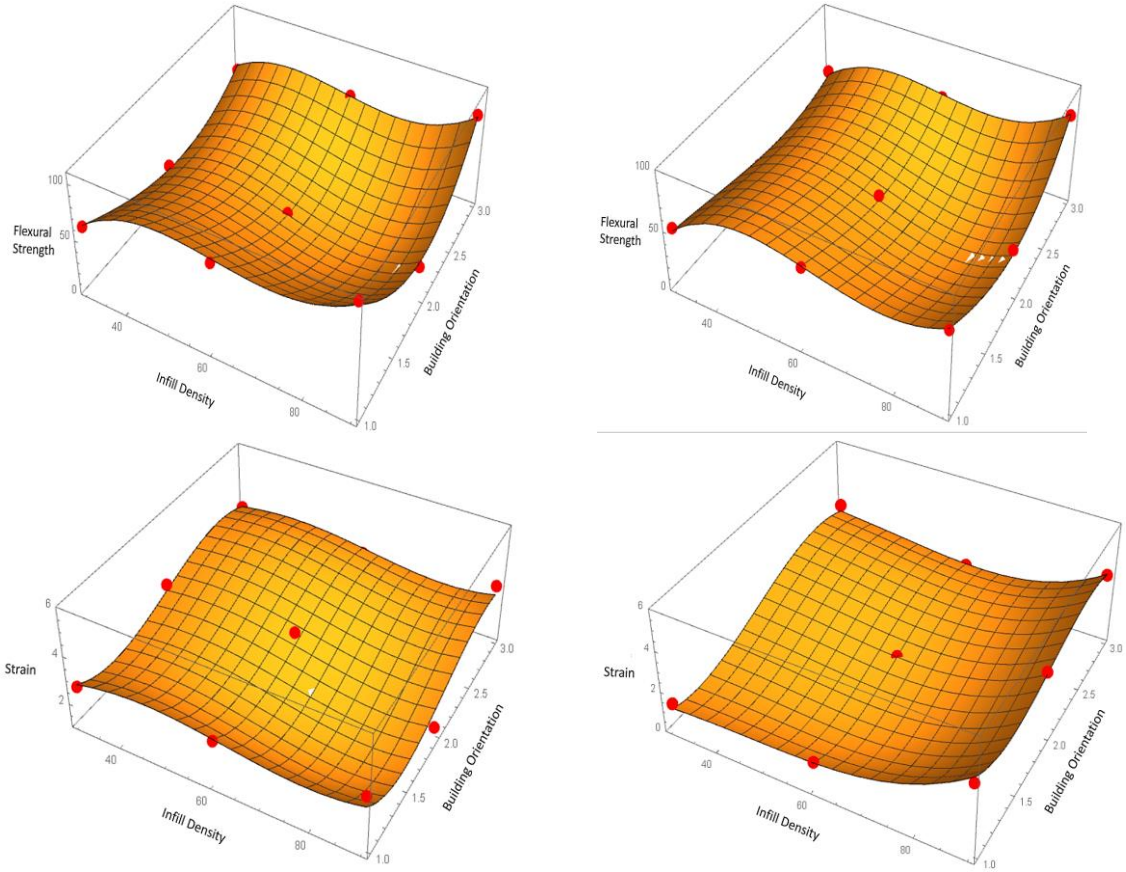

Figure 2. 3D plot representations of experimental data and recommended mathematical model

Figure 2 represents the experimental results and proposed mathematical models to express them. In this figure, it is seen that the effect of infill density and building orientation on strength and strain behavior of 3d printed PLA material subjected to flexural loading. While the polynomial model is enough to describe mathematical phenomena regarding strength results, hybrid model including logarithmic and polynomial expression have been used to explain the strain behavior.

Table 4. Results of optimization problems

Problem	Objective	Constraints	Optimization Algorithm	UFS (MPa)	ST (%)	x_1	x_2	x_3
1	Max UFS	$x_1 \in \{1, 2\}$, $x_3 \in \{1,2,3\}$, $30 \leq x_2 \leq 90$	DE	99.666	3.253	1	90	1
			NM	99.666	3.253	1	90	1
2	Min ST	$x_1 \in \{1, 2\}$, $x_3 \in \{1,2,3\}$, $30 \leq x_2 \leq 90$	DE	73.955	1.102	2	47	1
			NM	73.955	1.102	2	47	1
3	Min ST	$x_1 \in \{1, 2\}$, $x_3 \in \{1,2,3\}$, $30 \leq x_2 \leq 90$ UFS > 85 MPa	NM	85.013	2.775	1	42	1
				85.769	2.786	1	43	1
				86.388	2.797	1	44	1
				85.644	3.186	1	83	1
				87.078	3.196	1	84	1
				99.666	3.253	1	90	1
				85	3.473	1	90	3

Table 4 denotes the results of three separate problems involving different optimization scenarios for 3d printed PLA material. In problem 1, ultimate flexural strength is selected as objective function and its value is maximized under design constraints. In Problem 2 and 3, strain is considered as objective function and the values of design variables: infill pattern (x_1), infill density (x_2), building orientation (x_3) that minimized strains are found. According to the results given in Table 4, it is seen that maximum strength is obtained as 99.66 MPa and minimum strain is found as 1.102 %. When the maximum strength is selected as the objective, it is clearly seen that the design parameters infill pattern and building orientation must be a cubic pattern (x_1=1) and flat orientation (x_3=1), respectively. When a similar evaluation is made for problems where strain is selected as the objective function, it is seen that the gyroid pattern (x_1=2) causes minimal strain. The flat is an appropriate orientation to obtain the best design in both strength and strain problems. In contrast to orientation, infill density and infill pattern can get distinct values for strength and strain problems. Experimental results given in Table 2 have shown that if the strength value is desired to be above 85 MPa, the strain value must be a minimum of 3.2 (%). The optimization results given in Table 4 show that when a design with a strength of 85 MPa is desired, the strain value should be at least 2.78%. It is also noteworthy that the infill density providing desired strength condition is 44%. This result shows that it is possible to obtain a lower strain and more lightweight design using optimization.

Conclusions

This study presents optimization of FDM process parameters such as infill pattern, infill density, building orientation using Nelder-Mead and Differential Evaluation methods to determine maximum ultimate flexural strength and minimum ultimate strain of PLA specimens. Three different optimization scenarios were selected to solve the problems. Third-order polynomial model and hybrid model were employed as an objective function to define physical phenomena regarding flexural strength and strain, respectively. It was found that (i) maximum flexural strength as 99.66 MPa using a cubic pattern, flat orientation, and 90 % infill density, (ii) minimum ultimate strain as 1.102 % for gyroid pattern, flat orientation, and 47 % infill density. Also, employing flat direction as building orientation design parameter have provided the best results in both ultimate flexural strength and ultimate strain problems. In future studies, mechanical behaviors of PLA material for design parameters printing speed, layer thickness, bed temperature, printing temperature and infill patterns such as triangle, honeycomb, Hilbert curve, rectilinear can be investigated using optimization techniques.

References

[1] Bowyer A. RepRap. Available from: https://reprap.org/wiki/RepRap[Accessed on: 2020 Dec 21]
[2] Rao VDP, Rajiv P, Geethika VN. Effect of fused deposition modelling (FDM) process parameters on tensile strength of carbon fibre PLA. Mater. Today: Proceedings 2019; 18:2012–8. doi: 10.1016/j.matpr.2019.06.009
[3] Torres J, Cotelo J, Karl J, Gordon AP. Mechanical Property Optimization of FDM PLA in Shear with Multiple Objectives. JOM 2015 Mar; 67:1183–93. doi: 10.1007/s11837-015-1367-y
[4] Lee B, Abdullah J, Khan Z. Optimization of rapid prototyping parameters for production of flexible ABS object. J. Mater. Process. Technol. 2005 Oct; 169:54–61. doi: 10.1016/j.jmatprotec.2005.02.259
[5] Ning F, Cong W, Qiu J, Wei J, Wang S. Additive manufacturing of carbon fiber reinforced thermoplastic composites using fused deposition modelling. Compos. B. Eng. 2015 Oct; 80:369–78. doi: 10.1016/j.compositesb.2015.06.013
[6] Alafaghani A, Qattawi A, Alrawi B, Guzman A. Experimental Optimization of Fused Deposition Modelling Processing Parameters: A Design-for-Manufacturing Approach. Procedia Manuf. 2017; 10:791–803.doi: 10.1016/j.promfg.2017.07.079
[7] Rajpurohit SR, Dave HK. Analysis of tensile strength of a fused filament fabricated PLA part using an open-source 3D printer. Int. J. Adv. Manuf. Technol. 2018 Nov; 101:1525–36.doi:10.1007/s00170-018-3047-x
[8] Fernandes J, Deus A, Reis L, Vaz M, Leite M. Study of the influence of 3D printing parameters on the mechanical properties of PLA. Proceedings of the 3rd International Conference on Progress in Additive Manufacturing 2018
[9] Aydin L, Artem HS, Oterkus S, eds. Designing Engineering Structures Using Stochastic Optimization Methods. CRC Press, 2020 Apr. doi:10.1201/97804292895762
[10] Savran M, Aydin L. Stochastic optimization of graphite-flax/epoxy hybrid laminated composite for maximum fundamental frequency and minimum cost. Eng. Struct. 2018 Nov; 174:675–87. doi: 10.1016/j.engstruct.2018.07.043

Fotovoltaik Jeneratörlerin Boyutlandırılması için Sayısal Yöntemlerle birlikte Sezgisel Yöntemlerin Optimizasyonu

Harris J. N. Welepe[1], Hüseyin Günerhan, Levent Bilir*
[1,2]Ege Üniversitesi, Makine Mühendisliği Bölümü, 35100-Bornova-Izmir, Türkiye
[3]Yaşar Üniversitesi, Enerji Sistemleri Mühendisliği Bölümü, 35230-Bornova-Izmir, Türkiye
**Corresponding author: harrisharrismail@gmail.com*

Özet

Bu çalışma, elektrik enerjisi talebi profili haftanın günleri arasında büyük değişimler gösterdiğinde, bir fotovoltaik jeneratörün boyutlandırılması için sayısal yöntemlerle birlikte sezgisel yöntemlerin optimizasyonu ile ilgilenmektedir. Gerçekten de, sezgisel yöntemler nispeten basit denklemler kullanıp ancak belirli bir bölge için yıl boyunca gelen güneş ışınımının en düşük aylık ortalama değerine (en olumsuz ay) ve elektrik enerjisi talebini tam olarak karşılamak için bu ayın en yüksek elektrik enerjisi talebine dayanmaktadır. Bu durum, üretilen elektrik enerjisinin yüksek maliyetini ve zayıf bir yatırım geri dönüşünü üreten fotovoltaik jeneratörlerin aşırı boyutlandırılmasına neden olmaktadır. Sayısal yöntemler aşırı boyutlandırma problemini tamamen çözmese de, özellikle sahip oldukları şey, fotovoltaik jeneratörün sağlayabildiği elektrik enerjisi, elektrik enerjisi talebi ve batarya elemanlarının şarj durumu (Bataryada mevcut olan enerji) arasında saatlik veya günlük bir enerji dengesi entegre etmeleridir. Bu çalışmada önerilen kombinasyon yöntemi, Kamerun'da Douala şehrinde bulunan Hayvansal Üretimlerin Geliştirilmesi ve İşletilmesi Şirketi olan SODEPA'nın (Société de Développement et d'Exploitation des Productions Animales) aydınlatması için elektrik enerjisi ihtiyaçlarını karşılayabilen bir fotovoltaik jeneratörün boyutlandırılması için kullanılmıştır. Bulgular, önerilen boyutlandırma yöntemiyle elde edilen fotovoltaik panellerin toplam gücünün, ve daha yüksek bir güvenilirlikle birlikte batarya elemanlarının toplam kapasitesinin, modifikasyon olmadan kullanılan sezgisel yöntemlerin formülleriyle elde edilenlerden sırasıyla 3,26 kattan daha az ve 1,18 kattan daha yüksek olduklarını göstermektedir.

Anahtar Kelimeler: sezgisel yöntemler, sayısal yöntemler, haftalık elektrik enerjisi talebi, aşırı boyutlandırma, zayıf boyutlandırma

Semboller

C_{bat}	:	sezgisel yöntemlerinde batarya elemanlarının toplam kapasitesi, Ah
$C_{bat,0}$	:	önerilen yöntemde batarya elemanlarının toplam kapasitesi, Ah
C_J	:	haftalık elektrik enerjisi talebinin günlük ortalaması, Wh
C_{ji}	:	i gününde günlük elektrik enerjisi talebi, Wh
C_{jmax}	:	maksimum günlük elektrik tüketimi, Wh
C_{jnew}	:	önerilen yöntemde batarya elemanlarının toplam kapasitesinin hesaplanmasında yeni otonomili günlük tüketimi, Wh
d_M	:	batarya deşarj derinliği
E_j	:	en olumsuz ayın aylık ortalama günlük ışınımı, kWh/m^2/g
i	:	gün numarası
k	:	düzeltme katsayısı
N_{aut}	:	otonomi günleri sayısı
P_{PV}	:	sezgisel yöntemiyle hesaplanan fotovoltaik panellerin toplam gücü, W
$P_{PV,0}$	:	önerilen yöntemde fotovoltaik panellerin toplam gücü, W
V_{bat}	:	batarya elemanlarının toplam voltajı, V
η_{bat}	:	batarya verimi
η_i	:	dönüştürücü verimi
η_{reg}	:	regülatör verimi

Giriş

Güneş enerjisinin elektrik enerjisine fotovoltaik panellerle dönüştürülmesi, her geçen gün popüler hale gelen çok yaygın bir teknolojidir. Bununla birlikte, bu teknoloji, fotovoltaik jeneratörleri bazen aşırı bazen zayıf boyutlandırma problemiyle karşı karşıyadır. Tasarımcıların hedeflerine, geniş bir süre boyunca mevcut tüm meteorolojik verilere bağlı aranan güvenilirlik ve hassasiyet derecelerine, enerji talebinin profiline bağlı olarak fotovoltaik jeneratörlerin çeşitli boyutlandırma yöntemleri vardır. Bu çalışma, ağa bağlı olmayan, yani izole veya otonom fotovoltaik sistemlere odaklanmaktadır. Bu tip bir sistem için, [1] üç grup fotovoltaik jeneratörü boyutlandırma yöntemi tanımlamıştır: sezgisel yöntemler, sayısal yöntemler ve analitik yöntemler. Sezgisel yöntemler genellikle en az güneş ışınımını alan ay (en olumsuz ay) yöntemleri olarak adlandırılır, çünkü bu yöntemlerle boyutlandırma yılın en olumsuz ayının ortalama aylık gelen güneş ışınımının değerinden yapılmaktadır. [1] 'e göre, bu yöntemle boyutlandırma ortalama yıllık gelen güneş ışınımının değeri ile de yapılabilmektedir. Bu yöntemlerin derhal dezavantajı, eğer güneş ışınımı yıl boyunca büyük ölçüde dalgalanırsa, sırasıyla yıllık ortalamadan daha yüksek veya düşük güneş ışınımının değerlerine sahip aylarda, sistemin aşırı veya zayıf boyutlandırılmış bulanacağı olmaktadır. Zayıf boyutlandırma güvenilirliğini düşürürken, aşırı boyutlandırma ise üretilen elektrik enerjisinin maliyeti ve yatırım geri dönüşü zamanını yükselttiğini hatırlamak önemlidir. Sayısal ve analitik yöntemler, çok daha karmaşık olma dezavantajı ile sistemlerin aşırı ve zayıf boyutlandırma oranını azaltmak için geliştirilmiştir. Sayısal yöntemler, fotovoltaik jeneratörün sağlayabildiği elektrik enerjisi, elektrik enerjisi talebi ve batarya elemanlarının şarj durumu (Bataryada mevcut olan enerji) arasında saatlik veya günlük bir enerji dengesine dayanırken, analitik yöntemler ise fotovoltaik jeneratörün boyutları ile istenen güvenilirliğini bağlayan denklemlere ve bu jeneratörün bulunduğu yerin bir fonksiyonu olan bu denklemlerin katsayılarını bulma zorluğunun dezavantajı ile dayanmaktadır [1]. Bu çalışma, sezgisel yöntemler nispeten basit denklemlere dayandığından haftanın günleri arasında büyük değişiklikleri gösteren bir haftalık elektrik enerjisi talebi profili için onların bir optimizasyonunu önermektedir. Gerçekten de sezgisel yöntemler, boyutlandırma hesaplamalarında maksimum günlük enerji tüketiminin kullanılmasını önermektedir. Bundan dolayı hafta boyunca çok dalgalanan günlük elektrik enerjisi talebi için maksimum günlük enerji talebini kullanan bir boyutlandırma, en olumsuz ay boyunca bile fotovoltaik jeneratörün aşırı boyutlandırılmasını ağırlaştıracaktır. Bu nedenle, sezgisel yöntemlerin optimize edilmiş bir boyutlandırmasını elde etmek için sezgisel yöntemlerin ve sayısal yöntemlerin hesaplama ilkelerinin birleştirilmesi söz konusu olacaktır. Bu optimizasyon, Kamerun'da Douala şehrinde bulunan Hayvansal Üretimlerin Geliştirilmesi ve İşletilmesi Şirketi olan SODEPA'nın (Société de Développement et d'Exploitation des Productions Animales) aydınlatması için elektrik enerjisi talebinin profiline uygulanacaktır.

Malzeme ve Yöntemler

Bu bölümde, genellikle fotovoltaik jeneratörlerin boyutlandırılması için sezgisel yöntemlerin bağlantıları ve bu çalışma çerçevesinde önerilen yöntemin sunulması söz konusudur. Fotovoltaik panellerin toplam gücünü ve kurulacak batarya elemanlarının toplam kapasitesini hesaplamak istenilmekte, çünkü önerilen optimizasyon bu iki miktarın değerlendirilmesinde bulunmaktadır.

Jeneratörün Sezgisel Yöntemlerle Boyutlandırılması

Kurulacak fotovoltaik panellerin toplam gücü P_{PV}, aşağıdaki formülle ifade edilmektedir [1-3]:

$$P_{PV} = \frac{C_{jmax}}{k \times \eta_{reg} \times \eta_{bat} \times \eta_i \times E_j} \quad \text{(W)} \tag{1}$$

C_{jmax} : maksimum günlük elektrik tüketimi, Wh
η_{reg} : regülatör verimi
η_{bat} : batarya verimi
η_i : dönüştürücü verimi
E_j : en olumsuz ayın aylık ortalama günlük ışınımı, kWh/m^2/g
k : aşağıdakileri dikkate alan düzeltme katsayısı:

- Hava belirsizliği
- Mevsim boyunca fotovoltaik panellerin düzeltilmemiş eğimi

- Fotovoltaik panellerin çalışma noktası
- Kablolar ve bağlantılar kayıpları.

Batarya elemanlarının C_{bat} toplam kapasitesi, maksimum günlük elektrik tüketimi C_{jmax}, istenen otonomi N_{aut} günleri sayısı, batarya elemanlarının V_{bat} volt cinsinden toplam voltajı, bataryanın η_{bat} verimi ve bataryanın d_M deşarj derinliğinin bir fonksiyonudur. Şu ilişki ile ifade edilmektedir:

$$C_{bat} = \frac{C_{jmax} \times N_{aut}}{V_{bat} \times \eta_{bat} \times d_M} \quad \text{(Ah)} \tag{2}$$

Fotovoltaik Jeneratörün Önerilen Yöntemle Boyutlandırılması

Bu çalışmada önerilen yöntem, fotovoltaik panellerin P_{PV} toplam gücü ve batarya elemanlarının C_{bat} toplam kapasitesinin sezgisel yöntemlerinin formülleriyle hesaplamalarının maksimum günlük elektrik tüketimine dayandığı gözleminden başlamaktadır. Böylece, yılın en olumsuz ayı için (en düşük güneş ışınımına sahip ay) bile, haftanın günleri arasında günlük elektrik tüketimi büyük ölçüde değişirse fotovoltaik jeneratör aşırı boyutlandırılmış bulunacaktır. Bu çalışmanın konusu olan SODEPA için durum öyledir. Bu şirket için, aydınlatma için elektrik enerjisi talebi veya tüketimi profili yılın tüm haftaları için neredeyse aynıdır, ancak günlük talebi veya tüketimi hafta boyunca günden güne büyük ölçüde değişmekte.

0, 1, 2, 3, 4, 5, 6 sayıları, sırasıyla Pazartesi, Salı, Çarşamba, Perşembe, Cuma, Cumartesi ve Pazar günlerine verilir. C_{ji}, aydınlatma için i ∈ {0, 1, 2, 3, 4, 5, 6} gününde günlük elektrik enerjisi talebini ifade eder. Haftalık elektrik enerjisi talebinin günlük ortalaması olan C_J günlük talebi olarak alınır. Önerilen yöntemle fotovoltaik panellerin toplam gücü $P_{PV,0}$ aşağıdaki formülle ifade edilir:

$$P_{PV,0} = \frac{C_J}{k \times \eta_{reg} \times \eta_{bat} \times \eta_i \times E_j} \quad \text{(W)} \tag{3}$$

$$C_J = \frac{\sum_{i=0}^{6} C_{ji}}{7} \quad \text{(Wh)} \tag{4}$$

Böylece fotovoltaik paneller, günlük olarak C_J enerjisini sağlayacak şekilde boyutlandırılır; bu, gerçek talebi karşılamak için haftanın gününe göre bazen çok küçük, bazen çok büyük bir değerdir. Bu nedenle, fotovoltaik panellerin daha az enerji sağlayacağı günlerde elektrik enerjisi talebinin her zaman sağlanabilmesi için depolamanın (tüm batarya elemanları) uygun şekilde boyutlandırılması gerekmektedir. Bunun için sadece batarya elemanlarının toplam kapasitesinin hesaplanmasında yeni bir otonomili günlük tüketimin C_{jnew} değerini hesaplayacak bir algoritma geliştirmek gereklidir. Bu büyüklük, sezgisel yöntemlerin bağlantısında $C_{jmax} \times N_{aut}$ ifadesinin yerini alacaktır. Bu algoritmanın gelişimi aşağıdaki hususlara dayanmaktadır:

- Bir gün, güneş doğuşundan başlayıp sonraki günün güneş doğuşunda biter.
- Depolama için 02 günlük bir otonomi talep edilir. Yani bir gün sonunda depolama, öndeki iki günde güneş ışınımı yetersiz ise o günlerin elektrik enerjisi talebini karşılamak için yeterli enerjiye sahip olmalıdır. Böyle bir otonomi kavramı, sezgisel yöntemlere kıyasla depolama güvenilirliğini arttırmaktadır.
- Bir haftanın 7 günü vardır ve pazartesiden pazara gitmektedir.

C_{bi}, depolamanın i'inci günün sonunda içermesi gereken enerjiyi belirtir. C_J, fotovoltaik panellerin günde kaplaması gereken haftanın ortalama günlük tüketimidir. Bu i'inci günün sonunda fotovoltaik panellerden elde edilen ve depolanan G_i (pozitif veya negatif olabilir) enerji kazancı şu ilişki ile ifade edilmektedir: $G_i = C_J - C_{ji}$

Algoritma aşağıdaki gibidir:

1- Bir gün seçilmekte. $C_{bi} = C_{ji+1} + C_{ji+2} = C_{Jnew}$'in başlangıç değeri, çünkü i günün sonunda, sonraki i+1 ve i+2 iki günün otonomini sağlamak için depolamanın yeterli enerjiye sahip olması gerekmektedir.

Not: i+j, j ∈ {1, 2, 3, 4, 5, 6}, bir sayı değildir. Endekste taşıyan miktarın i'inci gününden sonraki j'inci günün miktarını olduğunu belirtmekte.

2- $C_{bi+1} = C_{bi} + G_i$, i+1 gününün sonunda depolama içereceği enerjidir.

3- İlerleyen i+2 et i+3 günlerinin otonomini sağlamak için eksik olacak enerji şu ifadeyle belirlenir: $Eksiklik = \left(C_{ji+2} + C_{ji+3} \right) - C_{bi+1}$.

- Eksiklik> 0 ise, takip eden bu iki günün otonomileri garanti edilmez. Bu sorunu düzeltmek için önceki C_{Jnew}'in değerine $Eksiklik$ değeri eklenir ve C_{bi+1}'in yeni değeri şudur: $C_{bi+1} = C_{ji+2} + C_{ji+3}$. Böylece eksiklik iptal edilir. Algoritma 2. adımından şimdi C_{bi+2} ile tekrar yürütülüp C_{bi+6}'na kadar devam eder.
- Eksiklik < 0 ise, takip eden bu iki günün otonomileri sağlanacaktır. C_{bi+1}, $C_{bi} + G_i$ olan aynı değerini tutar. Algoritma 2. adımından şimdi C_{bi+2} ile tekrar çalıştırılıp C_{bi+6}'na kadar devam eder.

Algoritma i günüyle başlattığında C_{Jnew}'in değeri şudur: $C_{Jnew}(i) = C_{ji+1} + C_{ji+2} + pozitif eksikliklerin\ toplamı.$

Tüm algoritma tekrar yürütülür, şimdi i+1 gününü, sonra i+2 gününü seçererek ve i+6 gününe kadar devam eder. Ve her karşılık gelen $C_{Jnew}(i+j)_{1\le j\le 6}$'in değeri bulunur. Son olarak, C_{Jnew}'in değeri $C_{Jnew}(i+j)_{0\le j\le 6}$ değerlerinin maksimum değeridir.

Dikkate alınması gereken önemli bir nokta şöyledir: bir i günün sonunda, depolama sonraki i+1 ve i+2 günlerinin talebini karşılamak için yeterli enerjiye sahip olur, batarya elemanları tamamen şarj edildi, i+1 günü boyunca birkaç zaman (çok veya az olsa da) için enerji tüketimi fotovoltaik panellerin ürettiği elektrik enerjiden daha az olursa, ek enerji depolamak artık mümkün olmayacaktır ve önceki algoritmada açıklanan G_i kazancı bozulacaktır. Bunu düzeltmek için, fotovoltaik panellerin günde kaplaması gereken haftanın ortalama günlük tüketimi ya da onların günlük ürettiği elektrik enerji olan C_J, C_{Jnew}'e eklenmelidir. Bu, depolamanın güvenilirliğini sağlar.

Sonunda depolamanın ya da batarya elemanlarının $C_{bat,0}$ toplam kapasitesi şu bağlantıyla ifade edilir:

$$C_{bat,0} = \frac{C_{Jnew} + C_J}{V_{batt} \times \eta_{bat} \times d_M} \tag{5}$$

$$C_{Jnew} = Max\left[C_{Jnew}(i+j)_{1\le j\le 6}\right] \tag{6}$$

Sezgisel Yöntemlerle Önerilen Yöntemin Karşılaştırılması

Elde edilen fotovoltaik panellerin toplam güçleri ile batarya toplam kapasiteleri arasında aşağıdaki ilişkiler değerlendirilerek bir karşılaştırma yapılabilmektedir.

$$\frac{P_{PV}}{P_{PV,0}} = \frac{C_{jmax}}{C_J} \tag{7}$$

$$\frac{C_{bat}}{C_{bat,0}} = \frac{C_{jmax} \times N_{aut}}{C_{Jnew} + C_J} \tag{8}$$

$$C_{jmax} = Max\left(C_{ji}, i \in \{0,1,2,3,4,5,6\}\right) \tag{9}$$

Bulgular ve Tartışma

Tablo 1, şirketin hafta boyunca aydınlatması için günlük elektrik tüketimini göstermektedir.

Tablo 1. Şirketin hafta boyunca aydınlatması için günlük elektrik tüketimi [3]

Günler:	Pazartesi	Salı	Çarşamba	Perşembe	Cuma	Cumartesi	Pazartesi
Günlük tüketim (Wh) :	16271	4344	16271	2558	16271	11931	2184

Bu tüketimlerin günlük ortalaması C_J = 9975.7143 Wh'dir. Maksimum tüketim C_{jmax} = 16271 Wh'dir.

Şirketin bulunduğu bölgenin güneş ışınımının verilerine de ihtiyaçlar duyulmaktadır. O bölgenin güneş ışınımının kesin verilerinin olmamasından bulunduğu Douala şehrinden genel veriler kullanılmaktadır (Tablo 2). Bu güneş ışınımının verileri RESTCREEN 4 yazılımından gelmektedir.

Tablo 2. Douala şehrinde enlemi, fotovoltaik panellerin en uygun eğimi, aylık ortalama günlük güneş ışınımı [4]

Aylar:	Ocak	Şubat	Mart	Nissan	Mayıs	Haziran
Ortalama günlük güneş ışınımı kWh/m^2/g:	5,41	5,36	4,88	4,55	4,37	3,91
Aylar:	Temmuz	Ağustos	Eylül	Ekim	Kasım	Aralık
Ortalama günlük güneş ışınımı kWh/m^2/g:	3,41	3,04	3,44	3,7	4,3	5,05
Enlem: 4,1° N		Fotovoltaik panelleri en uygun eğimi: 10° güneye bakan				

Bu nedenle en olumsuz güneş ışınımı $E_j = 3{,}04$ kWh/m^2/g'dir. Boyutlandırma için aşağıdaki değerler seçilir: $k = 0{,}8$; $\eta_{reg} = 0{,}95$; $\eta_{bat} = 0{,}9$; $\eta_i = 0{,}9$; $N_{aut} = 2$; $d_M = 0{,}8$, $V_{bat} = 48$ V. Hesapladıktan sonra Tablo 3 elde edilir.

Tablo 3. Fotovoltaik jeneratörün boyutlandırılmasının sonucu

Büyüklük	Değerler		
C_{jmax} (Wh) :	16271		
C_J (Wh):	9975,7143		
C_{Jnew} (Wh):	28202		
N_{aut} (Wh):	2		
	Sezgisel yöntemler, P_{PV}	Önerilen yöntem, $P_{PV,0}$	Oran, $\frac{P_{PV}}{P_{PV,0}}$
Fotovoltaik panellerin toplam gücü (Wh):	18041,322	5530,5474	3,26
	Sezgisel yöntemler, C_{bat}	Önerilen yöntem, $C_{bat,0}$	Oran, $\frac{C_{bat}}{C_{bat,0}}$
Batarya elemanlarının toplam kapasitesi (Ah):	941,6088	1104,67923	0,85 ≅ 1/1,18

Bu tablo, $\frac{P_{PV}}{P_{PV,0}}$ ve $\frac{C_{bat}}{C_{bat,0}}$ oranlarının değerlerinden önerilen yöntemin formülüyle hesaplanan fotovoltaik panellerin toplam gücünün sezgisel yöntemlerin formülüyle hesaplanandan 3,26 kattan daha az olduğunu göstermekte ve daha yüksek bir güvenilirlikle batarya elemanlarının toplam kapasitesinin sezgisel yöntemlerin formülüyle hesaplanandan biraz (1,18) daha yüksek olduğunu göstermektedir.

Bu sonuç önemlidir ve şirketin aydınlatması için önerilen yöntem sayesinde üretilen elektrik enerjisinin maliyeti ve yatırımın geri dönüş zamanının önemli ölçüde düşebileceğini göstermektedir. Önerilen yöntemin, sezgisel yöntemler gibi, yılın en düşük aylık ortalama güneş ışınımının değerini kullandığını belirtmek önemlidir. Böylece, daha yüksek güneş ışınımına sahip aylarda, fotovoltaik jeneratör aşırı boyutlandırılmış bulunacak ve kullanılmadığı takdirde üretilebilecek fazla olan enerji kaybolacaktır. Bu aylarda şirket, uygun bir enerji yönetimi oluşturarak bazı elektrikli ekipmanlarını da

örneğin ofis ekipmanlarını (bilgisayarlar, buzdolapları, klimalar, vb.), fotovoltaik jeneratörle besletebilir. Böyle bir enerji yönetimi, enerji maliyetini ve fotovoltaik jeneratörün geri dönüş zamanını en aza indirecektir.

Sonuç

Bu çalışmanın amacı, elektrik enerjisi talebi profili haftanın günleri arasında büyük değişimlerle haftalık olduğunda, bir fotovoltaik jeneratörün boyutlandırılması için sayısal yöntemlerle birlikte sezgisel yöntemlerin optimizasyonu önermek olmuştu. Bu çalışmadan, bu çalışmanın konusu olan şirket için önerilen optimizasyon yöntemiyle elde edilen fotovoltaik panellerin toplam gücünün ve daha yüksek bir güvenilirlikle birlikte batarya elemanlarının toplam kapasitesinin, sezgisel yöntemlerin formülleriyle elde edilenlerden sırasıyla 3 kattan daha az ve biraz daha yüksek olduklarını göstermektedir. Ancak, sezgisel yöntemler gibi önerilen yöntem en olumsuz ayın ortalama güneş enerjisinin değerine dayandığından, fotovoltaik jeneratörün daha yüksek güneş enerjisi alan aylarda asışı boyutlandırılacağını belirtmek önemlidir. Bu aylar boyunca jeneratör, şirketin aydınlatması için gereken enerji talebinden daha fazla elektrik enerjisi üretebilecektir. Bu elektrik enerji üstünden yararlanmak için, jeneratör, elektrik düğmeli bir sistemle bu aylarda aydınlatmaya ek olarak şirketin diğer elektrik yüklerini (bilgisayarlar, klimalar, ofis buzdolapları, vb.) besleyebilecektir. Böyle bir tasarım, yıl boyunca fotovoltaik jeneratör tarafından üretilen elektrik enerjisi maliyetini önemli ölçüde azaltacaktır.

Referanslar

[1] Khatib T, Mohamed A, Sopian K. A Review of Photovoltaic Systems Size Optimization Techniques. Renewable and Sustainable Energy Reviews 2013 (vol. 22, p. 454–465).
[2] Trahi F. Prédiction de l'Irradiation Solaire Globale pour la Région Tizi-Ouzou par les Réseaux de Neurones Artificiels : Application pour le Dimensionnement d'une Installation Photovoltaïque pour l'alimentation du Laboratoire de Recherche LAMPA. Mémoire de Magister publié, 2011. Université Mouloud Mammeri de Tizi-Ouzou, Alger.
[3] Welepe HJ. Etude d'une Initiative Technique d'Acquisition de l'Autonomie Energétique par le Solaire Photovoltaïque et la Biomasse à la SODEPA de Douala. Mémoire d'Ingénieur des Travaux, 2013. Ecole Nationale Supérieure Polytechnique de Maroua, Maroua.
[4] RETScreen 4. Versiyonu (2013): İklim verileri yazılımı.

Manufacturing and Modeling of Hybrid Polymer Composites by Using Multiple-Nonlinear Regression Analysis

*Muhammed Yılmaz, Melih Savran, Mustafa Öncül, Kutlay Sever**
Izmir Katip Çelebi University, Department of Mechanical Engineering, Izmir, Turkey
**Corresponding author: kutlay.sever@ikcu.edu.tr*

Abstract

In this study, artichoke stem particles (AS) and wollastonite mineral (W) were used as an organic and inorganic fillers in order to improve the mechanical properties of polypropylene (PP). In this regard, PP-based composites containing AS and W were produced as non-hybrid and hybrid materials using a high-speed thermokinetic mixer. Mechanical properties of polymer composites were investigated by the tensile test. Experimental results reveal that the highest elastic modulus for PP-W and the highest tensile strength for PP were obtained while the lowest ultimate strain value was gained using PP-W-A. Then, multiple nonlinear regression analysis was employed to determine the effect of weight ratios of wollastonite mineral and artichoke stem particles in polypropylene on elastic modulus, tensile strength and ultimate strain. Experimental results were expressed second order (tensile strength), third order (elastic modulus) and fourth order (ultimate strain) mathematical models. The results show that the proposed models have well fitted with the experimental results. The coefficient of determination (R2) values were found between 0.95 and 1 in all models. Also, boundedness check control of the proposed models which gives information about whether models are realistic or not was carried out by calculating the maximum and minimum values produced by the relevant model.

Keywords: multiple-nonlinear regression, hybrid polymer composites

Introduction

Natural fibers are increasingly used as filler or reinforcement in polymers in the production of composite materials due to their advantages such as being renewable, having low density, non-toxicity and low cost. Natural fibers find themselves as an alternative to synthetic fibers in many areas such as automotive industry, construction industry and daily use materials in applications that do not require high strength. In addition, the use of natural fiber filled polymer composites is limited by their poor thermal properties. To overcome this situation, the availability of mineral filler materials that improve thermal performance in natural fiber filled polymer composites has been the subject of this research. In this study, artichoke stem particles and wollastonite (W) were used as organic and inorganic fillers to improve the mechanical and thermal properties of polypropylene (PP).

Studies for the recycling of materials that are easily found in nature and considered as waste have increased in recent years. One of the main purposes of these studies is to reduce the environmental impact of these wastes. Polymer matrix composites are reinforced with woody cellulosic materials such as kenaf, sisal, jute, ramie, sugar cane, coconut fiber to reduce production costs and possible environmental damage [1–5]. In addition, agricultural wastes such as vine stem, olive pomace, corn, wheat, rice, almond shell and lignocellulose-rich corn cob were used as reinforcement/filling material [6–12]. Although such non-hybrid studies are very common in the literature, the number of studies on agricultural waste and mineral filled hybrid composites is limited. With the use of hybrid structures, it is aimed to provide many important features in engineering design such as reducing material weight, increasing strength, reducing production costs, improving thermal properties, and ensuring easy recycling of materials [13].

Materials and Methods

Polypropylene were used as matrix material and artichoke stem particles and wollastonite were used as filling/reinforcing elements within the scope of this work for manufacturing composite materials. PP copolymer used in experimental studies (PP, LG Chem M 1500, Korea) supplied by İzmir Education Health Industry Investment Inc. (Manisa, Turkey). PP copolymer has a melting temperature of 230 °C/2.16 kg, a flow index of 16 g/10 minutes and a density of 0.9 g/cm^3. Artichoke stems were

obtained from the products left as agricultural waste from the fields in Çiğli, İzmir. Wollastonite used in experimental studies (TREMIN 939-300 needle-shaped wollastonite, D50=37 μm, L/D=6, untreated, density=2.85 g/cm and Mohs hardness=4.5) was obtained from the KAOLIN Industrial Minerals Inc. (İstanbul, Turkey).

PP matrix composites were produced with a laboratory scale high-speed thermokinetic mixer. AS, W and PP were physically mixed in a total of seventy grams before being put into the mixer chamber and the mixture was put into the mixer chamber. In the mixer operating at 2000 rpm, the mixture was kept for about 25-30 seconds until it became a dough. Composite plates are produced by the method of hot pressing the dough by hot and cold press. Table 1 shows the mixing ratios of the materials.

Table 1. The mixing ratios of the materials

Trial	Material	Wollastonite (wt %)	Artichoke stem (wt %)
1	PP	0	0
2	PP-10AS	10	0
3	PP-20AS	20	0
4	PP-30AS	30	0
5	PP-10W	0	10
6	PP-20W	0	20
7	PP-30W	0	30
8	PP-3W-7AS	7	3
9	PP-7W-3AS	3	7
10	PP-5W-5AS	5	5
11	PP-10W-10AS	10	10
12	PP-14W-6AS	6	14
13	PP-6W-14AS	14	6
14	PP-15W-15AS	15	15
15	PP-21W-9AS	9	21
16	PP-9W-21AS	21	9

Mechanical tests were carried out according to "ASTM D638" standards on "Shimadzu AGS-X" tensile testing machine. During the tensile test, the cross-head speed was determined as 50 mm/min. The tests were repeated at least five times for each type of material produced to increase the sensitivity of the tests. Test results were determined according to the average values, taking into account the standard deviations.

Regression Analysis

The researchers try to find the most appropriate models which correctly estimate the results obtained using experimental or numerical methods. Regression analysis is one of the statistical methods used for this purpose. There is distinct type of mathematical models to estimate relationship between independent and dependent parameters. Among these, models including only linear functional terms are appropriate for problems that are non-complex and having few independent variables. In case the relationship between parameters is nonlinear, a regression model consisting of advanced mathematical functions would be more suitable to many engineering processes [14]. In the literature, the most commonly used criteria for evaluating model success is coefficient of determination. R^2 consists of two parameters that show the relationship between predicted-observed and observed-mean values and are named as the sum of square error and the total sum of square, respectively. The fact that the R^2 value is close to 1 indicates that the proposed mathematical model very well defines the phenomena.

$$SSE = \sum_{i=1}^{n}(x_i - \hat{x}_i)^2 \quad (1)$$

$$SST = \sum_{i=1}^{n}(x_i - x_{mean})^2 \quad (2)$$

$$R^2 = 1 - \frac{SSE}{SST} \quad (3)$$

where $x_i, , x_{mean,}$ $\hat{x}_i$ and n show observed, mean, predicted values and the number of rows, respectively.

Results and Discussion

In this section, various regression models have been proposed for PP-based hybrid materials design. In the modelling phase, experimental data, some of which were produced within the scope of this study, and some obtained from the study conducted by Sever and Yılmaz [15] were used. Considered PP-based hybrid composite includes artichoke stem and wollastonite mineral as filler. The effect of weight ratio of AS and W fillers regarding elastic modulus, ultimate tensile strength, and ultimate strain is investigated experimentally. After that 12 distinct regression models with two parameters have been tested in terms of fitting performance.

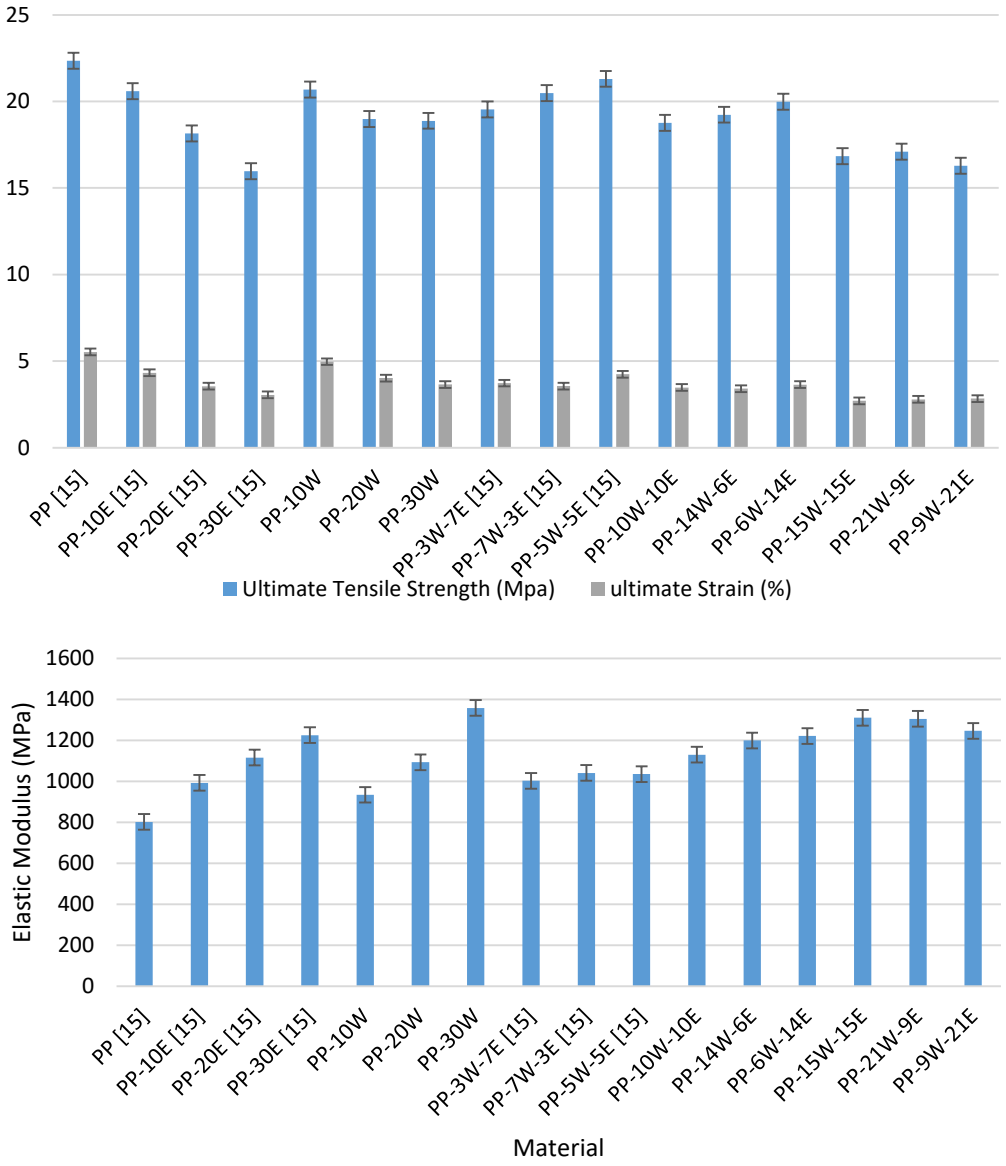

Figure 1. Mechanical properties of PP-based hybrid materials

Figure 1 shows experimental results regard with mechanical properties of PP-based hybrid materials with different weight ratio of AS and W fillers. It is clearly seen that the hybridization process negatively affected the strength performance of the PP material, non-hybrid PP material gives the best results (22.34 MPa) in terms of ultimate strength. When the elastic modulus and strain results are evaluated, it can be

said that while hybridization of PP with 30% W provides the highest elastic modulus, hybridization of PP with 15% W and 15% AS gives the lowest strain design.

Multiple nonlinear regression analysis was used to describe phenomena mathematically regarding elastic behaviour of PP-based hybrid composites. Four distinct models and their fitting performance were compared with each other.

Mathematical Models for Elastic Modulus

Model 1 (fifth order polynomial)

$$Y = 801.6 + 23.04x_1 - 0.7127x_1^2 + 0.05279x_1^3 - 0.002737x_1^4 + 0.00004797x_1^5 + 16.36x_2 + 4.502x_1x_2 - 1.326x_1^2x_2 + 0.1346x_1^3x_2 - 0.003301x_1^4x_2 - 0.361x_2^2 + 0.8592x_1x_2^2 - 0.1052x_1^2x_2^2 + 0.0008965x_1^3x_2^2 - 0.01527x_2^3 - 0.04608x_1x_2^3 + 0.00385x_1^2x_2^3 + 0.002335x_2^4 + 0.0004718x_1x_2^4 - 0.00004482x_2^5$$

Model 2 (third order rational)

$$Y = \frac{17.83+783.4x_1+10036.x_1^2-196.1x_1^3-1283.x_2-14918.x_1x_2+171.3x_1^2x_2-1553.x_2^2+63.24x_1x_2^2+159.1x_2^3}{0.02224+17.87x_1+8.242x_1^2-0.1809x_1^3-18.64x_2-15.91x_1x_2+0.2274x_1^2x_2+1.17x_2^2+0.1519x_1x_2^2+0.05974x_2^3}$$

Model 3 (third order trigonometric)

$$Y=279.3 + 8.723\mathrm{Cos}[x_1] + 298.9\mathrm{Cos}[x_1]^2 - 2.066\mathrm{Cos}[x_1]^3 + 13.81\mathrm{Cos}[x_2] + 122.1\mathrm{Cos}[x_1]\mathrm{Cos}[x_2] - 88.45\mathrm{Cos}[x_1]^2\mathrm{Cos}[x_2] + 273.8\mathrm{Cos}[x_2]^2 - 111.2\mathrm{Cos}[x_1]\mathrm{Cos}[x_2]^2 + 6.739\mathrm{Cos}[x_2]^3 + 29.41\mathrm{Sin}[x_1] + 169.9\mathrm{Cos}[x_1]\mathrm{Sin}[x_1] - 78.91\mathrm{Cos}[x_1]^2\mathrm{Sin}[x_1] - 187.3\mathrm{Cos}[x_2]\mathrm{Sin}[x_1] - 49.58\mathrm{Cos}[x_1]\mathrm{Cos}[x_2]\mathrm{Sin}[x_1] + 26.5\mathrm{Cos}[x_2]^2\mathrm{Sin}[x_1] + 441.3\mathrm{Sin}[x_1]^2 + 138.2\mathrm{Cos}[x_1]\mathrm{Sin}[x_1]^2 + 145.\mathrm{Cos}[x_2]\mathrm{Sin}[x_1]^2 + 65.66\mathrm{Sin}[x_1]^3 + 24.02\mathrm{Sin}[x_2] - 218.3\mathrm{Cos}[x_1]\mathrm{Sin}[x_2] + 25.03\mathrm{Cos}[x_1]^2\mathrm{Sin}[x_2] + 76.52\mathrm{Cos}[x_2]\mathrm{Sin}[x_2] - 59.11\mathrm{Cos}[x_1]\mathrm{Cos}[x_2]\mathrm{Sin}[x_2] - 65.56\mathrm{Cos}[x_2]^2\mathrm{Sin}[x_2] + 72.17\mathrm{Sin}[x_1]\mathrm{Sin}[x_2] - 355.3\mathrm{Cos}[x_1]\mathrm{Sin}[x_1]\mathrm{Sin}[x_2] - 322.2\mathrm{Cos}[x_2]\mathrm{Sin}[x_1]\mathrm{Sin}[x_2] + 40.49\mathrm{Sin}[x_1]^2\mathrm{Sin}[x_2] + 487.3\mathrm{Sin}[x_2]^2 + 157.6\mathrm{Cos}[x_1]\mathrm{Sin}[x_2]^2 + 117.8\mathrm{Cos}[x_2]\mathrm{Sin}[x_2]^2 + 65.69\mathrm{Sin}[x_1]\mathrm{Sin}[x_2]^2 + 53.88\mathrm{Sin}[x_2]^3$$

Model 4 (third order polynomial)

$$Y = 801.6 + 24.73x_1 - 0.6392x_1^2 + 0.009467x_1^3 + 22.17x_2 + 1.198x_1x_2 - 0.04765x_1^2x_2 - 0.9281x_2^2 - 0.02881x_1x_2^2 + 0.02688x_2^3$$

Table 2 denotes the fitting and boundedness performance of mathematical models using to estimate elastic behaviour of PP-based hybrid composites. The most important parameter showing the usability of a mathematical model in the literature is the value of R^2. When the results are examined, it will be seen that except that Model 4 all models R^2 values are 1. If we made a model selection taking into account only the R^2 value, we could think that all the models explain the process well. However, R^2 alone does not correctly define the phenomena of the process. Further, boundedness check control of the proposed models which gives information about whether models are realistic or not should be carried out. We can see if there is a functional limitation (bounded) by calculating the maximum and minimum values produced by the relevant model.

Table 2. Fitting performance and boundedness of models for elastic modulus

Model	R^2	Max.	Min.
Model 1 (fifth order polynomial)	1	1399.29	801.6
Model 2 (third order rational)	1	2194.14	-31020
Model 3 (third order trigonometric)	1	1653.29	377.42
Model 4 (third order polynomial)	0.97	1357.23	801.6

In this context, it has been accepted that the results of polynomial models Model 1 and Model 4 are suitable for the nature of the problem by expert researchers in production and material selection. However, the view that Models 2 and 3 give results that cannot be obtained experimentally came to the fore.

Figure 2 represents 3D plot of polynomial, rational and trigonometric models which are the best fit in the experimental results. When the graphics are examined, it is seen that the models accurately predict all the experimental data. However, as stated when evaluating the results of Table 2, a high R^2 value does not always give accurate information about the usability of the proposed model. Whether the mathematical model gives correct information should be checked with criteria other than R^2. In problems where the number of design variables is one or two, an evaluation can be made by examining the model's results graphically. Since the weight ratios of artichoke and wollastonite materials in the hybrid structure are selected as two design variables in the problem addressed in this study, it is possible to evaluate the mathematical models graphically. Rational and trigonometric models (Model 2 and Model 3) have many local maximum and minimum points, which insignificant changes in design parameters make a non-negligible difference in results. On the contrary, polynomial models (Model 1 and Model 4) show a stable and consistent distribution within the specified range of design parameters. Therefore, these models are appropriate to estimate mathematical phenomena regarding elastic modulus of PP-based hybrid composite.

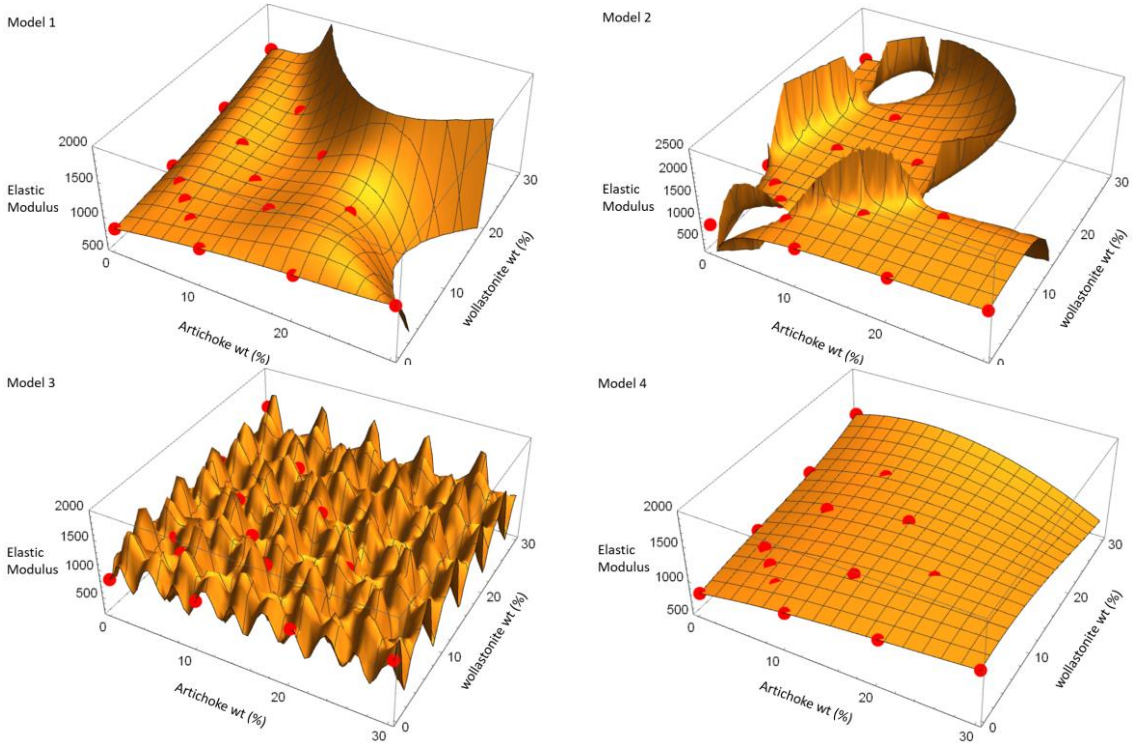

Figure 2. 3D plot representations of experimental data and recommended mathematical model for elastic modulus

Proposed mathematical models to describe phenomena regarding ultimate tensile strength of PP-based hybrid composites. Four distinct models and their fitting performance were given as follow.

Mathematical Models for Ultimate Tensile Strength

Model 1 (sixth order polynomial)

$$Y = 22.34 - 0.1237x_1 - 0.01134x_1^2 + 0.00002776x_1^3 + 0.0001375x_1^4 - (9.586 \times 10^{-6})x_1^5 + (1.76 \times 10^{-7})x_1^6 - 0.09966x_2 + 0.02216x_1x_2 - 0.01042x_1^2x_2 - 0.01065x_1^3x_2 + 0.0009603x_1^4x_2 - 0.00002011x_1^5x_2 - 0.008408x_2^2 + 0.01434x_1x_2^2 + 0.0215x_1^2x_2^2 - 0.0009108x_1^3x_2^2 - (1.304 \times 10^{-7})x_1^4x_2^2 - 0.0007965x_2^3 - 0.01181x_1x_2^3 - 0.0009454x_1^2x_2^3 +$$

$0.00003689x_1^3x_2^3 + 0.0001704x_2^4 + 0.000916x_1x_2^4 + (2.702 \times 10^{-6})x_1^2x_2^4 - (8.699 \times 10^{-6})x_2^5 - 0.00001807x_1x_2^5 + (1.399 \times 10^{-7})x_2^6$

Model 2 (second order rational)

$$Y = \frac{3141.8 - 51.011x_1 - 0.94323x_1^2 - 118.64x_2 - 2.0546x_1x_2 + 0.1594x_2^2}{140.62 - 0.81531x_1 - 0.076061x_1^2 - 4.1694x_2 - 0.19421x_1x_2 - 0.033376x_2^2}$$

Model 3 (third order trigonometric)

$$\begin{aligned}Y = {} & 4.622 + 0.7108\text{Cos}[x_1] + 6.661\text{Cos}[x_1]^2 + 1.155\text{Cos}[x_1]^3 + 0.7972\text{Cos}[x_2] - \\ & 1.973\text{Cos}[x_1]\text{Cos}[x_2] + 1.73\text{Cos}[x_1]^2\text{Cos}[x_2] + 6.162\text{Cos}[x_2]^2 + 1.341\text{Cos}[x_1]\text{Cos}[x_2]^2 + \\ & 1.134\text{Cos}[x_2]^3 + 0.2348\text{Sin}[x_1] + 2.5\text{Cos}[x_1]\text{Sin}[x_1] - 1.035\text{Cos}[x_1]^2\text{Sin}[x_1] - \\ & 1.444\text{Cos}[x_2]\text{Sin}[x_1] - 1.021\text{Cos}[x_1]\text{Cos}[x_2]\text{Sin}[x_1] + 1.34\text{Cos}[x_2]^2\text{Sin}[x_1] + 4.167\text{Sin}[x_1]^2 - \\ & 2.086\text{Cos}[x_1]\text{Sin}[x_1]^2 + 0.2159\text{Cos}[x_2]\text{Sin}[x_1]^2 + 0.6172\text{Sin}[x_1]^3 + 0.001065\text{Sin}[x_2] - \\ & 2.13\text{Cos}[x_1]\text{Sin}[x_2] + 1.414\text{Cos}[x_1]^2\text{Sin}[x_2] + 1.698\text{Cos}[x_2]\text{Sin}[x_2] - \\ & 0.2111\text{Cos}[x_1]\text{Cos}[x_2]\text{Sin}[x_2] - 1.467\text{Cos}[x_2]^2\text{Sin}[x_2] + 5.109\text{Sin}[x_1]\text{Sin}[x_2] - \\ & 8.071\text{Cos}[x_1]\text{Sin}[x_1]\text{Sin}[x_2] - 9.091\text{Cos}[x_2]\text{Sin}[x_1]\text{Sin}[x_2] - 5.494\text{Sin}[x_1]^2\text{Sin}[x_2] + \\ & 5.08\text{Sin}[x_2]^2 + 0.4327\text{Cos}[x_1]\text{Sin}[x_2]^2 - 0.7113\text{Cos}[x_2]\text{Sin}[x_2]^2 - 3.866\text{Sin}[x_1]\text{Sin}[x_2]^2 + \\ & 0.3384\text{Sin}[x_2]^3\end{aligned}$$

Model 4 (third order polynomial)

$$\begin{aligned}Y = {} & 22.34 - 0.2984x_1 + 0.01022x_1^2 - 0.0002481x_1^3 - 0.1546x_2 + 0.02779x_1x_2 - \\ & 0.001013x_1^2x_2 - 0.004468x_2^2 - 0.0008286x_1x_2^2 + 0.0001926x_2^3\end{aligned}$$

Table 3 denotes the fitting and boundedness performance of mathematical models using to estimate ultimate tensile strength (UTS) of PP-based hybrid composites. According to results, sixth order polynomial, second order rational and third order trigonometric models show the best fitting performance in terms of R^2. However, rational and trigonometric models contain maximum and minimum values that cannot be encountered in practice. For this problem, ultimate tensile strength which gives information about the resistance of the material under tensile loading does not get a negative value. In addition to this, experimental results display that the minimum value of UTS is obtained as 16 MPa. Namely, the minimum strength value (7.38 MPa) obtained by Model 1 does not seem realistic. Because of all these reasons, the third-order polynomial model (Model 4), which has a more straightforward structure and produces more realistic values, is recommended in PP-based hybrid composite material design where strength is considered an important parameter.

Table 3. Fitting performance and boundedness of models for ultimate tensile strength

Model	R^2	Max.	Min.
Model 1 (sixth order polynomial)	1	30.66	7.38
Model 2 (second order rational)	1	22.34	-15.06
Model 3 (third order trigonometric)	1	28.98	-0.31
Model 4 (third order polynomial)	0.95	22.14	15.89

Figure 3 demonstrates 3D plot of polynomial, rational and trigonometric models which are the best fit in the experimental results with respect to concerning ultimate tensile strength. As mentioned above, graphical demonstration gives an important idea to us concerning mathematical model selection. The rational model, which has many discontinuities and extreme values, is not a suitable model to express strength mathematically. It is decided that although the trigonometric model shows well fit with the experimental results, it is not a suitable model taking into account expert opinions. For similar reasons,

Model 1 cannot be used either. In this regard, it can be said that third order polynomial model is the most appropriate model that gives the realistic results.

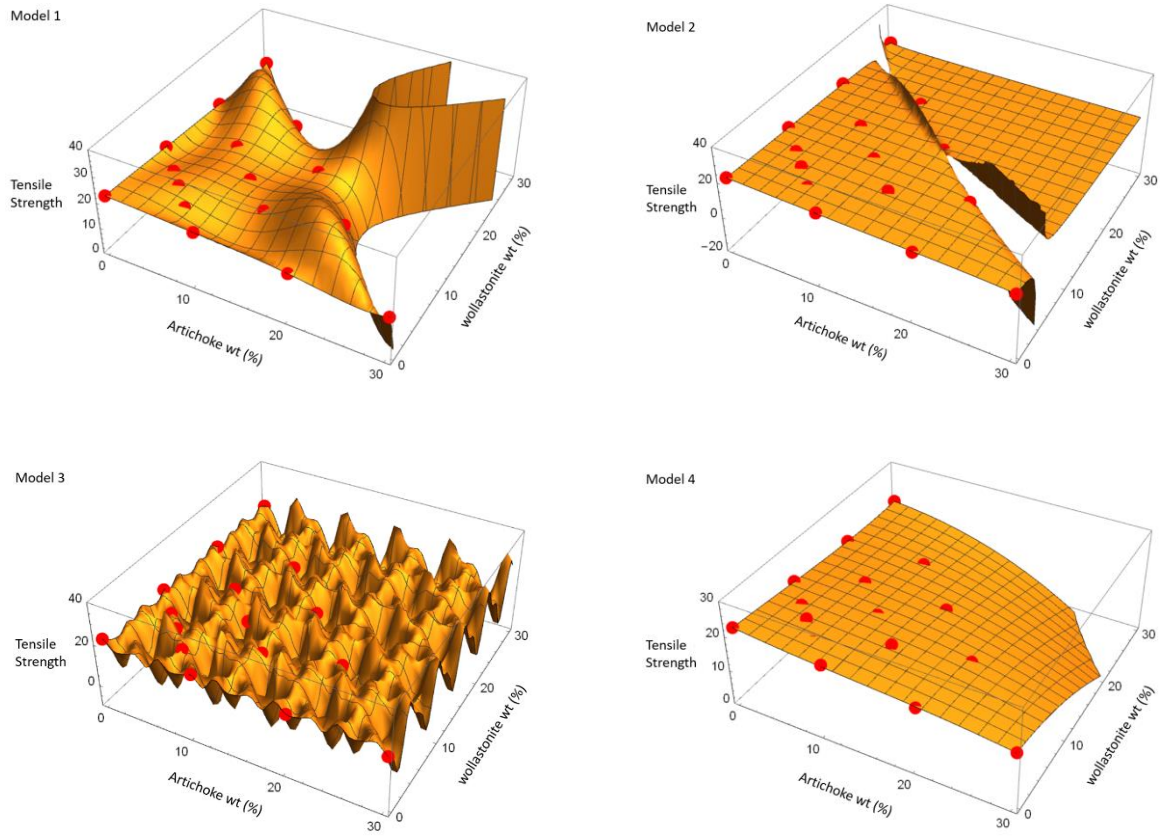

Figure 3. 3D plot representations of experimental data and recommended mathematical model for ultimate tensile strength

In order to define physical phenomena regarding ultimate strain of PP-based hybrid composites, four distinct mathematical models and their fitting performance were given as follow.

Mathematical Models for Ultimate Strain

Model 1 (sixth order polynomial)

$$Y = 5.52 - 0.1422x_1 + 0.00196x_1^2 - 0.0004241x_1^3 + 0.00008384x_1^4 - (4.667 \times 10^{-6})x_1^5 + (7.816 \times 10^{-8})x_1^6 - 0.05474x_2 - 0.02993x_1x_2 + 0.007392x_1^2x_2 - 0.006162x_1^3x_2 + 0.0004825x_1^4x_2 - (9.539 \times 10^{-6})x_1^5x_2 - 0.001292x_2^2 - 0.002668x_1x_2^2 + 0.01165x_1^2x_2^2 - 0.0004904x_1^3x_2^2 + (8.529 \times 10^{-7})x_1^4x_2^2 - 0.0001888x_2^3 - 0.005781x_1x_2^3 - 0.0004778x_1^2x_2^3 + 0.00001849x_1^3x_2^3 + 0.00007167x_2^4 + 0.0004986x_1x_2^4 - (4.091 \times 10^{-8})x_1^2x_2^4 - (4.948 \times 10^{-6})x_2^5 - 0.00001018x_1x_2^5 + (9.358 \times 10^{-8})x_2^6$$

Model 2 (third order rational)

$$Y = (-8.7426 \times 10^6 - (5.9254 \times 10^8)x_1 - (1.506 \times 10^9)x_1^2 + (4.6272 \times 10^7)x_1^3 - (6.7693 \times 10^8)x_2 + (3.0311 \times 10^9)x_1x_2 + (1.3337 \times 10^8)x_1^2x_2 - (1.7382 \times 10^9)x_2^2 - (8.0405 \times 10^7)x_1x_2^2 + (1.4135 \times 10^8)x_2^3)/(-1.5835 \times 10^6 + (1.3053 \times 10^9)x_1 - (5.3328 \times 10^8)x_1^2 + (1.4823 \times 10^7)x_1^3 + (2.0706 \times 10^9)x_2 + (1.2855 \times 10^6)x_1x_2 + (6.9078 \times 10^7)x_1^2x_2 - (7.3308 \times 10^8)x_2^2 + (2.4002 \times 10^7)x_1x_2^2 + (4.4705 \times 10^7)x_2^3)$$

Model 3 (third order trigonometric)

$$Y = 0.921 + 0.2069\text{Cos}[x_1] + 1.408\text{Cos}[x_1]^2 + 0.3694\text{Cos}[x_1]^3 + 0.1811\text{Cos}[x_2] - 0.3544\text{Cos}[x_1]\text{Cos}[x_2] + 0.5762\text{Cos}[x_1]^2\text{Cos}[x_2] + 1.342\text{Cos}[x_2]^2 + 0.5977\text{Cos}[x_1]\text{Cos}[x_2]^2 + 0.2719\text{Cos}[x_2]^3 + 0.03054\text{Sin}[x_1] + 0.5365\text{Cos}[x_1]\text{Sin}[x_1] - 0.406\text{Cos}[x_1]^2\text{Sin}[x_1] - 0.3352\text{Cos}[x_2]\text{Sin}[x_1] + 0.005495\text{Cos}[x_1]\text{Cos}[x_2]\text{Sin}[x_1] + 0.237\text{Cos}[x_2]^2\text{Sin}[x_1] + 0.6831\text{Sin}[x_1]^2 - 0.9424\text{Cos}[x_1]\text{Sin}[x_1]^2 - 0.1696\text{Cos}[x_2]\text{Sin}[x_1]^2 + 0.1425\text{Sin}[x_1]^3 - 0.05898\text{Sin}[x_2] - 0.4338\text{Cos}[x_1]\text{Sin}[x_2] + 0.2482\text{Cos}[x_1]^2\text{Sin}[x_2] + 0.6653\text{Cos}[x_2]\text{Sin}[x_2] + 0.4743\text{Cos}[x_1]\text{Cos}[x_2]\text{Sin}[x_2] - 0.7262\text{Cos}[x_2]^2\text{Sin}[x_2] + 1.119\text{Sin}[x_1]\text{Sin}[x_2] - 0.7263\text{Cos}[x_1]\text{Sin}[x_1]\text{Sin}[x_2] - 1.424\text{Cos}[x_2]\text{Sin}[x_1]\text{Sin}[x_2] - 1.304\text{Sin}[x_1]^2\text{Sin}[x_2] + 0.803\text{Sin}[x_2]^2 - 0.1215\text{Cos}[x_1]\text{Sin}[x_2]^2 - 0.3062\text{Cos}[x_2]\text{Sin}[x_2]^2 - 0.7467\text{Sin}[x_1]\text{Sin}[x_2]^2 + 0.07127\text{Sin}[x_2]^3$$

Model 4 (fourth order polynomial)

$$Y = 5.52 - 0.1943x_1 + 0.01213x_1^2 - 0.0005466x_1^3 + (8.891 \times 10^{-6})x_1^4 - 0.1006x_2 - 0.07173x_1x_2 + 0.006727x_1^2x_2 - 0.0001407x_1^3x_2 + 0.008007x_2^2 + 0.004726x_1x_2^2 - 0.0002343x_1^2x_2^2 - 0.000555x_2^3 - 0.00007394x_1x_2^3 + 0.00001102x_2^4$$

Table 4 denotes the fitting and boundedness performance of mathematical models using to estimate ultimate strain of PP-based hybrid composites. Although it has a lower R^2 value as in models expressing elastic modulus and strength, fourth order polynomial model is the most appropriate model to mean the experimental results related to strain. Graphical representation in Figure 4 supports this idea.

Table 4. Fitting performance and boundedness of models for ultimate strain

Model	R^2	Max.	Min.
Model 1 (sixth order polynomial)	1	9.01	-0.53
Model 2 (third order rational)	1	36.58	-16.92
Model 3 (third order trigonometric)	1	5.82	-0.46
Model 4 (fourth order polynomial)	0.95	5.52	2.70

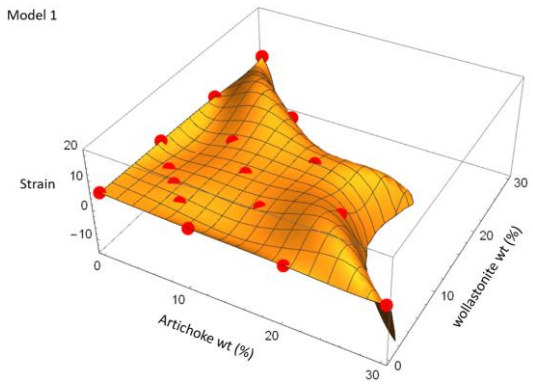

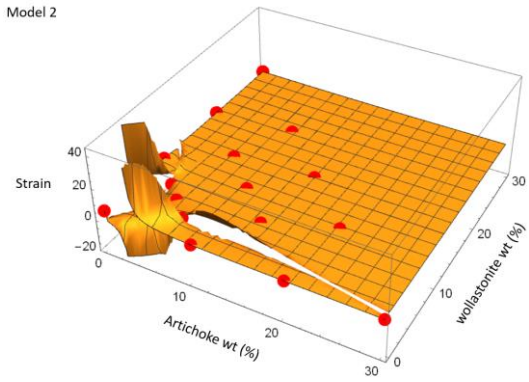

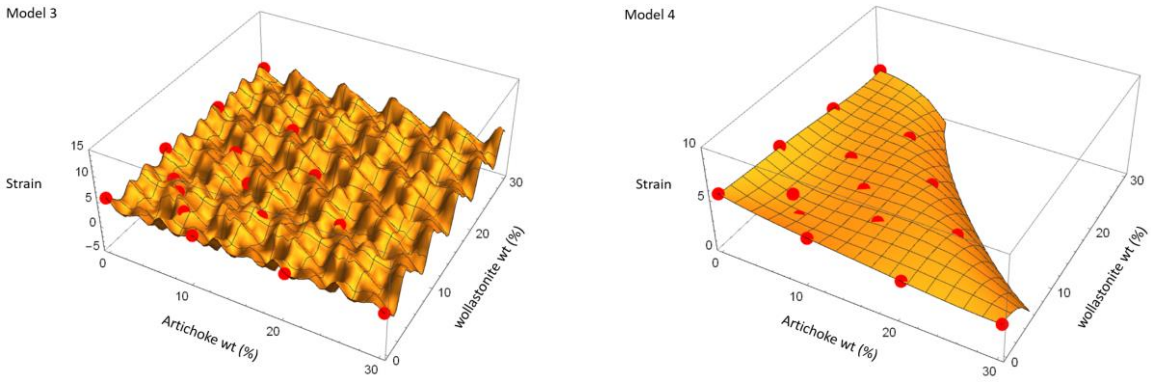

Figure 4. 3D plot representations of experimental data and recommended mathematical model for ultimate strain

Conclusion

In this study, artichoke stem particles (AS) and wollastonite mineral (W) were used as an organic and inorganic fillers in order to improve the mechanical properties of polypropylene (PP). PP-based hybrid composites, including different proportions of artichoke stem particles and wollastonite mineral, were mathematically modeled using the data regarding elastic modulus, ultimate strength, and strain obtained from the experimental study. The most important parameter showing the usability of a mathematical model in the literature is the value of R^2. In this study, the primary purpose is to show that it is always possible to create a model with an R^2 value of 1. In this regard 9 different polynomials, rational and trigonometric non- linear models whose R^2 value is equal to 1 are given. However, a high value of R^2 itself does not always mean a good fit, and it does not define the entire physical phenomena of the engineering process. Graphically results given in the study denote that R^2 is not enough standalone criterion to evaluate the mathematical models. It has been specified that other criteria are needed in the evaluation of the models. It is impossible to obtain a realistic functional structure in cases where models are not examined in terms of stability. To overcome this drawback, the functions that produce value only within the physical limits by inspecting the boundedness of each candidate model have been admitted as successful. In the light of these evaluations, it was seen that only polynomial models fulfill the necessary success criteria.

References

[1] Saba N, Paridah MT, Jawaid M. Mechanical properties of kenaf fibre reinforced polymer composite: A review. Constr Build Mater. 2015 Feb;76:87–96.
[2] Xu Y, Wu Q, Lei Y, Yao F. Creep behavior of bagasse fiber reinforced polymer composites. Bioresour Technol. 2010 May;101(9):3280–6.
[3] Sever K, Sarikanat M, Seki Y, Erkan G, Erdoğan ÜH, Erden S. Surface treatments of jute fabric: The influence of surface characteristics on jute fabrics and mechanical properties of jute/polyester composites. Ind Crops Prod. 2012 Jan;35(1):22–30.
[4] Rong MZ, Zhang MQ, Liu Y, Yang GC, Zeng HM. The effect of fiber treatment on the mechanical properties of unidirectional sisal-reinforced epoxy composites. Compos Sci Technol. 2001 Aug;61(10):1437–47.
[5] Verma D, Gope PC. The use of coir/coconut fibers as reinforcements in composites. In: Biofiber Reinforcements in Composite Materials [Internet]. Elsevier; 2015 [cited 2021 Jun 8]. p. 285–319. Available from: https://linkinghub.elsevier.com/retrieve/pii/B9781782421221500101
[6] Kılınc AC, Atagur M, Ozdemir O, Sen I, Kucukdogan N, Sever K, et al. Manufacturing and characterization of vine stem reinforced high density polyethylene composites. Compos Part B Eng. 2016 Apr;91:267–74.
[7] Kaya N, Atagur M, Akyuz O, Seki Y, Sarikanat M, Sutcu M, et al. Fabrication and characterization of olive pomace filled PP composites. Compos Part B Eng. 2018 Oct;150:277–83.
[8] Nourbakhsh A, Ashori A. Wood plastic composites from agro-waste materials: Analysis of mechanical properties. Bioresour Technol. 2010 Apr;101(7):2525–8.

[9] Yao F, Wu Q, Lei Y, Xu Y. Rice straw fiber-reinforced high-density polyethylene composite: Effect of fiber type and loading. Ind Crops Prod. 2008 Jul;28(1):63–72.
[10] Essabir H, Nekhlaoui S, Malha M, Bensalah MO, Arrakhiz FZ, Qaiss A, et al. Bio-composites based on polypropylene reinforced with Almond Shells particles: Mechanical and thermal properties. Mater Des. 2013 Oct;51:225–30.
[11] Mengeloglu F, Karakus K. Thermal Degradation, Mechanical Properties and Morphology of Wheat Straw Flour Filled Recycled Thermoplastic Composites. Sensors. 2008 Jan 24;8(1):500–19.
[12] Guimarães JL, Frollini E, da Silva CG, Wypych F, Satyanarayana KG. Characterization of banana, sugarcane bagasse and sponge gourd fibers of Brazil. Ind Crops Prod. 2009 Nov;30(3):407–15.
[13] Mattos BD, Misso AL, de Cademartori PHG, de Lima EA, Magalhães WLE, Gatto DA. Properties of polypropylene composites filled with a mixture of household waste of mate-tea and wood particles. Constr Build Mater. 2014 Jun;61:60–8.
[14] Aktaş LT, Aydın L. Stochastic optimization and modeling of high-velocity impact tests on high-temperature carbon–carbon composites. SN Appl Sci. 2021 Mar;3(3):313.
[15] Sever K, Yılmaz M. Evaluation of Mechanical and Thermal Properties of Artichoke Filled Polypropylene Composites: Influence of Wollastonite Hybridization. Emerg Mater Res. 2020 Jun 1;9(2):1–6.

An Improved Control Arm Design for a Commercial Vehicle

Sinan Yıldırım[1,2,], Ufuk Çoban[1], Mehmet Çevik[3]*
[1]BMC Automotive, Test and Validation Dept., İzmir, Turkey
[2]Izmir Kâtip Çelebi Univ., The Graduate School of Natural and Applied Sciences, Izmir, Turkey
[3]Izmir Kâtip Çelebi Univ., Dept. of Mechanical Engineering, Izmir, Turkey
**Corresponding author: sinanyildirim92@gmail.com*

Abstract

Suspension linkages are one of the fundamental structural elements in each vehicle since they connect the wheel carriers i.e. axles to the body of the vehicle. Moreover, the characteristics of suspension linkages within a suspension system can directly affect driving safety, comfort and economics. Beyond these, all these design criteria are bounded to the package space of the vehicle. In last decades, suspension linkages have been focused on in terms of design development and cost reduction. In this study, a control arm of a diesel public bus was taken into account in order to get the most cost-effective design while improving the strength within specified boundary conditions. Due to the change of the supplier, the control arm of a rigid axle was redesigned to find an economical and more durable solution. The new design was analyzed first by the finite element analysis software Ansys and the finite element model of the control arm was validated by physical tensile tests. The outputs of the study demonstrate that the new design geometry reduces the maximum Von Mises stress 15% while being within the elastic region of the material in use and having found an economical solution in terms of supplier's criteria.

Keywords: automotive engineering, control arm, suspension systems, finite element analysis

Introduction

In the contemporary vehicle design in automotive industry, it is getting more important to take customer's needs as the basis of design criteria [1]. This remark leads engineers to deal with the vehicle design of today, which is directly linked to driving dynamics, driving comfort and driving safety.

As a holistic approach and as a subsystem of the vehicle, suspension system is one of the systems that covers those three main parameters. The suspension forms a bridge between the vehicle and the road. Neglecting inertial, powertrain and aerodynamic forces, all external forces come to the vehicle through a contact patch between tire and the road in various directions and loading cases.

In this study, the control arm of a diesel public bus was taken into account in order to get the most cost-effective design while improving the strength within specified boundary conditions. Due to the change of the supplier, the control arm of a rigid axle was redesigned to find an economical and more durable solution. In that sense, it was necessary to validate the new control arm design with respect to an appropriate design within specified boundary conditions, a more durable design and a cost-effective solution.

Recent studies [2-6] show that the control arm of a vehicle was investigated in terms of weight and cost reduction, which was linked to the safety, driving dynamics and driving comfort.

Methodology

Initially, the scope of the study was clarified according to the specifications. As the specifications of the study was about investigations on the control arm of the rigid axle, only the control arm itself was considered. Materials of the study was then justified to perform the investigations on it. The critical sub-part of the control arm was determined and its material was confirmed by a tensile test performed in the company laboratory. Then, the existing control arm design was validated performing both physical test and a structural analysis on ANSYS Workbench environment. Results were investigated and a new design on a critical region on the simulation was developed. A finite element analysis (FEA) of the new design was also performed. The results of the reference and new designs were compared as well as the production cost. The use of FEA for weight and cost reduction of industrial machine parts are studied by many researchers [7-10].

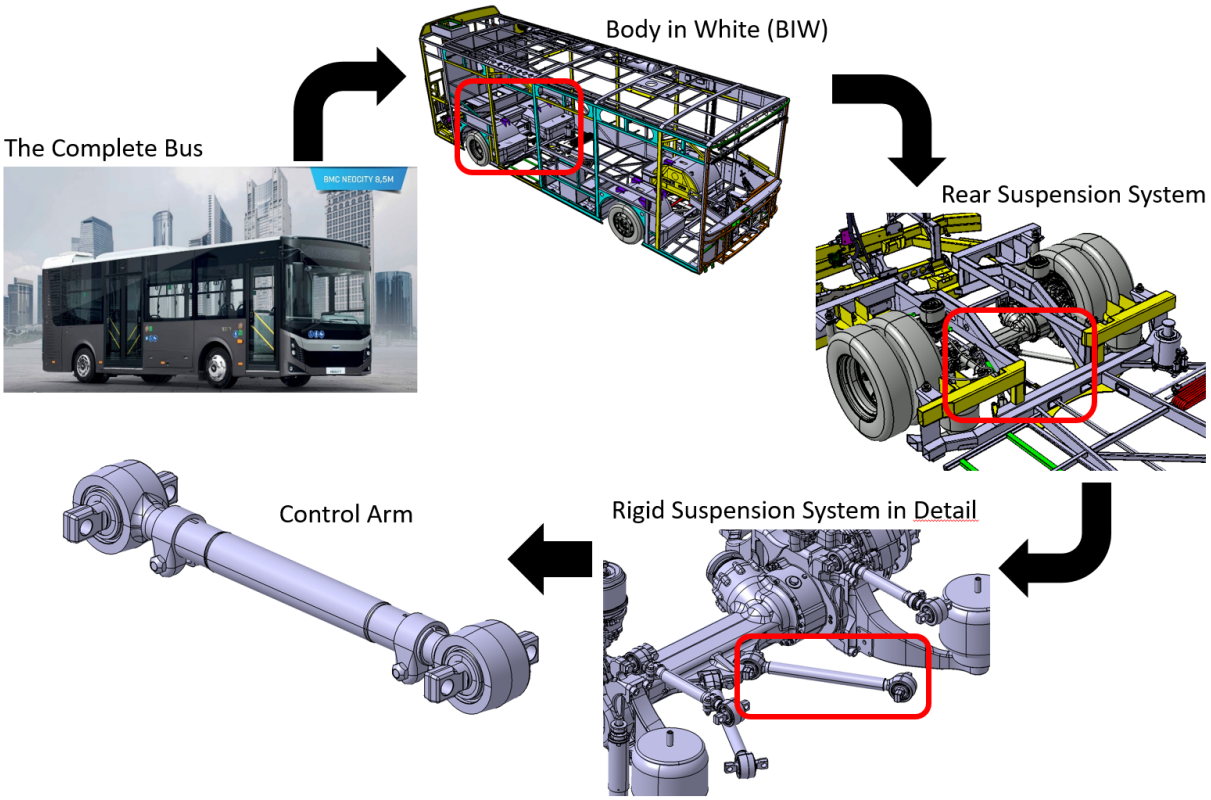

Figure 1. An overview of the design

The geometrical scope of the study covers only one of the control arms used in the public bus as seen in Figure 1. The axle body was accepted as out of the control volume or as a rigid body so that the rest of the system can be neglected.

Materials used in the study were denoted in Figure 2. The hub of the control arm was made of C-1050, the joint connecting the control arm to the axle body was made of a forged steel whose yield strength is higher than the bolts in use in that region.

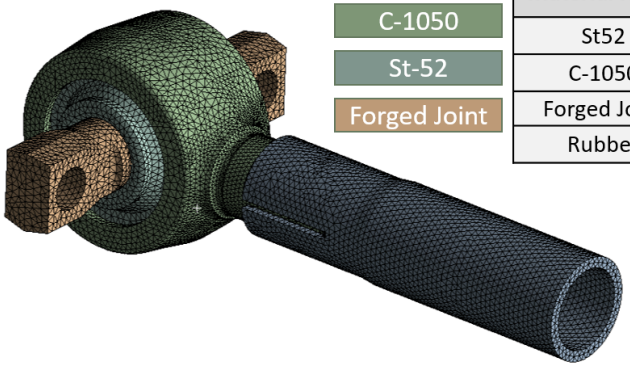

Material Name	Yield Strength [MPa]	Ultimate Strength [MPa]
St52	355	500
C-1050	380	600
Forged Joint	1080	1200
Rubber	Shore: 68	

Figure 2. Materials used in the design

The control arm was connected to the axle body with two DIN6921 M18x60 G10.9 hex bolts with a tightening torque of 440Nm. Moreover, as the yield strength of a bolt with a quality of 10.9 is 900MPa while the yield strength of the hub is 380MPa, the hub was determined as the critical part. Therefore, those hex-bolts were neglected in this study.

Tensile test of the hub was material C-1050 steel was performed and the stress-strain diagram is shown in Figure 3.

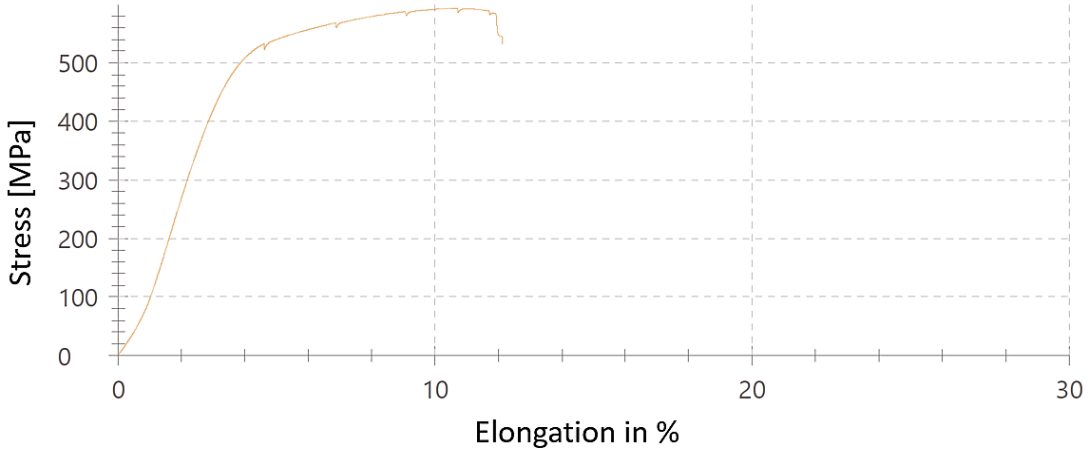

Figure 3. Stress-strain diagram of C-1050 steel used for the hub

Although there is a rubber element within the hub, the rubber material with 68 Shore was generalized as if it was St-52 material since the focus of the study is not elastoplastic or hyperelastic behavior of the control arm. This generalization was used both during the tensile test of the C-1050 material and the FEA steps to be told afterwards.

For the friction between sub-parts of the study, the frictional coefficient was taken 0.2 in FEA. Loading conditions were obtained from the "MSC Adams", a Multi Body Dynamics (MBD) software, for the Control Arm both to be used in the physical test and FEA simulation. For this information, the "Vehicle Dynamics contribution" team within BMC automotive has been worked with. Accordingly, the axial force on the control arm was obtained as 156kN under the vehicle's longitudinal shock loading condition. Regarding this loading condition, it was aimed to observe whether the control arm breaks or any possible plastic deformation happens in the test to be carried out by the supplier company.

Findings from Adams MBD software were compared with the characteristics of other tested vehicles and these results were found to be consistent. Based on this, road loads of other loading conditions were taken into consideration. In that sense, Pothole Braking, which is one of the loads where the axial force is most obvious to the control arm, is defined for the control of the safety conditions in the elastic region within the limits of yield strength, since it exposes the vehicles to a 2g load in the x-axis. Loading information was presented in Table 1.

Table 1. Loading conditions derived by MSC Adams

	X [N]	**Y [N]**	**Z [N]**
Longitudinal Shock	155.6 E+03	-1.64	-1.2 E+03
Pothole Braking	51.6 E+03	0	2.9 E+03

For FEA analysis as seen in Figure 4, a fixed support was defined from the bolt holes of the joint (shown in blue). Tensile displacement was applied to catch the target axial force from the symmetrically cut section of the control arm pipe profile (shown in yellow). The same procedure was applied to the physical test of the control arm.

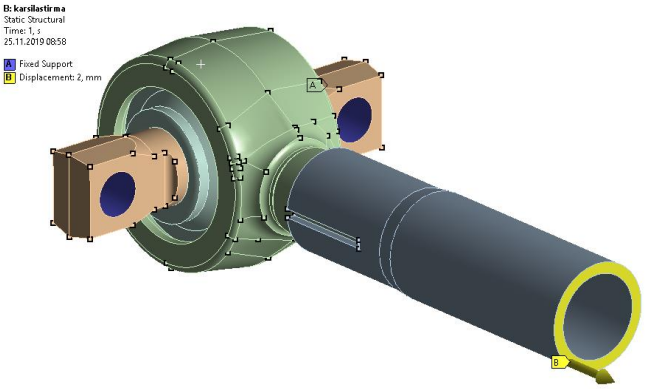

Figure 4. Boundary conditions of the system

Results

Control arm analyses were verified with the part pull test performed at the supplier company and the benchmark with identical loadings of the control arms used in diesel buses.

An axial drawbar load of 156kN, corresponding to the definition of longitudinal shock (acceleration axes x: 3g, y: 0, z: -1g) taken from the vehicle dynamics team, was given and the control arm was tested under this force. As a result of the test performed with 156 kN longitudinal shock tensile force, plastic deformation was observed in the knuckle region of the part, as seen in Figure 5. However, no rupture occurred in the piece (see Figure 6).

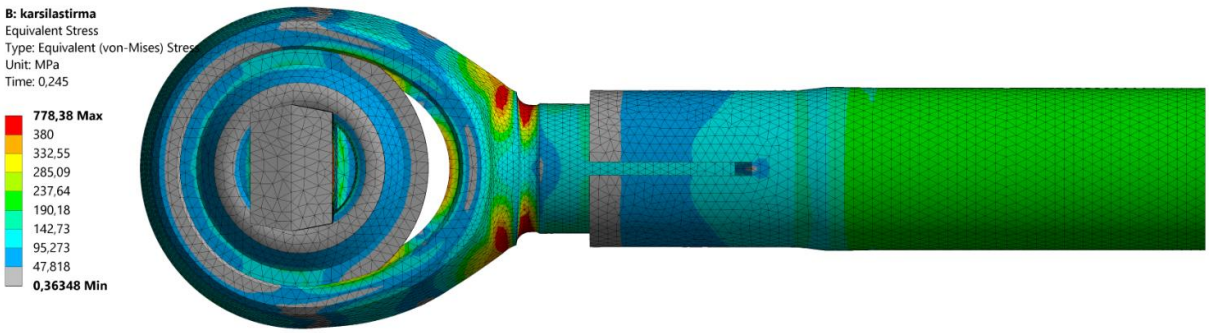

Figure 5. Deformation behavior of the part according to longitudinal shock results

Figure 6. Test specimen after the tensile test

In order to understand whether similar plastic deformation will be seen in the analyses and to confirm the test, analysis was performed with the longitudinal shock load. According to the analysis results, the deformation form on the part coincides with the test result when the same conditions are met. The similarity can be easily understood by comparing Figures 5 and 6.

The results have been compared with the equivalent control arm variation of the bus due to its structural similarities. The structural comparison of the control arm and the 8.5m drawbars is presented in Figure 7, with the main difference being the radius forms in the knuckle of the hub. Since the radius transition of the existing tool is more dramatic, the stress build-up is higher (Figure 8).

A comparison was performed because of the structural similarities between reference design and the new design. The main difference lays on the radius region on the hub. The main difference was at the radius forms in the knuckle of the hub (Figure 8). Since the radius transition of the existing tool is more dramatic, the Von-Mises stress was higher.

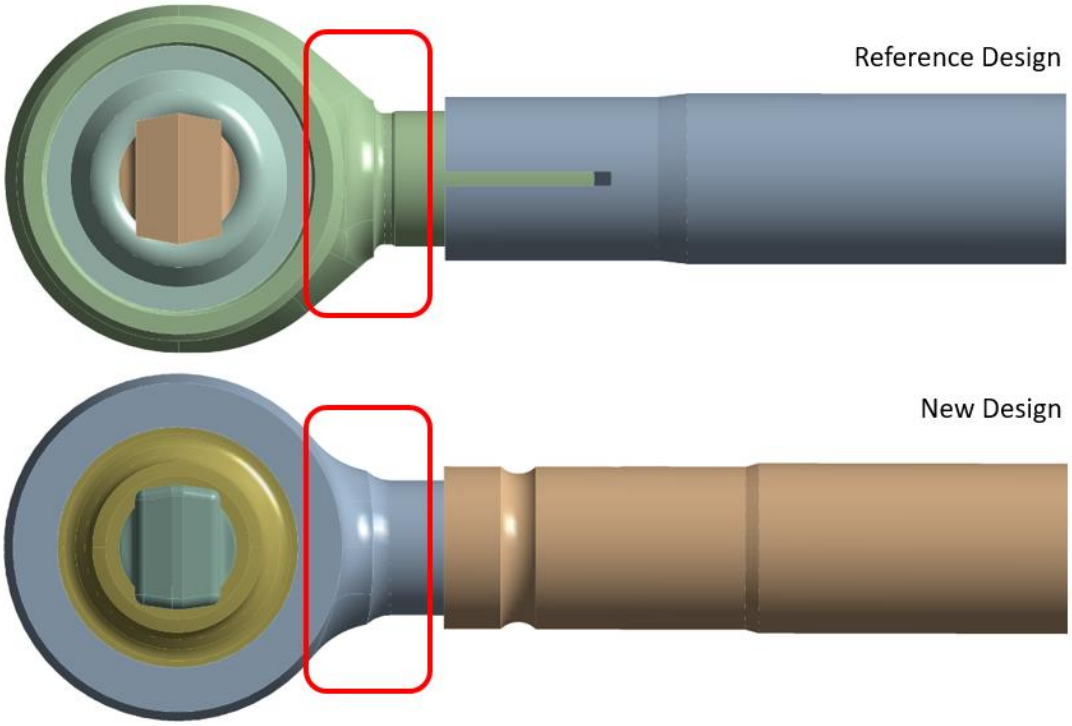

Figure 7. Geometric comparison between existing and the new designs

When the Longitudinal Shock results are compared, a distributed Von Mises stress of around 700MPa was observed in the control arm of the current vehicle. In contrast, the Von Mises stress is around 465 MPa in the new design. It is understood that the control arm will continue to provide the road-body connection as a result of the front shock loading according to the static vehicle load (Figure 8). For the longitudinal shock, the ultimate strength of the material was considered instead of yield point.

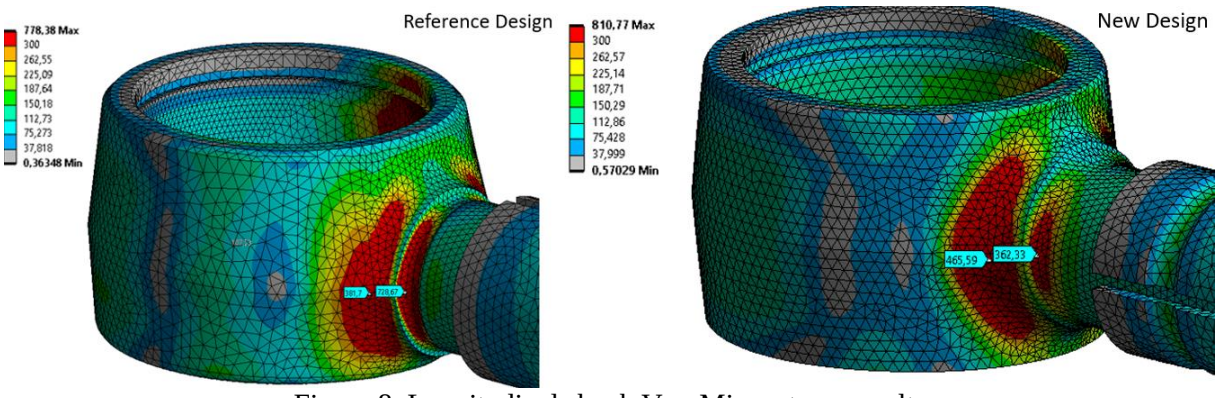

Figure 8. Longitudinal shock Von Mises stress results

Considering the elastic behavior of the control arm, pothole braking loading condition with an axial force of 51.6kN was applied to two systems (reference and new design). The resulting Von Mises stress on the reference design was found 320MPa with a safety factor of 1.18. On the other hand, the new design faced with 270MPa of Von Mises stress on the radius of the hub with a safety factor of 1.40 (Figure 9).

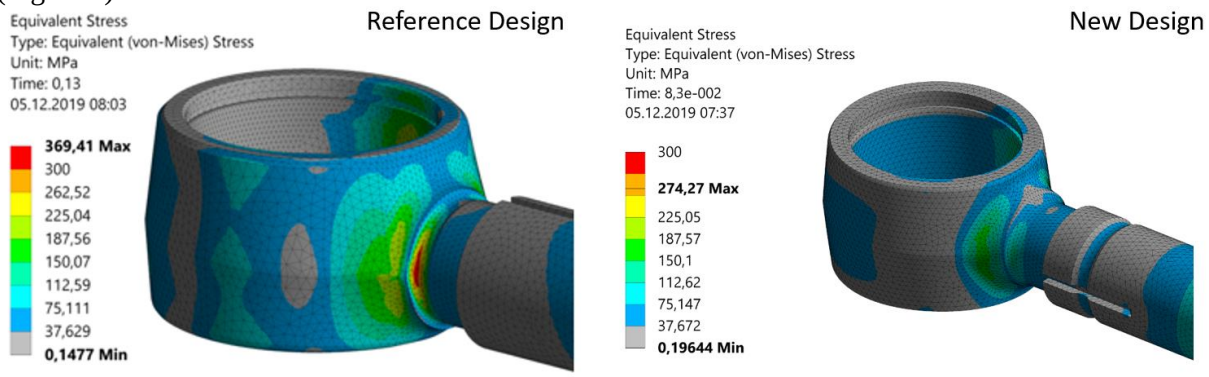

Figure 9. Pothole braking Von Mises stress results

The comparison in pothole braking loading condition between two design levels was done on the stess-strain curve of the C-1050 hub material (see Figure 10).

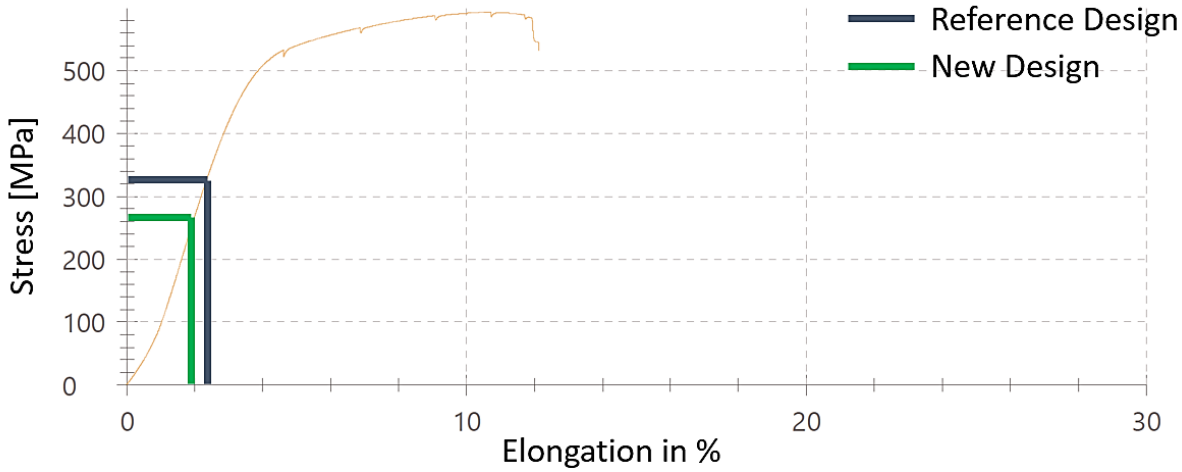

Figure 10. Von Mises Stresses in pothole braking results on stress-strain plot of C-1050

Discussion and Conclusion

It has been observed that under the longitudinal shock condition (x: 3g, y: 0, z: -1g) coming from the vehicle dynamics, 156kN axial force is applied to the drawbar. Longitudinal shock for rupture scenario and pothole braking loading condition for elastic zone behavior were evaluated. In the Pothole Braking loading condition (x: 2g, y: 0, z:-3g), the evaluation was made with the axial loading on the control arm.

According to the results of longitudinal shock and tensile test, no rupture was observed.

Von Mises stress and plastic strain values are consistent with the definition of elasto-plastic material and non-linear quasi-static analysis conditions originating from geometric nonlinearity. Thus, it has been evaluated that the axle will be securely connected to the body and axle after this loading.

As a result of the studies, a structural strength comparison was made between the control arm used in the reference buses and the new control arm. The results of the new control arm in pothole braking loading condition were found to be 15% better than the results of the reference geometry. Accordingly, the evaluation is presented in Table 2.

Table 2. Evaluation of pothole braking in terms of the safety factor

Design Levels	Pothole Braking	
	Von Mises [MPa]	Safety Factor
New Design	320	1.18
Reference Design	270	1.40

The new design fulfilled the requirements of the supplier, which brings a cost-effective solution in trade.

References

[1] Heißing B, & Ersoy M (Eds.). (2011). Chassis Handbook. Vieweg+Teubner.
[2] Song B-C, Park Y-C, Kang S-W, & Lee K-H (2009). Structural optimization of an upper control arm, considering the strength. Proceedings of the Institution of Mechanical Engineers, Part D: Journal of Automobile Engineering, 223(6), 727–735.
[3] Lee D-C, & Lee J-I (2003). Structural optimization concept for the design of an aluminium control arm. Proceedings of the Institution of Mechanical Engineers, Part D: Journal of Automobile Engineering, 217(8), 647–656.
[4] Ramli MN, Sulaiman S, Azizul MA. Implementation of Weight Reduction Method for Lower Front Control Arm without Reducing the Safety Factor. J of Design for Sust. And Env. 2020; 2(2):1-6
[5] Goudra BM, Gowda N. Structural Analysis and Comparison of control Arm using SAE J2340 and Kevlar 49/Epoxy Fabric. Int Res J of Eng &Tech 2018; 5(8)
[6] Billur S, Raju GU. Mass Optimization of Automotive Radial Arm Using FEA for Modal and Static structural Analysis. IOP Conf. Ser.: Mater. Sci. Eng. 2021; 1116 012113.
[7] Sunar Ö, Çevik M. Tek katlı yaprak yaylarda sonlu elemanlar yöntemi ile yorulma analizi. Celal Bayar University Journal of Science 2015; 11(1): 1-6.
[8] Krishna AGL, Kumar KMS. Analytical and Finite Element Solution of Tractor Brake Link to Achieve Weight and Cost Reduction. Applied Mechanics and Materials 2019; 895: 307-312.
[9] Kankariya NKP, Pimple SS. Three Piece Wheel Rim Weight Reduction by Finite Element Analysis. International Journal of Engineering Research & Technology 2020; 9(4): 440-442.
[10] Reddy PSK, Nagaraju Ch. Weight optimization and Finite Element Analysis of Composite automotive drive shaft for Maximum Stiffness. Materials Today Proceedings 2017; 4(2): 2390-2396.

Approximate Solutions of Nonlinear Pendulum with Fractional Damping

Sümeyye Sınır[1], Bengi Yıldız[2], B. Gültekin Sınır[3]*
[1]Izmir Katip Çelebi University, General Coordination Office of Projects, Izmir, Turkey
[2]Bilecik Şeyh Edebali University, Department of Mathematics, Bilecik, Turkey
[3]Manisa Celal Bayar University, Department of Civil Engineering, Manisa, Turkey
**Corresponding author: sumeyye.sinir@ikc.edu.tr*

Abstract

Because of many real problems are better characterized using fractional-order models, fractional calculus has recently become an intensively developing area of calculus not only among mathematicians but also among physicists and engineers as well. Fractional oscillator and fractional damped structure have attracted the attention of researchers in the field of mechanical and civil engineering [1-6].

This study is dedicated mainly a pendulum with fractional viscous damping. The mathematic model of pendulum is a cubic nonlinear equation governing the oscillations of systems having a single degree of freedom, via Riemann-Liouville fractional derivative. The method of multiple scales is performed to solve the equation by assigning the nonlinear and damping terms to the ε-order. Finally, the effects of the coefficient of a fractional damping term on the approximate solution are observed.

Keywords: fractional derivative, fractional damping, method of multiple time scales, perturbation method

Introduction

In recent years, nonlinear phenomena have been successfully modeled using the theory of derivatives and integrals of fractional order in many areas of science and engineering, such as dynamic systems, mathematical biology, optimal control, mechanics, and so on [1-6, 8, 11-13, 14, 16, 21]. Fractional calculus is known as one of the generalizations of the classical calculus which is the main reason for using fractional calculus. Although there are many mathematically acceptable and common fractional derivative definitions such as Riemann-Liouville, Caputo, Grünwald-Letnikov, Marchaud, Coimbra, Canavati, Riesz and so on [9-10, 15, 17-18], two type of them, namely Riemann-Liouville and Caputo, are mostly used in problem formulations.

Since the fractional damper more accurately represents the behavior of viscoelastic materials, fractional oscillator and fractional damped structure have attracted considerable interest from researchers in the field of mechanical and civil engineering [5, 19-20].

Physical structures can be modeled nonlinearly and so the mathematical equations of nonlinearly modeled structures are included nonlinear terms. Perturbation methods are widely used to get approximate analytical solutions of these systems, and they can be used for the analysis of these mechanical systems whose behaviour is described by vicsoelastic models with fractional derivatives. For this purpose, many different perturbation methods have been developed. Of these, the method of multiple time scales is one of the most well-known methods [5-7].

Determining the behavior of physical structures is important in many fields, especially in engineering. Physical systems are considered in the literature to be single degree of freedom, multi degree of freedom and continuous systems and solutions of mathematical models of single freedom systems have been done by perturbation as well as by many methods [6-7].

Because of when doing research in a new field, firstly its effects on single degree of freedom systems are examined is common approach. Also, in this study, the model of pendulum which is a primary (simple) mechanical system with fractional viscous damping is introduced. The multiple time scales method is applied directly to the equation of motion. The method is chosen is convenient for nonlinear differential equations. The approximate solution of the equation is calculated and the effects of the coefficient of a fractional damping are observed from the solution.

Equation of Motion

In this study, it is aimed to investigate a pendulum with fractional viscous damping [1,6], which is a nonlinear equation governing the oscillations of systems having a single degree of freedom, via Riemann-Liouville fractional derivative.

$$\ddot{\theta} + 2\hat{\mu}D^{\alpha}(\theta) + \omega_0^2 \sin(\theta) = 0 \quad (1)$$

where θ is an angle of the displaced pendulum, ω_0 is natural frequency of the pendulum, $\hat{\mu}$ is the damping coefficient and D^{α} denotes α order fractional derivative.

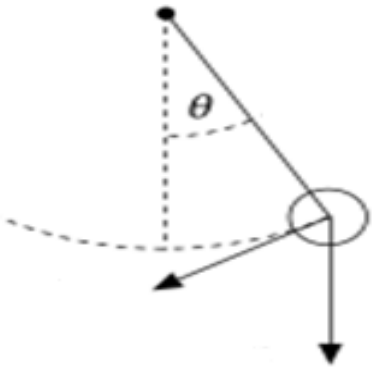

Figure 1. Displacement of a pendulum

We seek an approximate solution of Eq. (1) that is uniformly valid near $\theta = 0$ and that accounts for nonlinear effects. To this end we expand $\sin(\theta)$ and retain only the first two term, consequently Eq. (1) with cubic nonlinearities and damping defined by Riemann-Liouville fractional derivative becomes as following,

$$\ddot{\theta} + 2\hat{\mu}D^{\alpha}(\theta) + \omega_0^2 \left(\theta - \frac{1}{6}\theta^3\right) = 0 \quad (2)$$

Solution

The method of multiple scales is performed to solve the equation by assigning the nonlinear and damping terms to the ε-order. Eq. (2) is solved by using method of multiple time scale to determine a first order perturbation solution for small ε. Assuming a first order expansion, we write:

$$\theta(t,\varepsilon) = \varepsilon\theta_1(T_1, T_2, T_3, \dots) + \varepsilon^2\theta_2(T_1, T_2, T_3, \dots) + \varepsilon^3\theta_3(T_1, T_2, T_3, \dots) + \cdots \quad (3)$$

Here, θ_1, θ_2 and θ_3 are are the displacement functions at order ε, ε^2 and ε^3. Time scales are in the following form

$$T_1 = \varepsilon t,\ T_2 = \varepsilon^2 t,\ T_3 = \varepsilon^3 t, \quad (4)$$

Here, T_0 is fast time scale and T_1, T_2, T_3 are slow time scales characterizing the modulations of the amplitude and phase. The relationship related to time derivatives can be written as

$$\frac{d}{dt} = D_0 + \varepsilon D_1 + \varepsilon^2 D_3 + \cdots \quad (5)$$

$$\frac{d^2}{dt^2} = D_0^2 + 2\varepsilon D_0 D_1 + \varepsilon^2(D_1^2 + 2D_0 D_2) + \cdots \quad (6)$$

$$\left(\frac{d}{dt}\right)^{\alpha} = (D_0 + \varepsilon D_1 + \varepsilon^2 D_3 + \cdots)^{\alpha} = D_0^{\alpha} + \varepsilon\alpha D_0^{\alpha-1} D_1 + \cdots \quad (7)$$

where $D_n = \frac{\partial}{\partial T^n}$ [4]. The damping term is considered ε^2order and so $\hat{\mu} = \varepsilon^2\mu$ to concern with lightly damped motion.

For calculating the fractional derivative of the exponential function, the following formula is introduced [1-5],

$$D_{RL}^{\alpha} e^{i\omega t} = (i\omega)^{\alpha} e^{i\omega t} \quad (8)$$

where i denotes complex number $\sqrt{-1}$. This formula can be valid only in the case if the Riemann-Liouville fractional-order derivative are defined as follows [5]

$$D_{RL}^{\alpha} f(t) = \frac{1}{\Gamma(1-\alpha)} \frac{d}{dt} \int_{-\infty}^{t} \frac{f(s)}{(t-s)^{\alpha}} ds \tag{9}$$

On the other hand, D^{α}, $D^{\alpha-1}$, $D^{\alpha-2}$represent the Riemann-Liouville fractional derivatives in time t. Substituting Equations (3)-(7) into the Equation (2), we get the equations in the following for third order of ε by neglecting higher orders.

$$O(\varepsilon): \quad D_0^2\theta_1 + \omega_0^2\theta_1 = 0 \tag{10}$$

$$O(\varepsilon^2): \quad D_0^2\theta_2 + \omega_0^2\theta_2 = -2D_0D_1\theta_1 \tag{11}$$

$$O(\varepsilon^3): \quad D_0^2\theta_3 + \omega_0^2\theta_3 = -2D_0D_1\theta_2 - D_1^2\theta_1 - 2D_0D_2\theta_1 - 2\mu D_0^{\alpha}\theta_1 + \frac{\omega_0^2}{6}\theta_1^3 \tag{12}$$

The solution of Equation (10) has the following general form

$$\theta_1 = A_1(T_1, T_2)e^{i\omega_0 T_0} + \bar{A}_1(T_1, T_2)e^{-i\omega_0 T_0} \tag{13}$$

where A_1 and $\bar{A}_1$ are complex conjugate functions. Substituting (13) into the Eq. (11), we obtain

$$D_0^2\theta_2 + \omega_0^2\theta_2 = -2i\omega_0 D_1 A_1 e^{i\omega_0 T_0} + c.c. \tag{14}$$

where *c.c.* is the complex conjugate part to the preceding terms. Eliminating secular terms in Eq. (14).

$$D_1 A_2 = 0 \tag{15}$$

where $A_1 = A_1(T_2)$ obtained from solution of Eq. (15). The solution of Eq. (14) has the following general form.

$$\theta_2 = A_2(T_1, T_2)e^{i\omega_0 T_0} + \bar{A}_2(T_1, T_2)e^{-i\omega_0 T_0} \tag{16}$$

where A_2 and $\bar{A}_2$ are complex conjugate functions.

$$D_0^2\theta_3 + \omega_0^2\theta_3 = -2i\omega_0 D_1 A_2 e^{i\omega_0 T_0} - 2i\omega_0 D_2 A_1 e^{i\omega_0 T_0} - 2\mu(i\omega_0)^{\alpha} A_1 e^{i\omega_0 T_0} + \frac{\omega_0^2}{2} A_1^2 \bar{A}_1 e^{i\omega_0 T_0} + c.c + N.S.T. \tag{17}$$

where NST stands for the terms that will not bring secular terms into the solutions. Eliminating secular terms in Eq. (17).

$$D_1 A_2 + D_2 A_1 - i\mu\omega_0^{\alpha-1} i^{\alpha} A_1 + \frac{i\omega_0}{4} A_1^2 \bar{A}_1 = 0 \tag{18}$$

and considering the formula:

$$i^{\alpha} = cos\left(\frac{\alpha\pi}{2}\right) + i\, sin\left(\frac{\alpha\pi}{2}\right) \tag{19}$$

we get:

$$D_1 A_2 + D_2 A_1 - i\mu\omega_0^{\alpha-1}\left(cos\left(\frac{\alpha\pi}{2}\right) + i\, sin\left(\frac{\alpha\pi}{2}\right)\right) A_1 + \frac{i\omega_0}{4} A_1^2 \bar{A}_1 = 0 \tag{20}$$

$D_1 A_2 = 0$ thence $A_2(T_2)$is obtained. Then, Eq. (18) is written as following form:

$$D_2 A_1 - i\mu\omega_0^{\alpha-1}\left(cos\left(\frac{\alpha\pi}{2}\right) + i\, sin\left(\frac{\alpha\pi}{2}\right)\right)A_1 + \frac{i\omega_0}{4}A_1^2\bar{A}_1 = 0 \tag{21}$$

Considering the polar form of the function $A_1(T_2)$:

$$A_1(T_2) = \frac{1}{2}a(T_2)e^{i\beta(T_2)} \tag{22}$$

From Eq. (21) we obtain:

$$D_2 a + iaD_2\beta - i\mu\omega_0^{\alpha-1}\left(cos\left(\frac{\alpha\pi}{2}\right) + i\, sin\left(\frac{\alpha\pi}{2}\right)\right)a + \frac{i\omega_0}{16}a^3 = 0 \tag{23}$$

Separating the resulting equation into the real and imaginary parts,

$$\Re: \quad D_2 a + \mu\omega_0^{\alpha-1} sin\left(\frac{\alpha\pi}{2}\right)a = 0 \tag{24}$$

$$\Im: \quad D_2\beta - \mu\omega_0^{\alpha-1} cos\left(\frac{\alpha\pi}{2}\right)a\frac{i\omega_0}{16}a^3 = 0 \tag{25}$$

are obtained.

Integrating Eqs. (24) and (25) yields:

$$a(T_2) = a_0 e^{-\mu\omega_0^{\alpha-1} sin\left(\frac{\alpha\pi}{2}\right)T_2} \tag{26}$$

$$\beta(T_2) = \frac{\omega_0}{32}\frac{a_0^2 e^{-2\mu\omega_0^{\alpha-1} sin\left(\frac{\alpha\pi}{2}\right)T_2}}{\mu\omega_0^{\alpha-1} sin\left(\frac{\alpha\pi}{2}\right)} + \mu\omega_0^{\alpha-1} cos\left(\frac{\alpha\pi}{2}\right)T_2 + \beta_0 \tag{27}$$

and substituting the obtained results (Eqs. (26) and (27)) into Eq. (22) and considering $T_0 = t$ and $T_1 = \varepsilon t$, $T_2 = \varepsilon^2 t$, the solution of equation is obtained as:

$$\theta(t,\varepsilon) = \varepsilon a_0 e^{-\mu\omega_0^{\alpha-1} sin\left(\frac{\alpha\pi}{2}\right)\varepsilon^2 t} e^{i\left(\omega_0 t + \frac{\omega_0 a_0^2 e^{-2\mu\omega_0^{\alpha-1} sin\left(\frac{\alpha\pi}{2}\right)\varepsilon^2 t}}{32\,\mu\omega_0^{\alpha-1} sin\left(\frac{\alpha\pi}{2}\right)} + \mu\omega_0^{\alpha-1} cos\left(\frac{\alpha\pi}{2}\right)\varepsilon^2 t + \beta_0\right)} + O(\varepsilon^3) \tag{28}$$

Conclusion

A pendulum with fractional viscous damping is considered. The mathematical model of pendulum is a cubic nonlinear equation governing the oscillations of systems having a single degree of freedom, via Riemann-Liouville fractional derivative. The method of multiple scales is performed to solve the equation by assigning the nonlinear and damping terms to the ε-order. Finally, the nonlinear frequency of a pendulum with fractional viscous damping that has a cubic nonlinear equation is dependent on amplitude and the damping coefficient and also α order fractional derivative, as it is observed from solution.

References

[1] Rossikhin YA, Shitikova MV. Application of Fractional Calculus for Dynamic Problems of Solid Mechanics: Novel Trends and Recent Results. Appl. Mech. Rev. 2010;63(1): 010801 (52 pages)
[2] Rossikhin YA, Shitikova MV, Shcheglova TA. Nonlinear dynamics of a fractionally damped oscillator. In: Applied Mechanics in Americas 12. Proc. 10th Pan American Congress of Applied Mechanics. Cancun, Mexico, January 7–11, 2008; 223–226.
[3] Rossikhin YA, Shitikova MV, Shcheglova TA. Forced vibrations of a nonlinear oscillator with weak fractional damping. Journal of Mechanics of Materials and Structures 2009; 4 (9): 1619–163.
[4] Rossikhin YA, Shitikova MV. New approach for the analysis of damped vibrations of fractional oscillators. Shock and Vibration 2009; 16 (4):365–387.
[5] Sınır BG, Dönmez Demir D. The analysis of nonlinear vibrations of a pipe conveying an ideal fluid. European Journal of Mechanics-B/Fluids, 2015; 52:38–44.
[6] Nayfeh AH, Mook DT. Nonlinear Oscillations. New York: John Wiley & Sons, Inc.; 1995.
[7] Nayfeh AH. Introduction the Perturbation Methods. Wiley 2011.
[8] Carpinteri A, Mainardi F. Fractals and fractional calculus in continuum mechanics, vol. 378. Springer, 2014.
[9] Coimbra CF. Mechanics with variable-order differential operators. Annalen der Physik, 2003; 12(11-12):692–703.
[10] De Oliveira EC, Tenreiro Machado JA. A review of definitions for fractional derivatives and integral. Mathematical Problems in Engineering, 2014.
[11] Duan J-S. Time-and space-fractional partial differential equations. Journal of Mathematical Physics, 2005; 46(1):013504.
[12] Hilfer R. et al. Applications of fractional calculus in physics, vol. 35. World scientific Singapore (2000).
[13] Kilbas AA, Srivastava HM, Trujillo JJ. Theory and applications of fractional differential equations, vol.204. Elsevier, 2006.
[14] Magin RL. Fractional calculus in bioengineering, vol. 2. Begell House Redding, 2006.
[15] Miller KS, Ross B. An introduction to the fractional calculus and fractional differential equations. Wiley, 1993.
[16] Monje CA, Chen Y, Vinagre B M, Xue D, Feliu-Batlle V. (2010). Fractional-order systems and controls: fundamentals and applications. Springer Science & Business Media.
[17] Oldham K, Spanier J. The fractional calculus theory and applications of differentiation and integration to arbitrary order. Elsevier. 1974.
[18] Podlubny I. Fractional differential equations: an introduction to fractional derivatives, fractional differential equations, to methods of their solution and some of their applications. Elsevier. 1998.
[19] Rossikhin YA, Shitikova MV. Application of fractional calculus for dynamic problems of solid mechanics: novel trends and recent results. Applied Mechanics Reviews, 2010; 63(1).
[20] Rossikhin YA, Shitikova MV. On fallacies in the decision between the caputo and riemann–liouville fractional derivatives for the analysis of the dynamic response of a nonlinear viscoelastic oscillator. Mechanics Research Communications, 2012; 45:22–27.
[21] Yang, X.-J. Advanced local fractional calculus and its applications. World Science Publisher 2012.

Design and Production of Man Powered Olive Harvest Machine

Ahmet Aktan, Burak Akkaya, Suat S. Şanlı, Uğur Kemiklioğlu
Doğuş University, Mechanical Engineering Department, Istanbul, Turkey
**Corresponding author: ahmet_aktan_2492@hotmail.com*

Abstract

Today, agricultural sector develops in many areas. So, we have decided to make a project that can bring facileness by using the developing technology. We aimed to harvest the olives easily to work in these agricultural areas with a mechanical machine. We knew that there are many olive trees in our country and that people spend a lot of time collecting olives in these trees and they work costly. Therefore, we decided to design a machine that would also protect the environment by reducing the cost that would lead to saving. We met with many people and companies who went to the machine production industry and made studies in this field. Based on this information, we have decided to make a mechanism that works with shaking tree branch thanks to the gear system. As a result of our work, we think that this mechanism will be operated in a healthy manner and ready for production. The mechanism requires 159.2 N.m of torque, 1620 N force and 1 ~1.7 kW of manpower.

Keywords: novel design, olive harvest, unbalancing, vibration

Introduction

Olive cultivation has an important commercial position in our country. Olive harvesting methods are very important for olive cultivation. Various olive harvesting machine inventions and some methods have been developed from past to present, working with an energy like that engine, electricity, wind using shaking method [1-6].

The aim of this study is to produce mechanic olive harvesters that are manpower-powered in the olive growing sector, taking reference to the gasoline-powered olive harvesters. In this context, we uncover a product that is less costly, economical, and environmentally conscious, working with manpower without the need for any fossil fuels.

The system consists of three main components. These are the power supply part (motion lever and 1/3 ratio chain gear) [7], shaft part (shaft and joint) and circular motion part (1/1 conical gearbox, unbalanced mass and hook). Here's how the system torques. The chain gear group in the power supply will rotate with the help of the dialing lever to produce 159.2 N.m of Torque. With the help of the joint in the drivetrain, it will transfer angular rotational motion to the circular motion unit with the help of shaft. With the help of 1/1 conical gear in the circular motion unit [8], the direction of movement will change by 90 degrees and the unbalanced mass attached to the conical gear shaft will begin to rotate. As a result of this rotation, the hook attached to the tree branch will shake the branch and the olives will be poured from the branch and the harvest process will be completed. The constraints we need in the system are producing 60 rpm, using 1 Kw of manpower and producing 159.2 N.m of Torque.

Design of the Olive Harvest Machine

The machine we designed consists of three main parts: power supply unit, shaft and circle motion unit. We have modeled the bicycle gear system in the creation of the power supply unit. Taking the differential system used in automobiles as an example, we decided to use a bevel gear set operating at 90^o and 1/1 transmission ratio to change the direction of circular movement from the shaft to circle motion unit.

Circular motion unit

In this part, we obtain a circular vibration movement with the centrifugal forces that we create with unbalanced forces as seen in Figure 1.

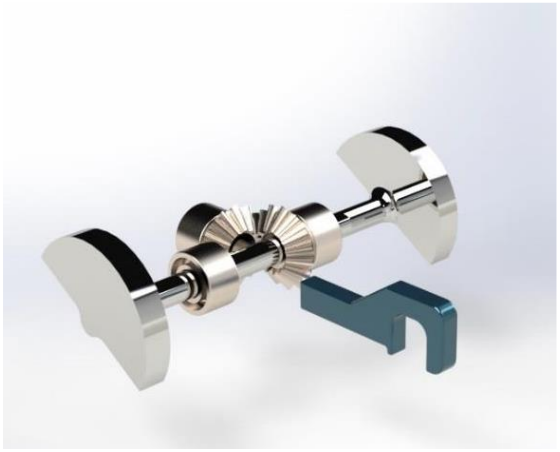

Figure 1. Demonstration of circular motion unit

Circular motion unit consists of a hook and two unbalanced masses. This unit transmits the rotary motion from shaft to unbalanced masses via bevel gears.

Unbalanced mass: The design of unbalanced mass is given Figure 2. The unbalanced mass will be produced from sheet metals via laser cutter machine.

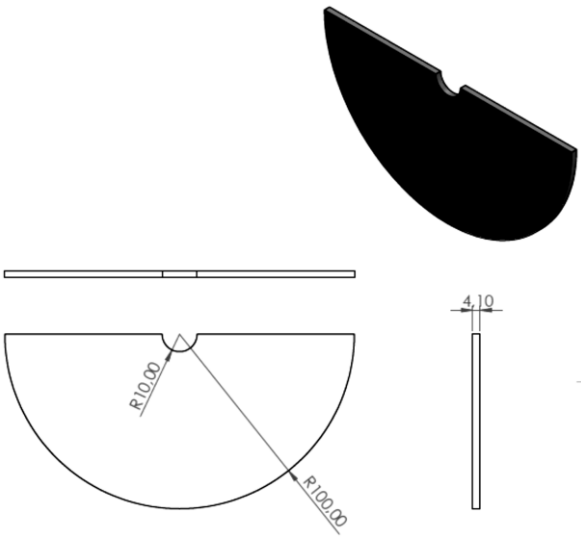

Figure 2. Technical drawing of unbalanced mass

Bevel gearbox: The bevel gear we use in our system is M4 and has 15 gears. The hole diameter is 20 mm and the connecting shaft length is 16 cm [8]. The technical drawing of bevel gear is given in Figure 3.

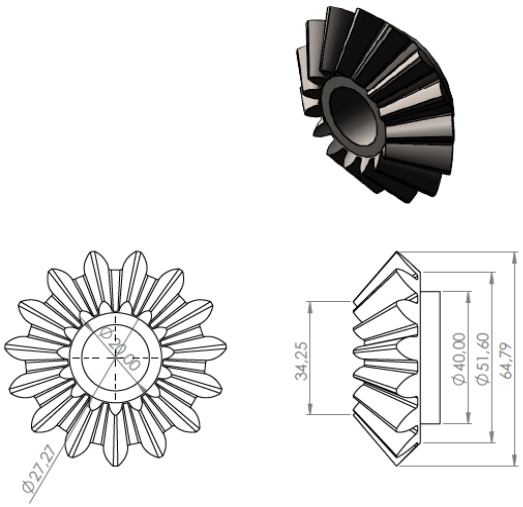

Figure 3. Technical drawing of bevel gear

Hook: The hook part transmits the rotational movement to the tree branches by making circular motion with the force coming from unbalanced masses and bevel gears. The technical drawing of hook part is given in Figure 4.

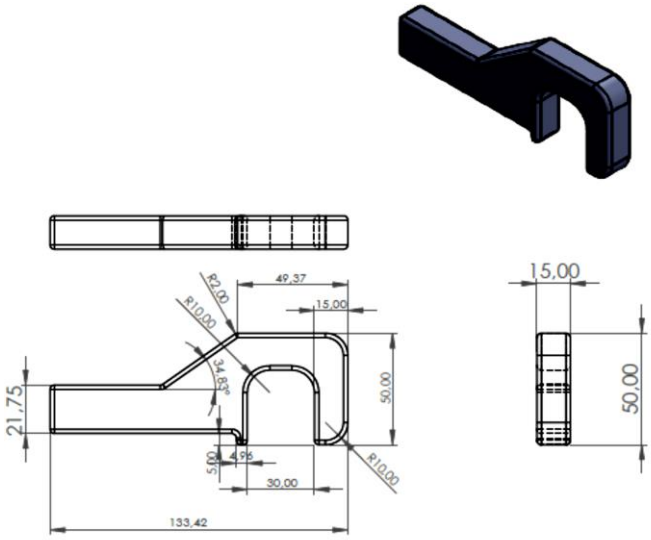

Figure 4. Technical drawing of hook part

Shaft part

The shaft, which is intended to be used in this design, will transmit the human power to the circular motion unit. The shaft has a diameter of 20 mm and a length of 2 m. A hook joint will be used in the middle of the shaft to prevent angular deformation that will occur in the shaft with the rotational movement.

Power supply unit

In this unit, the torque required for proper operation of the harvesting machine is 159.2 N.m and the angular speed is 180 rpm. The maximum energy a person can produce in a minute is 1.7 Kw and the continuous energy is 1 Kw.

We will use 1/3 ratio and 45/15 teeth number in chain gear design [7]. The 60 g / min produced on the big gear will increase to 18 rpm on the small gear and the torque value will be transmitted to the circular drive unit with the help of the shaft.

The chain sprockets in our system are fixed to the connection plate by bearing. Two connection plates are used in power supply unit and the unit will be mounted to each other with four bolts and nuts as seen in Figure 5.

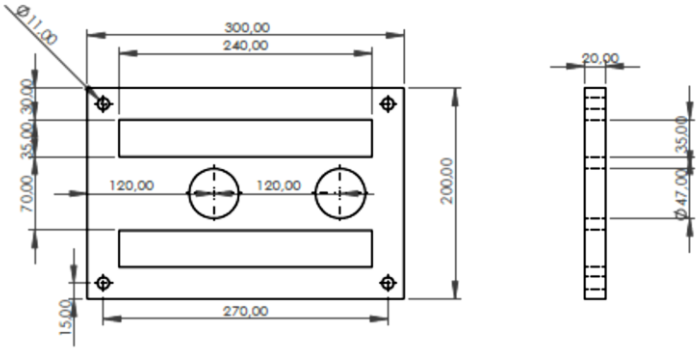

Figure 5. Technical drawing of power supply plates

Production of the Olive Harvest Machine

Production of the olive harvest machine designed within the scope of the study will be made of metal parts. Power supply plates and unbalanced masses will be produced from 10 mm thick sheet metal. These parts will be cut with a laser cutting machine. The hook joint will be fixed using the grooved assembly method at the exact center of the shaft. The production demonstration on of the olive harvest machine is shown in Figure 6.

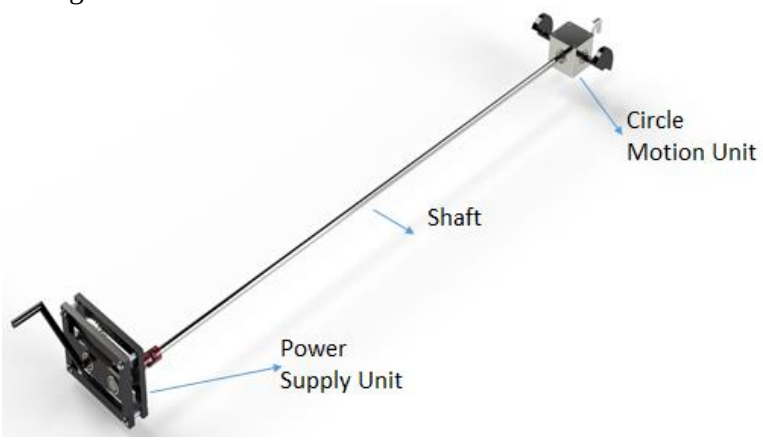

Figure 6. Demonstration of man powered olive harvest machine

Conclusion

In this project, which we designed and researched, we determined that we would achieve very high efficiency. We have evaluated this efficiency among ourselves.

- We have seen that we can make our project with as low cost as possible.
- We asked people and got ideas. This project has become a real curiosity for agricultural people, and they are interested.
- Many people aspire to buy this machine with the promised features.

In line with these demands, our belief in our project increased more. We aimed to develop our product much more until the completion of our project. We met many tradesmen, teachers, and trade people in industry and school. We received suggestions about developing our project.

References

[1] Porta C, Rostan H, Bonadeo P. 2003: Olive harvesting machine, US20050034441A1.
[2] Georgoulis G. 2009: Olive harvesting device, EP2119340A2.
[3] Boultadakis I. 2003: Olive tree shaker-harvester, WO2004057943A1.
[4] Pelagio M, da Costa T. 1999: Wind machine for harvesting and gathering olives, US6609359B1.
[5] Drusiani F. 1990: Tool for olive-picking, US5099637A.
[6] Rabalakos A., Rabalakos A. 2005: Olive trees beating machine for olive crop collection, EP1749435B1.
[7] http://yavuzlardisli.com/FILE/88a7218df5f8a054757caee7a40726b0.pdf (Retrieved 24.12.2019)
[8] https://www.norelem.com.tr/xs_db/DOKUMENT_DB/www/NORELEM/DataSheet/tr/22/22430_Datasheet_16061_Konik_di_li_arklar_elik_aktarma_oran_1_1_frezelenmi_di_li_tertibat_d_z_di_li_kavrama_a_s_20_--tr.pdf (Retrieved 24.12.2019)

Investigation of Quasi-Static Punch-Shear Behavior of Acorn Powder Reinforced Composites

Halis Kandaş[1], Okan Özdemir[2]*
[1]The Graduate School of Natural and Applied Sciences, Department of Mechanical Engineering, Tınaztepe Campus, Izmir, Turkey
[2]Dokuz Eylül University, Engineering Faculty, Department of Mechanical Engineering, Tınaztepe Campus, Izmir, Turkey
**Corresponding author: haliskandas1@gmail.com*

Abstract

In this study, the effect of different amounts of acorn powder reinforcement on the quasi-static penetration behavior of glass fiber reinforced composites was investigated. Glass fiber used in this study is 0˚/90˚ stitched E-glass fiber with a density of 600 g/m^2. The sizes of acorn powders used as particle reinforcements are between 10 to 40 micrometers. Powders were cleansed from impurities with a sodium hydroxide solution. Cleaned powders mixed with epoxy resin by using mechanical mixing method. Thereafter, resin mixture was applied to glass fiber with hand lay-up method and composite plate was produced by vacuum bag method. Quasi-static penetration tests were performed at room temperature. As quasi-static penetration speed, 1, 10 and 20 mm/minute was selected. Force and energy results of composites compared with each other.

Keywords: particle reinforced composites, bio-composites, glass fiber, quasi-static penetration

Introduction

Composite materials are mostly made out of petrochemical-based materials. But these materials pose a serious environmental pollution problem due to their insolubility in nature [1]. Therefore, produced bio-composites using biodegradable and renewable natural materials have been recently preferred [2]. Even though, forests considered as most important sources of natural materials, they are disappearing due to usage for wood supply. Because of that, the current investigations which use natural materials have focused on side product materials as reinforcement [3].

When the studies in the literature are examined, different fibers and different particle reinforcements were used together as reinforcement material only in a few studies. In these studies, it was concluded that different proportions of particle reinforcements positively affect the mechanical properties of fiber reinforced composites [4].

Recently, many investigations have been made on composites with different material stacking sequences under various loading rates and boundary conditions. These investigations showed that laminated composite structures are sensitive to impact of external loading conditions [5]. Therefore, impact properties of glass/epoxy composites have been a subject for many researches. The main goal of this study is optimizing these materials for using in different applications by understanding their characteristic properties and energy dissipating impact damage mechanisms [6].

In this study, composite materials have been manufactured with both fiber and particle reinforcement. As a particle reinforcement material, acorn powder, which is a natural reinforcement material, were used at different ratios. Stitched glass fiber laminates were also used as fiber reinforcement material. Because of above mentioned reasons, quasi-static punch shear test responses of composites were investigated at different particle ratios.

Material and Method

In manufacturing of composite laminates, acorn powders with 10-40 µm size and 0/90 stitched 600 gr/m^2 glass fibers were used. As a matrix material F-1564 epoxy and F3487 hardener were used. The picture of materials used in manufacturing of composite panels is given in Figure 1.

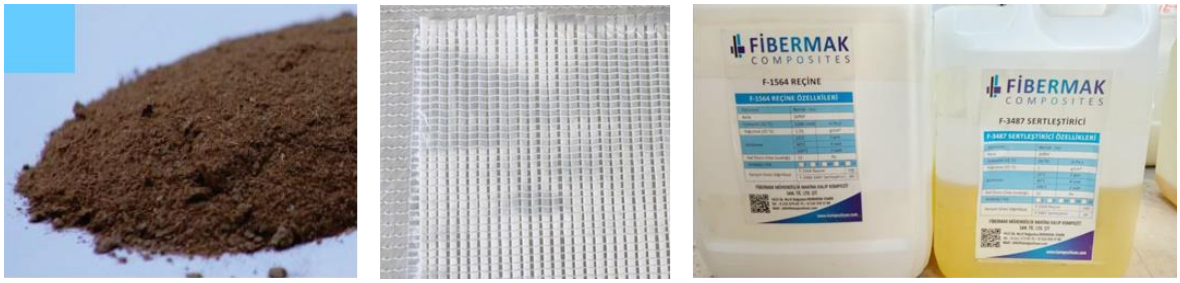

Figure 1. Acorn powder, 0/90 stitched glass fiber, F-1564 epoxy and F3487 hardener

Acorn powder has to be purified before using since it's a natural material. For this aim, grinded acorn powder chemically treated in a 1.6mol 1^{-1} sodium hydroxide aqueous solution for 48 hour. Acorn powder cleanse from contamination such as dust and other materials. Purified acorn powder left to dry for 96 hours shown in Figure 2.

Figure 2. Acorn powder purification process

Prepared acorn powder was added gradually to the respective epoxy resin and hardener and mixed mechanically at room temperature. In manufacturing of composites, hand lay-up method was preferred. Firstly, the matrix-particle mixture was applied to each layer of the composites in order to ensure homogeneous disturbance of mixture. After that, these composite laminates were taken to vacuum bag as shown in Figure 3. Vacuum bagged structure was cured for 8 hours at 80°C.

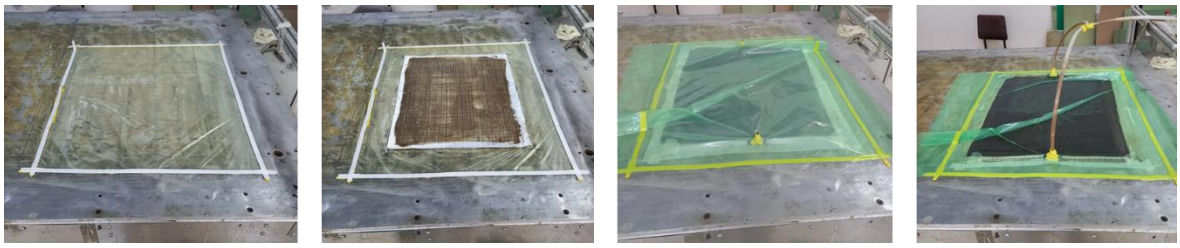

Figure 3. Composite plate manufacturing processes

After particle and fiber reinforced composite plates were manufactured, they cut to 100 x 100 mm. Cutting process was performed by using water refrigerated diamond blade to prevent composites have any unnecessary damage. All manufacturing and sizing processes are given in Figure 4.

Figure 4. Composite specimen sizing processes

In this study, quasi-static punch-shear tests were performed with hemispherical shaped cross head with a 12.7 mm diameter. These quasi-static punch-shear tests were carried out at 1 mm/min and 10

mm/min speeds in Shimadzu universal testing machine. The equipments and machine used in the experimental study are given in Figure 5.

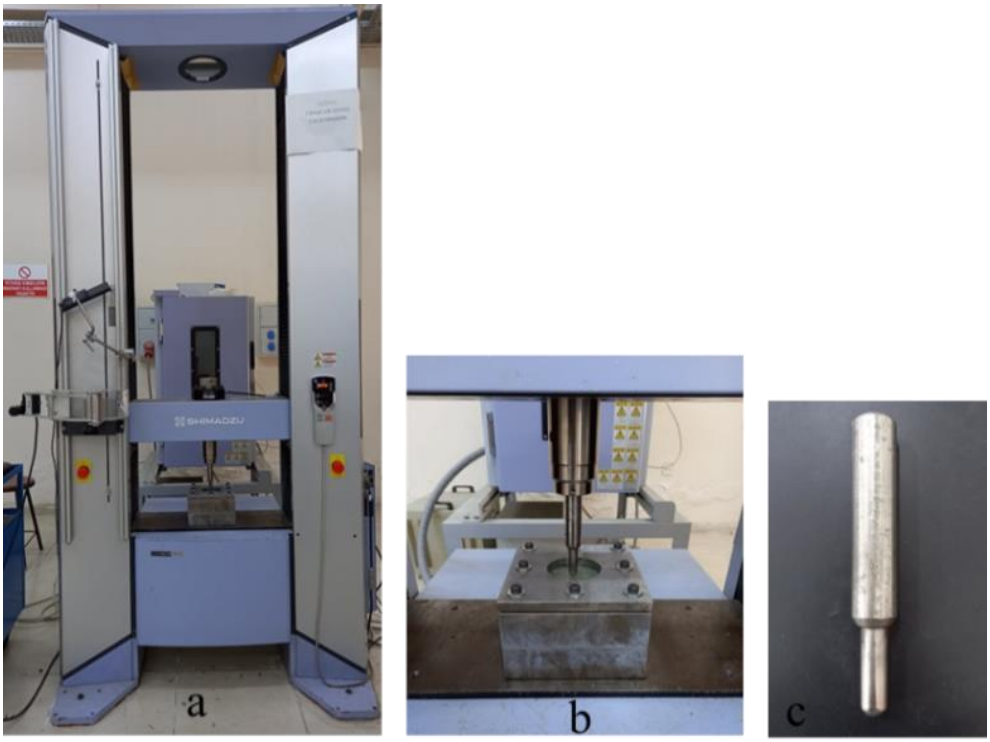

Figure 5. a) Shimadzu universal testing machine, b) quasi-static punch-shear apparatus and c) cross head.

Results and Discussions

This research focuses on the effect of particle reinforcements in glass fiber reinforced composites. Quasi-static punch shear test was selected in order to investigate the perforation behavior of composites. Force – deformation curves obtained from the quasi-static punch-shear tests of %0, %2 and %4 particle reinforced composites are shown in Figure 6. It can be observed from the figure that curves increase linearly at the beginning of test and initial parts of curves start separate from each other along with rising test speed. Contact force of composites decreases drastically after plugging point and stabilizes at a certain value after tip of cross-head move out from back of composite plate. After this point friction create resistance effect against the cross head.

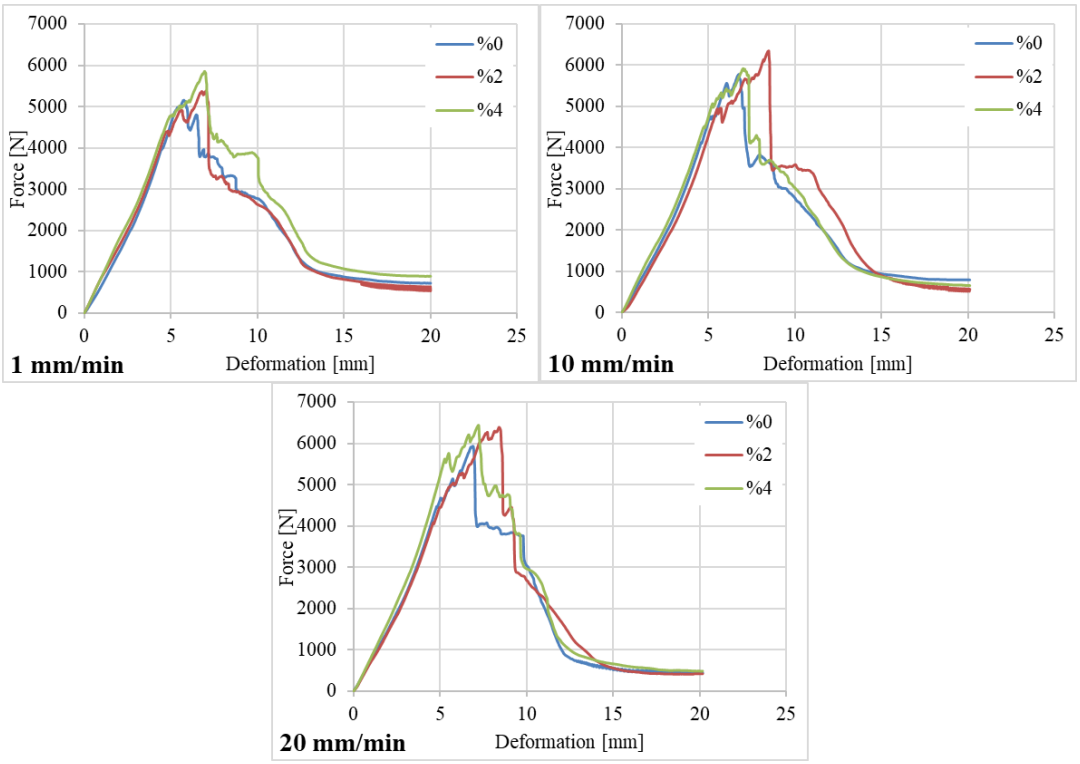

Figure 6. Force – Deformation curves of quasi-static punch-shear tests

In order to evaluate the quasi-static punch-shear strengths of particle reinforced composites maximum penetration force graphs are given in Figure 7 and values are given in Table 1. According to the Figure 7, maximum penetration forces of each composite group increase with increasing test speed. Additionally maximum penetration forces of composites get higher values at higher particle reinforcement ratios.

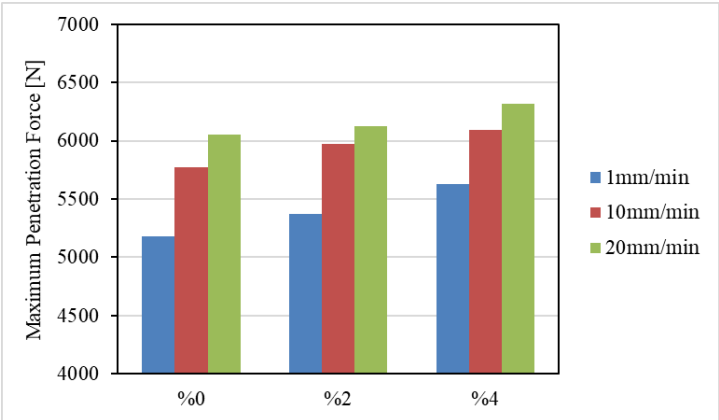

Figure 7. Maximum Penetration Forces of quasi-static punch-shear tests

Table 1. Maximum Penetration Forces of quasi-static punch-shear tests

	0 %	2 %	4 %
1 mm/min	5177 N	5371 N	5630 N
10 mm/min	5771 N	5972 N	6097 N
20 mm/min	6051 N	6127 N	6320 N

In order to understand the energy behavior of composites in quasi-static tests better, energy-deformation curves are given in Figure 8. In energy – deformation curves, effect of particle

reinforcement ratio seen better after initial part of curves. Especially, after fiber plugging point curves differentiate from each other more distinctively.

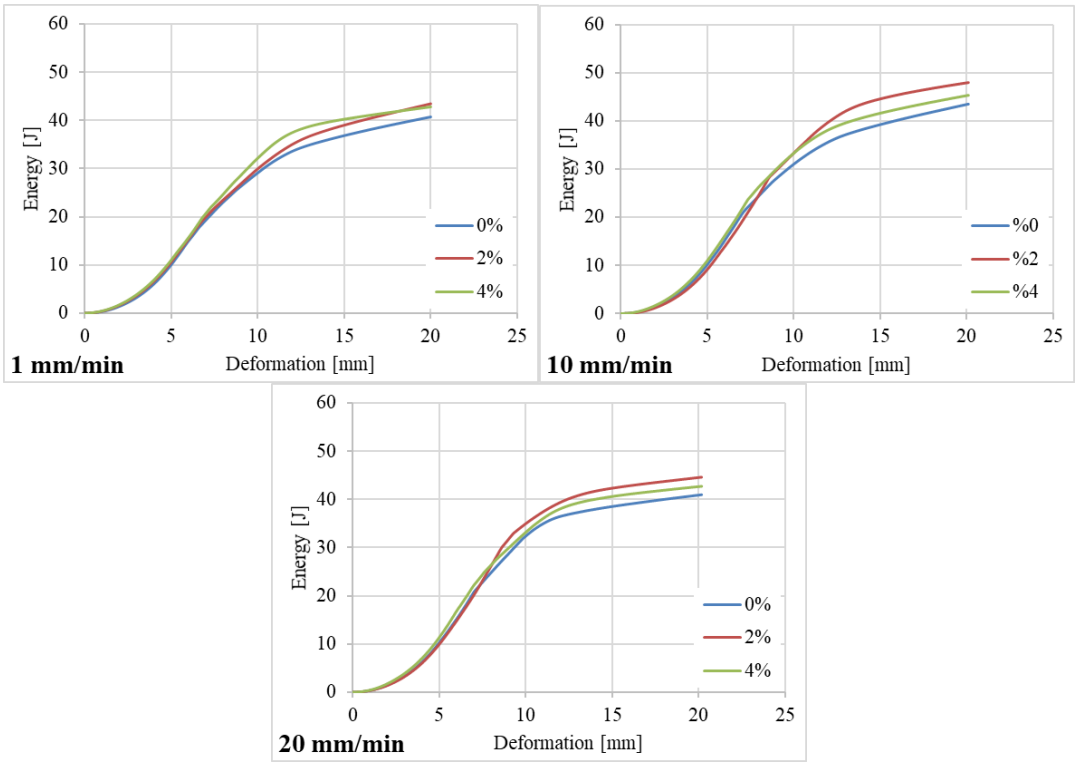

Figure 8. Energy – Deformation curves of quasi-static punch-shear tests

Fiber plugging and rapture point of composites is a critical point for quasi-static punch-shear tests. Because of that, absorbed energy graphs and values of quasi-static punch-shear tests at fiber rapture point given in Figure 9 and Table 2. It can be seen in Figure 9 that energy value of each composite group at fiber rapture point increases with test speed. Furthermore, absorbed energy of composites at fiber rapture point gets higher values at higher particle reinforcement ratios.

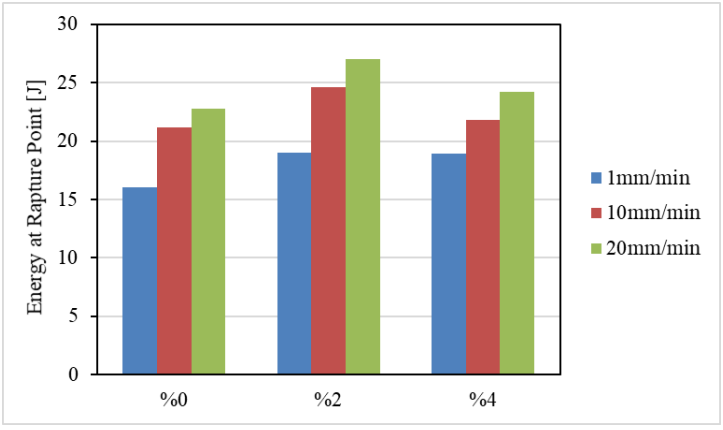

Figure 9. Absorbed energy of quasi-static punch-shear tests at fiber rapture point

Table 2. Absorbed energy of quasi-static punch-shear tests at fiber rapture point

	0 %	2 %	4 %
1 mm/min	16 J	19 J	18,9 J
10 mm/min	21,2 J	24,6 J	21,8 J
20 mm/min	22,8 J	27 J	24,2 J

Quasi-static punch-shear tests were lasted at 20mm deformation point. Absorbed energy graphs and values of quasi-static punch-shear tests at 20mm deformation point given in Figure 10 and Table 3. It can be seen from the Figure 10 that absorbed energy value of each composite group increase when test speed increases 1 to 10mm/min, but it starts to decrease when test speed reaches 20 mm/min.

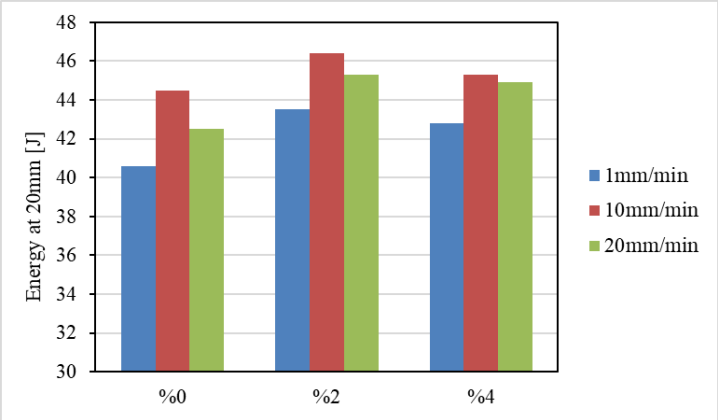

Figure 10. Absorbed energy of quasi-static punch-shear tests at 20mm deformation

Table 3. Absorbed energy of quasi-static punch-shear tests at 20mm deformation

	0 %	2 %	4 %
1 mm/min	40,6 J	43,5 J	42,8 J
10 mm/min	44,5 J	46,4 J	45,3 J
20 mm/min	42,5 J	45,3 J	44,9 J

Conclusions

In this study, the effect of different amounts of acorn powder reinforcement on the quasi-static penetration behavior of glass fiber reinforced composites was investigated experimentally. The quasi-static penetration tests were carried out at 1, 10 and 20 mm/minute cross-head speeds. The obtained conclusion can be summarized as:

- Maximum contact force of composites increases with particle reinforcement.
- Absorbed energy at rapture point gets higher value at %2 particle reinforcement but this value starts to decrease at %4 particle reinforcement.
- Total absorbed energy at 20mm deformation have similar response to absorbed energy at rapture point while particle reinforcement increases.
- Maximum contact force and absorbed energy value at rapture point increases while penetration speed increases.

References

[1] Bledzki AK, Jaszkiewicz A. Mechanical performance of biocomposites based on PLA and PHBV reinforced with natural fibers—A comparative study to PP. Composites Science and Technology 2010; 70(12): 1687-1696.

[2] Kılınç AC, Atagur M, Ozdemir O, Sen I, Kucukdogan N, Sever K, Seydibeyoglu O, Sarikanat M, Seki Y. Manufacturing and characterization of vine stem reinforced high density polyethylene composites. Composites Part B: Engineering 2016; 91: 267–74.

[3] Agayev S, Ozdemir O. Fabrication of high-density polyethylene composites reinforced with pine cone powder: mechanical and low velocity impact performances. Materials Research Express 2019; 6(4): 045312.

[4] Singh K, Kand Rawat P. Mechanical behavior of glass/epoxy composite laminate with varying amount of MWCNTs under different loadings. Materials Research Express 2018; 5(5): 055012.

[5] Taghizahed SA, Liaghat G, Niknejad A, Pedram A. Experimental study on quasi-static penetration process of cylindrical indenters with different nose shapes into the hybrid composite panels. Journal of Composite Materials 2018; 53(1): 107-123.
[6] Erkendirici Ö, Haque BZ. Quasi-static penetration resistance behavior of glass fiber reinforced thermoplastic composites. Composites Part B 2012; 43: 3391-3405.

Investigation of the Effects of Core Thickness on Low Velocity Impact Behaviors of Aluminum Honeycomb Composites

Kasım Karataş[1], Okan Özdemir[2]*
Dokuz Eylül University, The Graduate School of Natural and Applied Sciences, Department of Mechanical Engineering, Tınaztepe Campus, Izmir, Turkey
Dokuz Eylül University, Engineering Faculty, Department of Mechanical Engineering, Tınaztepe Campus, Izmir, Turkey
**Corresponding author: ksm.krts43@gmail.com*

Abstract

Honeycomb structures are used where the weight to strength ratio is important. They are also preferred to absorb the energy from the blows received. In this study, low velocity impact behavior of aluminum honeycomb composites with different core thicknesses were investigated. Aluminum honeycombs used in this study are AL3003 honeycombs of 10 mm and 15 mm thicknesses. Glass fiber reinforced epoxy sheets with a thickness of 2 mm were used as the surface sheet material. Composite plates were produced by vacuum infusion method. The upper and lower face plates were cut in dimensions of 100x100 mm. The cut plates were attached to the core material with adhesive and a sandwich structure was formed. After bonding, low velocity impact tests were performed on these test samples at 40J, 100J and 160J energy levels using the composite CEAST Fractovis Plus impact testing machine. According to the results obtained from the impact tests, at higher energy levels, 15 mm thick composites have 10-15% higher energy absorption capacity than 10 mm.

Keywords: sandwich composite, low velocity impact, aluminum honeycomb, epoxy adhesive

Introduction

A sandwich structure consists of a core structure that acts as an energy absorber and a thin sheet metal or fiber-reinforced composite faceplate [1]. The important properties of honeycomb sandwich structures, which are classified as sandwich composites, such as high impact energy absorption, bending stiffness and high strength/weight have increased their use in the aviation, marine and automotive industries in recent years [2]. It has also been seen in previous studies that the core takes on the task of absorbing energy in the sharing of the impact applied to sandwich composites [3].

For the production of the composite, it was planned to use fiber reinforced plate as the plate material and hexagonal aluminum honeycombs were chosen for the core material. The reason why E-glass epoxy composites are used in the production of plate composites in this study is the reason why glass fibers, which are widely used in the composite industry, are preferred due to their low cost, high impact resistance, high tensile strength and resistance to chemicals [4-6]. Ozdemir et al. [7] has shown in their research, core-thickness has a noticeable effect on the impact behavior. In the sandwich structures, small fiber cracks and matrix cracks occurred on the surface plate at low energy levels, while damage increased at higher impact energy levels. The small thickness core had no significant effect on the contact force and hardness of the sample. They saw that when the core thickness increased, the energy absorption ability increased. In sandwich composite with honeycomb core, the cell wall thickness and the side length of the honeycomb core have significant effects on the impact load, but compared with the surface layer, it has been observed that they do not have a large effect on energy absorption for the perforation condition [8]. In the studies on the effect of honeycomb core thickness, the total damage height of sandwich composites with different honeycomb core wall thicknesses under the same impact load did not affect much, but the effect of core heights on energy absorption was observed. While the wall thickness and cell size significantly affect the peak strength, the core height has little effect on the peak strength of the sandwich composite [9].

In this study, the low velocity impact behavior of sandwich composites formed by glass epoxy composite sheet and aluminum honeycomb with different core thicknesses was investigated. The responses of sandwich composites produced using E-glass epoxy composite plates and aluminum honeycomb at different energy values (40J, 100J and 160J) were investigated. For each energy type,

low-speed impact tests were performed on different core thicknesses and necessary graphics were drawn.

Methodology

Materials

Aluminum honeycombs used in this study are AL3003 honeycombs with 10 mm and 15 mm thickness. E-glass fiber woven laminate with a density of 300 g/m^2 is used for the production of upper and lower face sheets. As matrix material epoxy resin (F-1564) and hardener (F3487) at a ratio of 1/3 were used in the bonding process.

Figure 1. **a)** Aluminum Honeycombs and **b)** E-Glass Fiber Woven

Manufacturing

In the first stage, glass epoxy plates at 2 mm thickness were produced. The vacuum assisted resin infusion method used for production of composite face sheets. Composite plates consist of three-layer woven glass fiber laminate. All layers are set up and wrapped with vacuum bagging film with sealing tape from the edges to the heater plate. Resin inlet and vacuum channel are hermetically connected to both sides of the bag.

As seen in the Figure 2, the pipes placed on both sides are closed with a vacuum bag. After opening the vacuum and pulling the air inside, leakage control is done. If there is no leakage after the control, the mixture of epoxy and hardener is prepared with a ratio of 1/3 of the hardener epoxy. After that, the plate is produced by curing at 80 °C for 8 hours. Finally, the plate was cut to dimensions of 100 mm x 100 mm.

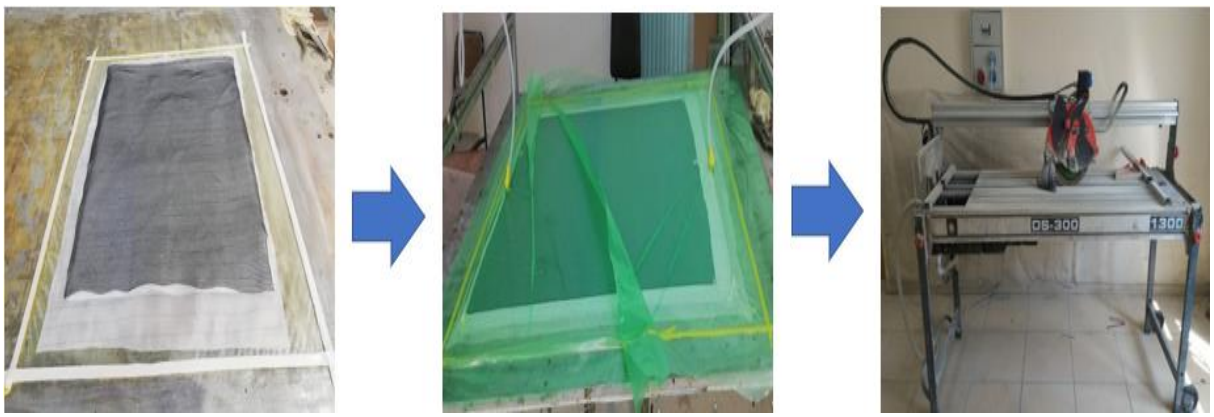

Figure 2. Manufacturing processes of face sheet plate

After the plate production process was completed, the bonding process is started to form the sandwich structure. In order to use equal adhesive for each sample in the bonding process, an injector

was used and the density of adhesive is 200 gr/m^3 and evenly distributed on the surface with the help of a brush. bonding process is shown in Figure 3.

Last process, the surface sheets bonded with core structure honeycombs are put into the oven at 80 ˚C for 8 hours to cure the Adhesive. The curing process was carried out separately (2 stages) for the two plates in order to prevent the adhesive applied to the upper layer from accumulating by flowing from the cell walls to the bottom plate during the curing process [10]. At the end of this process, sandwich composite sample was produced. The bonding process of the surface sheet plates and the core is shown in the Figure 3.

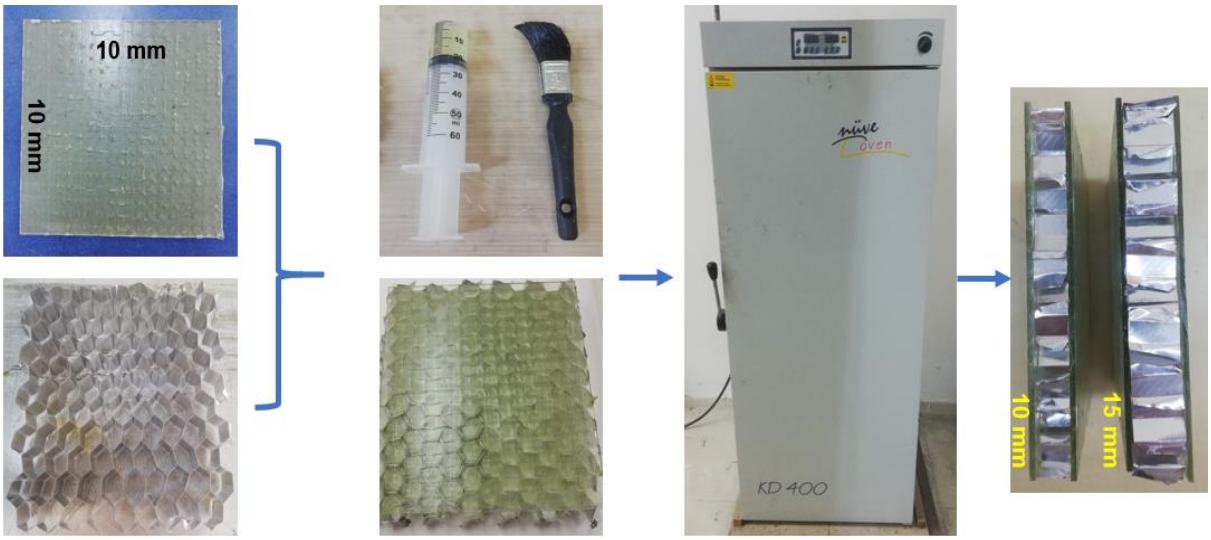

Figure 3. Manufacturing processes of face sheet plate and core bonding process

Low Velocity Impact Test

Impact tests were performed with a CEAST-Fractovis Plus impact testing machine. In the impact tests, hemispherical impactor with a dimeter of 20 mm with a load capacity of 22 kN is used. Low velocity impact tests were performed at room temperature under the impact energy level of 40J, 100J and 160 J according to ASTM D3763 standards (Figure 4).

Figure 4. **a)** CEAST-Fractovis Plus impact testing machine, **b)** Impactor

Results

In this research, impact test was performed at 40 J, 100 J, 160 J energy levels; each test was repeated at least 3 repetitions. Contact force-deformation and energy-time graphs were obtained as a result of the averages of these 3 repetitions. Contact force and deformation graph are given for two different core thicknesses in Figure 5. At 40 J impact energy level, rebounding case was observed in both core thicknesses. Penetration case at 100 J for 10 mm and 15 mm thickness were seen. But at 160 J energy level, the impactor pierced the upper and lower surfaces of the composites, revealing the perforation condition.

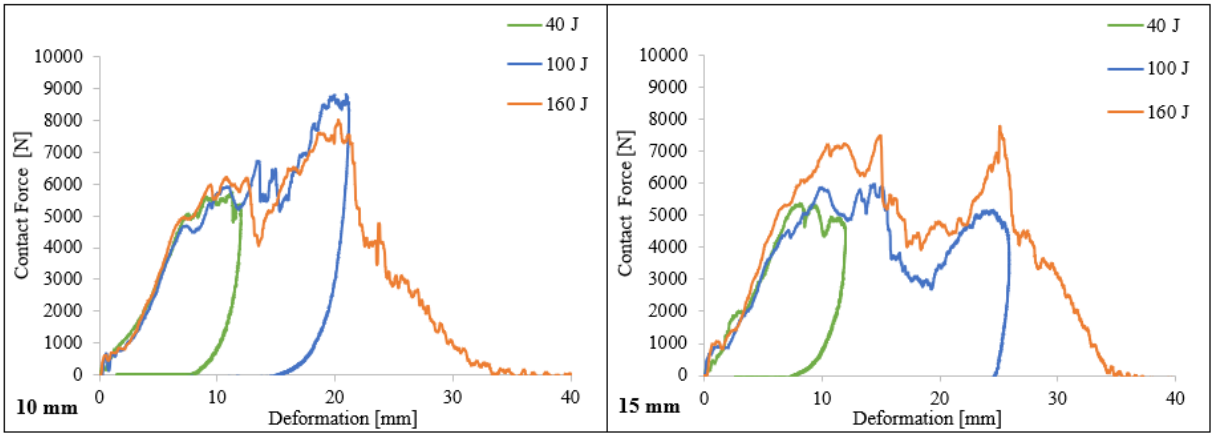

Figure 5. Contact force – Deformation diagrams of 10 mm and 15 mm core thickness

In Table 1 and Figure 6, the maximum contact forces at the determined energies are given for both thicknesses. As a result, the contact force at 100 J energy level with a core thickness of 10 mm is 50% higher than that of 15 mm.

Table 1. Maximum contact force [N]

Impact Energy [J]	Max.Contact Force [N] (10 mm Core)	Max. Contact Force [N] (15 mm Core)
40 J	5684	5449
100 J	9371	6227
160 J	7799	7306

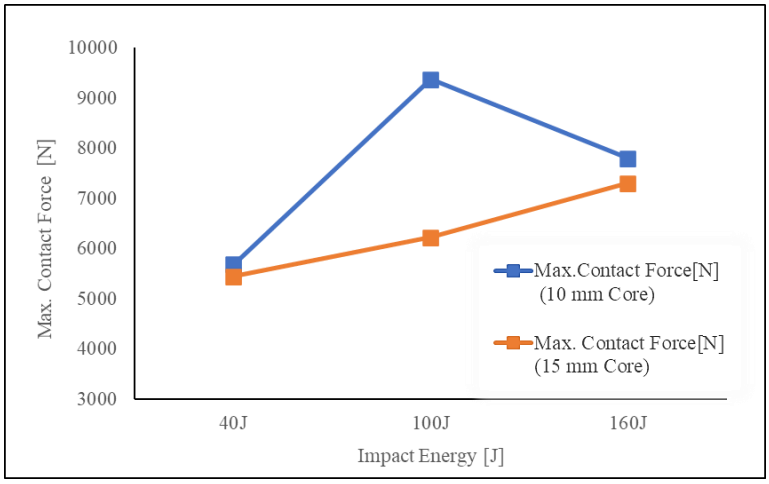

Figure 6. Maximum contact force diagrams of 10 mm and 15 mm core thickness

Energy-time graphs of 10 mm and 15 mm cell thickness composites are given in Figure 7. Although the absorbed energy values for both thicknesses were the same at low energy levels, the composite with 15 mm core thickness at high energies (160 J) absorbed 12% more energy.

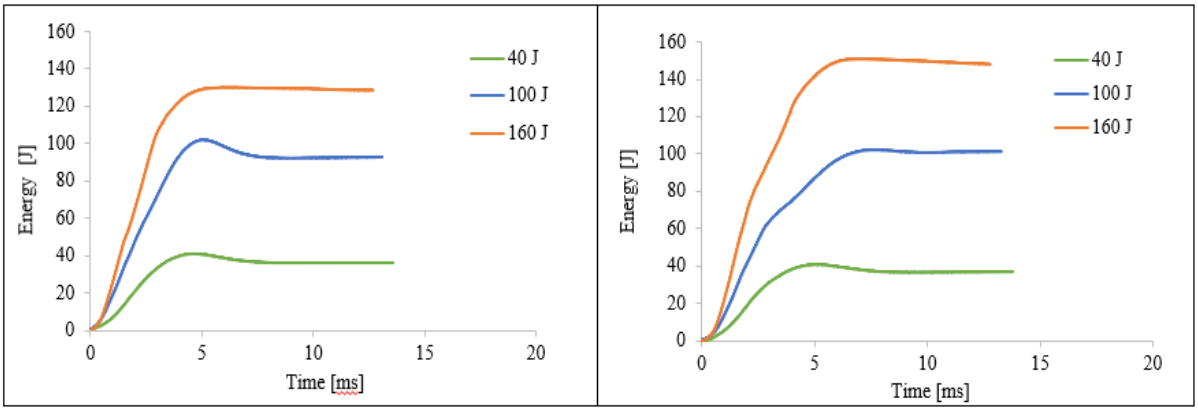

Figure 7. Energy - Time diagrams of 10 mm and 15 mm core thickness

In order to understand the energy interactions, the absorbed energy–impact energy diagrams of the structure are given in Figure 8 and Table 2. As can be seen, the composite with a core thickness of 15 mm absorbs much energy than 10 mm.

Table 2. Absorbed Energy-Impact Energy [J]

Impact Energy [J]	Absorbed Energy (10 mm Core)	Absorbed Energy (15 mm Core)
40	36,15	36,62
100	92,18	100,00
160	129,95	150,78

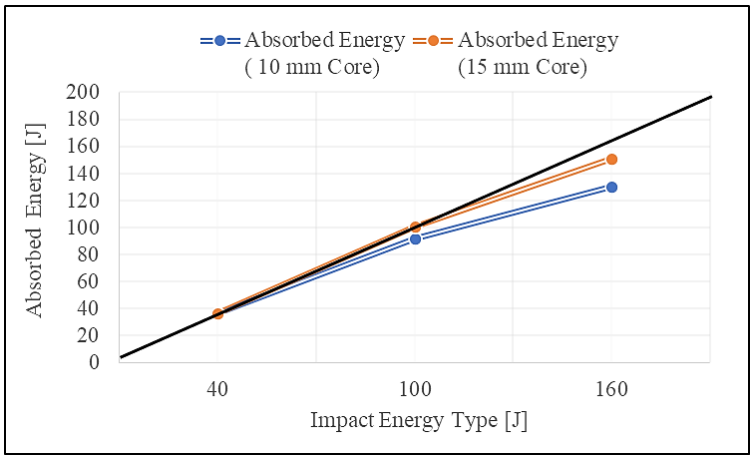

Figure 8. The energy profile curves of sandwich composites with various core thicknesses

Conclusions

In this study, the impact response of a sandwich composite formed with aluminum honeycombs with different core thickness and glass fiber - epoxy composite plates was investigated experimentally. In the experiments, impact tests were carried out with hemispherical shaped impactors at 40J, 100J and 160J energy values. The results are as follows.

- At 40J impact energy, the contact force is equal in both thicknesses. At higher energy levels, the contact force is higher in a composite with a core thickness of 10mm.

- Energy absorbed at 40J impact energy did not change according to thickness. At higher energy levels (100J-160J), 15mm thick composites have 10-15% higher energy absorption capability than 10 mm.
- As the core thickness increases, specimens starts to lose their rigidity. As a result of this, maximum contact force value decreases while contact time and maximum deflection values increase.
- Also, in the higher core thicknesses, the specimens absorbed more energy. Therefore, penetration energy region seen in the wide energy ranges.

References

[1] Xiong, Jian, et al. Sandwich structures with prismatic and foam cores: a review. Advanced Engineering Materials 2019; 21(1): 1800036.
[2] He, Meifeng, Wenbin Hu. A study on composite honeycomb sandwich panel structure. Materials & Design 29.3 (2008): 709-713.
[3] Griškevičius, Paulius, et al. Experimental and numerical study of impact energy absorption of safety important honeycomb core sandwich structures. Materials Science (Medžiagotyra) 16.2 (2010): 119-123.
[4] Belingardi, Giovanni, Roberto Vadori. Low velocity impact tests of laminate glass-fiber-epoxy matrix composite material plates. International Journal of Impact Engineering 27.2 (2002): 213-229.
[5] Rahman MM, et al. Improvements in mechanical and thermo-mechanical properties of e-glass/epoxy composites using amino functionalized MWCNTs. Composite Structures 94.8 (2012): 2397-2406.
[6] Abdel-Magid, Beckry, et al. The combined effects of load, moisture and temperature on the properties of E-glass/epoxy composites. Composite Structures 71.3-4 (2005): 320-326.
[7] Ozdemir O, Karakuzu R, Al-Shamary AKJ. Core-thickness effect on the impact response of sandwich composites with poly (vinyl chloride) and poly (ethylene terephthalate) foam cores. Journal of Composite Materials 49.11 (2015): 1315-1329.
[8] Mitrevski T, Marshall IH, Thomson RS, Jones, R. (2006). Low-velocity impacts on preloaded GFRP specimens with various impactor shapes. Composite Structures, 76, 209–217.
[9] Xuea X, Zhanga C, Chenb W, Wua M, Zhaoa J. (2019) Study on the impact resistance of honeycomb sandwich structures under low-velocity/heavy mass. Composite Structures 26: 111223.
[10] Anderson T, Madenci E. Experimental investigation of low-velocity impact characteristics of sandwich composites. Composite Structures 2000; 50(3): 239-247.

Fonksiyonel Derecelendirilmiş Malzemelerin Mekanik Karakterizasyonu

*Uğur Özmen**, *B. Burak Özhan*
Manisa Celal Bayar Üniversitesi, Makine Mühendisliği Bölümü, Manisa, Türkiye
**İletişimden sorumlu yazar: ugur.ozmen@cbu.edu.tr*

Özet

Ağırlığına oranla yüksek dayanım ve rijitliğe sahip olmalarından dolayı birçok uygulama alanı bulunan tabakalı kompozit malzemeler, tabakalar arası temas kuvvetlerinin yarattığı etkilerden dolayı karşı koyabileceklerinden daha düşük yüklerde hasara uğramaktadırlar. Bu problemi tamamen ortadan kaldırmak adına malzeme (yapı) fonksiyonel derecelendirilme ile üretilmektedir. Fonksiyonel derecelendirilmiş malzemeler (FDM) belirli bir doğrultuda değişen malzeme özelliklerine sahip yüksek performanslı malzemelerdir. Bu malzemeler, özelliklerin keskin olarak değiştiği ara yüzeyleri ortadan kaldırarak bu yüzeyler arası temas kuvvetlerinin yarattığı hasarları en aza indirir. Bu benzersiz özelliklerinden dolayı birçok uygulama alanında hızla yayılmaktadır. Bu çalışmada dört farklı polimer malzeme kullanılarak eklemeli imalat yöntemi ile fonksiyonel derecelendirilmiş malzemeler üretilmiş, çekme testi ile mekanik özellikleri tespit edilmiş ve sonuçlar karşılaştırılmıştır. Fonksiyonel derecelendirilmiş malzemelerin mekanik özellikleri en büyük çekme dayanımı, elastisite modülü ve kopma uzaması sonuçları ile değerlendirilmiştir.

Anahtar Kelimeler: fonksiyonel derecelendirilmiş malzemeler, mekanik karakterizasyon

Giriş

Birbirinden bağımsız birden fazla malzemenin bir araya gelmesi ile elde edilen kompozit yapılar, içerisinde bulunan malzemelerin kendilerine özgü özelliklerini tek bir yapıda ortaya koymasıyla oldukça ilgi çekmektedir. Kimi zaman yüksek mekanik özellikler sergilerken kimi zaman yüksek ölçüde ısıl özellikler ortaya koyan kompozit malzemeler, havacılıktan inşaata, ulaşımdan elektroniğe kadar birçok alanda kullanılmaktadır. Bu yapılar içerisinde yer alan takviye malzemesinin şekil ve yerleştirilmesine göre elyaflı, parçacıklı, tabakalı ya da karma kompozit malzemeler olarak sınıflandırılabilirler. Kompozit malzemelerin bir alt dalı olan tabakalı kompozit malzemeler, farklı doğrultularda yönlendirilebilir ve bir veya birden fazla doğrultuda yüksek mukavemet ve ısıl davranış sergilerler. Birden fazla tabakanın bir araya gelmesi ile oluşan bu yapılarda, birbirinden farklı özelliklerdeki tabakaların arasındaki temas (kontakt) kuvvetlerinin yarattığı hasar, asıl yapının gösterebileceği yüksek dayanıma engel olmaktadır. Bu problemi ortadan kaldırmak adına malzemeler arasındaki geçişin bir fonksiyona bağlı olarak yapıldığı fonksiyonel derecelendirilmiş malzemeler, tabakaları ve tabakalar arasındaki temas kuvvetlerini kaldırarak asıl yapının performansını artırmaktadır. Fonksiyonel derecelendirilmiş malzeme, 1984 yılında Japonya'da gerçekleştirilen bir projede ortaya atılmış ve havacılık sektörü için termal bariyer malzemesi üretilmiştir [1]. O günden bu yana fonksiyonel derecelendirilmiş malzemeler konusunda çalışmalar yapılmaya devam etmektedir. Geleneksel yöntemlerde olduğu gibi fonksiyonel derecelendirilmiş malzemelerin üretimi konusunda da henüz netlik yoktur. Fonksiyonel derecelendirilmiş malzemelerin üretiminde fiziksel ve kimyasal yöntemler kullanılmaktadır [2]. Fiziksel ve kimyasal buhar biriktirme ve püskürtme yöntemlerinde buhar sıvılaştırarak kimyasal reaksiyona girmesi ve ya dönüşmesi sağlanarak katı malzeme elde edilir [3-4]. Kullanımı sırasında zehirli gazın açığa çıktığı buhar biriktirme yöntemleri ise çoğunlukla kaplamalarda kullanılan bir üretim yöntemidir [5]. Metal ve metal türevi malzemelerle fonksiyonel derecelendirilmiş malzemeler elde etmek için toz metalürjisi yöntemi çok kullanılmaktadır [6-8]. Belirlenen bir fonksiyona bağlı olarak üretim öncesinde bir araya getirilen toz tabakaları, basınç altında sinterlenerek üretilir [8]. Fonksiyonel olarak derecelendirilmiş malzemelerin üretiminde önemli bir yeri olan eklemeli imalat yönteminde, elde edilecek fonksiyonel derecelendirilmiş malzemeye ait detaylar bilgisayar yardımı ile sağlanmaktadır. Eklemeli imalat yönteminin en büyük avantajları çok detaylı malzeme geometrisi oluşturmaya ve malzeme bileşenini kontrol etmeye izin vermesidir [9-10].

Bu çalışmanın temel amacı, farklı özelliklerdeki birçok polimer malzeme ile oluşturulmuş fonksiyonel derecelendirilmiş malzemeleri eklemeli imalat yöntemi ile üretmek ve mekanik özelliklerini tespit etmektir. Bu amaçla fonksiyonel derecelendirilmiş malzemelerin eklemeli imalat yöntemi ile

üretimi yapılmıştır. Ardından bu malzemelerin mekanik davranışını anlayabilmek için çekme testleri gerçekleştirilmiştir. Üretimde, ABS (akrilonitril bütadien stiren), PLA (polilaktik asit), PETG (polietilen tereftalat) ve PA (naylon) polimerler kullanılmıştır. Farklı polimerlerle üretilen fonksiyonel derecelendirilmiş malzemeler çekme testleri ile deneysel olarak analiz edilmiştir.

Üretim Yöntemi ve Çekme Testi

Bu bölümde, fonksiyonel derecelendirilmiş malzemelerin mekanik karakterizasyonu için kullanılan numunelerin üretim yöntemi ve gerçekleştirilen çekme testinin detayları anlatılacaktır.

Üretim Yöntemi

Bu çalışmada kullanılan fonksiyonel derecelendirilmiş malzemelerin üretiminde eklemeli imalat yöntemi ile çalışan üç boyutlu yazıcı teknolojisi kullanılmıştır. Endüstride yer alan üç boyutlu yazıcılar çoğunlukla tek bir malzemeyi üretmeye imkan verir ve üretim sırasında kullanılan malzemelerin değiştirilmelerine izin vermezler. Fakat bu çalışmanın amacı, birden fazla malzemeyi aynı anda üretebilmektir. Bu amaç için birden fazla malzemeyi aynı anda üretmeye imkan veren üç boyutlu yazıcı oluşturulmuş ve Tablo 1'de yer alan parametre değerleri kullanılarak üretimler gerçekleştirilmiştir.

Tablo 1. Üç Boyutlu Yazıcıda Kullanılan Üretim Parametre Değerleri

Parametre	Değer
Nozzle çapı	1.0 mm
Duvar çizgi sayısı	1
Yazma sıcaklığı	230°C
Tabla sıcaklığı	65°C
Doluluk oranı	%100
Çizgi oryantasyonu	45°
Katman kalınlığı	0.1 mm
Yazma hızı	60 mm/s

Fonksiyonel derecelendirilmiş malzemeleri üretirken kullanılan ve kalınlık doğrultusunda derecelendirilmeyi ifade eden fonksiyon ve güç yasası indisi (üst indis) k Denklem 1'de görülmektedir.

$$E(z) = (E_T - E_B)\left(\frac{z}{h} + \frac{1}{2}\right)^k + E_B \quad (1)$$

Çekme Testi

Çekme testleri (Şekil 1) ASTM D638 standartlarına göre ABS (Akrilonitril Bütadien Stiren), PLA (Polilaktik Asit), PETG (Polietilen Tereftalat Glikol) ve PA(Poliamid), homojen malzemeleri ve ABS/PA, PLA/PA ve PETG/PA fonksiyonel derecelendirilmiş malzemeler için gerçekleştirilmiştir. Testler, video ekstansometre kullanılarak yapılmış, ekstansometrenin ölçeceği kısmın kesit ve uzunluk değerleri bilgisayara girilmiştir. Tüm numunelerin çekme testi 1 mm/dk hızla yapılmıştır. Bu çekme testi ile en büyük (maksimum dayanım), elastisite modülü ve kopma uzaması değerleri elde edilmiştir. Bu veriler ile ilgili değerlendirme Bölüm 3'de sonuçlar bölümünde yapılmıştır.

Şekil 1. Çekme Testi

Sonuçlar ve Değerlendirme

PLA, ABS, PETG, PA polimer malzemeleri ve k=1 güç yasası endeksine göre üretilmiş PLA-PA, ABS-PA ve PETG-PA fonksiyonel derecelendirilmiş malzemeleri için yapılan çekme testi sonucunda elde edilen maksimum çekme dayanımı değerleri Şekil 2'de verilmiştir. PLA, ABS, PETG ve PA malzemelerinin maksimum çekme dayanımları birbirine oldukça yakındır. PLA-PA, ABS-PA ve PETG-PA fonksiyonel derecelendirilmiş malzemelerin maksimum çekme dayanımları ise tek üretilen malzemelerden daha düşüktür. PLA, ABS ve PETG filamentler, tekil haldeki üretimlerine kıyasla PA filament ile iyi yapışma sağlayamadığından maksimum çekme dayanımı değerlerinde azalma görülmektedir. PA ilavesi PLA'nın maksimum çekme dayanımı değerini %37 düşürürken bu değer ABS için %22 ve PETG için %12'dir. Bir başka deyişle PETG-PA malzemeleri diğer malzemelere kıyasla daha iyi yapışma yüzeylerine sahiptir.

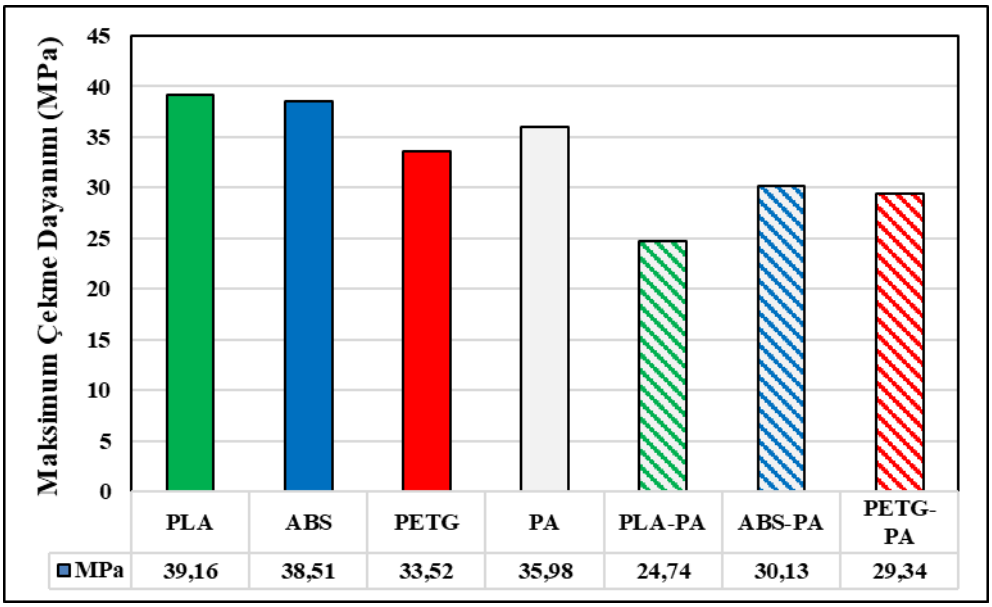

Şekil 2. Maksimum Çekme Dayanımı Grafiği

Saf halde üretilen PLA, ABS, PETG ve PA numunelere ve PLA-PA, ABS-PA ve PETG-PA fonksiyonel derecelendirilmiş malzemelere ait elastisite modülü değerleri Şekil 3'de görülmektedir. PLA-PA, ABS-PA ve PETG-PA fonksiyonel derecelendirilmiş malzemelerin elastisite modülü değerleri, PLA, ABS, PETG malzemelere ait elastisite modülü değerleri ile PA elastisite modülü değeri arasındadır. Üretilen numunelerdeki ilgili malzemeler eşit hacimde bulunmaktadır. Örneğin PLA-PA numunelerinde eşit hacimde PLA ve PA malzemeleri yer almaktadır. Bu nedenle PLA-PA fonksiyonel derecelendirilmiş malzemenin elastisite modülü değeri beklendiği gibi PLA ve PA tekil malzemelerinin elastisite modülü değerlerinin hemen hemen tam ortasında yer almaktadır. Fakat PETG-PA fonksiyonel

derecelendirilmiş malzemenin elastisite modülü değeri PETG ve PA malzemelerinin elastisite modülü değerinden daha yüksektir. Bu iki malzemenin birbirine daha iyi yapışması yüksek dayanımı ve dolayısıyla yüksek elastisite modülünü sağlamıştır.

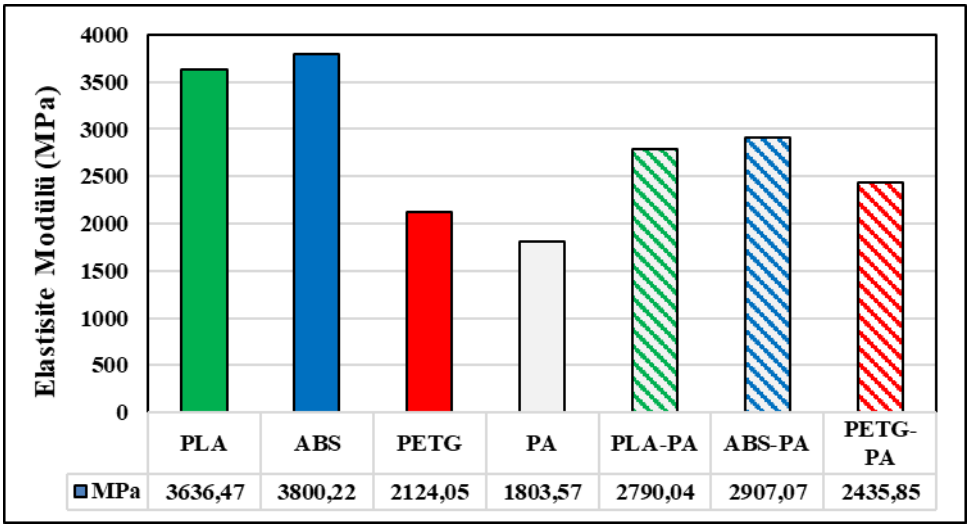

Şekil 3. Elastisite Modülü Grafiği

Çekme testi sonucunda elde edilen kopma uzaması değerleri için sonuçlar (Şekil 4), elastisite modülüne benzer şekilde elde edilmiştir. PLA-PA, ABS-PA ve PETG-PA fonksiyonel derecelendirilmiş malzemelerinin kopma uzaması değerleri PLA, ABS, PETG ve PA malzemelerinin kopma uzaması değerlerinden daha düşüktür. Fonksiyonel derecelendirilmiş numunelerin malzeme uyumsuzluğu, yapışma sorunları, tekil malzemelere kıyasla daha az şekil değiştirebilme özelliğine sahip olmasına neden olmaktadır. En düşük kopma uzaması değeri PLA-PA fonksiyonel derecelendirilmiş malzemede, en yüksek kopma uzaması değeri ise PETG-PA malzemelerinde görülmektedir.

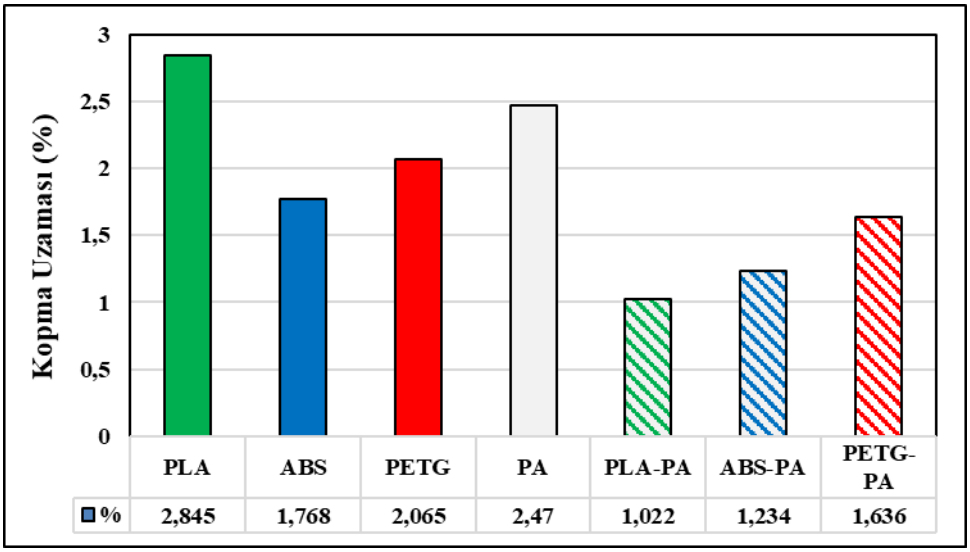

Şekil 4. Kopma Uzaması Grafiği

Teşekkür

Bu çalışma, Manisa Celal Bayar Üniversitesi Bilimsel Araştırma Projeleri Koordinasyon Birimi tarafından 2019/139 proje numarası ile desteklenmiştir.

Referanslar

[1] Koizumi M. FGM activities in Japan. Compos Part B Eng 1997. https://doi.org/10.1016/s1359-8368(96)00016-9.
[2] Gupta A, Talha M. Recent development in modeling and analysis of functionally graded materials and structures. Prog Aerosp Sci 2015. https://doi.org/10.1016/j.paerosci.2015.07.001.
[3] Groves JF, Wadley HNG. Functionally graded materials synthesis via low vacuum directed vapor deposition. Compos Part B Eng 1997. https://doi.org/10.1016/s1359-8368(96)00023-6.
[4] Mahamood RM, Akinlabi ET, Shukla M, Pityana S. Functionally graded material: An overview. Lect. Notes Eng. Comput. Sci., 2012.
[5] Knoppers GE, Gunnink JW, Van Den Hout J, Van Vliet WP. The reality of functionally graded material products. Proc Solid Free Fabr Symp 2004.
[6] Nemat-Alla MM, Ata MH, Bayoumi MR, Khair-Eldeen W. Powder Metallurgical Fabrication and Microstructural Investigations of Aluminum/Steel Functionally Graded Material. Mater Sci Appl 2011. https://doi.org/10.4236/msa.2011.212228.
[7] Watari F, Kondo H, Tamura Y, Yokoyama A, Omori M, Hirai T, et al. Fabrication and properties of titanium nitride and titanium nitride/apatite functionally graded material for abrasion resistant implant. Trans. - 7th World Biomater. Congr., 2004.
[8] Zhu J, Lai Z, Yin Z, Jeon J, Lee S. Fabrication of ZrO2-NiCr functionally graded material by powder metallurgy. Mater Chem Phys 2001. https://doi.org/10.1016/S0254-0584(00)00355-2.
[9] Lin X, Yue TM. Phase formation and microstructure evolution in laser rapid forming of graded SS316L/Rene88DT alloy. Mater Sci Eng A 2005. https://doi.org/10.1016/j.msea.2005.05.024.
[10] Moon J, Caballero AC, Hozer L, Chiang YM, Cima MJ. Fabrication of functionally graded reaction infiltrated SiC-Si composite by three-dimensional printing (3DPTM) process. Mater Sci Eng A 2001. https://doi.org/10.1016/s0921-5093(00)01282

Design and Production of a New Smaller Diameter Axial Bearing Subjected to High Wear Loads

Sinan Dayı, Mehmet Çevik
İzmir Kâtip Çelebi Univ., Department of Mechanical Engineering, Izmir, Turkey
**Corresponding author: sinan.dayi@zf.com*

Abstract

In the steering system of a passenger car, one of the essential components is the tie rod, and the sub-assembly component is the inner tie rod, which is subject to static and dynamic bearing loads. These bearing loads are the key points to ensure the inner tie rod's performance and total lifetime. A significant drop in the inner tie rod's performance can cause uncomfortable driving conditions and noise during driving. Most of the designs are developed over-safe with bigger ball sizes to fulfill the defined requirements. On the other hand, over-safe design can cause higher prices.

In this study, a new small diameter axial bearing system is developed subjected to high wear loads on the inner tie rod. Three design parameters are considered: press force, tempering method, and tempering temperature. A smaller ball diameter design is created during the development phase. After the manufacturing, the inner tie rods are tested concerning the wear test and setting behavior under the maximum loading test. Results have been compared with a bigger ball size design. By changing the production and assembly parameters, optimum assembly conditions have been defined. Functional measurements before and after testing have validated the new smaller ball diameter design for serial usage.

Keywords: Steering system, inner tie rod, axial bearing

Introduction

The steering system is the system that transmits the circular motion from the steering wheel to the wheels linearly with the help of steering gear. The most crucial mechanical connection part of the steering system is the rods. The tie rod's most crucial function is transmitting the linear motion from the steering system to the knuckle.

The tie rod is an essential part of the steering system and a critical component from the safety point of view. It conducts the connection between the wheel and the steering system. A tie rod is simply an assembly of the inner tie rod and outer tie rod connected by a thread connection and a counter nut. By the thread connection, the tie rod length can be adjusted.

Tie rods can be damaged in many ways during operating, and these damages mostly cannot be recognized. One of these damages is the plastic bearing's wear or breakage inside the inner and outer tie rod assembly.

A steering system consists of the steering wheel, steering column, intermediate shaft, power steering pump, rack & pinion steering gear, tie rod, and the steering knuckle. The tie rod is connected to the steering knuckle by ball joints. The intermediate shaft rotates with the steering wheel's rotational movement applied by the driver. As a result, power is transmitted to the steering gear. Rotational movement applied from the steering wheel by the driver is converted into linear motion by a gearbox. It transmits this linear motion over the tie rod to the knuckle and wheels.

The systems used to guide the vehicles have developed from past to present. More complex, easy-to-use systems have replaced simple systems. One of the most commonly used mechanical steering system designs is the rack and pinion steering system, and they are mostly used in light vehicles.
In driving conditions, the wheels also move vertically parallel to the steering axis; this system is under the influence of a force in the third dimension. Therefore, the use of ball joints in rods is required. The inner tie rod, located at the steering gear side, has an axial ball joint, while the outer tie rod on the knuckle side has a radial ball joint as shown in Figure 1. With the help of the ball joints, the left and right horizontal movement and the up and down vertical movement of the wheel can be provided.

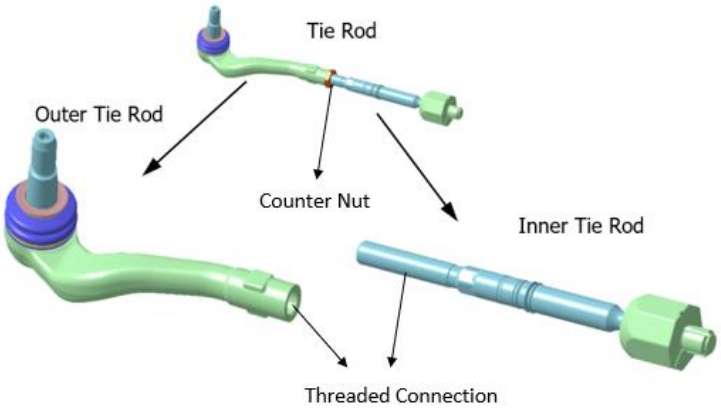

Figure 1. Outer tie rod, inner tie rod, and counter nut [1]

Inner tie rod includes axial housing, axial ball stud and plastic ball race. Figure 2 shows the assembly components of the inner tie rod. The inner tie rod is manufactured by the cold forging method. During the assembly of these single components by pressing operation, axial housing is subjected to plastic deformation under high load. The axial ball stud cannot easily get out of the axial housing. The ball stud can stay up to 40 kN pull-out force without separation from the axial housing [1].

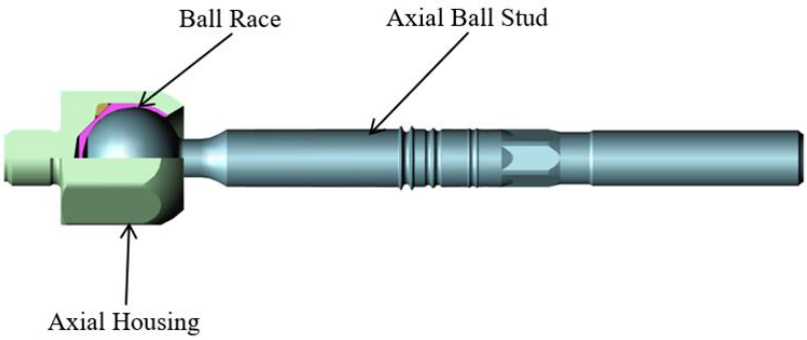

Figure 2. Inner tie rod subcomponents

Shende and Padole [2] examined the steering mechanisms of heavy commercial vehicles. They stated that sudden loads caused the most significant effect causing damage to the rod occur during steering the wheels. They calculated the fatigue performance and durability life with the finite element method and determined that the bushes they add to the rod geometry reduce stresses. In automobiles, ships, aircraft wings and fuselages, turbines, nuclear reactors and other machine components subjected to cyclic loading, fatigue is the major threat and has come into question with the technological development [3]. Flores et al. [4] investigated the effects of the joint gap on mechanical systems. They have seen that vibration and wear cause durability problems and stated that if the gaps are modelled as lubricated, the forces formed are more regular. Zhao et al. [5] presented a method to predict the effect of the amount of gap in the rolling joints on wear. The elastic elements are modelled based on the absolute node coordinate formulation method, and the contact forces of the hinge components are calculated by the continuous contact method. Mohamed et al. [6] aimed to determine the automotive pre-order system's workload under real conditions. The workloads were obtained by data collection operations on the test track. The information obtained from sensors such as accelerometer, wheel force sensor, and strain-gage were recorded with data collection systems.

Polyoxymethylene (POM) material is used most commonly in inner tie rod ball joints [7]. Polyacethylene is also referred to as polyoxymethylene. The plastic material POM belongs to the thermoplastics group. It has a partial crystal structure with a high degree of crystallization (up to 80% of the crystal content of the homopolymerisate). POM has many outstanding characteristics that prove to be the best bearing material for the axial joints. Chen et al. [8] investigated the friction and wear behaviour of polyoxymethylene/linear low-density polyethylene/ethylene-acrylic-acid blends. Results

showed that the friction and wear properties of POM were significantly improved after an amount of linear low-density polyethylene (LLDPE) and ethylene/acrylic acid copolymers (EAA) was added. Kırlı [9] investigated POM material properties used in ball joints and studied on a model to create a finite element analysis model. Gao et al. [10] investigated contact of polymer-stainless steel with wear and friction tests. As a result of their analysis, they found that during the friction process, on surfaces complex chemical reactions occur.

In industry, preliminary experimental studies are generally performed in order to achieve favorable designs, aiming to decrease costs. The main goal of these studies is to minimize the number of prototypes and the testing period required to start mass production. The effective parameters are investigated in such studies [11, 12].

Material and Method

In this study, a new small diameter axial bearing is designed to resist high wear loads. After assembly, the pressing force for joint assembly is defined, the tempering method and temperature are determined to maintain the appropriate stiffness value to meet the wear loads of the axial bearing. Besides, the functional values as articulation torque (M_k), axial travel (S_{ax}), stiffness ($C_{min,ax}$) of the assembled inner tie rods are measured by experimental studies, and their wear behaviour is examined.

The effects of the standard pressing force and different tempering methods on the part's stiffness value are investigated. The inner tie rod assemblies with high stiffness are subjected to the wear test and the wear test results are compared, and an optimized design is obtained.

In the scope of the study, setting behaviour under maximum loading is also tested by the setting test. In this test, inner tie rods are loaded at maximum loading for three load cycles, and then functional measurements described below are applied. Production and testing of the inner tie rods are done in ZF Lemförder Aks Modülleri San. ve Tic. A.Ş. Laboratories, Izmir.

The following materials are used in this thesis study.

Housing: C15 according to EN 10277-2 (Bright steel products standard), case-hardened steel, manufactured externally by cold forging. Commonly used in the automotive market.

Ball stud: 30MnVS6 according to DIN EN 10267 (Ferritic-pearlitic steels for precipitation hardening from hot-working temperature), micro-alloy steel, manufactured externally by cold forging. No additional heating process is needed after forging which brings cost advantage.

Ball race: plastic component POM. Commonly used in the automotive market.

The geometry of the components of inner tie rod is shown in Figure 3. These chosen single part materials mentioned above for each are the most commonly used in the market for inner tie rod production.

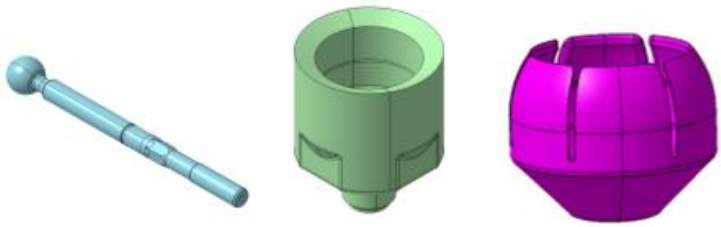

Figure 3. Part of the inner tie rod assembly, from left to right: ball stud, housing and ball race.

Inner tie rod assembly components are ball stud, housing, and ball race. The components assembly process is shown in Figure 4.

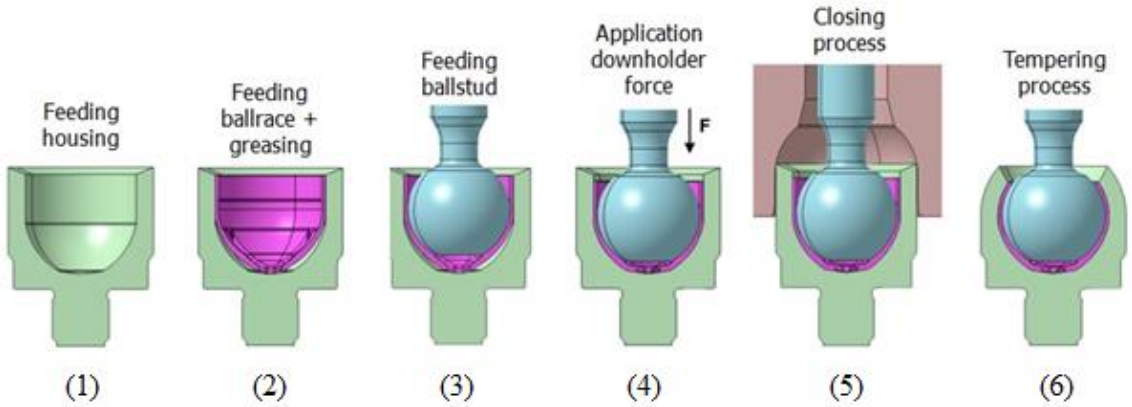

Figure 4. Inner tie rod assembly process

In this study assembly process number 3 ball tempering (only if ball tempering method is selected), number 5 closing force and number 6 oven tempering (only if oven tempering method is selected) are considered, and parameters are defined accordingly. Assembly on round table can provide around 30 assemblies per minute.

The tempering process enables the assembled housing, ball stud, and ball race to make surface contact with the temperature's effect, which is more suitable for the assembly parts. The articulation torque values of ball joints without the tempering process are high due to the high friction force. Therefore, to reach the desired torque values, the tempering is applied on complete inner tie rod or only on ball stud; thus, required articulation torque values are reached. Nevertheless, as a result of this heat treatment, while torque values decrease, axial and radial deflection increases. Therefore, tempering temperature and duration should be determined according to the inner tie's functional conditions. There are two methods for the tempering process which are applied in this study:

(i) Oven Tempering: The complete inner tie rod is heated up to a defined temperature for a defined duration in the oven tempering option. Oven tempering is applied after the complete assembly of the inner tie rods. During oven tempering, assembled inner tie rods lay on a tray, and the complete inner tie rod is heated up to a specific temperature. The main drawback with oven tempering is that, unnecessary areas of the inner tie rod are also heated up such as the ball stud shaft. This has no adverse effect on the ball stud but causes high energy consumption.
(ii) Ball Tempering : Only the spherical ball is heated up to a defined temperature for a defined duration in the ball tempering option. The difference between oven tempering and ball tempering is that, in the ball tempering the ball is heated before feeding the ball stud during the assembly process.

Both tempering methods are investigated in this study.

In the scope of our study, a new smaller ball diameter, Ø26 mm axial bearing (ball joint) is developed. For the functional measurements, spring travel (S_{ax}), stiffness ($C_{min,ax}$), articulation torque (M_k) acceptance criteria are defined according to global ball joint standard. The new Ø26 mm axial bearing is compared with the current series product, a Ø29 ball size axial bearing which has a larger ball diameter. Ball diameter Ø29 inner tie rod is also measured for spring travel, stiffness, articulation torque for comparison purpose.

The study's target is to get the same functional performance from Ø26 ball size, which is already achieved by Ø29 ball size. For this purpose, 12 Ø29 ball size, and 180 Ø26 ball size samples in a total of 192 inner tie rod samples are manufactured, and functional performances are measured. According to the preliminary measurement results, 12 Ø29 ball size samples in 1 batch and 48 Ø26 ball size samples in 4 batches were used to focus on further wear and setting test. Each batch contains 12 samples, the first 6 samples are used for the setting test, and the second 6 are used for the wear test.

Inner tie rods are numbered according to the ball size, batch no, and sample no. New smaller ball diameter Ø26 inner tie rods are produced according to three production parameters: press force, tempering method, and tempering temperature. During the test sample manufacturing, three different test groups are created. For each group creation, a new functional diagram is created.

The chosen inner tie rods variants are given in Table 1, for each variant 12 inner tie rods are manufactured, and functional performances measured.

Table 1. Inner tie rod production variants

Batch No	Press Force	Tempering Method	Tempering Temperature
1	Min press force + 20 kN	Oven	Initial
2	Min press force + 20 kN	Oven	Initial + 10°C
3	Min press force	Ball	Initial
4	Min press force + 10 kN	Ball	Initial

Functional properties of the inner tie rod assembly are spring travel, stiffness, articulation torque. These properties are spesific for every single assembly, for this reason, all assemblies are measured before and after testing.

The effect of different assembly and tempering parameters (press force, tempering method and tempering temperature) on the friction moment of the inner tie rod axial bearing was investigated by the articulation torque measurement. The axial spring travel is measured by a special measurement device. The test sample is attached to the machine's piston rod using connecting elements. The housing of the test sample is firmly fixed on the machine table. Measurement device is used to apply the axial force on the inner tie rod from ball stud to housing direction. By applying the defined axial force, the ball stud ball area inside the joint moves in the axial direction. The travel of the ball inside the joint is recorded.

The setting test is performed to evaluate the plastic bearing performance at maximum force and under high temperature. In the wear test, the functional performance of the inner tie rod is investigated after the worn ball race. During the wear test, the force is applied in the axial direction of the tie rod. The inner tie rod direction is ensured by fixing the housing on the test rig to apply articulation angle and by clamping the ball stud to apply the axial force. The joint area is heated up to 80°C in heat chamfer.

Inner tie rods are tested according to the block cycle defined in Table 2. This block cycle is repeated 8 times for the sample.

Table 2. Wear test block cycle

Test Load [kN]	Frequency [Hz]	Articulation Angle [°]	Temperature [°C]	Cycle
±8884	2	14	80	1250
±7625	4	14	80	2500
±5724	4	14	80	2500
±4464	2	14	80	6250
±3276	1	14	80	25.000
±2468	2	14	80	25.000

Results and Discussions

In this section, the experimental results are evaluated. First, the reference sample of Ø29 ball size design results is evaluated. Since Ø29 ball diameter is tested only for reference to the new smaller ball joint production, all functional measurements before and after setting and wear tests are evaluated as acceptable.

For Batch 1 of test samples, production is done with “min press force +20 kN” pressing force for pressing operation. Inner tie rods are tempered in the oven at the initial temperature. Red colored cells show unacceptable results.

According to the results given in Table 3, sample numbers 26.1.1, 26.1.5, and 26.1.6 did not fulfill the requirement of M_k before setting test. Inner tie rods were tested only for information and samples fulfill the requirement after the test. However, because of unacceptable results before the test, samples are evaluated as unacceptable. Also, a wear test is not performed on these samples. Thus, either press force “min press force +20 kN” is high or tempering temperature is not high enough to ensure acceptable torque results before testing.

Table 1. Batch 1 functional measurements of Ø26 ball size before and after the setting test

Sample No	Before Setting Test			After Setting Test			Evaluation
	S_{ax} [mm]	$C_{min,ax}$ [kN/mm]	M_k [Nm]	S_{ax} [mm]	$C_{min,ax}$ [kN/mm]	M_k [Nm]	
26.1.1	0,02	229	3,9	0,23	6,3	0,7	NOT OK
26.1.2	0,03	197	3,5	0,22	6,6	0,6	OK
26.1.3	0,02	264	3,3	0,23	6,3	0,6	OK
26.1.4	0,02	229	2,8	0,27	4,8	0,5	OK
26.1.5	0,02	230	3,8	0,24	5,5	0,6	NOT OK
26.1.6	0,02	269	3,7	0,22	6,5	0,5	NOT OK

Then Batch 2 is tested. Press force "min press force +20 kN" is applied again, tempering temperature is increased by 10°C to ensure the pre-test measurements for Mk to be acceptable. Higher tempering temperature can adjust the M_k to decrease. The results are shown in Tables 4 and 5.

Table 4. Batch 2 functional measurements of Ø26 ball size before and after the wear test

Sample No	Before Wear Test			After Wear Test			Evaluation
	S_{ax} [mm]	$C_{min,ax}$ [kN/mm]	M_k [Nm]	S_{ax} [mm]	$C_{min,ax}$ [kN/mm]	M_k [Nm]	
26.2.1	0,03	172	3,5	0,07	22	1,1	OK
26.2.2	0,03	150	3,1	0,07	31	0,8	OK
26.2.3	0,03	165	3,1	0,06	30	0,9	OK
26.2.4	0,02	181	3,0	0,06	42	1,1	OK
26.2.5	0,02	199	3,2	0,06	46	1,1	OK
26.2.6	0,03	187	3,2	0,06	54	1,4	OK

Table 5. Batch 2 functional measurements of Ø26 ball size before and after the setting test

Sample No	Before Setting Test			After Setting Test			Evaluation
	S_{ax} [mm]	$C_{min,ax}$ [kN/mm]	M_k [Nm]	S_{ax} [mm]	$C_{min,ax}$ [kN/mm]	M_k [Nm]	
26.2.7	0,03	187	3,5	0,39	2,4	0,3	OK
26.2.8	0,03	191	3,5	0,35	2,7	0,5	OK
26.2.9	0,03	177	3,1	0,28	3,3	0,4	OK
26.2.10	0,03	195	3,5	0,32	3,4	0,5	OK
26.2.11	0,03	207	3,3	0,29	3,1	0,4	OK
26.2.12	0,03	179	3,5	0,30	3,5	0,5	OK

According to pre-test measurements of the wear test, it is evident that torque measurement results are still close to the upper limit but decreased in respect to the Batch 1 results. This means that a 10°C tempering temperature increase is decreasing the torque to the required level by keeping the pressing force constant. Evaluation after wear test is also acceptable according to functional measurement results. Setting test pre-and post-test measurement results are also evaluated as acceptable. Thus, for Ø26 ball joint production parameters; "min press force +20 kN" press force, Initial +10°C oven tempering temperature fulfills the requirements and can be used for series production.

After the first results stated for oven tempering, Batch 3 is tested which was tempered at the ball area. Assembly is done by using Min press force and the tempering method has been updated to ball tempering. (See Tables 6 and 7)

Table 6. Batch 3 functional measurements of Ø26 ball size before and after the wear test

Sample No	Before Wear Test			After Wear Test			Evaluation
	S_{ax} [mm]	$C_{min,ax}$ [kN/mm]	M_k [Nm]	S_{ax} [mm]	$C_{min,ax}$ [kN/mm]	M_k [Nm]	
26.3.1	0,03	137	1,3	0,07	50	0,6	OK
26.3.2	0,03	156	0,8	0,07	47	0,5	OK
26.3.3	0,03	201	1,2	0,05	80	1,0	OK
26.3.4	0,03	167	0,9	0,06	55	0,6	OK
26.3.5	0,03	195	1,1	0,05	76	1,2	OK
26.3.6	0,02	225	1,2	0,05	94	1,2	OK

Table 7. Batch 3 functional measurements of Ø26 ball size before and after the setting test

Sample No	Before Setting Test			After Setting Test			Evaluation
	S_{ax} [mm]	$C_{min,ax}$ [kN/mm]	M_k [Nm]	S_{ax} [mm]	$C_{min,ax}$ [kN/mm]	M_k [Nm]	
26.3.7	0,03	152	1,1	0,44	1,7	0,4	NOT OK
26.3.8	0,03	183	1,1	0,18	5,1	0,4	OK
26.3.9	0,03	156	1,0	0,49	1,7	0,4	NOT OK
26.3.10	0,03	171	1,1	0,44	1,9	0,3	NOT OK
26.3.11	0,03	171	1,2	0,45	1,9	0,3	NOT OK
26.3.12	0,03	187	1,4	0,47	1,7	0,3	NOT OK

According to the results in Tables 6 and 7, pre and post measurements of the wear test fulfills the requirements. Usage of lower press force decreased the inner stress at ball joint which resulted in acceptable measurement values of M_k. On the other hand, pre-test measurements of setting test were evaluated as acceptable. After testing, axial travel S_{ax} has increased more than the allowed limit and in respect to S_{ax} measurements stiffness $C_{min,ax}$ has decreased more than the allowed limit. Five out of 6 samples are evaluated as unacceptable. This means that a reduction in press force decreased the pre-torque performance inside the requirement. Also, after the wear test, all functional values are within the limit because wear on the ball race was within allowed limits. However, deformation on ball race after setting test caused unacceptable results at S_{ax} and $C_{min,ax}$. The travel of the ball stud inside the joint is more than allowed. Thus, Min press force is not enough to ensure a safe design.

For the final test trials, Batch 4 is tested concerning the Batch 3 results. The outcome from Batch 3 results showed that Min press force is not enough to fulfill the requirements. For increased performance and acceptable evaluation, press force has been increased to Min press force + 10 kN. According to pre-test measurements of wear test, results are in the middle range of the requirement. This means that increase in press force is also increasing the pre-test torque results. Evaluation after wear test is also acceptable according to functional measurement results. Setting test pre-and post-test measurement results are also evaluated as acceptable. Thus, for Ø26 ball joint production parameters; Min press force + 10 kN, initial ball tempering temperature fulfills the requirements and can be used for series production. (See Tables 8 and 9)

Table 8. Batch 4 functional measurements of Ø26 ball size before and after the wear test

Sample No	Before Wear Test			After Wear Test			Evaluation
	S_{ax} [mm]	$C_{min,ax}$ [kN/mm]	M_k [Nm]	S_{ax} [mm]	$C_{min,ax}$ [kN/mm]	M_k [Nm]	
26.4.1	0,02	273	2,1	0,04	135	1,7	OK
26.4.2	0,02	235	2,2	0,04	125	1,8	OK
26.4.3	0,02	235	2,1	0,04	109	1,5	OK
26.4.4	0,02	276	2,0	0,04	135	1,5	OK
26.4.5	0,02	293	2,1	0,04	102	1,2	OK
26.4.6	0,02	228	1,9	0,05	93	1,3	OK

Table 9. Batch 4 functional measurements of Ø26 ball size before and after the setting test

Sample No	Before Setting Test			After Setting Test			Evaluation
	S_{ax} [mm]	$C_{min,ax}$ [kN/mm]	M_k [Nm]	S_{ax} [mm]	$C_{min,ax}$ [kN/mm]	M_k [Nm]	
26.4.7	0,02	242	2,4	0,15	6,5	0,6	OK
26.4.8	0,02	253	1,8	0,13	6,2	0,4	OK
26.4.9	0,02	267	2,0	0,12	7,1	0,6	OK
26.4.10	0,02	242	2,3	0,11	7,3	0,5	OK
26.4.11	0,02	222	2,0	0,11	7,8	0,5	OK
26.4.12	0,02	250	2,3	0,14	7,7	0,5	OK

Conclusion

In this study, a smaller diameter plastic bearing was designed and manufactured instead of the relatively large diameter plastic bearing, which is still in use. Thus, it is aimed to lighten the product and reduce its cost. The functional values specified by the current standards and the products have been determined.

The new Ø26 ball diameter inner tie rod samples were assembled in 3 different groups with different assembly force, tempering type and tempering temperatures. All variations of all three groups were tested for their functional performance and the best 4 variations were selected for wear and setting.

The test samples are tested in the wear test device at the loading of the road simulating conditions. All samples were subjected to wear test under load, simulating road conditions in the test device. Functional values were measured both before and after the setting test, and the results were compared, as was done in the wear test.

For Batch 1, only the setting test was performed because the articulation torque in three parts exceeded the allowable range of 0.5 - 3.5 Nm with the values 3.9, 3.8, 3.7 Nm. Although functional measurements obtained after the setting test were within the expected range, the results before the test were out of range, as a result of the evaluation, it was determined that the tempering temperature should be increased and the wear test was not continued.

For Batch 2, tempering temperature was increased by 10 ° C and functional values were measured. As all functional measurements before tests are within the specified range, wear and setting tests have been carried out for this batch. Since the values obtained after the tests meet the acceptance criteria, this batch has been evaluated as having suitable assembly parameters for series production.

For Batch 3, the tempering method was ball tempering instead of oven tempering. In the measurements before the test, all samples were evaluated as in the range of acceptance criteria. Wear tests and setting tests were carried out. After the wear tests, functional values were measured again, and it was seen that all values met the acceptance criteria. After the setting tests, five out of six pieces could not meet the axial displacement and stiffness criteria. This occurred because of excessive wear of the plastic bearing and it was decided that the press force during assembly should be increased.

The Batch 4 samples are again assembled by ball tempering and with 10 kN more press force than batch samples. According to the measurements made, it has been observed that the functional values of

all parts before the test are within the acceptance criteria and the tests can be continued. Since functional values meet the acceptance criteria after the wear and setting tests, this batch has been evaluated as having the appropriate assembly parameters for series production.

As a result of the study, the production methods of the Batch 2 and Batch 4 samples were determined as appropriate for series production. In both batches, reduction of around 10% in weight and reduction of around 8% in costs were achieved. In this case both Batch 2 and Batch 4 are preferred for serial production according to tempering method. If oven tempering will be performed then Batch 2 is preferred, if ball tempering will be performed then Batch 4 is preferred.

Acknowledgment

The authors thank to ZF Lemförder Aks Modülleri San. ve Tic. A.Ş. for providing production and testing possibilities during the study.

References

[1] Heißing B, Ersoy M. Chassis Handbook. 1st Edition. Wiesbaden: Vieweg+Teubner; 2011.
[2] Shende A, Padole V. Failure analysis and fatigue life improvement of modified steering mechanism (Tie-Rod) of heavy commercial vehicles using FEA. International Journal for Scientific Research & Development 2016; 4(07): 283-284.
[3] Köksal NS, Kayapunar A, Çevik M. Fatigue analysis of a notched cantilever beam using ANSYS workbench, Proceedings Book of the Fourth International Conference on Mathematical and Computational Applications, 2013, Manisa, Turkey, 111-118.
[4] Flores P, Ambrosio J, Claro JCP, Lankarani HM, Koshy CS. A study on dynamics of mechanical systems including joints with clearance and lubrication. Mechanism and Machine Theory 2006; 41(3): 247-261.
[5] Zhao B, Zhang Z-N, Dai X-D. Prediction of wear at revolute clearance joints in flexible mechanical systems. Procedia Engineering 2013; 68:661-7.
[6] Mohamed EAAE, Yusuff MA, Wahab DA, Application of rain flow cycle counting in the reliability prediction of automotive front corner modüle system, 16th International Conference on Industrial Engineering and Engineering Management, 2009, 709-712.
[7] Sarıkaya A. Modelling and control of power assisted steering systems (master's thesis). İstanbul Technical University, Institute of Science and Technology, 2007. https://tez.yok.gov.tr/
[8] Chen J, Cao Y, Li H. Investigation of the friction and wear behaviors of polyoxymethylene/linear low-density polyethylene/ethylene-acrylic-acid blends. Wear 2006; 260 (11–12): 1342-48.
[9] Kırlı O. Determining mechanical properties of the steering joint ball race material acetal/polyoxymethylene (POM) at compression loading and different temperatures with experimental and numeric simulation (doctoral thesis). Ege University Graduate School of Natural and Applied Science, Izmir, 2009. https://tez.yok.gov.tr/
[10] Gao J, Mao S, Liu J, Feng D. Tribochemical effects of some polymers/stainless steel. Wear 1997; 212(2): 238-243.
[11] Sunar Ö, Çevik M. Tek katlı yaprak yaylarda sonlu elemanlar yöntemi ile yorulma analizi. Celal Bayar University Journal of Science 2015; 11(1): 1-6.
[12] Essienubong IA, Ikechukwu O, Ebunilo PO, Ikpe EE. Static analysis on a vehicle tie rod to determine the resulting buckling displacement. International Journal of Industrial and Manufacturing Systems Engineering 2016; 1(1): 16-24.

Finite Element Vibration Analysis of a Functionally Graded Plate

Alif Ngimbi Diambu[1], Mehmet Çevik*
[1]Izmir Katip Çelebi University, The Graduate School of Natural and Applied Sciences, Dept. of Mechanical Engineering, Izmir, Turkey
Izmir Katip Çelebi University, Department of Mechanical Engineering, Izmir, Turkey
**Corresponding author: anasroudine1@gmail.com*

Abstract

Functionally Graded (FG) materials are recent types of engineering materials Fdeveloped as a solution for applications where a couple of relevant properties of different materials are desired in a single continuous composite structure. In these materials, properties are patterned in a way to insure a gradient and continuous property transition direction-wise. This study is a contribution in the literature among other studies but provides an additional understanding of FG Plate structures vibrational behavior in terms of natural frequencies and modal shapes. For this end, an FG plate is modelized and analyzed using Ansys APDL. Two boundary conditions (all sides clamped "CCCC" and two parallel sides clamped with two others free "CCFF") for the same plate element and two power law indices "n" are considered. Results are compared with those in the literature and conclusions are drawn accordingly.

Keywords: Functionally graded (FG) plate, natural frequencies, modal shapes, Ansys APDL

Introduction

Functionally Graded (FG) materials are one of the brilliant engineering developments of the last century. These materials' structure mimics natural materials characterized by a smooth and continuous property transition from one side to another. The purpose here is to take benefit from different materials properties and bring a solution to the "delamination phenomena" [1] observed in laminated composites characterized by interlaminar stress concentration. The most common material combination is metals for their good fracture toughness and ceramics for their low thermal conductivity. Therefore, the material can thus resist high-temperature conditions while maintaining toughness.

By reviewing the literature, it's found out that a substantial number of researches with the concern of FG plate has been carried out. Merdaci et al. [2] performed a free vibration analysis of ceramic-metal FG rectangular solar plates with porosities using high-order shear theory by studying the influence of variance of material properties in terms of the porosity factor on the natural frequencies of solar FG plates. Amirpour et al. [3] carried out a numerical and experimental study on free vibration of 3D-printed polymeric FG plates. Gehlot et al. [4] studied the harmonic analysis of stiffened FG plate using FEM, where the vibration behavior of different stiffened laminated plate by varying the thickness of plate, height of stiffener, and the number of stiffeners employed on the plate was presented. Rao et al. [1] performed a study on finite element modeling and analysis of FG composite shell structures and investigated the influences of important parameters on the responses of FG shell structures. Diambu and Çevik [5] performed a study on finite element analysis of a FG plate under pressure, as a model for gas turbine blades. In the master thesis by Ghassabi [6], the free vibration analysis of FG rectangular nano-plates considering spatial variation of the nonlocal parameter was investigated; the purpose was to present a nonlocal elasticity-based method for free vibration of FG rectangular nano-plates. Kwak et al. [7] analyzed a novel solution method for free vibration analysis of FG arbitrary quadrilateral plates with hole. In their study, a new meshfree moving least squares-Tchebychev (MLST) shape function was proposed to analyze the free vibration characteristics of FG arbitrary quadrilateral plate with hole. Hassan and Kurgan [8] conducted research on modeling and buckling analysis of rectangular plates in ANSYS. Makwana and Panchal [9] published a review of stress analysis of FG material plate with cut-out. Gupta et al. [10] studied natural frequency of FG plates resting on elastic foundation using finite element method, with the purpose of finding the influence of volume fraction index, and foundation parameters on the vibration behavior of FG materials plates resting on two parameter Pasternak foundation. Bendine et al. [11] on structural modeling and active vibration control of smart FG material plate through ANSYS, present a methodology to use the software Ansys in modeling and active

vibration control of a FG plate with upper and lower surface-bonded piezoelectric layers. Zaoui et al. [13] carried out the fundamental frequency analysis of FG plates with temperature-dependent properties based on improved exponential-trigonometric two-dimensional higher shear deformation theory, for the purpose of providing a computational method to analyze free vibrations of advanced composite plates in thermal environments according to the higher-order shear deformation theory. Elaikh and Abed [14] conducted a study on semi-analytic solution for stability and free vibration of FG material micro-pipe conveying fluid where an analytical solution is presented for free vibration of a FG material micro-pipe conveying fluid on the basis of the Euler beam model and the modified coupled stress theory.

For systems under dynamic loading conditions, accurate frequency and mode shape determination is very important for the safety and durability of structures. In the present study, vibration analysis of a FG square plate is performed using Ansys APDL. The FG plate natural frequencies with respect to the power index and two different boundary conditions (all sides clamped "CCCC" and two parallel sides clamped with two others free "CCFF") for variable non-dimensional thickness (a/h) are investigated.

Problem Definition

The problem studied is a plate model made of ceramic and metal. The upper side is made of ceramic and the bottom is made of steel. Properties change within the thickness from ceramic to steel gradually and continuously according to the power law distribution. A 300x300x4 mm plate is considered (Figure 1). The thickness is incremented by 4mm while the other dimensions are constant. Two boundary conditions are considered. The first considers a totally clamped plate (CCCC) and the second has two parallel sides clamped while the other two are free (CCFF). In order to study the influence of the power law index on the natural frequency, two power law index values "n" are considered (n=1 and n=1.5).

General Concepts on Plate Theory and FG Plate

Reddy [12] defines a plate as "a structural element with planform dimensions that are large compared to its thickness and is subjected to loads that cause bending deformation in addition to stretching". Different authors define the concept of thin and thick plates. Equations of plate theories are related to this concept. Rao et al. [1] consider a plate (square) as thick, for the ratio of the length (a) to the thickness (h) higher than 10, and thin for a/h less than 100.

There are a couple of theories developed for plates in the literature. Classical Plate Theory (CPT) is valid for vibration analysis of rectangular thin plates but doesn't consider shear deformation (Kirchhoff hypothesis) which leads to inaccurate results [3]. It overestimates frequencies while underestimating deflections. Many researchers have exploited First-order Shear Deformation Theory (FSDT) which includes the effects of transverse shear deformation by the introduction of a shear correction factor. Several other High-order Shear Deformation Theories have been proposed to avoid the use of the shear correction factor including the Third-order Shear Deformation Theory (TSDT), Sinusoidal Shear Deformation Theory (SSDT) and Hyperbolic High-order Shear Deformation Theory (HHSDT).

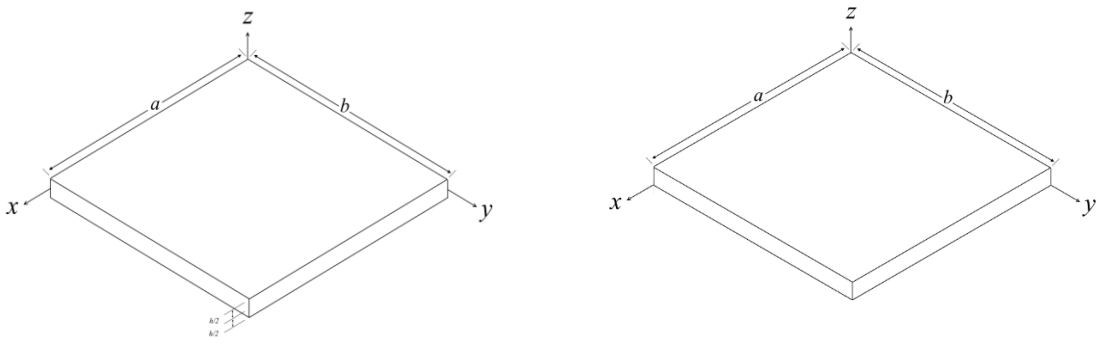

(a) (b)

Figure 1. The geometry of the FG plate: (a) Reference at the midheight (b) Reference at the bottom (considered for this study)

Some fundamental equations are necessary to study plate problems.

Displacement Fields

The generalized form of the displacement field is given as [6]:

$$\begin{cases} u(x,y,z,t) = u_0(x,y,t) - z\frac{\partial w_0}{\partial x} + f(z)(\emptyset_x + \frac{\partial w_0}{\partial x}) \\ v(x,y,z,t) = v_0(x,y,t) - z\frac{\partial w_0}{\partial y} + f(z)(\emptyset_y + \frac{\partial w_0}{\partial y}) \\ w(x,y,z,t) = w_0(x,y,t) \end{cases} \quad (1)$$

Here, u, v and w are displacement components in x, y and z directions respectively and u_0, v_0 and w_0 are displacements of a point on mid-plane; $\emptyset_x$ and $\emptyset_y$ are respectively the rotations of a transverse normal about y and x axis. $f(z)$ represents the shape function defining the transverse shear stress and strain distribution through the thickness of the plate and t is the time. Note that u_0 and v_0 are associated with extensional deformation of the plate while w_0 denotes the bending deflection [12]. $f(z)$ is defined according to different theories.

In the Classical Plate Theory (Kirchhoff theory):

$$f(z) = 0; \quad (2)$$

In Mindlin plate theory (First-Order Shear Deformation Theory):

$$f(z) = z; \quad (3)$$

In the Third-Order Shear Deformation Theory:

$$f(z) = z(1 - \frac{4z^2}{3h^2}); \quad (4)$$

If the Kirchhoff theory is applied, for the case of thin plate for instance, (1) becomes:

$$\begin{cases} u(x,y,z,t) = u_0(x,y,t) - z\frac{\partial w_0}{\partial x} \\ v(x,y,z,t) = v_0(x,y,t) - z\frac{\partial w_0}{\partial y} \\ w(x,y,z,t) = w_0(x,y,t) \end{cases} \quad (5)$$

The strains associated with the displacement field can be computed using either nonlinear strain-displacement relations (Consider second order derivatives in Taylor expansion) or the linear strain-displacement relations (Consider first order terms in Taylor expansion). In theory of elasticity (small strains and small rotations), strain field corresponding to the displacements is given as:

$$\begin{cases} \varepsilon_{xx} = \frac{\partial u}{\partial x} \\ \varepsilon_{yy} = \frac{\partial v}{\partial y} \\ \varepsilon_{zz} = \frac{\partial w}{\partial z} \\ \varepsilon_{xy} = \frac{1}{2}\left(\frac{\partial u}{\partial y} + \frac{\partial v}{\partial x}\right) \\ \varepsilon_{yz} = \frac{1}{2}\left(\frac{\partial v}{\partial z} + \frac{\partial w}{\partial y}\right) \\ \varepsilon_{xz} = \frac{1}{2}(\frac{\partial u}{\partial z} + \frac{\partial w}{\partial x}) \end{cases} \quad (6)$$

Exploiting the CPT at this point, (6) becomes:

$$\begin{cases} \varepsilon_{xx} = \frac{\partial u_0}{\partial x} - z\frac{\partial^2 w_0}{\partial x^2} \\ \varepsilon_{yy} = \frac{\partial v_0}{\partial y} - z\frac{\partial^2 w_0}{\partial y^2} \\ \varepsilon_{zz} = \frac{\partial w}{\partial z} = 0 \\ \varepsilon_{xy} = \frac{1}{2}\{(\frac{\partial u_0}{\partial y} + \frac{\partial v_0}{\partial x}) - 2z\frac{\partial^2 w_0}{\partial x 0 \partial y}\} \\ \varepsilon_{yz} = 0 \\ \varepsilon_{xz} = 0 \end{cases} \quad (7)$$

Constitutive Equations

The linear constitute relations of FG plate are given as [13]:

$$\begin{Bmatrix} \sigma_x \\ \sigma_y \\ \tau_{yz} \\ \tau_{xz} \\ \tau_{xy} \end{Bmatrix} = \begin{bmatrix} Q_{11} & Q_{12} & 0 & 0 & 0 \\ Q_{12} & Q_{22} & 0 & 0 & 0 \\ 0 & 0 & Q_{44} & 0 & 0 \\ 0 & 0 & 0 & Q_{55} & 0 \\ 0 & 0 & 0 & 0 & Q_{66} \end{bmatrix} \begin{Bmatrix} \varepsilon_x \\ \varepsilon_y \\ \gamma_{yz} \\ \gamma_{xz} \\ \gamma_{xy} \end{Bmatrix} \quad (8)$$

$$Q_{11} = Q_{11} = \frac{E(z)}{1-\nu^2(z)} \quad (9)$$

$$Q_{12} = \nu(z)\frac{E(z)}{1-\nu^2(z)} \quad (10)$$

$$Q_{12} = \frac{E(z)}{2(1+\nu(z))} \quad (11)$$

Since the effect of variation of Poisson's ratio on the response of FG plates is very small [3], ν is assumed to be constant. Therefore, only the Young modulus (E) and the density (ρ) are considered to be variable.

Governing Equations

Hamilton's principle is used to obtain the governing differential equations:

$$\int_0^t (\delta U + \delta V - \delta) dt = 0 \quad (12)$$

This equation is the dynamic version of the virtual displacements (minimum total potential energy) [12]. In the equation, U is the strain energy, V is the work done by applied forces and $K$is the kinetic energy.

Methodology

The approach used in this study consist of modelling the FG plate in Ansys APDL as separated small sublayers, gluing them, applying material properties to each sublayer, meshing, applying boundary conditions and pressure on the ceramic side and solving in terms of natural frequencies (Modal Analysis).

Material properties including the Young modulus and density are function of the thickness coordinate and their variations are described as follows:

$$E(z) = E_c V_c(z) + E_s V_s(z), \quad (13)$$

$$\rho(z) = \rho_c V_c(z) + \rho_s V_s(z), \quad (14)$$

where "c" stands for ceramic and "s" for steel. $V(z)$ is the volume fraction defined as:

$$V(z) = (\frac{z}{h})^n \quad (15)$$

$$V_c(z) = (\frac{z}{h})^n \quad (16)$$

$$V_s(z) = 1 - V_c(z) \quad (17)$$

Table 1 presents the properties of the materials used for this study.

Table 1. FG plate material properties

Material Designation	E (GPa)	Poisson's ratio ν	ρ(kg/m^3)
Ceramic (Alumina: Al_2O_3)	320.2	0.3	3970
Steel	207.78	0.3	8166

For n=1 and n=1.5, material property gradients are as follows:

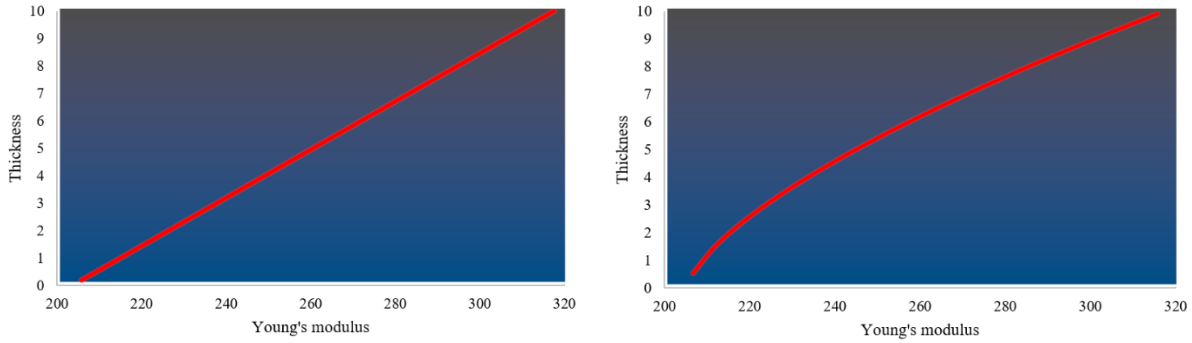

(a) (b)

Figure 2. Material property gradient in FGP with n=1 (a) et n=1.5 (b)

Figure 2 presents the FG plate properties gradient for 2 power indices. In (a), there is a linear distribution of properties while in (b), there is a powered distribution. Remembering that the bottom of the plate was made of steel, this comes to say that steel properties are dominant for n=1.5.

The element type used in this study is the solid-shell type element (Solsh190) for the reason that it combines the benefits of solid elements and shell elements at one. This element provides good results, closer to the FSDT [8]. Therefore, it includes strain assumptions which prevents locking phenomenon when modeling thin plates while being able to model thick plates as well. This is important for this study providing that the ratio a/h of the plates to study covers thin and moderately thick plates.

The diagram in Figure 3 resume the steps used in this study for modeling and analyzing the FG plate in Ansys APDL.

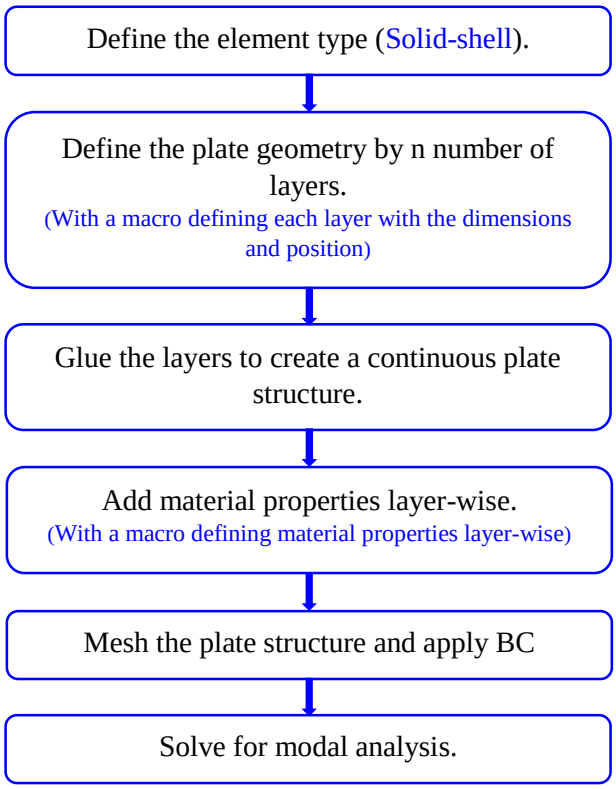

Figure 3. FG plate analyzing steps in Ansys APDL.

These steps were used by Diambu and Çevik [5] to study the deflection of a cantilever plate and results were validated.

FE Analysis Results

The FE analysis is performed for the square plate with 300x300x4 mm initial dimensions, for n=1 and n=1.5, CCCC and CCFF boundary conditions and thickness varying from 4 to 40 mm. Natural frequencies of the first three modes for CCCC boundary conditions and n=1 are presented in Table 2 and the change of natural frequency with respect to length/thickness ratio is illustrated in Figure 4. Although the plate has symmetric geometry, the material property is not symmetric when considering the in-plane material stiffness variation. Thus; the full FG plate has been considered in the FE model.

Table 2. Natural frequencies for the three first modes (CCCC, n=1)

Thickness (h in mm)	a/h ratio	Natural Frequency (Hz)		
		Mode 1	Mode 2	Mode 3
40	7.50	4342.6	8058.2	11100
36	8.33	4008.8	7535.1	10450
32	9.38	3650.6	6952.7	9712.9
28	10.71	3267.7	6306.1	8879.8
24	12.50	2860	5591.4	7940
20	15.00	2428.3	4806.4	6884.8
16	18.75	1974.2	3951.9	5709.3
12	25.00	1500.2	3032.2	4415.3
8	37.50	1010	2056.7	3014.3
4	75.00	508.28	1039.9	1530.7

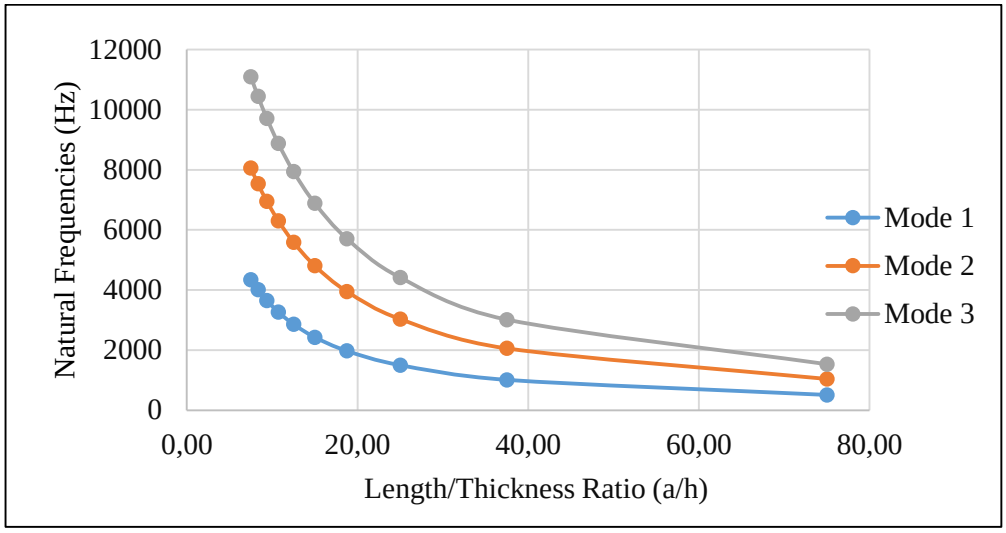

Figure 4. Length/thickness ratio vs. natural frequencies for CCCC boundary conditions and n=1

Natural frequencies of the first three modes for CCCC boundary conditions and n=1.5 are presented in Table 3 and the change of natural frequency with respect to length/thickness ratio is illustrated in Figure 5.

Table 3. Natural frequencies for the three first modes (CCCC, n=1.5)

Thickness (h in mm)	a/h ratio	Natural Frequency (Hz)		
		Mode 1	Mode 2	Mode 3
40	7.50	4128.4	7651.8	10535
36	8.33	3812.4	7158.2	9921.8
32	9.38	3473	6608	9226.5
28	10.71	3109.7	5996.2	8439.3
24	12.50	2722.6	5319.1	7549.9
20	15.00	2390.9	4729.5	6771.6
16	18.75	1880.2	3762.4	5433.9
12	25.00	1428.9	2887.3	4203.4
8	37.50	961.54	1957.8	2869
4	75.00	482.34	986.82	1452.6

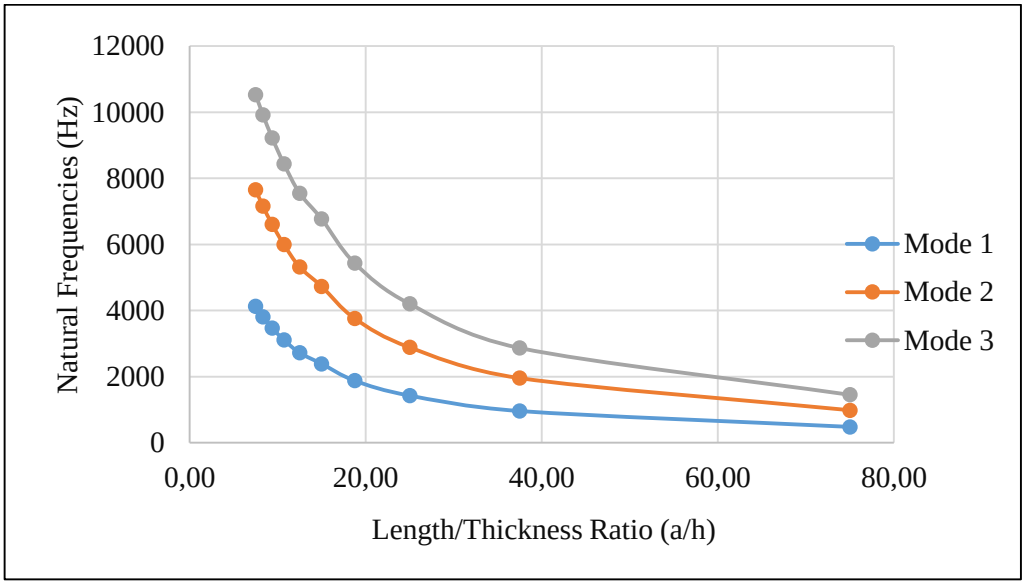

Figure 5. Length/thickness ratio vs. natural frequencies for CCCC boundary conditions and n=1.5

Natural frequencies of the first three modes for CCFF boundary conditions and n=1 are presented in Table 4 and the change of natural frequency with respect to length/thickness ratio is illustrated in Figure 6.

Table 4. Natural frequencies for the three first modes (CCFF, n=1)

Thickness (h in mm)	a/h ratio	Natural Frequency (Hz)		
		Mode 1	Mode 2	Mode 3
40	7.50	2796.2	3216.2	5087.9
36	8.33	2566.1	2963.7	4707.4
32	9.38	2322.9	2693.9	4297.8
28	10.71	2066.9	2406.8	3857.9
24	12.50	1798.5	2102.7	3387
20	15.00	1518.8	1782.5	2885.4
16	18.75	1226.8	1442.9	2349.5
12	25.00	929.96	1099	1795.4
8	37.50	624.22	739.78	1213.2
4	75.00	313.57	372.44	612.45

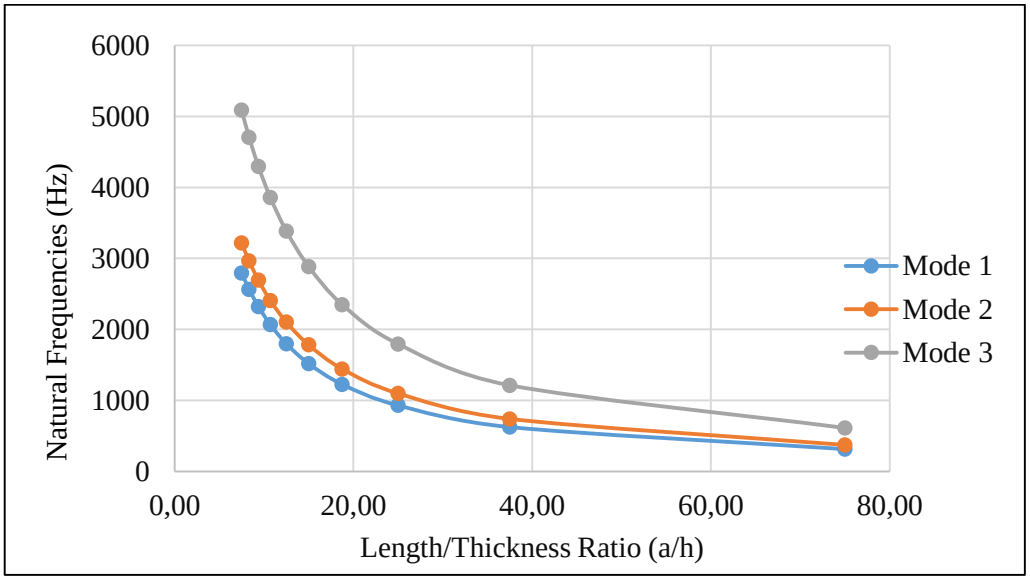

Figure 6. Length/thickness ratio vs. natural frequencies for CCFF boundary conditions and n=1

Natural frequencies of the first three modes for CCFF boundary conditions and n=1.5 are presented in Table 5 and the change of natural frequency with respect to length/thickness ratio is illustrated in Figure 7.

Table 5. Natural frequencies for the three first modes (CCFF, n=1.5)

Thickness (h in mm)	a/h ratio	Natural Frequency (Hz)		
		Mode 1	Mode 2	Mode 3
40	7.50	2659.7	3058.9	4840.9
36	8.33	2424.6	2789.4	4454.1
32	9.38	2210.9	2563.7	4090.6
28	10.71	1967.8	2291.1	3672.6
24	12.50	1712.7	2002.1	3225
20	15.00	1495.8	1755.2	2840.7
16	18.75	1170.5	1378.5	2242.1
12	25.00	885.82	1046.7	1710
8	37.50	594.28	704.27	1154.9
4	75.00	297.58	353.43	581.19

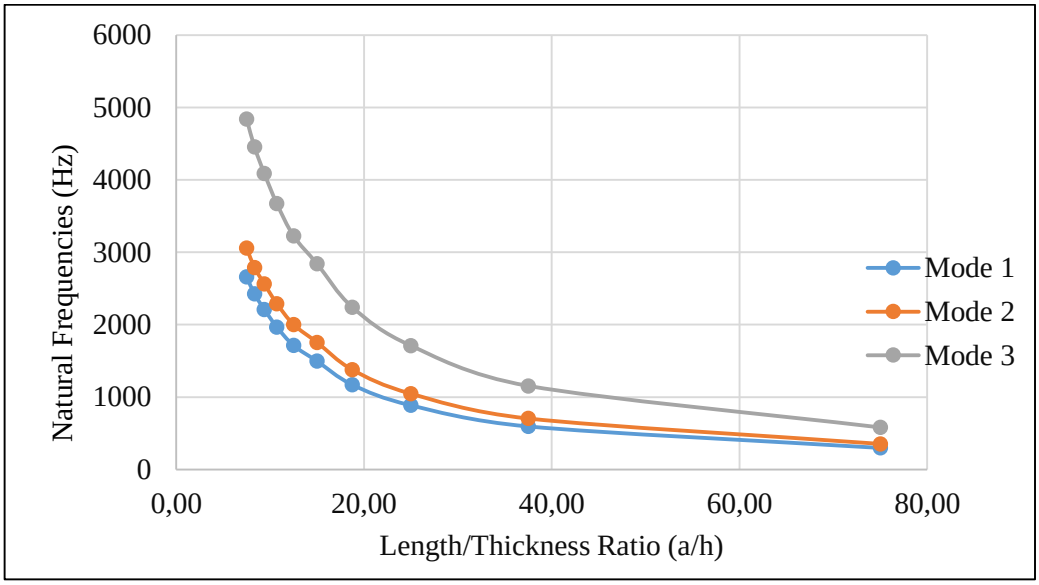

Figure 7. Length/thickness ratio vs. natural frequencies for CCFF boundary conditions and n=1.5

Natural frequency curves of each mode are compared in Figure 8 for given boundary conditions and power index values.

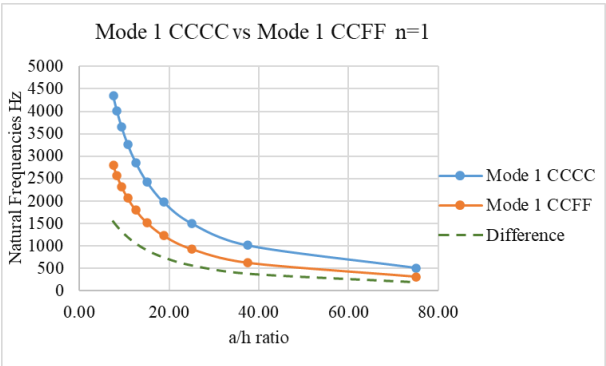

(a) mode 1 CCCC vs mode 1 CCFF for n=1

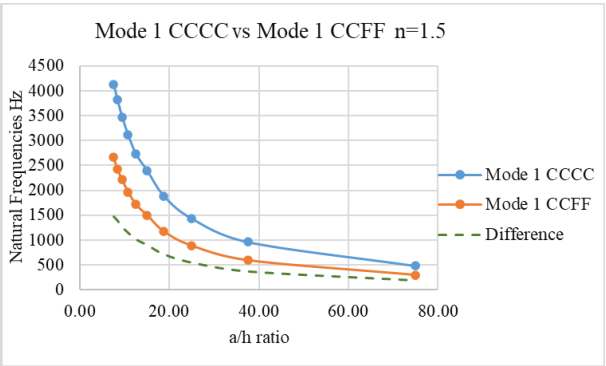

(b) mode 1 CCCC vs mode 1 CCFF for n=1.5

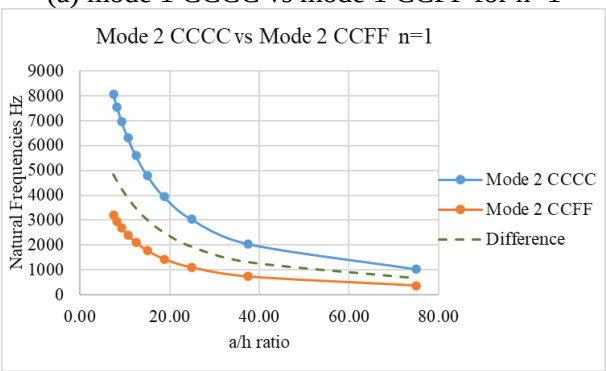

(c) mode 2 CCCC vs mode 2 CCFF for n=1

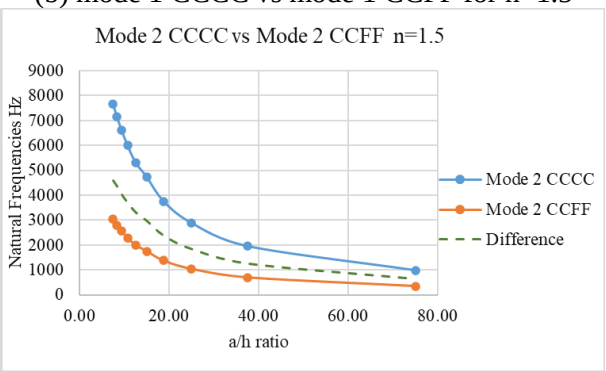

(d) mode 2 CCCC vs mode 2 CCFF for n=1.5

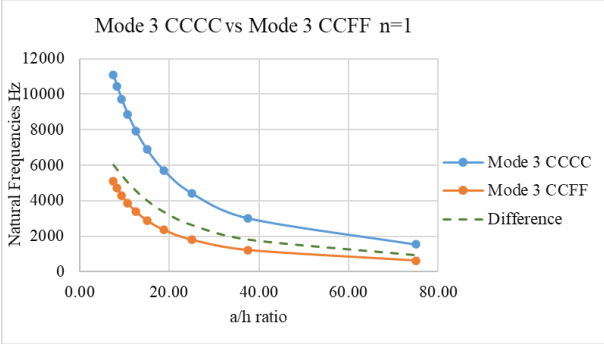

(e) mode 3 CCCC vs mode 3 CCFF for n=1

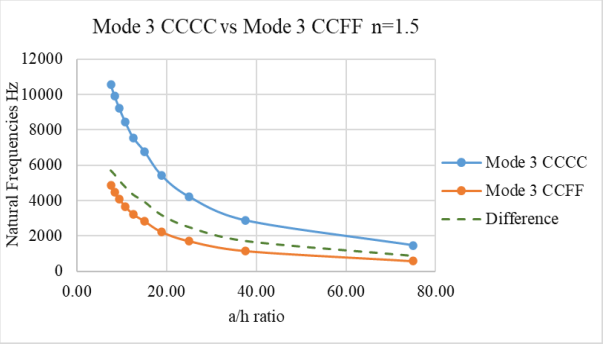

(f) mode 3 CCCC vs mode 3 CCFF for n=1.5

Figure 8. Comparison of natural frequency curves

Since most of engineering designs are based on first natural frequencies, we focused on the comparison of the first natural frequency in Figure 9.

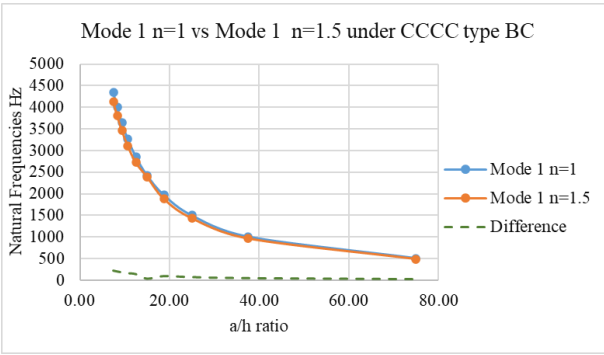

(a) CCCC mode 1, n=1 vs n=1.5

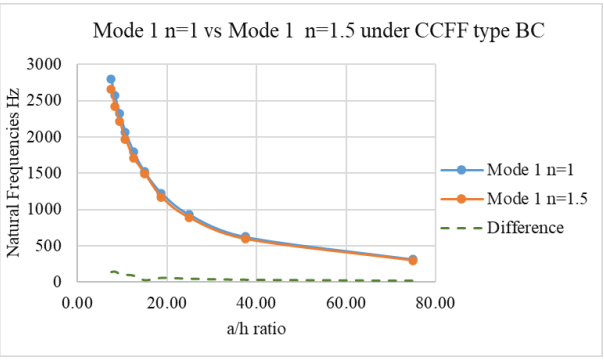

(b) CCFF mode 1, n=1 vs n=1.5

Figure 9. Comparison of mode 1 natural frequency curves

Finallly mode shapes of some selected cases are shown in Figure 10.

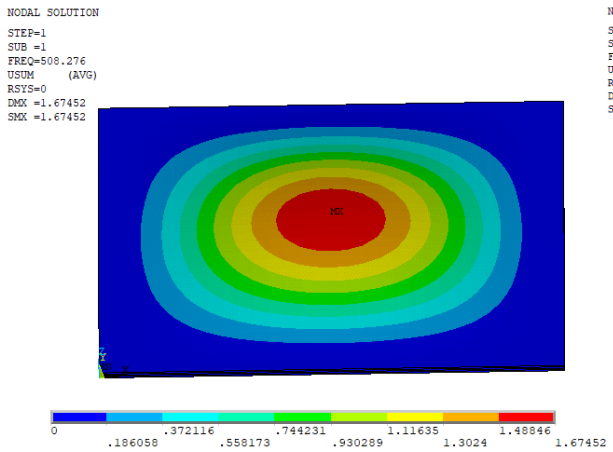

(a) CCCC; n=1; mode 1; h=4mm

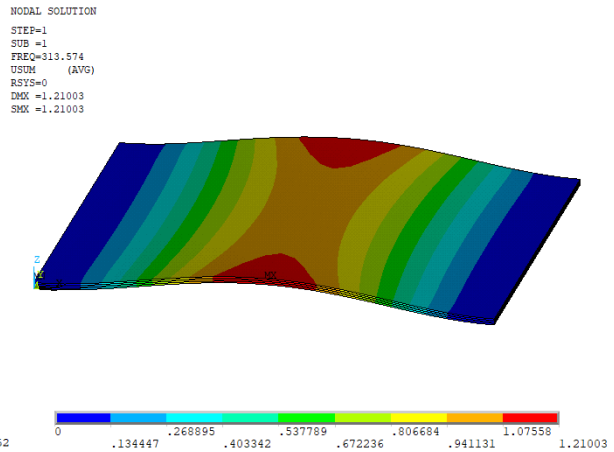

(b) CCFF; n=1; mode 4; h=4mm

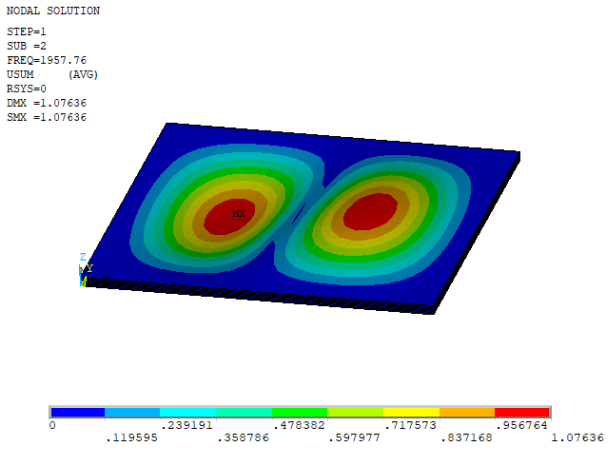

(c) CCCC; n=1.5; mode 2; h=8mm

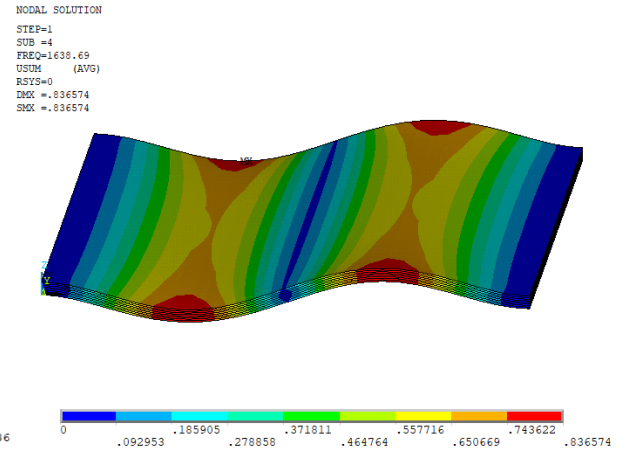

(d) CCFF; n=1.5; mode 4; h=8mm

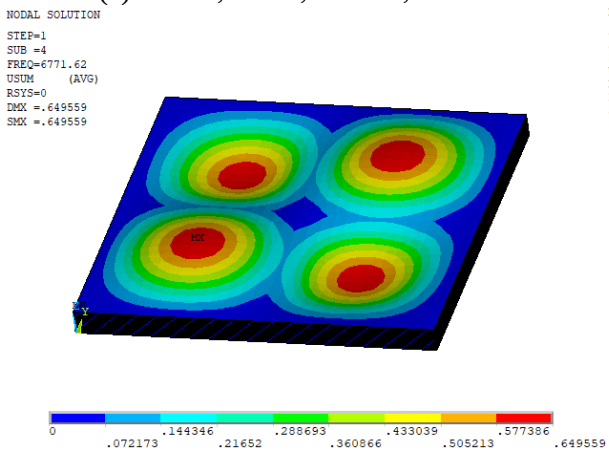

(e) CCCC; n=1.5; mode 4; h=20mm

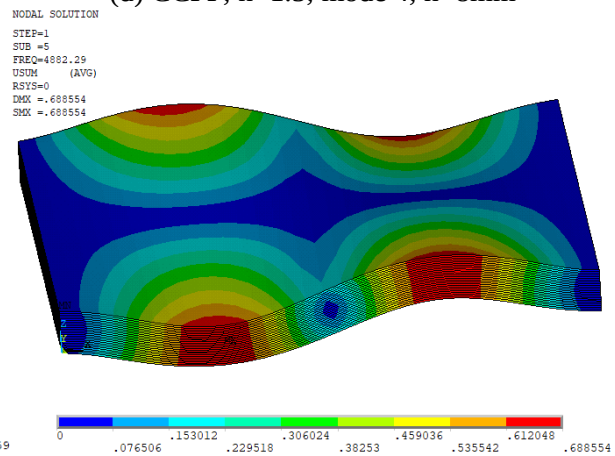

(f) CCFF; n=1.5; mode 5; h=24mm

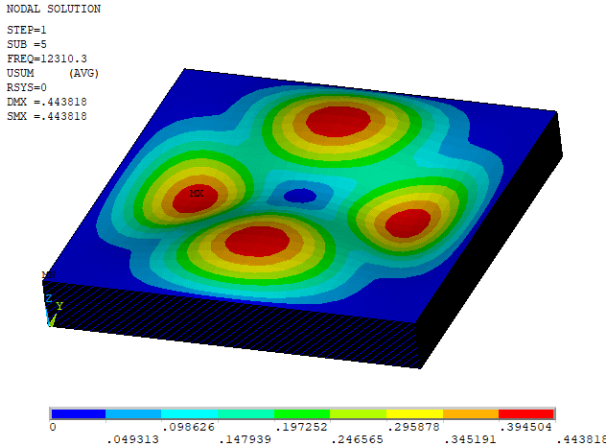

(g) CCCC; n=1.5; mode 4; h=40mm

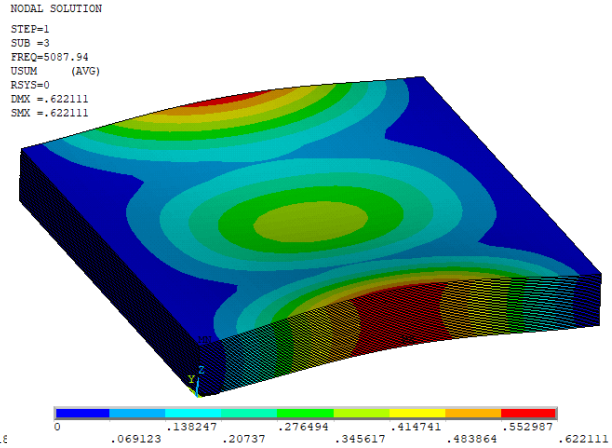

(h) CCFF; n=1; mode 3; h=40mm

Figure 10. Mode shapes of some selected cases

Conclusion

This study focused on modal frequency analysis of a 300x300mm square FG plate using Ansys APDL. The variation of non-dimensional length-to-thickness ratio (a/h) was investigated for different thicknesses of the plate model, with two power law indices n=1 and n=1.5, and two boundary conditions –CCCC and CCFF. The following conclusion can be drawn from the results of the current analysis:

- For all the cases without exception, natural frequency decreases for increasing a/h ratio and the values of the three first natural frequencies get closer (converge to each other) for thin plates (high a/h ratio).
- The influence of the power index n is moderated for higher value of the ratio (a/h). The thinner is the plate, the lesser is the difference between the same nth frequencies.

- First natural frequencies for two identical plates under the same boundary conditions have close values but the plate having higher n index value has lower natural frequency values. This comes to say that natural frequency decreases for increasing power index n.
- Comparing Figure 8 with Figure 9, it can be observed that the boundary conditions have a big influence on the natural frequencies of plates when compared to the power index n. However, playing on the power index n while manufacturing FG material would help to customize the end product in order to meet the expected results. In some previous studies, FG material prototype manufacturing process was guided by codes that ensure the generation of an evenly distributed material pattern in the structure that obey the power law targeted. The same procedure can be exploited for low budget FG sample manufacturing.

References

[1] Rao DK, Blessington PJ, Tarapada R. Finite element modeling and analysis of functionally graded (FG) composite shell structures. Procedia Engineering 2012; 38:3192-3199. doi: 10.1016/j.proeng.2012.06.370

[2] Merdaci S, Mostefa AH, Merazi M, Belghoul H, Sabrina B, Hadjira H. Free vibration analysis of ceramic-metal functionally graded rectangular solar plates with porosities using high-order shear theory: Solar plate FG composed of (Al/Al2O3) and (Al/ZrO2) influence by porosity, 11th International Renewable Energy Congress (IREC), 2020; 1-5.

[3] Amirpour M, Bickerton S, Calius E, Mace BR, Das R. Numerical and experimental study on free vibration of 3D-printed polymeric functionally graded plates. Composites Structures 2018; 189: 192-205. doi.org/10.1016/j.compstruct.2018.01.056

[4] Gehlot P, Sharma AK, Rajawat AS. Harmonic analysis of stiffened functionally graded plate using FEM. Materials Today: Proceedings 2018; 5: 5145–5153.

[5] Diambu AN, Çevik M. Finite element analysis of a functionally graded plate. Third International Students Science Congress Proceedings 2019: 517-523.

[6] Ghassabi AA. Free vibration analysis of functionally graded rectangular nano-plates considering spatial variation of the nonlocal parameter. MSc Thesis 2017, Middle East Technical University, Turkey.

[7] Kwak S, Kim K, Jong G, Kim Y, Ri C. A novel solution method for free vibration analysis of functionally graded arbitrary quadrilateral plates with hole. Journal of Vibration Engineering & Technologies 2021. https://doi.org/10.1007/s42417-021-00327-5.

[8] Hassan A, Kurgan N. Modeling and buckling analysis of rectangular plates in ANSYS, International Journal of Engineering & Applied Sciences 2019; 11(1): 310-329. http://dx.doi.org/10.24107/ijeas.531011.

[9] Makwana AB, Panchal KC. A review of stress analysis of functionally graded material plate with cut-out. International Journal of Engineering Research & Technology 2014; 3(3): 2020-2025.

[10] Gupta A, Talha M, Chaudhari VK. Natural frequency of functionally graded plates resting on elastic foundation using finite element method. Procedia Technology 2016; 23: 163-170. doi.org/10.1016/j.protcy.2016.03.013

[11] Bendine K, Boukhoulda BF, Nouari M, Satla Z. Structural modeling and active vibration control of smart FGM plate through ANSYS. International Journal of Computational Methods 2017; 14(4). doi: 10.1142/S0219876217500426

[12] Reddy JN. Theory and analysis of elastic plates and shells. New York: CRC Press; 2007.

[13] Zaoui FZ, Ouinas D, Tounsi A, Olay JAV, Achour B, Touahmia M. Fundamental frequency analysis of functionally graded plates with temperature-dependent properties based on improved exponential-trigonometric two-dimensional higher shear deformation theory. Archive of Applied Mechanics 2021; 91:859–881. https://doi.org/10.1007/s00419-020-01793-1

[14] Elaikh THE, Abed NM. Semi-analytic solution for stability and free vibration of functionally graded (FG) material micro-pipe conveying fluid. International Journal of Energy and Environment 2018; 9(6): 563-580

[15] Sınır S, Çevik M, Sınır BG. Nonlinear free and forced vibration analyses of axially functionally graded Euler-Bernoulli beams with non-uniform cross-section. Composites Part B: Engineering 2018; 148: 123-131. doi.org/10.1016/j.compositesb.2018.04.061

Stochastic Optimization of TiO2-Graphene Nanocomposite by Using Neuro-Regression Approach for Maximum Photocatalytic Degradation Rate

*Kemal Bartu Aydın[1]**, *Levent Aydin[2]*, *Fethullah Güneş[3]*
[1,3]Izmir Kâtip Çelebi University, Department of Materials Science and Engineering, Izmir, Turkey
[2]Izmir Kâtip Çelebi University, Department of Mechanical Engineering, Izmir, Turkey
**Corresponding author: bartua3@gmail.com*

Abstract

TiO_2 is one of the most common materials for photocatalytic applications due to its stability, affordability, and photoactive efficiency. However, it has some drawbacks, such as limited solar radiation response and quick recombination of excitons. Using graphene could be one of the methods to enhance the photocatalytic properties of TiO_2. This study intends to optimize the photocatalytic performance of TiO_2/Graphene (TiO_2/G) nanocomposite by using neuro-regression analysis. In the analysis, the effect of some hydrothermal synthesis parameters, namely, amount of graphene oxide, ethanol/water ratio, and hydrothermal reaction time on the photocatalytic activity of TiO_2/G nanocomposite, have been investigated. The parameters were determined from a literature study focused on overcoming the drawbacks of TiO_2 by combining it with graphene oxide. Nelder-Mead, Simulated Annealing, Differential Evolution, and Random Search algorithms are used to obtain the optimum synthesis parameters for maximum photocatalytic activity in the optimization process. The results are indicated that all algorithms give the realizable value for design variables and photodegradation rate.

Keywords: photocatalytic activity, hydrothermal process, stochastic optimization, neuro-regression approach

Introduction

Photocatalysts have become an option recently for many kinds of applications such as air purification and water treatment. In this field, the challenges are that improving reaction rate and photocatalytic activity. TiO_2 is one of the most suitable semiconductor materials for photocatalyst due to its chemical stability, non-toxicity, affordability, and so on [1]. Nevertheless, they have drawbacks, such as quick exciton recombination rate and limited visible light response [2-5]. To make this technology applicable for commercial applications, its disadvantages must be eliminated [6]. To improve photocatalytic performance, a combination of TiO_2 with carbon-based materials came to the fore recently. Especially graphene-derived materials are among the most promising candidates among carbon-based materials due to their extraordinary properties such as zero band-gap energy and electron mobility [7-12]. Graphene can contribute to the structure to improve photocatalytic activity in two respects: by ensuring the uniform dispersion of nanoparticles in the structure, and the other one is that by decreasing exciton recombination rate through acting as an electron acceptor [6,13].

Nanocomposite structure properties have lots of parameters depending on the applicational area. With the increase of the effect of the parameters on the performance of the nanocomposite, theoretical models come forward as an alternative to reduce time- and cost-consuming. Recently, some approaches such as multi-gene genetic programming (MGGP) and artificial neural networks (ANN) have been rising methods among soft computing techniques [14-19]. Many investigations in the literature related to modeling and optimizing nanocomposite materials for several applicational areas [20-24]. Regression analysis, RSM kind approaches are generally used to obtain a model function that includes the interaction between parameters and the results of all experimental possibilities. However, this kind of non-hybrid approach is insufficient to optimize complex engineering problems due to not examining the accuracy of the proposed model adequately. Therefore, it is necessary to apply more realistic methods to solve and optimize this kind of problem. It is seen that estimating the phenomena in realistic and reliable ways by utilizing hybrid approaches of regression analysis and ANN algorithm would be helpful to further optimization problems [25-28].

In this context, it aims to present a systematic perspective to find solutions to solve the inadequacy problem of the current methods and define and optimize the engineering problem in a realistic way. Hence, it is intended to optimize the photocatalytic activity of the TiO_2/Graphene (TiO_2/G) nanocomposite affected by the amount of ethanol/water (EtOH/water) ratio, graphene oxide (GO)

content, and hydrothermal reaction time. These effects were taken into consideration as design variables of the problem. To make a comparison, the whole parameters were determined from a literature study focused on overcoming the drawbacks of TiO_2 by combining with GO [6]. For this reason, neuro-regression-based modeling was performed to acquire a reliable objective function for the problem. Nelder-Mead (NM), Simulated Annealing (SA), Differential Evolution (DE), and Random Search (RS) algorithms are used to maximize the 2-hydroxyterephthalic acid (HTPA) degradation rate.

Methods

In the present study, non-linear neuro-regression analysis was first carried out to acquire a mathematical model to determine the HTPA formation rate of the TiO_2/G nanocomposite affected by design variables which are EtOH/Water ratio, graphene oxide content, and hydrothermal reaction time. In the analysis context, the total number of data, which was 20, was divided into two parts as 75% of them were training, and the remaining amount is testing data. First, training data were utilized to form a model to be an objective function of the problem. And then, to examine whether the model is appropriate, determination coefficients ($R^2_{training}$, $R^2_{training\text{-}adjusted}$, and $R^2_{testing}$) values were obtained firstly by the following equations:

$$R^2 = 1 - \frac{SS_{res}}{SS_{tot}} \tag{1}$$

$$R^2_{adjusted} = 1 - \left[\left(\frac{n-1}{n-k-1}\right) x\,(1-R^2)\right] \tag{2}$$

where

$$SS_{tot} = \sum_i (y_i - \bar{y})^2 \tag{3}$$

and

$$SS_{res} = \sum_i (y_i - f_i)^2 \tag{4}$$

where, $\bar{y}$ is the mean of the output values and f_i is the prediction by the proposed model for corresponding inputs. The parameters *n* and *k* represent the number of observations and the number of independent variables, respectively. In this step, $R^2_{training}$, $R^2_{training\text{-}adjusted}$, and $R^2_{testing}$ values being above 0.85 would be sufficient for an appropriate model.

After examining the model's accuracy by considering the relevant R^2 values, the boundedness check is the next step. In this process, the boundaries of the objective function as the minimum and maximum values to determine whether the proposed model is meaningful in the manner of engineering phenomena. If the proposed model gives realistic values, it can be interpretable as bounded, so the model is appropriate.

In this study, whole modeling and optimization procedures were performed via Wolfram Mathematica 11. Here, the functions of NMaximize and NMinimize were used to find constrained global optimum values. HTPA formation rate maximization by using stochastic algorithms (NM, DE, SE, and RS) is the main objective of this study. It is noted that these algorithms work independently from each other. A detailed assessment of these algorithms can be found in the study by Rao, S. S [29]. Within the scope of this paper, RS, SA, DE, and NM algorithms were briefly explained as follows:

Random Search is a method based on generating a population of random starting points. It converges to a local minimum by using a local optimization method from each starting point, and the best local minimum is chosen as a solution. The main advantage of this algorithm is that it enables to the acquisition of the global optimum for non-convex, non-differentiable objective functions containing continuous, discrete domains, or a mix of them for large-scale problems [30].

Simulated Annealing is one of the most popular methods, originating from the physical process of annealing. Annealing is a type of heat treatment process wherein a metal is heated to a high temperature and allowed to cool slowly. In the SA algorithm, it is ensured the structure to settle on a better global

optimum point. It also has an advantage as solving several optimization problems such as continuous, discrete, or mixed-integer [30].

Differential Evolution is a type of method that maximizes or minimizes the design problem iteratively. Although it permits alternative and convergent global optimum solutions, it is not assured to find the global optimum. It includes initialization, mutation, crossover, and selection steps [30].

Nelder-Mead is an optimization method that enables the maximum or maximum response of objective function for the unconstrained optimization problem. Thus, it can give reasonable results for problems that do not have many local minima in practical use [30].

Problem Definition

In the present study, the effect of design parameters i) EtOH/water ratio, ii) GO content, and iii) hydrothermal reaction time on the photocatalytic performance of TiO_2/G nanocomposite were investigated. The single objective optimization approach is used to maximize the HTPA formation rate through different direct search methods, including the stochastic optimization approach (DE, SA, NM, RS). A detailed explanation about the problem is given as follow:

Find

v, v ϵ [4.55, 105.00]
g, g ϵ [0.06, 1.24]
t, t ϵ [0.23, 24.00]

Maximizing

K(v, g, t)

Constraints

Scenario 1 $4.55 \leq v \leq 105.00,\ 0.06 \leq g \leq 1.24,\ 0.23 \leq t \leq 24.00$

Scenario 2 $4.55 \leq v \leq 105.00,\ 0.06 \leq g \leq 1.24,\ 0.23 \leq t \leq 24.00$ {v, g, t} ϵ Integers

***Design* variables**

v, g, t

where v, g, and t represent Et/OH water ratio, graphene oxide content, and hydrothermal reaction time, respectively. HTPA formation rate is the objective function of the problem represented as K.

Results and Discussion

In this section, results of the optimization problem within the scope of the current study are given. Neuro-regression modeling and stochastic optimization methods are employed to solve the problem. In the modeling stage, the data are divided into 75% for training and 25% for testing data. The multiple non-linear regression model is constituted using training data, and the remained ones are utilized for testing. The training and testing data with the corresponding HTPA formation rate values are given in Table 1 [6].

Multiple non-linear regression model for HTPA formation rate (K) is given as follows:

$$K = 0.123727 - 0.00245074v - 0.161525g + 0.00735434t + 0.0873669 \ln v + 0.0537129 \ln g + 0.00158895 \ln t$$

Table 1. Training and testing data with their corresponding observed response [6]

	Experimental Run	EtOH/Water (v/v %)	GO Content (wt. %)	Reaction Time (h)	Rate (min^{-1}) K
Training	1	55.00	0.06	12.00	0.27
	2	55.00	0.65	24.00	0.40
	3	105.00	0.65	12.00	0.20
	4	4.55	0.65	12.00	0.22
	5	55.00	1.24	12.00	0.25
	6	55.00	0.65	0.23	0.21
	7	85.00	0.30	5.00	0.27
	8	25.00	0.30	5.00	0.23
	9	55.00	0.65	12.00	0.32
	10	55.00	0.65	12.00	0.29
	11	55.00	0.65	12.00	0.31
	12	55.00	0.65	12.00	0.30
	13	85.00	1.00	19.00	0.28
	14	55.00	0.65	12.00	0.32
	15	25.00	1.00	19.00	0.32
Testing	16	25.00	1.00	5.00	0.23
	17	85.00	0.30	19.00	0.33
	18	55.00	0.65	12.00	0.29
	19	85.00	1.00	5.00	0.18
	20	25.00	0.30	19.00	0.35

The accuracy of the model is shown in Table 2. The results of R^2 for training and testing data are found as 0.9953 and 0.9552, respectively. In addition, $R^2_{\text{training-adjusted}}$ value of the model is 0.9293.

Table 2. Results of accuracy check of the proposed model

Data	Number of Data	R^2	$R^2_{adjusted}$	Minimum K (min^{-1})	Maximum K (min^{-1})
Training	15	0.9953	0.9293	0.11155	0.417288
Testing	5	0.9552	-		

In order to determine whether the fitted regression model is bounded, the boundedness control stage has been performed by checking the maximum and minimum values taken by the model in the search space of design variables specified in this study. As it is seen from the accuracy check, the minimum and maximum values of K are obtained as 0.11155 min^{-1} and 0.417288 min^{-1}, respectively. Thus, the proposed model gives realistic results for relevant engineering phenomena, and hence, it can be interpretable as bounded.

Table 3 and Table 4 show the optimum HTPA formation rate utilizing stochastic optimization methods (NM, SA, DE, and RS) considering the continuous and integer search spaces, respectively. In Table 3, all design variables are assumed to be real numbers, and the search space is continuous. It is seen that despite all optimization methods that work independently from each other, they give the same HTPA formation rate value as 0.417288 min^{-1}. Additionally, design variable values are nearly identical to each other due to four different stochastic algorithms.

Table 3. Results of the optimization problem considered in continuous search space

Optimization Methods	Design Variables			Formation Rate (K) (min^{-1})
	EtOH/Water Ratio (v/v %)	GO Content (wt. %)	HT Reaction Time (h)	
NM	35.6492	0.332535	24	0.417288
SA	35.6493	0.332537	24	0.417288
DE	35.6493	0.332535	24	0.417288
RS	35.6492	0.332535	24	0.417288

On the other hand, Table 4 denotes the optimum design of TiO_2/G nanocomposite for photocatalytic activity by the same optimization algorithms, considered in integer search space. Obtained values for the HTPA formation rate are not the same but close to each other as almost 0.37 min^{-1}.

Table 4. Results of the optimization problem considered in integer search space

Optimization Methods	Design Variables			Formation Rate (K) (min^{-1})
	EtOH/Water Ratio (v/v %)	GO Content (wt. %)	HT Reaction Time (h)	
NM	36	1	24	0.36861
SA	37	1	24	0.368553
DE	36	1	24	0.36861
RS	53	1	24	0.360739

The comparison of our proposed results with the results in the reference article has been shown in Table 5 [6]. It is seen that the objective function has higher values than that of the reference study.

Table 5. Result comparison with the reference article

Study	Design Variables			Formation Rate (K) (min^{-1})
	EtOH/Water Ratio (v/v %)	GO Content (wt. %)	HT Reaction Time (h)	
Reference Study [6]	51.49	0.48	19	0.36
Our study (continuous)	35.65	0.33	24	~ 0.42
Our study (integer)	36	1	24	~ 0.37

Conclusion

Consequently, it is intended to design and optimize TiO_2-G nanocomposite materials for photocatalytic activity in this study. In this context, optimization of photocatalytic performance of the nanocomposite affected by EtOH/water ratio, GO content, and hydrothermal reaction time was studied. It is found that the proposed model ensured better results than that reference study. A hybrid approach, neuro-regression, was utilized to acquire an appropriate model. More critical thing than found results, the phenomena is defined as an optimization problem. Then more reliable model was proposed because of checking its accuracies in many respects, such as $R^2_{\text{training-adjusted}}$, R^2_{testing}, and boundedness of the model instead of checking only determination coefficients.

Additionally, four different stochastic algorithms, which worked independently from each other, gave nearly HTPA formation rate results as 0.42 min^{-1} (in continuous search space) and 0.37 min^{-1} (in integer search space) for optimum design. Therefore, this paper demonstrated that the stochastic optimization algorithms give a reasonable estimation for the phenomena by neuro-regression-based modeling. It is envisaged that this systematic approach would make realistic predictions for further studies related to nanomaterials production for any application area.

References

[1] Nakata K, Fujishima A. TiO_2 photocatalysis: Design and applications. Journal of Photochemistry and Photobiology C: Photochemistry Reviews. 2012; 13: 169-189.
[2] Tang B, Chen H, Peng H, Wang Z, Huang W. Graphene modified TiO_2 composite photocatalysts: mechanism, progress and perspective. Nanomaterials. 2018; 8: 105.
[3] Liang D, Cui C, Hu H, Wang Y, Xu S, Ying B, Li P, Lu B, Shen H. One-step hydrothermal synthesis of anatase TiO_2/reduced graphene oxide nanocomposites with enhance photocatalytic activity. Journal of Alloys and Compounds. 2014; 582: 236-240.
[4] Kim H, Moon G, Monllor-Satoca D, Park Y, Choi W. Solar photoconversion using Graphene/TiO_2 composites: nanographene shell on TiO_2 core versus TiO_2 nanoparticles on graphene sheet. The Journal of Physical Chemistry. 2012; 116(1): 1535-1543.
[5] Zhao D, Sheng G, Chen C, Wang X. Enhanced photocatalytic degradation of methylene blue under visible irradiation on graphene@TiO_2 dyade structure. Applied Catalysis B: Environmental. 2012; 111-112: 303-308.
[6] Fattahi A, Liang R, Kaur A, Schneider O, Arlos MJ, Peng P, Servos M, Zhou N. Photocatalytic degradation using TiO_2-graphene nanocomposite under UV-LED illumination: Optimization using response surface methodology. Journal of Environmental Chemical Engineering. 2019; 7: 103366.
[7] Inagaki M, Kojin F, Tryba B, Toyoda M. Carbon-coated anatase: the role of the carbon layer for photocatalytic performance. Carbon. 2005; 43(8): 1652-1659.
[8] Wang H, Robinson JT, Diankov G, Dai H. Nanocrystal growth on graphene with various degrees of oxidation. Journal of the American Chemical Society. 2010; 132: 3270-3271.
[9] Zhang LL, Xiong Z. Pillaring chemically exfoliated graphene oxide with carbon nanotubes for photocatalytic degradation of dyes under visible light irradiation. ACS Nano. 2010; 4(11): 7030-7036.
[10] Geim AK. Graphene: status and prospects. Science. 2009; 324(5934): 1530-1534.
[11] Güneş, F. A direct synthesis of Si-nanowires on 3D porous graphene as a high-performance anode material for Li-ion batteries. RSC Adv. 2016; 6: 1678-1685.
[12] Chang J, Jin M, Yao F, Kim TH, Le VT, Yue H, Gunes F, Li B, Ghosh A, Xie S, Lee YH. Asymmetric Supercapacitors Based on Graphene/MnO_2 Nanospheres and Graphene/MoO_3 Nanosheets with High Energy Density. Adv. Funct. Mater. 2013; 23: 5074-5083.
[13] Zhou K, Zhu Y, Yang X, Jiang X, Li C. Preparation of graphene-TiO_2 composites with enhanced photocatalytic activity. New Journal of Chemistry. 2011; 35(2): 353-359.
[14] Gopalakrishnan K, Kim S, Ceylan H, Khaitan SK. Natural selection of asphalt mix stiffness predictive models with genetic programming. St. Louis, Missouri: ANNIE 2010, Artificial Neural Networks in Engineering; 2010.
[15] Desai CK, Shaikh A. Prediction of depth of cut for single-pass laser micro-milling process using semi-analytical, ANN and GP approaches. Int. J. Adv. Manuf. Technol. 2012; 60: 865–882
[16] Gandomi AH, Alavi AH. A new multi-gene genetic programming approach to nonlinear system modeling. Part I: materials and structural engineering problems, Neural Comput. Appl. 2012; 21: 171–187.
[17] Gandomi AH, Alavi AH. A new multi-gene genetic programming approach to nonlinear system modeling. Part II: geotechnical and earthquake engineering problems, Neural Comput. Appl. 2012; 21: 189–201.
[18] Rezaei M, Eftekhari M, Mahin S, Ranjbar M. A CO_2-oil minimum miscibility pressure model based on multi-gene genetic programming. Energy Expl. Exploit. 2013; 31: 607–622.
[19] Muduli PK, Das SK. CPT-based seismic liquefaction potential evaluation using multi-gene genetic programming approach. Ind. Geotech. J. 2014; 44(1): 86-93.
[20] Nasouri K, Shoushtari AM. Designing, modeling and manufacturing of lightweight carbon nanotubes/polymer composite nanofibers for electromagnetic interference shielding application. Composites Science and Technology. 2017; 145: 46-54.
[21] Chang BP, Akil HM, Affendy MG, Khan A, Nasir RBM. Comparative study of wear performance of particulate and fiber-reinforced nano-ZnO/ultra-high molecular weight polyethylene hybrid composites using response surface methodology. Mater. Des. 2014; 63: 805-819.

[22] Ayoubi-Feiz B, Sheydaei M, Karimi M. Visible light photoelectrocatalysis for wastewater treatment using bifacial N-TiO_2/Graphene/Ho_2O_3/Titanium nanocomposite: Artificial neural network modelling and evaluation of ozone addition. Process Safety and Environmental Protection. 2019; 127: 56-65.
[23] Hassani A, Khataee A, Fathinia M, Karaca S. Photocatalytic ozonation of ciprofloxacin from aqueous solution using TiO_2/MMT nanocomposite: Nonlinear modelling and optimization of the process via artificial neural network integrated genetic algorithm. 2018; 116: 365-376.
[24] Mohammad A-T, Abdulhameed AS, Jawad AH. Box-Behnken design to optimize the synthesis of new crosslinked chitosan-glyoxal/TiO_2 nanocomposite: Methyl orange adsorption and mechanism studies. International Journal of Biological Macromolecules. 2019; 129: 98-109.
[25] Polatoğlu İ, Aydın L, Nevruz BÇ, Özer S. A Novel Approach for the Optimal Design of a Biosensor. Analytical Letters. 2020; 53(9): 1428-1445.
[26] Polatoğlu İ, Aydin L. A new design strategy with stochastic optimization on the preparation of magnetite cross-linked tyrosinase aggregates (MCLTA). Process Biochemistry. 2020; 99: 131-138.
[27] Aktaş LT, Aydın L. Stochastic optimization and modelling of high-velocity impact tests on high-temperature carbon-carbon composites. SN Applied Sciences. 2021; 3; 313.
[28] Ceylan AB, Aydın L, Nil M, Mamur H, Polatoğlu İ, Sözen H. A new hybrid approach in selection of optimum establishment location of the biogas energy production plant. Biomass Conversion and Biorefinery. 2021.
[29] Rao S S. Engineering optimization: theory and practice: John Wiley & Sons. 2019.
[30] Savran M, Aydin L. Stochastic optimization of graphite-flax/epoxy hybrid laminated composite for maximum fundamental frequency and minimum cost. Engineering Structure. 2018; 174: 675–687.

Investigation of the Wear Behavior of AA6082 Against Different Counterparts

*Safiye İpek Ayvaz**, *Mehmet Ayvaz*
Manisa Celal Bayar University, Turgutlu Vocational School, Manisa, Turkey
Manisa Celal Bayar University, Manisa Technical Sciences Vocational School, Manisa, Turkey
**Corresponding author: safiye.ipek@cbu.edu.tr*

Abstract

In this study, the effect of different counterparts on the wear resistance of AA6082 aluminum alloy was investigated. In tests using pin-on-disk method, 6 mm diameter Al_2O_3, 100Cr6 and WC-6Co balls were used as counterparts. The tests were carried out using 500 m sliding distance and 5N load. The lowest specific wear rate was measured as $7.58x10^{-4}$ mm^3/Nm in WC-6Co / AA6082 couple, and the highest value was measured as $9.71x10^{-4}$ mm^3/Nm in 100Cr6/AA6082 couple. In the Al_2O_3/AA6082 couple, the specific wear rate of the AA6082-T6 sample was determined as $8.23x10^{-4}$ mm^3/Nm. While it was observed that the dominant wear type in the 100Cr6/AA6082 pair was abrasive wear, oxidation wear and oxide tribofilm were detected in the WC-6Co/AA6082 and Al_2O_3/AA6082 couple besides the abrasive wear.

Keywords: AA6082, wear, pin-on-disc

Introduction

Friction occurs between two materials moving relative to each other. As a result of friction, material loss, that is, wear, occurs [1,2]. The systems in which wear, and friction events occur are called "Tribological System". Tribological system consists of main body, counterpart, interface, load, motion and environmental conditions. In tribological systems, many mechanical, physical and chemical properties of the counter element, the abrasive, and the main material, that is, the abraded material, affect the wear process [3].

Aluminum and its alloys are used in many sectors such as automobile, defense, shipbuilding, and aerospace, thanks to their superior properties such as high specific strength, easy workability, and high corrosion resistance [4,5]. However, the low wear resistance of aluminum and its alloys creates an effect that limits their use. However, the machine elements in which aluminum alloys are used in these sectors work within the tribological system. 6XXX series Al-Mg-Si alloys are aluminum alloys suitable for general use with their features such as aging, weldability, easy formability, and machinability [6,7]. One of the commonly used alloys for 6XXX series alloys is AA6082.However, there is not enough data to reveal the effects of the counter element, which is an important part of the tribological system, on the tribological properties of AA6082.

In this study, the tribological properties of AA6082 aluminum alloy against WC-6Co, Al_2O_3 and 100Cr6 balls were investigated.

Materials and Methods

The chemical composition and mechanical properties of the AA6082-T6 alloy used in the study are presented in Tables 1 and 2, respectively [8]. Samples were cut 30 mm in diameter and 10 mm in height in precision cutting device. After cutting, the samples were cleaned in an ultrasonic bath. Then, the samples were sanded with 100-1200 µm abrasives in the polishing device and their surfaces were polished with 3 and 1 µm diamond polishers.

Table 1. The chemical composition of the AA6082-T6

Mn	Fe	Mg	Si	Cu	Zn	Cr	Other	Al
0.40-1.00	<0.50	0.60-1.20	0.70-1.30	<0.10	<0.20	<0.25	<0.15	Balance

Table 2. The mechanical properties of the AA6082-T6

Yield strength (MPa)	Tensile strength (MPa)	Elongation (%)	Hardness (HB)
0.40-1.00	<0.50	0.60-1.20	0.70-1.30

Wear tests were performed on the CSM Tribometer tester. The tests were carried out using the pin-on-disc method in accordance with ASTMG99-17 standards. In the wear tests, 100Cr6, Al_2O_3 and WC-6Co balls with 6 mm diameter were used as counter elements. Tests using 500 m sliding distance, 0.15 m/sec sliding speed and 5 N load were performed at room temperature and ~ 55-60% relative humidity. After the wear tests, the worn surface examinations were performed using Clemex image analysis and Nikon SMZ745T stereo microscope.

Results and Discussion

In Figure 1, the change in friction coefficient depending on the sliding distance of 100Cr6, Al_2O_3 and WC-6Co counter elements and AA6082 friction pairs is seen. The coefficient of friction in all samples reached equilibrium after a sliding distance of approximately 150 m. The average friction coefficients-μ were determined as 0.53 in the 100Cr6 / AA6082 couple, 0.54 in the Al_2O_3 / AA6082 couple, and 0.50 in the WC-6Co/ AA6082 couple.

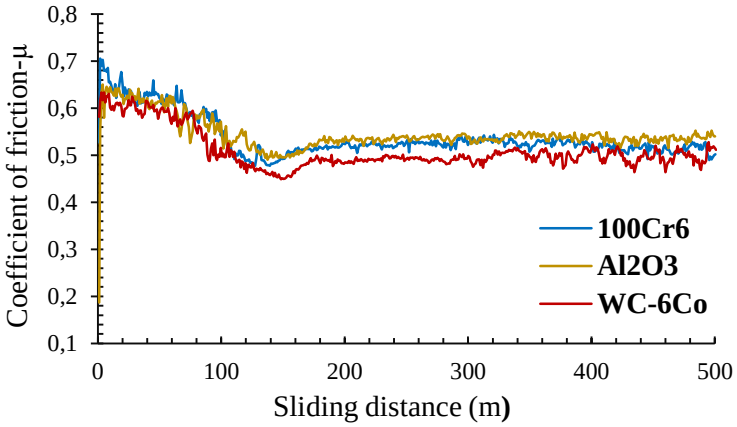

Figure 1. The Change in friction coefficient depending on the sliding distance

In Figure 2, the specific wear rates of AA6082 aluminum alloy against 100Cr6, Al_2O_3 and WC-6Co counter elements are given. The determined specific wear values are compatible with the literature [9]. However, contrary to expectations, the lowest specific wear rate was observed in the WC-6Co / AA6082 pair, while the highest value was measured in the 100Cr6 / AA6082 pair. In the examinations, it was observed that 100Cr6 counter element wear was higher than WC-6Co ball. As a result, it was determined that the contact area between 100Cr6 / AA6082 material pairs was higher than the other pairs. Increasing contact area, on the other hand, increases the specific wear rate of AA6082 in 100Cr6 / AA6082 couple at 500 m sliding distance.

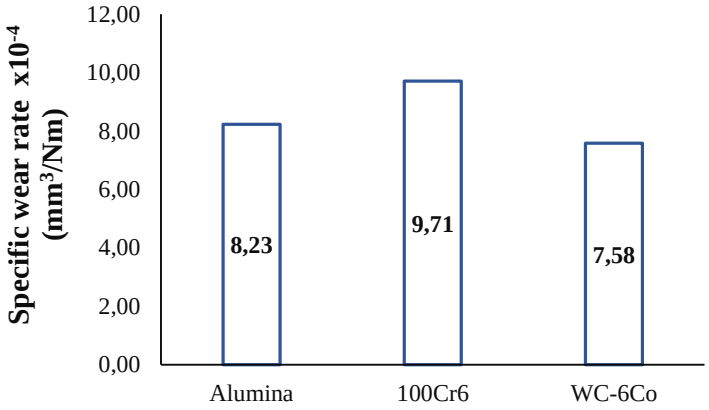

Figure 2. The specific wear rates of AA6082 Aluminum alloy against 100Cr6, Al_2O_3 and WC-6Co parts

Figure 3 shows the worn surface image of AA6082 in the 100Cr6-AA6082 pair. When the worn surface was examined, it was seen that the dominant wear type was abrasive wear. The wear track width was found to be 1553 µm on average. In addition to AA6082 abrasive wear, oxidation wear was observed in some areas in the Al_2O_3-AA6082 couple (Figure 4). Oxidation wear is a cyclical wear in the form of oxidation of worn surfaces and wear residues, forming tribofilms on the surface, and re-disruption of this oxidized tribofilm surface as the tribological process continues. The oxide tribofilm formed on the surface is quite hard compared to the main material. This was an effect that reduced the specific wear rate in these samples. Apart from abrasive and oxidation wear, delamination wear, cracks and fractures were also seen (Figure 5). The plastic deformation rates of the surface and the region just below the surface are different. As a result, nucleation occurs under the surface and nucleation causes cracks. Cracks growing parallel to the surface cause delamination wear in the process [10]. The mean wear track width in these samples was measured as 1467.1 µm.

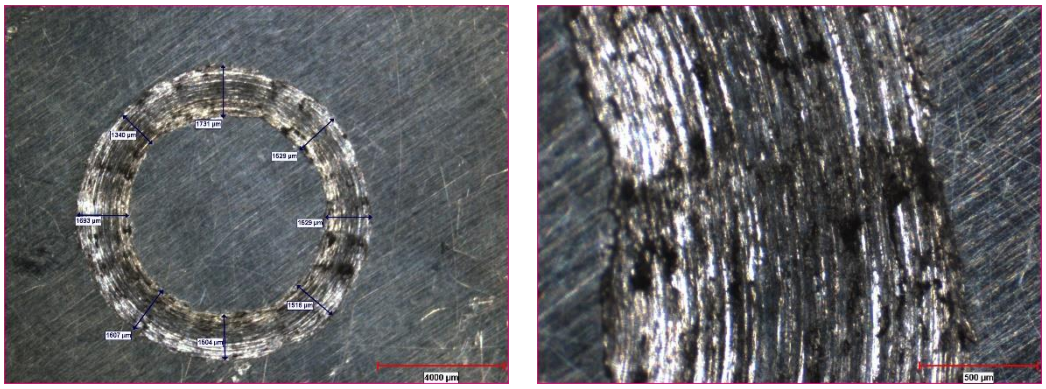

Figure 3. The worn surface image of AA6082 in the 100Cr6-AA6082 Couple

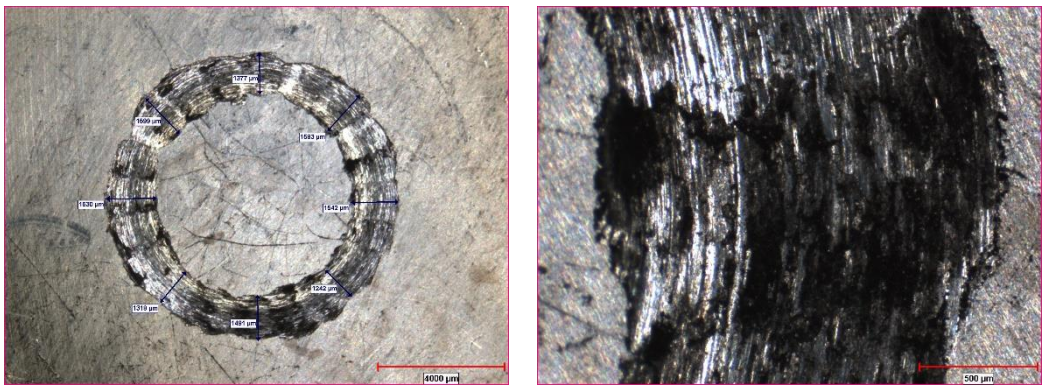

Figure 4. The worn surface image of AA6082 in the Al_2O_3-AA6082 Couple

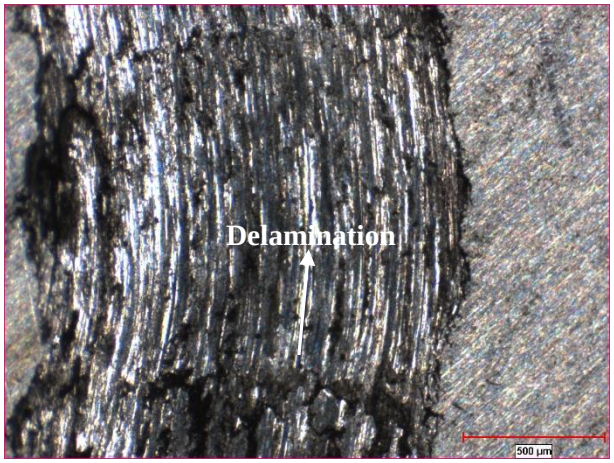

Figure 5. The delamination wear on AA6082 in the Al_2O_3-AA6082 Couple

AA6082 abrasive wear, delamination and oxidative wear types were also observed in the WC-6Co-AA6082 couple. Wear residues are oxidized in the course of time. These oxides residues are mechanically compressed by the counter element and form a protective layer on the surface that acts as a lubricant [11]. This surface cuts the metal-to-metal contact and reduces adhesive wear [12]. It was also observed that the side surfaces of the wear trace were forced to plastic flow. For this reason, the oxide film layer forms a mechanism that reduces wear. The average wear track width was measured as 1439.7 µm.

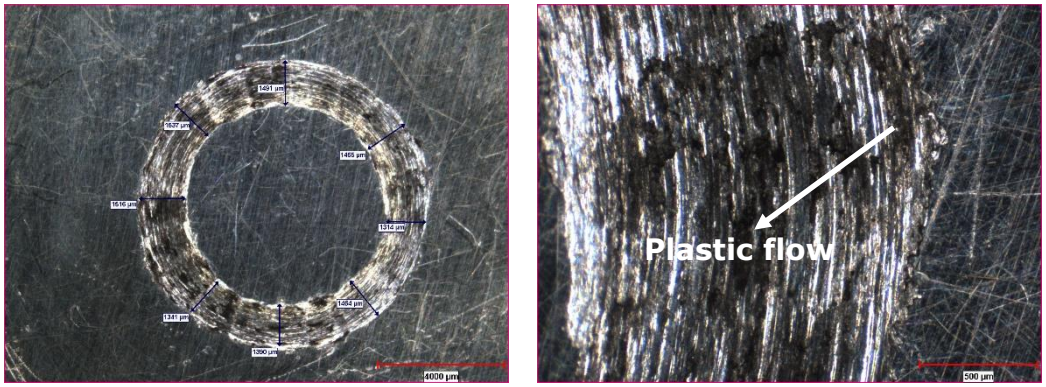

Figure 6. The worn surface image of AA6082 in the WC-6Co-AA6082 Couple

Conclusion

In this study, the effects of 100Cr6, Al_2O_3, WC-6Co counter elements on the tribological properties of AA6082-T6 aluminum alloy were investigated. The detected results are:

- Average friction coefficients (µ) were determined as 0.53 in 100Cr6/AA6082 couple, 0.54 in Al_2O_3/AA6082 couple and 0.50 in WC-6Co/AA6082 couple.
- The lowest specific wear rate was measured in the WC-6Co/AA6082 pair ($7.58x10^{-4}$ mm^3/Nm), while the highest value was measured in the 100Cr6/AA6082 pair ($9.71x10^{-4}$ mm^3/Nm). In the Al_2O_3/AA6082 couple, the specific wear rate of the AA6082-T6 sample was determined as $8.23x10^{-4}$ mm^3/Nm.
- The predominant wear type seen in the 100Cr6/AA6082 pair is abrasive wear.
- Besides abrasive wear, oxidation wear and oxide tribofilm were observed in the WC-6Co/AA6082 and Al_2O_3/AA6082 couple. Thanks to this oxidized tribofilm, the specific wear rate of the AA6082-T6 sample in these sample pairs decreased compared to the 100Cr6/AA6082 couple.

References

[1] B.S. Ünlü, L. Paralı, A.M. Pınar, Pin-disc, Pin-plate, Pin-ring, Journal-bearing Wear Test Rig Design and Manufacturing, 5. Uluslararası İleri Teknolojiler Sempozyumu (IATS'09), 13-15 Mayıs 2009, Karabük, Türkiye.
[2] R. Koç, Bilgisayar Kontrollü Aşınma Test Cihazı Tasarımı ve İmalatı, 2. Ulusal Tasarım İmalat ve Analiz Kongresi, 11-12 Kasım 2010, Balikesir, Türkiye.
[3] Y. Soyda, (2016). Elektrikli ve konvansiyonel otomobil tribolojisi: Yeni eğilimler ve uygulamalar, Dicle Üniversitesi Mühendislik Fakültesi Mühendislik Dergisi, 7(3), 527-536.
[4] S.V. Prasad, R. Asthana, (2004). Aluminum metal–matrix composites for automotive applications: tribological considerations, Tribology Letters, 17(3), 445-453.
[5] M. Ayvaz, (2020). characterization and tribological Properties of Novel AlCu4.5SiMg alloy–(B4C/TiO2/nGr) quaternary hybrid composites sintered via microwave, Metals and Materials International. https://doi.org/10.1007/s12540-020-00894-4
[6] Heat Treating of Aluminum Alloys, ASM Handbook, Volume 4: Heat Treating, 841-879, 1991.
[7] J. R. Davis: Aluminium and aluminium alloys, 351-416, 1993, Materials Park, OH, ASM International.
[8] 6082 Alüminyum Kimyasal Bileşimi, Seykoç Alüminyum, 2017, Türkiye.
[9] S. Das, L. Pelcastre, J. Hardell, B. Prakash, (2013). Effect of static and dynamic ageing on wear and friction behavior of aluminum 6082 alloy, Tribology International, 60, 1-9.
[10] Nam P. Suh (1997). An overview of the delamination theory of Wear. Wear, 44, 1-16.
[11] X. Y. Li, K. N. Tandon, (2000). Microstructural characterization of mechanically mixed layer and wear debris in sliding wear of an Al alloy and an Al based composite, Wear 245, 148-161.
[12] M. Varenberg, G. Halperin, I. Etsion, (2002). Different aspects of the role of wear debris in fretting Wear, Wear, 252, 902-910.

Preparation of Chitosan Based Hydrogels Functionalized by Mesoporous Silica/Zinc Oxide Nanoparticles

Ahmet Aykaç[1,2*], *İzel Ok*[2]
[1]*Izmir Katip Çelebi University, Faculty of Engineering and Architecture, Department of Engineering Sciences, Balatcık, 305620, Çiğli, Izmir, Turkey*
[2]*Izmir Katip Çelebi University, The Graduate School of Natural & Applied Sciences, Department of Nanoscience & Nanotechnology, Balatcık, 35620, Çiğli, Izmir, Turkey*
**Corresponding author: ahmet.aykac@ikcu.edu.tr*

Abstract

Hydrogels are biocompatible and swollen materials that have been used as a wound dressing for years. Among them, chitosan-based hydrogels have become popular in the wound healing process owing to their low toxic, biocompatible, biodegradable, antibacterial properties. Chitosan (CS) has been used either as a pure form or incorporated with polymers or nanoparticles to increase antimicrobial activity and stability. In this context, zinc oxide nanoparticles (ZnO NPs) have been used to enhance antibacterial activity and mesoporous silica nanoparticles (MSN) have been employed to develop mechanical strength and control of drug release time. In this study, we report the synthesis and fully characterizations of ZnO NPs, MSN and the hydrogel by using dynamic light scattering (DLS), scanning electron microscopy (SEM), Fourier transform infrared spectroscopy (FTIR). We have also prepared and characterized chitosan-based hydrogels functionalized by MSNs and ZnO NPs.

Keywords: hydrogel, chitosan-based hydrogel, zinc oxide nanoparticles, mesoporous silica nanoparticles, wound healing

Introduction

Wound infection is a considerable problem in the wound healing process. Because these infections result in delay wound healing [1]. According to studies, an ideal wound dressing should carry properties such as having developed mechanical properties, keeping the moisture in the healing environment, being biocompatible, maintaining barriers to microorganisms [2,3]. In this regard, hydrogels have been commonly used wound dressing for years. Hydrogels are biocompatible material with three-dimensional (3D), cross-linked polymeric networks which can absorb a high amount of water and can swell without dissolving. They are widely used for many biomedical applications such as drug delivery, tissue engineering, wound dressing, etc. [4,5]**.** Among them, chitosan-based hydrogels as a pure form or in combinations with nanoparticles have become popular day by day in order to inhibit microbial growth and increase mechanical properties.

Chitosan is a linear, cationic natural polysaccharide that is derived by the deacetylation of chitin. Chitosan has been commonly used in biomedical applications owing to its low toxicity, antibacterial activity, wound healing properties, biocompatibility, biodegradability, high water permeability, affinity to chemical modifications [6-8]. Over the years, chitosan has been incorporated with polymers or nanoparticles to enhance antimicrobial activity and stability. Zinc oxide (ZnO) is one of these nanoparticles which are chosen for a combination of CS. Because ZnO is not only biocompatible and low toxic but also has antibacterial activity, high stability, and photocatalytic properties [1,9]. Besides antibacterial properties of the hydrogel, the development of mechanical properties is another important point. For this approach, MSN are one of the most be interested nanoparticles, especially as drug carriers. MSN have several advantages such as large surface area, high pore volume, tunable pore size, nontoxicity, and allowing easy surface functionalization. Also, MSN contribute to the control of drug release, and this provides them to be preferred drug loading and carrying applications [10,11].

Taking into consideration the advantages of CS, ZnO, and MSN, in this study, we aimed to synthesis ZnO/CS-based hydrogel reinforced with MSN as can be seen in Figure 1. After the obtained the hydrogel, we characterized the ZnO NPs, MSN and the hydrogel by techniques such as Fourier transform infrared spectroscopy (FTIR), dynamic light scattering (DLS), and scanning electron microscopy (SEM).

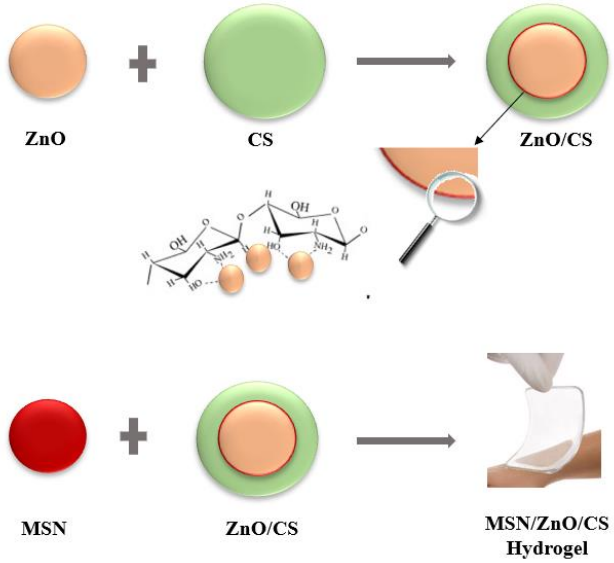

Figure 1. ZnO/CS-based hydrogel reinforced with MSN

Material and Methods

Materials

Zinc acetate dihydrate (Zn $(CH_3CO_2)_2 2H_20$), sodium hydroxide (NaOH), acetic acid (CH_3COOH), chitosan (low MW), cetyltrimethylammonium bromide (CTAB), ammonium hydroxide NH_4OH were purchased from Sigma Aldrich. Tetraethyl orthosilicate (TEOS, 99% was supplied form abcr, GmbH. Ethanol (C_2H_5OH, 99,9 %) was purchased from Isolab Chemicals and ammonium nitrate (NH_4NO_3) was purchased from Carlo Erba Reagents. Distilled water was used for preparation of solutions. All chemicals were of analytical grade and they were used without further purification.

Preparation of ZnO Nanoparticles

ZnO NPs were synthesized by precipitation method. Briefly, 0,219 gr of Zn $(CH_3CO_2)_2 2H_20$ was dissolved in 50 ml distilled water at room temperature. 2 M NaOH solution was added drop wise until pH is 11 and the solution was kept stirring for 2h at room temperature which lead a formation of white precipitate. The white precipitate washed with distilled water for three times to remove unreacted chemicals. Finally, the precipitations were dried in oven for overnight at 80˚C [12,13].

Preparation of ZnO/CS Core/Shell Structure

The ZnO NPs were dissolved in 10 mL of 1% CH_3COOH. Certain amount of CS added into the solution and the mixture was sonicated for 30 min. Following it, 1 M NaOH drop by drop was added until the solution pH reaches to 11. The solution was kept magnetic stirring for 3h at 65 °C. Finally, the white precipitations were washed with distilled water three times and dried in an oven at 80◦C overnight [6,14].

Preparation of MSN

MSN prepared by slight modifications as described in our previous study [15]. Briefly, 0, 32 gr CTAB was dissolved in 110 mL distilled water. 2 ml of TEOS and 52 mL of ethanol absolute, and 2 mL of NH_4OH were added into the solution. The mixture was stirred for 3h to produce a white precipitate. After the reaction, white precipitations were washed with NH_4NO_3 several times. And then collected the white precipitations were washed with ethanol [11].

Preparation of MSN/ZnO/CS Hydrogel

First of all, certain amount of prepared MSN was dissolved in 9 ml acetic acid (1M) solution. And then adequate amount of prepared ZnO/CS powder was then dissolved in the acidic suspension by kept stirring at 50 ◦C for 24h. The viscous solution was transferred into petri dishes and dried overnight and then at 80◦C overnight too. Also, pure chitosan hydrogel and ZnO/CS hydrogel were also prepared as control samples following the same process [16].

Characterizations

The particle size distribution of ZnO NP and MSN were determined by DLS (Marvern Nano ZS90 Zetasizer). Also, MSN and pure CS based hydrogel were identified using FTIR (Thermo Scientific Nicolet iS50 FTIR Spectrometry). FTIR spectral reading was carried out in the range from 500 to 4000 cm^{-1}. The morphology of nanostructures determined by SEM **(**Carl Zeiss 300VP).

Results and Discussion

Fourier Transform Infrared Spectroscopy

The FTIR spectrum of MSN and CS-based hydrogel were presented in Figure 2. FTIR spectrum of MSN shows a broad band at 3646 cm^{-1}, attributed to O-H stretching while the band at 1058 cm^{-1} refers the silica groups. The FTIR spectrum of pure CS- based hydrogel shows a broad band at 3253 cm^{-1}, attributed to O-H stretching, the band at 2922 cm^{-1} refers - CH_2 aliphatic groups while the band at 1635 cm^{-1} shows N-H bending vibration. Also, the band at 1538 cm^{-1} refers to N-O stretching.

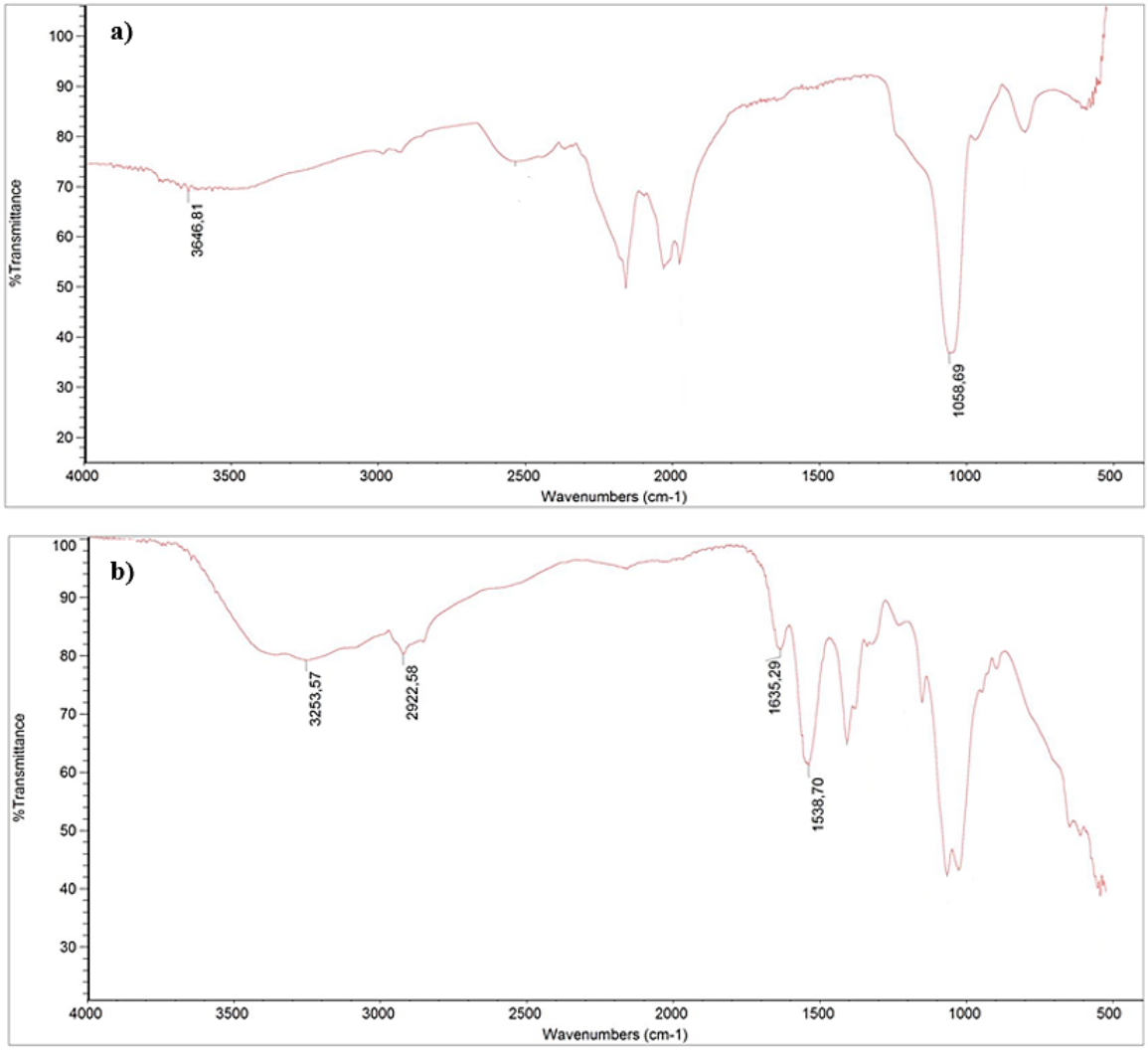

Figure 2. a) FTIR spectra of mesoporous silica nanoparticles (MSN), b) FTIR spectra of chitosan hydrogel

Dynamic Light Scattering Analysis

The size distributions of MSN and ZnO NP were exhibited in Figure 3. According to DLS analysis results, the average hydrodynamic diameter of MSN dispersed in water is between 300-400 nm and average hydrodynamic diameter of ZnO NPs dispersed in ethanol is between 110-150 nm.

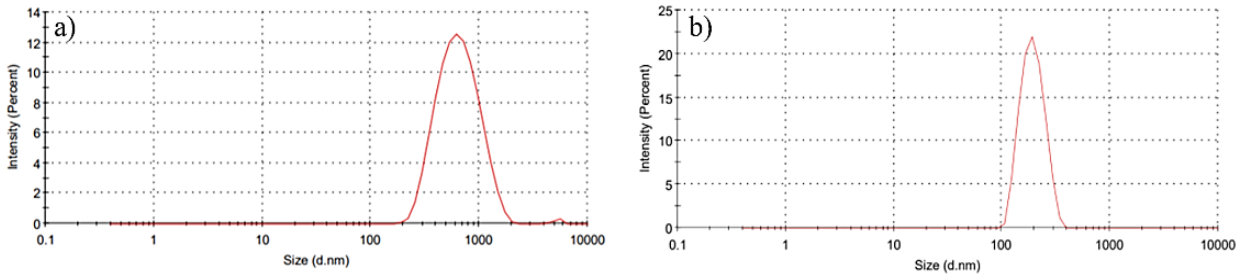

Figure 3. The size distribution of a) MSNs and b) ZnO NP

Scanning Electron Microscopy Analysis

The morphologies of the MSN, ZnO NPs, CS-based hydrogel and ZnO/CS-based hydrogel were determined by SEM. As shown in Figure 4, the nanoparticles were mainly monodispersed and spherical shape. Moreover, the morphologies of hydrogels with CS and ZnO/CS NPs were determined.

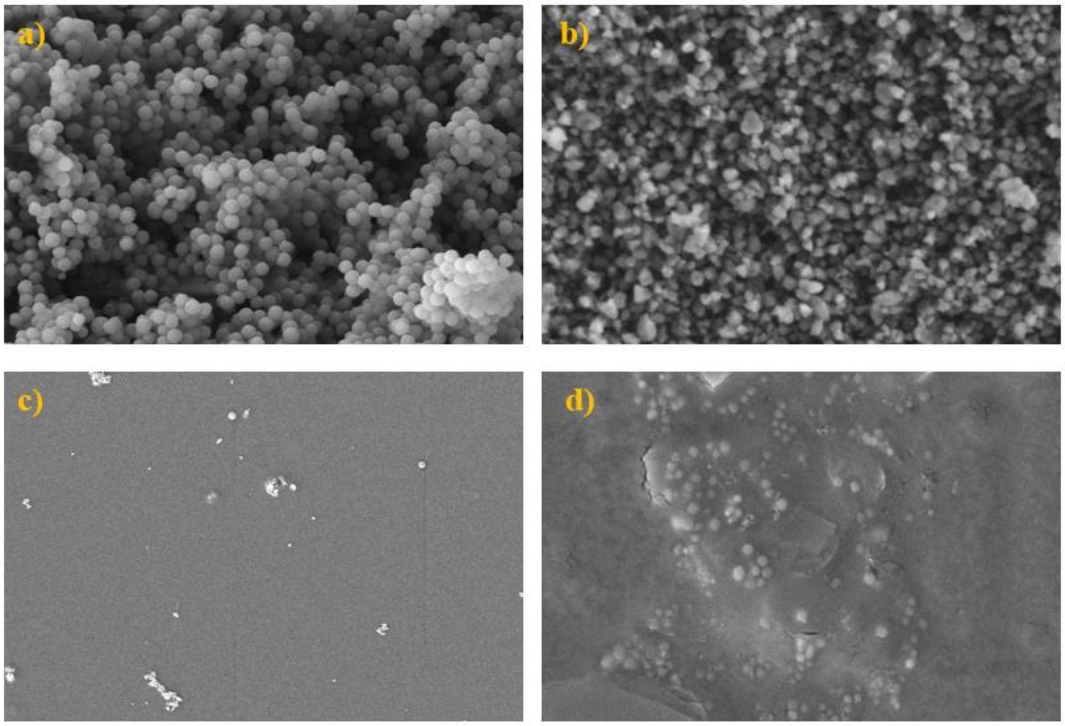

Figure 4. SEM analysis of a) MSNs, b) ZnO NPs, c) CS-based hydrogel and d) ZnO/CS-based hydrogel

Conclusion

In this study, we performed an MSN-reinforced ZnO/CS-based hydrogel synthesis. First of all, we successfully synthesized and characterized ZnO NPs approximately 110-150 nm in size and MSN in between 300-400 nm in size. Characterization studies showed that the synthesized nanoparticles were spherical and mainly monodisperse. Following it, we combined ZnO NP with CS to obtain a core/shell nanostructure. Afterwards, we carried out studies to strengthen the ZnO/CS-based hydrogel structure with MSN and reported its characterization. Many studies in the literature indicate that hydrogels are promising candidates in wound healing applications. Herein, we aimed to synthesis CS-based hydrogels more functional by doping with nanoparticles, and we think that the nanostructure has the potential to be used in wound healing applications due to its antibacterial properties and mechanical development.

References

[1] Sudheesh Kumar PT, Lakshmanan V-K, Anilkumar T V, Ramya C, Reshmi P, Unnikrishnan AG. Flexible and microporous chitosan hydrogel/nano ZnO composite bandages for wound dressing: in vitro and in vivo evaluation. ACS Appl Mater Interfaces. 2012;4(5):2618–29.
[2] Napavichayanun S, Amornsudthiwat P, Pienpinijtham P, Aramwit P. Interaction and effectiveness of antimicrobials along with healing-promoting agents in a novel biocellulose wound dressing. Mater Sci Eng C. 2015;55:95–104.
[3] Rakhshaei R, Namazi H. A potential bioactive wound dressing based on carboxymethyl cellulose/ZnO impregnated MCM-41 nanocomposite hydrogel. Mater Sci Eng C. 2017;73:456–64.
[4] Wahid F, Yin J-J, Xue D-D, Xue H, Lu Y-S, Zhong C, vd. Synthesis and characterization of antibacterial carboxymethyl Chitosan/ZnO nanocomposite hydrogels. Int J Biol Macromol. 2016;88:273–9.
[5] Hamidi M, Rostamizadeh K, Shahbazi M-A. Hydrogel nanoparticles in drug delivery. Içinde: Intelligent Nanomaterials: processes, properties, end applications. Wiley-VCH; 2012. s. 585–624.
[6] Li L-H, Deng J-C, Deng H-R, Liu Z-L, Xin L. Synthesis and characterization of chitosan/ZnO nanoparticle composite membranes. Carbohydr Res [Internet]. 2010;345(8):994–8. Available at: http://www.sciencedirect.com/science/article/pii/S0008621510001151
[7] Kaushik A, Khan R, Solanki PR, Pandey P, Alam J, Ahmad S, vd. Iron oxide nanoparticles–chitosan composite based glucose biosensor. Biosens Bioelectron. 2008;24(4):676–83.
[8] Al-Naamani L, Dobretsov S, Dutta J. Chitosan-zinc oxide nanoparticle composite coating for active food packaging applications. Innov Food Sci Emerg Technol. 2016;38:231–7.
[9] Yadollahi M, Farhoudian S, Barkhordari S, Gholamali I, Farhadnejad H, Motasadizadeh H. Facile synthesis of chitosan/ZnO bio-nanocomposite hydrogel beads as drug delivery systems. Int J Biol Macromol. 2016;82:273–8.
[10] Kwon S, Singh RK, Perez RA, Abou Neel EA, Kim H-W, Chrzanowski W. Silica-based mesoporous nanoparticles for controlled drug delivery. J Tissue Eng. 2013;4:2041731413503357.
[11] Zhao P, Liu H, Deng H, Xiao L, Qin C, Du Y, vd. A study of chitosan hydrogel with embedded mesoporous silica nanoparticles loaded by ibuprofen as a dual stimuli-responsive drug release system for surface coating of titanium implants. Colloids Surfaces B Biointerfaces [Internet]. 2014;123:657–63. Available at: http://www.sciencedirect.com/science/article/pii/S092777651400544X
[12] Gnanasangeetha D, Saralathambavani D. One Pot Synthesis of Zinc Oxide Nanoparticles via Chemical and Green Method. Res J Mater Sci. 2013;1(7):1–8.
[13] Javed R, Rais F, Fatima H, Haq I ul, Kaleem M, Naz SS, vd. Chitosan encapsulated ZnO nanocomposites: Fabrication, characterization, and functionalization of bio-dental approaches. Mater Sci Eng C [Internet]. 2020;116:111184. Available at: https://doi.org/10.1016/j.msec.2020.111184
[14] AbdElhady MM. Preparation and Characterization of Chitosan/Zinc Oxide Nanoparticles for Imparting Antimicrobial and UV Protection to Cotton Fabric. Int J Carbohydr Chem. 2012:1–6.
[15] Students I, Congress S. Preparation and Characterization of Chitosan-Based Hydrogels Reinforced by Mesoporous Silica Nanoparticles. :447–52.
[16] Zhu M, Zhu Y, Zhang L, Shi J. Preparation of chitosan/mesoporous silica nanoparticle composite hydrogels for sustained co-delivery of biomacromolecules and small chemical drugs. Sci Technol Adv Mater [Internet]. 23 Temmuz 2013;14(4):45005. Available at: https://pubmed.ncbi.nlm.nih.gov/27877598

Çinko Oksit (ZnO) Nanoparçacıklarla Katkılandırılarak Üretilen Feldspatik Cam-Seramiklerin Karakterizasyonu

Ahmet Aykaç[1], Gizem Kestane[1], Mücahit Sütçü[1,2]*
[1] İzmir Katip Çelebi Üniversitesi, Fen Bilimleri Enstitüsü, Nanobilim ve Nanoteknoloji Anabilim Dalı, Balatçık, 35620, Çiğli, İzmir, Türkiye
[2] İzmir Katip Çelebi Üniversitesi, Fen Bilimleri Enstitüsü, Malzeme Bilimi ve Mühendisliği Anabilim Dalı, Balatçık, 35620, Çiğli, İzmir, Türkiye
**İletişimden sorumlu yazar e-mail: ahmet.aykac@ikcu.edu.tr*

Özet

Seramikler farklı oranlarda olmak üzere feldspat, kuvars ve kilden oluşmaktadır. Feldspatik içerikli cam seramikler, yapılarının amorf ve kristal fazlar içermesi nedeniyle özellikle dental uygulamalarda tercih edilmektedir. Nanoteknoloji tıp, ambalaj paketleri, inşaat, boya, nanosensör, elektronik uygulamalar, ilaç taşıyıcı sistemler, biyobozunur malzemeler, yenilenebilir filmler gibi çok çeşitli uygulamalarda kullanılmaktadır. Nanoteknolojinin insan hayatına girmesiyle endüstriyel alanda yeni nesil malzemeler üretilmeye başlamıştır. Nanopartiküller boyutları 100 nanometreden küçük parçacıklar olarak adlandırılmaktadır ve yüksek yüzey alanı/hacim oranına sahip olmaları nedeniyle birçok uygulama alanında tercih edilmektedir. Özellikle çinko oksit (ZnO) nanoparçacıklar eşsiz fiziksel ve kimyasal özelliklere sahip olduğu için elektronik, piezoelektrik ve optik cihazların yanı sıra gaz sensörleri, biyosensörler, güneş pilleri, kozmetik ürünleri gibi birçok alanda kullanılmaktadır. Çalışmada feldspatik esaslı cam seramik malzemesinin ZnO NP ile katkılandırılarak üretilmesi amaçlanmıştır ve bu amaçla feldspatik esaslı cam seramik malzemesinin karakterizasyon çalışmaları yürütülmüştür. Feldspatik esaslı amorf cam tozu, çöktürme yöntemiyle sentezlenen ZnO NP ile %0.1 ile %1 oranları arasında katkılandırılarak ZnO NP/Feldspatik cam seramik malzemesi elde edilmiştir. ZnO NP ve feldspatik cam seramikten elde edilen numuneler, homojen bir şekilde karıştırıldıktan sonra 40^{O}C'de etüvde bekletilerek preslenmiştir. Preslenen numuneler amorf halden kısmi kristallendirilmesi için iki kademeli ısıl işlem ile cam-seramik hale getirilmiştir. Üretilen numunelerin karakterizasyon çalışmaları kapsamında taramalı elektron mikroskobu (SEM) ile nanoparçacıkların yüzey morfolojileri, X-ışını kırınımı analizi (XRD) ile malzemenin kristallografik özellikleri, eş zamanlı termal analiz sistemi (SDT) ile malzemenin ağırlık değişimi ve ısı akışı gibi özellikleri sıcaklığın ve zamanın fonksiyonu olarak, parçacık boyut analizi (DLS) ile nanoparçacıkların boyutları incelenmiştir. Tüm bu çalışmalar ışığında ZnO NP ile katkılandırılmış cam seramik malzemesinin ülkemiz ekonomisine katkı sağlayacağına ve yapılacak olan yeni çalışmalara ışık tutacağına inanıyoruz.

Anahtar Kelimeler: cam seramik, çinko oksit (ZnO) nanoparçacık, nanoparçacık sentezi

Giriş

Seramikler bir veya daha fazla metalin, metal olmayan element ile birleşmesi ve sinterlenmesi sonucu oluşan inorganik bileşiklerdir ve farklı oranlarda olmakla birlikte tüm seramiklerde temel yapı feldspat, kuvars ve kilden oluşmaktadır [1]. M.Ö. 6000 tarihli Çatalhöyük buluntuları tarihteki ilk seramikler olarak anılırken son arkeolojik buluntular insanoğlunun henüz yerleşik yaşama geçmeden önce yani kap kacak yapmaya başlamadan önce, kilden idol heykeller yaptığını ortaya koymuştur. Kurutulmuş, ya da düşük ısıda pişirilmiş toprak idollerin en eski tarihli olanları Mezolitik Dönem'e (M.Ö. 14.000-9000) aittir. Örneğin Kahramanmaraş'ın Direkli Mağarasında son yıllarda bulunan kilden kadın figürini Anadolu'da bu çağa ait tek örnektir (Şekil 1) [2]. Seramikler inert olmaları, renk stabiliteleri, yüksek aşınma dirençleri, su absorbe etmemeleri, ağız dokuları tarafından çok iyi tolere edilmeleri ve estetik özellikleri nedeniyle diş hekimliği uygulamalarında yaygın bir şekilde kullanılmaktadır [3,4]. Sabit protezlerde estetik amaçla kullanılan tüm materyaller arasında, doğal dişle renk uyumunun en iyi sağlandığı materyal seramiktir [5]. Seramikler mikro yapılarına göre; camsı seramikler, katkı içeren cam seramikler ve polikristalin seramikler olarak üç grup altında sınıflandırılmıştır [6]. Cam seramikler, camların kontrollü kristalizasyonu ile oluşan amorf ve kristal fazlara sahip malzemelerdir ve diş hekimliği uygulamalarının yanı sıra ısıya dayanıklı malzemelerde, çok düşük veya sıfır genleşme katsayılı ev mutfak gereçlerinde, fırın üst katmanlarında, silindirlerde,

tüpler ve diğer elemanlarda, ışık hassasiyeti sergileyen gaz boşaltım panellerinde, inkjet yazıcılarda, akışkan aparatlarda, manyetik kayıt disklerinde, tıpta kullanılan biyomalzemelerde (suni kemikler, kafa ve boğaz cerrahisinde orta kulak cihazları ya da implantlar, enjeksiyon parçacıkları vs.), elektrik ve elektronik sanayide yarı iletkenlerin elektrik yalıtım bileşenlerinde, ısı izolatörlerinde, vakum sızdırmazlık parçalarında, mikro-elektronik altlıklarda, sıvı kristal ekranlarda, kaplamalarda, teleskop aynalarında, optik fiber sistemlerindeki ara yüz lenslerinde, otomatik yaklaştırma yapabilen kameralarda kullanılan lenslerde vb. çok çeşitli kullanım alanları göstermektedir [7].

Şekil 2'de cam seramiklerin diş hekimliği uygulamalarında kullanımını gösteren bir örnek gösterilmiştir.

Şekil 1. Mezolitik Dönem pişmiş toprak idol, Kahramanmaraş Direkli Mağarası [8]

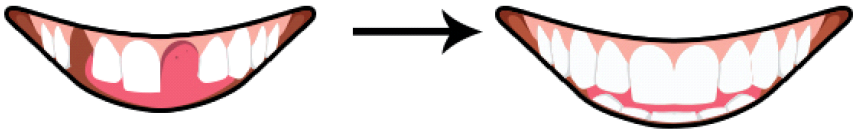

Şekil 2. Diş seramiği uygulaması ile yerine yerleştirilmesi hedeflenen diş

Her geçen gün artan teknoloji ile seramik alanında nano malzeme kullanımı son yıllarda ilgi çekmektedir ve böylelikle nanoteknolojinin de yardımıyla endüstriyel alanda yeni nesil malzemeler üretilmeye başlamıştır. Nanoparçacıklar boyutları 100 nanometreden küçük parçacıklar olarak adlandırılmaktadır ve yüksek yüzey alanı/hacim oranına sahip olmaları nedeniyle birçok uygulama alanında tercih edilmektedir. Nanoparçacıklar, kendi içerisinde organik, inorganik, karbon bazlı olarak sınıflandırılabilmektedir. İnorganik nanoparçacık türlerinden biri olan metal oksit nanoparçacıklardan özellikle çinko oksit (ZnO) nanoparçacıklar eşsiz fiziksel ve kimyasal özelliklere sahip olduğu için elektronik, piezoelektrik ve optik cihazların yanı sıra gaz sensörleri, biyosensörler, güneş pilleri gibi birçok alanda kullanılmaktadır [9]. Geniş bant aralığına sahip yarı iletkenliği, yüksek mekanik, termal ve kimyasal kararlılığı, yüksek bağlanma enerjisi, düşük fiyatı, elektriksel, optoelektronik ve piezoelektrik özellikleri, uygun elementlerle depolandığında gösterdiği yüksek iletkenlik özelikleri ZnO nanoyapılarının çok geniş uygulama alanlarında kullanımını mümkün kılmaktadır [10,11].

Bu çalışmada feldspatik cam seramiklerin ZnO NP ile katkılandırılarak üretilmesi amaçlanmıştır. ZnO NP'ler laboratuvar ortamında sentezlendikten sonra belirli oranlarla cam seramik tozu ile homojen bir şekilde karıştırılarak ve ısıl işlem uygulanarak yeni nesil bir diş seramiği üretilmesi hedeflenmiştir (Şekil 3).

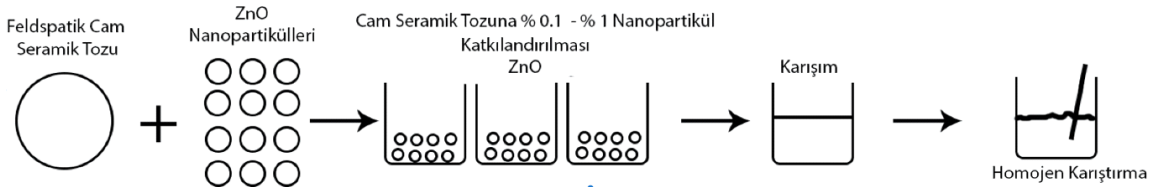

Şekil 3. Çalışmanın basamaklarını gösteren akım şeması.

Materyal ve Metot

Deneysel çalışmalar kapsamında materyal olarak çinko asetat dihidrat ($Zn(CH_3CO_2)_2.2H_2O$), sodyum hidroksit (NaOH), polivinil alkol (PVA), etil alkol Sigma-Aldrich'ten temin edilmiştir. Feldspatik içerikli camsı toz ise ticari olarak temin edilmiştir. Tüm kimyasallar analitik saflıkta kullanılmıştır ve çözelti hazırlanmasında saf sudan yararlanılmıştır.

Çalışmada kullanılan yöntemler kapsamında ZnO NP sentezi, ZnO NP ile feldspatik cam seramik tozunun katkılandırılması, pelet oluşumu ve karakterizasyon çalışmaları yürütülmüştür.

Çinko Oksit (ZnO) Nanoparçacık Sentezi

50 ml saf suda 0.219 gr çinko asetat dihidrat ($Zn(CH_3CO_2)_2.2H_2O$) çözdürülmüştür ve 10 ml saf suda 2M, 0.8 gr sodyum hidroksit (NaOH) çözdürülerek pH 11 oluncaya kadar damla damla çözeltiye (çinko asetat dihidrat içerisine) eklenmiştir. 2 saat daha 50°C'de karıştırıldıktan sonra saf su ile birkaç kez yıkanmış ve son olarak etüvde 24 saat 80°C'de kurutulmuştur [12].

Çinko Oksit Nanoparçacıklar ile Feldspatik Cam Seramik Tozunun Katkılandırılması

Laboratuvar ortamında sentezlendikten sonra elde edilen ZnO NP'ler %0.1 ile %1 aralığında olacak şekilde 5 adet (0 mg, 2.5 mg, 5 mg, 7.5 mg, 10 mg) numune hazırlanmıştır ve 5 adet 1 gr feldspatik cam seramik tozu ile homojen bir şekilde agat havanda karıştırılmıştır. Karıştırma işlemi sırasında toz haldeki karışıma PVA ve etil alkol eklenmiştir ve numune kuruması amacıyla 40°C'de etüvde 1 saat bekletilmiştir.

Pelet Oluşumu

Feldspatik cam seramik tozu ve ZnO NP ile katkılandırılan numuneler 10 bar basınç yardımıyla preslenmiştir ve pelet formuna getirilmiştir. Pelet forma getirilen numunelerin son olarak karakterizasyon çalışmaları yürütülmüştür.

Bir sonraki aşamada ise, pelet formdaki numuneler amorf halden kısmi kristallendirilmesi için iki kademeli ısıl işlem ile cam-seramik hale getirilmiştir.

Karakterizasyon Çalışmaları

Karakterizasyon çalışmaları kapsamında, taramalı elektron mikroskobu (SEM) ile nanoparçacıkların yüzey morfolojileri, X-ışını kırınımı analizi (XRD) ile malzemenin kristallografik özellikleri, eş zamanlı termal analiz sistemi (SDT) ile malzemenin ağırlık değişimi ve ısı akışı gibi özellikleri sıcaklığın ve zamanın fonksiyonu olarak ve parçacık boyut analizi (DLS) ile nanoparçacıkların boyutları incelenmiştir.

Tartışma ve Sonuçlar

Parçacık Boyut Analizi (DLS)

ZnO NP'lerin boyut dağılımı şekil 4'te gösterilmiştir. Elde edilen sonuçlara göre ZnO NP'lerin boyutunun yaklaşık 100-120 nm civarında olduğu görülmektedir. ZnO NP'lerin parçacık boyut dağılımı Marvern Nano ZS90 Zetasizer cihazı ile belirlenmiştir.

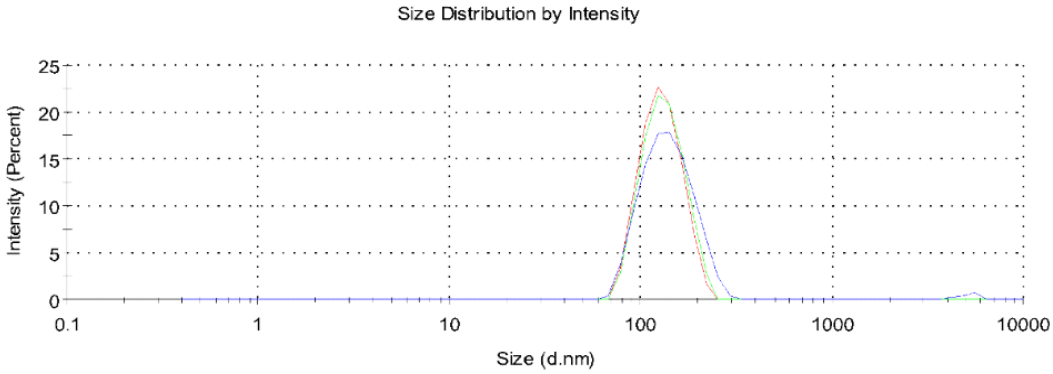

Şekil 4. ZnO NP'lerin DLS (Parçacık Boyut Analizi) sonuçları

Taramalı Elektron Mikroskobu (SEM) Analizi

SEM analizi sonuçları Şekil 5a ve Şekil 5b'de gösterilmiştir. ZnO NP'lerin küresel bir morfolojiye sahipken cam seramik tozunun amorf bir yapıya sahip olduğu gözlemlenmiştir. Ayrıca ZnO NP'lerin boyutları 70-80 nm aralığında, feldspatik cam seramik tozunun boyutu ise 15 µm olarak rapor edilmiştir. ZnO NP ve feldspatik cam seramik tozunun yüzey morfolojileri Carl Zeiss 300VP cihazı ile belirlenmiştir.

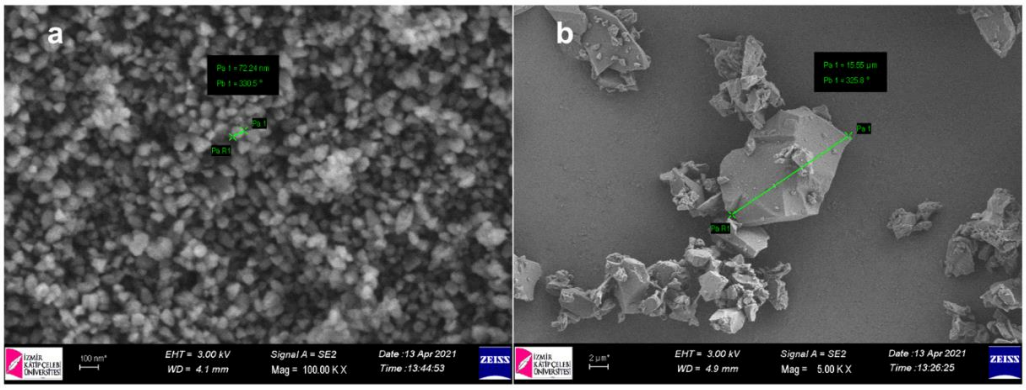

Şekil 5. (a) ZnO NP'lerin SEM (Taramalı Elektron Mikroskobu) Analizi sonucu (b) Feldspatik cam seramik tozunun SEM (Taramalı Elektron Mikroskobu) Analizi sonucu

X-Işını Kırınımı (XRD) Analizi

X-ışını kaynağından (Cu) alfa (α), beta (β) parçacıkları üretilerek bir numune üzerine yönlendirilmesi ve yönlendirilen parçacığın numunenin kristal yapısına bağlı olarak yansıma açılarının belirlenmesi prensibine dayanmaktadır ve Bragg prensibinin temelidir. XRD analizi sonuçlarına göre malzemenin vermiş olduğu pik değeri belirlenmiştir. Şekil 6'da görüldüğü gibi 15-40 2 theta degree aralığında pik verdiği görülmüştür. Geniş tümsek form yapının amorf olduğunu göstermektedir. 27° deki ana pik, amorf yapı içindeki kristal feldspatik bir fazın oluşmaya başladığını göstermektedir. Bu kristal fazın lösit kristal içerikli bir faz olduğu tespit edilmiştir. Çalışmada XRD Analizi sonuçları, Bruker D2 Phaser cihazı ile ölçülmüştür. Feldspatik camsı tozun %100 amorf olmadığı az bir miktar kristal içerdiği anlaşılmaktadır.

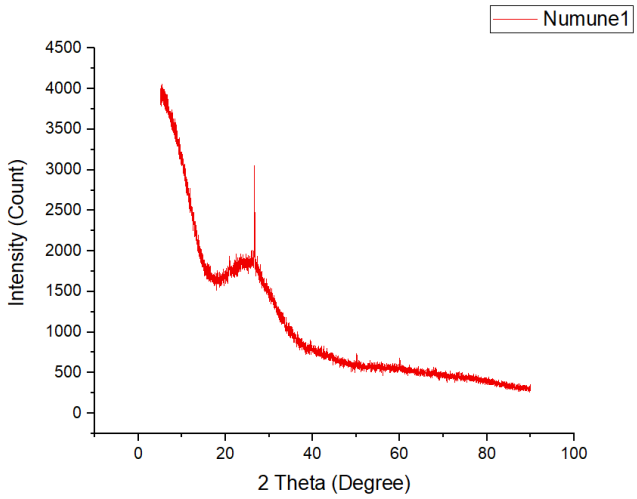

Şekil 6. Feldspatik cam seramik tozunun XRD (X-Işını Kırınımı) Analizi sonucu

Eş Zamanlı Termal Analiz Sistemi (SDT)

Malzemelerin ağırlık değişimi ve ısı akışı eş zamanlı olarak sıcaklığın veya zamanın bir fonksiyonu olarak ölçülmüştür. Bu analiz yardımıyla malzeme içerisindeki nem, uçucu, katkı maddesi oranları da belirlenebilmektedir. Şekil 7a'da feldspatik cam seramik tozunun sıcaklık(ºC)-kütle(mg) grafiği, Şekil 7b'de ise feldspatik cam seramik tozunun sıcaklık(ºC)-kütle değişimi(%) grafiği görülmektedir. Numuneler, 0 ila 900 ºC arasındaki sıcaklık derecesi 10 ºC / dakika olan bir TA TGA-SDT Q600 ve TA DSC Q200kullanılarak karakterize edilmiştir.

Çalışmada faz değişim sıcaklığını gösteren grafik şekil 7c'de verilmiştir ve buna göre 400-550ºC sıcaklıkta bir faz değişimi olduğu sonucuna varılmıştır.

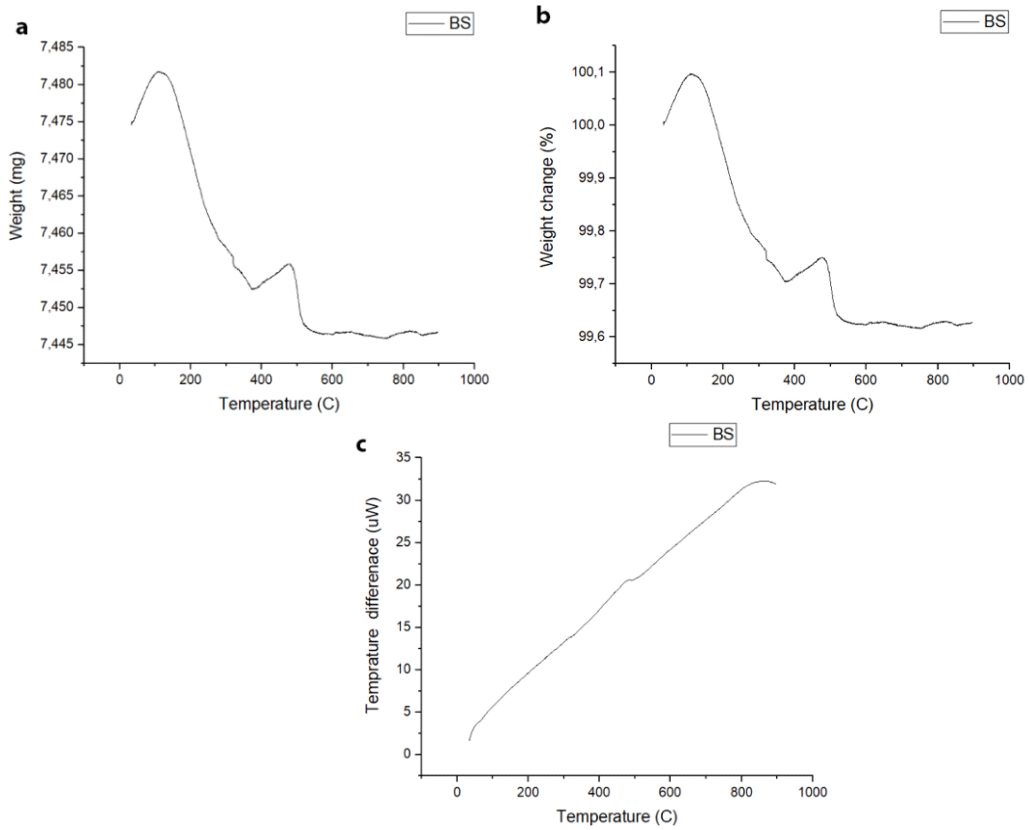

Şekil 7. (a) Feldspatik cam seramik tozunun SDT (Eş Zamanlı Termal Analiz) sonucuna göre sıcaklık(ºC)-kütle(mg) grafiği. (b) Feldspatik cam seramik tozunun SDT (Eş Zamanlı Termal Analiz)

sonucuna göre sıcaklık(ºC)-kütle değişimi (%) grafiği. (c) Feldspatik cam seramik tozunun SDT (Eş Zamanı Termal Analiz) sonucuna göre faz değişimini gösteren grafik.

Sonuçlar

Çalışmada çöktürme yöntemi kullanılarak yaklaşık 80-100 nm boyutlarında küresel morfolojiye sahip ZnO NP'lerin sentezi ve sonrasında ZnO NP ile feldspatik cam seramik tozunun %0.1 ile %1 aralığında katkılandırılması işlemleri gerçekleştirilmiştir. Katkılandırılan numuneler basınç yardımıyla pelet forma getirilmiştir. Çalışmada son olarak elde edilen numunelerin karakterizasyon çalışmaları gerçekleştirilmiş olup DLS ve SEM analizleri ile parçacık boyutu ve morfolojisi, XRD analizi ile kristallografik özellikleri, SDT analizi ile faz değişim sıcaklığı ile ilgili bilgiler elde edilmiştir. DLS analizi ile nanoparçacıkların parçacık boyutlarının 100 nm civarında ve eşit boyutlarda olduğu sonucuna ulaşılmıştır. SEM analizi sonucuna göre ise ZnO NP'lerin boyutu 70-80 nm aralığında ve küresel morfolojide, feldspatik cam seramik tozunun boyutu ise 15 µm ve amorf bir yapıda olduğu gözlemlenmiştir. XRD analizine göre 15-40 2 theta degree aralığında pik verdiği görülmüştür. Feldspatik camsı tozun %100 amorf olmadığı az bir miktar kristal içerdiği anlaşılmıştır. SDT analizi sonucuna göre ise sıcaklık, kütle değişimi dikkate alınarak ölçülmüştür ve 400-550ºC sıcaklıkta bir faz değişimi olduğu sonucuna varılmıştır. Tüm bu çalışmalar ışığında, dental seramik üretimi tamamlanmıştır. Çalışmanın devamı olarak numunelerin antibakteriyel yönden ve mekanik açıdan incelenebileceği düşünülmektedir. Bu çalışma, bilimsel çalışmalara ışık tutacak ve bu alanda yapılan yeni çalışmalara kaynakça oluşturacak ve ayrıca ticari ürüne dönüştürülebilmesi durumunda ülke ekonomisine katkı sağlama potansiyeli olan bir çalışmadır.

Referanslar

[1] Volpato CAM, Fredel MC, Philippi AG, Petter CO. Ceramic Materials and Color in Dentistry. Wunderlich W, ed. Ceramic Materials. Rijeka: Sciyo; 2010: 155-174.
[2] Yücel Ç., (2018). Tarih Öncesi İnsan Biçimli Figürinler Hakkında Genel Bir Değerlendirme., Dicle Üniversitesi Sosyal Bilimler Enstitüsü Dergisi, (21), 228-239.
[3] Lawn BR, Deng Y, Lloyd IK, Janal MN, Rekow ED, Thompson VP. Materials design of ceramic-based layer structures for crowns. J Dent Res 2002;81(6):433-8.
[4] Vult von Steyern P, Carlson P, Nilner K. All-ceramic fixed partial dentures designed according to the DCZirkon technique. A 2-year clinical study. J Oral Rehabil. 2005; 32 (3): 180-7.
[5] Shillingburg HT, Hobo S, Whitsett LD, Jacobi R, Brackett SE. All ceramic restorations. In: Bateman LA, ed. Fundamentals of Fixed Prosthodontics. 3 rd ed. London Quintessence Publishing Co. Inc; 1997. p.433-55.
[6] Kelly Jr, Benetti P. Ceramic Materials in Dentistry: Historical Evolution and Current Practice, Australian Dental Journal, 2011, 56:(1 Suppl): 84–96. doi: 10.1111/j.1834-7819.2010.01299.x
[7] Karasu B. Türkiye'de Cam ve Cam-Seramikler, TSE Standart Ekonomik ve Teknik Dergi, Yıl: 51, Sayı: 598, Mart 2012.
[8] Yücel Ç. (2018). Tarih Öncesi İnsan Biçimli Figürinler Hakkında Genel Bir Değerlendirme., Dicle Üniversitesi Sosyal Bilimler Enstitüsü Dergisi, (21), 228-239.
[9] Hassan M, Afify AS, Ataalla M, Mohammed A, Staneva A, Dimitriev Y, Tulliani JM. 2016. Preparatıon and Characterizatıon of A Zinc Oxide nanopowder Supported onto Inorganıc Clay, Journal of Chemical Technology and Metallurgy, 51, 168-172.
[10] Romeo R, Leinen D, Dalchiele EA, Ramos-Barrado JR, Martin F. 2006. The effects of zinc acetate and zinc chloride precursors on the preffered crystalline orientation of ZnO and Al-doped ZnO thin films obtained by spray Pyrolysis, The Solid Films, 5151, 1942-1949.
[11] Ergin B, Ketenci E, Atay F. 2009. Characterization of ZnO films obtained by ultrasonic spray pyrolysis technique, International Journal of Hydrogen Energy, 34, 5249-5254.
[12] Gnanasangeetha D, SaralaThambavani D. 2013, Research Journal of Material Sciences 1 (7), 1-8.

Doğal Liflerin Özelliklerine Atmosferik Plazma İşleminin Etkileri

Huda Alattas[*], *Aslı Demir*
Ege Üniversitesi, Tekstil Mühendisliği Bölümü, İzmir, Türkiye
**İletişimden sorumlu yazar e-mail: asli.demir@ege.edu.tr*

Özet

Maddenin dördüncü hali olarak kabul edilmekte olan plazma, iyonlar, elektronlar, serbest radikaller, fotonlar, uyarılmış ve uyarılmamış haldeki nötr atomlar ve moleküller oluşturmaktadır. Fizikokimyasal modifikasyonlardan olan plazma, materyalin, temel özelliklerini değiştirmeden sadece yüzeyde çeşitli modifikasyonların oluşmasını sağlamaktadır. Günümüzde kâğıt endüstrisinde, biyoloji ve biyomedikal, materyal aşındırma veya sertleştirme teknolojisinde, uzay sanayisinde, yarı iletken teknolojisinde, elektronik cip yapımında, iletişim teknolojisinde, elmas yapımında, kaplama ve dekorasyon teknolojisinde, sterilizasyon ve arıtma sistemlerinde, güneş enerjisi ve optik sanayisinde, otomobil ve tekstil endüstrisi gibi birçok alanda kullanılmaktadır. Plazma teknolojisi doğal liflerin gerek ön terbiyesi gerekse boyama ve bitim işlemlerinde klasik yöntemlere kıyasla hem enerji hem kimyasal madde tüketimi açısından bir çok avantaja sahiptir. Çevresel tedbirlerin öneminin arttığı günümüzde plazma teknolojisi ekolojik bir yöntem olarak geleceğe yönelik bir uygulamadır.

Hidrofilik veya hidrofobik özellik kazandırma, özellikle kaplama ve kompozit uygulamalarında adhezyonun iyileştirilmesi ve tekstil yüzeylerine istenen fonksiyonel özelliklerin kazandırılması amacıyla uygulanan plazma işlemiyle yüzey modifikasyonu, son yıllarda birçok araştırmacının ilgisini çekmektedir. Özellikle giderek artan çevresel endişeler nedeniyle tekstil endüstrisinde plazma teknolojisi çok daha güncel bir yöntem olarak karşımıza çıkmaktadır. Geleneksel yaş kimyasal işlemlere alternatif ekonomik ve ekolojik bir yöntem olan plazma sadece materyalin yüzeyinde etkili olduğu için, lifin temel özelliklerini bozmadan, su gereksinimi olmadan, çok az veya hiç kimyasal kullanmadan tekstil materyallerine fonksiyonellik kazandırmasının yanında işlemler esnasında herhangi bir kirlenme ve toksik atık açığa çıkmadığı için de son derece avantajlı bir yöntemdir. Bu derlemenin amacı: atmosferik basınç plazma teknolojisinin doğal liflere uygulanmasını ve işlem sonrası bu liflerin kimyasal ve morfolojik özelliklerinde meydana gelen değişimlerin, temas açısı ölçümü ve SEM gibi farklı yöntemlerle yapılan karakterizasyonlarının incelenmesidir.

Anahtar Kelimeler: atmosferik basınç plazma, yüzey modifikasyonu, doğal lifler, tekstil

Giriş

"Her şey oluşturuldu, kalıplanmış", Yunancada "Plazma" sözcüğü anlamına gelmektedir. Sir William Crooks, plazma kavramını 1879'da "maddenin dördüncü hali" olarak ileri sürmüştür. Amerikalı kimyager Irving Langmuir ilk olarak 1928'de "plazma" terimini kullanmıştır. Plazma, serbest radikaller, elektronlar ve ağır parçacıklar gibi reaktif türlerin karışımını içermektedir. Bu yüzey modifikasyonu için eşsiz bir ortam sağlamaktadır [1].

Son yıllarda, plazma işleme teknolojisi, konvansiyonel kimyasal işleme tekniklerine ekonomik ve ekolojik olarak sağlıklı bir alternatif olarak görüldüğünden, tekstil endüstrisinde daha fazla ilgi çekmiştir [1-3]. Mevcut standart bitim işlemleri ile karşılaştırıldığında, plazma kimyasal, su ve enerji kullanımını azaltmada önemli bir avantaja sahiptir. Ayrıca, temel tekstil özelliklerini değiştirmeden tipik tekstil kaplamaları elde etme imkanı sunarmaktadır [4]. Plazma işleminin etkinliği, substratın doğası ve işlem çalışma koşulları gibi çeşitli faktörlere bağlıdır. Plazma teknolojisini çok farklı yüzey özellikleri elde etmek için kullanılmaktadır: Yüzey enerjisinin ve ıslatabilme özelliğinin ayarlanması, hidrofilleştirme, hidrofoblaştırma, oleofoblaştırma (kir ve yağ önleyici etki), çok işlevli kaplamalar (örneğin asitli, bazlı, yapışkan veya ayırıcı) veya biyoaktif kaplamalar (antimikrobik, mantar önleyici) [2].

Atmosferik basınç termal olmayan plazma teknolojisi, tekstil endüstrisinin ihtiyacını karşılamak üzere geliştirilmiştir [1]. Atmosferik plazma standart atmosfer basıncında (y100 kPa) çalışmaktadır. Çevredeki havayı kullanan açık sistemler vardır. Aynı zamanda, şartlandırılmış bir reaktördeki sistemler de mümkündür, bunlar genellikle nitrojen gazı gerektirmektedirler, ancak bazen (ilave) bir soy gazına ihtiyaç duyulmaktadır. Açık sistemler için, plazmaya hangi maddelerin enjekte edildiğine dikkat edilmelidir. Bu nedenle, işlem aralığı düşük basınçlı plazmalar kadar büyük değildir. Öte yandan, bu

sistemler, endüstriyel bakış açısından önemli bir avantaj olan mevcut bağlantı hatlarına kolayca entegre edilmektedir. Tekstillerin atmosferik basınç plazma (APP) işleminde çeşitli teknolojik ve makine unsurları yer almaktadır (şekil1). Tekstilde uygulanacak dört ana tip atmosferik basınç plazması vardır: korona deşarjı, dielektrik bariyer deşarjı (DBD), atmosferik basınç kızdırma deşarjı (APGD) ve atmosferik basınçlı plazma jeti (APPJ) [3]. APP, özel yüzeyler için yüzey aşındırmasından plazma polimerizasyonuna kadar geniş bir yelpazede tekstil uygulamalarına sahiptir. Plazma işlemi, temel özelliklerini değiştirmeden yüzey kimyası ve topografyasında değişiklikler getirebilmektedir [1].

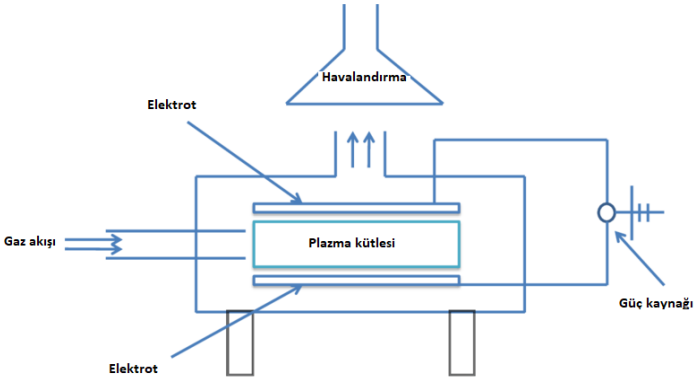

Şekil 1. APP sisteminin şematik diyagramı

Yapılmakta olan substratın derinliği y10 nm veya daha azıyla sınırlıdır. Bu, plazmanın sadece substratın en dıştaki ince tabakasını etkilediği, yani gerçek bir yüzey modifikasyon tekniği olduğu anlamına gelmektedir. Bunun pozitif bir yanı (temel özellikleri etkilenmez), aynı zamanda negatif olanı vardır (yüzey kirlenmesi plazma işlemi için zararlı olabilir) [4]. Plazmanın yüksek yüzey spesifik aktivitesi nedeniyle, plazma işleminden sonra tekstillerin fiziksel, kimyasal ve morfolojik özelliklerini incelemek şarttır [1]. Plazma ile işlenmiş bazi doğal lifler, adezyon geliştirme, yüzey topografisinin modifikasyonu, hidrofilik özelliklerin geliştirilmesi gibi farklı karakterizasyon teknikleri kullanılarak bu çalışmada ele alınmıştır.

Tekstil Özelliklerine Plazma Uygulamalarının Etkisi

Plazma uygulamaları, yüzey enerjisinin modifikasyonu, yüzey topoğrafyasının modifikasyonu, adezyonunn iyileştirilmesi ve yüzey temizliği de dahil olmak üzere çeşitli amaçlar için tekstil alanında uygulanmasını sağlar. Bu bölüm, plazmalı işlemi yöntemlerini kullanarak tekstillerin işlevselleştirilmesine yönelik çok sayıda akademik araştırma çabalarını özetlemektedir. Burada sunulan uygulamaların sayısı ne tam ne de tam kapsamlı değil, sadece APP teknolojisinin tekstil işlemeye yararlılığını ve olası uygulamalarını gösteren bir uygulama örneği.

Hidrofilik Özelliklerin Geliştirilmesi

Plazma işleminin yüzey enerjisini arttırdığı ve tekstil substratlarının hidrofilik özelliklerini geliştirdiği gösterilmiştir. Yüzey enerjisindeki değişiklikler esas olarak, plazmada veya post plazma reaksiyonları sırasında kumaş yüzeyleri üzerinde polar fonksiyonel grupların oluşmasından kaynaklanır. Geliştirilmiş ıslatma özelliklerinin sonuçları, çoklu ve tekstil imalatına büyük ilgi göstermektedir. Bununla birlikte, tekstil malzemelerinin heterojen yapısı göz önüne alındığında, plazmalı yüzeylerin ıslatılabilirliğinin değerlendirilmesi genellikle ıslanma süresi ve fitilleme gibi dolaylı yöntemlerle yapılmaktadır [3].

Bhat ve diğ. [5], atmosferik hava plazma işleminden sonra gri pamuklu kumaşların ıslanabilirliği ve sertleşmesinde önemli bir artış gözlemlemişlerdir. Bu etki, hava plazması nedeniyle polar grupların sokulmasına bağlanmıştır. Lam ve diğ. [9], oksijen gazını kullanarak atmosferik plazmada pamuklu kumaş işlemi üzerinde çalışmışlar. Plazma ön işleminden sonra C atomik yüzdesinin oksijen atomu yüzdesinin artmasına neden olduğu ve bunun da pamuklu kumaşın hidrofilisitesinin iyileşmesine yol açtığı bulunmuştur. Naebe ve diğ. [10], nispeten kısa bir maruz kalma süresine sahip yün kumaşın atmosferik basınç plazma işleminin kovalent olarak bağlanmış lipit tabakasını yün yüzeyinden etkin bir şekilde çıkardığını bulmuşlardır. Plazma ile muamele edilmiş kumaş ıslanabilirliği arttırdı ve lifler daha

fazla pürüzlülük göstermiştir. XPS analizi, oksijen ve azot konsantrasyonlarında anlamlı artışlar ve karbon konsantrasyonunda azalma ile çok daha hidrofilik bir yüzey göstermiştir (Tablo 1). Benzer sonuçlar, helyum ve oksijen / helyum APPJ ile işlem görmüş yün kumaşlar kullanılarak, Xu ve diğ. [11] tarafından da elde edilmiştir.

Tablo 8. İşlem görmemiş ve plazma işlem görmüş kumaşın nispi atomik konsantrasyonu

Elementler	Carbon (C_{1s})	Oxygen (O_{1s})	Nitrogen (N_{1s})	Sulphur (S_{2P})	C_{1s} / N_{1s}
Binding Energy (eV)	284.0	530.0	399.0	167.0	
Untreated	73.8	13.8	9.9	2.4	7.5
Plasma Treated	54.2	26.9	15.3	2.6	3.5

Vila ve diğ. [15], yerba mate boyası ile boyanmış ipek kumaşların yüzey modifikasyonu için dielektrik bariyer deşarjı (DBD) plazma muamelesi üzerinde çalışmıştır. Temas açısı ölçümlerinin sonuçları, modifiye kumaşta hidrofilikliğin plazma işlemi ile arttırıldığını göstermiştir. Tablo 2, 6000 W dak m^{-2}'nin dozajının, hidrofilikliği arttırmada en etkili olduğu statik temas açısı için sonuçları göstermektedir, çünkü açının 2350°'ye önemli bir düşüşünü sağlamıştır.

Tablo 9. Statik temas açısı

	No treated	**2000 W min m^{-2}**	**4000 W min m^{-2}**	**6000 W min m^{-2}**	**Degummed**
Static contact angle	141.38°	105.46°	102.96°	23.50°	104.62°

Hidrofobik İşlevselleştirme

Suya dayanıklı kumaşların üretimi uzun zamandır çok sayıda araştırmayı çeken ilginç bir konudur. Plazma işlemi, nefes alabilirlik gibi kumaşın orijinal özelliklerini önemli ölçüde etkilemeyen ancak yüzeye çok düşük bir yüzey enerjisi kazandıran hidrofobik bir kaplama oluşturmak için kullanılabilir, bu, kumaşı su geçirmez veya kir tutmaz hale getirmektedir [3].

Tsoi ve diğ. [6], atmosferik basınçlı oksijen plazmanın yaşlanma etkisini kullanarak pamuklu dokuma kumaşın hidrofobik modifikasyonunu indüklediğini göstermiştir. Fourier Transform Infrared Spectroskopi çalışmaları, yaşlanma üzerine, polimer yüzeyinde hidrofobik alifatik hidrokarbonların oluşmasıyla yüzey polaritesinin tersine döndüğünü ortaya koymuştur. Ayrıca, oksijen plazma modifiye pamuklu kumaşın ticari su itici ajanlara benzer bir dereceye ulaştığını da bulmuşlardır. Görüldüğü gibi, (Tablo 3), kontrol kumaşı ve plazma ile işlenmiş pamuklu kumaşların su iticilik derecelerini göstermektedir. Yazarlar, oksijen plazma işleminin, pamuklu ürünlere çevre dostu bir şekilde hidrofobiklik kazandırmanın alternatif bir yolunu sağlayabileceği sonucuna varmışlardır.

Tablo 10. Su iticilik derecelendirme

Sample	Rating
Control	0
O_2-plasma treated (under optimum condition)	90
Water repellent agent finished	90

Parida ve diğ. [8], atmosferik basınçtaki stiren / helyum glow plazmanın sert yıkama işleminden sonra bile pamuk tekstil kumaşına dayanıklı hidrofobik işlevsellik kazandırabileceğini göstermiştir. Bu durum, stiren parçaları ve pamuklu kumaşın selüloz molekülleri arasındaki doğrudan kimyasal reaksiyona bağlanmıştır. Ayrıca, yüksek derecede hidrofobiklik elde etmek için stirenin parçalanma

derecesini kontrol etmek için daha düşük frekans ve daha düşük deşarj voltajının gerekli olduğu bulunmuştur.

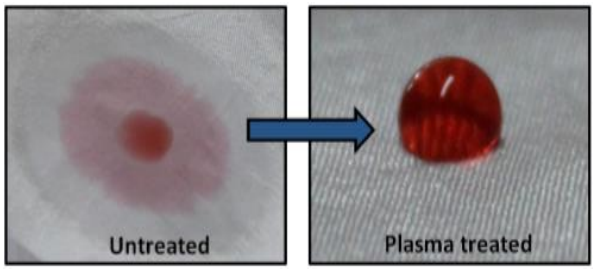

Şekil 2. Hidrofilik ipeğin plazma işlemiyle hidrofobik ipeğe dönüştürülmesi

Kale ve diğ. [12], atmosferik basınç plazma ile güçlendirilmiş hekzametildisiloksan (HMDSO) kimyasal buhar biriktirme özelliğine sahip pamuk ve polyester kumaşlara iyi su itici özelliklerin verildiğini bildirmiştir. Püskürtme derecesi, suyla ıslanmaya karşı iyi direnç gösterir. Yazarlar, HMDSO plazma polimerize ince filmlerinin, giyim ve ev eşyası tekstillerinde hidrofobik kaplamalar gibi çok sayıda uygulama için kullanılabileceği sonucuna varmıştır. Benzer şekilde Vinisha ve diğ. [13], plazma ile polimerize edilmiş (pp) HMDSO birikiminin, ipeğin hidrofobik yapısını önemli ölçüde arttırdığını vurgulamıştır. Kaplama süresinin ve gücün HMDSO kaplı ipek kumaşlar üzerindeki etkileri araştırılmıştır. Pp-HMDSO kaplı ipek kumaş yüzeyinin su temas açısı, güç ve kaplama zamanının bir fonksiyonu olarak ölçülmektedir. Kumaş yüzeyi, kaplamadan sonra hidrofobiklikte bir gelişme göstermektedir. Kaplanmamış kumaş durumunda, su damlası hızlı bir şekilde emilir, HMDSO kaplı kumaş durumunda ise su damlası, maksimum 140 surface temas açısına sahip kumaş yüzeyinde kalmaktadır. Teli ve diğ. [14], atmosferik basınç helyum-flüorokarbon (He-FC) plazma işleminin, Dut ipeğinin hidrofobik değişimini indükleyebildiğini göstermiştir (şekil 2). Bu sonuç, Taramalı elektron mikroskobu (SEM) tarafından ortaya konan fiber yüzeyinde florokarbon tabakasının birikmesine atfedilebileceğini göstermiştir (Şekil 3).

Yüzey Topografyasının Modifikasyonu

Tekstillerin yüzey kimyasını değiştirmenin yanı sıra, plazma işlemleri yüzey topografyasını değiştirebilmektedir. Bu, enerjik plazma türleri tarafından tekstil yüzeyinin balistik bombardımanından kaynaklanır ve bu da malzeme yüzeyinden moleküllerin ısıtılmasına ve / veya çıkarılmasına neden olabilmektedir [3].

Goud [7], yün dokuma kumaşı atmosferik hava DBD plazması ile işledi ve indüklenen yüzey morfolojisi değişikliklerinin plazma işleme parametrelerine bağlı olduğunu gözlemlemiştir. Aslında, aktif türün plazmadaki yünü substrat üzerine aşındırma etkisinin uygulanan voltaj ile doğru orantılı olduğu ve elektrodlar arası boşluk ile ters orantılı olduğu bulunmuştur. Bu sonuç, elektrot aralığının azalması ve / veya elektrot boyunca voltajın artmasıyla, aktif gaz türlerinin toplam gaz türüne oranının daha yüksek olacağı, böylece kumaşın yüzeyine yoğun bir işlem uygulanacağı ve böylece Daha yüksek pürüzlendirme ile sonuçlanmaktadır (Şekil 4). Boonla ve Saikrasun [20], hem oksijen hem de argon plazma işlemlerinin özellikle ipek lifi yüzeyini pürüzlendirdiğini ve indüklenen yüzey pürüzlülüğünün plazma işlem süresi ile arttığını keşfetmiştir.

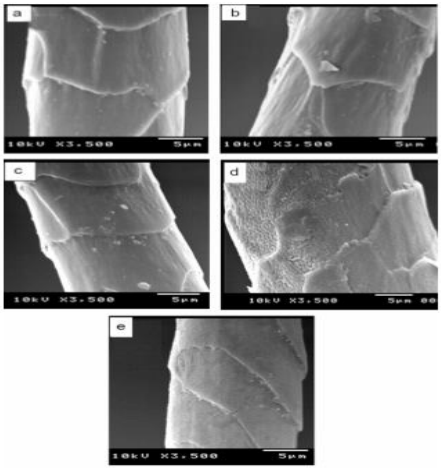

Şekil 4. Yün lifinin SEM görüntüleri (a) işlenmemiş yün, (b) 2 mm aralıklı 4.0 kV'da plazma işlemi, (c) 4 mm aralıklı 4.0 kV'da plazma işlemi, (d) 2 mm aralıklı 5.5 kV'da plazma işlemi, ve (e) 4 mm aralıklı 5.5 kV'da plazma işlemi

Bhat ve diğ. [5], gri pamuklu kumaşlara, atmosferik hava DBD plazması ile hava ve helyum gazı karışımı işlem uygulamıştır. Yüzeydeki ağırlık kaybının Aşındırma etkisine bağlı olduğunu gözlemlediler. Aşındırmanın sonucu SEM kullanılarak yapılan yüzey gözlemiyle desteklenebilmektedir. Şekil 5'ten görülebilir, yüzey morfolojisinin plazma işleminden dolayı değiştiği görülmektedir. Şimdi, lifin yüzeyini hasarlı veya aşınmış gibi görünüyor. Bu, bazı maddelerin aşındırma yoluyla çıkarılmasından kaynaklanmaktadır.

Adezyon geliştirme

Plazma malzemeleri, ıslanabilirliğini ve yüzey pürüzlülüğünü arttırmak için etkili bir şekilde kullanılabilmektedir. Bu potansiyel etkiler, yüzey işleme olmadan kullanılamayan tekstil substratları ve adezyon arasındaki yapışmayı ve böylece iyileştirilmiş malzeme özelliklerine yol açmaktadır [3].

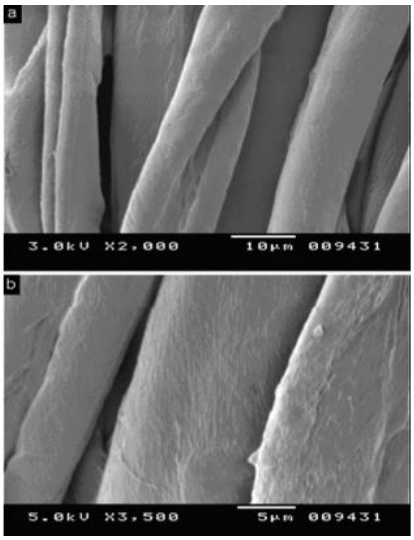

Şekil 5. Pamuklu kumaşın yüzey morfolojisi a) işlenmemiş b) plazma ile işlenmiş

Oliveira ve diğ. [16], hava DBD plazması ile muamele edildikten sonra bir yün kumaşta bir dolgunun (padding) işlemi ile uygulanan faz değiştirme materyali (PCM) mikrokapsüllerinin yapışmasını incelemiştir. Plazma işleminin PCM mikrokapsüllerinin yün yıkama yüzeyine yapışmasını, hatta birkaç yıkama işleminden sonra bile arttırdığını bulmuşlardır. Yazarlar, DBD plazma işleminin, PCM mikrokapsülleriyle tamamlanan tekstil ürünlerinin fonksiyonel performansını arttırmak, daha dayanıklı özellikler elde etmek ve bu nedenle yenilikçi tekstillerin sürdürülebilirliğine katkıda bulunmak için mükemmel bir çözüm olarak kabul edilebileceği sonucuna varmıştır.

Vasiljevic ve diğ. [17], düşük basınçlı su buharı plazma ön işleminin, FAS kaplamanın yapışmasını arttıracak ve aynı zamanda yıkama dayanıklılığını arttıracak selüloz kabarcıkları üzerindeki etkili Fl üroalkilfonksiyonel siloksan (FAS) ağının etkin konsantrasyonunu arttırdığını bildirmiştir. Bozacı ve diğ. [19], ketenli kumaşlar ile yüksek yoğunluklu polietilen (HDPE) ve doymamış polyester arasındaki ara yüz yapışmasını iyileştirmek için çeşitli plazma güçleri altında argon ve hava atmosferik basınçlı plazma ile muamele edilmiş keten lifleri. Argon plazma ile muamele edilmiş keten liflerin ve HDPE matrisinin arayüzey yapışmasının, havayla muamele edilmiş ve muamele edilmemiş bal mumuna göre daha üstün olduğunu bulmuşlardır. Ayrıca, plazma gücü arttırılarak arayüzey adezyonu daha da arttırılmıştır. Bu sonuç, XPS ve SEM ölçümlerinde belirtildiği gibi pürüzlülüğün artması ve polar fonksiyonel grupların ketenli yüzeylere sokulması ile ilişkilendirilebilmektedir. Naebe ve diğ. [10], yün kumaşın Atmosferik plazma işleminin, SPM analizi ile ölçülen daha fazla pürüzlülük ve yapışma ile kumaş ve liflerin ıslanabilirliğinin artmasına neden olduğunu bulmuşlardır. SPM yapışma çalışmaları, her bir lifin farklı kısımlarında alınan ölçümlerden değerlendirildiği gibi, hem plazma ile muamele edilmiş liflerde hem de muamele edilmemiş kontrol liflerirnde önemli farklılıklar göstermiştir. Bununla birlikte, plazma ile muamele edilmiş lifin ortalama yapışması muamele edilmemiş lifinkinden önemli ölçüde daha yüksekti. Tablo 4, 24 saat şartlandırmadan sonra işlemden geçirilmemiş bir lif ve bir plazma işlem görmüş lif üzerindeki altı farklı alan için ortalama yapışma değerlerinin değişimini göstermektedir. Bhushan ve Jung'a göre [18], elde edilen daha yüksek su afinitesi, prob ucu ile lif numunesi arasında bir su köprüsü oluşma olasılığını arttırmaktadır, artmış menisküs kuvveti, uç ve numune arasında daha fazla yapışmaya neden olmaktadır. Ek olarak, daha yüksek su afinitesinin uç ve numune arasındaki gerçek temas alanını etkilemesi muhtemeldir ve yapışmayı daha da arttırmaktadır.

Tablo 11. İşlemden geçirilmemiş ve plazma ile muamele edilmiş lifleri ortalama yapışma değerleri (her lifin yüzeyinin altı farklı parçasından alınmıştır)

Sample	Area						Mean	STDEV
	1	2	3	4	5	6		
Untreated	83.3	37.1	81.2	37.8	84.2	76.3	66.7	22.8
Plasma Treated	127.3	146.7	135.8	146.1	156.2	121.8	133.8	13.0

Boyama ve baskı özelliklerinin iyileştirilmesi

Tekstil ıslak işleminde bir ön işlem olarak plazmanın uygulanması, tekstil malzemelerinin boyama ve baskı özelliklerini avantajlı bir şekilde geliştirebilmektedir. Bu sayede ıslatılabilirlik ve kılcallık iyileştirmesi, yüzey alanının arttırılması, yüzeylerdeki reaktif yerlerin oluşturulması ve diğer pek çok işlem, plazma çalışma koşullarına bağlı olarak en önemli etkiye katkıda bulunabilmektedir [3].

Boonla ve Saikrasun [20], ipekle lak boyamanın adsorpsiyon kinetiği ve termodinamiği üzerindeki plazma ile muamele edilmiş ipek yüzeylerinin etkisini incelemiştirler. İpek yüzeylerinin oksijen ve argon plazması kullanılarak işlenmesi, esas olarak, amid-II rasgele bobinden amid-I b-tabaka yapısına olan konformasyon değişikliğini göstermiştir. İpek yüzeyleri özellikle oksijen ve argon plazma işlemleriyle pürüzlendirildi ve artan plazma işlem süresi ile yüzey pürüzlülüğünün arttığı bulunmuştur.

Dengede adsorbe edilen boya miktarına dayanarak, adsorpsiyon kapasitesi, plazma ile ön işlemden geçirilmiş numuneler için çok geliştirilmiştir ve ipek üzerinde lak boyama için adsorpsiyon kapasitesinin en iyi şekilde Ar-muamele edilmiş ipek numunesi kullanılarak bulunmuştur (şekil6).

Chvalinova ve Wiener [21], atmosferik basınçta difüzif düzlemsel yüzey bariyeri dşarj plazmasının (DCSBD), yün kumaşların asit boya absorpsiyonu miktarını arttırdığını ve daha iyi boyanabilirlik ve basılabilirliğe yol açtığını göstermiştir. Yazarlar, yünün plazma işleminin gelecekte yün boyama ve baskı için ıslak ön işlem işlemlerinin yerini alabileceği sonucuna varmıştır. Ratnapandian ve diğ. [22], Acacia bitki ailesinden elde edilen doğal boyaların yün üzerine sürekli uygulanması için plazma işleminin ve dolgunun (padding) uygulanabilir bir kombinasyon olduğunu vurgulamıştır.

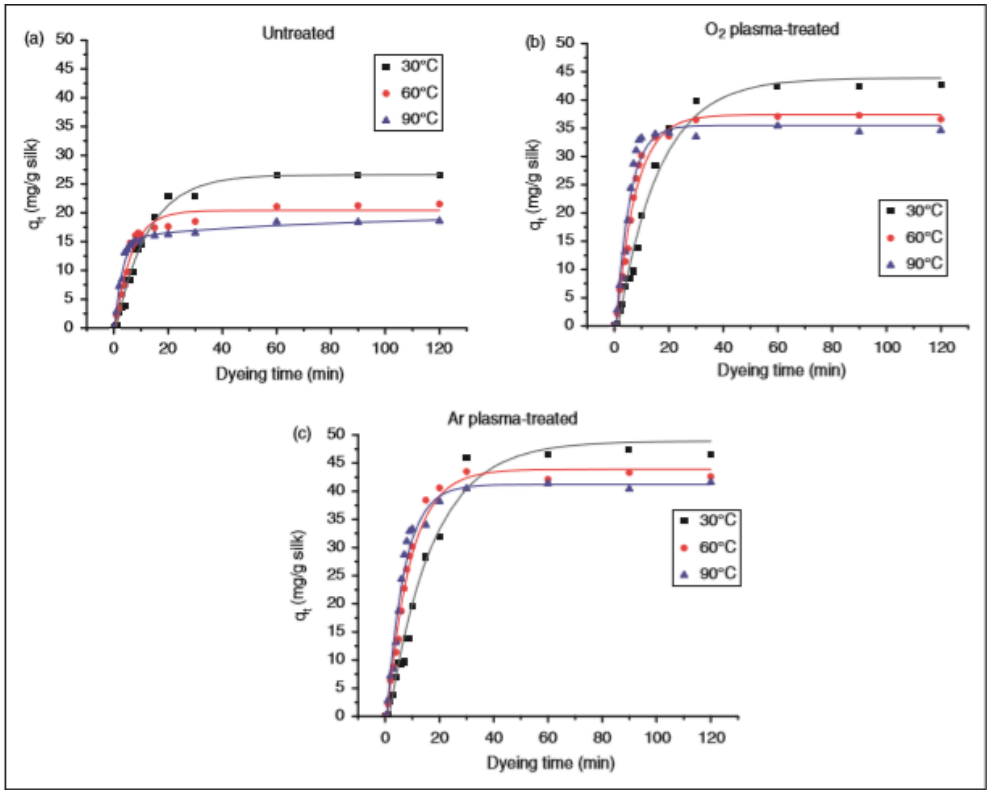

Şekil 6. Boyama (temas) süresinin lak boyanın muamele edilmemiş ipek (a), O2 plazma ile muamele edilmiş ipek (b) ve Ar plazma ile muamele edilmiş ipek (c) üzerine 30, 60 ve 90 ° C'deki (boyama koşulları: C0 500¼Ì mg / 1, malzemeler-likör oranı 100 :1¼Ì, pH 3.0¼Ì

Aslında, kullanılan helyum ve helyum/azot (% 95/5) gazları için muamele edilmemiş numuneye kıyasla, plazma ile muamele edilmiş yün substratı üzerinde% 30'a kadar boya emiliminde artış gözlenmiştir. Geliştirilmiş boya alımı, plazma işlemiyle uzun süreli yüzey değiştirmesine (aşındırma) bağlanmıştır. Aynı zamanda, boyanmış plazma ile muamele edilmiş numunelerin yıkama, sürtünme ve ışık haslığı, iyi haslık derecelerine adil bir şekilde vererek değerlendirilmiştir.

Özel Fonksiyonlar Kazandırma

Farklı tipteki plazma gazları ile plazma işlemi, antimikrobiyal, keçeleşmezlik, kendi kendini temizleme işlevi, UV koruma, alevlenmeyi geciktirci gibi tekstil malzemelerine özel fonksiyonlar kazandırabilmektedir. Bu etkiler mikro yüzeyde yüzey modifikasyonları ile tekstillerin hacim özelliklerini etkilemeden sağlanmaktadır [3].

Antibakteriyel Etkisi

Muller ve diğ. [23], pamuklu kumaşların dielektrik bariyer deşarjlarıyla dezenfekte edilmesini incelemiş ve bazı örneklerde mikroorganizma popülasyonunda belirgin bir azalma olduğunu gözlemlemiştir. Sterilizasyona ek olarak, plazma işlemleri ayrıca antimikrobiyal ve antibakteriyel işlevler sağlayabilir veya antimikrobiyal terbiye işlemlerinde yardımcı olabilir. Yazarlar, teklif edilen DBD konfigürasyonlarının ve yöntemlerinin nispeten basit tasarımlarının, onlara açıklanan uygulama alanlarındaki geleneksel temizleme yöntemlerini değiştirme potansiyeli sağladığı sonucuna varmıştır. Su tüketiminden tasarruf etmek ve deterjan kullanmadan tekstil temizleme prosedürü geliştirmek yardımcı olabilir. Palaskar ve diğ. [24], ped-kurutma yöntemiyle nano TiO2 / SiO2 içeren atmosferik basınç plazması ile pamuklu kumaşın çok fonksiyonlu bir şekilde işlenmesinin, mükemmel antibakteriyel özellikler kazandırmasına ve pamuklu kumaşa kolayca bakılmasına yol açtığını göstermiştir. İşlemden geçirilmemiş bakteri ve nano $Ti0_2$ ile işlenmiş numune üzerinde bakteri kullanmıştırlar. Tablo 5'teki sonuçlara göre, plazma ve nano TiO_2 ile işlenmiş numunenin, hem gram-pozitif hem de gram-negatif bakterilere karşı mükemmel antibakteriyel aktiviteye sahip olduğunu ve

plazma ön aktivasyonu ile %0.5 nano $Ti0_2$ ile %100'e ulaşabileceğini göstermektedir. Bu nedenle, plazma işleminin tekstil malzemesinin işlevsel özelliklerini arttırdığı ve etkili işlem için daha az kimyasal gerektirdiği sonucuna varılabimektadir.

Tablo 12. Antibakteriyel test sonuçları

Sample	% Reduction	
	S. aureus	*K. pneumonia*
Control cotton	No reduction	No reduction
TiO_2 0.5% without plasma	43.85	44.54
TiO_2 0.5% plasma	99.95	99.96
TiO_2 1% without plasma	96.24	99.56
TiO_2 1% plasma	99.99	99.99

Güç Tutuşurluk

Shahidi [25], nanoclay işleminin ardından azot plazma işleminin, pamuklu kumaşın alev geciktirici özelliklerini arttırdığını vurgulamıştır. Aslında, N_2 plazma/nanoclay ile muamele edilmiş pamuk için kömür verim değerinin, tam yanmadan sonra %12'ye çıktığı bulunmuştur (Tablo 6). LOI (Sınırlı Oksijen İndeksi) değerleri için de benzer gelişmeler sağlanmıştır. Muamele edilen numunelerin geliştirilmiş alev geciktiriciliği, alev oluşumuyla pamuklu kumaşlar arasında ısı, enerji ve O2 iletimini engelleyebilecek char oluşumunu ilerletmek için daha önce Nanoclay'ın ayrışmasına bağlanmıştır. Palaskar ve diğ. [24], He-O_2 plazma ön işleme tabi tutulmuş pamuklu kumaşta TiO_2 / SiO_2 nanokompozit kullanılmasının, alev geciktiriciliğini yeterince geliştirdiğini ve numunelerin ısıl stabilitesinin işlenmemiş numunelerle karşılaştırıldığını vurgulamıştır.

Tablo 13. Char verimi ve muamele edilmemiş, nanoclay ile muamele edilmiş, plazma ile muamele edilmiş, plazma / nanoclay ile muamele edilmiş numunelerin LOI değerleri

Sample	LOI	Char yield (%)
Untreated	18.5	1.9
Nanoclay treated	22.5	10.21
N_2 plasma treated	21.8	8.7
N_2 plasma/nanoclay treated	23.5	12

Sonuç

Atmosferik basınç plazma işlemi tekstil yüzeylerini çeşitli şekillerde uyglanabilmektedir ve tekstil yüzeyine istenen fonksiyonel özellikleri kazandırabilmektedir. Örneğin, tekstilin plazma ile işlenmesi ıslanabilirliği, boyanabilirliği, hidrofilikliği, adezyon geliştirebilir ve tekstil maddelerine özel işlevler kazandırması sağlayabilmektedir. Plazma işlemesiyle tekstilin özel özelliklerini etkilemeden kimyasal, fiziksel ve morfolojik değişiklikler meydana getirmektedir. Plazma işlemi, kuru ve çevre dostu bir işlem olmanın eşsiz avantajlarını sunmaktadır.

Kaynaklar

[1] Kale HK, Desai AN. (2010) Atmospheric pressure plasma treatment of textiles using non-polymerising gases, Indian Journal of Fibre and Textile Research 36(3):289-299.
[2] Freudenberg Forschungsdienste KG web sitesi, erişim 3 Aralık 2018.
[3] Abd Jelil R. (2015) A review of low-temperature plasma treatment of textile materials, J Mater Sci, 50:5913–5943.
[4] Buyle G. (2009) Nanoscale finishing of textiles via plasma treatment, Materials Technology, 24(1):46-51.

[5] Bhat NV, Bharati RN, Gore AV. (2011) Effect of atmospheric pressure air plasma treatment on desizing and wettability of cotton fabrics, Indian J Fiber Text Res, 36:42–46.
[6] Tsoi WYI, Kan CW, Yuan CWM. (2011) Using ageing effect for hydrophobic modification of cotton fabric with atmospheric pressure plasma, BioResources, 6:3424–3439.
[7] Goud VS. (2012) Influence of plasma processing parameters on mechanical properties of wool fabrics Indian Journal of Fibre & Textile Research, 37:292–298.
[8] Parida D, Jassal M, Argawal AK. (2012) Functionalization of cotton by in situ reaction of styrene in atmospheric pressure plasma zone, Plasma Chem Plasma Process, 32:1259–1274.
[9] Lam Y, Kan C, Yuen C. (2011), Physical and chemical analysis of plasma-treated cotton fabric subjected to wrinkle-resistant finishing, Cellulose, 18:493–503.
[10] Naebe M, Denning R, Huson M, Cookson G, Wang XP. (2011) Ageing effect of plasma treated wool , Journal of the Textile Institute, 102(12):1086-1093.
[11] Xu H, Peng S, Wang C, et al. (2009) Influence of absorbed moisture on antifelting property of wool treated with atmospheric pressure plasma, J Appl Polym Sci, 113:3687–3692.
[12] Kale KH, Palaskar SS, Kasliwal PM. (2012) A novel approach for functionalization of polyester and cotton textiles with continuous online deposition of plasma polymers, Indian Journal of Fibre & Textile Research, 37:238–244.
[13] Vinisha Rani K, Chandwani N, Kikani P, Nema SK, Kumar Sarma A, Sarma B. (2018) Hydrophobic surface modification of silk fabric using plasma-polymerized HMDSO, Surface Review and Letters, 25(2).
[14] Teli MD, Kartick Samanta K, Pandit P, Basak S, Gayatri TN. (2015), Hydrophobic Silk Fabric using Atmospheric Pressure Plasma, International Journal of Bioresource Science, 2(1).
[15] Vila NT, Ferreira A, Silva M, Fernandes M, Fiori S. (2017) Surface Modification of Silk by (DBD) Dielectric Barrier Discharge Treatment for Dyeing with Natural Dye Yerba Mate, Elsevier, Procedia Engineering, 200: 170–177.
[16] Oliveira FR, Fernandes M, Carneiro, N. et al (2013) Functionalization of wool fabric with phase-change materials microcapsules after plasma surface modification, J Appl Polym Sci 128:2638–2647.
[17] Vasiljevic J, Gorjanc M, Tomsic, B. et al (2013) The surface modification of cellulose fibres to create super-hydrophobic, oleophobic and self-cleaning properties, Cellulose, 20:277–289.
[18] Bhushan B, Jung YC. (2008) Wetting, adhesion and friction of superhydrophobic and hydrophilic leaves and fabricated micro/nanopatterned surfaces, Journal of Physics: Condensed Matter, 20:1-24.
[19] Bozacı E, Sever K, Sarıkanat M. et al (2013) Effects of the atmospheric plasma treatments on surface and mechanical properties of flax fiber and adhesion between fiber–matrix for composite materials, Compos Part B 45:565–572.
[20] Boonla K, Saikrasun S. (2013) Influence of silk surface modification on via plasma treatments on adsorption kinetics of lac dyeing on silk, Textile Research Journal, 83:288–297.
[21] Chvalinova R, Wiener J. (2008) Sorption Properties of wool fibers after plasma treatment, Chem Listy, 102:1473–1477.
[22] Ratnapandian S, Wang L. (2011) Effect of atmospheric plasma treatment on pad-dyeing of natural dyes on wool, Journal of Fiber Bioengineering and Informatics, 4:267–276.
[23] Muller S, Zahn RJ, Koburger T. et al (2010) Smell reduction and disinfection of textile materials by dielectric barrier discharges, Natural Science Journal, 2:1044–1048.
[24] Palaskar SS, Desai AN, Shukla SR. (2016) Development of multifunctional cotton fabric using atmospheric pressure plasma and nano-finishing, The Journal of The Textile Institute, 107:3, 405-412.
[25] Shahidi S. (2014) Novel method for ultraviolet protection and flame retardancy of cotton fabrics by low-temperature plasma, Cellulose 21:757–768.

The Contribution of Riparian Zone on Urban Ecosystems through Climate Change Urban Adaptation Process

Hande Gündel[1], Ayşe Kalaycı Önaç[2]*
Izmir Katip Çelebi University, Engineering and Architecture Faculty, Department of Urban Regeneration, Izmir, Turkey
Izmir Katip Çelebi University, Engineering and Architecture Faculty, Department of City and Regional Planning, Izmir, Turkey
**Corresponding author: handegundel9@gmail.com*

Abstract

The riparian zone plays a crucial role in the development and transformation of cities. This zone dramatically changes cities both ecologically and economically and is one of the cornerstones of the future scenarios of the city. These areas constitute significant emphasis throughout the city by providing wildlife, improving the water quality, reducing flood areas, and creating social activity areas in the city. Besides, it influences land use, transportation, energy efficiency, social life. The riparian zones are one of the most significant components of the cities that mitigate the climate change effects. Because, the existence of water creates microclimatic conditions around the cities and this conserves the heat island effect, greenhouse effect, and also air pollution. The deterioration of the sustainability of this important backbone throughout the city causes an important loss in terms of urban ecosystems. Because it is an important connection of natural life and urban life, and any deterioration causes two important characters to be separated from one another. In this regard, ensuring water management in the city is a crucial issue in terms of urban habitat. In the scope of this study, research was conducted on the contribution of riparian zone to the urban ecosystem and also how the presence of this backbone system in the city transforms the urban areas was discussed.

Keywords: riparian zone, urban ecosystem, climate change

Introduction

The Concept of Riparian

Riparian comes from the term 'Riparius'. The word of Riparian consists of the Latin 'ripa', shore or bank, and significant ecological systems, natural, societal, and ecosystem services. Biotic communities on the shores of streams and lakes are indicated the term 'Riparian' (Naiman & D´ecamps, 1997). These areas provide a rich kind of services to the environment and humans and also their unique characteristics are related to water, soil, and vegetation. Their waterbodies support to increase the levels of soil moisture and thus, it leads to unique vegetation assemblages (Iakovoglou, Zaimes, & Gounaridis, 2014). Therefore, riparian zones are defined as interfaces between aquatic ecosystems and terrestrial landscapes. Riparian vegetation performs support opportunities for ecological functions such as the provision of habitat and food for many species, regulation of shade and water temperature, control of nutrient and sediment input into streams, provision of corridors for the movement of biota, and stabilization of riverbanks (Pascacio, Argueta, Castillo-Uzcanga, & Ramírez-Marcial, 2018). Besides, this zone plays a crucial role in the ecological balance of a riparian area. The riparian area can be defined as a traditional semiterrestrial zone extending from the edges of water bodies to the edges of upland communities and regularly interacts with river water, flow alterations, sediment, and nutrients (Baniya, et al., 2019) and also it forms a corridor between land and water permitting animals to travel among different biomes. The effective riparian zone involves very kind of plant species, aquatic and terrestrial wildlife. It also provides to maintain water levels, temperatures and prevents erosion (Figure 1) (Watersheds Canada, 2016).

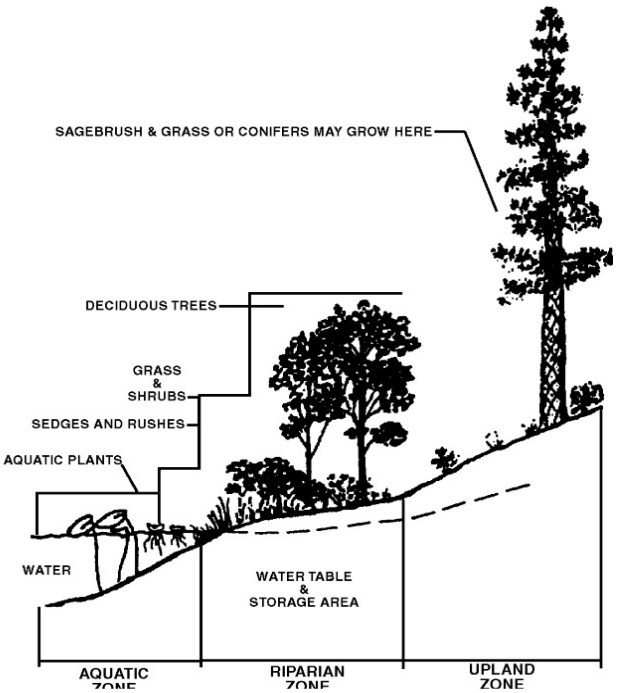

Figure 8. Riparian Zone defined

Up to now, riparian zones have been scrutinized from different perspectives based on hydrologic, topographic, edaphic, and vegetative criteria. Generally, riparian classification systems stay focused on a few selected attributes of riparian areas, such as hydric soil or hydrophilic plant associations (Gregor, Swanson, M cKee, & Cummins, 1991). In addition, these zones benefit humans as an ecosystem service. They provide flood protection, chemical runoff uptake, and associated improvements to water quality, and create recreation, shade, and green space in urbanized areas. This zone can support more water and chemical runoff that can be taken by younger forests, sparsely treed forests, shrubs, or grasslands. When the riparian area enhances the stream ecosystem by supporting linear terrestrial habitat for wildlife, and also, riparian vegetation stabilizes stream banks and limits erosion and transport of sediment in the waterbody (Figure 2). This corridor develops the stream ecosystem with organic matter for ecological production, canopy production, and decreasing the fluctuation in water temperature and light levels (Weilert, 2018).

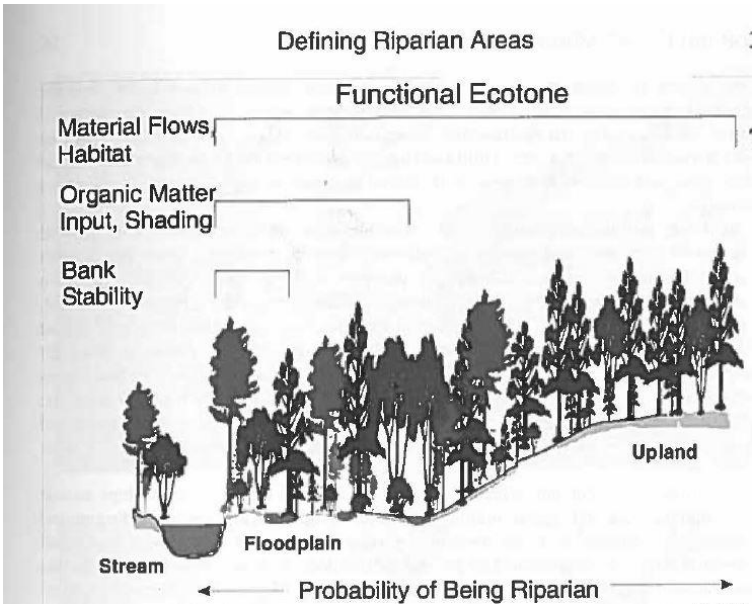

Figure 9. The functions of Riparian Zone

The value of Riparian Areas

Riparian areas enhance streambank, channel, shoreline stability, water quality, and stream temperature. They support crucial habitats for many species of mammals, birds, reptiles, fish, amphibians, and insects. Besides, they include water storage and preservation, nutrient and food input to the aquatic system

These areas play a significant role in recreation, tourism, forest products, hunting, biological diversity, fishing (Figure 3) (North Central Region Forest Management Guide, 2006).

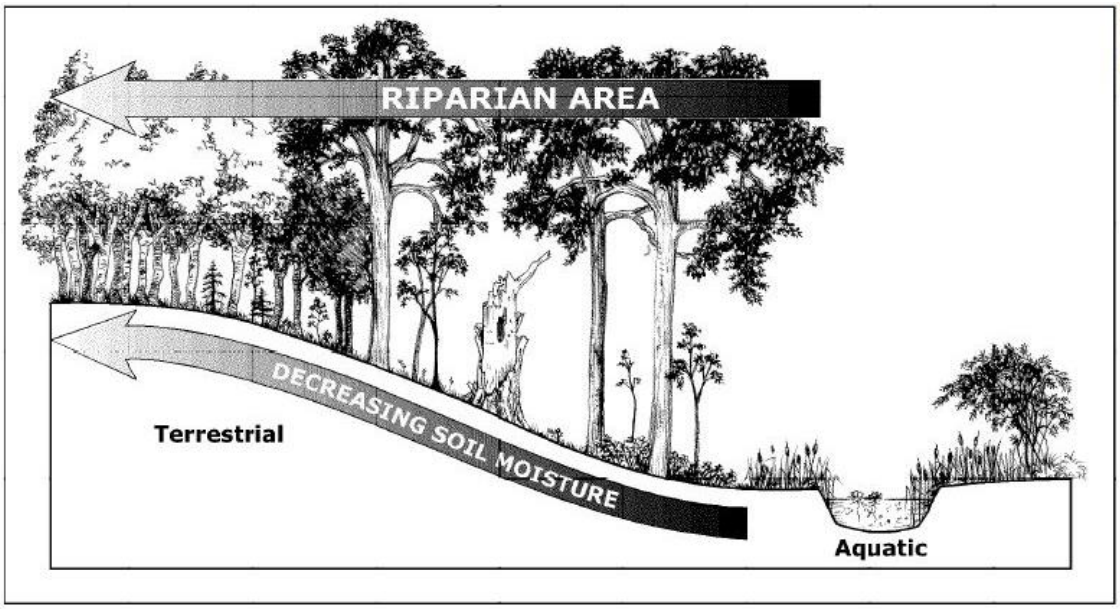

Figure 10. Transition from Aquatic to Terrestrial habitat in a Riparian Area

Riparian Zone and Climate Change

The phenomenon of climate change alters drastically natural resource management. It is observed to lead to augmented frequency and severity of extreme weather events, and also it causes severe floods and more intense droughts. Besides, this phenomenon leads to higher air temperatures and, higher surface water temperature. It alters hydrological regimes and causes extreme flooding events, as a result, changed seasonal patterns of precipitation and run-off. (Seavy, et al., 2009). Changes in sulfate aerosol emissions and greenhouse gas like carbon dioxide are related to future population growth, socio-economic development, energy sources, and technological progress. Because of climate change, carbon dioxide concentrations increase in the atmosphere, changes in air temperature affect water temperature, and also, air temperature influences the timing of key hydrological events and the amount of prescription falling as rain and snow (Tillmann & Siemann, 2011). Both the biological and physical compositions can be affected by excessive water and insufficient flows due to climate change. Until now, it has been observed riparian ecosystems such as river flow, snowpacks, temperature have been influenced because of this problem. Drought causes a decrease in the ability of plants to photosynthesize and reduce enough moisture for germination or the seasonal flooding required by flood-adapted species like cottonwood. Besides, the deficiency of seasonal flooding and groundwater level influences negatively cottonwood reproduction and establishment. In addition, these, drought also affects native riparian species (Figure 4) (Poff, Koestner, Neary, & Henderson, 2011).

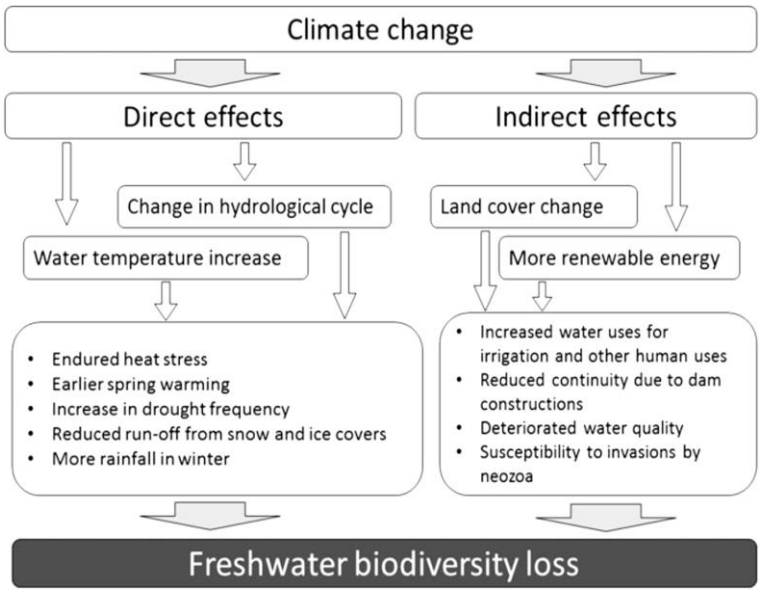

Figure 11. Direct and indirect climate change effects on freshwater biodiversity in rivers

Climate is a crucial driver for ecosystem processes; indeed, freshwater ecosystems as thermal and hydrological regimes are connected to climate. Therefore, heat exchange and atmospheric energy fluxes directly affect river water temperature, and also it is one of the most significant factors in the chemo-physical environment of aquatic organisms. In addition, runoff through the amount and type of precipitation is affected by climate and temperature. The results of future climate change in freshwater ecosystems are linked to the rate and magnitude of change both imply absolute change and the increasing variation among extremes (Pletterbauer, Melcher, & Graf, 2018).

Most riparian plants can be adapted to geomorphic disturbances, hydrologic, and tolerate not only seasonal but also annual variation in environmental conditions. Therefore, riparian species might be more resilient to the augmented flooding and drought regions. Besides, for the preservation of biodiversity from climate change, connectivity in landscape planning and reserve design is very significant and popular advice. The phenomenon of connectivity is crucial for both the conservation of the ecological processes and evolutionary adaptations to climate change (Seavy, et al., 2009).

Riparian ecosystems involve ecological, socioeconomic, and cultural functions, and also, the most of functions are significant both locally and affect physical, chemical, and biological components and processes in the landscape. These functions contribute energy between neighbor aquatic and terrestrial ecosystems and the regulation of exchanges of materials. These systems include crucial habitat functions and augment the diversity of species pools at the regional scales. Restoration activities like riparian vegetation are the most important for decreasing building adaptive capacity and sensitivity, and also the aim of restoration is the protection, restitution, and enhancement of riparian ecosystem services and functions (for example, temperature regulation of instream habitats) (Capon, et al., 2013). Riparian systems play a critical role in climate change adaptation. Riparian inventions decrease directly warming, stressors, develop resilience by supporting habitat and energetic subsidies (Thomas, Griffiths, & Ormerod, 2016).

Case Studies on Riparian Systems

Urban riverfront landscapes play a significant role in the uniqueness of a city. For all waterfront landscapes, waterfront landscapes are charming, and also urban waterfront regions' planning and landscape design is the most studied in recent years. Besides, many design projects are studied (Song, 2013).

Chicago Riverfront Design

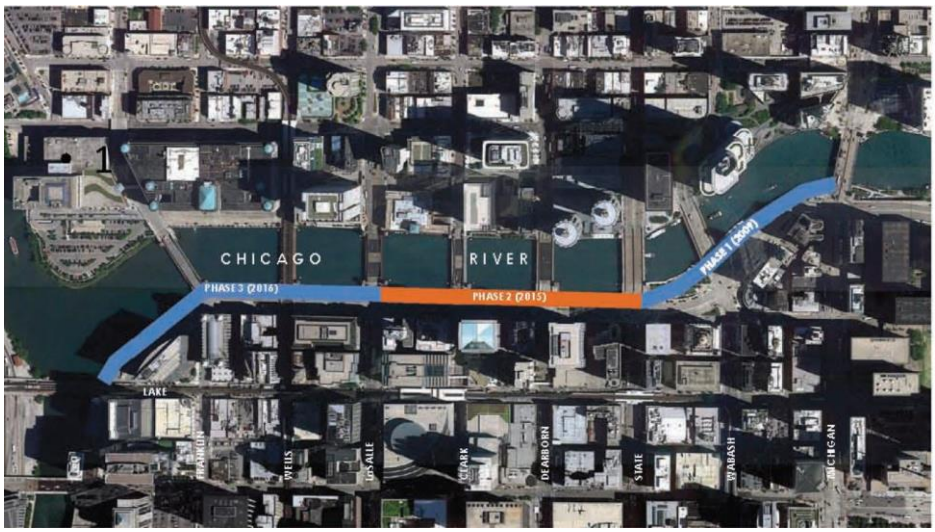

Figure 12. Chicago Riverwalk Project

Chicago's developments are related to trade through industrial and transportation in the 1800s and 1900s. In 1836, Chicago as a city was founded, and in these years, the Chicago River began to become contaminated due to industrial pollution and a sewage outlet. After the environmental movements in the 1960s and 1970s, storm and sewer systems were built. Water Reclamation District constructed the Deep Tunnel. In 1979, Friends of the Chicago River supported better environmental and people-friendly policies. With these developments, in the 1990s, various guidelines, plans, and studies were prepared and the department of Transportation of Chicago confirmed a plan which is related to the south bank to the US Department of Transportation's Volpe National Transportation Center (Figure 6). This plan covered a 25-foot extension in the river, the construction of under-bridges (Asla, 2015). This project was started by Mayor Richard Daley in 1998, and the planner, the project manager was Ms. Ferhat Zerin. All length of the river is about 30 miles from the north neighborhood to the industrial area to the south. The project involves many sections of the Riverwalk, parks, and plazas (Figure 5) (Ginkgo planning & design inc, 2015).

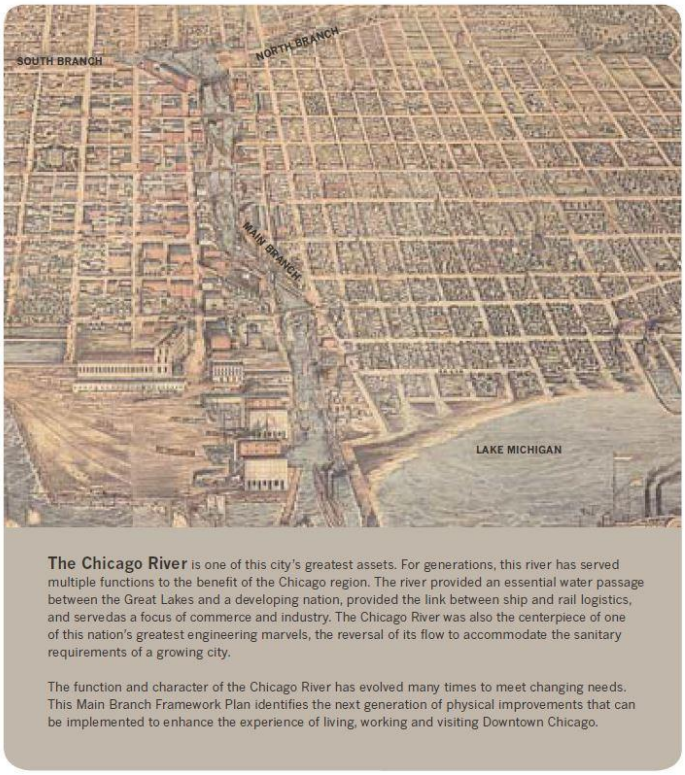

Figure 13. The history of Chicago River

The Chicago Riverwalk plays a significant role in the ecological, recreational, and economic benefits of the city. Phases two and three involve five blocks between State Street and Franklin Street, the plans cover a pedestrian connection along the river (Figure 7). This project develops downtown Chicago by giving visitors and residents of Chicago and also presents recreation and leisure in the heart of the city.

Figure 14. Pedestrian connection

The ecologically sensitive design aims to enhance water quality, enabling people to interact with the river, and also, the floating wetlands support a variety of habitats for aquatic life, besides, it provides children an outdoor classroom for learning about fauna, fish, and critters. Creating Park space contributes to a healthy and happy environment for all city dwellers (Rudy Bruner Award Project Data, 2017) (Figure 8).

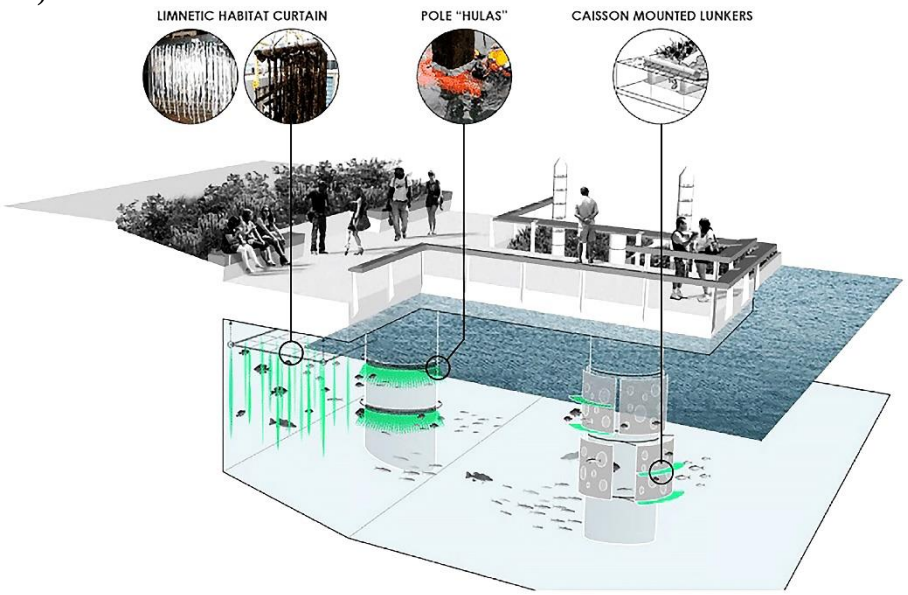

Figure 15. Underwater infrastructure

Los Angeles Riverfront Design

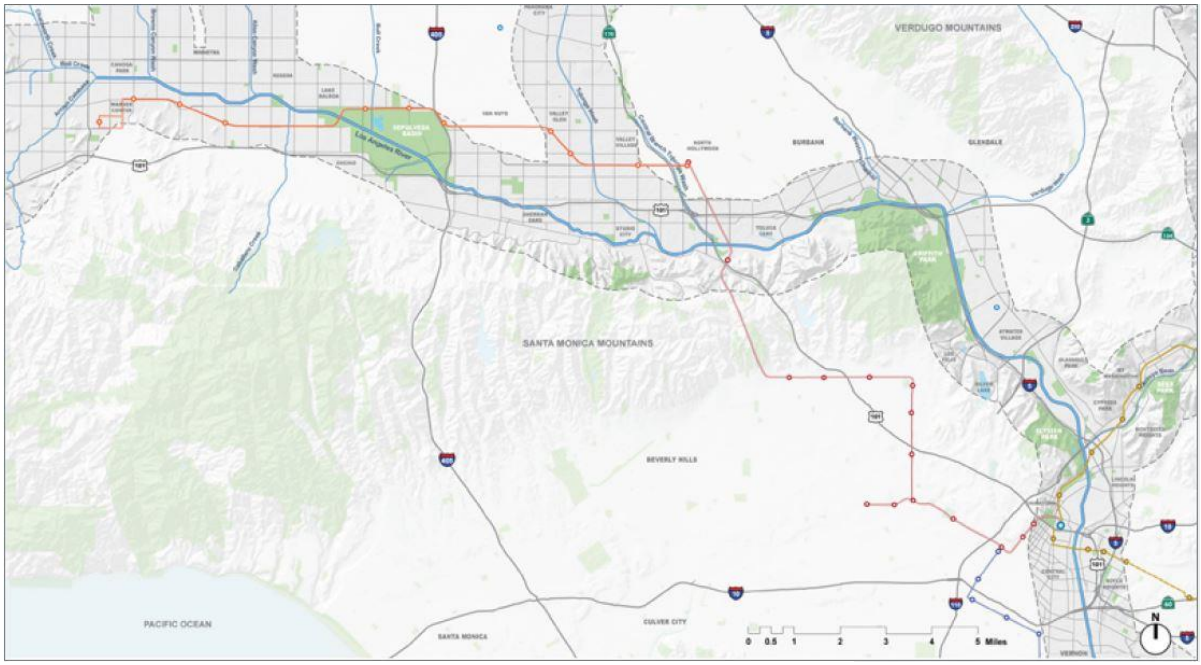

Figure 16. Los Angeles River

The Los Angeles River flows almost 51 miles is located in the San Fernando Valley region of the City of Los Angeles to Long Beach Harbor and the Pacific Ocean. The first 32 miles of the River is the intersection of 10 Council Districts, 20 Neighborhoods Councils, and 10 community planning areas. The project includes bridges, parks, bicycle paths, pedestrian trails, recreational amenities, public education, litter removal, job creation, community development, tourism, civic pride, water quality

(Figure 10-11). The Los Angeles River Revitalization Master Plan gives opportunities such as a renewal of the River's environmental qualities (Rebirth of the L. A. River, 2006).

Water preservation is one of the crucial activities for the Los Angeles County Department of Public Works. The county's policy aims to protect the winter stormwater runoff possible, considering the runoff quantity and quality, capacities of spreading groundwater conditions, geologic, and grounds (Los Angeles County Flood Control District, 2004). The widths and heights of the Los Angeles River system cover flood control. The public row in the Los Angeles River involves the channel and adjacent land, also these Row widths permit flood control maintenance personnel and vehicles to access the channel (Los Angeles County Public Service that Works, 2004) (Figure 12).

Figure 17. Riverfront design

Figure 18. Social activities

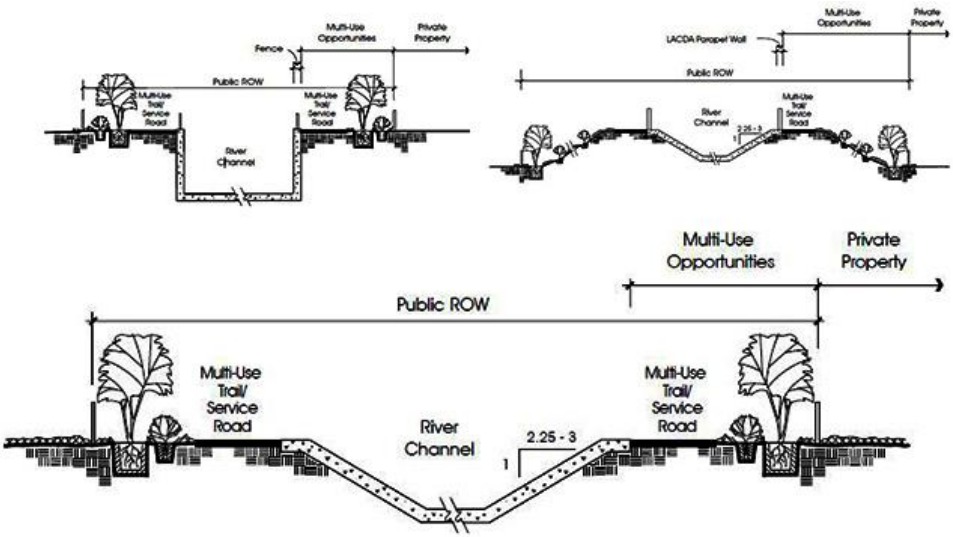

Figure 19. Channel diagram

The Guadalupe River Project

There is a long history of winter flooding in this river. In recent years, economic investments have started to increase drastically for flood protection, coupled with the community's desire for open space. The Flood control project was completed in 2004 in San Jose, and also this project presents recreational amenities to the local community, ecologic sound system, and habitat restoration (Figure 13) (Otto, McCormick, & Leccese, 2004).

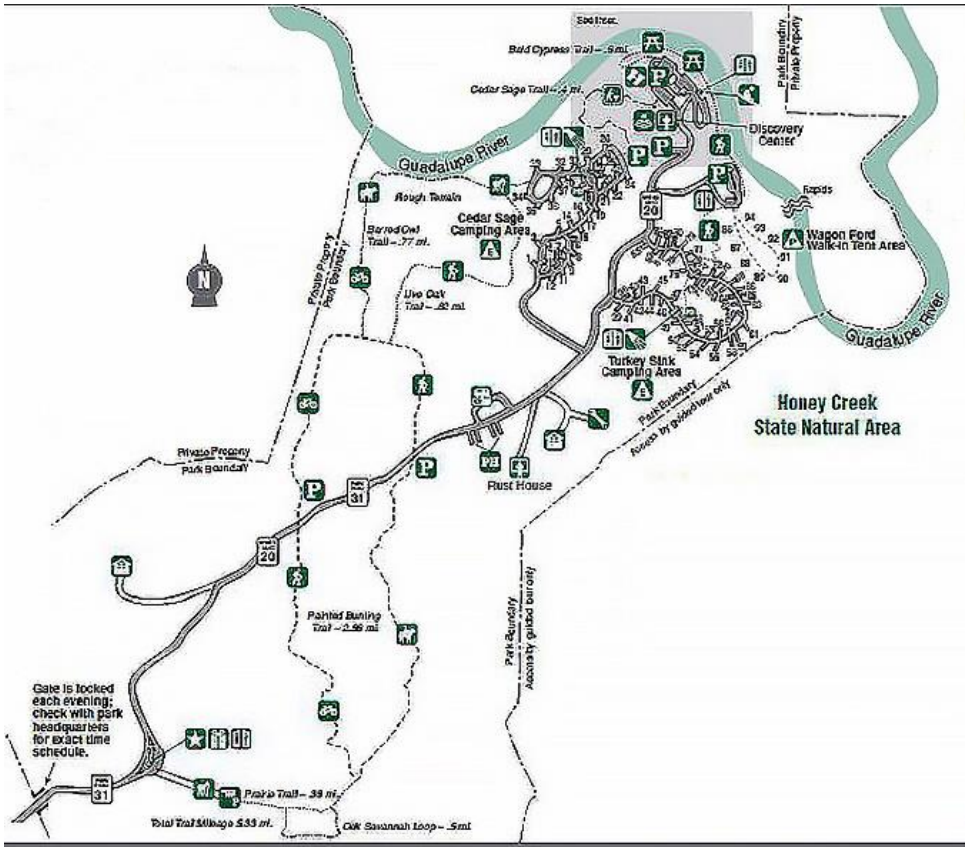

Figure 20. The Guadalupe River Project

According to Molina-Navarro et. all (2015), this project aims to reduce the climate change effect, and therefore, the river will decrease the climate change effect by around -%45 in the short term and -%60 in the long term. Besides, the river protects native fish habitat, native species, and maintains a natural riparian corridor (Figure 14) (Otto, McCormick, & Leccese, 2004).

Figure 21. The Guadalupe River Project

Conclusion

Climate change causes the demonstration of hydrologic, ecologic balance in the whole urban area. Besides, it brings about sea-level rise, flood risk, heat island in the earth surface, and accordingly, environmental, social, and economic conditions start to be influenced dramatically. Greenhouse gas emissions such as carbon dioxide, methane, nitrogen dioxide, hydrofluorocarbons, perfluorocarbons, sulfur hexafluoride started to accumulate in the atmosphere, fossil fuels, changes in land use,

deforestation caused the problem of climate change. (T.C Çevre ve Şehircilik Bakanlığı, 2012). Because of the problems, adaptation programs for climate change began to be developed. The most essential steps are the United Nations Framework Convention on Climate Change (UNFCCC), Kyoto Protocol (KP), Intergovernmental Panel on Climate Change (IPCC), and the European Climate Change Program (ECCP) (Batan and Toprak, 2015). In addition, most adaptation projects based on water conservation have been developed. The protection of water quality becomes an important issue for cities. The duties of riverfront design are to prevent climate change effect, protect urban habitat and sustain natural condition throughout the city.

These projects, like other riverfront projects, involve quality of life, restoration of riverbanks, sustainability, and accessibility. The most important features of it are to provide accessibility in the surrounding of the river. Water management strategies are applied and emphasized in these projects. Riparian systems have the potential to decrease the adverse effects of climate change. These systems can protect urban habitat and ecosystem services in urban areas by enhancing the water cycle. If effective project design can be constructed in all cities, sea-level rise, heat island effect, and flood risk will be prevented. Therefore, river systems are crucial in urban habitat, water is essential to sustain life.

References

[1] A Texas State Park. (2021). Guadalupe River. Texas State Parks.
[2] Asla 2015. Walking the Riverwalk: Connecting People to the Chicago River. Chicago: Annual Meeting & Expo.
[3] Baniya, M., Asaeda, T., Fujino, T., Jayasanka, S., Muhetaer, G., Li, J. (2019). Mechanism of Riparian Vegetation Growth and Sediment Transport Interaction in Floodplain: A Dynamic Riparian Vegetation Model (DRIPVEM) Approach. WATER, 1-13.
[4] Batan, M., Toprak, Z. F. (2015). Küresel iklim değişikliğinin olumlu etkileri ve bu etkilerin iklim değişikliğine uyum kapsamında değerlendirilmesi. Mühendislik Dergisi, 6, pp. 93 - 102.
[5] Capon, S., Chambers, L., Nally, R., Naiman, R., Marshall, N., Pittock, J., . Williams, S. (2013). Riparian Ecosystems in the 21st Century: Hotspots for Climate Change Adaptation. Ecosystems, 359-381.
[6] Chicago Riverwalk Development Committee. (2009). Chıcago Rıverwalk. Chicago: Chicago Department of Zoning and Planning | Chicago Department of Transportation.
[7] T.C Çevre ve Şehircilik Bakanlığı. (2012). İklim Değişikliği ve Türkiye. Ankara: Çevre Yönetimi Genel Müdürlüğü İklim Değişikliği Dairesi Başkanlığı.
[8] Ginkgo Planning & Design inc. (2015). Regional Plan Chicago River Master Plan. Chicago: Ginkgo planning & design inc.
[9] Gregor, S., Swanson, F., M cKee, W., Cummins, K. (1991). An ecosystem perspective of Riparian Zones. Bioscience, 540-551.
[10] Iakovoglou, V., Zaimes, G. N., Gounaridis, D. (2014). Managıng Healthy Rıparıan Areas In Urban Settıngs Of. Protection and restoration of the environment XI Sustainable architecture and planning Conference Paper, 2169-2178.
[11] llhardt, B., Verry, E., Palik, B. (2000). Defining Riparian Areas. In E. e. Verry, Riparian management in forests of the continental eastern United States (pp. 23-42). New York: Lewis Publishers.
[12] Los Angeles County Flood Control District. (2004, January). Los Angeles River Master Plan. Retrieved from Public Works Los Angeles County: http://ladpw.org/wmd/watershed/la/larmp/LARMP-07%20Flood%20Management%20and%20Water%20Conservation.pdf
[13] Los Angeles County Public Service that Works. (2004, January). Los Angeles River Master Plan Lanscaping Guidelines and Plant Palettes. Retrieved from Landscape Guidlines Edits: http://ladpw.org/wmd/watershed/LA/LAR_planting_guidelines_webversion.pdf
[14] Molina-Navarro, E., Martínez-Pérez, S., Sastre-Merlín, A., Ramírez-Hernández, J., Sastre-Merlín, A., Mungaray-Moctezuma, A. (2015). Hydrological modeling and climate change impacts in an agricultural semiarid region. Case study: Guadalupe River basin, Mexico. Elseiver, 29-42.
[15] Naiman, R., & D´ecamps, H. (1997). The Ecology of Interfaces: Riparian Zones. Annu. Rev. Ecol. Syst., 621-58.

[16] North Central Region Forest Management Guide. (2006, May 25). United States Department of Agriculture. Northern Research Station: https://www.nrs.fs.fed.us/fmg/nfmg/docs/mn/Riparian.pdf
[17] Otto, B., McCormick, K., Leccese, M. (2004). Ecological Riverfront Design: Restoring Rivers, Connecting Communities. Washington, DC: American Planning Association.
[18] Pascacio, E., Argueta, A., Castillo-Uzcanga, M., Ramírez-Marcial, N. (2018). Influence of land use on the riparian zone condition along an urban-rural gradient on the Sabinal River, Mexico. Botanical Sciences, 180-199.
[19] Pletterbauer, F., Melcher, A., Graf, W. (2018). Climate Change Impacts in Riverine Ecosystems. Riverine Ecosystem Management, Aquatic Ecology Series 8, 203-223.
[20] Poff, B., Koestner, K., Neary, D., Henderson, V. (2011). Threats To Rıparıan Ecosystems In Western North America: An Analysis of Existing Literature. Journal of The American Water Resources Association, 1 - 14.
[21] Rebirth of the L. A. River. (2006). Los Angeles River Revitalization master Plan. Los Angeles: City of Los Angeles, Department of Public Works, Bureau of Engineering.
[22] Rudy Bruner Award Project Data. (2017). Chicago Riverwalk. Chicago: BNP Media.
[23] San Jose Redevelopment Agency. (2002). Guadalupe River Park. California: San Jose Redevelopment Agency .
[24] Seavy, N., Gardali, T., Golet, G., Griggs, F., Howell, C., Kelsey, R., . . . Weigand, J. (2009). Why Climate Change Makes Riparian Restoration More Important than Ever: Recommendations for Practice and Research. Ecological Restoration, 330-338.
[25] Song, Y. (2013). Application of Ecological Engineering Method in Urban Waterscape Design. Journal of Landscape Reseach, 5-6.
[26] Thomas, S., Griffiths, S., Ormerod, S. (2016). Beyond cool: adapting upland streams for climate change using riparian woodlands. Global Change Biology, 310-324.
[27] Tillmann, P., Siemann, D. (2011). Climate Change Effects and Adaptation Approaches in Freshwater Aquatic and Riparian Ecosystems in the North Pacific Landscape Conservation Cooperative Region. U.S: The U.S. Fish and Wildlife Service Region 1 Science Applications Program.
[28] Watersheds Canada. (2016, February). Watersheds. https://watersheds.ca/wp-content/uploads /2016/02/The-Riparian-Zone-Final.pdf
[29] Weilert, T. (2018). Urban Riparian Areas: Ecological and Streamside-Ordınance Assessments. PhD Thesis. Kansas City, Missouri, Columbia.
[30] Url-1:https://watersheds.ca/wp-content/uploads/2016/02/The-Riparian-Zone-Final.pdf

Biyofilik Tasarım Kriterleri Bağlamında Ofis Tasarımı

Ahenk Karci Demirkol[1], Ayşe Kalaycı Önaç[2]*
İzmir Kâtip Çelebi Universitesi, Kentsel Dönüşüm Bölümü, Çiğli Ana Kampüs, İzmir, Türkiye
** İletişimden sorumlu yazar: ahnkkarci@gmail.com*

Özet

Çevreden gelen uyaranlar insanlar tarafından farkında olmadan algılanır ve bunun sonucunda ortaya çıkan tepkiler insanların yaşam kalitesini etkiler. Biyofili kavramı, insanların doğal çevre ve yaşayan diğer canlılar ile doğuştan gelen içgüdüsel bir bağı olduğunu ifade etmektedir. Doğal ortamlar ve doğal materyaller kullanılarak tasarlanan mekanların insanların mental ve fiziksel sağlıkları üzerine restoratif etkileri bulunmaktadır. Biyofilik tasarım ise, günümüzde ki yapılı çevrede doğal bir yaşam alanı yaratarak, insanların sağlık ve refah düzeylerini artırmayı amaçlamaktadır.

Sanayi devriminden sonra artan kurumsal şirketlerin mekân ihtiyacına cevap vermek için ofis mekanları ortaya çıkmıştır. Günümüzde, insanların günlük rutininin önemli bir bölümünü çalışma hayatı oluşturmaktadır. Dolayısıyla insanlar zamanlarının büyük bir bölümünü kapalı ofis ortamlarında geçirmektedirler. Bu nedenle ofis tasarımları önem taşımaktadır.

Sağlık, insanların sadece fiziksel olarak değil zihinsel olarak da kendilerini iyi hissetme hali olarak tanımlanır. Sağlık üretkenliği etkilemektedir, bu sebeple çalışma ortamları tasarımları büyük önem taşımaktadır. Sağlıklı çalışma ortamları doğa ile iç içe tasarlanan, sürdürülebilir malzemelerin kullanıldığı, termal konforun sağlandığı, iyi hava kalitesine sahip, ergonomi standartları dikkate alınarak tasarlanmış mekanlar olarak tanımlanabilirler.

Günümüzde, yapılı çevreler insanları doğadan koparan önemli bir etmendir. Biyofilik tasarım, doğal unsurların iç mekanlara entegre edilmesine katkıda bulunacak tasarım ilkeleri sunarak bu kopuşun önüne geçerek insanların hayat kalitesini artırmayı hedeflemektedir. Biyofilik tasarımın ilkeleri; çevresel niteliklerin kullanılması, doğal formların kullanılması, doğal dokuların ve süreçlerin kullanılması, ışığın kullanılması, mekânsal ilişkilerin sağlanması ve insan doğa ilişkilerinin mekanlara yansıtılması şeklinde özetlenebilir. Biyofilik tasarım, mimaride yeni bir akım olmasına rağmen, insan sağlığı, ekoloji ve sürdürülebilirlik ilkelerini de kapsamaktadır. Biyofilik tasarımın temel amacı, insanın doğa ile bağını sağlayarak doğal unsurları barındıran mekanlar dizayn etmektir.

Biyofilik tasarım kriterleri çerçevesinde tasarlanmış ofis ortamları; çalışanlar üzerinde konsantrasyon artırıcı, stres düşürücü etkiye sahiptir. Ayrıca doğal unsurlar ve materyaller kullanıldığı için iç mekân çevre kalitesini de artırmaktadır. Biyofilik tasarım ilkeleri doğrultusunda tasarlanmış ofis ortamları, çalışanların sağlıklarını ve yaratıcılıklarını pozitif yönde etkilemektedir. Buna bağlı olarak, çalışanların üretkenlikleri ve çalışma hayatı kaliteleri artmaktadır.

Çalışmada, öncelikle biyofili ve biyofilik tasarım unsurları, literatür çalışması ışığında açıklanmıştır. Daha sonra biyofilik ofis tasarımı unsurlarına göre Amazon Seattle Ana Merkezi değerlendirilmiştir. Son olarak da biyofilik tasarım unsurlarının ofis tasarımlarına ve çalışma alanlarına entegre edilmesini sağlayan öneriler sunulmuştur.

Anahtar Kelimeler: ofis tasarımı, biyofilik tasarım, biyofilik ofis tasarımı

Giriş

Artan kentleşme insanların doğa ile ilişkisinin azalmasına neden olmaktadır. Günümüzde insanlar zamanının yaklaşık %90'ını kapalı alanlarda geçirmektedir. Bu durum insanlar üzerinde olumsuz etkiler yaratmaktadır. Fiziksel çevre dolaylı olarak insanların ruh sağlığını da etkilemektedir. Olumsuz yapılı çevre koşullarından dolayı insanların, kaygı düzeyi ve yorgunluk düzeyleri artmaktadır. Buna bağlı olarak insanların sosyal ilişkilerinde de olumsuzluklar ortaya çıkmaktadır [1]. Özellikle sanayi devriminden sonra artan kurumsal şirketlerin mekân ihtiyacına cevap vermek için ofis mekanları ortaya çıkmıştır. Bundan dolayı özellikle modern kentlerdeki çalışma alanları da bu yönde değişim göstermiştir. Çimen (2008)'in belirtiği üzere ofis, insanların grup halinde ya da bireysel olarak çalıştıkları küçük ya da büyük ölçekli mekanlar olarak tanımlanabilir [2].

Küreselleşme, teknolojik gelişmeler ve tasarım anlayışındaki değişimler ofis tasarımlarına da yansımıştır. Günümüzde fonksiyonellikten uzak, sadece göze hitap eden ofis tasarımları yerine; çalışanların motivasyonunu, konforunu ve verimliliğini artıran, sağlıklarını olumsuz yönde etkilemeyen

ofis tasarımlarına yönelim artmıştır. Ofis iç mekanlarının tasarımındaki hiyerarşik düzen yerine çalışan odaklı tasarım kararlarına önem verilmektedir. Özellikle teknolojik gelişmeler ofis tasarımlara büyük ölçüde yansımıştır. Bilgiye ulaşmanın ve paylaşmanın çok önemli bir unsuru olan ofis teknolojileri iç mekân tasarımlarının kurgulanmasında önemli bir etken olmaktadır [3].

Günümüzde, insanların günlük rutininin önemli bir bölümünü çalışma hayatı oluşturmaktadır. Dolayısıyla insanlar zamanlarının büyük bir bölümünü kapalı ofis ortamlarında geçirmektedirler. Bu nedenle ofis tasarımları önem taşımaktadır. Kapalı ortamlarda fazla zaman geçiren insanlarda bu ortamların neden olduğu olumsuz etkiler görülmektedir [4]. Bu bağlamda teknolojik özellikle kaynaklar kullanılırken, çalışanları doğal ortamdan koparmadan doğa ve teknolojiyi birleştiren dengeli mekanlar yaratmak büyük önem taşımaktadır.

Stephen Kellert'e göre doğal sistemin bozulmasının önemli bir nedeni de günümüz mimarı tasarım yaklaşımlarıdır. Bu yaklaşımların insanı doğadan kopuşunu hızlandıran önemli bir etken olduğunu vurgulamaktadır [5]. Biyofilik tasarım, kısaca insanların mental ve fiziksel sağlıklarını artırmak amacıyla doğal unsurların ve desenlerin mimari tasarımlarda uygulanması olarak tanımlanabilir [6]. Biyofilik tasarım ilkelerinin mimari tasarımlarda başarılı bir şekilde uygulanması yapılı çevrenin sürdürebilirliğini sağlarken, insanlarının mental ve fiziksel sağlıklarını da pozitif yönde etkilemektedir [7].

Biyofilik tasarım kriterlerini barındırarak tasarlanmış ofis mekanlarının çalışanlar üzerindeki etkileri incelendiğinde; performans artışı, üretkenlik ve konsantrasyon artışı, pozitif duygu durumu artışı gibi hayat kalitesini artırıcı nitelikle faydalar sağladığı saptanmıştır [8–11] .

Bu çalışmada, Biyofilik tasarım açıklanarak biyofilik tasarımın kriterleri incelenmiştir. Bu kriterler ışığında dünyada biyofilik tasarım ilkeleri iyi bir örnek olarak gösterilen "Amazon Seattle Ana Merkezi" değerlendirilmiştir. Ayrıca ofis mekanlarına ve çalışma alanlarına biyofilik tasarım unsurlarının kolaylıkla entegre edilmesine yönelik öneriler geliştirilmiştir.

Yöntem ve Materyal

Çalışmanın yöntemi başlıca üç aşamadan oluşmaktadır (Şekil 1).

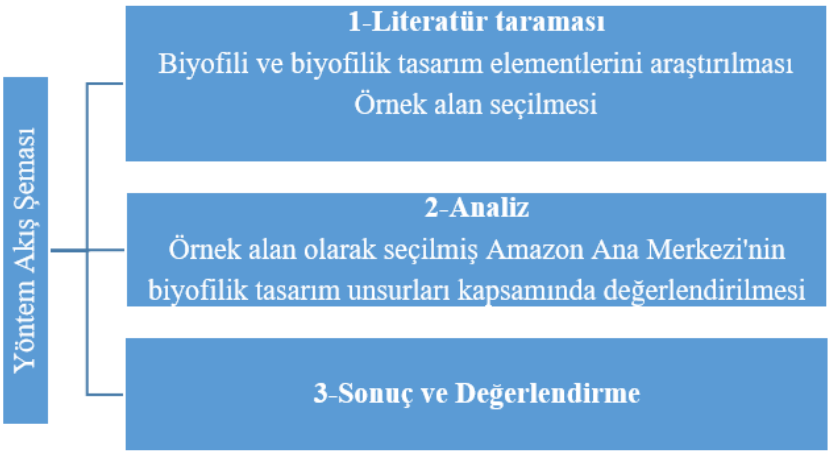

Şekil 1. Yöntem akış şeması

Çalışmanın ilk aşamasında kapsamlı bir literatür taraması gerçekleştirilmiş, çalışma konusu ile ilgili yapılmış bilimsel çalışmalar incelenmiştir. Literatür taramasından elde edilen veriler doğrultusunda biyofilik tasarım unsurları belirlenmiştir (Tablo 1). Dünyada biyofilik tasarımın iyi bir örneği olarak gösterilen Amazon'un Seattle'da bulunan ana merkezi örnek alan olarak seçilmiştir. Çalışmanın ikinci aşamasında ise, örnek alan biyofilik tasarım unsurlarına göre incelenmiştir. Çalışmanın son aşamasında, Amazon Ana Merkezi, biyofilik tasarım unsurları formuna göre değerlendirilmiştir. Çalışmanın son aşamasında biyofilik tasarım unsurları kapsamında ofis mekanlarının iyileştirilmesine yönelik uygulanabilir öneriler geliştirilmiştir.

Araştırmanın materyalleri, konuya ilişkin çalışmaların yer aldığı uluslararası, ulusal ve internet kaynaklarının yanı sıra, araştırma için özgün olarak hazırlanmış, değerlendirme formundan oluşmaktadır.

Biyofili ve Biyofilik Tasarım Kavramları

Biyofili kelimesi eski Yunanca'da bio: yaşam veya canlılarla ilgili ve phila: bir şeye karşı duyulan sevgi, eğilim kelimelerinden türetilmiştir. Biyofili kavramının temeli Antik Yunan'da 'yaşama-canlılara karşı duyulan sevgi' anlamına gelmektedir [12].

Biyofili fikri, insanın evrimi anlayışına dayanmaktadır. İnsan tarihinin %99'undan fazlasında, insanlar diğer canlılarla iç içe, avcı-toplayıcı gruplar halinde yaşamışlardır. İnsan beyni makinelerin düzenlediği bir dünyada değil, biyo-merkezli bir dünyada evrimleşmiştir. Günümüzdeki modern hayat, insanlık tarihi için oldukça yenidir. Bundan dolayı insanlarda o dünyaya ait izlerin silindiğini görmek imkânsızdır [7].

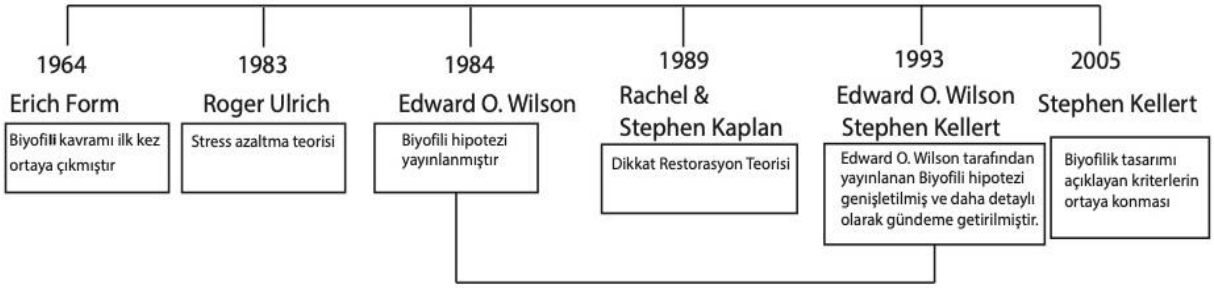

Şekil 2. Biyofili kavramının gelişimi ve etkileyen teoriler

Şekil 2'de doğanın insan üzerindeki restoratif etkileri ve biyofilik tasarım kavramı ile ilgili yapılmış çalışmalar ve teoriler kronolojik olarak sıralanmıştır.

Biyofili kavramı ilk olarak 1964 yılında psikolog Erich From tarafından doğayı sevme eğilimi olarak tanımlanmıştır [13].

1983 yılında Roger Ulrich'ın ortaya koyduğu stres azaltma teorisinde, doğanın stres ve olumsuz duygu durumlarını azaltıcı etkileri olduğu belirtilmiştir [14].

1984 yılında ise biyolog Edward O. Wilson 'Biophilia' kitabında biyofiliyi 'insanın yaşama ve yaşam süreçlerine karşı olan doğuştan gelen eğilimi' olarak tanımlamıştır. Wilson (1984) biyofili hipotezini, doğa ile insanın kalıtsal olarak bağlantısı olduğundan dolayı doğanın insanların fiziksel ve mental sağlığı için gereklik olduğunu savunmaktadır [13].

Kaplan ve Kaplan (1989)'in Dikkat restorasyon teorisinde, insanların doğada vakit geçirdikten, hatta doğayı izledikten sonra bile konsantrasyon düzeylerinde artış olduğu belirtilmektedir [15].

1993 yılında Edward O. Wilson ve Stephen Kellert tarafından Biyofili Hipotezi genişletilerek ''Biophilia'' kitabı yayınlanmıştır.

2005 yılında ise Stephen Kellert "Building for Life: Designing and Understanding the Human-Nature Connection" isimli kitabında biyofilik tasarım kavramı tanıtılmış ve doğanın mimarı tasarımlar vasıtasıyla insanlar tarafından deneyimlenmesini amaçlayan 60'tan fazla tasarım kriteri geliştirmiştir [16].

Evrimsel süreç boyunca insanın hayatta kalma ve neslini devam ettirme şansı doğa koşullarına adaptasyon başarısıyla doğrudan ilgilidir. Bu süreçte insan doğa koşullarını içselleştirerek gelişmiştir. Bunun sonucunda insan ile doğa arasında kolektif bir bağ ve yakınlık hissi oluşmuştur. Bu bağ biyofilik tasarımın temelini açıklamaktadır. Orr (2002)'a göre insanlar doğal unsurların daha fazla bulunduğu ortamlara daha iyi uyum sağlamaktadır. Bu bağlam 'doğa' biyofilik tasarım anlayışını şekillendirmektedir [17].

Kellert, biyofilik tasarımın planlaması için çok yönlü hiyerarşik bir çerçeve geliştirmiştir. Biyofilik tasarımın 6 temel unsuru bulunmaktadır. Bu unsurlar; çevresel özellikler, doğal şekiller, doğal desenler ve süreçler, ışık ve mekan, mekan temelli ilişkiler, evrimleşmiş insan- doğa ilişkileridir. Bu unsurların 70'in üzerinde tasarım özelliği bulunmaktadır [18].

Kellert ve Calabrese (2015) biyofilik tasarım unsurlarını daha yalın bir hale getirmişlerdir. Bu unsurlar ve onlara ulaşmak için gerekli tasarım stratejileri Tablo 1'de özetlenmiştir.

Tablo 1. Biyofilik tasarım elementleri ve tasarım stratejileri

	Tasarım unsurları	Tasarım Stratejileri
Doğanın doğurudan deneyimi	Işık	Cam duvar, iç mekân penceresi, yansıtıcı renk ve materyal kullanmak
	Hava	Açılan pencereler, teknolojik sistemler (havalandırma, hava temizleyici vb.)
	Su	Su kütleleri, çeşmeler, akvaryumlar (temiz ve hareketli olursa birden çok duyuya hitap eder)
	Bitki varlığı	İç mekân bitkileri, yeşil çatılar, yeşil duvarlar
	Hayvanlar	
	Hava	Açılabilir pencereler, teknolojik havalandırma imkanları
	Doğal peyzajlar ve ekosistemler	Ekosistemler, inşa edilmiş sulak alanlar, orman sırları ve otlaklar, simüle su ortamları, gözlem kuleleri
	Ateş	Şömine kuzine
Doğanın dolaylı deneyimi	Doğal görüntüler	Bitki-hayvan-doğal peyzaj-su-jeolojik konulu tablo, resim, video, bilgisayar simülasyonu, heykel,
	Doğal materyaller	Ahşap, taş, yün, pamuk, deri vb.
	Doğal renkler	Özellikle toprak tonları, doğal renkler, yapay kontrast oluşturan renklerden kaçınılmalı
	Doğal ışık ve hava simülasyonu	Doğal ışık ve havaya yakın.
	Doğal şekiller ve formlar	Sütunlarda bulunan yaprak benzeri desenler, bina cephelerindeki bitki şekilleri, kumaşlara ve kaplamalara dokunan hayvan kopyaları vb.
	Doğal şekil ve formların taklit edilmesi	Doğadaki şekil ve formların soyutlanması, yaratıcı ve fantastik şekilde taklit edilmesi
	Bilgi zenginliği	Fırsat sunan, bilgi açısından zengin
	Değişim, yaş, zamanın patinası	Yaşlanan malzemeler, değişen hava koşulları, zamanın geçişi hissi
	Doğal geometriler	Geometrik şekiller, fraktallar, altın oran, Fibonacci dizisi
	Biyomimikri	Doğada canlılar tarafından kullanılan ve insan ihtiyaçlarına cevap verecek şekilde adapte edilebilir. Örümcek ağının yapısal mukavemeti, termik tepeciklerin ısı kontrolü vb.
Mekanın deneyimi	Manzara ve sığınma	Pencere, kapalı alan
	Organize edilmiş karmaşıklık	Karmaşık niteliklere sahip olma eğiliminde, organize ve düzenli deneyimlenen mekanlar
	Parçaların bütüne entegrasyonu	Odak noktası bulunan parçaların bütün oluşturduğu mekanlar
	Mobilite ve yön bulma	Net anlaşılan yollar,
	Mekâna kültürel ve ekolojik bağlılık	Yerli fauna flora, kültürü yansıtan tasarımlar

Biyofilik Tasarım Kriterlerine Göre tasarlanmış Örnek Ofis Mekanının Değerlendirilmesi

Biyofilik tasarım kriterleri kullanılarak çalışanlar için onarıcı ve üretkenliği teşvik eden mekanlar yaratılması amacıyla tasarlanmış olan Amazon Seattle Ana Merkezi çalışmanın örnek alanı olarak seçilmiştir.

Amazon Seattle Ana Merkezi

Amazon'un Seattle'da bulunan ana merkezi eskiden depo ver tersanelerden oluşan bir mahallede inşa edilmiştir. Alan teknoloji merkezine mümkün oldukça çevresiyle uyum içinde dönüştürülmüştür. Şekil 3'de görülen merkez 24.000'den fazla çalışanı barındırmakta olan 3,3 milyon metrekarelik bir

alanda kurulmuştur. Üç yüksek katlı kule, orta yükseklikte bir kule ve çok amaçlı "Kubbe" binasından oluşmaktadır [19-20].

Şekil 3. Amazon Ana Merkezinin havadan görünüşü [19]

Amazon Ana Merkezi önceden rezervasyon şartıyla halka açıktır. Şekil 4'de görülen doğal formlar ve desenler kullanılarak tasarlamış Kubbe konstrüksiyonlarında yürüyüş yolları, doğrusal olmayan kavisli geçiş alanları bulunmaktadır. Kubbelerde 40.000'den fazla bitki türü bulunmaktadır (Şekil 3). Kubbeler çalışanlarına doğal aydınlatmalı, bitkilerle çevrili alışmış kapalı toplantı odalarının ve ofislerin yerine doğa ile iç içe çalışma alanı imkânı sunmaktadır [19-21]. Kubbeler özellikle çok güçlü evrimleşmiş insan-doğa ilişkisine olanak sağlamaktadır.

Şekil 4. Amazon Ana Merkezinde bulunan kubbe konstrüksiyonları [19]

Mekanın ortak alanlarında dönen sanat sergileri, temalı binalar ve odalar, bağımsız yerel satıcılar bulunmaktadır. Ayrıca çalışanların veya ziyaretçilerin yanlarında evcil hayvanları olan köpeklerini getirmelerine de olanak sağlanmaktadır [20]. Şekil 4'de görüldüğü gibi mekanların tasarımda doğal materyaller kullanılmış, doğal şekiller ve formlar taklit edilmiş, doğal ve yapay ışığa yer verilmiştir.

Şekil 4. Amazon Ana Merkezi ortak alan [20,22]

Zemin katta bulunan kamusal alan Amazon Ana Merkezi'nin kültürel bir kimliğe bürünmesine hizmet etmektedir (Şekil 5). Bu alan kent sakinlerine park ve köpek parkı olarak da hizmet vermektedir [20]. Birbirine bağlı yürüyüş yolları ve ağaç evler, görünüşte kaotik bitki türleriyle çevrili olsa da düzenli bir alan hiyerarşisi sağlamaktadır.

Tablo 2. Amazon Ana Merkezi'nin biyofilik tasarım elementlerine göre değerlendirilmesi

	Biyofilik tasarım elementleri	
Doğanın doğrudan deneyimi	Işık	✓
	Hava	✓
	Su	✓
	Bitki varlığı	✓
	Hayvanlar	✓
	Hava	✓
	Doğal peyzajlar ve ekosistemler	✓
	Ateş	×
Doğanın dolaylı deneyimi	Doğal görüntüler	✓
	Doğal materyaller	✓
	Doğal renkler	✓
	Doğal ışık ve hava simülasyonu	✓
	Doğal şekiller ve formlar	✓
	Doğal şekil ve formların taklit edilmesi	✓
	Bilgi zenginliği	✓
	Değişim, yaş, zamanın patinası	×
	Doğal geometriler	✓
	Biyomimikri	×
Mekânın deneyimi	Manzara ve sığınma	✓
	Organize edilmiş karmaşıklık	✓
	Parçaların bütüne entegrasyonu	✓
	Mobilite ve yön bulma	✓
	Mekâna kültürel ve ekolojik bağlılık	Ekolojik bağlılık

Şekil 5. Amazon Ana Merkezi kamusal alan ve köpek parkı [23]

Sonuç ve Değerlendirme

Amazon Seattle Ana Merkezi Tablo 1'de belirtilmiş kriterler kapsamında değerlendirilmiştir. Değerlendirme sonuçları Tablo 2'de belirtilmiştir. Amazon Ana Merkezi Tablo 2'de görüldüğü gibi biyofilik tasarım elementleri kapsamında genel olarak değerlendirildiğinde söz konusu tasarım unsurlarının çoğunu içermektedir. Değerlendirilmiş olan örnek alan oldukça başarılı bir biyofilik tasarım örneğidir.

Biyofilik tasarımın temel amacı, insanların yaşamakta olduğu yapılı çevre ile doğa ilişkisinin sürdürülmesidir. Bu bağlamda, yapılı çevre ile oluşturulmuş yaşam alanlarına doğadan ilham alınarak taklit edilen görsel ve duyusal uyaranlar da dahil edilir. Amazon Ana Merkezi örneğinde görüldüğü gibi tasarıma sadece doğa entegre edilmemiş, doğada bulunan unsurlar da taklit edilerek doğanın insanlar tarafından hatırlanması sağlanmıştır.

Kaplan (1995)'in belirtiği gibi, insanlar doğada vakit geçirdikten ve doğanın sahnelerine baktıktan sonra konsantrasyon seviyelerinde artış gözlenmektedir. Özellikle iş yerlerinde doğal unsurların kullanılması çalışanların performansını artırmaktadır.

Yapılmış olan literatür taraması ışığında biyofilik tasarım unsurları barındırarak tasarlanmış ofis mekanları çalışanların performans, konsantrasyon artışı ve pozitif duygu durumu artışı gibi hayat kalitesini artırıcı nitelikte etkileri olduğu görülmüştür. [8–11] . Bundan dolayı özellikle ofis gibi çalışma ortamlarında doğal unsurların kullanımı hayat kalitesini artırmaktadır. Bu yönde herkes tarafından kolaylıkla uygulanabilir bazı uygulamalar önerilmiştir. Bunlar;

- Canlı bitki varlığının çalışma ortamlarında bulundurulması
- Renk seçiminde çarpıcı kontrastlardan kaçınılmalıdır
- Özellikle toprak renklerinin ofis tasarımlarında kullanılması
- Deri, ahşap, pamuk gibi doğal materyal kullanımı
- Doğal malzemelerden yapılmış ve doğayı hatırlatıcı objelerin kullanımı
- Su kütlelerinin bulundurulması (akvaryum, küçük süs havuzu vb.)
- Doğal patern ve fraktalları taklit eden şekillerin kullanımı

Güneş ışığı alan yerlerin tercih edilmesi veya iyi düzeyde gün ışığını taklit eden aydınlatma elemanlarının kullanımı.

Kentleşme ile birlikte insanların doğadan koptuğu bu günlerde doğa ile ilişkinin tekrar sağlanmasına yönelik tasarım anlayışları oldukça önem taşımaktadır. Çalışma mekanları tasarımlarında biyofilik tasarım unsurlarının bulundurulmasının insanların hayatlarındaki olumlu etkileri düşünüldüğünde, yapılı çevrede bu tasarım unsurlarına mümkün olduğunca yer verilmesi gerektiği düşünülmektedir.

Kaynaklar

[1] Evans GW, McCoy JM. When buildings don't work: The role of architecture in human health. Journal of Environmental psychology. 1998;18(1):85–94.
[2] Karaoğlu Tekin Ö. Paylaşımlı Ofislerin İç Mekan Tasarım Anlayışları, 2019.
[3] Noraslı M, Doğan RK. Çağdaş Ofis Tasarımı Bağlamında Bee Rendering Tasarım Ofisi. Artium. 2020;8(1):1–10.
[4] Mendell MJ. Non-specific symptoms in office workers: A review and summary of the epidemiologic literature. Indoor Air. 1993;3(4):227–36.
[5] Gray T, Birrell C. Are biophilic-designed site office buildings linked to health benefits and high performing occupants? International journal of environmental research and public health. 2014;11(12):12204–22.
[6] Molthrop E. Biophilic design: A review of principle and practice. Environmental Sciences, Spring 2011. 2011;37–9.
[7] Kellert S, Calabrese E. The practice of biophilic design. London: Terrapin Bright LLC. 2015;
[8] Sanchez JA, Ikaga T, Sanchez SV. Quantitative improvement in workplace performance through biophilic design: A pilot experiment case study. Energy and Buildings. 2018;177:316–28.
[9] Raanaas RK, Evensen KH, Rich D, Sjøstrøm G, Patil G. Benefits of indoor plants on attention capacity in an office setting. Journal of Environmental Psychology. 2011;31(1):99–105.
[10] Han K-T, Ruan L-W. Effects of indoor plants on self-reported perceptions: a systemic review. Sustainability. 2019;11(16):4506.
[11] Shoemaker CA, Randall K, Relf PD, Geller ES. Relationships between plants, behavior, and attitudes in an office environment. HortTechnology. 1992;2(2):205–6.
[12] Şenozan MI. İnsan-Mekan-Doğa Etkileşiminin Sürdürülebilir Bir Öğretisi Olarak Biyofilik Tasarım. Mimar Sinan Güzel Sanatlar Üniversitesi Basılmamış Yüksek Lisans Tezi İstanbul. 2018.
[13] Myers MG. Visual Art as a Restorative, Placed-Based Biophilic Coping Mechanism in the Workplace: A Case Study. Kent State University; 2020.
[14] Ulrich RS. Aesthetic and affective response to natural environment. In: Behavior and the natural environment. Springer; 1983. p. 85–125.
[15] Adamson K, Thatcher A. Do Indoor Plants Improve Performance Outcomes?: Using the Attention Restoration Theory. In: Congress of the International Ergonomics Association. Springer; 2018. p. 591–604.
[16] Kellert SR. Building for life: designing and understanding the human-nature connection. Building for life: designing and understanding the human-nature connection: Island Press; 2005. 250.
[17] Bayraktaroğlu ÖE. Mimarlıkta ekosistem düşüncesiyle tasarlamak. Fen Bilimleri Enstitüsü; 2014.
[18] Kellert SR. Dimensions, elements, and attributes of biophilic design. Biophilic design: the theory, science, and practice of bringing buildings to life. 2008;3–19.
[19] Amazon Opens The Spheres - [Internet]. [cited 2021 May 8]. Available from: https://www.world-architects.com/en/architecture-news/headlines/amazon-opens-the-spheres
[20] Amazon Headquarters Seattle: Coolest Office Features | Built In Seattle [Internet]. [cited 2021 May 8]. Available from: https://www.builtinseattle.com/2019/03/08/coolest-features-amazon-seattle-headquarters
[21] Nelson B. Americans have a nature problem. Is "biophilic design" the solution? [Internet]. 2018 [cited 2021 May 8]. Available from: https://www.nbcnews.com/mach/science/new-biophilic-buildings-use-quirky-features-bring-nature-indoors-ncna853996
[22] Amazon.com Opens Its Own Rainforest in Seattle | Voice of America - English [Internet]. [cited 2021 May 9]. Available from: https://www.voanews.com/silicon-valley-technology/amazoncom-opens-its-own-rainforest-seattle
[23] Gallery of Aerial Imagery Depicts Iconic Modern and Contemporary Architecture in a New Perspective-24 [Internet]. [cited 2021 May 9]. Available from: https://www.archdaily.com/942298/aerial-imagery-depicts-iconic-modern-and-contemporary-architecture-in-a-new-perspective/5ee26a17b35765c6d80003c6-aerial-imagery-depicts-iconic-modern-and-contemporary-architecture-in-a-new-perspective-image?next_project=no

Hayvanların Sağlıklı ve Doğal Gelişiminin Desteklenmesinde Yeni Bir Vizyon; Arı Ürünleri

Mustapha Ndimballan [1*], *Banu Yücel* [2]
[1]*Ege Üniversitesi, Fen Bilimleri Enstitüsü, Bornova-İzmir/Türkiye*
[2]*Ege Üniversitesi Ziraat Fakültesi Zootekni Bölümü, Bornova- İzmir/Türkiye*
**İletişimden sorumlu yazar: ndimssta@gmail.com*

Özet

Son yıllarda, doğal ürünlerle beslenme bilincindeki artış, arı ürünlerinin popüleritesini giderek arttırmaktadır. Dünyada, arı ürünlerinin gıda, tarım ve hayvancılıkta kullanımı için çeşitli çalışmalar yapılmaktadır. Bununla birlikte, gelişmekte olan ülkelerde, hayvansal protein sağlamak için kümes hayvanlarına ve hayvansal ürünlere talep artmaktadır. Hayvan yeminde kullanılan antibiyotikler konusundaki endişeler sebebi ile 2006 yılında Avrupa Birliği tarafından antibiyotiklerin ve büyüme destekleyicilerin kaldırılmasına karar verilmiş ve diğer doğal yem katkı maddelerinin kullanımına önem verilmiştir. Bu nedenle araştırmacılar, hayvan sektöründeki büyüme, yem kullanımı, et kalitesi ve bağışıklık sistemine etkileri bakımından büyük öneme sahip doğal ürünler bulma konusunda büyük çaba sarf etmişlerdir. Geçtiğimiz son on yıllık dönemde, hayvanların performansını ve bağışıklığını arttırmak için antibiyotiklerin yerine doğal ürünlerin kullanımı teşvik edilmiştir. Arı ürünlerinin üretiminde, işlenmesinde, pazarlanmasında ve kullanım aşamalarında arı ürünlerinin güvenilirliği sadece beslenme açısından değil, aynı zamanda daha sık olarak belirtilen Apiterapi (arı ürünlerinin sağlığın korunmasında ve tedavisinde kullanılması) uygulamalarında da son yıllarda önem kazanmıştır. Doğal beslenme bilincinin giderek artması, doğal ürün tüketimine yönelimin artmasına neden olmuştur. Bal, propolis, arı poleni, arı zehiri, arı sütü ve apilarnil, beslenmenin yanı sıra çeşitli hastalıkların tedavisinde ve önlenmesinde de etkili bir şekilde kullanılmaktadır. Bu çalışmada, hayvancılık sektöründe kullanılan arı ürünlerinin fonksiyonel özellikleri, hayvan beslemede kullanımı, biyo-yararlılığı, dikkat edilmesi gereken hususlar, hayvanların sağlıklı gelişimi için sağlayacağı potansiyel vizyon ve arı ürünleri üzerine yapılmış olan bilimsel çalışmalar tartışılmıştır.

Anahtar Kelimeler: bal arısı, bal, propolis, arı poleni, arı zehiri, arı sütü, apilarnil

Giriş

Son yıllarda, doğal ürünlerle beslenme bilincindeki artış, arı ürünlerinin popüleritesini artırmaktadır. Dünyada, arı ürünlerinin gıda, tarım ve hayvancılıkta kullanımını geliştirmek için çeşitli çalışmalar yapılmaktadır. Türkiye, zengin nektar kaynakları, uygun iklim koşulları ve güçlü genetik çeşitliliğe sahip olması sebebi ile yüksek arıcılık potansiyeline sahiptir. Buna rağmen, bal dışındaki arı ürünlerinin üretimi ve kullanımı istenilen düzeyde değildir. Doğal tamamlayıcı ürünler, sağlıkta refahı sağlama amacıyla ve bazı hastalıkların olası tedavi yöntemlerinde büyük ölçüde uygulanmaktadır. Son yıllarda, hayvanların performansını iyileştirmek ve bağışıklığını arttırmak için de antibiyotiklere alternatif olarak doğal ürünlerin kullanılması teşvik edilmiştir. Arı ürünlerinin önemi ve arı ürünlerinin üretimindeki, işlenmesindeki, pazarlanmasındaki ve kullanım aşamalarındaki güvenirliliği, sadece beslenme aşamasında değil, aynı zamanda Apiterapi (arı ürünlerinin sağlığın korunmasında ve tedavisinde kullanılması) uygulamalarında da son yıllarda önem kazanmıştır.

Günümüzde Apiterapi adı verilen bu uygulamalar, tıp dünyasında tamamlayıcı/destekleyici tedavi olarak kabul edilmektedir. Apiterapi uygulamaları, uzun vadeli bilimsel araştırmaların ve doğal tedavi anlayışının sonuçlarına dayanmaktadır. Bal, propolis, polen, arı zehiri ve arı sütü, insan beslenmesinde ve çeşitli hastalıkların tedavisinde veya önlenmesinde sıklıkla etkili bir şekilde kullanılmaktadır. Bununla birlikte hayvanlarda apiterapi uygulamalarına odaklanan çok az sayıda çalışma vardır. Arıların korunmasına yönelik ilginin artması ile birlikte, arı ürünlerinin de daha fazla önem kazanacağı bilinmektedir. Hayvanlarda aşırı antibiyotik kullanımı, bir gıda güvenliği ve halk sağlığı sorunudur. Arı ürünlerinin kullanımı, artan sıklıkta ortaya çıkan antibiyotiğe dirençli türlerin tedavisinde alternatif bir yöntem olabilecektir. Vitamin, mineral ve sağlıklı yağlar bakımından zengin arı ürünlerinin yem katkısı olarak kullanımı ile bu ürünlerin hali hazırda kullanılmakta olan mineral-vitamin karışımlarından çok

daha iyi gıda takviyeleri haline gelebileceği veya ıslah çalışmalarında tamamlayıcı ürün olarak kullanılabileceği belirtilmiştir (1). Arı ürünlerinin biyo-yararlanımının sentetik ilaçlardan daha yüksek olduğuna dikkat edilmelidir. Yapılan birçok çalışma, arı ürünlerinin hayvanların üretim performansını ve sağlığını önemli ölçüde etkilediğini belirtmektedir. Bal, polen, arı sütü, arı zehiri, propolis, arı ekmeği ve apilarnil gibi arı ürünleri, hayvan beslenmesinde, üremesinde ve sağlığında farklı uygulama şekillerinde ve miktarlarında yaygın olarak kullanılmaktadır. Bu sunuda, hayvancılık sektöründe arı ürünlerinin kullanımındaki son gelişmeler ve yenilikçi kullanım olanakları tartışılmış, konuyla ilgili mevcut bilgiler değerlendirilmiş ve gelecekteki araştırmalar için bir perspektif oluşturulması amaçlanmıştır.

Arı Sütü ve Hayvancılıkta Kullanımı

Arı sütü, 5 ila 15 günlük işçi arıların alt çene (mandibular) ve hipofaringal bezlerinden salgılanan, ana arı gözlerindeki larvaların beslenmesinde kullanılan bir maddedir. Arı sütü, ana arı gözlerine aşılama yapıldıktan 36-48 saat sonra toplanan ve pelte kıvamında, açık sarı-krem renkli, kendine has bir kokusu ve keskin tada sahip bir gıdadır. Bileşiminde bulunan birçok farklı bilinen ve bilinmeyen biyolojik işleve sahip maddeler, arı sütünün biyomedikal etkisinde önemli rol oynamaktadır. Arı sütünün yapısında proteinler, lipitler, karbonhidratlar, kül, P, Na, K, Ca, Mg, polen, C, D ve E vitaminleri ve B vitaminlerinin tamamı ile diğer bazı vitaminler vardır. Arı sütünde 1.3-2 µg/g B1 Vitamini, 7.5-10 µg/g B2 vitamini, 2-8 µg/g B6 Vitamini, 2-3 µg/g H Vitamini ve 3-5 µg/g düzeyinde C Vitamini bulunmaktadır (2).

Arı sütünün hayvan sağlığı üzerindeki etkilerinin belirlenmesi için birçok araştırma yapılmıştır. Bu araştırmaların sonuçlarına göre arı sütü yüksek kolajen içeriği nedeniyle hayvanlarda kıkırdak dokusunun gelişimini arttırmakta, içerdiği kalsiyum ve selenyum miktarı nedeniyle kemik ve diş yapısını güçlendirmekte, ayrıca kan hücrelerini, kalp ve karaciğer dokularını korumaktadır. Ayrıca içeriğindeki potasyum varlığından dolayı kaslar ve sinir sistemi üzerinde güçlendirici etkilere sahiptir (3). Arı sütünün bıldırcınlarda göğüs, böbrek, bacak ve karaciğer dokularında toplam çoklu doymamış yağ asidi oranını arttığı bildirilmektedir. Ayrıca, koyunlarda üreme veriminin arıtılmasında ve üreme problemlerinin çözümünde sentetik hormonların doğal kaynaklı alternatifi olarak arı sütü önerilmektedir (4).

Propolis ve Hayvancılıkta Kullanımı

Propolis bal arıları tarafından toplanan ağaç kabukları, yaprakları ve bitki salgılarının, bal arıları tarafından kendi enzimlerini ve bal mumu ekleyerek oluşturdukları kuvvetli reçinemsi, yapışkan özellikli bir maddedir (5).Propolisin yapısında bulunan maddeler bal mumu (%7), polen (%5), reçine - polifenolik fraksiyon (%55), aromatik uçucu yağlar (%30) ve diğer küçük bileşenler (%3), vitaminler (A, C, D, E ve B1, B2 ve B6), niasin, folik asit, demir, kalsiyum, bakır, nikel, çinko, magnezyum, manganez, vanadyum, stronsiyum ve kobalt gibi bazı mikro ve makro minerallerdir. Ana bileşenler fenolik bileşikler, flavonoidler ile bunların terpenler ve esterleridir (6). Ek olarak, propolis glukozidazları içerir. Propolis flavonoidleri; flavonoller, flavonlar, izoflavonlar ve flavanonlar dihidroflavonoller gibi birçok alt gruba aittir (7).

Propolisin, kuluçka özelliklerini ve yumurtadan çıkan civciv performansını olumsuz etkilememesi nedeni ile, kuluçkalık yumurta dezenfeksiyonunda halihazırda kullanılan sentetik kimyasallara potansiyel bir alternatif olarak kullanılabileceği düşünülebilir. Bu sonuçlar, propolisin ölüm oranını azaltma yeteneğini bildiren ve bu bulguları, toplam protein, kolesterol ve amino asitin kan seviyelerinde değişikliklere neden olan besinlerin emiliminde ve metabolizmasındaki hayati rolüne bağlayan Abdel-Rahman ve Mosaad (8) tarafından güçlü bir şekilde desteklenmiştir. Aynı araştırıcılar ayrıca, yukarıdaki olumlu etkilerin, propolisin makrofaj ve lenfatik doku fonksiyonlarının aktivitesi gibi bağışıklık tepkilerini arttırma kabiliyeti ile ilişkili olabileceğini de belirtmiştir.

Yücel ve arkadaşları (5)'na göre kanatlılarda rasyona propolis eklenmesi, yumurta üretimini, kan bileşenini ve hematolojik parametreleri geliştirmeye yardımcı olmaktadır. Etlik piliç yetiştirciliğinde yüksek canlı ağırlık artışı ve optimum yemden yararlanma oranı hedeflenir. Açıkgöz ve arkadaşları (9), propolisin "doğal bir antibiyotik" olması sebebi ile, etlik piliç besiciliğinde kötü hijyenik koşullarda propolisin olumlu etki gösterebileceğini; bu nedenle de propolisin özellikle etlik piliçlerin bağışıklık

sistemi üzerinde antimikrobiyal özelliklerini belirlemek için daha kapsamlı araştırmaların yapılmasının gerekliliğini belirtmişlerdir.

Propolisin küçükbaş hayvanların bağışıklık sistemi üzerine etkilerini irdeleyen sınırlı sayıda çalışma bulunmaktadır. Kızgınlık döneminde Brezilya kırmızı propolisinin etanolik ekstraktının Santa Inês koyunlarına (3 g / dişi / gün) oral yoldan verilmesi, toplam lökositleri, toplam protein ve globulin konsantrasyonlarını azaltırken, trigliseritleri düzeyi ile glutamat oksaloasetat transaminaz ve glutamat piruvat transaminaz enzimlerinin aktivitelerini arttırdığı bildirilmiştir (10).

Besin takviyesi olarak arı ürünlerinden faydalanabilecek diğer ruminant hayvanlar büyükbaş hayvanlardır. Büyükbaş hayvancılıkta, ruminantların vücutlarındaki sindirim süreçleri ve enerji dengesi belirgindir. Yoğun süt ve et üretimi ile ilişkili olan birçok hastalık; zayıf beslenme, süt üretim süreci veya besi sürecinde yüksek enerji ve mineral kayıplarının yol açtığı metabolik kökenli hastalıklardır. Rumendeki fermantasyon süreci hem bakteri hem de protozoa olan probiyotik organizmaların etkisine dayanmaktadır. Bu nedenle, mide bölümlerindeki organizma sayıları, organizma türlerinin bileşimi ve uygun geçişi önemlidir. Hastalıklar, yararlı mikrofloranın düşük seviyesinde olmasından veya istenmeyen patojenik mikroorganizmaların ortaya çıkmasından kaynaklanabilmektedir.

Zawadzki ve arkadaşları (11) tarafından yapılan bir çalışmada, monensin (300mg/ hayvan/gün) ve propolis ekstraktı (35 g/hayvan/gün) içeren yemler 84 gün boyunca boyunca buzağılara verilmiş ve ağırlık artışı, yem tüketimi ve karkas özelliklerindeki değişimler irdelenmiştir. Propolis ekstraktı tüketen buzağılarda canlı ağırlık ve kesim sonrası karkas ağırlığı artmış ve yemden yararlanma iyileşmiştir. Propolisin süt verimi ve kalitesi üzerine etkilerini belirmek amacıyla da çalışmalar yürütülmüştür. Aguiar ve arkadaşları (12) tarafından yapılan bir çalışmada, toplam günlük propolis alımı 19.2 g olarak belirlenmiştir. Sonuçlar, propolis takviyesi ile beslenen ineklerde sütte protein içeriğinin daha yüksek olduğunu ve aynı zamanda ineklerin daha yüksek bir süt verimine sahip olduğunu göstermektektedir. Propolisin yem alımı, yağ içeriği ve sütteki somatik hücre sayısı üzerinde önemli bir etkisi belirlenmemiştir. Perinatal dönemde ineklerde flavonoidlerin, süt devedikenindeki *(Sylybum marianum*) silimarin (3-hidroksiflavon) ile benzer bir etkiye sahip olabileceği belirtilmektedir. Ayrıca propolis insanlarda karaciğer hastalıklarını tedavi etmek için kullanılan bir hepatoprotektör görevini üstlenmektedir. Hepatoprotektörün ineklere perinatal dönemde uygulandığı çalışmalar, ineklerin enerji dengesi, postpartum durumu ve üretkenlik üzerindeki olumlu etkisini ortaya koymuştur. Propolisin hepatoprotektif ve kandaki yağ azaltma aktivitesi, sığırlarda kritik bir dönem olan perinatal dönemde beslenmesinde iyi bir uygulama olabilir. Propolis takviyesi ile, lipid uygulamasında bir iyileşme ve karaciğer hücrelerinin daha iyi korunması, özellikle iyi beslenen inekleri etkileyen yağlı inek sendromu veya yakın zamanda buzağılayan ineklerde görülen ketozis gibi birçok tıbbi bozukluğu önleyebileceği belirtilmektedir.

Yücel ve arkadaşları (5) tarafından yapılan çalışmada, yeni doğan buzağılara 2 cc (%96 etil alkol çözeltisi ile hazırlanmış) propolis verilmiş ve buzağılarda propolisin ishal üzerindeki etkileri incelenmiştir. Araştırmada, bir aylık süreç içerisinde, toplam 20 buzağı (10 dişi ve 10 erkek) kullanılmış, buzağıların ağırlığı doğumda, birinci haftada, üçüncü haftada ve deneme sonunda kaydedilmiştir. Deney sırasında farklı fiziksel parametreler de ölçülmüş ve toplam canlı ağırlık artışı ortalamasının dişi buzağılar için sırasıyla 10.95 ve 13.75 kg, kontrol ve propolis gruplarında erkek buzağılar için sırasıyla 16.04 ve 16.47 kg olduğu bildirilmiştir. Günlük canlı ağırlık artışları, dişi buzağılar için 312.88 ve 392.83g, kontrol ve propolis gruplarında erkek buzağılar için sırasıyla 458.31 ve 470.31 g olarak ölçülmüştür. Bu sonuçlardan propolisin buzağılarda ishali önlediğini ve canlı ağırlık artışını ve büyümesini iyileştirdiğini ortaya koymaktadır. Önceki çalışmalarda da desteklendiği gibi, propolisin birçok patojenik bakteri türünün ortadan kaldırılmasındaki etkinliği nedeniyle yeni doğan buzağı diyaresinde hem önleyici hem de tedavi edici olarak kullanılabileceğini belirterek, hayvan gelişimini teşvik ettiği öngörülmektedir.

Polen ve Hayvancılıkta Kullanımı

Polen, bal arıları (*Apis mellifera* L.) tarafından çeşitli botanik kaynaklardan toplanan çiçekli bitkilerin erkek üreme hücreleridir (13). Arı poleni, çiçekli bitkilerin erkek üreme hücreleri tarafından üretilen polenin, bal arıları (*Apis mellifera* L.) tarafından toplanırken yapıştırılma ve korunması amacıyla içerisine nektar veya bal ile glukoz oksidaz gibi enzimler eklenmesi ile oluşan doğal bir arı ürünüdür. Bal arıları, poleni az miktarda ağız salgısı veya nektarla karıştırır ve arka bacaklarındaki polen

sepetleri ile kovana taşırlar. Polen sepetindeki polenler tuzaklar kullanılarak toplanır ve kurutulduktan sonra farmasötik, kozmetik veya beslenme alanlarında kullanım için bir hammadde haline gelir. Besleyici ve terapötik özellikleri nedeniyle, arı poleni kullanılarak yapılan preparatlar besin takviyesi olarak kullanılır (14). Arı poleninin, gıda ve/veya hayvan yemi olarak kullanımının önemli bir potansiyele sahip olduğu ve insan beslenmesinde kullanılabileceği bildirilmiştir. Arı poleni, antimikrobiyal, antifungal, antioksidan, anti-radyasyon, hepatoprotektif, kemoprotektif, kemopreventif ve antienflamatuar aktivitelerin en belirgin olduğu, sağlığı destekleyen bir gıda olarak tanımlanır.
Arı poleninin, piliçlerin büyüme, performans ve iç fonksiyonları üzerindeki olumlu etkileri çeşitli çalışmalarla vurgulanmıştır (15,16,17). Wang ve arkadaşları (15) tarafından yapılan çalışmada, %1.5 arı poleni takviyesi ile beslenmiş tavuklarda duodenum, jejunum ve ileumun ince bağırsak villerinin, kontrol grubuna göre daha uzun ve kalın olduğu görülmüştür. Araştırmacılar, farkın erken gelişim sırasında, özellikle de ilk iki hafta boyunca daha önemli olduğunu belirtmişlerdir. Bu durum yüzde olarak özetlendiğinde, arı poleni villus uzunluğunu duodenumda %29.4 ve %37.1, jejunumda %28.1 ve %33.7, ileumda ilk iki haftada (sırasıyla birinci ve ikinci hafta) %16.2 ve %18.6 oranında artırmıştır. Ayrıca, polenle beslenen grupta ince bağırsak bezlerinin gelişiminin daha yüksek bir yoğunlukta olduğu ve ilk iki haftada arı poleni uygulamasını takiben bezlerin yoğunluğunda önemli bir artış olduğu rapor edilmiştir.

Evcil hayvanların rasyonlarına eklenen polenin büyüme hızını arttırdığı, sindirimi kolaylaştırdığı ve hayvanlara daha sağlıklı bir görünüm verdiği belirtilmektedir. Yarış atlarının rasyonlarına eklenen polenin, performansı artırdığı, genel durumu iyileştirdiği ve yem kullanımını geliştirdiği belirlenmiştir. Atlarda arı poleni ile beslenen gruplarda göz sulanması, alerji ve stres gibi problemler azalmış, vücut canlılığı ve performansı artmıştır. Bu sonuçlar, aynı zamanda, yem veya suya taze polen ilavesinin doğal bağışıklık sistemini güçlendirdiğini, enerji verdiğini ve sindirimi desteklediğini belirten Stangaciu (3) tarafından da desteklenmiştir.

Arı Zehiri ve Hayvancılıkta Kullanımı

Bal arısı zehiri (apitoksin) bal arısının karın boşluğunda bulunan zehir bezlerinde üretilir. Zehir kesesinde depo edilir (18). Arı zehiri renksiz, asidik bir sıvıdır. Arılar, kendilerini tehdit altında hissettiklerinde iğnelerini kullanarak sokma yolu ile zehirlerini enjekte ederler. Arı zehiri, enzimler, şekerler, mineraller ve amino asitler dahil olmak üzere hem anti-enflamatuar hem de enflamatuar bileşikler içerir. Aktif kısmı, lokal iltihaplanmaya neden olan ve antikoagülan olarak işlev gören bir protein karışımını içerir. Arı zehiri, histamin, feromonlar, enzimler, peptitler, amino asitler ve diğer asitlerin bir karışımıdır. Mevcut ana enzimler fosfolipaz A, hiyalüronidaz ve lesitinazdır; ana peptitler mellitin, apamin ve peptit 401 iken, arı zehiri sitotoksiktir. Arı zehiri, kalp ve adrenal bezleri uyarırken sinir sistemini inhibe etmektedir.

Arı zehirinin kullanımı, glukokortikoidlerin yardımıyla, enflamatuar artritin ilerlemesini yavaşlatabilmektedir. Krylov ve Bardahcieva (19) tarafından yapılan bir deneyde, köpeklerde kornea hasarının, %0.06 arı zehiri içeren bir merhem uygulandıktan sonra arı zehirinin yüksek biyo-uyarıcılığı sayesinde, kontrol grubuna göre daha hızlı ve daha kaliteli bir iyileşme gösterdiğini belirtmişlerdir. Bu sonuçlar, arı zehirinin yüksek biyostimülatif, antiseptik ve antienflamatuar etkilerine atfedilmektedir.
Süt ineklerinde arı zehiri uygulamasının mastitise karşı terapötik etkisinin başarılı olduğu yapılan çalışmalar ile kanıtlanmıştır. Han ve arkadaşları (20) tarafından yapılan çalışmada, mastitisli süt ineklerinin meme somatik hücre sayıları (SCC) değerlendirilmiştir. Bu çalışmaların sonuçlarına göre, arı zehirinin enjeksiyon olarak kullanılmasının, hayvan sağlığı uygulamalarında viral enfeksiyon, artritis ve mastitise karşı güvenli ve etkili bir alternatif olabileceği belirtilebilir.

Bal ve Hayvancılıkta Kullanımı

Bal, en fazla bilinen arı ürünlerindendir. Türk Gıda Kodeksine göre bal; bitki nektarlarının, bitkilerin canlı kısımlarının salgılarının veya bitkilerin canlı kısımları üzerinde yaşayan bitki emici böceklerin salgılarının bal arısı tarafından toplandıktan sonra kendine özgü maddelerle birleştirerek değişikliğe uğrattığı, su içeriğini düşürdüğü ve petekte depolayarak olgunlaştırdığı doğal üründür. Balın yapısında; şekerler, su ve organik asitler, mineral tuzlar, vitaminler, proteinler, fenolik bileşikler, yağlar ve serbest amino asitler gibi diğer minör bileşikler, laktonlar, vitaminler (B1, B2, C ve nikotinik asit), polen, balmumu ve pigmentler bulunmaktadır (21).

Bal, antibakteriyel özelliği nedeniyle hayvanlarda yara iyileşmesine yardımcı olabilmekte ve antibiyotiğe dirençli suşlar dahil olmak üzere enfekte olan bakterileri hızla temizlemektedir. Bal, antibakteriyel özelliğinden dolayı cilt dokusuna derinlemesine hızlı bir difüzyon geliştirilebilmekte ve böylece derin yerleşimli enfeksiyonlara ulaşabilmektedir. Balın ozmotik etkisi, yara yatağını temizlemekte, nemli ve temiz tutmaktadır. Baldaki hidrojen peroksit insülin benzeri bir etkiye sahip olması nedeniyle yara iyileşmesini desteklemektedir. Balın ayrıca atlardaki yaraların tedavisinde de etkili olduğu kanıtlanmıştır. Atlarda, çoğunlukla bacaklarının alt kısımlarında meydana gelen yaralar, metisiline dirençli *Staphylococcus aureus* (MRSA), *Staphylococcus aureus, Escherichia coli, Streptococcus equi,* metisiline dirençli *Staphylococcus epidermis* (MRSE) ve *Pseudomonas aeruginosa* türleridir. Pollock (2013) tarafından yapılan bir çalışmada, test edilen 11 çeşit baldan sekizinin tüm suşlara karşı etkinlik gösterdiği ve en iyi sonuçların manuka balı ve hafifçe ısıtılmış bal ile elde edildiği belirtilmiştir. Manuka balının yüksek terapötik etkinliği birçok çalışma ile doğrulanmıştır (22).

Apilarnil ve Hayvancılıkta Kullanımı

Apilarnil biyolojik olarak aktif özelliklere sahip bir arı ürünüdür. Apilarnil, erkek arı larvalarının pupa döneminde geçmeden önceki 3-7 günlük larval safha dönemleridir (23). Apilarnil, hasat edilen larva homojenatının süzülmesi ve toz haline getirilmesi ile elde edilir. Apilarnil homojen ve sütümsü kıvamda olan, sarımsı gri renkte, ekşi tatta bir maddedir. Kolayca olgunlaşır ve dondurucuda ham halde saklanır. Su (%65-75), proteinler (%9-12), karbonhidratlar (%6-12), yağ asitleri ve lipitler (%3.5-8) K, Na, Ca, Mg mineralleri (%1-1.5) içerir. Amino asitler (treonin, lösin, izolösin, metiyonin) ve ayrıca testosteron, prolaktin, progesteron ve östradiol gibi seks hormonları bulunur (Stangaciu, 1999). Varroa‟ların (arı parazitleri) erkek arı gözlerinde daha fazla bulunması nedeniyle erkek arı gözlerinin bulunduğu petekler kesilir ve arıcılar tarafından atılır. Apilarnil, erkek arı gözlerinden alınarak elde edilir; öğütme (ezme, öğütme), homojenizasyon, filtrasyon ve liyofilizasyon işlemlerinden geçirilir. Ancak bu işlemden sonra apilarnil uygun şekilde saklanabilir ve / veya kullanılabilir (3).

Yapılan çalışmalar, apilarnilin antiviral, bağışıklık sistemi arttırıcı, anabolik stimülatör özelliği de dahil olmak üzere birçok yararlı özelliğe sahip olduğunu ve iştahı, vücudun enerjisini, canlılığını ve rejeneratif gücünü arttırdığını göstermiştir. Aynı zamanda erkeklerde testosteron salgılanmasını uyaran yüksek düzeyde protein ve aktif bileşenler içermesi sebebi ile hayvansal üretimde bir yem takviyesi olarak kullanımı önemlidir. Apilarnil, spermin miktarı ve kalitesi üzerinde doğrudan bir etki yaratarak damızlık erkek hayvanların daha uzun süre kullanılmasını sağlamaktadır. Apilarnil, erkeklerde androjenik hormonların varlığı nedeniyle spermatogenezin uyarılmasına yardımcı olur. Bu nedenle apilarnilin hem androjenik hem de anabolik etkilere sahip olması ve büyümeyi ve cinsel gelişimi teşvik etmek için ilaçlara ve kimyasallara doğal bir alternatif olarak düşünülmesi beklenmektedir (23).

Apilarnil uygulamasının broylerlerde büyüme performansı ve eşeysel gelişim üzerindeki etkisini belirlemek için bazı çalışmalar yapılmıştır. Yücel ve arkadaşları (23) tarafından 17 günlük 40 pilicin (Ross-308) kullanıldığı bir deneyde, 5 günlük bir adaptasyon süresi verilen hayvanlar tartılmış, kontrol ve tedavi gruplarına ayrılmış ve kafeslere konulmuştur. Araştırmacılar, deneyin sonunda büyüme döneminde (22 ila 42 gün arasında) 4 gr/gün apilarnilin erkek piliçlere uygulanmasının vücut ağırlığı, yem alımı ve yem dönüşüm oranı üzerinde etki göstermediğini, bununla birlikte, ibik uzunluğu ve sakal uzunluğu gibi ikincil cinsiyet özellikleri üzerinde gelişimin kaydedildiğini belirtmişlerdir

Altan ve arkadaşları (24) tarafından yapılan çalışmada, apilarnil uygulamasının büyüme performansı üzerinde olumsuz bir etkisi olmadığı, bununla birlikte kan şekeri ve kolesterol konsantrasyonlarını düşürdüğü, cinsel olgunlaşmayı uyardığı ve korkuyu azalttığı görülmüştür.

Sonuç

Çalışmalardan elde edilen veriler değerlendirildiğinde, hayvansal üretimde arı sütü, propolis, polen, bal, arı zehiri ve apilarnil gibi arı ürünlerinin kullanımının sentetik kimyasallar ve antibiyotiklerden arı sağlıklı yaşama daha fazla fayda sağladığı görülmektedir. Arı ürünleri, antioksidan, antifungal, antibakteriyel gibi bağışıklık artırıcı özellikleri ile daha güvenli ve sağlıklıdır. Ancak, arı ürünlerinin içeriğindeki kimyasal ve biyoaktif bileşiklerin farklı canlı türlerinin organizmaları üzerindeki etkileri yeterince bilinmemektedir. Arı ürünlerinin ve izole bileşiklerin yararlarını ve etki mekanizmalarını kanıtlamak için daha fazla araştırma ve çalışmalara ihtiyaç duyulmaktadır. Arı ürünlerinin hayvancılıkta uygulanma olanaklarının geliştirilmesi için etki mekanizmalarını ortaya koyan detaylı bilimsel

çalışmalara gereksinim vardır. Arı ürünlerinin yem katkı maddesi olarak kullanımının hayvansal üretimde pratik bir beslenme stratejisi sunabileceği sonucuna varılabilmektedir. Kullanılacak arı ürünlerinin kalitesinin ve standardizasyonunun iyileştirilmesi, arı ürünlerinin yapısal karmaşıklığı ve değişkenliği için güvenilir ve öngörülebilir bir temel oluşturmak açısından önemlidir. Arı ürünlerinin daha yaygın olarak üretiminin ve kullanımının arıcılar için kârlı hale gelebileceği ve üretimin artabileceği öngörülmektedir.

Kaynaklar

[1] Premratanachai P, Chanchao, C. Review of the anticancer activities of bee products. *Asian Pac. J. Trop. Biomed*. 2014; 4 (5): 337-344.
[2] Benfenati L. Sabatini, AG. Nanetti A. Composizione in sali minerali della gelatina reale, Apicoltura. 1986; 2: 129-143.
[3] Stangaciu S. Apitherapy course notes, Constanta apitherapy research hospital, Bucuresti-Romania.1999.
[4] Gimenez-Diaz B, Emsen E, Emsen E, Kutluca M, Koycegiz F. Improved reproductive response of sheep in intrauterine insemination program with the use of royal jelly. African Journal of Biotechnology. 2012; 11(61):12518-12521
[5] Yücel B, Önenç A, Kaya A, Altan Ö. Effects of propolis administration on growth performance and neonatal diarrhea of calves. SOJ Veterinary Sciences, 2015; 1(1):102-106.
[6] Nolkemper S, Reichling J, Sensch KH, Schnitzler P. Mechanism of herpes simplex virus type 2 suppression by propolis extracts. Phytomedicine. 2010;17 (2): 132-138.
[7] Bankova V. Chemical diversity of propolis and the problem of standardization. J. Ethnopharma. 2005; 100 (1-2): 114-117.
[8] Abdel-Rahman MA, Mosaad GM. Effect of propolis as additive on some behavioral patterns, performance and blood parameters in Muscovy broiler ducks. J. Adv. Vet. Res. 2013;3 (2): 64-68.
[9] Açıkgöz Z. Yücel B, Altan Ö. The effects of propolis supplementation on broiler performance and feed digestibility. Arch. Geflügelkunde.2005; 69(3): 117-122.
Morsy AS, Soltan YA, Elzaiat HM, Sallam SMA, Alencar SM, Louvandini H, Abdalla AL. Effect of two types of Brazilian propolis extracts on rumen gas and methane production and truly degradability in vitro, Middle East and North Africa Journal of Animal Science 2011; 4 (1): 446 – 456.
[10] Zawadzki F, Prado IN., Marques JA, Zeoula LM., Rotta PP, Sestari BB, Valero MV, Rivaroli DC. Sodium monensin or propolis extract in the diets of feedlot-finished bulls: effects on animal performance and carcass characteristics. J. Anim. Feed Sci. 2011; 20, 16-25.
[11] Aguiar SC, Cotica SM, Boeing JS, Samensari RB, Santos GT, Visantianer JV, Zeoula LM. Effect of feeding phenolic compounds from propolis extracts to dairy cows on milk production, milk fatty acid composition, and the antioxidant capacity of milk, Animal Feed Science and Technology. 2014; 193: 148-154.
[12] Oliveira MC, Silva DM, Loch FC, Martins PC, Dias DMB, Simon GA. Effect of bee pollen on the immunity and Tibia characteristics in broilers. Brazilian Journal of Poultry Science. 2010; 15: 323-328
[13] Brindza J, Gróf J, Bacigálová K, Ferianc P, Tóth, D. Pollen microbial colonization and food safety. Acta Chimica Slovaca. 2010; 3: 95102.
[14] Wang J, Li S, Wang Q, Xin B, Wang H. Trophic effect of bee pollen on small intestine in broiler chickens. Journal of Medicinal Food. 2007; 10: 276-280.
[15] Cheng Y. Effect of bee pollen on the growth of immune organs of miscellaneous broilers. Animal Husbandry and Feed Science. 2009; 30: 23-24.
[16] Haščík P, Elimam I, Garlík J, Kačániová M, Čuboň J, Bobko M, Vavrišinová K, Arpášová H. The effect of bee pollen as dietary supplement on meat chemical composition for broiler Ross 308. Acta Universitatis Agriculturae et Silviculturae Mendelianae Brunensis. 2013; 61: 71-76.
[17] Kokuludağ A. Arı zehiri içeriği ve tıbbi özellikleri. Arı Ürünleri ve Sağlık (Apiterapi). Editör: Akçiçek, E., Yücel, B. İzmir: Sidas Yayınları, 2015.
[18] Krylov NV, Bardahchieva LV. The use of ungapiven in veterinary surgery. The XXXVth. Apimondia Congress, 1-6 September, Antwerp- Belgium, 1997: 205.

[19] Han SM, Lee KG, Yeo HJ, Hwang SJ, Chenoweth PJ, Pak SC. Somatic cell count in milk of bee venom treated dairy cows with mastitis. Journal of Applied Animal Scence. 2009; 1 (4):104-109.
[20] Molan PC. The antibacterial activity of honey 2. Variation in the potency of the antibacterial activity. Bee World. 1992; 73 (2): 59-76.
[21] Bansal V, Medhi B, Bandhi P. Honey – A remedy rediscovered and its therapeutic utility. Kathmandu Univ. Med. J.2005; 3(11): 305-309.
[22] Yücel B, Açıkgöz Z, Bayraktar H, Şeremet Ç. The Effects of Apilarnil (Drone Larvae) Administration on Broiler Performance and Secondary Sex Characteristics. Journal of Animal and Veterinary Advances. 2011; 10(17): 2263-2266.
[23] Altan Ö, Yücel B, Açıkgöz Z, Şeremet Ç, Kösoğlu M, Turgan N, Özgönül AM. Apilarnil reduces fear and advances sexual development in male broilers but has no effect on growth. British Poultry Science. 2013;54(3):355-361.

Doğal Ekosistemin Sürdürülebilirliği Açısından Bal Arısı ve Çevre İlişkilerinin Değerlendirilmesi

Mustapha Ndimballan [1*], *Banu Yücel* [2]
[1]*Ege Üniversitesi, Fen Bilimleri Enstitüsü, Bornova-İzmir/Türkiye*
[2]*Ege Üniversitesi Ziraat Fakültesi Zootekni Bölümü, Bornova- İzmir/Türkiye*
**İletişimden sorumlu yazar: ndimssta@gmail.com*

Özet

Belirli bir alandaki canlı ve cansız çevrenin karşılıklı ilişkileri sonucu oluşan ve süreklilik gösteren ekolojik sistemlere "ekosistem" denilmektedir. Ekolojik dengenin korunmasında önemli bir alana sahip olan ve doğadaki en gelişmiş sosyal böceklerden olan bal arıları besin gereksinimlerini karşılamak amacıyla çiçekli bitkiler ve meyve ağaçlarından polen ve nektar toplarken bitkilerin döllenmesine, biyoçeşitliliğe ve ürün artışına katkıda bulunmaktadırlar. Bitkilerin tozlaşması rüzgarla (anemofoli), böceklerle (entomofoli) özellikle de bal arıları ile gerçekleşmektedir. Böylece içinde arı bulunan bahçelerde, tarım arazilerinde ve bitkisel alanlarda döllenme oranı ve tohum tutma çok yüksek olmaktadır. Arılar yoğun uçuşlarıyla rüzgara ve diğer böceklere kıyasla bu döllenmeyi başarıyla gerçekleştirmektedir. Bal arılarının tozlaşmaya katkısı, bitkisel ürünlerin kalite ve kantitesi üzerine olumlu etki yaratmakta, pek çok endemik ve tıbbi bitkinin üretilmesine, toprak erozyonunu önleme, seralarda hormon ve açık tarım arazilerinde insektisit kullanımını azaltmakta, dolayısıyla doğal yaşamın sürdürülebilirliğine ve ülkesel ekonomiye önemli katkı sağlamaktadır. Arıların ekolojik dengedeki hassas konumlarını etkileyen birçok faktör vardır. Bunların sebebi genel olarak ne yazık ki insanların yanlış davranışlarının ve teknolojik gelişmelerin sonuçlarıdır. Bal arıları havadaki CO2 seviyesini azaltarak ekolojik dengenin korunmasına yardımcı olmaktadır. Küresel ısınma, iklim değişikliği, çarpık kentleşme, rüzgar enerji santralleri, yaygın mobil ve kablosuz teknolojilerinin kullanımı, elektromanyatik radyasyonun çoğalması çevre koşullarını, bir başka deyişle sürdürülebilir yaşam şartlarını olumsuz etkilediği gibi, yaşamın olmazsa olmaz değeri bal arılarını da büyük ölçüde tehdit etmektedir. Bu konuda ivedi stratejik, ekonomik ve idari tedbirlerin alınması önem taşımaktadır.

Anahtar Kelimeler: bal arısı, sürdürülebilir ekosistem, çevre, doğal yaşam

Giriş

İnsan var oluşundan bu yana, doğadan yararlanmıştır. Ancak gelişen teknolojinin olanaklarıyla, doğayı sınırsızca kullanmaya, ona zarar vererek tüketmeye başlamıştır. Çevreye verilen bu zararlar, doğanın kendini yenileyebilme özelliği nedeniyle başlangıçta önemsenmemiş, hatta çevrenin doğal döngüsü ile bu kirliliği yok edeceği düşünülmüştür. Zaman içinde çevreye bırakılan kirliliğin nicel ve nitel olarak artması, çevrenin kendini yenileyebilme özelliğinin çok üstüne çıkmış ve çevre hızla bozulmaya başlamıştır (1).

Çevreyi oluşturan temel unsurlar olan; hava, su ve toprak arasında, ekolojik bir denge ve çok yönlü bir etkileşim bulunmaktadır. Bu nedenle hava, su ve toprak unsurlarından herhangi birinin kirlenmesi, diğerlerini de olumsuz etkilemektedir. Bir başka deyişle, kirlenme sadece kullanıldığı alanda sınırlı kalmamaktadır. Bu ekolojik etkileşimde, arı gibi tozlayıcıların etkisi büyüktür. Bal arısı da dahil olmak üzere, arıların belki de en önemli işlevleri, doğada çeşitli yabani ve kültür bitkilerinin tozlaşmasını sağlayarak, birçok bitki türlerinin soylarını devam ettirmelerine ve yeryüzüne yayılmalarına yardımcı olmalarıdır. Bitkileri gıda ve yuva yapma yeri olarak kullanan pek çok hayvan türü de bal arılarından dolaylı olarak yararlanmaktadır (2).

Son yıllarda, çevresel kaynaklı sorunların yarattığı olumsuz etkiler başta bal arıları olmak üzere pek çok canlı türünün yaşamını tehdit etmektedir. Tarımda kullanılan pestisidler, bal arıları hastalık ve zararlıları ile mücadelede kullanılan kimyasallar, çevre kirliliği, arılar arası doğal rekabete dayalı ilişkiler, radyasyon, iklimsel değişmeler ve küresel ısınma, son yıllarda ciddi arı kayıplarına yol açan ancak nedeni kesin olarak belirlenemeyen "koloni çökme bozukluğu" (CCD veya Maria Celeste Sendromu), bal arısı kolonileri için önemli çevresel sorunlar olarak görülmektedir (3).

Kimyasallar (Pestisit, Herbisit, İnsektisit)

Hızla artan dünya nüfusunun besin ihtiyacını karşılayabilmek için, kültür bitkilerinde ürün kayıplarına neden olan yüzlerce hastalık ve zararlılar ile sürekli mücadele, kaçınılmaz bir zorunluluk halinde devam etmektedir. 1940'larda DDT' nin bitkisel üretimde kullanılmaya başlanılmasıyla kimyasal savaş önem kazanmaya başlamış ve giderek daha fazla tür ve miktarda insektisit tarım alanlarında kullanılır hale gelmiştir. Bitkisel tozlaşmada çok önem taşıyan bal arıları ve yaban arıları ise, tarım ilaçlarından olumsuz yönde etkilenmektedir. Bitki üzerine bulaşan insektisit ile doğrudan temas eden arılar, kovana geri dönüş sırasında uçuşa geçememekte veya kovana ulaşsa dahi, kovan önünde ölmektedirler. Çoğu arı zehirlenmesi, bitkiler çiçeklenme döneminde iken kullanılan insektisitler ile gerçekleşir. Böcek öldürücü tozlar, tarlacı arıların arka bacaklarında taşıdıkları polenlere yapışır (4). Böcek öldürücü (insektisit) ilaçların arıları zehirlemesi, nektar ve polen toplanması sırasında; ağız, temas ve solunum olmak üzere üç yolla meydana gelmektedir. Arı zehirlenmesinin en çok görülen belirtisi, kovan önünde aşırı miktarda ölü arı yığınlarının görülmesidir. Diğer bir belirti ise kovandaki tarlacı arı populasyonunun azalmasıdır. Çoğu pestisid, arıların saldırganlığının artmasına yol açar. Klorlu hidrokarbonlara ve organofosfatlı insektisitlere maruz kalan arılarda uyuşukluk, felç, anormal davranışlar, nektar özünü kusarak çıkarma, dilin dışarı doğru çıkması gibi belirtiler görülür. Kovan önünde dolaşan fakat uçamayan arılar gözlenir. Arsenik, metil parathoin gibi kimyasallar ile zehirlenmede kovan önünde ölü yavrular gözlenir. Petek gözlerine gerekli bakımı yapan arıların sayısının yetersiz olması nedeniyle larva ölümleri gerçekleşir. Bazı durumlarda tüm kovandaki arılar ölebilir. Ana arı polen ile yuvaya getirilen, özellikle yavaş etki gösteren kimyasallar (arsenik gibi) tarafından olumsuz etkilenebilir, hareketlerinde anormallik ve yumurta veriminde azalma görülebilir. Zayıflayan kolonilerin pek çoğu kış mevsimini geçiremez ve ölür (4).

Zararlılar

Tüm canlılarda olduğu gibi birçok hastalık ve zararlı, arıların yaşamlarını tehdit etmektedir. Çevre kirliliği, atık maddeler ve gazların neden olduğu küresel ısınma, gezgin arıcılığın yoğunluğu, koloni bakım ve yönetiminde yapılan yanlış uygulamalar, bal arısı hastalık ve zararlılarının hızla yayılmasına neden olmaktadır. Bugün bal arılarına en çok zarar veren parazit *Varroa jacobsoni'dir.* Varroa; kovanda ergin arı populasyonunun azalmasına, yavru gelişmesinde gerilemeye, kuluçka petek gözlerinde düzensizliğe, hastalık etmeni patojenlerin gelişmesine, arıların kovanı terk etmesine, bal veriminde düşmeye, ileri boyutta kovanın sönmesine neden olan tehlikeli bir dış parazittir (5).

Doğa Kaybı

Doğanın zarar görmesi, arı topluluklarını büyük derecede etkiler. Doğa yıkımının ana nedenleri: mono-kültürel ekim, meraların aşırı otlatılması, sulama ve arazilerin temizlenmesidir.

Doğal bitki örtüsünün yok olması, bal arısı popülasyonlarının çöküşüne sebep olabilir. Arılar geniş, sürekli, birbirine bağlı, uygun doğal bitki örtüsüne ihtiyaç duyar. Küçük ölçekli habitatlar, bal arılarının yayılma kabiliyetini ve yuva bölgelerinin sayısını, mevcut besin kaynaklarını azaltır (6).

Çevresel Kirlilik

Bal arıları, bitkilerden nektar ve polen toplayarak beslenirler. Bu sebeple çevre ile sürekli ilişki içerisinde bulunurlar. Bu faaliyetlerini gerçekleştirirken, çevrede bulunan bazı kimyasal madde ve atıkları da, topladıkları çiçek tozları ile birlikte yuvalarına taşırlar. Tabiatta çevreyi kirleten atık ve toksik maddeler (genellikle endüstriden çıkan dumanlar, araçlardan yayılan gazlar, tarımda zararlılarla mücadelede kullanılan ilaçlar) çevrede bulunan bitkiler tarafından emilerek depolanırlar. Daha önce de vurgulandığı üzere, çevreye yayılan toksik nitelikteki atık maddeler, bal arılarını zehirlemektedir. Büyük bölümü antropolojik faktörler sonucu (kentleşme, endüstrileşme, enerji üretimi, mobil kaynaklar ve diğer kirleticiler) ortaya çıkan hava kirliliğinin önemli sonuçlarından biri de, ağır metal kirliliğidir. Baca ve egzoz gazlarından kaynaklanan atmosferdeki ağır metal kirliliği insan, hayvan ve bitkiler için çeşitli olumsuzlukları da beraberinde getirmiştir. Bu olumsuz şartlardan bitkilerin sadece vejetatif organları değil aynı zamanda generatif organları da etkilenmektedir. Bunlardan biri de erkek üreme hücresi olan; polenlerdir. Kadmiyum, kobalt, bakır, çinko, kurşun, nikel ve civa gibi çeşitli ağır metal katyonlarının, doğrudan polenleri, dolaylı olarak da bunlarla beslenen bal arılarını olumsuz yönde etkilediği bilinmektedir (2).

Arılar farklı türden çiçeklerin polenlerini topladığı için, bitki bünyesinde fazla miktarda bulunan ağır metal, arıların vücudunda ve bu bitkilerin nektarlarından ürettikleri balların içeriğinde, toksik ağır metal konsantrasyonun da artmasına neden olmaktadır. Sanayi tesisleri ve kent alanlarının ürettiği kimyasal atıklar; toprağın asitleşmesine, mevcut ve potansiyel yeraltı ve yerüstü su kaynaklarının kirlenmesine, biyolojik aktivitelerin azalmasına, toprak yapısının olumsuz etkilenmesine yol açmaktadırlar. Bu maddeler, bitkilerin topraktaki besin maddelerinden yeterince yararlanamamasına ve bitki gelişimini yavaşlatarak verimlilikte azalmaya, yetiştirilen ürünlerde bazı mikro besin maddelerinin toksik düzeylere ulaşmasına neden olmaktadırlar. Anılan olumsuzluklar, bal arılarının temiz polen ve nektar kaynakları bulmalarını zorlaştırmaktadır (3).

Rekabete Dayanan İlişkiler

Bal arıları için diğer önemli bir sorun da; bal üretimini artırmak amacıyla dış ülkelerden getirilen yabancı bal arısı ırklarından kaynaklanmaktadır. İthal edilen arı ırkları, yerli ırkların yaşam bölgelerini kısıtlamakta, yerli gen kaynaklarımızın giderek yok olmasına yol açmaktadır. İthal edilen koloniler, yerli ekotiplerle bitkisel kaynakların kullanımı ve yuva yeri bakımından rekabete girebilir, doğal floradaki bitkilerin polinasyonunu engelleyebilir, parazit ve patojenlerin taşınmasına ve yerli ekotiplerle çiftleşerek genetik açılmalara neden olabilirler.

Küresel Isınma

Küresel ısınma önümüzdeki yüzyılın en önemli çevre gündemlerinden biri olacaktır. Küresel iklimde meydana gelecek değişmeler, arılar da dahil pek çok hayvanın davranışını ve yaşam tarzlarını etkileyebilecektir. Arıların küresel ısınma sonucu, çevrede oluşacak değişimlere nasıl bir fizyolojik tepki verecekleri ya da uyum gösterecekleri konusunda çok fazla bir bilgi yoktur. Küresel ısınma, genellikle çevresel şartları değiştirerek dolaylı yoldan arılara etki etmektedir. Küresel ısınmanın doğaya en önemli etkisi, iklimlerde meydana getirdiği değişimlerdir. İklimde meydana gelen değişimler aynı zamanda canlıların yaşadığı çevrenin karakterlerini de değiştirecek ve bu değişimler de o ekolojik ortamda yaşayan arı toplumlarının davranışlarını dolaylı olarak etkileyecektir. Ekolojik sistemin bitki örtüsünde küresel ısınmanın bir sonucu olarak ortaya çıkacak değişimler, bitki örtüsü ile etkileşim içinde bulunan arı topluluklarını da olumsuz değişikliğe zorlayacaktır. Küresel ısınmaya bağlı olarak ortaya çıkan iklim değişiklikleri bitkiler üzerine birkaç yolla etki eder. Kurak ve yarı kurak alanların genişlemesine ek olarak, yaz kuraklığının süresinde ve şiddetindeki artışlar çölleşme sürecini hızlandıracak ve birçok bitki türü kuruyup, yok olacaktır. İlkbaharda meydana gelmesi gereken çiçeklenmenin zamanlaması değişebilecek, üretici değişen sıcaklıklara göre ektikleri ürünün cinsini ve dikilme zamanını ayarlamaya çalışacaktır. Böylece arıların gezdiği birçok bitki türünün çiçeklenme dönemleri değişeceği için, arılar bundan olumsuz yönde etkilenecektir. Bunun yanı sıra hava sıcaklığında ve neminde meydana gelen değişiklikler, bal arılarının biyolojik ve davranışsal özelliklerini de değiştirebilecektir (1).

Mevsimsel değişiklikler ile yabani arı ırklarının yayılışı etkilendiği için, yabani arılar ile bal arıları arasındaki rekabet artacaktır. Yabani arıların yeni alanlara yayılması ve popülasyonlarının aşırı artması, bitkisel kaynakların kullanımı ve yuva yeri bulmada doğal polinatörler ile rekabet yaşanmasına, parazit ve patojenlerin taşınmasına, doğal floranın polinasyonunun azalmasına ve yerel türler ile melezleşerek bu türlerin yok olmasına neden olabilecektir. Bal arıları, mevsim koşullarından ve ani ısı değişikliklerinden oldukça fazla etkilendiğinden ötürü, arı kayıplarında artma beklenebilir. Küresel ısınma nedeniyle, kışların "sıcak" geçmesi, bitkilerin kış mevsiminde gereksinim duydukları yeterli "soğuklanma"'nın gerçekleşmemesine neden olabilir. Bu da, ilkbaharda bitkilerin anılan nedenle yeterli polen ve nektar üretememelerine yol açabilir. Çevrede yeterli nektar ve polen olmaması durumunda bal arıları kolonileri, gelecek generasyonun sürekliliğinin sağlanması amacıyla, kovanlarında bal olması halinde bile, kovanı terk etme yoluna gitmektedirler. Bu durum bal arılarının ne kadar hassas "biyoindikatörler" olduğunu ortaya koymaktadır. Bir başka deyişle bal arıları, nektar akımı döneminde, çevrede nektar ve polen kaynaklarının ne derece yeterli olup olmadığını en hassas şekilde belirleyebilmekte, yaşamlarını planlayabilmektedirler (3).

Koloni Çökme Bozukluğu (CCD)

Son aylarda medyayı son derece meşgul eden ve arıcılar arasında tedirginlik yaratan koloni çökme bozukluğunun (CCD) nedeni halen kesin olarak bilinemese de, bunu tetikleyen bir çok olasılık üzerinde durulmaktadır. Bunlar arasında: dış parazitler, ergin ve yavru hastalıkları, bilinen yada bilinmeyen patojenler, ergin arıların yetersiz beslenmesi, GDO'lu tarım, genetik çeşitliliğin azlığı, ergin arılarda

görülen stres unsurları, bal ve balmumundaki ilaç kalıntıları, tarımsal mücadelede kullanılan yeni kimyasallar, baz istasyonlarından yayılan radyasyon gibi etmenler yer almaktadır. Koloni çökme bozukluğunu araştıran bilim adamları, kovana dönemeyen arıları toplayıp yaptıkları incelemelerde, arıların bal midesinde yüksek düzeyde bakteri, virüs ve mantar bulmuştur. Yapılan çalışmalarda, şiddetli enfeksiyonun toksik etkinin yüksekliğine bağlı olarak bal arılarında bağışıklık sistemini çökerttiği belirlenmiştir. Kovanların sık yer değiştirmesine bağlı olarak arılarda meydana gelen stresin, arıların hastalıklara karsı hassaslaşmasına ve diğer hastalık ve parazitlere karsı duyarlı hale gelmesine neden olabileceği belirtilmektedir. CCD'nin en belirgin özelliği, sağlıklı görünen kovanlardaki ergin arıların bir gece içerisinde ölüm belirtisi göstermeksizin, ortadan kaybolmasıdır.

Kovanda ana arıyı ve yavruları arkada bırakarak giden ergin arılar kovana geri dönmemekte ve kovandaki ergin arı sayısı giderek azalmaktadır. Oysa ki arı davranışını bilenler, bunun son derece sıra dışı bir olay olduğunu anlayacaklardır. Bu kovanlar ergin arı sayısındaki azalmaya bağlı olarak yetersiz beslenme nedeniyle güçsüz düşmekte, ana arıları olsa dahi yok olmaktadırlar. Dolayısı ile bu kadar büyük ölçekte ve ani bal arısı kaybı, CCD'nin incelenmesini zorlaştırmaktadır. Ayrıca kovanın da hastalık taşıdığına dair bir ipucu da yoktur. Günümüze dek kesin nedeni anlaşılamamakla beraber, CCD konusunda çalışan bilim adamları, varroa ve hastalıklarla mücadeleden, GDO'lu tarım alanlarına, bitkisel mücadelede kullanılan ilaçlardan, baz istasyonlarından yayılan radyasyona dek pek çok konuyu göz önüne alarak, CCD kuşkusu altındaki arılıklarda alınması gereken önlemlerle ilgili görüşlerini açıklamışlardır (4).

CCD, görülen arılıklarda, kaybedilen kovanlardaki arıların güçlü kovanlarla birleştirilmesi kesinlikle önerilmemektedir. Şayet CCD, enfeksiyonla ilgili bir etmene dayanıyorsa, bu işlem sağlıklı kolonilerin de kaybına neden olabilecektir. CCD'nin Nosema gibi sinsi ilerleyen ergin arı hastalıkları ile ilgili bir bağlantısı olduğundan da kuşkulanılmaktadır. Çünkü, CCD kuşkusu ile otopsi yapılan arıların bal midelerinde görülen mantar sporları, nosemanın buna yol açmış olabileceği kuşkusunu artırmaktadır. Özellikle nosema sporu taşıyan kolonilerde, diğer hastalık etmeni patojenlere karşı duyarlılık da oldukça yüksektir. Bu durumda enfekte kolonilerin saptanması, karantinaya alınarak fumagilinli şeker şurubu ile besleme yapılarak tedavi edilmesi önerilmektedir. Şayet kolonide Varroa aşırı yüksek düzeyde ise, arıların malpighi tüpleri üzerinde olumsuz etki yaratan kuvvetli kimyasalların (okzalik asit, fluvalinate, coumaphos, amitraz, apistan) kullanımından kaçınılmalıdır. Bu kimyasalların kullanımından sonra kovanların kimi zaman hızla boşalması, ana arıda dölsüzlük gibi sorunlar da gündeme gelmektedir. Ayrıca, varroanın taşıyıcı görevini üstlendiği kimi virüslerin de etkisinin olduğundan kuşkulanılmaktadır.

Mısır, pamuk, soya, kanola, ayçiçeği tarlalarına götürülen kovanlarda CCD'nin daha fazla görülmesi, son zamanlarda bu bitkilere uygulanan değişik pestisid uygulamalarının bal arıları üzerinde olumsuz etki yaratmış olabileceğini de ortaya koymaktadır. Anılan bitkilere uygulanan "neonikotinoidler", bitkilere zarar veren emici böceklerin kontrolünde kullanılan sistemik insektisitlerdir. Bu grup insektisitler son dönemde çok yaygın olarak kullanılmakta olup, çok düşük dozda dahi, bal arıları üzerine olumsuz etki yaratmaktadır. Kovana getirilen nektar ve polenle beslenen genç arılar bundan daha fazla etkilenmekte, larvaların beslenmesini aksatmakta, CCD'li kovanlarda terk edilmiş larvalı çerçeveler dikkat çekmektedir. Ergin tarlacı arılar ise, neonikotinoid grubu insektisitlerin etkisi ile hafıza kaybına uğramakta, yön bulma yeteneklerini yitirmektedir. Bağışıklık sistemleri zayıflamakta ve hastalıklara daha açık hale gelmektedir. Etki aylar sonra da meydana gelebilmektedir.

Yapılan çalışmalar, imidacloprid gibi sistemik insektisitlerin arılarda davranış bozukluğuna neden olduğunu, arıların yön bulma yeteneklerini yitirdiklerini, hafızalarını kaybettiklerini ve kovana dönmekte zorlandıklarını ortaya koymaktadır. Bunu tetikler nitelikte, artan baz istasyonlarından yayılan radyasyon dalgalarının, arıların yön bulma yeteneklerini olumsuz yönde etkilediğini ortaya koyan çalışmalar da bulunmaktadır. Bütün bunların yanı sıra ümit vaadeden bir ipucu ise, CCD'in yerli ekotiplerde, ithal arılara göre daha az görülmesi, bu arıların bölgedeki ekolojiye daha yüksek uyum yetenekleri bulunması nedeniyle bağışıklık sistemlerinin de güçlü olması avantajıdır. Belki de bu bulgu, yıllarca empoze edilen, ancak bir türlü istenilen başarının yakalanamadığı "ithal arılarla" arıcılık yerine, yerli ekotipler üzerinde yapılması gereken ıslah çalışmalarının hızlanması ve geliştirilmesi için dikkat çekici olarak değerlendirilmelidir.

Sonuç

Bütün dünyada çeşitli nedenlerle arı kayıplarının görüldüğü bir gerçektir. Ümit vaadeden bulgu ise, yerli ekotiplerde, ithal arılara göre daha az arı kaybı görüldüğü gerçeğidir. Bu arıların bölgedeki ekolojiye daha yüksek uyum yetenekleri bulunması nedeniyle bağışıklık sistemlerinin de daha güçlü olduğu görülmektedir. Belki de bu bulgu, yıllarca empoze edilen, ancak bir türlü istenilen başarının yakalanamadığı "ithal arılarla" arıcılık yerine, yerli ekotipler üzerinde yapılması gereken ıslah çalışmalarının hızlanması ve geliştirilmesi için dikkat çekici olarak değerlendirilmelidir. Bal arılarının yaşamdaki önemleri yadsınamaz bir gerçektir. Giderek yaşanması zorlaşan çevresel koşulların bal arıları üzerinde yarattığı olumsuz etkiler, aynı zamanda dünyamızın da geleceğini yok etmektedir. Yaşamımıza ekonomik ve biyolojik olarak çok önemli katkıları olan bal arısının yaşamsal döngüdeki sürekliliğini sağlayabilmek, çevresel sorunların en az düzeye indirilme çabasını gerektirmektedir.

Kaynaklar

[1] Akbulut S. Küresel Isınmanın Böcek Popülasyonları Üzerine Muhtemel Etkileri, Çevre ve Koruma Dergisi 2000, 25-27.
[2] Kevan PG. Pollinators as Bioindicators of The State of The Environment: Species, Activitiy and Diversity, Agriculture, Ecosystems & Environment. 1999; 74(1-3): 373-393.
[3] Celi G, Maccagnani B. Honey Bees as Bioindicators of Environmental Pollution, Bulletin of İnsectology.2003; 137-139.
[4] Hooven L, Sagili R, Johansen E. How to reduce bee poisoning from pesticides. A Pasific Northwest Extension Publication, PNW 591, 2005.
[5] Akyol E, Korkmaz A. Bal arısı (*Apis mellifera*) Zararlısı Varroa destructor'un Biyolojisi, Uludağ Arıcılık Dergisi. 2005; 122-127.
[6] Çetin U. Isı değişimlerinin Arı Kayıplarına Etkileri, Uludağ Arıcılık Dergisi. 2004; 171-174.

Congress Photo Gallery / Kongre Fotoğraf Galerisi


LIVE
on Custom Live Streaming Service
İZMİR KÂTİP ÇELEBİ ÜNİVERSİTESİ
İZMİR Uluslararası Misafir Öğrenci Derneği
www.sciencecon.org
INTERNATIONAL
STUDENTS
SCIENCE
CONGRE
Mehmet Çevik


LIVE
on Custom Live Streaming Service
Murat Yulek


Üniversite Araştırmaları Platformu

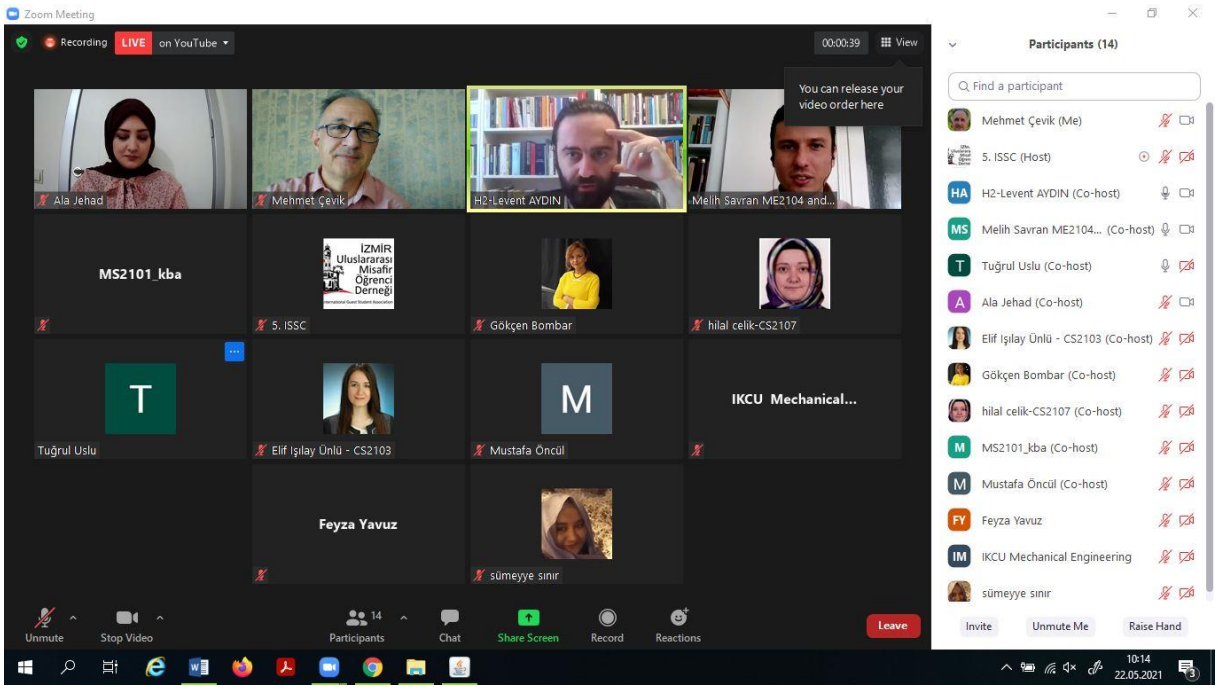
Zoom Meeting
Recording LIVE on YouTube
00:00:39
View
You can release your video order here
Participants (14)
Find a participant
Ala Jehad
Mehmet Çevik
H2-Levent AYDIN
Melih Savran ME2104 and...
MS2101_kba
5. ISSC
Gökçen Bombar
hilal celik-CS2107
Tuğrul Uslu
Elif Işılay Ünlü - CS2103
Mustafa Öncül
IKCU Mechanical...
Feyza Yavuz
sümeyye sınır
Mehmet Çevik (Me)
5. ISSC (Host)
H2-Levent AYDIN (Co-host)
Melih Savran ME2104... (Co-host)
Tuğrul Uslu (Co-host)
Ala Jehad (Co-host)
Elif Işılay Ünlü - CS2103 (Co-host)
Gökçen Bombar (Co-host)
hilal celik-CS2107 (Co-host)
MS2101_kba (Co-host)
Mustafa Öncül (Co-host)
Feyza Yavuz
IKCU Mechanical Engineering
sümeyye sınır
Unmute
Stop Video
Participants
Chat
Share Screen
Record
Reactions
Leave
Invite
Unmute Me
Raise Hand
10:14
22.05.2021

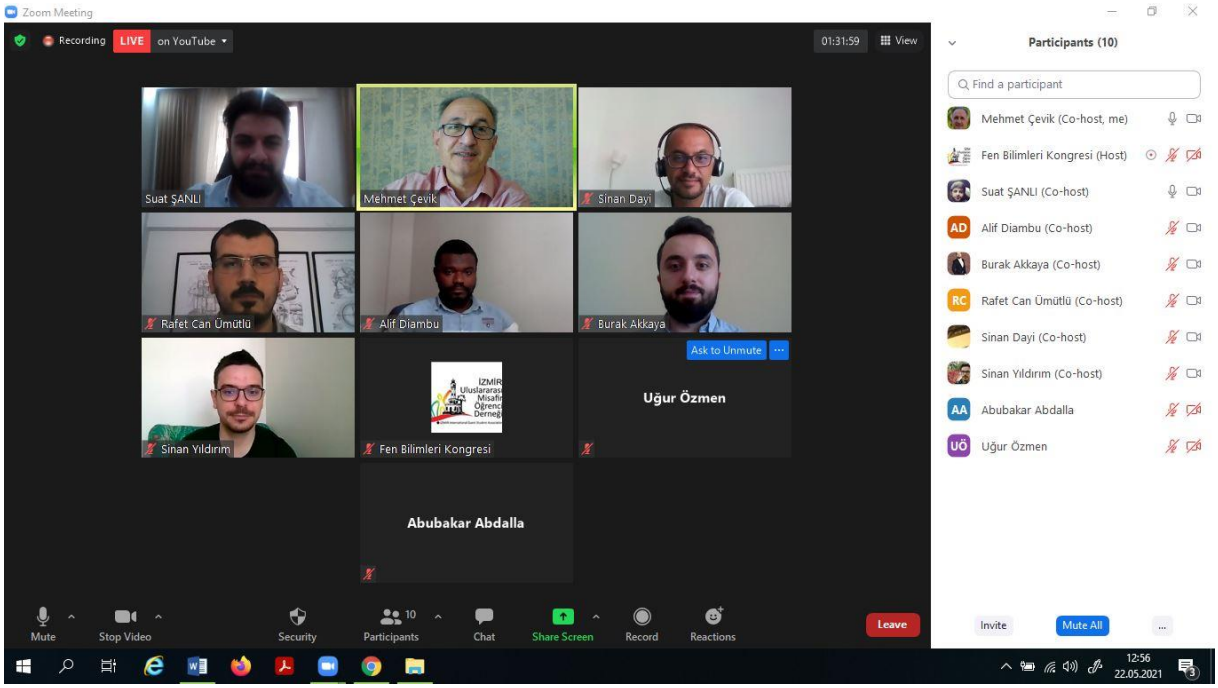
Zoom Meeting
Recording LIVE on YouTube
01:31:59
View
Participants (10)
Find a participant
Suat ŞANLI
Mehmet Çevik
Sinan Dayi
Rafet Can Ümütlü
Alif Diambu
Burak Akkaya
Ask to Unmute
Sinan Yıldırım
Fen Bilimleri Kongresi
Uğur Özmen
Abubakar Abdalla
Mehmet Çevik (Co-host, me)
Fen Bilimleri Kongresi (Host)
Suat ŞANLI (Co-host)
Alif Diambu (Co-host)
Burak Akkaya (Co-host)
Rafet Can Ümütlü (Co-host)
Sinan Dayi (Co-host)
Sinan Yıldırım (Co-host)
Abubakar Abdalla
Uğur Özmen
Mute
Stop Video
Security
Participants
Chat
Share Screen
Record
Reactions
Leave
Invite
Mute All
12:56
22.05.2021

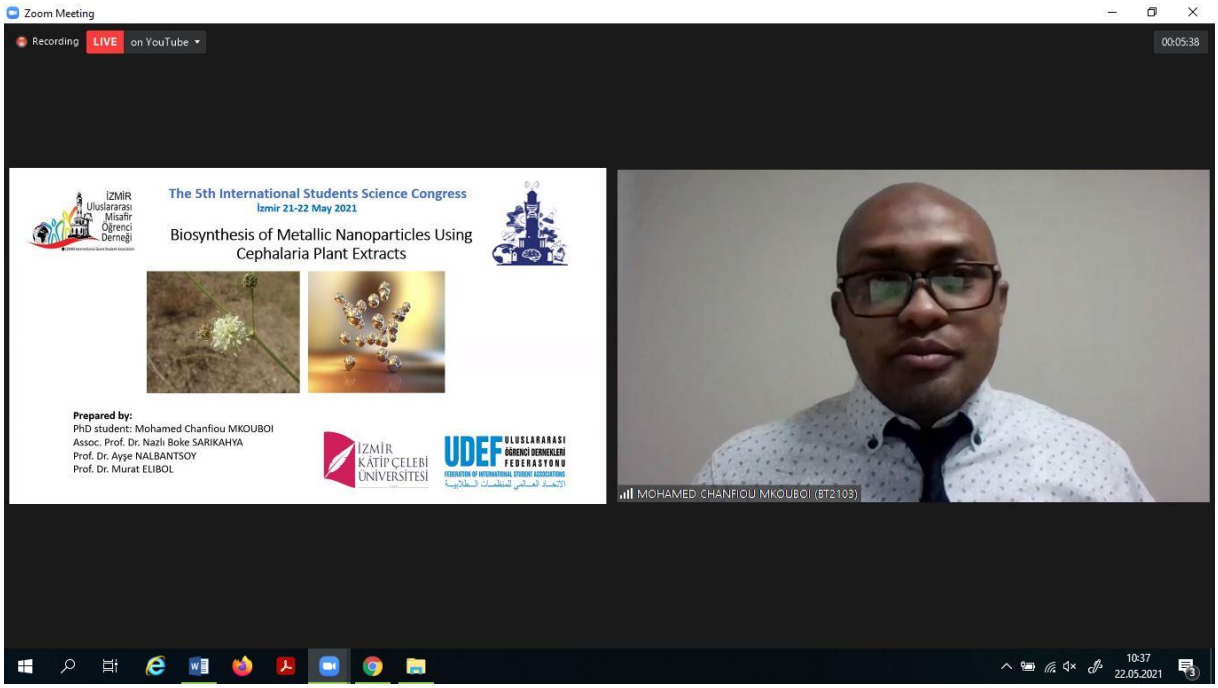
Zoom Meeting
Recording
LIVE
on YouTube
00:05:38
The 5th International Students Science Congress
İzmir 21-22 May 2021
Biosynthesis of Metallic Nanoparticles Using Cephalaria Plant Extracts
Prepared by:
PhD student: Mohamed Chanfiou MKOUBOI
Assoc. Prof. Dr. Nazlı Boke SARIKAHYA
Prof. Dr. Ayşe NALBANTSOY
Prof. Dr. Murat ELIBOL
MOHAMED CHANFIOU MKOUBOI (BT2103)
10:37
22.05.2021

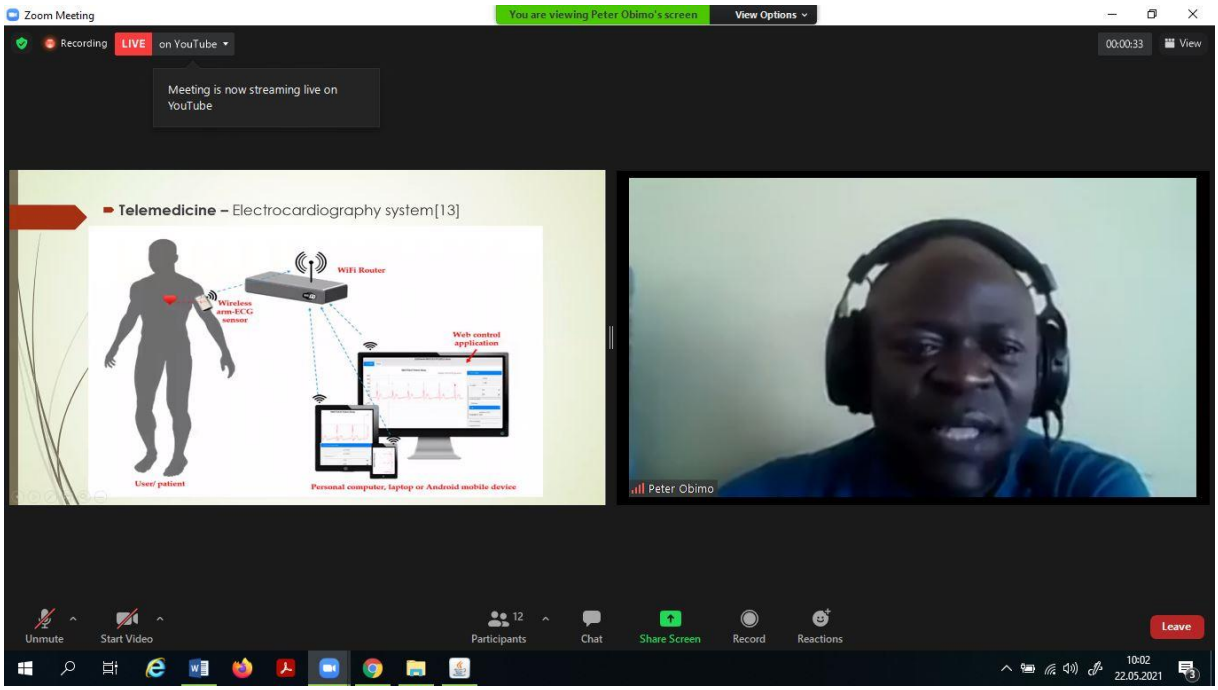
Zoom Meeting
You are viewing Peter Obimo's screen
View Options
Recording
LIVE
on YouTube
00:00:33
View
Meeting is now streaming live on YouTube
Telemedicine – Electrocardiography system[13]
WiFi Router
Wireless arm-ECG sensor
Web control application
User/ patient
Personal computer, laptop or Android mobile device
Peter Obimo
Unmute
Start Video
Participants
12
Chat
Share Screen
Record
Reactions
Leave
10:02
22.05.2021

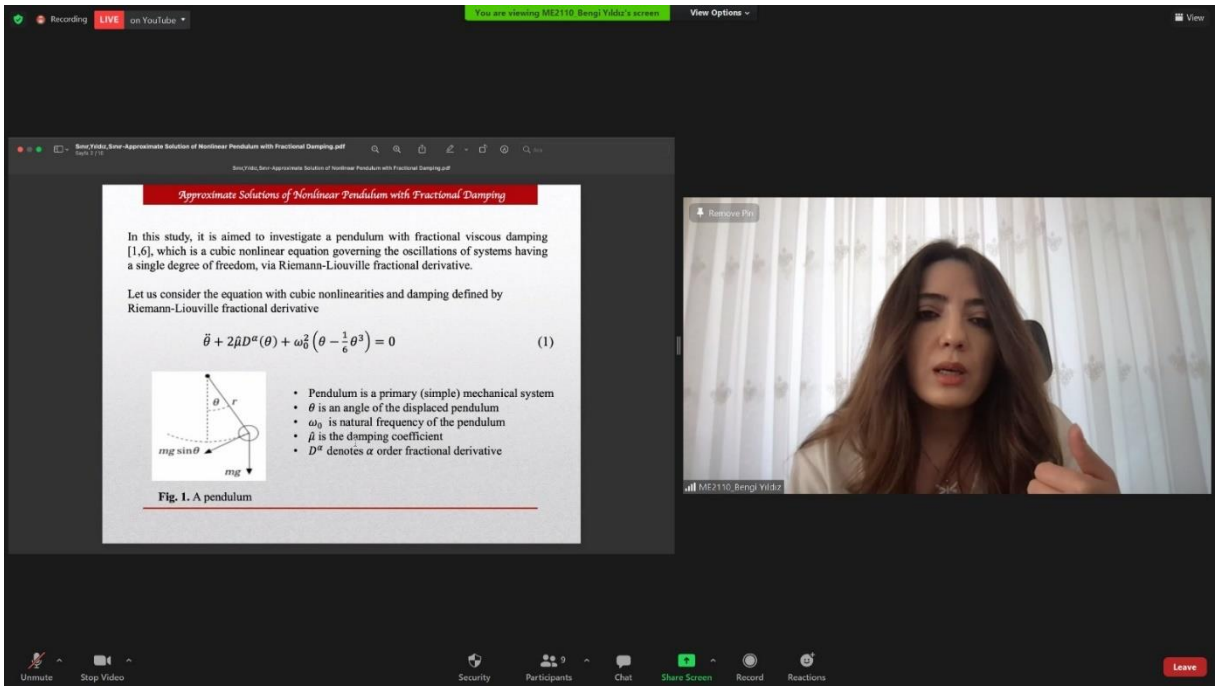
Recording LIVE on YouTube
You are viewing ME2110 Bengi Yildiz's screen
View Options
View
Approximate Solutions of Nonlinear Pendulum with Fractional Damping
In this study, it is aimed to investigate a pendulum with fractional viscous damping [1,6], which is a cubic nonlinear equation governing the oscillations of systems having a single degree of freedom, via Riemann-Liouville fractional derivative.
Let us consider the equation with cubic nonlinearities and damping defined by Riemann-Liouville fractional derivative
$\ddot{\theta} + 2\hat{\mu}D^{\alpha}(\theta) + \omega_0^2\left(\theta - \frac{1}{6}\theta^3\right) = 0$ (1)
Pendulum is a primary (simple) mechanical system
θ is an angle of the displaced pendulum
ω_0 is natural frequency of the pendulum
$\hat{\mu}$ is the damping coefficient
D^{α} denotes α order fractional derivative
Fig. 1. A pendulum
Remove Pin
ME2110_Bengi Yildiz
Unmute
Stop Video
Security
Participants
Chat
Share Screen
Record
Reactions
Leave

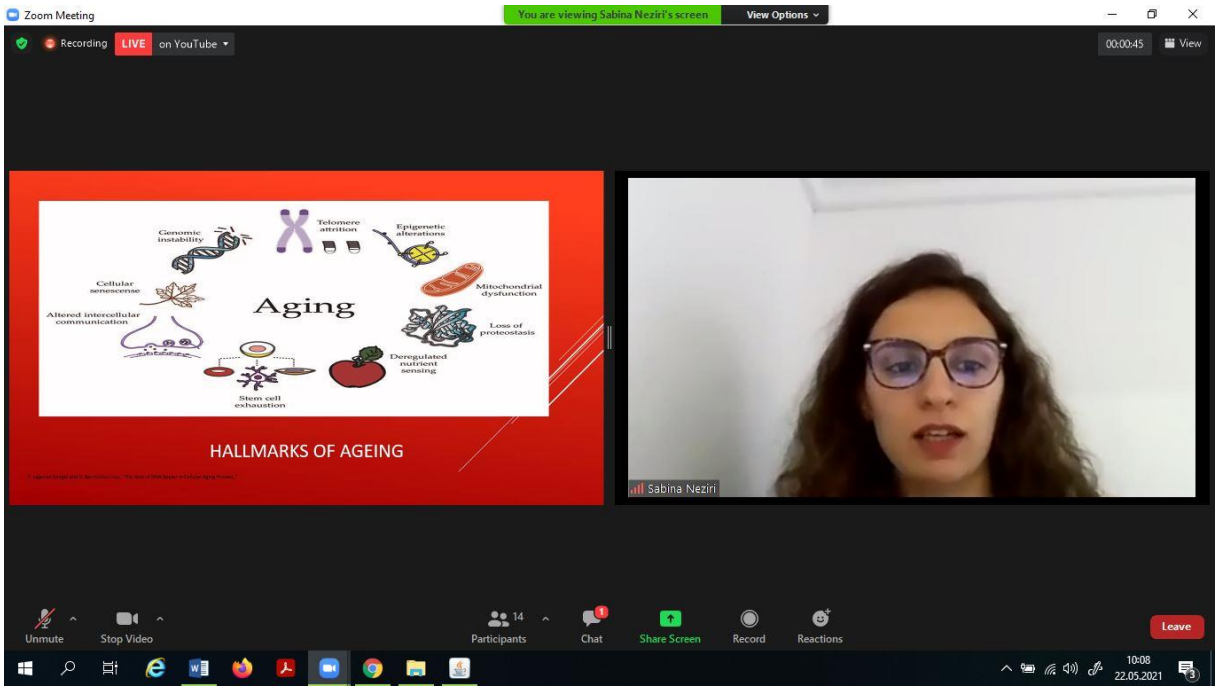
Zoom Meeting
You are viewing Sabina Neziri's screen
View Options
Recording LIVE on YouTube
00:00:45
View
Genomic instability
Telomere attrition
Epigenetic alterations
Cellular senescence
Aging
Mitochondrial dysfunction
Altered intercellular communication
Loss of proteostasis
Deregulated nutrient sensing
Stem cell exhaustion
HALLMARKS OF AGEING
Sabina Neziri
Unmute
Stop Video
14
Participants
Chat
Share Screen
Record
Reactions
Leave
10:08
22.05.2021

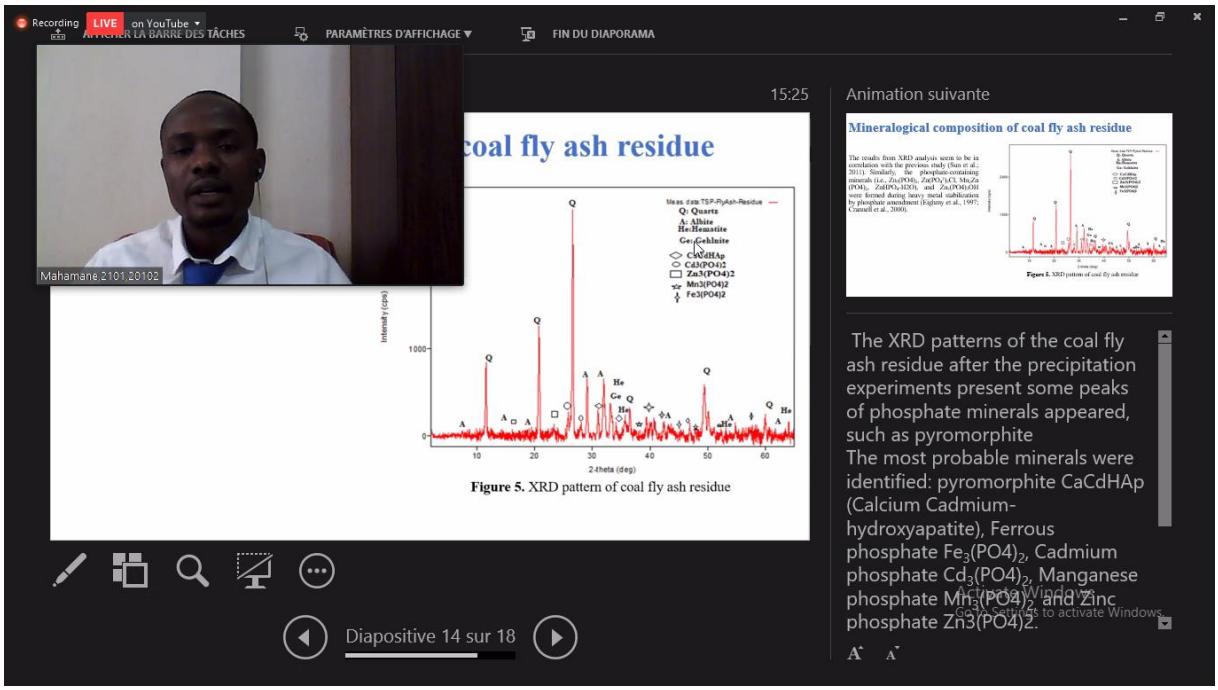
Recording LIVE on YouTube
PARAMÈTRES D'AFFICHAGE
FIN DU DIAPORAMA
15:25
Mahamane 2101 20102
coal fly ash residue
Figure 5. XRD pattern of coal fly ash residue
Animation suivante
Mineralogical composition of coal fly ash residue
The XRD patterns of the coal fly ash residue after the precipitation experiments present some peaks of phosphate minerals appeared, such as pyromorphite
The most probable minerals were identified: pyromorphite CaCdHAp (Calcium Cadmium-hydroxyapatite), Ferrous phosphate Fe3(PO4)2, Cadmium phosphate Cd3(PO4)2, Manganese phosphate Mn3(PO4)2 and Zinc phosphate Zn3(PO4)2.
Diapositive 14 sur 18


Zoom Meeting
You are viewing Omar QASIM ES2101's screen
View Options
LIVE on YouTube
00:00:40
View
6. Parameters of The Windmill's Efficiency
12
6.A The Effect of Solidity & Blade Number
Duquette et al [18] tested effect of solidity and the number of blades on the efficiency of the rotor, they tested separate rotors, with the same diameter of 510 mm, under controlled conditions in a wind tunnel.
They found that raising the number of blades from 3 to 12, while retaining a constant strength of 10%, decreased aerodynamic efficiency & power , due to low Reynolds number effects, although wind tunnel blockage impacted results.
5/22/2021
5. ISSC Congress
Mehmet Çevik
Murat Tuyan
5. ISSC Congress
EL2102-Hande...
GE2101_ABDULH...
Richard Roben S...
Sarah Waleed
Omar QASIM ES2101
Abdiaziz Hussein
Unmute
Start Video
Participants
Chat
Share Screen
Record
Reactions
Leave
14:36
22.05.2021

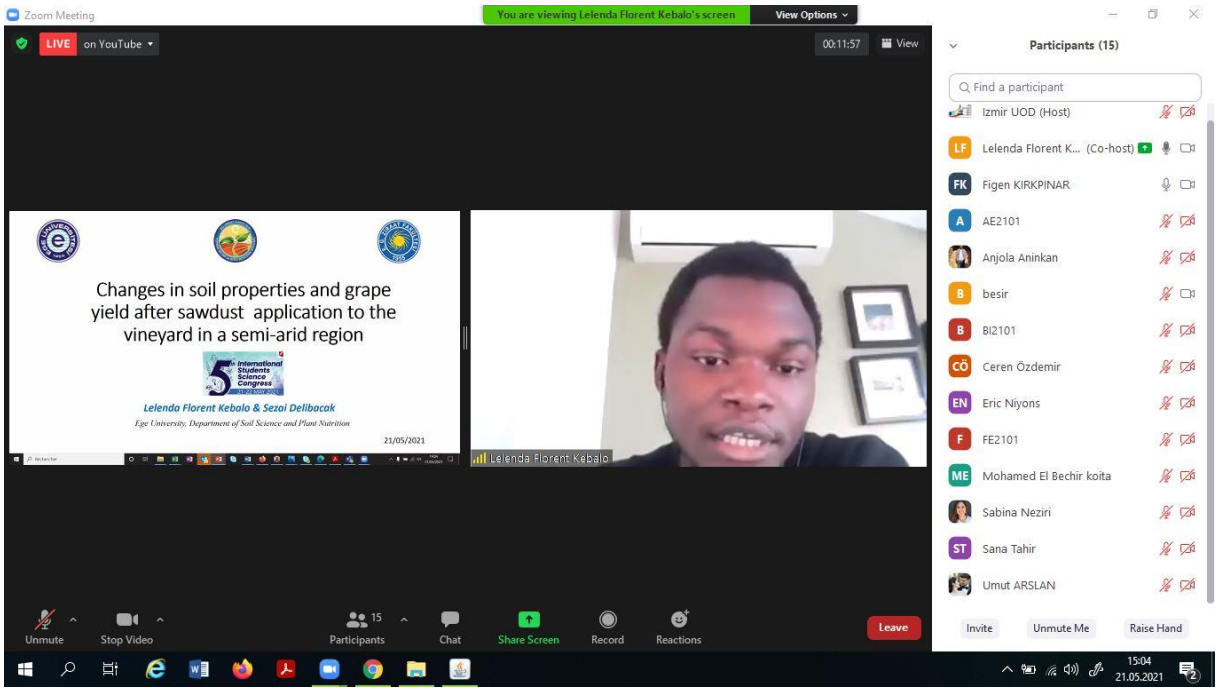
Zoom Meeting
You are viewing Lelenda Florent Kebalo's screen
View Options
LIVE on YouTube
00:11:57
View
Changes in soil properties and grape yield after sawdust application to the vineyard in a semi-arid region
Lelenda Florent Kebalo & Sezai Delibacak
Ege University, Department of Soil Science and Plant Nutrition
21/05/2021
Lelenda Florent Kebalo
Participants (15)
Find a participant
Izmir UOD (Host)
Lelenda Florent K... (Co-host)
Figen KIRKPINAR
AE2101
Anjola Aninkan
besir
BI2101
Ceren Özdemir
Eric Niyons
FE2101
Mohamed El Bechir koita
Sabina Neziri
Sana Tahir
Umut ARSLAN
Invite
Unmute Me
Raise Hand
Unmute
Stop Video
Participants
Chat
Share Screen
Record
Reactions
Leave
15:04
21.05.2021

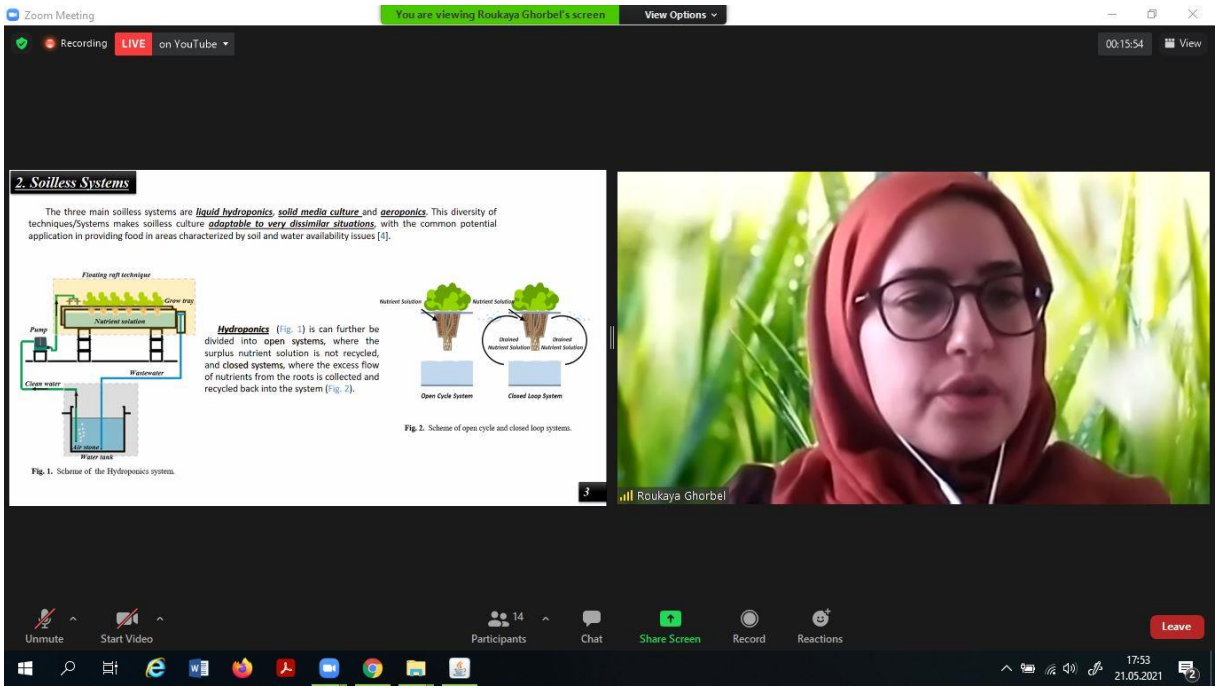
Zoom Meeting
You are viewing Roukaya Ghorbel's screen
View Options
Recording
LIVE on YouTube
00:15:54
View
2. Soilless Systems
The three main soilless systems are liquid hydroponics, solid media culture and aeroponics. This diversity of techniques/Systems makes soilless culture adaptable to very dissimilar situations, with the common potential application in providing food in areas characterized by soil and water availability issues [4].
Floating raft technique
Grow tray
Nutrient solution
Pump
Wastewater
Clean water
Air stone
Water tank
Fig. 1. Scheme of the Hydroponics system.
Hydroponics (Fig. 1) is can further be divided into open systems, where the surplus nutrient solution is not recycled, and closed systems, where the excess flow of nutrients from the roots is collected and recycled back into the system (Fig. 2).
Nutrient Solution
Drained Nutrient Solution
Open Cycle System
Closed Loop System
Fig. 2. Scheme of open cycle and closed loop systems.
3
Roukaya Ghorbel
Unmute
Start Video
Participants
Chat
Share Screen
Record
Reactions
Leave
17:53
21.05.2021

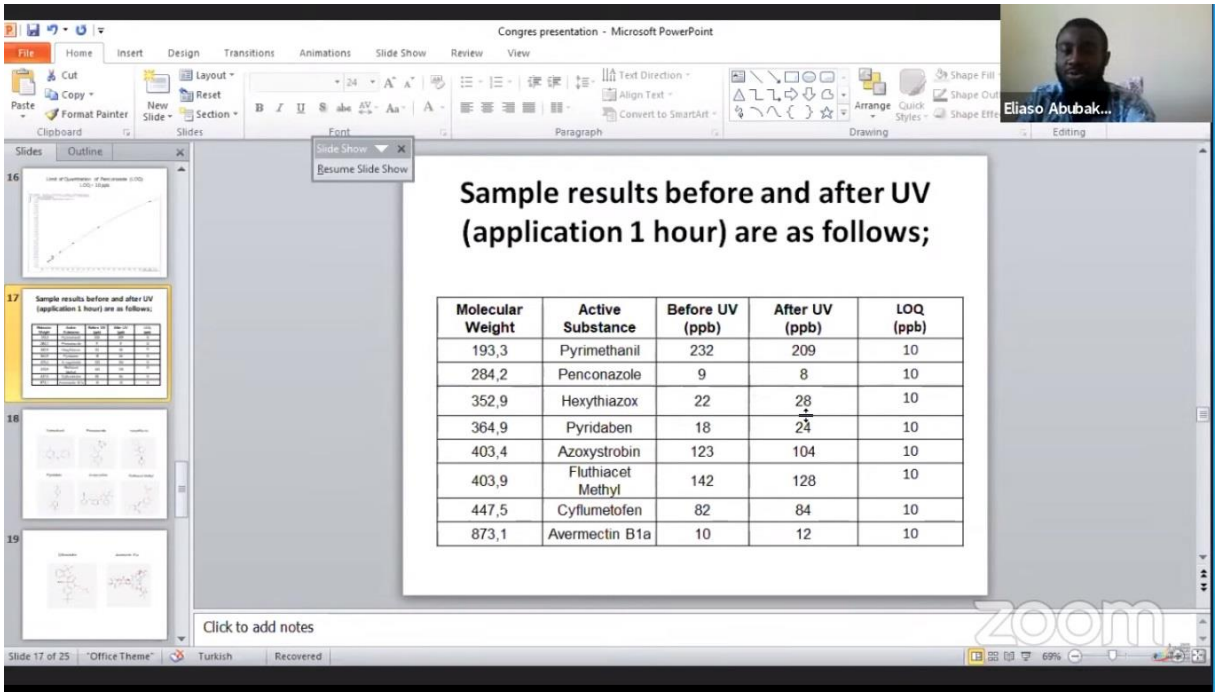

Molecular Weight	Active Substance	Before UV (ppb)	After UV (ppb)	LOQ (ppb)
193,3	Pyrimethanil	232	209	10
284,2	Penconazole	9	8	10
352,9	Hexythiazox	22	28	10
364,9	Pyridaben	18	24	10
403,4	Azoxystrobin	123	104	10
403,9	Fluthiacet Methyl	142	128	10
447,5	Cyflumetofen	82	84	10
873,1	Avermectin B1a	10	12	10

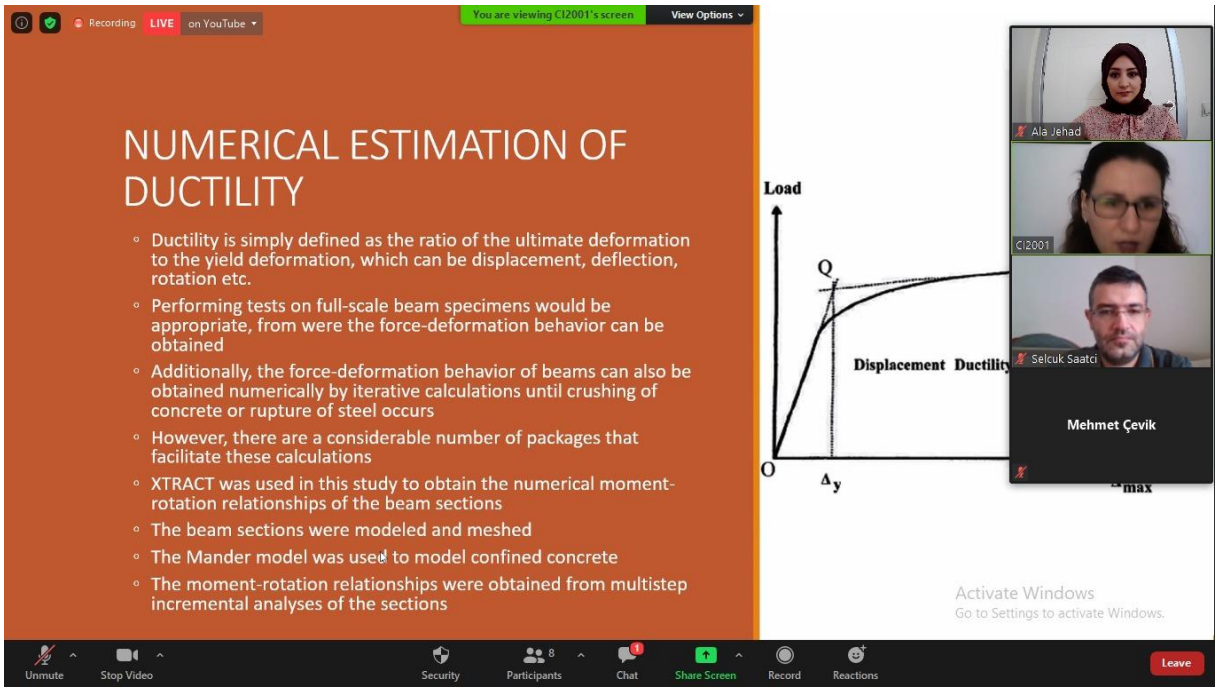


Recording...
LIVE
on YouTube
View
B. G. SINIR
İzmir UOD
Mehmet Çevik
Halis KANDAŞ
Bengusu erdal
Faruk Özger
Cihan Canıbek
Ala Jehad
EC2102-Peter Obimo
Eric Niyons
Ceren Özdemir
furkan emrem
ME2103-Kırmızıgöl-Acarer
Elf Işılay Ünlü
erman
M. Mustafa BAHŞI
Uğur Özmen
Kasım Karataş
Hadya TAŞÇI
Mustafa Öncül
5. ISSC Congress
Gökçen Bombar
Mohamed El Bechir koita
Ebru Taşkaya
sümeyye sınır
Ask to Unmute
Unmute
Stop Video
Security
Participants
Chat
Share Screen
Pause/Stop Recording
Reactions
More
End

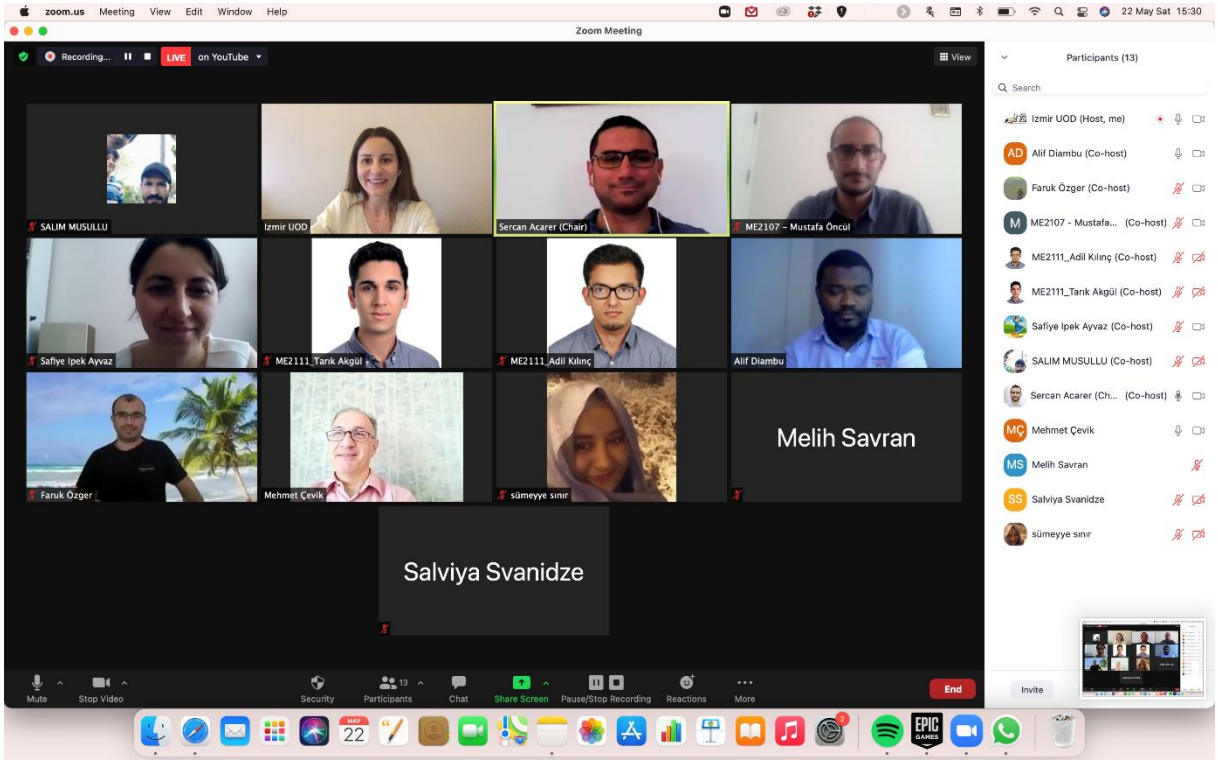
zoom.us
Meeting
View
Edit
Window
Help
22 May Sat 15:30
Zoom Meeting
Recording...
LIVE
on YouTube
View
SALIM MUSULLU
İzmir UOD
Sercan Acarer (Chair)
ME2107 – Mustafa Öncül
Safiye İpek Ayvaz
ME2111_Tarık Akgül
ME2111_Adil Kılınç
Alif Diambu
Faruk Özger
Mehmet Çevik
sümeyye sınır
Melih Savran
Salviya Svanidze
Participants (13)
Search
İzmir UOD (Host, me)
Alif Diambu (Co-host)
Faruk Özger (Co-host)
ME2107 - Mustafa... (Co-host)
ME2111_Adil Kılınç (Co-host)
ME2111_Tarık Akgül (Co-host)
Safiye İpek Ayvaz (Co-host)
SALIM MUSULLU (Co-host)
Sercan Acarer (Ch... (Co-host)
Mehmet Çevik
Melih Savran
Salviya Svanidze
sümeyye sınır
Mute
Stop Video
Security
Participants
Chat
Share Screen
Pause/Stop Recording
Reactions
More
End
Invite

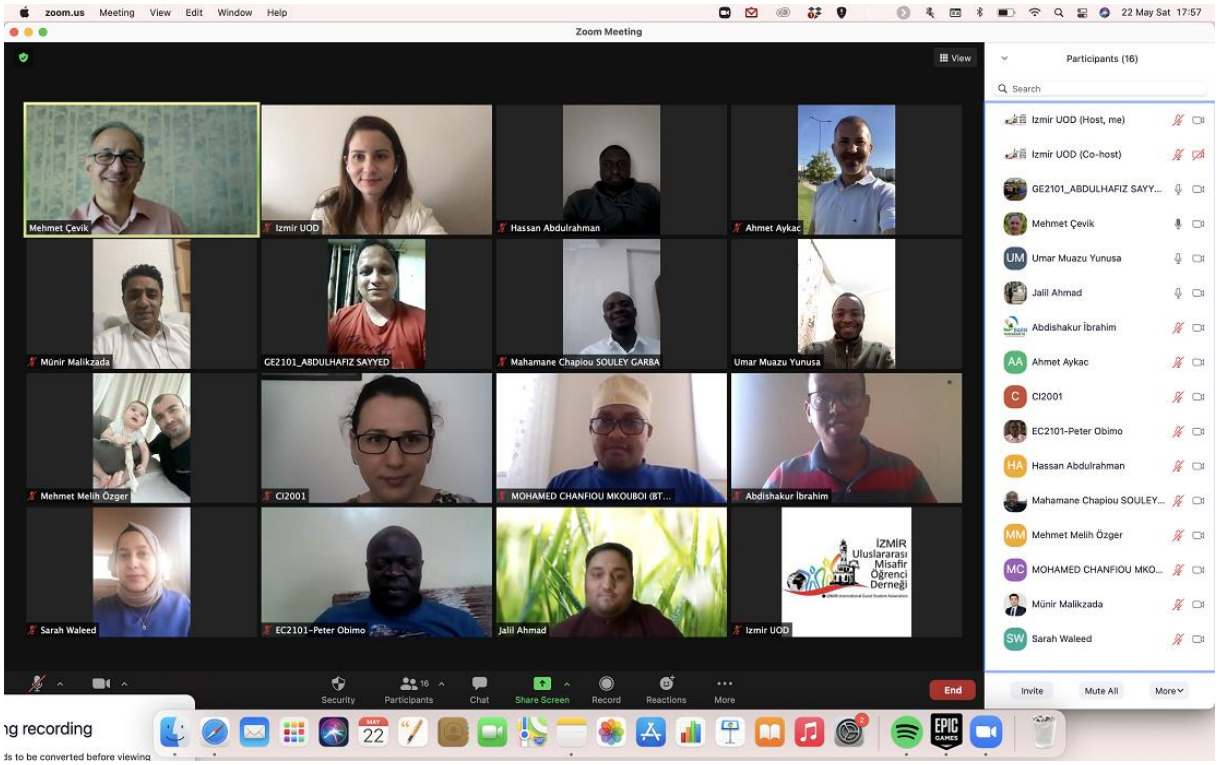
Zoom Meeting
Participants (16)
Mehmet Çevik
Izmir UOD
Hassan Abdulrahman
Ahmet Aykac
Münir Malikzada
GE2101_ABDULHAFIZ SAYYED
Mahamane Chapiou SOULEY GARBA
Umar Muazu Yunusa
Mehmet Melih Özger
CI2001
MOHAMED CHANFIOU MKOUBOI (BT...
Abdishakur İbrahim
Sarah Waleed
EC2101-Peter Obimo
Jalil Ahmad
Izmir UOD
End

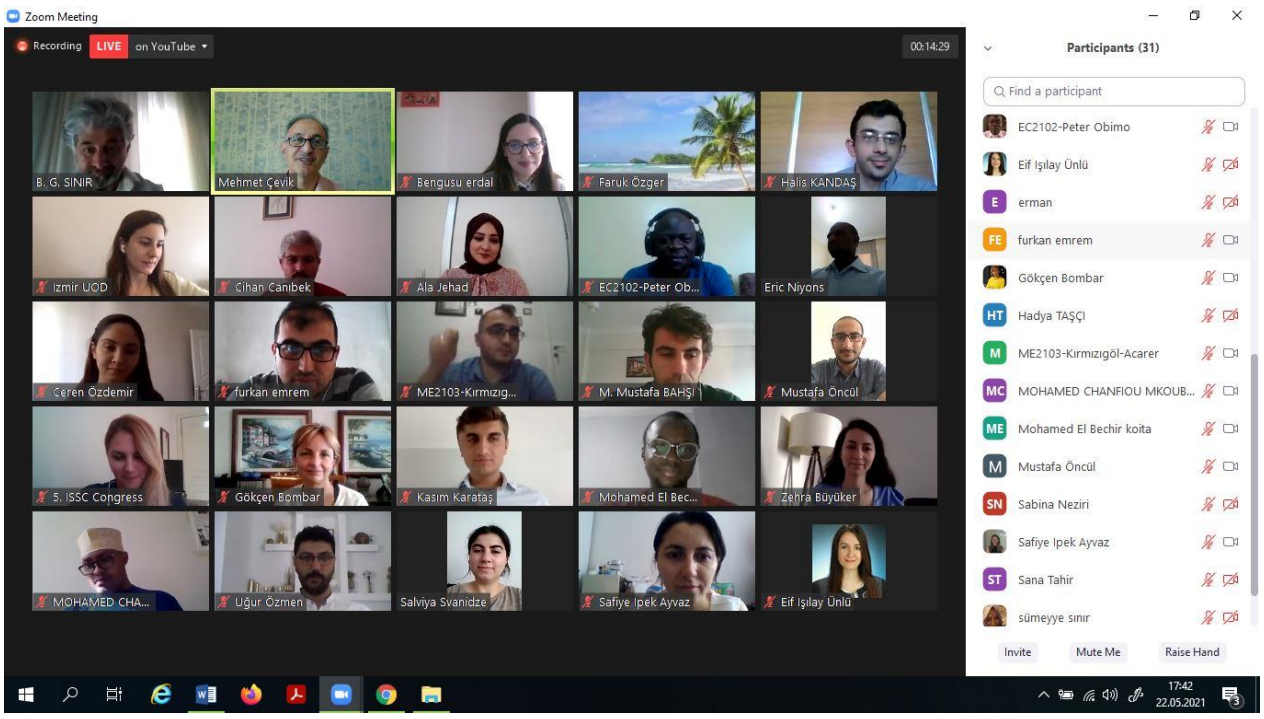
Zoom Meeting
Recording LIVE on YouTube
00:14:29
Participants (31)
Find a participant
B. G. SINIR
Mehmet Çevik
Bengusu erdal
Faruk Özger
Halis KANDAŞ
Izmir UOD
Cihan Canibek
Ala Jehad
EC2102-Peter Ob...
Eric Niyons
Ceren Özdemir
furkan emrem
ME2103-Kırmızıg...
M. Mustafa BAHŞİ
Mustafa Öncül
5. ISSC Congress
Gökçen Bombar
Kasım Karataş
Mohamed El Bec...
Zehra Büyüker
MOHAMED CHA...
Uğur Özmen
Salviya Svanidze
Safiye Ipek Ayvaz
Eif Işılay Ünlü
EC2102-Peter Obimo
Eif Işılay Ünlü
erman
furkan emrem
Gökçen Bombar
Hadya TAŞÇI
ME2103-Kırmızıgöl-Acarer
MOHAMED CHANFIOU MKOUB...
Mohamed El Bechir koita
Mustafa Öncül
Sabina Neziri
Safiye Ipek Ayvaz
Sana Tahir
sümeyye sınır
Invite
Mute Me
Raise Hand
17:42
22.05.2021

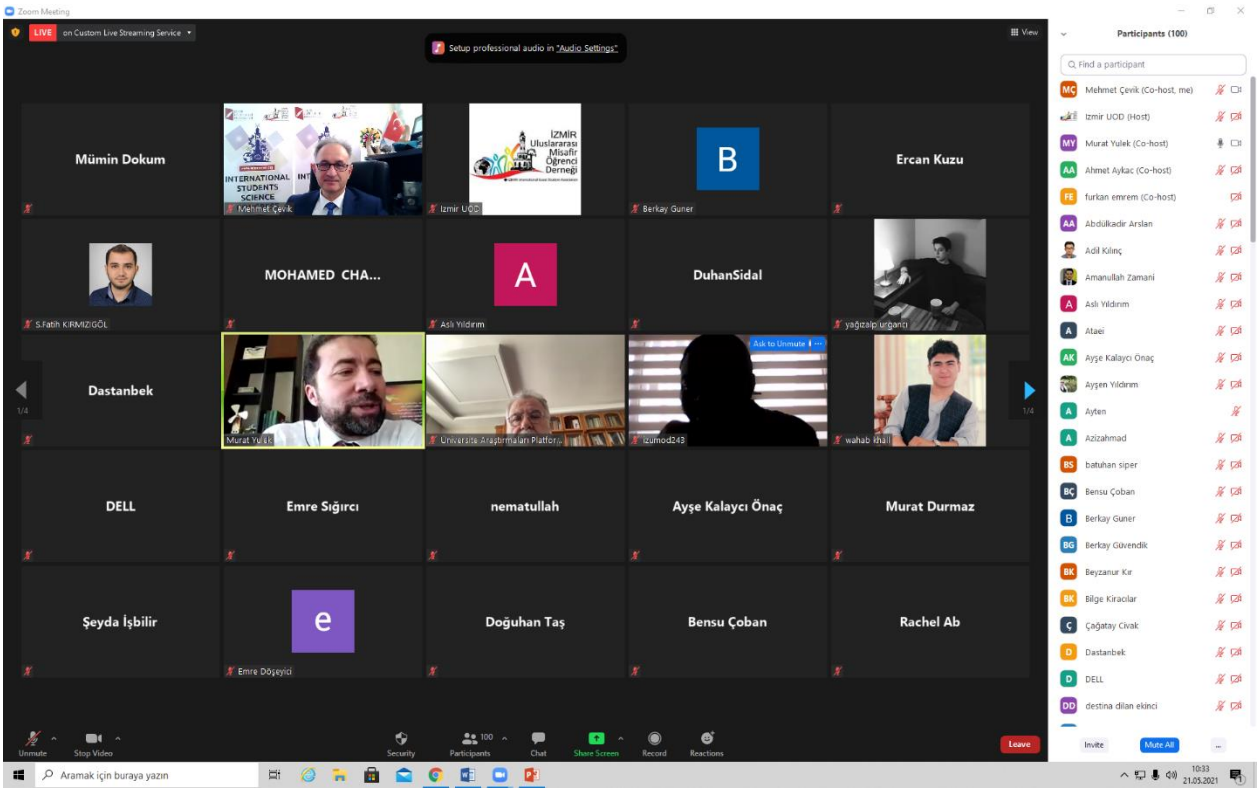
Mümin Dokum
Ercan Kuzu
MOHAMED CHA...
DuhanSidal
Dastanbek
DELL
Emre Sığırcı
nematullah
Ayşe Kalaycı Önaç
Murat Durmaz
Şeyda İşbilir
Doğuhan Taş
Bensu Çoban
Rachel Ab
Participants (100)

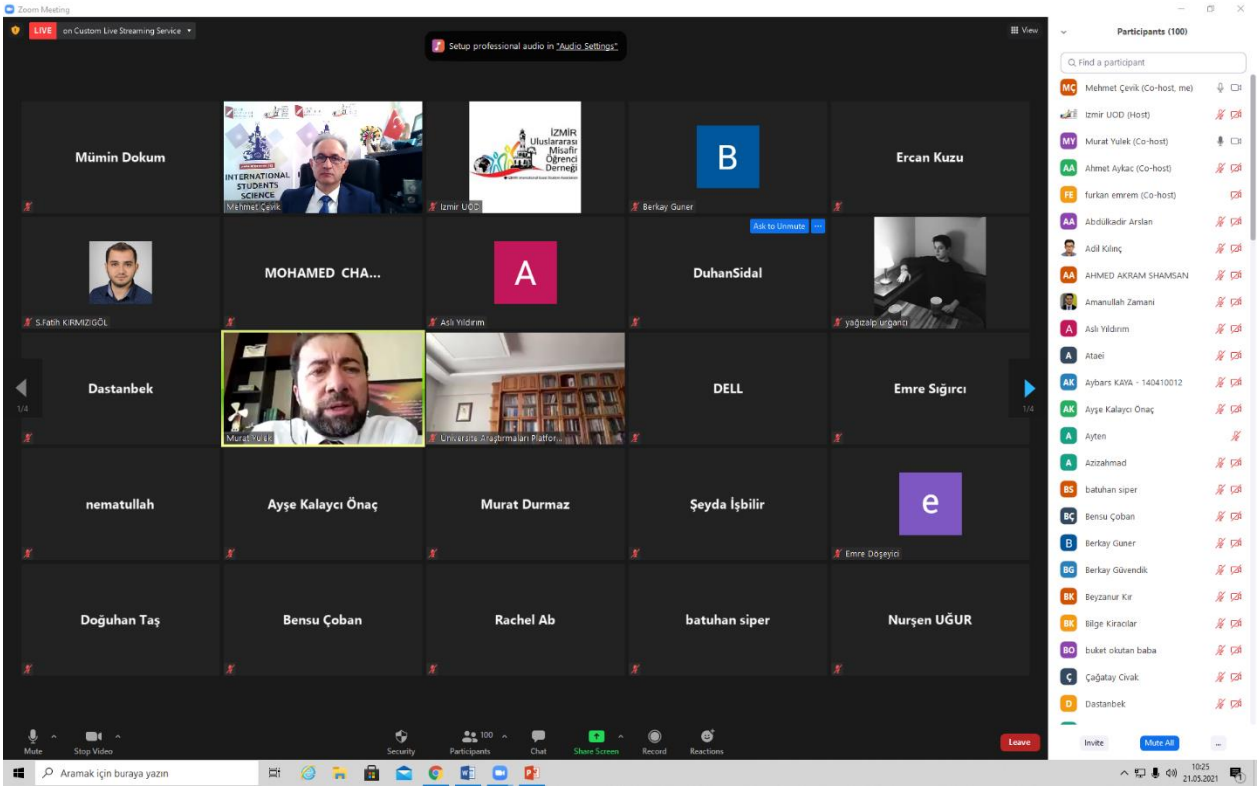
Mümin Dokum
Ercan Kuzu
MOHAMED CHA...
DuhanSidal
Dastanbek
DELL
Emre Sığırcı
nematullah
Ayşe Kalaycı Önaç
Murat Durmaz
Şeyda İşbilir
Doğuhan Taş
Bensu Çoban
Rachel Ab
batuhan siper
Nurşen UĞUR
Participants (100)